Syntheses in Limnogeology 1

Michael Elliot Smith
Alan R. Carroll *Editors*

Stratigraphy and Paleolimnology of the Green River Formation, Western USA

EXTRAS ONLINE

Springer

Syntheses in Limnogeology

Volume 1

Series Editors

Michael R. Rosen
Department of Geological Sciences and Engineering,
University of Nevada, Reno, Nevada, USA

Elizabeth Gierlowski-Kordesch
Department of Geological Sciences,
Ohio University, Athens, Ohio, USA

Aims and Scope

The aim of this book series is to focus on syntheses or summaries of modern and/or ancient lake systems worldwide. Individual books will present as much information as is available for a particular lake basin or system of basins to offer readers one distinct reference as a guide to conduct further work in these areas. The books will synthesize the tectonics, basin evolution, paleohydrology, and paleoclimate of these basins and provide unbiased new interpretations or provide information on both sides of controversial issues. In addition, some books in the series will synthesize special topics in limnogeology, such as historical records of pollution in lake sediments and global paleoclimate signatures from lake sediment records.

More information about this series at http://www.springer.com/series/10029

Michael Elliot Smith • Alan R. Carroll
Editors

Stratigraphy and Paleolimnology of the Green River Formation, Western USA

Springer

Editors
Michael Elliot Smith
School of Earth Science
and Environmental Sustainability
Northern Arizona University
Flagstaff, AZ, USA

Alan R. Carroll
Department of Geoscience
University of Wisconsin-Madison
Madison, WI, USA

Additional material to this book can be downloaded from http://extras.springer.com.

ISSN 2211-2731 ISSN 2211-274X (electronic)
Syntheses in Limnogeology
ISBN 978-94-017-9905-8 ISBN 978-94-017-9906-5 (eBook)
DOI 10.1007/978-94-017-9906-5

Library of Congress Control Number: 2015943673

Springer Dordrecht Heidelberg New York London

Cover illustration: View north towards carbonate mounds at the contact between the Wilkins Peak Member and overlying Laney Member of the Green River Formation near the southern edge of the Greater Green River Basin in southwest Wyoming. Flaming Gorge Reservoir can be seen in the background to the left of gently dipping mudstone strata of the Laney Member (photograph taken by Michael Elliot Smith, 2004)

Printed on acid-free paper

Springer Science+Business Media B.V. Dordrecht is part of Springer Science+Business Media (www.springer.com)

Preface

This book was originally conceived at a dinner meeting with Beth Gierlowski-Kordesch, Kevin Bohacs and Mike Rosen in Portland, Oregon during the GSA annual meeting of 2009. Its purpose is two-fold: (1) to provide a logical starting point to its strata; and (2) to showcase the wealth of sedimentary geology currently being conducted on its strata. Our hope is that the reader can efficiently discover a wealth of accumulated knowledge and at the same get a snapshot of the current cutting edge of sedimentary research on lacustrine depositional systems.

Our gratitude goes out to all of the contributors and reviewers of this volume.

Flagstaff, AZ, USA — Michael Elliot Smith
Madison, WI, USA — Alan R. Carroll
February, 2015

Contents

Introduction to the Green River Formation

1

Michael Elliot Smith and Alan R. Carroll

Abstract

The Green River Formation of Wyoming, Colorado and Utah contains an important record of the paleogeography, climate and lakes in the Rocky Mountains region during the Early Eocene epoch. Its have been a source of inspiration for paleolimnologists since before the term paleolimnology came to exist. Its strata contain fossil faunas and flora, extensive resources of trona and kerogenous shale, and one of the most complete records of the Early Eocene Climatic Optimum. Emerging geochronology has permitted correlations of the Green River Formation between the structural basins that contain it, and is beginning to bring to tempo and origins of the pronounced cyclity exhibited by the Green River Formation into focus. Each of the 11 subsequent chapters of this book presents a suite of detailed stratigraphic and sedimentologic investigations of the Green River Formation within the Green River Formation basins.

1.1 A Rich Lacustrine Archive of the Early Eocene Earth

The Green River Formation is a complex amalgam of Eocene lacustrine strata that was deposited within a series of intermontane basins surrounding the Uinta Uplift during the end phases of Laramide basement deformation in the U.S. foreland (Fig. 1.1). Since it was first named by the Hayden survey in 1869, the Green River Formation has been the subject of over 2,500 publications. Its strata occupy four structural basins arrayed around the Uinta Uplift: the Greater

M.E. Smith (✉)
School of Earth Science and Environmental Sustainability, Northern Arizona University, 602 S. Humphreys, Flagstaff, AZ 86011, USA
e-mail: michael.e.smith@nau.edu

A.R. Carroll
Department of Geoscience, University of Wisconsin-Madison, 1215 W. Dayton St., Madison, WI 53706, USA
e-mail: carroll@geology.wisc.edu

M.E. Smith, A.R. Carroll (eds.), *Stratigraphy and Paleolimnology of the Green River Formation, Western USA*, Syntheses in Limnogeology 1, DOI 10.1007/978-94-017-9906-5_1

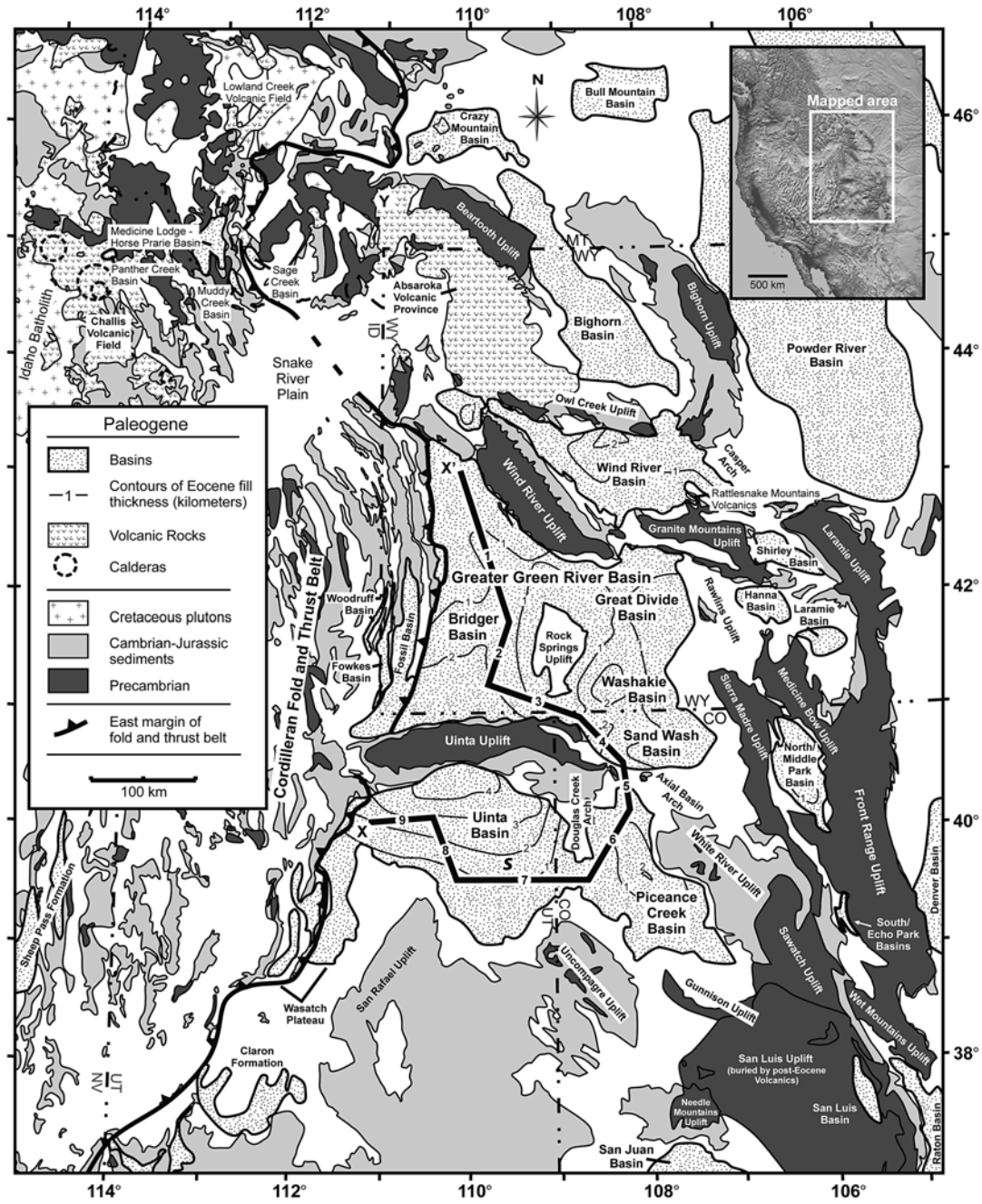

Fig. 1.1 Map showing the location of Eocene basins and basin-bounding uplifts (Adapted from Smith et al. 2008). The location of the Skyline 16 core from which the Skyline tuff was sampled from is indicated by an ***S*** (cf. Fig. 1.4)

Green River; Fossil; Piceance Creek; and Uinta basins (Fig 1.1), record a great variety of depositional environments (i.e., lake depth, lake water chemistry, and paleobiology), and interfinger extensively with predominantly alluvial facies of the Wasatch, DeBeque, Colton, Bridger and Uinta Formations (Fig. 1.2). In this volume alone, more than 100 distinct Green River Formation lithofacies are described and interpreted.

The Green River Formation was deposited during the most geologically recent period of unusually warm climate (cf. Smith et al. 2014),

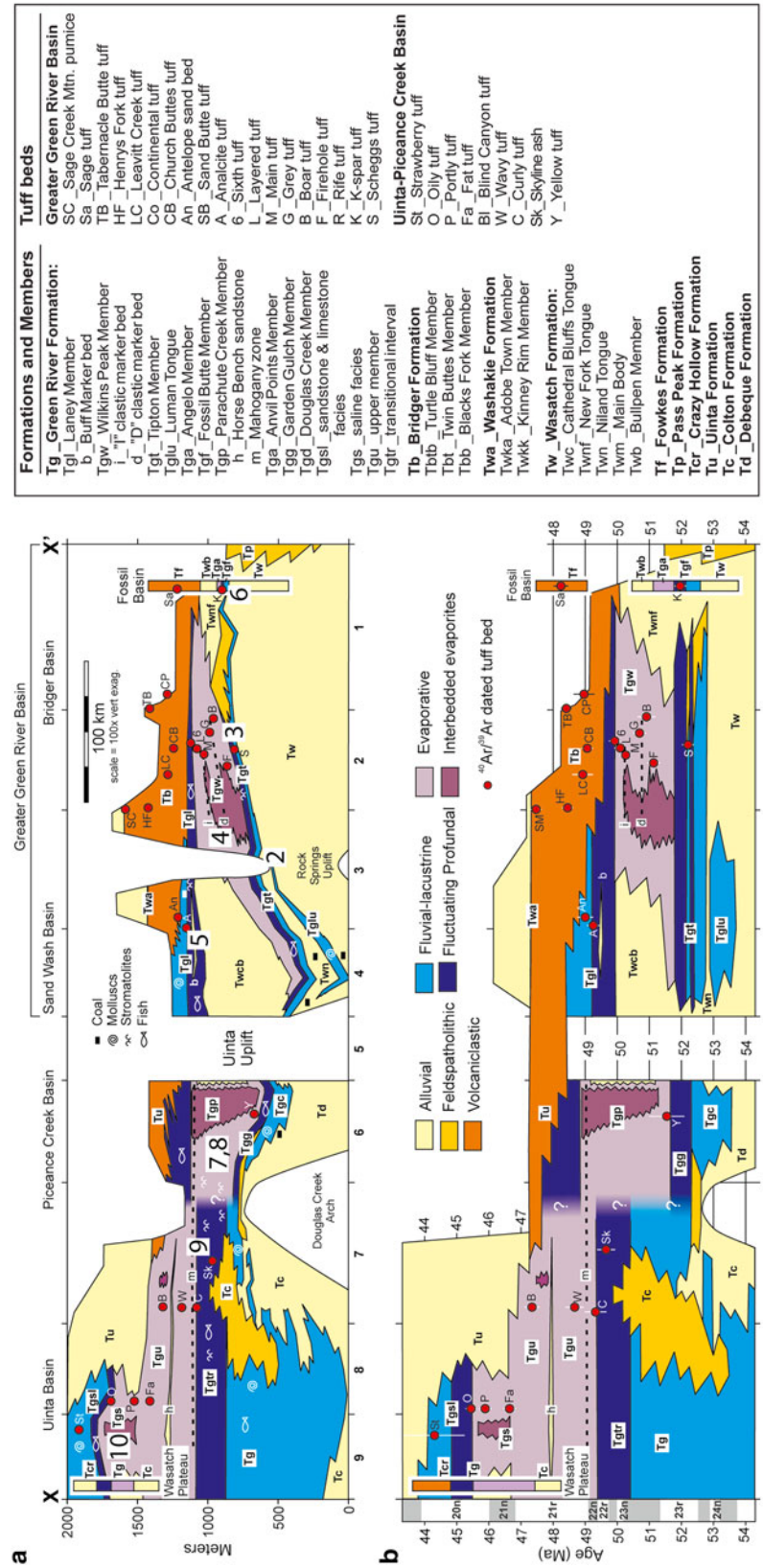

Fig. 1.2 Lithostratigraphic and time stratigraphic cross sections of Eocene strata in the Greater Green River, Piceance, and Uinta Basins along cross section X-X′ (see Fig. 1.1) showing the stratigraphic position of facies associations, structural features, and dated tuff beds. Cross section line was chosen in order to intersect area of thickest sediment accumulation, sites of bedded evaporites, and principle sills. Inset columns with white background depict stratigraphy and chronostratigraphy of the Green River Formation in the Fossil Basin and Wasatch Plateau regions (Modified from Smith et al. (2008) with the updated magnetostratigraphy and geochronology of Smith et al. (2014))

and as such it provides a valuable opportunity to examine the mode and tempo of past episodes of global warming. A number of studies have concluded that fluctuations in Eocene lake levels were caused by Milanovitch-scale orbital forcing of climate (Fischer and Roberts 1991; Roehler 1993; Machlus et al. 2008; Meyers 2008; Aswasereelert et al. 2013) or by shorter-period climatic oscillations related to ENSO or sunspots (Bradley 1929; Ripepe et al. 1991). The actual mechanisms by which any these putative forcing signals were transferred into Green River Formation strata remain enigmatic however.

Green River Formation strata and their alluvial equivalents also contain an unparalleled fossil treasure trove, famous for its well preserved vertebrate (both terrestrial and aquatic) and plant remains that have been preserved within its finely laminated strata (MacGinitie 1969; Grande 1984; Wilf 2000). It is also host to several rich and varied assemblages of trace fossils (see Chap. 12 of this volume). Vertebrate fossils collected from alluvial strata laterally equivalent to the Green River Formation throughout the Laramide broken foreland province have been utilized to define the North American land mammal "ages" (Wood et al. 1941), which have been refined and subdivided by subsequent paleontologic investigations (cf. Robinson et al. 2004). Though vertebrate fossils are rare to entirely absent in the Green River Formation itself, a great number of vertebrate faunas have been collected from Green River Formation-equivalent alluvial strata assigned to the Wasatch, DeBeque, Colton, Bridger and Uinta Formations (Osborn 1895; Morris 1954; McGrew and Roehler 1960; McGrew and Sullivan 1970; Gunnell and Bartels 1994, 1999; Gunnell 1998; Zonneveld et al. 2000) and indicate that the Green River Formation spans the Wasatchian, Bridgerian and Uinta land mammal ages (Fig. 1.2; cf. Smith et al. 2008).

The Green River Formation has also stimulated considerable interest due to its rich endowment of economic resources. Its potential to generate oil via retort of organic-rich mudstone has been recognized since at least 1916, when federal Naval Oil Shale Reserves were designated by Woodrow Wilson in Colorado and Utah. Recent U.S.G.S. estimates put the total in situ resource magnitude in Colorado, Utah, and Wyoming at approximately 4.3 trillion barrels of oil (Johnson et al. 2011), an amount 2.5 times greater than the currently proven oil reserves of the world. However, it remains unclear how much of this resource (if any) will be commercially exploited, or whether the environmental consequences of its use would outweigh the benefits. Although very rich, Green River Formation oil shale is generally too thermally immature to act as a conventional petroleum source rock across most of its area, except in the northern Uinta basin. There, oil generated from the lower Green River Formation accounted for approximately 30 million barrels of production in 2014 (Utah Division of Oil, Gas, and Mining).

The other main economic resource of the Green River Formation is soda ash, which is mined primarily in the form of trona (cf. Wiig et al. 1995). Trona deposits in the Bridger basin of Wyoming represent the single largest soda ash deposit in the world, and with more than 17 million metric tons of production in 2013 (U.S.G.S. 2013 Minerals Yearbook).

1.2 A Century and a Half of Geologic Inquiry

Wilmot H. Bradley's pioneering work on the Green River Formation during the 1920s through 1970s set a high bar for subsequent workers (Sears and Bradley 1924; Bradley 1926, 1928, 1929, 1931, 1964, 1974), and set the stage for the types of questions that are still being investigated nearly a century later (i.e., stratigraphic packaging, lacustrine sedimentology, and the identification of climate cycles from vertical facies stacking patterns).

During the 1950s through 1990s, and great number of scientists from the U.S. Geological Survey, industry and academia brought the Green River Formation into much greater focus by differentiating, mapping and correlating its member-scale units and lithofacies (Donovan 1950; Duncan and Belser 1950; Dane 1954; Picard 1955; Bradley 1959; Picard 1959; Culbertson 1961, 1965, 1966, 1971, 1998; Donnell 1961; Stuart 1963; Love 1964; Wiegman 1964; Hansen 1965; Sanborn and Goodwin 1965; Roehler 1968; Oriel and Tracey 1970; Trudell et al. 1970;

Wolfbauer 1971; Cashion and Donnell 1972, 1974; Roehler 1973; West 1973; Duncan et al. 1974; O'Sullivan 1974; Trudell et al. 1974; Fouch 1976; Burnside and Culbertson 1979; Surdam and Stanley 1979, 1980; Sullivan 1980; Dyni 1981, 1996; Johnson 1984, 1985; Dyni et al. 1985; Roehler 1985; Rowley et al. 1985; Hail 1987, 1990, 1992; Franczyk et al. 1989; Roehler 1991, 1992, 1993; Franczyk et al. 1992; Remy 1992; and works cited within; Buchheim 1994; Wiig et al. 1995; Buchheim and Eugster 1998). These efforts were aided by an extensive coring program funded by both industry and the U.S. Energy Research and Development Administration. Several of these cores are still available at the U.S.G.S. core repository in Denver, Colorado.

During the 1970s and early 1980s, detailed sedimentologic investigation of the Wilkins Peak Member of the Green River Formation in Wyoming revealed that a significant proportion of its lithofacies were accumulated on lake fringing playa rather than within a deep stratified lake (Eugster and Surdam 1973; Wolfbauer 1973; Wolfbauer and Surdam 1974; Eugster and Hardie 1975; Surdam and Wolfbauer 1975; Smoot 1978, 1983). The application of the playa-lake model to other members of the Green River Formation has proven less successful, however, because much of the Green River Formation, including portions of the Wilkins Peak Member, does in fact record deep lake conditions.

The Green River Formation was influential in the conception and development of the lake type concept (Carroll and Bohacs 1999; Bohacs et al. 2000), which relates lacustrine lithofacies and stacking patterns to the long term balance between precipitation, evaporation, and basinal accommodation. The criteria used for lake type subdivision of its strata are summarized in Table 1.1.

Since the advent of the new century, investigations of the Green River Formation have taken advantage of new radioisotopic dating methods (Smith et al. 2008, 2010, cf. Table 1.2), sedimentology and ichnology (cf. Chap. 12), stable and radiogenic isotopic proxies (Doebbert et al. 2010, 2014), and the application of sequence- and cyclo-stratigraphy to its strata (Bohacs et al. 2007; Machlus et al. 2008; Aswasereelert et al. 2013). Radioisotopic geochronology ($^{40}Ar/^{39}Ar$ and U-Pb) in particular has facilitated viewing the Green River lake system as a whole in a paleogeographic context (Fig. 1.3). This volume contains nine chapters (Chaps. 2, 3, 4, 5, 6, 7, 8, 9, 10) that explore the member-scale stratigraphy and lithofacies of the Green River Formation within the individual basins it occupies (Fig. 1.2), and the two final Chaps. (11 and 12) which address the paleoenvironmental implications of evaporite deposits and ichnofossils from a regional perspective.

Acknowledgments We thank Michael Vanden Berg, Lauren P. Birgenheiler, and the Utah Geological Survey for kindly providing a core sample of the Skyline tuff. Laser fusion $^{40}Ar/^{39}Ar$ geochronology for the Skyline tuff was conducted by Brian Jicha and Brad S. Singer the University of Wisconsin-Madison. National Science Foundation grants EAR-0230123, EAR-0114055 and EAR-0516760, the Donors of the Petroleum Research Fund of the American Chemical Society, Chevron, and ConocoPhillips kindly provided funding for the geochronology and stratigraphy summarized in Figs. 1.1, 1.2, and 1.3.

Table 1.1 Criteria for classification of lake type in Green River Formation strata

Basin type	Facies Association	Typical facies	Stratigraphic stacking	Fauna	Hydrologic interpretation
Overfilled	Fluvial-lacustrine	Sandstone, coal, massive to laminated mudstone, coquina limestone	Dominantly progradational	Molluscs common, occasional fish	Freshwater "open" lake
Balanced Filled	Fluctuating profundal	Predominantly organic rich laminated mudstone, stromatolites, oolites	Mixed aggradational/ progradational	Fish, ostracodes	Fluctuating salinity, intermittently open/closed lake
Underfilled	Evaporative	Na-rich evaporites, may include basin interior alluvial units and palustrine mudstone	Aggradational	Fauna absent	Hypersaline "closed" lake

Table 1.2 $^{40}Ar/^{39}Ar$ ages for Eocene strata in the Laramide foreland province

Location Sample	Stratigraphy	Dated Material	Method	flux monitor	Age (Ma)	±2σ[a]	±2σ[b]	References
Greater Green River Basin								
Scheggs tuff	Tipton Member	san	fus	TCs	52.22	±0.09	±0.35	Smith et al. (2008, 2010)
Rife tuff	”	san	fus	”	51.62	±0.30	±0.45	”
Firehole tuff	Wilkins Peak Member	san	fus	”	51.41	±0.21	±0.39	”
Boar tuff	”	san	fus	”	51.14	±0.24	±0.41	”
Grey tuff	”	san	fus	”	50.86	±0.21	±0.39	”
Main tuff	”	san	fus	”	50.28	±0.09	±0.34	”
Layered tuff	”	san	fus	”	50.12	±0.09	±0.34	”
6th tuff	”	bio	ih	”	49.93	±0.10	±0.34	”
Analcite tuff	Laney Member	san	fus	”	49.25	±0.12	±0.34	”
Antelope sandstone	”	san	fus	”	49.00	±0.19	±0.37	”
Church Butte tuff	Bridger Formation	san	fus	”	49.06	±0.09	±0.33	”
Leavitt Creek tuff	”	san	fus	”	48.93	±0.28	±0.42	”
Henrys Fork tuff	”	san	fus	”	48.45	±0.08	±0.32	”
Tabernacle Butte tuff	”	san	fus	”	48.41	±0.08	±0.32	”
Sage Creek tuff	”	san	fus	”	47.46	±0.08	±0.32	”
Continental tuff	”	san	fus	”	48.97	±0.28	±0.42	”
Fossil Basin								
K-spar tuff	Fossil Butte Member	san	fus	”	51.98	±0.09	±0.35	”
Sage tuff	Fowkes Formation	san	fus	”	48.23	±0.17	±0.36	”
Piceance Creek Basin								
Yellow tuff	Parachute Creek Mb.	san	fus	”	51.56	±0.52	±0.62	”
Uinta Basin								
Skyline ash	Parachute Creek Mb.	san	fus	FCs	49.58	±0.28	±0.32	***This study*** (cf. Fig. 1.4 and Table 1.3)
Curly tuff	”	bio	ih	TCs	49.32	±0.30	±0.44	Smith et al. (2008, 2010)
Wavy tuff	”	bio	ih	”	48.67	±0.23	±0.39	”
Blind Canyon tuff	”	bio	ih	”	47.33	±0.18	±0.36	”
Fat tuff	Saline member	bio	ih	”	46.63	±0.13	±0.33	”
Portly tuff	”	bio	ih	”	45.86	±0.14	±0.33	”
Oily tuff	”	bio	ih	”	45.42	±0.10	±0.31	”
Strawberry tuff	sandstone and limestone member	san	fus	”	44.27	±0.93	±0.97	”

(continued)

Table 1.2 (continued)

Location Sample	Stratigraphy	Dated Material	Method	flux monitor	Age (Ma)	±2σ[a]	±2σ[b]	References
Wind River Basin								
Halfway Draw tuff	Wind River Formation	san	fus	”	52.07	±0.10	±0.35	”
Wagon Bed tuff	Wagon Bed Formation	san	fus	”	47.99	±0.12	±0.33	”
Bighorn Basin								
Willwood ash	Willwood Formation	san	fus	”	52.91	±0.12	±0.36	Smith et al. (2004)

Notes: All ages calculated relative to the 28.201 Ma age for FCs using the equations of Kuiper et al. (2008) and Renne et al. (1998), and are shown with 2σ analytical and fully propagated uncertainties. Mineral dated: san – sanidine, bio – biotite. Analysis type: ih – weighted mean of concordant plateau ages from incremental heating experiments, fus – weighted mean of multiple laser fusions. Neutron flux monitors: *TCs* Taylor Creek Rhyolite sanidine, *FCs* Fish Canyon Tuff sanidine, Cf. Smith et al. (2008) for analytical details

[a]Analytical uncertainty

[b]Fully propagated uncertainty for preferred age

Table 1.3 $^{40}Ar/^{39}Ar$ results for Skyline tuff single crystal laser fusion experiments

$^{40}Ar/^{39}Ar$	$^{37}Ar/^{39}Ar$	$^{36}Ar/^{39}Ar$	$^{40}Ar^*$ $\times10^{-14}$ mol	$^{40}Ar^*$ %	K/Ca	Apparent age ± 2σ Ma
3.669 ± 0.009	0.00305 ± 0.00185	0.000317 ± 0.000074	0.19	97.4	141	50.25 ± 0.65
4.763 ± 0.011	0.04946 ± 0.00312	0.004088 ± 0.000109	0.17	74.7	9	50.01 ± 0.93
4.012 ± 0.010	0.03922 ± 0.00198	0.001600 ± 0.000088	0.20	88.3	11	49.79 ± 0.76
4.079 ± 0.008	0.02443 ± 0.00139	0.002002 ± 0.000059	0.30	85.5	18	49.05 ± 0.52
3.657 ± 0.010	0.06422 ± 0.00397	0.000256 ± 0.000121	0.11	98.1	7	50.40 ± 1.02
3.937 ± 0.008	0.01221 ± 0.00210	0.001347 ± 0.000071	0.23	89.9	35	49.75 ± 0.62
3.867 ± 0.008	0.00993 ± 0.00218	0.001191 ± 0.000096	0.17	90.9	43	49.42 ± 0.82
4.419 ± 0.011	0.01673 ± 0.00287	0.002851 ± 0.000117	0.16	81.0	26	50.28 ± 0.99
4.435 ± 0.010	0.02423 ± 0.00290	0.003170 ± 0.000123	0.15	78.9	18	49.21 ± 1.04
4.006 ± 0.009	0.08356 ± 0.00343	0.001772 ± 0.000095	0.19	87.1	5	49.04 ± 0.81
4.496 ± 0.010	0.09342 ± 0.00393	0.003342 ± 0.000110	0.18	78.2	5	49.42 ± 0.93
4.644 ± 0.010	0.02280 ± 0.00227	0.003790 ± 0.000100	0.21	75.9	19	49.55 ± 0.85
4.269 ± 0.008	0.01886 ± 0.00214	0.002632 ± 0.000099	0.19	81.8	23	49.10 ± 0.84
4.697 ± 0.009	0.07262 ± 0.00376	0.004373 ± 0.000112	0.21	72.6	6	47.96 ± 0.94
Inverse isochron age	49.78 ± 0.55					
$^{40}Ar/^{39}Ar$ intercept	288.2 ± 17.3	MSWD	1.52	**Weighted mean age**		**49.58 ± 0.28**

Notes: All ages calculated relative to 28.201 Ma for the Fish Canyon tuff sanidine (Kuiper et al. 2008); using the decay constants of Min et al. (2000); uncertainties in Ar isotope ratios are reported at 1σ analytical precision, uncertainties in ages are reported at 2σ analytical precision. Corrected for ^{37}Ar and ^{39}Ar decay, half lives of 35.2 days and 269 years, respectively. $J = 0.0078430 \pm 0.00000701$; $\mu = 1.0060$. Italics indicate analysis that were excluded from weighted mean age calculations

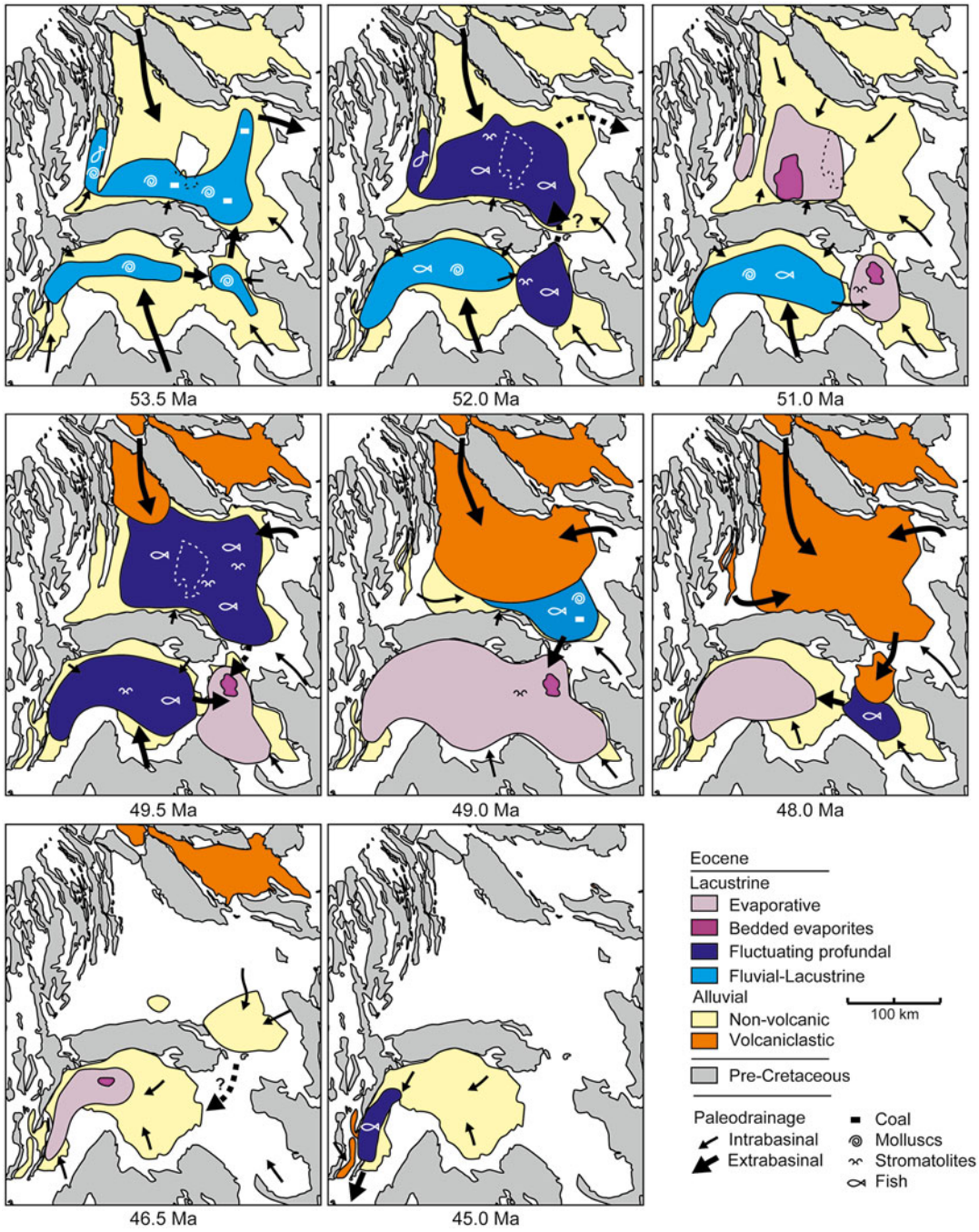

Fig. 1.3 Annotated synoptic maps showing paleohydrologic configuration of the Green River Formation lakes at 8 discrete times between 53.5 and 45 Ma (updated from Smith et al. 2008). Time slices were selected to highlight major hydrologic configurations of Green River Formation lake system (cf. Smith et al. 2008). Note that knowledge of the continuity of lacustrine deposition in the central Greater Green River Basin is limited by the absence of Eocene strata atop the Rock Springs uplift (*dashed outline*).

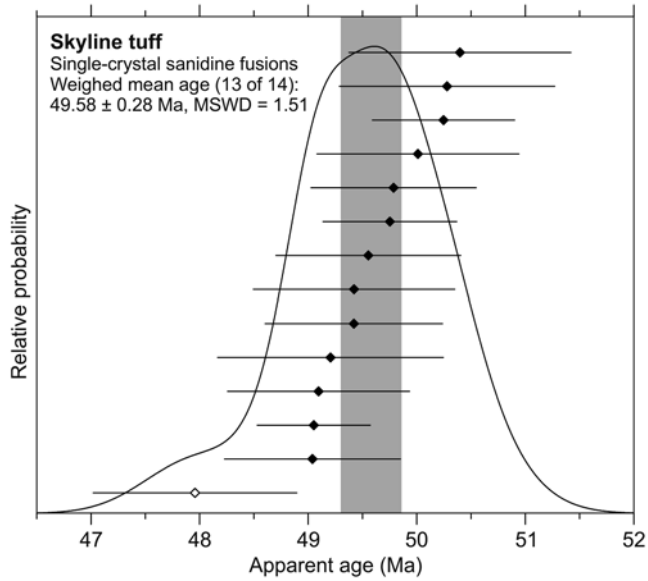

Fig. 1.4 Cumulative probability plot of $^{40}Ar/^{39}Ar$ laser fusion analyses of single sanidine from the Skyline tuff. The airfall ash was sampled from profundal facies of the R-4 oil shale zone in the Skyline 16 core in the R-4 oil shale zone (depth: 890.67–890.93 ft) in the Eastern Uinta Basin: (11S 25E sec. 10) 661506E, 4414904 N (UTM zone 12)

References

Aswasereelert W, Meyers SR, Carroll AR, Peters SE, Smith ME, Feigl KL (2013) Basin-scale cyclostratigraphy of the Green River Formation, Wyoming. Geol Soc Am Bull 125:216–228

Bohacs KM, Carroll AR, Neal JE, Mankiewicz PJ (2000) Lake-basin type, source potential, and hydrocarbon character: an integrated sequence-stratigraphic-geochemical framework. In: Gierlowski-Kordesch EH, Kelts KR (eds) Lake basins through space and time, Studies in Geology 46. American Association of Petroleum Geologists, Tulsa, pp 3–34

Bohacs KM, Grabowski GJ, Carroll AR (2007) Lithofacies architecture and variations in expression of sequence stratigraphy within representative intervals of the Green River Formation, Greater Green River Basin, Wyoming and Colorado. Mt Geol 44:39–60

Bradley WH (1926) Shore phases of the Green River Formation in northern Sweetwater County, Wyoming. U.S. Geological Survey professional paper 140-D, pp 121–131

Bradley WH (1928) Algae reefs and oolites of the Green River Formation. U.S. Geological Survey professional paper 154, pp 203–223

Bradley WH (1929) The varves and climate of the Green River epoch. U.S. Geological Survey professional paper 158-E, 110 p

Bradley WH (1931) Origin and microfossils of the oil shale of the Green River Formation of Colorado and Utah. U.S. Geological Survey professional paper 168, 58 p

Bradley WH (1959) Revision of stratigraphic nomenclature of Green River Formation of Wyoming. Am Assoc Pet Geol Bull 43:1072–1075

Bradley WH (1964) The geology of the Green River Formation and associated Eocene rocks in southwestern Wyoming and adjacent parts of Colorado and Utah. U.S. Geological Survey professional paper 496-A, 86 p

Bradley WH (1974) Oocardium tufa from the Eocene Green River Formation of Wyoming. J Paleontol 48:1289–1290

Buchheim HP (1994) Eocene fossil lake, Green River Formation, Wyoming: a history of fluctuating salinity. In: Renaut RW, Last WM (eds) Sedimentology and geochemistry of modern and ancient saline lakes, Special Publication 50. SEPM (Society for Sedimentary Geology), Tulsa, pp 239–247

Buchheim HP, Eugster HP (1998) Eocene Fossil Lake: the Green River Formation of Fossil Basin, southwestern Wyoming. In: Pitman JK, Carroll AR (eds) Modern & ancient lake systems; New problems and perspectives, Publication 26. Utah Geological Association, Salt Lake City, pp 191–208

Burnside MJ, Culbertson WC (1979) Trona deposits in the Green River Formation, sweetwater, Uinta, and

Lincoln counties, Wyoming. U.S. Geological Survey open-file report 79–737
Carroll AR, Bohacs KM (1999) Stratigraphic classification of ancient lakes: balancing tectonic and climatic controls. Geology 27:99–102
Cashion WB, Donnell JR (1972) Chart showing correlation of key units in the organic-rich sequence of the Green River Formation, Piceance Creek basin, Colorado, and Uinta basin, Utah. U.S. Geological Survey Oil and Gas Investigations Chart OC-65
Cashion WB, Donnell JR (1974) Revision of the nomenclature of the upper part of the Green River Formation, Piceance Creek Basin, Colorado, and Eastern Uinta Basin, Utah. U.S. Geological Survey bulletin 1394-G, 9 p
Culbertson WC (1961) Stratigraphy of the Wilkins Peak Member of the Green River Formation, Firehole Basin quadrangle, Wyoming. U.S. Geological Survey professional paper 424-D, pp 170–173
Culbertson WC (1965) Tongues of the Green River and Wasatch Formations in southeastern part of the Green River Basin, Wyoming. In: De Voto RH, Bitter RK (eds) Sedimentation of late Cretaceous and Tertiary outcrops, Rock Springs uplift. 19th annual field conference guidebook, Wyoming Geological Association, Casper, pp 151–155
Culbertson WC (1966) Trona in the Wilkins Peak Member of the Green River Formation, southwestern Wyoming. U.S. Geological Survey professional paper 550-B, pp 159–164
Culbertson WC (1971) Stratigraphy of the trona deposits in the Green River Formation, southwest Wyoming. Univ Wyo Contrib Geol 10:15–23
Culbertson WC (1998) Road log for the geology field trip of June 13, 1997, Geology and outcrops of the trona-bearing rocks of the Green River Formation. Wyoming State Geological Survey public information circular 40, pp 205–211
Dane CH (1954) Stratigraphic and facies relationships of upper part of Green River Formation and lower part of Uinta Formation in Duchesne, Uintah, and Wasatch Counties, Utah. Geol Soc Am Bull 38:405–425
Doebbert AC, Carroll AR, Mulch A, Chetel LM, Chamberlain CP (2010) Geomorphic controls on lacustrine isotopic compositions: Evidence from the Laney member, Green River Formation, Wyoming. Geol Soc Am Bull 122:236–252
Doebbert AC, Johnson CM, Carroll AR, Beard BL, Pietras JT, Rhodes-Carson MK, Norsted B, Throckmorton LA (2014) Controls on Sr isotopic evolution in lacustrine systems: Eocene Green River Formation, Wyoming. Chem Geol 380:172–179
Donnell JR (1961) Tertiary geology and oil-shale resources of the Piceance Creek Basin between the Colorado and White Rivers, northwestern Colorado. U.S. Geological Survey Bulletin 1082-L, pp 835–891
Donovan JH (1950) Intertonguing of Green River and Wasatch Formations in part of Sublette and Lincoln Counties, Wyoming. In: Harrison JW (ed) Southwest Wyoming. 5th annual field conference guidebook, pp 59–67
Duncan DC, Belser C (1950) Geology and oil-shale resources of the eastern part of the Piceance Creek Basin, Rio Blanco and Garfield counties, Colorado. U.S. Geological Survey oil and gas investigations map OM-119
Duncan DC, Hail WJ, Jr., O'Sullivan RB, Pipiringos GN (1974) Four newly named tongues of Eocene Green River Formation, northern Piceance Creek Basin, Colorado. U.S. Geological Survey Bulletin 1394-F, 13 p
Dyni JR (1981) Geology of the nacholite deposits and associated oil shales of the Green River Formation in the Piceance Creek Basin, Colorado. PhD thesis, University of Colorado, Boulder, 144 p
Dyni JR, Milton C, Cashion WB (1985) The saline facies of the upper part of the Green River Formation near Duchesne, Utah. In: Picard MD (ed) Geology and Energy Resources, Uinta Basin of Utah, Publication 12. Utah Geological Association, Salt Lake City, pp 51–60
Dyni, J. R., 1996, Sodium carbonate resources of the Green River Formation in Utah, Colorado, and Wyoming, U.S. Geological Survey open-file report 96–729, 39 p
Eugster HP, Hardie LA (1975) Sedimentation in an ancient playa-lake complex: the Wilkins Peak Member of the Green River Formation of Wyoming. Geol Soc Am Bull 86:319–334
Eugster HP, Surdam RC (1973) Depositional environment of the Green River Formation of Wyoming: a preliminary report. Geol Soc Am Bull 84:1115–1120
Fischer AG, Roberts LT (1991) Cyclicity in the Green River Formation (lacustrine Eocene) of Wyoming. J Sediment Petrol 61:1146–1154
Fouch TD (1976) Revision of the lower part of the tertiary system in the central and western Uinta Basin, Utah. U.S. Geological Survey Bulletin 1405-C, 7 p
Franczyk KJ, Pitman JK, Cashion WB, Dyni JR, Fouch TD, Johnson RC, Chan MA, Donnell JR, Lawton TF, Remy RR (1989) Evolution of resource-rich foreland and intermontane basins in eastern Utah and western Colorado: Salt Lake City, Utah, to Grand Junction, Colorado, July 20–24. In: American Geophysical Union field trip guidebook T324, Washington, D.C., 53 p
Franczyk KJ, Fouch TD, Johnson RC, Molenaar CM, Cobban WA (1992) Cretaceous and Tertiary paleogeographic reconstructions for the Uinta-Piceance Basin study area, Colorado and Utah. U.S. Geological Survey bulletin 1787-Q, 37 p
Grande L (1984) Paleontology of the Green River Formation, with a review of the fish fauna (second edition). Geological Survey of Wyoming Bulletin 63, 333 p
Gunnell GF (1998) Mammalian fauna from the lower Bridger Formation (Bridger A, Early Middle Eocene) of the southern Green River Basin, Wyoming. University of Michigan Contributions from the Museum of Paleontology 30:83–130

Gunnell GF, Bartels WS (1994) Early Bridgerian (middle Eocene) vertebrate paleontology and paleoecology of the southern Green River Basin, Wyoming. Univ Wyo Contrib Geol 30:57–70

Gunnell GF, Bartels WS (1999) Middle Eocene vertebrates from the Uinta Basin, Utah, and their relationship with faunas from the southern Green River Basin, Wyoming. In: Gillette DD (ed) Vertebrate paleontology of Utah, Miscellaneous Publication 99–1. Utah Geological Survey, Salt Lake City, pp 429–442

Hail WJ, Jr. (1987) Chart showing intertongued units of the Eocene Green River and Uinta Formations, northwestern Piceance Creek Basin, northwestern Colorado. U.S. Geological Survey Miscellaneous Investigations Series Map I-1797

Hail WJ, Jr. (1990) Geology of the lower Yellow Creek area, northwestern Colorado. U.S. Geological Survey Bulletin 1787-O, 45 p

Hail, W. J., Jr. (1992) Geology of the central Roan Plateau area, northwestern Colorado. U.S. Geological Survey Bulletin 1787-R, 26 p

Hansen WR (1965) Geology of the Flaming Gorge area Utah-Colorado-Wyoming. U.S. Geological Survey professional paper 490, 196 p

Hayden FV (1869) Preliminary field report of the United States Geological Survey of Colorado and New Mexico. U.S. Geological Survey of the Territories, third annual report, 155 p

Johnson RC (1984) New names for units in the lower part of the Green River Formation, Piceance Creek Basin, Colorado. U.S. Geological Survey bulletin 1529-I, 20 p

Johnson RC (1985) Early Cenozoic history of the Uinta and Piceance Creek basins, Utah and Colorado, with special reference to the development of Eocene Lake Uinta. In: Flores RM, Kaplan SS (eds) Cenozoic Paleogeography of the West Central United States. Rocky Mountain section, SEPM (Society for Sedimentary Geology) Rocky Mountain Paleogeography symposium 3, pp 247–276

Johnson RC et al. (2011) Oil shale resources of the Eocene Green River Formation, Greater Green River Basin, Wyoming, Colorado, and Utah. U.S. Geological Survey digital data series DDS–69–DD

Kuiper KF, Deino A, Hilgen FJ, Krijgsman W, Renne PR, Wijbrans JR (2008) Synchronizing rock clocks of Earth history. Science 320:500–504

Love JD (1964) Uraniferous phosphatic lake beds of Eocene age in intermontane basins of Wyoming and Utah. U.S. Geological Survey professional paper 474-E, 66 p

MacGinitie HD (1969) The Eocene Green River Flora of northwestern Colorado and northeastern Utah. University of California Publications in the Geological Sciences, vol 83, 230 p

Machlus ML, Olsen PE, Christie-Blick N, Hemming SR (2008) Spectral analysis of the lower Eocene Wilkins Peak Member, Green River Formation, Wyoming: support for Milankovitch cyclicity. Earth Planet Sci Lett 268:64–75

McGrew PO, Roehler HW (1960) Correlation of Tertiary units in southwestern Wyoming. In: McGookey DP, Miller DN, Jr. (eds) Overthrust Belt of Southwestern Wyoming and adjacent areas. Wyoming Geological Association 15th annual field conference guidebook, pp 157–158

McGrew PO, Sullivan R (1970) The stratigraphy and paleontology of Bridger A. Univ Wyo Contrib Geol 9:66–85

Meyers SR (2008) Resolving Milankovitchian controversies: the Triassic Latemar Limestone and the Eocene Green River Formation. Geology 36:319–322

Min K, Mundil R, Renne PR, Ludwig KR (2000) A test for systematic errors in $^{40}Ar/^{39}Ar$ geochronology through comparison with U-Pb analysis of a 1.1 Ga rhyolite. Geochim Cosmochim Acta 64:73–98

Morris WJ (1954) An Eocene fauna from the Cathedral Bluffs Tongue of the Washakie Basin, Wyoming. J Paleontol 28:195–203

Osborn HF (1895) Fossil mammals of the Uinta Basin. expedition of 1894. Am Mus Nat Hist Bull 7:71–105

O'Sullivan RB (1974) Chart showing correlation of selected restored stratigraphic diagram units of the Eocene Uinta and Green River Formations, east-central Piceance Creek Basin, northwestern Colorado. U.S. Geological Survey Oil and Gas Investigations Chart OC-67

Oriel SS, Tracey JI Jr. (1970) Uppermost cretaceous and Tertiary stratigraphy of Fossil Basin, southwestern Wyoming. U.S. Geological Survey professional paper 635, 53 p

Picard MD (1955) Subsurface stratigraphy and lithology of Green River Formation in Uinta Basin, Utah. Am Assoc Pet Geol Bull 39:75–102

Picard MD (1959) Green River and lower Uinta Formation subsurface stratigraphy in western Uinta Basin, Utah. In: Williams NC (ed) Guidebook to the geology of the Wasatch and Uinta Mountains, transition area. 10th annual field conference guidebook, International Association of Petroleum Geologists, Salt Lake City, pp 139–149

Remy RR (1992) Stratigraphy of the Eocene part of the Green River Formation in the south-central part of the Uinta Basin, Utah. U.S. Geological Survey Bulletin 1787-BB, 79 p

Renne PR, Swisher CC, Deino AL, Karner DB, Owens TL, DePaolo DJ (1998) Intercalibration of standards, absolute ages and uncertainties in $^{40}Ar/^{39}Ar$ dating. Chem Geol 145:117–152

Ripepe M, Roberts LT, Fischer AG (1991) ENSO and sunspot cycles in varved Eocene oil shales from image analysis. J Sediment Petrol 61:1155–1163

Robinson P, Gunnell GF, Walsh SL, Clyde WC, Storer JE, Stucky RK, Froehlich DJ, Ferrusquia-Villafranca I, McKenna MC (2004) Wasatchian through Duchesnean biochronology. In: Woodburne MO (ed) Late Cretaceous and Cenozoic Mammals of North America. Columbia University Press, New York, pp 106–155

Roehler HW (1968) Redefinition of Tipton Shale Member of Green River Formation of Wyoming. Am Assoc Pet Geol Bull 52:2249–2256

Roehler HW (1973) Stratigraphic divisions and geologic history of the Laney member of the Green River Formation

in the Washakie Basin in southwestern Wyoming. U.S. Geological Survey Bulletin 1372-E, 28 p

Roehler HW (1985) Geologic map of the Kinney Rim 30 x 60 minute quadrangle, Wyoming and Colorado. U.S. Geologic Survey Miscellaneous Investigations Series Map I-1615

Roehler HW (1991) Revised stratigraphic nomenclature for the Wasatch and Green River Formations of Eocene age, Wyoming, Utah, and Colorado. U.S. Geological Survey professional paper 1506-B, 38 p

Roehler HW (1992) Correlation, composition, areal distribution, and thickness of Eocene stratigraphic units, greater Green River basin, Wyoming, Utah, and Colorado. U.S. Geological Survey professional paper 1506-E, 49 p

Roehler HW (1993) Eocene climates, depositional environments, and geography, Greater Green River Basin, Wyoming, Utah, and Colorado. U.S. Geological Survey professional paper 1506-F, 74 p

Rowley PD, Hansen WR, Tweto O, Carrara PE (1985) Geologic map of the Vernal 1° x 2° quadrangle, Colorado, Utah, and Wyoming. U.S. Geological Survey miscellaneous investigations series map I-1526

Sanborn AF, Goodwin JC (1965) Green River Formation at Raven Ridge, Uintah county, Utah. Mt Geol 2:109–114

Sears JD, Bradley WH (1924) Relations of the Wasatch and Green River Formations in northwestern Colorado and southern Wyoming. U.S. Geological survey professional paper 132-F, pp 93–107

Smith ME, Carroll AR, Singer BS (2008) Synoptic reconstruction of a major ancient lake system: Eocene Green River Formation, Western United States. Geol Soc Am Bull 120:54–84

Smith ME, Chamberlain KR, Singer BS, Carroll AR (2010) Eocene clocks agree: Coeval $^{40}Ar/^{39}Ar$, U-Pb, and astronomical ages from the Green River Formation. Geology 38:527–530

Smith ME, Singer B, Carroll AR (2004) $^{40}Ar/^{39}Ar$ geochronology of the Eocene Green River Formation, Wyoming; reply. Geol Soc Am Bull 116:253–256

Smith ME, Carroll AR, Scott JJ, Singer BS (2014) Early Eocene carbon isotope excursions and landscape destabilization at eccentricity minima: green River Formation of Wyoming. Earth Planet Sci Lett 403:393–406

Smoot JP (1978) Origin of the carbonate sediments of the lacustrine Green River Formation (Eocene), Wyoming, U.S.A. In: Matter A (ed) Modern and ancient lake sediments, Special Publication 2. International Association of Sedimentologists, Blackwell Scientific Publishing, Oxford, pp 109–127

Smoot JP (1983) Depositional subenvironments in an arid closed basin; the Wilkins Peak Member of the Green River Formation (Eocene), Wyoming, U.S.A. Sedimentology 30:801–827

Stuart WJ, Jr. (1963) Stratigraphy of the Green River Formation west of the Rock Springs Uplift, Sweetwater County, Wyoming. M.Sc. thesis, University of Wyoming, Laramie, 51 p

Sullivan R (1980) A stratigraphic evaluation of the Eocene rocks of southwestern Wyoming. Wyoming Geological Survey report of investigations 20, 50 p

Surdam RC, Stanley KO (1979) Lacustrine sedimentation during the culminating phase of Eocene Lake Gosiute, Wyoming (Green River Formation). Geol Soc Am Bull 90:93–110

Surdam RC, Stanley KO (1980) Effects of changes in drainage-basin boundaries on sedimentation in Eocene Lakes Gosiute and Uinta of Wyoming, Utah, and Colorado. Geology 8:135–139

Surdam RC, Wolfbauer CA (1975) Green River Formation, Wyoming: a playa-lake complex. Geol Soc Am Bull 86:335–345

Trudell LG, Beard TN, Smith JW (1970) Green River Formation lithology and oil-shale correlations in the Piceance Creek Basin, Colorado. U.S. Bureau of Mines report of investigations 7357, 226 p

Trudell LG, Beard TN, Smith JW (1974) Stratigraphic framework of Green River Formation oil shales in the Piceance Creek Basin, Colorado. In: Murray DK (ed) guidebook to the energy resources of the Piceance Creek Basin, Colorado, Denver, Colorado. Rocky Mountain Association of Geologists, Denver, pp 65–69

West RM (1973) Geology and mammalian paleontology of the New Fork-Big Sandy area, Sublette County, Wyoming. Fieldiana: Geol 29, 193 p

Wiegman RW (1964) Late Cretaceous and early Tertiary stratigraphy of the Little Mountain area, Sweetwater County, Wyoming. M.Sc. thesis, University of Wyoming, Laramie, 53 p

Wiig SV, Grundy WD, Dyni, JR (1995) Trona resources in the Green River Basin, southwest Wyoming. U.S. Geological Survey open-file report OF 95-476, 91 p

Wilf P (2000) Late Paleocene-early Eocene climate changes in southwestern Wyoming: Paleobotanical analysis. Geol Soc Am Bull 112:292–307

Wolfbauer CA (1971) Geologic framework of the Green River Formation in Wyoming. Univ Wyo Contrib Geol 10:3–8

Wolfbauer CA (1973) Criteria for recognizing paleoenvironments in a playa-lake complex: the Green River Formation of Wyoming. In: Schell EM (ed) Symposium and core seminar on the geology and mineral resources of the Greater Green River Basin. 25th annual field conference guidebook, Wyoming Geological Association, Casper, pp 87–91

Wolfbauer CA, Surdam RC (1974) Origin of nonmarine dolomite in Eocene Lake Gosiute, Green River Basin, Wyoming. Geol Soc Am Bull 85:1733–1740

Wood HE II, Chaney RW, Clark J, Colbert EH, Jepson GL, Reedside JB, Stock C (1941) Nomenclature and correlation of the North American continental Tertiary. Geol Soc Am Bull 52:1–48

Zonneveld J-P, Gunnell GF, Bartels WS (2000) Early Eocene fossil vertebrates from the southwestern Green River Basin, Lincoln and Uinta counties, Wyoming. J Vert Paleontol 20:369–386

Initiation of Eocene Lacustrine Sedimentation in the Greater Green River Basin: Luman Member of the Green River Formation

2

Brooke Ann Norsted, Alan R. Carroll, and Michael Elliot Smith

Abstract

The Luman Member is the lowermost unit of the lacustrine Green River Formation, and provides an opportunity to examine in detail the initiation of lacustrine deposition within the Greater Green River Basin during the Early Eocene. Well-drained alluvial and fluvial strata of the Wasatch Formation are overlain by carbonaceous mudstone, channelized sandstone and isolated interbedded pond deposits of the lower Luman Member, which are in turn overlain by laterally extensive calcareous mudstone of the upper Luman Member, and together record a conformable progression alluvial to paludal to lacustrine environments. Here we describe alluvial, paludal and lacustrine lithofacies along a basin-scale transect through the Luman Member depocenter. Based on detailed correlation of Luman Member strata, freshwater lakes formed first in isolated regions of high subsidence to the east and west of the Rock Springs Uplift, then expanded and became more prone to carbonate deposition.

2.1 Introduction

Lacustrine systems commonly occur within and adjacent to active orogens. Uplifts are known to influence not only the distribution of lakes but also the character and architecture of lacustrine sedimentation patterns (e.g., Anadón et al. 1989; Sáez and Cabrera 2002). However, the interaction of large scale tectonic and climatic forcing on lacustrine depositional systems is poorly understood. Field exposures of the lacustrine Luman Member of the Green River Formation

B.A. Norsted • A.R. Carroll
Department of Geoscience, University of Wisconsin-Madison, 1215 W. Dayton St., Madison, WI 53706, USA

M.E. Smith (✉)
School of Earth Science and Environmental Sustainability, Northern Arizona University, 602 S. Humphreys, Flagstaff, AZ 86011, USA
e-mail: michael.e.smith@nau.edu

M.E. Smith, A.R. Carroll (eds.), *Stratigraphy and Paleolimnology of the Green River Formation, Western USA*, Syntheses in Limnogeology 1, DOI 10.1007/978-94-017-9906-5_2

along the southern margin of the Greater Green River Basin permit detailed observation of initiation and sedimentation in the context of growth of the Uinta and Rock Springs Uplifts.

This study examines sedimentology and stratigraphy of the Luman Member along an east-west cross-section that exposes the transgression of lacustrine facies over alluvial facies with the aim of constructing a genetic model for the embryonic stages of Lake Gosiute. Though ancient palustrine depositional environments are well described (cf. Sagri et al. 1989; Alonso-Zarza and Calvo 2000; Alonso-Zarza et al. 1992; Armenteros et al. 1997), less is known about the dynamics and stratal geometries associated with the transition from paludal to lacustrine environments.

2.2 Geologic Setting

2.2.1 Stratigraphic Framework

Terrestrial lithofacies within late Paleocene through the early Eocene strata in the southern part of the Greater Green River Basin record large-scale changes in accommodation and alluvial and lacustrine deposition that occurred in response to basin-bounding basement uplifts. The earliest Cenozoic deposits in the region consist of the Late Paleocene Fort Union Formation strata, which is comprised of sandstone and mudstone and sporadic coal beds that were deposited in fluvial, alluvial and limited paludal environments, respectively (McDonald 1972). The Fort Union Formation thickens to the north and east in the Greater Green River Basin, which likely records fluxurally-driven subsidence in response to growth of the Sierra Madre, Rawlins, and Wind River Uplifts (Beck et al. 1988). Overlying the Fort Union Formation are gray, green and red mudstones and light-gray to red sandstones were deposited in fluviatile and floodplain environments and constitute the Main Body of the Wasatch Formation (Roehler 1993). The Wasatch Formation is thickest in the south of the Greater Green River Basin, and thins to the north, indicating increased accommodation resulting from flexural loading by the Uinta Uplift coupled with high sediment supply rates in the southern part of the basin triggered by denudation of the Uinta Uplift (Roehler 1969). Overlying the Wasatch Formation (Fig. 2.1), the Green River Formation constitutes the deposits of Lake Gosiute, which occupied the 48,500 mi^2 of southwestern Wyoming in the early Eocene from 53 to 48 million years ago (Smith et al. 2008).

The term "Luman Tongue of the Green River Formation" was first applied by Pipiringos (1955) to a package of lacustrine strata within the upper part of the Wasatch Formation in the Great Divide sub-basin of the Greater Green River Basin. In its naming and in much of the subsequent literature, Luman strata have been considered a tongue. According to the North American Stratigraphic Code (1983), a tongue is "a wedging member that extends outward beyond a formation or wedges out within another formation." This definition implies lithological continuity between the tongue and the main body from which it is extending. Like all other members of the Green River Formation, on its margins, Luman strata exhibit intertonguing geometries with the adjacent Wasatch Formation. As a whole, however, the Luman is a lithologically distinct unit within the Green River Formation that is not laterally equivalent to any other parts of the GRF. We therefore adopt the term Luman Member for these deposits.

The Luman Member ranges in thickness from 10 to 125 m, however it is thickest in the southern part of the Greater Green River Basin in a trough that runs east-west, roughly parallel to the Uinta Mountains until bending to the northeast in the Washakie sub-basin (Roehler 1973). Complex intertonguing relationships and gradational transitions with both the overlying and underlying units contribute to significant lateral thickness gradients in the Luman Member thickness (Roehler 1987, this study; Culbertson 1965; Pipiringos 1955). The Luman Member is separated in many places from the Tipton Member and the rest of the Green River Formation proper by the Niland Tongue of the Wasatch Formation (Fig. 2.1). The Niland Tongue represents a return to widespread fluvial conditions before the

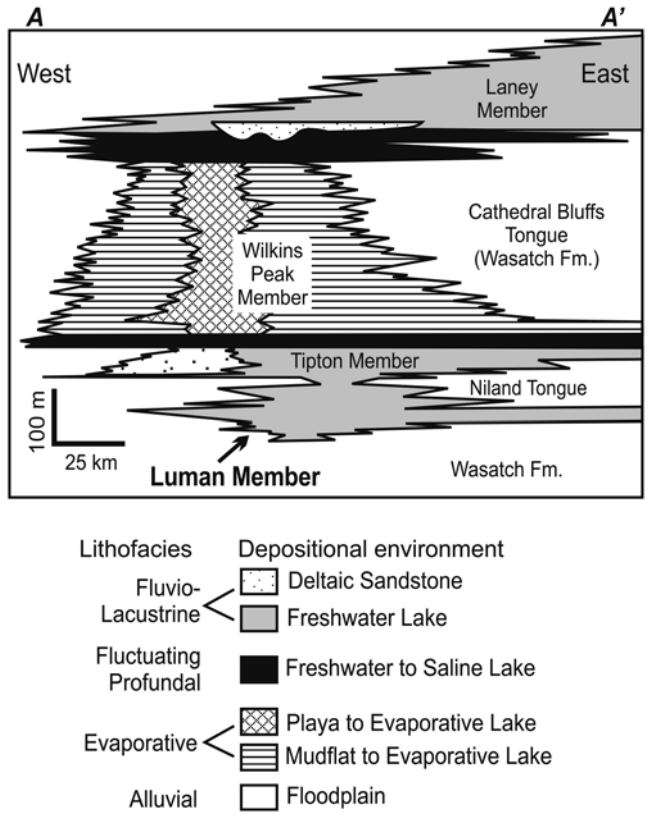

Fig. 2.1 Generalized cross-section illustrating the general stratigraphy of the Greater Green River Basin. The Luman Member is laterally equivalent to floodplain and fluvial deposits of the Wasatch Formation. Luman Member-equivalent strata contain mammals associated with the Lysitean subage of the Wasatchian North American land mammal age (Holroyd and Smith 2000) (Modified from Roehler 1991)

deposition of the Tipton Member of the Green River Formation.

2.2.2 Geochronology

Age determinations within the Greater Green River Basin are established through mammalian biostratigraphy and the $^{40}Ar/^{39}Ar$ dating of tuffs. At present, the Luman Member has not yielded any tuffs for dating, leaving biostratigraphy as the primary tool for age control in this unit. Within the early Eocene of southwestern Wyoming, Wasatchian and Bridgerian provincial Land Mammal ages (Wood et al. 1941) have been subdivided into several subzones based on mammalian and reptilian faunas (Gingerich and Clyde 2001; Gunnell and Bartels 1994; Robinson et al. 2004). Fossils found at Little Mountain, the Washakie sub-basin, and Tipton Buttes in laterally equivalent strata to the Luman Member correlate it to the Lysitean subage of the Wasatchian NALMA (McGrew and Roehler 1960; Holroyd and Smith 2000; Anemone 2001). A bentonite near the Lystitean – Lostcabinian boundary in the upper Willwood Formation in the Bighorn Basin yields a sanidine $^{40}Ar/^{39}Ar$ age of 52.91 ± 0.36 Ma (Wing et al. 1991; Smith et al. 2004, 2010), which provides a minimum age for Luman Member deposition (all ages shown with 2 s uncertainties relative to 28.201 Ma for FCs). Based on interpolation between the Lysitean-Lostcabinian age and the 52.22 ± 0.35 Ma sanidine $^{40}Ar/^{39}Ar$ age for the Scheggs tuff in the overlying Tipton Member

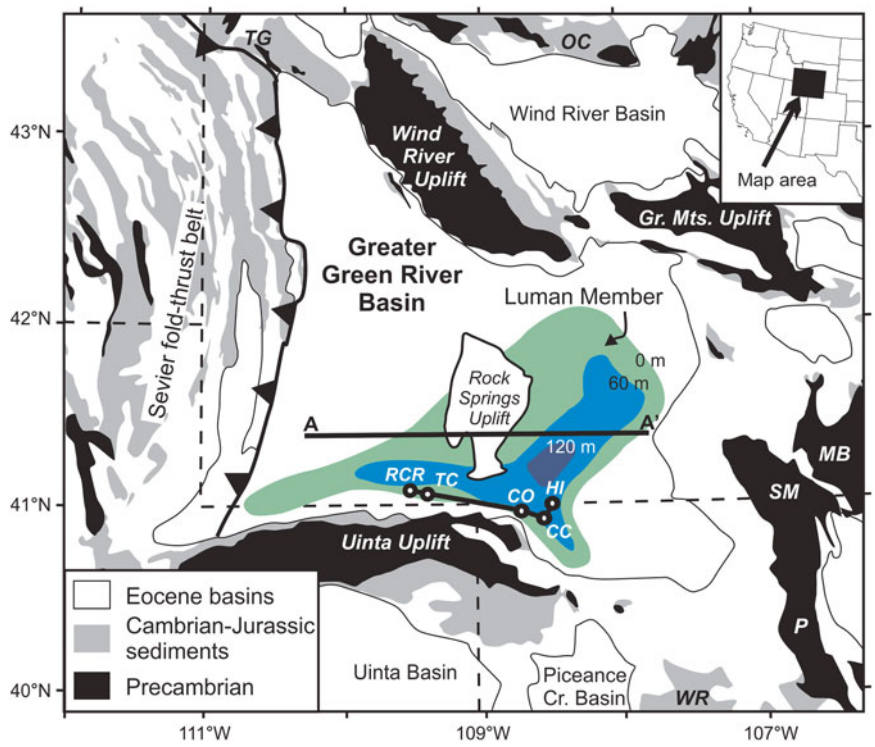

Fig. 2.2 Map showing the extent and tectonic context of the Luman Member of the Green River Formation in Wyoming and Colorado. Labels indicate the locations of measured sections and locales discussed in this report: Red Creek Rim (*RCR*); Telephone Canyon (*TC*); Colorado (*CO*); Canyon Creek (*CC*); and Hiawatha (*HI*). Luman Member maximum extent and thicknesses (in meters) are from Roehler (1993); base map modified from Witkind and Grose (1972). Abbreviations for Laramide uplifts: *TG* Teton-Gros Ventre; *OC* Owl Creek; *MB* Medicine Bow, *SM* Medicine Bow, *P* Park, *WR* White River. Cross section A is illustrated in Fig. 2.1. *Colors* correspond to thickness contours (see Carroll and Bohacs 2001)

(Smith et al. 2008, 2010), the duration of Luman Member deposition was ca. 400 ka, which translates to an average basin-center accumulation rate of ~150 μm/year.

2.2.3 Regional Tectonics

The Greater Green River Basin is bounded by the Sevier fold-thrust belt, and by Laramide-style basement uplifts (Fig. 2.2). These structures formed during the latest Cretaceous through early Cenozoic, with many experiencing late growth coeval with the deposition of the Green River Formation. Major movement along the Uinta-Sparks Fault, which bounds the north edge of the Uinta Uplift, occurred in the late Cretaceous to early Paleogene. Assuming that Phanerozoic strata were isopachous prior to uplift, angular unconformity and included fragments indicate that approximately 3 km of Cretaceous strata were eroded from parts of the Uinta Mountains prior to Paleocene deposition of the alluvial Fort Union Formation (Hansen 1965; Bradley 1995). Later early Eocene uplift is recorded by alluvial fan deposition (Crews and Ethridge 1993) and deformation and truncation of Wasatch and Green River Formation strata adjacent to the North Flank thrust, Sparks Ranch thrust and Uinta thrust (Roehler 1993; Hansen 1965, 1986; Bradley 1995). Coarse conglomerates north of the Uinta Uplift in Luman Member-equivalent deposits at Sugarloaf Butte and Richards Mountain imply steep gradients between the

basin floor and the crest of the Uinta Mountains during Luman time (Crews and Ethridge 1993; Rowley et al. 1985).

The Rock Springs Uplift (RSU) intersects with the Uinta Uplift and likely experienced growth during Luman Member deposition. The RSU is a north-south oriented anticlinal structure that lies in the south-central portion of the Greater Green River Basin (Gosar and Hopkins 1969), separating it into distinct subbasins to the east and west of it. Isopach mapping of upper Cretaceous Blair and Rock Springs Formation strata show thickening off the flanks of the uplift (Beaubouef et al. 1995). Syn-depositional movement along north-south trending faults on the west side of the Rock Springs Uplift is evident in large-scale lithofacies and thickness distributions of the upper Cretaceous Almond Formation (Van Horn 1979; Martinsen et al. 1995; Mongomery 1996). Additionally, the Paleocene Fort Union and Wasatch Formations, both of which underlie the Green River Formation, are observed to onlap the flanks of the uplift (Roehler 1965) which has been speculated to have been a topographic high during Green River Formation deposition (Bradley 1964; Roehler 1993). Isopach maps and depocenter depictions of the Green River Formation along the north flank of the Uinta Mountains show beds thinning with proximity to the Uinta Uplift, with depocenters on either side of its intersection with the Rock Springs Uplift (Burchfiel et al. 1992; Roehler 1993; Johnson and Anderson 2009; Mederos et al. 2005), implying either its active uplift or to less-rapid subsidence of the structure relative to adjacent subbasins.

2.2.4 Eocene Climate

Luman Member deposition occurred during the early Eocene just subsequent to the Paleocene-Eocene thermal maximum and prior to the early Eocene climatic optimum. Beginning in the late Paleocene, a warming trend led to frost-free conditions and a humid, warm-temperate to subtropical climate prior to and during deposition of the Green River Formation (MacGinitie 1969; Wilf 2000). Paleontologic records of continental flora and faunas suggest warm climates during the Eocene (Wolfe 1978; Wolfe and Poore 1982). Leaf-margin analyses of plant assemblages from the late Paleocene through the Early Eocene in the Greater Green River Basin indicate maximum temperatures in the Cenozoic were reached in middle Early Eocene time (Wilf 2000). During deposition of the Luman Member, plant assemblages from the Bighorn and Greater Green River Basins include tree ferns, palms and cycads, all of which are unable to survive prolonged freezes (Wing et al. 1991; Wilf 2000). Based on taxonomic affinities with modern plants and leaf margin analysis, mean annual temperatures in the Greater Green River Basin during deposition of the Luman Member are estimated to have been between 16 and 21 ° C (Greenwood and Wing 1995). Coals and ferns found in the Luman Member-equivalent Latham assemblage imply wet conditions in southwestern Wyoming during the Lysitean (Masursky 1962). Based on leaf-area analysis on leaf assemblages found within the Green River Formation, regional Eocene mean annual rainfall is estimated between 113 and 140 cm (Wilf 2000). Crocodilians have been identified in the Green River and Bridger Formations in southwestern Wyoming and northeastern Utah (Grande 1984) indicating a MAT >16 ° C (Markwick 1994).

2.3 Field Methodology and Results

To understand the sedimentology and stratigraphic relationships between the Luman Member and the Wasatch Formation, four vertical sections along a ~10 km transect were measured and described at 10 cm detail along an east-west transect in the southern part of the Greater Green River Basin (see section line in Fig. 2.2). Gamma ray scintillometry was conducted using a multi-channel spectrometer at the outcrop using an Exploranium GR-320 enviSpec hand-held spectrometer, with individual abundances of uranium, thorium, and potassium measured every 0.5 m. A detail photographic and

lithofacies investigation of a large, particularly well-exposed exposure of intertonguing lacustrine, paludal and alluvial facies was performed at Telephone Canyon.

2.3.1 Sedimentary Lithofacies

Lacustrine lithofacies within the Luman Member consist of mudstone; fossiliferous calcareous sandstone, and coquina (Pipiringos 1955, this study; Roehler 1993; Sklenar and Anderson 1985). These deposits alternate with coal, carbonaceous mudstone, and trough cross-bedded sandstone of fluvial and paludal origin (Figs. 2.3 and 2.4). This study identifies three major lacustrine lithofacies within the Luman Member and two associated lithofacies of fluvial-paludal origin. Gastropods, pelycopods and ostracodes found throughout the Luman Member support the interpretation of a freshwater depositional environment (Taylor 1972; Kuchta 2000).

Calcareous mudstone This facies consists of homogeneous gray to cream or brown calcareous mudstone that is infrequently thinly-laminated (Fig. 2.3a). The mudstone often contains ostracodes as well as both broken and complete mollusc shells. Within the Luman Member, calcareous mudstone may form low grade oil shale (Horsfield et al. 1994; Carroll and Bohacs 2001) and forms thick (1–15 m), recessive units generally bounded above and below by sand facies (Fig. 2.3). Crude 10 cm scale bedding is most common, with intervals of fine laminations (Fig. 2.4b).

Interpretation: Thinly-laminated strata are interpreted to represent of deposition in relatively deep or sheltered aquatic environments where disruption by wave action of biogenic activity is restricted (e.g. Anadón et al. 1989). The lack of pervasive laminated strata in the calcareous mudstone facies supports an interpretation of deposition in a moderately deep, yet dominantly unrestricted lacustrine setting during Luman time. Laminated facies likely are the result of deposition in the deepest part of Lake Gosiute during periods of higher lake levels or in more restricted settings within the lake.

Coquina Luman Member coquina is composed of limestone-cemented shells generally 1 to 3 cm in size and contain mollusc assemblages of *Goniobasis tenera*, *Viviparus* sp., and various unidentified unionid bivalves (Figs. 2.3b and 2.4c, h, i, j) (Hanley 1976; Kuchta 2000). Various degrees of transport are evident between different coquina beds. In general, shells are disarticulated and show mild breakage and rounding implying minimal transport. Thick (1 m) coquina beds can be traced for up to 5 km; thinner (2–10 cm) coquina beds are traceable less than 500 m.

Interpretation: These deposits are interpreted as sediment-starved stages of Lake Gosiute during which littoral and sublittoral shells were exposed and concentrated due to the winnowing of finer sediment. A possible analogous setting may exist in Lake Tanganyika, where shell communities live in the littoral zone and lake level fluctuations (on the order of ~10 m) expose shells to increased wave and wind action, winnowing finer sediment away and leaving broad, tabular shell lag surfaces. Hanley (1976) considers accumulations of *Goniobasis* and *Viviparus* shells in the Green River Formation indicative of littoral-lacustrine habitats where accumulations of these communities in coquinas record shoreline fluctuations, concentrating shells in widespread, tabular benches similar to those seen in the modern at Lake Tanganyika (Cohen 1989). Some coquinas cap bioturbated shoreface sandstone intervals, suggesting that molluscs were likely the burrowers.

Laminated sandstone This facies consists of horizontal to wavy non-parallel laminated, well-sorted, well-rounded, calcareous very-fine to fine-grained sandstone containing interbeds of coal and carbonaceous mudstone (Figs. 2.3c and 2.4e). Low-angle cross-stratification, wavy parallel bedding and wave ripples are commonly found in this facies. Iron nodules are occasionally present and often define bedding planes. Sandstone beds vary in thickness from 10 cm to 5 m and can be traced laterally within outcrops.

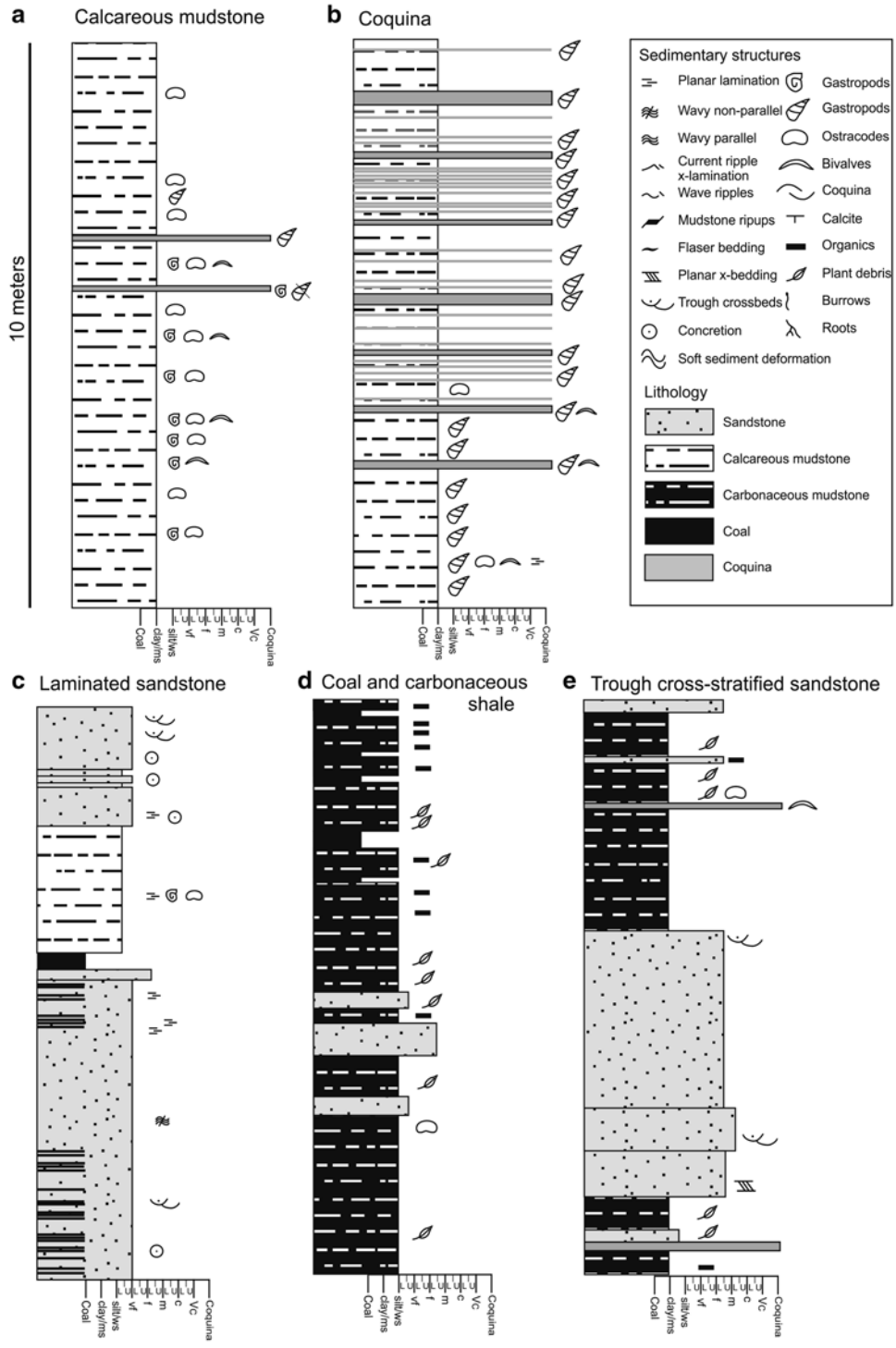

Fig. 2.3 Representative measured sections illustrating: (**a**) calcareous mudstone lithofacies from the Hiawatha section meters 108–118 (Chicken Creek SW 7.5′ quadrangle; NW1/4, NW1/4, NW1/4 Section 22, T12N, R100W); (**b**) interbedded coquina and calcareous mudstone lithofacies from the Hiawatha section meters 80–90 (Chicken Creek SW 7.5′ quadrangle; NW1/4, NW1/4, NW1/4 Section 22, T12N, R100W); (**c**) laminated sandstone from the Canyon Creek section meters 53–63 (Sugarloaf Butte 7.5′ quadrangle; NW1/4, NW1/4 Section 25, T12N, R101W); (**d**) coal and carbonaceous mudstone from the Colorado section meters 27–37 (Sparks 7.5′ quadrangle; SE1/4, NW1/4, SE1/4 Section 18, T12N, R101W); (**e**) trough cross-bedded sandstone from the Colorado section meters 27–37 (Sparks 7.5′ quadrangle; SE1/4, NW1/4, SE1/4 Section 18, T12N, R101W)

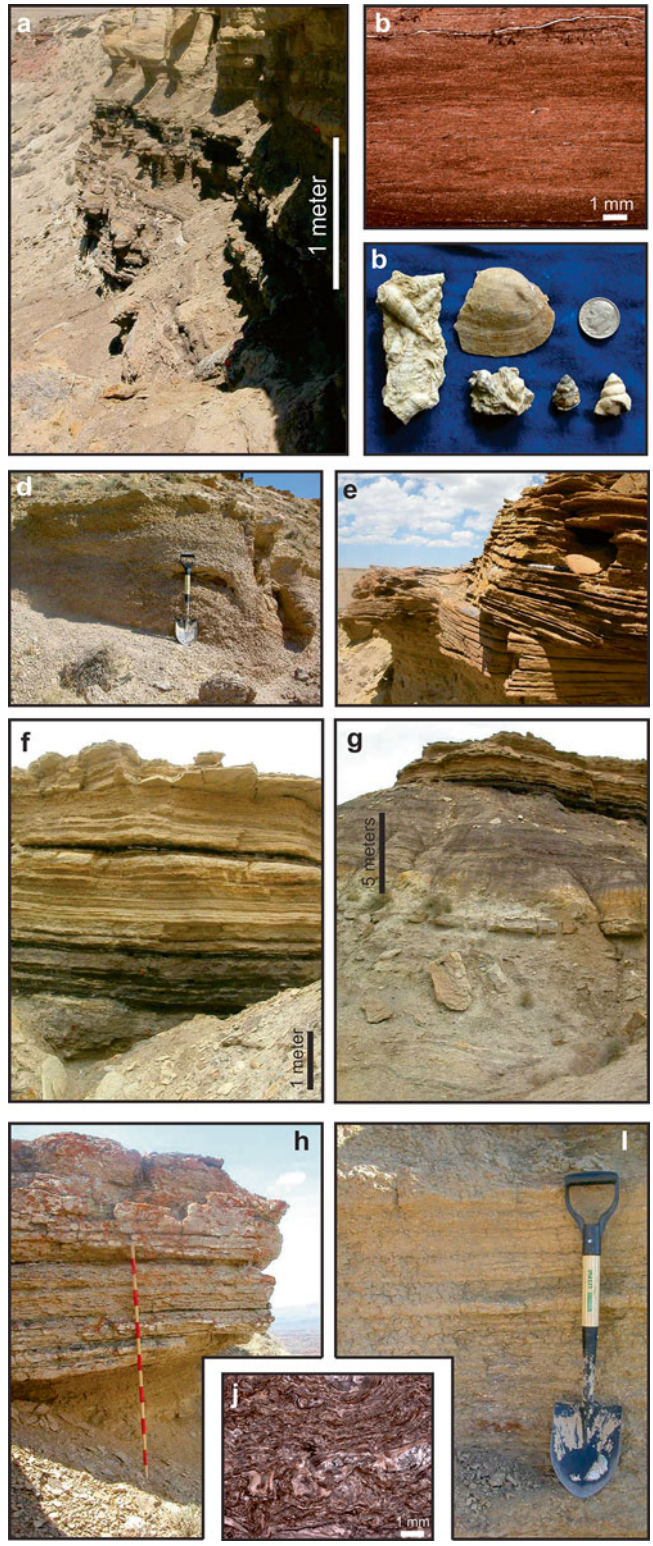
a
1 meter
b
1 mm
b
d
e
f
1 meter
g
5 meters
h
i
j
1 mm

Interpretation: We interpret these sandstone beds to be beach deposits. Sedimentary structures indicate wave action and well-sorted, well-rounded grains support a high energy environment. Repeated, sustained lake level rise and fall are represented by the alternation over the 1–8 m scale of these laminated sandstones with paludal coals and littoral shell-rich mudstones respectively (Figs. 2.4f and 2.5b).

Coal and carbonaceous mudstone This facies consists of vitrinitic to amorphous coals in beds that are often interbedded with carbonaceous mudstone and fine-grained sandstone (Figs. 2.3d and 2.4f). Generally 10–15 cm thick, these coal beds are laterally continuous for 100 m but are not useful as marker beds between stratigraphic sections. Millimeter-scale, planar-laminated mudstone contains carbonaceous matter of varying preservational quality. Unidentifiable plant material comprises the majority of the carbon content found in this facies. Root traces, woody debris, and invertebrate traces are also present.

Interpretation: Coal and carbonaceous mudstone are interpreted to represent overbank deposits and paludal, marginal lacustrine environments characterized by still water, abundant organic debris and reducing conditions. This type of environment is likely a complex of poorly-drained backswamps with networks of effective drainage systems where high sediment supply supports carbonaceous mudstone accumulation instead of thick coal bed formation (Flores 1981). Additionally, the deposition of non-laterally extensive or patchy coal deposits such as those seen in the Luman Member is generally restricted to nearshore and paludal environments and may be indicative of instable lake levels due to tectonic activity (Sáez and Cabrera 2002) and/or shoreline progradation (Bohacs et al. 2000).

Trough cross-bedded sandstone This fine to medium grained sandstone is often micaceous, hosting trough crossbeds and planar cross-lamination (Fig. 2.3e). This facies is often channelized at the meter scale, with cut-and-fill relationships and lateral accretion surfaces visible. Trough cross-bedded sandstone bodies typically cannot be traced more than approximately 5 m in outcrop and are replaced laterally by carbonaceous mudstone and coal. Individual channel bodies are commonly observable in outcrop, and are typically no more than 1 m thick. Amalgamated channel horizons are less common but can reach up to 5 m in thickness.

Interpretation: Trough cross-bedded sandstone is interpreted to represent fluvial sand deposited in alluvial systems adjacent to Lake Gosiute. Such fluvial-alluvial systems have been well-characterized (e.g., Miall 1988; Platt and Keller 1992) and contain lateral and vertical alternation between channel sand and overbank mud that record the lateral migration of fluvial channels across floodplains.

2.3.2 Stratigraphy

In many locations, an abrupt color change from red to drab gray-green occurs at the contact of the Main Body of the Wasatch Formation and the Luman Member (Fig. 2.5a). This color change is interpreted to represent a shift from oxidizing to reducing conditions of interstitial waters (cf. Walker 1967; Berner 1971), and corresponds to an increase in organic matter preservation and

Fig. 2.4 Photographs and photomicrographs of lithofacies described in this report: (**a**) Alternating calcareous mudstone and laminated sandstone on the meter scale; (**b**) photomicrograph of siliciclastic mudstone (UW1954/18); (**c**) representative fossils found within calcareous mudstone from Hiawatha section (*HI*); (**d**) shell-rich calcareous mudstone; (**e**) laminated sandstone at Canyon Creek section (*CC*) Sharpie for scale; (**f**) alternating coal (black) and carbonaceous mudstone (cream); (**g**) outcrop character of coal and carbonaceous mudstone at Colorado section (*CO*); (**h**) 2.5 m thick coquina bed capping Telephone Canyon (*TC*) and Red Creek Rim (*RCR*) sections. (**i**) Thinly-bedded coquina at Hiawatha section (*HI*); (**j**) Photomicrograph of coquina (UW1954/11)

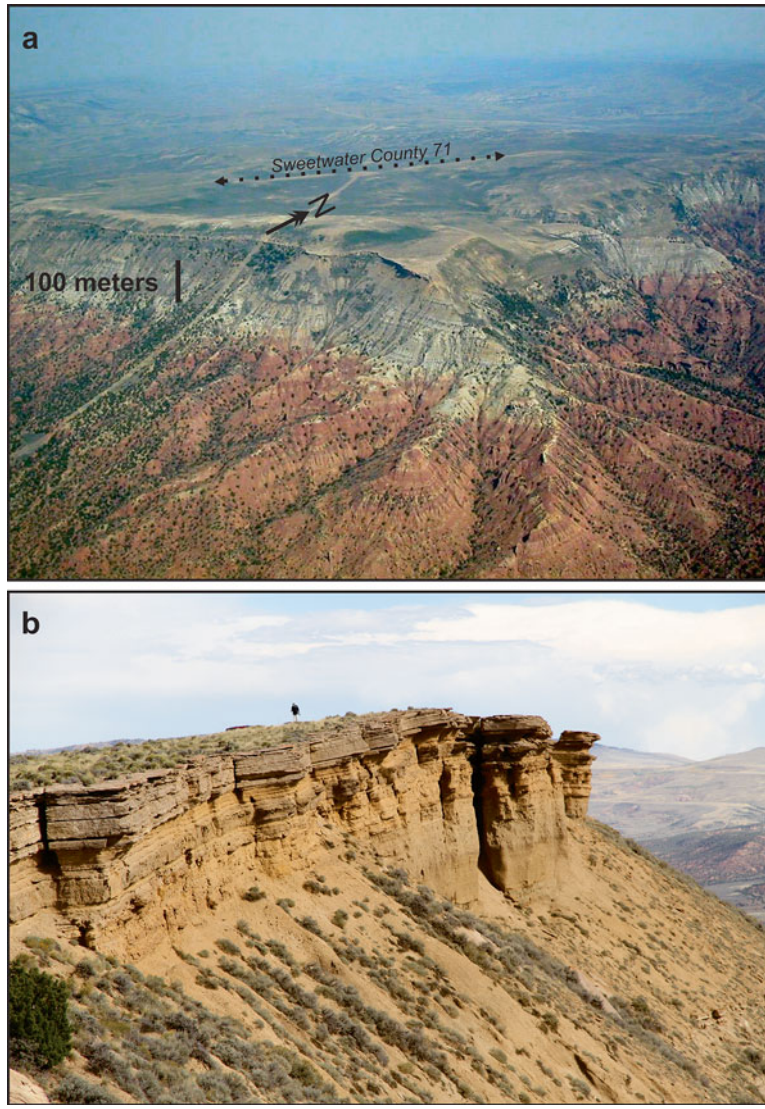

Fig. 2.5 Photographs of lithofacies transitions within the Luman Member of the Green River Formation: (**a**) oblique aerial photograph of the Wasatch Formation to Luman Member transition exposed along the Red Creek Rim. View is towards the north-northwest; (**b**) photograph of a ~10 m thick Luman Member shoreface succession consisting of silty mudstone that conformably grade into planar bedded sandstone. Approximately 2 m tall person for scale

likely a rise in the Eocene water table. Hence, the color change suggests a change in the hydrologic character of the basin and subsequently reflects the suitability for lacustrine environments to form in the basin. The preservation of this color change is significant as this process of oxidizing and reducing sediments is reversible. The retention of the red color indicates that the deposits lack metabolizable organic matter which preserves a high Eh. The transition into green-gray sediment signifies the addition of organic matter and the lowering of Eh, supporting reducing conditions. This would be seen as a rise in the water table relative to the ground surface during the transition from Wasatch to Luman time.

While this color change marks the contact between the Wasatch Formation and the Luman Member, the accompanying lithologic change is

gradual and conformable. Both local- (Fig. 2.6) and basin-scale stratigraphic correlations of the Luman Member and underlying Wasatch Formation indicate that this transition is commonly time transgressive (Figs. 2.6 and 2.7). The upper 'main body' of the Wasatch Formation contains mudstone and channelized sandstone while the lower portion of the Luman Member is composed primarily of carbonaceous mudstone and channelized sandstone with sporadic pond deposits ranging from 20 cm to 10 m in thickness. Roehler (Roehler 1993, 1965) suggested separating out this paludal stage of the Luman Member and creating another member of either the Green River Formation or Wasatch Formation to be called the Ramsey Ranch Member. This suggestion is not unreasonable and sedimentologic data from this study confirms that these stratigraphic relationships do exist. However, the Ramsey Ranch Member has not been critically accepted for use in the literature and herein this interval is considered part of the Luman Member.

At Telephone Canyon (TC) in the southern Green River Basin, a large-scale (2.5 km) facies changes within the Luman Member illustrates the embryonic stages of lacustrine deposition (Fig. 2.6). A channel complex containing a minimum of nine distinct channel bodies is located below lacustrine deposits. The channels are laterally replaced by red overbank mud which in turn is punctuated by thin, laterally restricted pond deposits. This channel-overbank-pond package observed at Telephone Canyon is likely coeval with the lowermost Luman Member sediments seen in the Red Creek Rim section (cf. Fig. 2.2). Widely dispersed paleoflow indicators within the channel complex imply deposition within a meandering river system, or alternatively a quasi-periodic alternation between axial and peripheral stream systems (Fig. 2.6).

Lateral thickness and facies changes suggest the influence of the Rock Springs Uplift on accommodation and paleogeography. Approximately 50 m of Luman Member lacustrine deposits overlie fluvial facies at Telephone Canyon, and are capped by a widely correlative 2.5 m thick coquina marker bed. At Red Creek Rim, 5 miles west, the thickness between the Wasatch Formation and the same coquina horizon is approximately 126 m. The difference is thickness may reflect greater accommodation at RCR relative to TC due to the latter being closer to the axis of the Rock Springs Uplift, and/or indicates that lacustrine conditions occurred earlier at RCR. In the latter scenario, while channel-fill and fluvial sediment were being deposited at Telephone Canyon, Red Creek Rim hosted an established, perennial lake. As the basin deepened, the small lake at Red Creek Rim expanded, flooding the surrounding lowlands which sloped gently up towards the Uinta Uplift, ultimately transgressing over the Telephone Canyon area. The coquina bed at the top of both of these sections marks the full expansion of Lake Gosiute and synchronous lacustrine deposition across both areas.

In the southern part of the Greater Green River Basin, adjacent to the Uinta Mountains, the upper contact of the Luman Member with overlying strata fluvial strata of the Niland Tongue of the Wasatch Formation is stratigraphically complex. Contacts between the Luman, Niland, and Tipton units are often difficult to establish; a situation exacerbated by conformable, gradational boundaries between units as well as similar definitions of each (Pipiringos 1955; Bradley 1964). Complex interfingering relationships of lacustrine, fluvial and alluvial strata make the identification and differentiation of the Luman Member and the overlying Niland Tongue (Wasatch Formation) particularly difficult in the southeastern part of the Green River sub-basin (Bradley 1964, 1959; Culbertson 1965; Roehler 1987). One to 5 m-thick fluvial or potentially shallow deltaic units interfinger with lacustrine strata near the top of the Luman Member at the majority of studied locations, but the strata never fully transition to alluvial (fluvial- and floodplain-deposited) lithofacies. In contrast, at the Colorado section (CO), which is nearest to axis of the Rock Springs Uplift, the top of the Luman Member is marked by a gradational transition to fully non-lacustrine fluvial and paludal facies, perhaps suggesting that the Rock Springs Uplift was a topographic high during the Eocene. Towards the basin center,

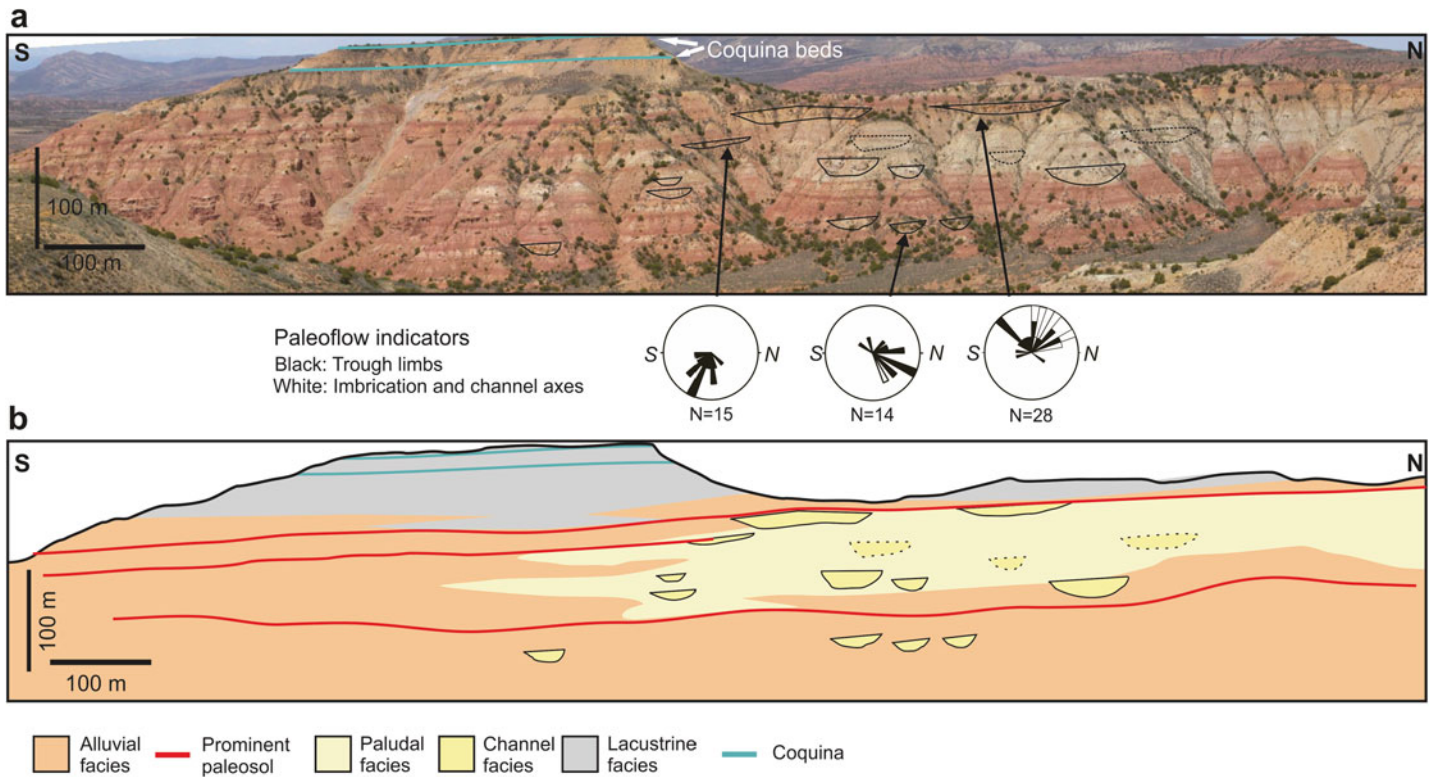

Fig. 2.6 Annotated field photograph illustrating stratigraphic geometries associated with the paludal-lacustrine transition between the Luman Member and underlying Wasatch Formation at Telephone Canyon (TC in Fig. 2.2)

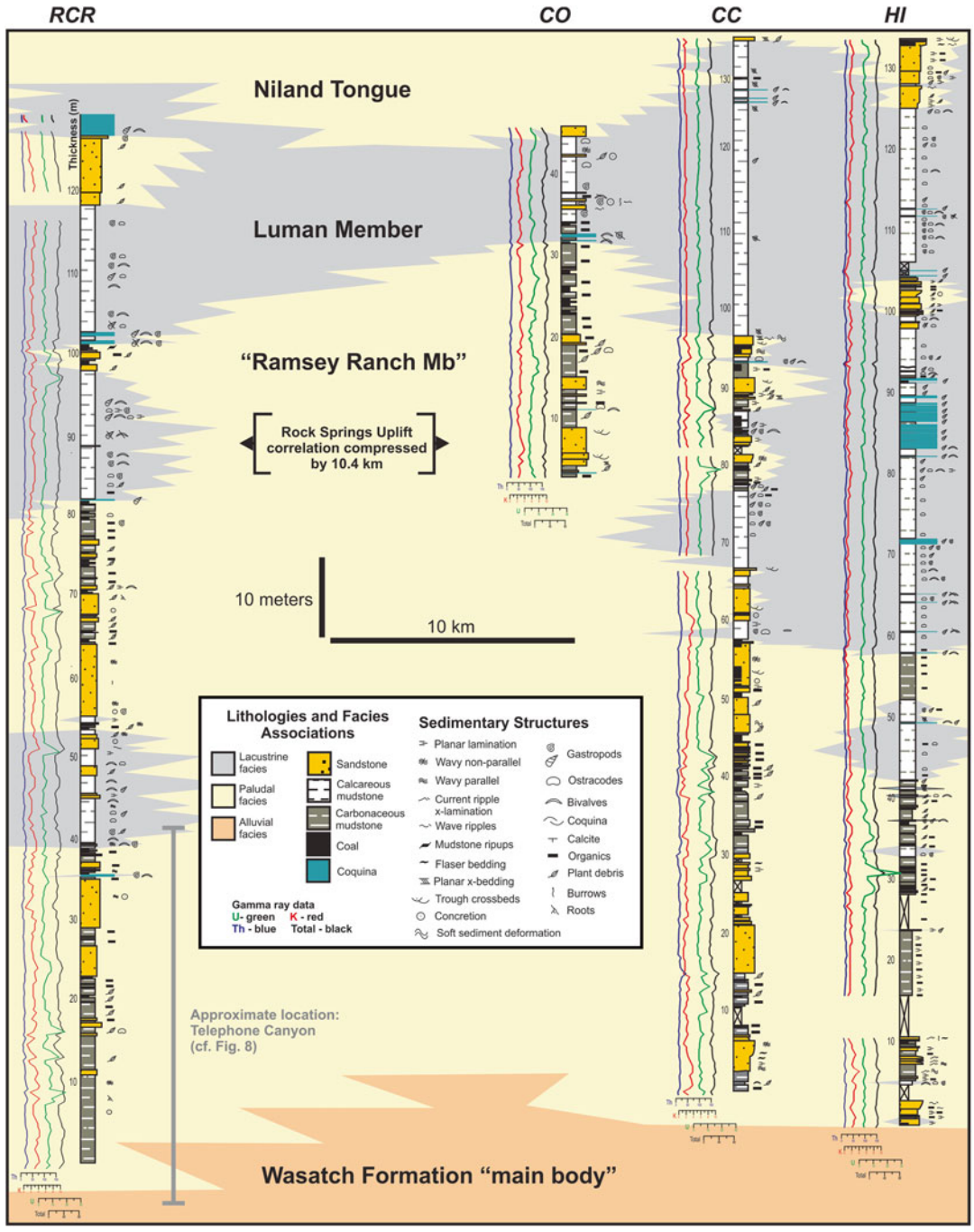

Fig. 2.7 East-west cross-section of the Luman Member in the southern part of the Greater Green River Basin (see Fig. 2.2 for location of section line)

the Niland Tongue thins and in many locations disappears, with Luman Member transitioning directly upwards into the Tipton Member.

2.4 Discussion

2.4.1 Initiation and Evolution of Lake Gosiute

Examination of the sedimentologic and stratigraphic relationships of the Wasatch Formation – Luman Member contact around Red Creek Basin reveals a conformable relationship between strata deposited from small, disconnected lakes and deposition of the Luman Member due to expansion of Eocene Lake Gosiute. We propose that the channel complex deposits seen at Telephone Canyon represent a fluvial inlet to an embryonic Lake Gosiute which later expanded to cover the surrounding floodplains. Likely during the inception of subsidence and the formation of Lake Gosiute there were many of these embryonic lakes in the southern portion of the Greater Green River Basin which later expanded and coalesced as subsidence deepened the Uinta trough (Fig. 2.8). Basin-scale stratigraphic stacking patterns observed in the Luman cross-section support this interpretation (Fig. 2.7). The cross-section reveals that in the lower half of the

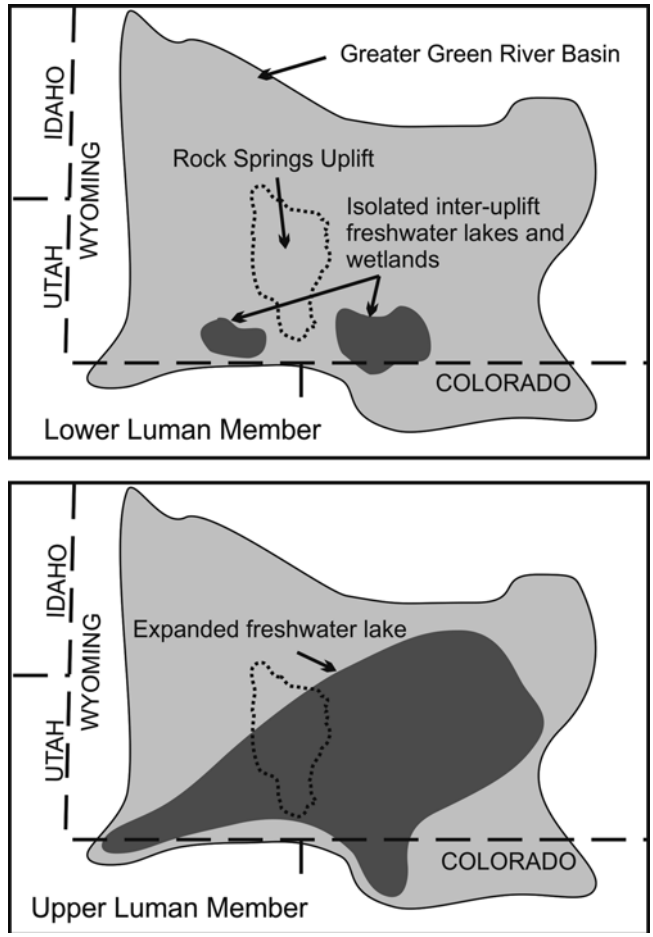

Fig. 2.8 Box model interpretive diagrams illustrating paleogeography and sedimentary facies during deposition of (**a**) lower Luman Member, and (**b**) upper Luman Member

Luman Member paludal facies dominate the depositional style of the basin with small, isolated ponds and lakes fed by axially draining feeder streams punctuating the vertical section.

Eocene rocks in the southern Greater Green River Basin record a conformable evolution from a well-drained fluvial and alluvial environment (Wasatch Formation) to a dominantly reducing paludal and eventually wave-influenced lacustrine environment (Luman Member, Green River Formation), clastic shorelines where streams entered the basin, and coquina-depositing carbonate shorelines between deltas. Due to their lateral continuity and vertical relationship to other lithofacies, coquinas may alternately have formed across entire shoreline in a non-Waltherian sense during interval of transgression. This first stage of Luman deposition occurred in a dominantly reducing environment, and consists of approximately half of the thickness of the Luman Member. Sediment supply rates in paludal environments are likely faster than those in deep water lacustrine environments, thus it is probable that this first stage of Luman Member deposition lasted less than half of the ~0.4 Ma duration of the Luman Member. Based on the distribution of lacustrine and alluvial strata in the lower Luman Member (Fig. 2.7) and broad-scale patterns of accumulation (Johnson and Anderson 2009), it seems likely that the Rock Springs Uplift was a topographic high during this time, creating two major depocenters on either side of the anticline. In the upper half of the Luman Member, previously small ponds coalesced and lacustrine deposits transgressed over the paleohigh created by the Rock Springs Uplift, and are recorded throughout the southern part of the basin with an arm extending to the northeast into the Great Divide sub-basin (Fig. 2.8). This expansion of lacustrine deposits coupled with the development of robust molluscan populations (Kuchta 2000) and low grade oil shale deposition (Horsfield et al. 1994) records the broad expansion of Lake Gosiute deposition over the entire study area.

Changes to sediment supply resulting from unroofing of basement structures may have contributed to the eventual dominance of lacustrine deposition in the Greater Green River Basin. Fluvial sedimentation during the Paleocene through early Eocene was likely promoted by high sediment efflux from easily erodable Cretaceous foreland basin strata (Carroll et al. 2006). Initiation of lacustrine deposition in the Greater Green River Basin followed the breaching of the core of the Uinta Uplift and the consequent integration of more resistant strata into the drainage basin. This likely decreased the sediment supply rate and allowed ponds to begin forming in the regions experiencing the greatest subsidence. As the basin deepened and sediment supply remained low, these ponds expanded, coalesced and transgressed over the surrounding floodplain, forming Lake Gosiute. The expansion of lacustrine environments across the region may also have been promoted by ongoing structural activity that increased potential accommodation in the basin by raising the basin spill point. In either scenario, actively forming structures appear to have guided the distribution of lacustrine and alluvial facies.

Acknowledgments We are grateful to Dana Geary, Anders Carlson, Patty Blankenberger, Rebecca Tedford, and Brandon Norsted for their assistance. Portions of this work were funded by the University of Wisconsin-Madison, Conoco, and Texaco.

References

Alonso-Zarza AM, Calvo JP (2000) Palustrine sedimentation in an episodically subsiding basin: the Miocene of the northern Teruel Graben (Spain). Palaeogeogr Palaeoclimatol Palaeoecol 160:1–21

Alonso-Zarza AM, Calvo JP, García del Cura MA (1992) Palustrine sedimentation and associated features – grainification and pseudo-microkarst – in the middle Miocene (Intermediate Unit) of the Madrid Basin, Spain. Sediment Geol 76:43–61

Anadón P, Cabrera L, Julià R, Roca E, Rosell L (1989) Lacustrine oil-shale basins in Tertiary grabens from NE Spain (Western European Rift System). Palaeogeogr Palaeoclimatol Palaeoecol 70:7–28

Anemone RL (2001) New paleogene faunas from the Great Divide Basin of southwestern Wyoming [abs.]. In: Ash AW, Wing SL (eds) Climate and biota of the early Paleogene. International meeting and field conference, Powell, WY, 3–8 July, 2001, National Museum of Natural History, Washington, D.C., p 2

Armenteros I, Daley B, García E (1997) Lacustrine and palustrine facies in the Bembridge Limestone (late Eocene Hamshire Basin) of Isle of Wight southern England. Palaeogeogr Palaeoclimatol Palaeoecol 128:111–132

Beaubouef RT, Bohacs KM, McLaughlin PP, Suter JR, Devlin WJ (1995) Sequence stratigraphy of coal-bearing strata, Upper Cretaceous, Washakie Basin, SW Wyoming. Soc Explor Geophys 65th annual international meeting, Society of Exploration Geophysicists, Tulsa, pp 841–843

Beck RA, Vondra CF, Filkins JE, Olander JD (1988) Syntectonic sedimentation and Laramide basement thrusting, Cordilleran foreland; Timing of deformation. In: Schmidt CJ, Perry WJ Jr (eds) Interaction of the Rocky Mountain Foreland and the Cordilleran Thrust Belt, vol 171, Geological Society of America Memoir., pp 465–487

Berner RA (1971) Principles of chemical sedimentology. McGraw-Hill, New York City, 240 p

Bohacs KM, Carroll AR, Neal JE, Mankiewicz PJ (2000) Lake-basin type, source potential, and hydrocarbon character: An integrated sequence-stratigraphic-geochemical framework. In: Gierlowski-Kordesch EH, Kelts KR (eds) Lake basins through space and time, vol 46, American Association of Petroleum Geologists Studies in Geology., pp 3–34

Bradley WH (1959) Revision of stratigraphic nomenclature of Green River Formation of Wyoming. Am Assoc Pet Geol Bull 43:1072–1075

Bradley WH (1964) The geology of the Green River Formation and associated Eocene rocks in southwestern Wyoming and adjacent parts of Colorado and Utah. U.S. Geological Survey professional paper 496-A, 86 p

Bradley MD (1995) Timing of the Laramide rise of the Uinta Mountains, Utah and Colorado. In: Jones RW, Winter GA (eds) Resources of Southwestern Wyoming. 45th annual field conference guidebook, Wyoming Geological Association, Casper, pp 31–44

Burchfiel BC, Cowan DS, Davis GA (1992) Tectonic overview of the Cordilleran orogen in the western United States. In: Burchfiel BC, Lipman PW, Zoback ML (eds) The Cordilleran orogen: conterminus U.S. Geology of North America, G-3. Geological Society of America, Boulder, pp 407–479

Carroll AR, Bohacs KM (2001) Lake-type controls on petroleum source rock potential in nonmarine basins. Am Assoc Pet Geol Bull 85:1033–1053

Carroll AR, Chetel LM, Smith ME (2006) Feast to famine: sediment supply control on Laramide basin fill. Geology 34:197–200

Cohen AS (1989) The taphonomy of gastropod shell accumulations in large lakes: an example from Lake Tanganyika, Africa. Paleobiology 15:26–45

Crews SG, Ethridge FG (1993) Laramide tectonics and humid alluvial fan sedimentation, NE Uinta Uplift, Utah and Wyoming. J Sediment Petrol 63:420–436

Culbertson WC (1965) Tongues of the Green River and Wasatch Formations in southeastern part of the Green River Basin, Wyoming. In: De Voto RH, Bitter RK (eds) Sedimentation of late Cretaceous and Tertiary outcrops, Rock Springs uplift. 19th annual field conference guidebook, Wyoming Geological Association, Casper, pp 151–155

Flores RM (1981) Coal deposition in fluvial paleoenvironments of the Paleocene Tongue River Member of the Fort Union Formation, Powder River Area, Powder River Basin, Wyoming and Montana. In: Ethridge FG, Flores RM (eds) Recent and ancient nonmarine depositional environments: models for exploration, Society of Economic Paleontologists and Mineralogists special publication no 31. Society of Economic Paleontologists and Mineralogists, Tulsa, pp 169–190

Gingerich PD, Clyde WC (2001) Overview of mammalian biostratigraphy in the Paleocene-Eocene Fort Union and Willwood Formations of the Bighorn and Clarks Fork Basins. In: Gingerich PD (ed) Paleocene-Eocene stratigraphy and biotic change in the Bighorn and Clarks Fork Basins, Wyoming., University of Michigan Museum of Paleontology Papers on Paleontology 33. University of Michigan Museum of Paleontology, Ann Arbor, pp 1–14

Gosar AJ, Hopkins JC (1969) Structure and stratigraphy of the southwest portion of the Rock Springs uplift, Sweetwater county, Wyoming: In: Lindsay JB (ed) Geologic guidebook of the Uinta Mountains: Utah's maverick range. 16th annual field conference guidebook, Intermountain Association of Geologists, Salt Lake City, pp 87–90

Grande L (1984) Paleontology of the Green River Formation, with a review of the fish fauna: Geological Survey of Wyoming bulletin 63, 333 p

Greenwood DR, Wing SL (1995) Eocene continental climates and latitudinal temperature gradients. Geology 23:1044–1048

Gunnell GF, Bartels WS (1994) Early Bridgerian (middle Eocene) vertebrate paleontology and paleoecology of the southern Green River Basin, Wyoming. Univ Wyo Contrib Geol 30:57–70

Hanley JH (1976) Paleosynecology of nonmarine mollusca from the Green River and Wasatch Formations (Eocene), southwestern Wyoming and northwestern Colorado. In: Scott RW, West RR (eds) Structure and classification of paleocommunities. Dowden, Hutchinson & Ross, Inc, Stroudsburg, pp 235–261

Hansen WR (1965) Geology of the Flaming Gorge area Utah-Colorado-Wyoming. U.S. Geological Survey professional paper 490, 196 p

Hansen WR (1986) History of faulting in the eastern Uinta Mountains, Colorado and Utah. In: Stone DS, Johnson KS (eds) New interpretations of Northwest Colorado geology. Rocky Mountain Association of Geologists 1986 symposium, pp 5–17

Holroyd PA, Smith KT (2000) Preliminary biostratigraphic evidence for age of the Wasatch and Green River Formations, Washakie Basin, Southwestern Wyoming. Geol Soc Am Abs Pro 32(7):498

Horsfield B, Curry DJ, Bohacs KM, Littke R, Rullkötter J, Schenk HJ, Radke M, Schaefer RG, Carroll AR, Isaksen G, Witte EG (1994) Organic geochemistry of freshwater and alkaline lacustrine sediments in the

Green River Formation of the Washakie Basin, Wyoming, U.S.A. Org Geochem 22:415–440
Johnson PL, Anderson DW (2009) Concurrent growth of uplifts with dissimilar orientations in the southern Green River Basin, Wyoming: Implications for Paleocene–Eocene patterns of foreland shortening. Rocky Mt Geol 44:1–16
Kuchta MA (2000) Paleoenvironmental significance of nonmarine mollusca in the Luman Tongue of the Green River Formation, Wyoming. M.Sc. thesis, University of Wisconsin–Madison, 63 p
MacGinitie HD (1969) The Eocene Green River flora of northwestern Colorado and northeastern Utah. University of California Publications in the Geological Sciences v. 83, 203 p
Markwick PJ (1994) "Equability", continentality, and Tertiary "climate": The crocodilian perspective. Geology 22:613–616
Martinsen RS, Christiansen GE, Olson MA (1995) Stratigraphy and lithofacies of the Almond Formation, Washakie and Great Divide Basins, Wyoming. In: Jones RW (ed) Resources of Southwestern Wyoming. Wyoming Geological Association 47th annual field conference guidebook, pp 297–310
Masursky H (1962) Uranium-bearing coal in the eastern part of the Red Desert area Wyoming. U.S. Geological Survey Bulletin 1099-B, 152 p
McDonald RE (1972) Eocene and Paleocene rocks of the southern and central basins. In: Mallory WW (ed) Geologic atlas of the Rocky Mountain region. Rocky Mountain Association of Geologists, Denver, pp 243–256
McGrew PO, Roehler HW (1960) Correlation of Tertiary units in southwestern Wyoming. In: McGookey DP, Miller DN, Jr. (eds) Overthrust belt of Southwestern Wyoming and adjacent areas. 15th annual field conference guidebook, Wyoming Geological Association, Casper, pp 157–158
Mederos S, Tikoff B, Bankey V (2005) Geometry, timing, and continuity of the Rock Springs uplift (WY) and Douglas Creek arch (CO): implications for uplift mechanisms in the Rocky Mountain foreland. Rocky Mt Geol 40:167–191
Miall AD (1988) Architectural elements and bounding surfaces in fluvial deposits; anatomy of the Kayenta Formation (Lower Jurassic), southwest Colorado. Sediment Geol 55:233–262
Mongomery SL (1996) Brady unit, Rock Springs uplift, Wyoming: migration and structural history. AAPG Bull 80:1535–1546
North American Commission on Stratigraphic Nomenclature (1983) North American stratigraphic code. Am Assoc Pet Geol Bull 67:841–875
Pipiringos GN (1955) Tertiary rocks in the central part of the Great Divide Basin, Sweetwater County, Wyoming. In: Anderman GG (ed) Green River Basin. 10th annual field conference guidebook, Wyoming Geological Association, Casper, pp 100–104
Platt NH, Keller B (1992) Distal alluvial deposits in a foreland basin setting-the Lower Freshwater Molasse (Lower Miocene), Switzerland: sedimentology, architecture and paleosols. Sedimentology 39:545–565
Robinson P, Gunnell GF, Walsh SL, Clyde WC, Storer JE, Stucky RK, Froehlich DJ, Ferrusquia-Villafranca I, McKenna MC (2004) Wasatchian through Duchesnean biochronology. In: Woodburne MO (ed) Late Cretaceous and Cenozoic Mammals of North America. Columbia University Press, New York, pp 106–155
Roehler HW (1965) Early Tertiary depositional environments in the Rock Springs uplift area. In: De Voto RH, Bitter RK (eds) Sedimentation of Late Cretaceous and Tertiary outcrops, Rock Springs uplift. 19th annual field conference guidebook, Wyoming Geological Association, Casper, pp 140–150
Roehler HW (1969) Stratigraphy and oil-shale deposits of Eocene rocks in the Washakie Basin, Wyoming. In: Barlow JA (ed) Symposium on Tertiary Rocks of Wyoming. 21st annual field conference guidebook, Wyoming Geological Association, Casper, pp 197–206
Roehler HW (1973) Mineral resources in the Washakie Basin, Wyoming, and Sand Wash Basin, Colorado. In: Schell EM (ed) Symposium and core seminar on the geology and mineral resources of the Greater Green River Basin. 25th annual field conference guidebook, Wyoming Geological Association, Casper, pp 47–56
Roehler HW (1987) Geological investigations of the Vermillion Creek coal bed in the Eocene Niland Tongue of the Wasatch Formation, Sweetwater County, Wyoming. U.S. Geological Survey professional paper 1314A-L, 202 p
Roehler HW (1991) Revised stratigraphic nomenclature for the Wasatch and Green River Formations of Eocene age, Wyoming, Utah, and Colorado. Professional paper 1506-B. U.S. Geological Survey, 38 p
Roehler HW (1993) Eocene climates, depositional environments, and geography, Greater Green River Basin, Wyoming, Utah, and Colorado. vol professional paper 1506-F. U.S. Geological Survey, 74 p
Rowley PD, Hansen WR, Tweto O, Carrara PE (1985) Geologic map of the Vernal 1° x 2° quadrangle, Colorado, Utah, and Wyoming. U.S. Geological Survey miscellaneous investigations series map I-1526, 1:250 000 scale
Sáez A, Cabrera L (2002) Sedimentological and palaeohydrological responses to tectonics and climate in a small, closed, lacustrine system: Oligocene As Pontes Basin (Spain). Sedimentology 49:1073–1094
Sagri M, Abbate E, Bruni P (1989) Deposits of ephemeral and perennial lakes in the Tertiary Daban Basin (Northern Somalia). Palaeogeogr Palaeoclimatol Palaeoecol 70:225–233
Sklenar SE, Anderson DW (1985) Origin and early evolution of an Eocene lake system within the Washakie Basin of southwestern Wyoming. In: Flores RM, Kaplan SS (eds) Cenozoic paleogeography of the West Central United States, Rocky Mountain Paleogeography Symposium 3. Rocky Mountain

Section, SEPM (Society for Sedimentary Geology), Denver, pp 231–245
Smith ME, Singer B, Carroll AR (2004) $^{40}Ar/^{39}Ar$ geochronology of the Eocene Green River Formation, Wyoming; Reply. Geol Soc Am Bull 116:253–256
Smith ME, Carroll AR, Singer BS (2008) Synoptic reconstruction of a major ancient lake system: Eocene Green River Formation, Western United States. Geol Soc Am Bull 120:54–84
Smith ME, Chamberlain KR, Singer BS, Carroll AR (2010) Eocene clocks agree: Coeval $^{40}Ar/^{39}Ar$, U-Pb, and astronomical ages from the Green River Formation. Geology 38:527–530
Taylor RS (1972) Paleoecology of ostracodes from the Luman Tongue and Tipton Member (early Eocene) of the Green River Formation, Wyoming. University of Kansas, Lawrence
Van Horn MD (1979) Stratigraphic relationships and depositional environments of the Almond and associated formations, east-central flank of the Rock Springs uplift. In: Field trip: Cretaceous of the Rock Springs uplift. Rocky Mountain section, Society of Economic Paleontologists and Mineralogists, Denver, pp 50–63
Walker TR (1967) Formation of red beds in modern and ancient deserts. Geol Soc Am Bull 78:353–368
Wilf P (2000) Late Paleocene-early Eocene climate changes in southwestern Wyoming: paleobotanical analysis. Geol Soc Am Bull 112:292–307
Wing SL, Bown TM, Obradovich JD (1991) Early Eocene biotic and climatic change in interior western North America. Geology 19:1189–1192
Witkind IJ, Grose LT (1972) Areal geologic map of the Rocky Mountain region and environs. In: Mallory WW (ed) Geologic atlas of the Rocky Mountain region. Rocky Mountain Association of Geologists, Denver, p 34
Wolfe JA (1978) A paleobotanical interpretation of Tertiary climates in the Northern Hemisphere. Am Sci 66:694–703
Wolfe JA, Poore RZ (1982) Tertiary marine and nonmarine climatic trends. In: Climate in Earth History. National Academy Press, Washington, D.C., pp 154–159
Wood HE II, Chaney RW, Clark J, Colbert EH, Jepson GL, Reedside JB, Stock C (1941) Nomenclature and correlation of the North American continental Tertiary. Geol Soc Am Bull 52:1–48

3 Lacustrine Sedimentology, Stratigraphy and Stable Isotope Geochemistry of the Tipton Member of the Green River Formation

Jennifer Walker Graf, Alan R. Carroll, and Michael Elliot Smith

Abstract

The Tipton Member of the Green River Formation occupies much of the Greater Green River Basin (GGRB) of Wyoming and Colorado. Long hypothesized to record a single shift from open to partly closed hydrology, new detailed stratigraphy and stable isotope geochemistry indicates that its strata record open, then partly closed, then open, then partly closed hydrology, which are each recorded by distinct transitions in facies associations, geochemistry, carbonate mineralogy, and organic content. Intervals of open hydrology occur coincident with the progradation of deltaic sandstones that are absent during the partly closed intervals, suggesting that environmental transitions were controlled by avulsions of the Idaho River. The first of these transitions occurs at the contact between the Scheggs bed and overlying Rife bed, and is thought to reflect the initial impoundment of Lake Gosiute. The Scheggs bed ranges from 23.5 to 36.5 m, and is characterized by fluvial-lacustrine lithofacies, calcitic mineralogy, an average Fischer Assay content of 7.6 gal./ton, and low $\delta^{18}O$ and $\delta^{13}C$ values (25.3‰ and 0.7‰, respectively). These deposits transition over a five meter interval to the overlying 2–15 m-thick lower Rife bed. The lower Rife bed is characterized by fluctuating profundal lithofacies, dolomitic mineralogy, an average Fischer Assay content of 17.6 gal./ton, and high $\delta^{18}O$ and $\delta^{13}C$ values (29.3 and 5.3‰). The lower Rife bed transitions up-section over a two meter interval into fluvial-lacustrine lithofacies

J.W. Graf (✉)
Encana Corporation,
370 17th St, Suite 1700, Denver, CO 80202, USA
e-mail: Jennifer.Graf@encana.com

A.R. Carroll
Department of Geoscience, University of Wisconsin-Madison, 1215 W. Dayton St., Madison, WI 53706, USA
e-mail: carroll@geology.wisc.edu

M.E. Smith
School of Earth Science and Environmental Sustainability, Northern Arizona University, 602 S. Humphreys, Flagstaff, AZ 86011, USA
e-mail: michael.e.smith@nau.edu

M.E. Smith, A.R. Carroll (eds.), *Stratigraphy and Paleolimnology of the Green River Formation, Western USA*, Syntheses in Limnogeology 1, DOI 10.1007/978-94-017-9906-5_3

of the 2.5–20 m thick middle Rife bed, which exhibits calcitic mineralogy, an average Fischer Assay content of 9.7 gal./ton, and low $\delta^{18}O$ and $\delta^{13}C$ values (23.0 and 1.9‰). The third and final transition, from the middle Rife bed to the upper Rife bed, occurs gradationally over 6 m of section. The 6.5–22 m-thick upper Rife bed is characterized by fluctuating profundal deposits, dolomitic mineralogy, an average Fischer Assay content of 19.2 gal./ton, and high $\delta^{18}O$ and $\delta^{13}C$ values (29.8‰ and 8.5‰, respectfully). We interpret this succession of abrupt changes in lithofacies and isotope geochemistry within the Tipton Member to reflect the diversion, recapture, and ultimate diversion of a major source(s) of water and sediment into the basin.

3.1 Introduction

The Green River Formation (GRF) in the Greater Green River Basin (GGRB) records the dynamic evolution of Eocene Lake Gosiute as it transitioned from originally open paleohydrology to closed and then finally back to open paleohydrology before its final infilling by alluvium (Fig. 3.1) (Carroll and Bohacs 1999; Smith et al. 2008). The Tipton Member, previously the Tipton Shale Member (Schultz 1920), contains a broad array of non-marine facies. It underlies the evaporative Wilkins Peak Member, and has been proposed to record a transition from a hydrologically open to hydrologically closed lake basin (Roehler 1993; Pietras et al. 2003). Despite a long history of field and core-based investigation and documentation (Pipiringos 1955; Schultz 1920; Roehler 1992; Oriel 1961), the detailed stratigraphy and depositional controls of Tipton Member remain incompletely understood. This study represents a basin-scale examination of the lithofacies, stratigraphic packaging, and stable isotope geochemistry of the Tipton Member along White Mountain in the eastern Bridger subbasin of the GGRB. We argue that the Tipton Member records two compositionally and isotopically distinct transitions from overfilled to balanced-fill conditions.

The Tipton Member was deposited within the GGRB, which is located in the foreland of the Sevier fold and thrust belt, and is bounded by Precambrian-cored, Laramide-style uplifts to the north, south and east (Fig. 3.1) (Dickinson et al. 1988; DeCelles 1994). Basement-involved arches divide the GGRB into the Washakie, Sand Wash, Great Divide, and Green River sub-basins, all of which contain Tipton Member strata. Fluvial deposits of the Luman Member of the GRF and Niland Tongue of the Wasatch Formation underlie the Scheggs bed, whereas evaporative facies of the Wilkins Peak Member overly the Rife bed (Fig. 3.2). The Tipton Member has been divided into two beds: the Scheggs bed and overlying Rife bed (Roehler 1991b), the contact between which is understood to reflect a transition from freshwater, overfilled conditions to more saline, balanced-filled conditions within the lacustrine system (Roehler 1993; Carroll and Bohacs 1999). The Farson Sandstone, an arkosic deltaic complex, laterally bounds and interfingers with the Tipton Member in the northern part of the basin (Roehler 1992), and is equivalent to coarse-grained alluvial strata of the Pass Peak Formation in the northwest GGRB (Smith et al. 2008; Steidtmann 1969). Principal Tipton Member lithologies include variably organic-rich calcareous mudstone and marlstone, fossil-bearing siltstone, ostracode and oolitic grainstone, stromatolite, and various sandstone lithofacies assigned to the Farson Sandstone. Its fossil assemblages include freshwater bivalves and gastropods, fish, plant fragments, and vertebrate and invertebrate trace fossils. The Tipton Member is Early Eocene in age, based on late Wasatchian faunas found within it and in equivalent strata, and sanidine $^{40}Ar/^{39}Ar$ ages for ash beds contained within it and the overlying Wilkins Peak Member (Smith et al. 2008). Assuming that the

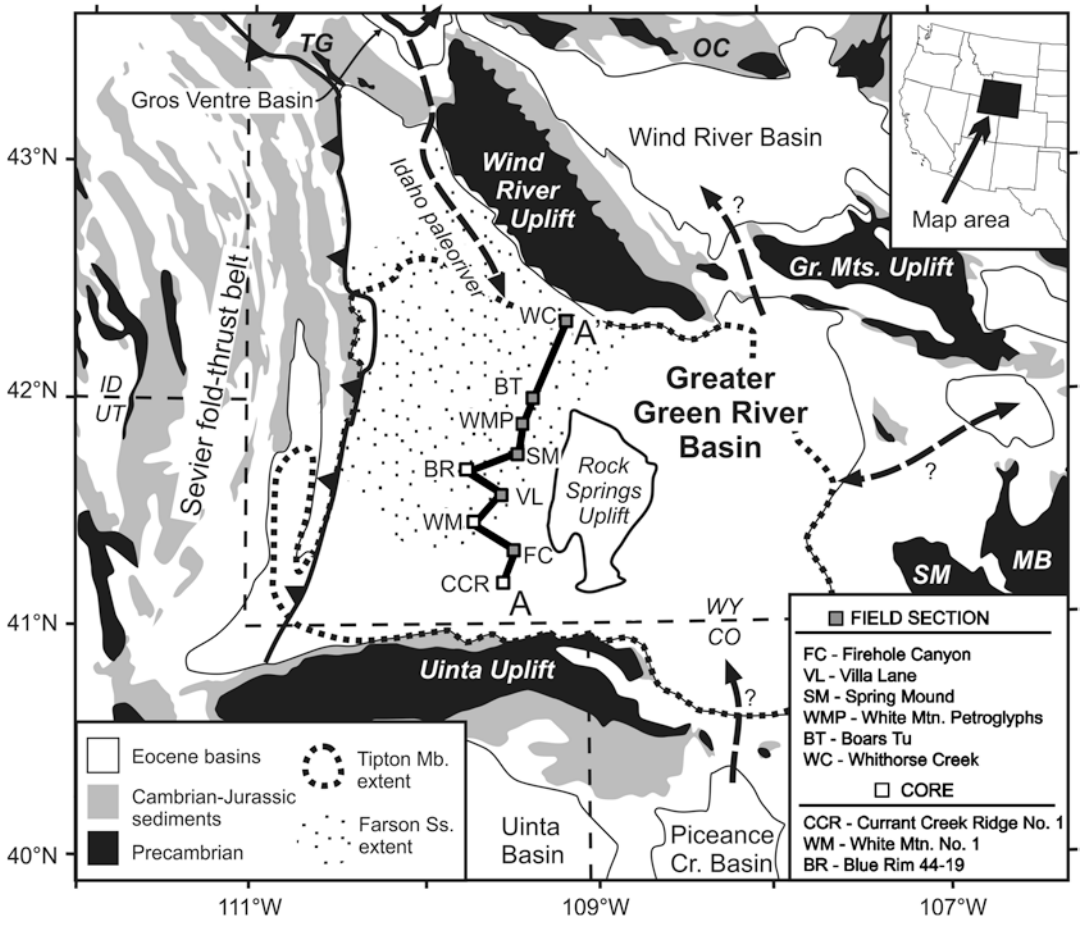

Fig. 3.1 Map showing the location of Eocene basins, basin-bounding uplifts, and measured sections (Base map modified from Witkind and Grose (1972). Abbreviations for Laramide uplifts: *TG* Teton-Gros Ventre, *OC* Owl Creek, *MB* Medicine Bow, *SM* Medicine Bow)

Scheggs bed represents 2/3 of the amount of time of the Lysitean mammalian subage, its deposition occurred over approximately 1.06 ± 0.43 m.y., (Smith et al. 2008, 2010). Based solely on their relative thicknesses, the Rife bed represents 0.60 ± 0.31 m.y. of deposition, whereas the Scheggs bed represents 0.46 ± 0.30 m.y.

3.2 Methods

3.2.1 Stratigraphic Analysis

Stratigraphic sections were chosen along a 150 km north–south cross-section through the GRB to document Lake Gosiute's evolution during deposition of the Tipton Member (Fig. 3.1). Five field sections were measured at decimeter-scale along the western and southwestern flanks of the Rock Springs Uplift along White Mountain and Flaming Gorge Reservoir. From the south to the north, they are Firehole Canyon (FC), Villa Lane (VL), Spring Mound (SM), White Mountain Petroglyphs (WMP), and Boar's Tusk (BT). An additional field section, Whitehorse Creek (WC), was modified from Pietras (2003) and incorporated into this study. Three cores supplement field data: the U.S. DOE/LETC Currant Creek Ridge No. 1 (CCR), U.S. ERDA White Mountain No. 1 (WM) and the Union Pacific Railroad Blue Rim 44-19 (BR). Locations of core and field sections are shown in Fig. 3.1.

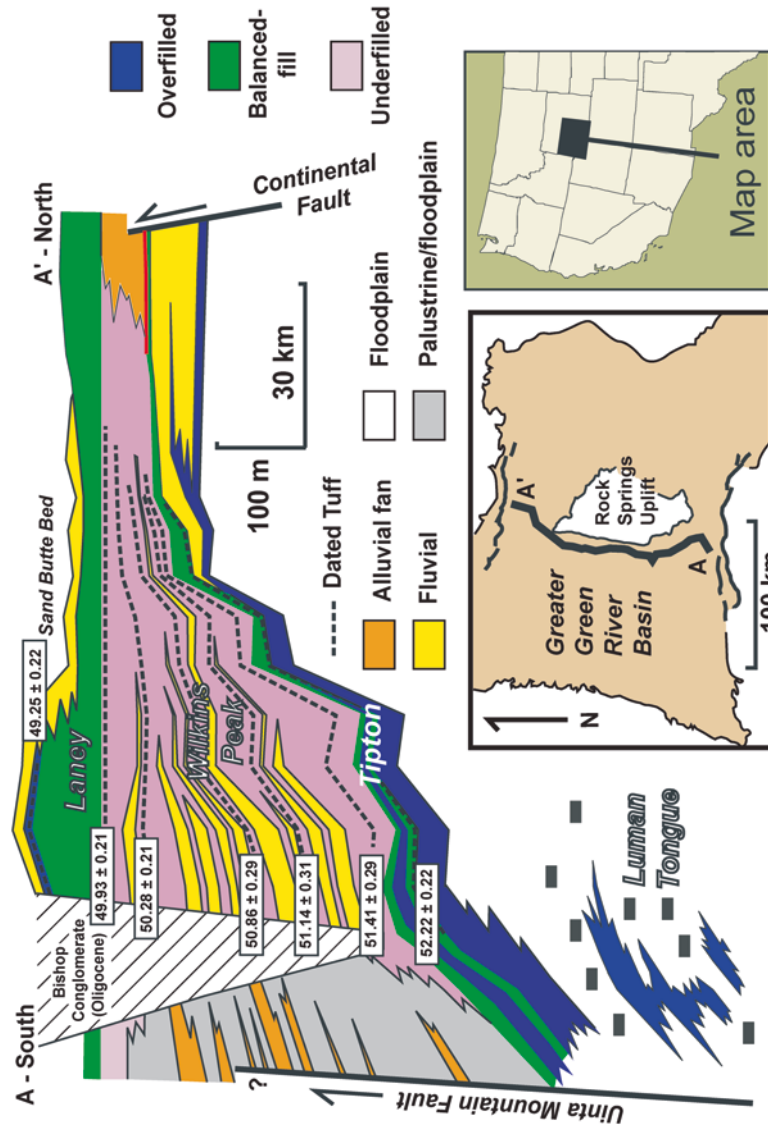

Fig. 3.2 Stratigraphy and associated lake-types of the Green River Formation in the Greater Green River Basin, Wyoming

3.2.2 Sampling

Field samples were collected primarily for comparative petrophysical analysis, and were not used for XRD and stable isotopic analysis due to observable effects of weathering. Samples from two cores, CCR and WM, were collected for XRD and stable isotopic analysis. The sample spacing and sample density of each core was concentrated on the Scheggs-Rife contact, as determined by lithofacies assemblages.

3.2.3 Mineralogy

The carbonate mineralogy of profundal mudstone samples from two cores (CCR and WM) was assessed using XRD analysis. Each sample was ground into fine powder, and a split of which was analyzed at the University of Wisconsin-Madison using a Sintag PAD V X-ray diffractometer using a Cu Kα x-ray source (λ = 1.5418 Å). The scans of 54 samples were run between 20 and 55 degrees 2-θ, a range that captures all relevant calcite and dolomite peaks. Step size was set at 0.02 degrees, with a step time of 1 s. The calcite-dolomite proportion of each sample was determined using the relative areas of dominant calcite peaks (those between 29.30 and 30.00 degrees 2-θ) and dolomite peaks (those between 30.40 and 31.10 degrees 2-θ) according to the relationship:

$$\%_{calcite} = \left[\frac{\sum A_{calcite\_peak}}{\left(\sum A_{calcite\_peak} + \sum A_{dolomite\_peak} \right)} \right] * 100$$

Based on this calculation, samples were categorized as dominantly calcitic (>80 % calcite), mixed (20–80 % calcite), or dominantly dolomitic (<20 % calcite).

3.2.4 Stable Isotopes

An additional split of each powdered sample was allocated for geochemical analysis. Samples were processed at the University of Michigan Stable Isotope Laboratory in Ann Arbor, Michigan where they were roasted in vacuo at 200 °C for 1 h to remove contaminants. Samples were then reacted at 77° ± 1 °C with 4 drops of anhydrous phosphoric acid for 8 min (12 min for dolomitic samples) in a Finnigan MAT Kiel IV preparation device coupled directly to the inlet of a Finnigan MAT 253 triple collector isotope ratio mass spectrometer. Maintained measured precision using this methodology is reported as better than 0.1 % for both carbon and oxygen isotope compositions. In this study, $\delta^{18}O$ data is reported relative to VSMOW, while $\delta^{13}C$ data is reported relative to VPDB. Where duplicate samples were run, averages weighted according to standard deviation were used.

3.3 Lithofacies

This study recognizes 13 lithofacies within the Tipton Member, as defined by lithology, organic content, sedimentary structures, biologic markers and paleo-flow indicators (Table 3.1).

Microlaminated kerogen-rich mudstone Laminated, organic-rich mudstone is the dominant lithofacies of the Rife bed, though it is also found to a lesser extent in the Scheggs bed. The mudstone is generally dark-brown to black in color. Discrete, rhythmic, variegated laminations are μm to mm in scale, and planar parallel (Fig. 3.4a). Interlaminations (mm- to cm-scale) of tan siltstone, tuff, and chert are found infrequently within sections. Fischer Assay oil yields range between 20 and 28 gal./ton (Roehler 1991a), qualifying these rocks as high-quality oil shale (Culbertson et al. 1980; Dana and Smith 1972). Well-preserved, intact fish fossils are present though infrequent. Occasional phosphatic concretions are preserved as both thin (mm-scale), lenticular bodies along lamination planes as well as irregularly shaped nodules around which overlying laminations are deformed. When associated with thin interbeds of sand, stromatolite, and ostracode and oolitic grainstone, cm-scale mud cracks are observed. In outcrop, this lithofacies forms pronounced cliffs that can be

Table 3.1 Tipton Member Lithofacies

Lithofacies	Description	Occurrence	Interpretation
Microlaminated kerogen-rich mudstone	Dark brown to black mudstone with μm- to mm-scale laminations, high kerogen content, no intact biologic markers; Fischer Assay yield of 20–28 Gal./ton	Primarily found in Zones B and D. It is present in meter-scale intervals throughout CCR and in the upper- most portion of WM's Zone C	Profundal deposition in anoxic water bottoms devoid of bioturbating benthic organisms
Laminated mudstone	Grey to brown mudstone with densely spaced, varigated, μm- to cm-scale laminations, including interlaminations of silt and tuff. Fish, ostracodes, burrows and coprolites are present; Fischer Assay yield of 9–22 Gal./ton	Observed in all zones of all sections, excluding WC	Profundal deposition in anoxic water bottoms devoid of bioturbating benthic organisms
Massive kerogen-rich mudstone	Dark brown to black mudstone with no visible laminations, high kerogen content, intermittent silt and kerogen-stained tuff interlaminations; Fischer Assay yield of 22–26 Gal./ton	Minor component of Zones B and D, though is infrequently observed throughout all Zones in CCR	Profundal deposition in anoxic water devoid of bioturbating benthic organisms
Massive mudstone	Grey mudstone with no visible laminations. Abundant gastropods and bivalves and infrequent burrows are present; Fischer Assay yield of 2–6 Gal./ton	Primary component of the basin- ward associations of Zones A and C	Littoral to sub-littoral deposition via hyperpycnal plumes during storms and/ or bioturbation of originally laminated mud
Fossiliferous siltstone	Grey or tan siltstone with gastropods and bivales (Scheggs) and fish (Rife) fossils. Laminations are low, density, mm- cm-scale with varied orientations	Found throughout all zones in CCR, BR, BT, WC. Primarily Zones A and B in WM, Zone C in VL, A and D in SM, and Zones A, C, and D in WMP	Littoral margi, pro-delta/ distal bar, or turbidite, depending on lithostratigraphic context
Delta foreset sandstone	Steeply-dipping (29 degrees) foresets of vF-F, subangular, well-cemented sand bearing cm-scale rip-ups of underlying silt	Observation is exclusive to the Farson Sandstone in Zone A at WMP	Deposition by grain flow avalanches down the front of a Gilbert-type delta
Trough cross-bedded sandstone	Vertically aggregated bed sets of vF to M sized, angular to subangular sand. Laminae dip 25 degrees and are distinguished by mica- rich laminae	Most prevalent sandstone architecture; Found in Zone A and C sands	Delta channel mouth bar deposition by ripples and dunes formed under unidirectional flow
Horizontally-bedded sandstone	Vertically aggregated, horizontal beds of vF sand that display slight fining upwards trend. Burrows, reed imprints are present	Frequent component of Zone A and C sands at WM, VL, SM, WMP, BT, and WC	Upper shoreface deposition at distributary terminii by unidirectional flow and/or swash zone deposition along beach faces

(continued)

Table 3.1 (continued)

Lithofacies	Description	Occurrence	Interpretation
Hummocky cross-stratified sandstone	Hummocked bed sets with 1–3 mm laminations dipping 15 degrees. Micaceous laminations and entrained fish debris are present	Observed in BR core and in Zone C at WMP field station	Storm-dominated lower shoreface
Climbing-rippled to wavy-bedded sandstone	Vertically aggregated, variably sinuous laminations of vF sand	Observed in Zone A of WMP and BT; Zone C in WMP	Delta-front deposition during period of high sedimentation
Massive sandstone	Grain-supported, vF-M sand lacking internal architecture. Rip-ups, burrows, floral material and fish debris are often present	More frequent Zone A sands (BR, VL, WMP, BT, and WC), but also observed in Zone C (BR and BT)	Liquefied delta slump/ debris flow deposition or intensely bioturbated delta front or lower shoreface deposit
Stromatolite	Brecciated isolated carbonate mounds (Scheggs) and laterally extensive stromatolites associated with green, mud-cracked, mineral-bearing siltstone (Rife)	Brecciated stromatolite exclusive to Zone A at SM. Laterally extensive stromatolites observed in Zone A of SM and Zone D in FC, SM, WMP and BT	Isolated tufa-travertive subaqueous spring deposits in the Scheggs bed; Widespread littoral stromatolitic carbonate deposition mediated by microbial mats in the Rife bed
Ostracode and ooid grainstone	Medium to coarse grain-sized, preserved as horizontal laminations and within vertical burrows, and often entrain silt rip-ups, fish debris and phosphatic resins	Found in the Rife Bed at CCR, BR, SM, WMP, and BT. Within the Scheggs bed, it is found only in CCR core. Observed in Zone A (CCR, SM), Zone B (CCR, BT), Zone C (BR), and Zone D (BR, SM, WMP)	Deposition of carbonate allochems in shallow, wave-agitated lake margin areas where Ca-rich stream/ spring waters and lake waters interacted

Notes: Abbreviations indicating modal grain size of sandstone: *M* medium, *F* fine, *vF* very fine.

traced laterally for tens of kilometers. Field sections weather blue in color, and are colloquially referred to as "blue beds".

Interpretation: Preservation of fine, densely spaced laminations suggests deposition from suspension in an area beneath wave base and where bottom currents were continuously slow or non-existent. The high rate of organic preservation, reflected by high Fischer Assay oil yields, is interpreted to reflect deposition within low-oxygenated or entirely anoxic water conditions (e.g. Demaison and Moore 1980). However, it is unresolved whether permanent chemical and thermal stratification of lake waters is necessary for generation of kerogen-rich laminated mudstone (i.e., oil shale). Citing the presence of fossil catfish within oil shale lithofacies of the Laney Member of the GRF, Buchheim and Surdam (1977) suggested that only fluctuating or semi-permanent lake stratification is necessary for oil shale deposition within the GRF. An alternative interpretation of the presence of bottom-dwelling catfish within oil shale, however, is that the corpse bloated, floated out to deeper areas of the lake where it sunk and then came to rest along anoxic bottom waters.

The small phosphatic nodules around which overlying laminae conform are interpreted as coprolites, an observation also reported in profundal sediments of the Tipton Member (Castro 1962) and the Laney Member (Fischer and Roberts 1991). This facies is interpreted to

represent profundal lacustrine deposition within a low-oxygenated, stratified lake conditions similar to those found within profundal zones of modern lakes Zurich (Bradley 1929; Kelts and Hsü 1978) and Tanganyika (Huc et al. 1990).

Laminated mudstone This lithofacies is represented in both the Scheggs and Rife beds as grey to brown mudstone. In most examples, variegated laminations range between mm to cm in scale (Fig. 3.3b). Upper and lower contacts of distinct laminae are variable, occurring as discrete planar, diffuse/gradational planar, or wavy/irregular. Infrequent mm- to cm-scale interlaminations of grey-tan silt and tuff are also present. Within the mudstone and siltstone inter-laminations, well-preserved fish fossils, ostracode molds, and compacted, vertical burrows are present. Tan, spherical nodules of silt onto which overlying laminae conform are observed with variable frequency. Fischer Assay oil yields range between 9 and 22 gal./ton (Roehler 1991a), classifying this lithofacies as low-quality oil shale (Culbertson et al. 1980; Dana and Smith 1972). Outcrop expression ranges from covered, gradual slopes to moderately high-angle cliffs.

Interpretation: The relatively diminished Fischer Assay oil yield of this lithofacies compared to that of the mm-laminated, organic-rich mudstone lithofacies suggests either diminished organic production, an increase in organic destruction and/or clastic dilution. The primary source of oil-shale kerogen in the GRF is autochthonous algae and bacteria (Tissot and Vandenbroucke 1983; Horsfield et al. 1994; Carroll and Bohacs 2001; Bohacs et al. 2000). During periods of sustained freshwater input, a corresponding increase in available oxygen may have increased degradation of these particulate organics (Horsfield et al. 1994), while increased inorganic sedimentation may have diluted preserved organic concentrations (cf. Carroll 1998). Alternatively, freshwater input has been attributed to the reduction of dissolved bicarbonate concentrations within a lake system, which ultimately decreases primary productivity (Horsfield et al. 1994). Collectively accounting for each possibility, this lithofacies is interpreted to reflect deposition during periods of freshwater input and low chemical and thermal stratification.

Massive kerogen-rich mudstone Massive, organic-rich mudstone is present in the Rife bed and, less frequently, in the Scheggs bed. This mudstone is typically dark-brown to dark grey in color. Laminations are not visible in hand samples or thin section, but may exist cryptically. Silty interbeds are rare, and thin (mm-scale) interlaminations of bitumen-saturated tuff and horizontal fracture-fills of dolomite are frequently observed. Fischer Assay yields range between 22 and 26 gal./ton (Roehler 1991a), qualifying this mudstone as high-quality oil shale (Culbertson et al. 1980; Dana and Smith 1972). Both core and field samples have a bituminous odor and are absent of well-preserved burrows, ostracode molds and fish fossils. Outcrop expression of this facies is pronounced cliffs that can be traced laterally for several kilometers.

Interpretation: Like the laminated organic-rich mudstone, above, preserved organic matter suggests sub-mixolimnium deposition in a chemically and thermally stratified lacustrine system in which there was an insufficient alternation in the delivery of micrite to create lamination. Massive kerogen-rich mudstone beds could also have been deposited by hypopycnal plumes basinward of sites of fluvial input or created via entrainment of organic rich mud during storm events (cf. Renaut and Gierlowski-Kordesch 2010).

Massive mudstone Massive mudstone is the dominant lithofacies of the Scheggs bed. It is almost exclusively light to medium grey in color, has no visible lamination, and generally preserves largely intact freshwater animals such as gastropods (2–4 cm) and bivalves (4–8 cm) (Fig. 3.3c and d), both of which commonly exhibit abrasion and removal of shell ornamentation. Ostracodes are abundant throughout, whereas vertical burrows occur infrequently. In the lower Scheggs bed, gastropods and bivalves are commonly silicified. Towards the upper Scheggs bed, however, gastropods become less frequent and articulated bivalves retain original aragonite mineralogy. The Fischer Assay oil

Fig. 3.3 Photographs of Tipton Member lithofacies: (**a**) Thinly laminated (μm to mm), organic-rich mudstone; (**b**) variably laminated (μm to cm) mudstone; (**c**) silicified *Goniobasis tenera* gastropods, which constitute the *Goniobasis* Marker bed; (**d**) freshwater bivalves preserved in the fossil-bearing siltstone lithofacies; (**e**) Gilbert-type foresets observed from the WMP section; (**f**) climbing ripples resulting from super-critical flow with both stoss- and lee-sides preserved; (**g**) injection feature where vF sand is injected into overlying F sand in the BR core; (**h**) concentric delamination of stromatolites which mark the Tipton-Wilkins Peak contact; and (**i**) brecciated stromatolites at the SM field section

yield of this lithofacies is low, ranging between 2 and 6 gal./ton (Roehler 1991a). Deep trenching (~0.5 m) did not reach un-weathered, intact section due to vegetated slopes. Abundant silicified float is, therefore, the primary facies identifier in the field. It should be noted that the observation of aragonitic fossils in the field was limited to the Villa Lane section, where a recent road cut had generated fresh exposure.

Interpretation: The absence of lamination within this lithofacies suggests either continuous sedimentation (Pasierbiewicz and Kotlarczyk 1997), or more likely the bioturbation of formerly laminated mud (Fischer and Roberts 1991; Demaison and Moore 1980) within a non-stratified lacustrine system (Bradley 1929, 1931; Carroll 1998). It may also reflect deposition by hyperpycnal plumes delivered to the lake center during periods of significant fluvial input or shoreface agitation by waves. The decreased kerogen content observed within this lithofacies is thought to reflect algal degradation resulting from increased oxygenation and decreased bicarbonate due to downstream outflow of lakewaters (Horsfield et al. 1994). This study interprets the massive mudstone lithofacies as littoral deposits within a freshwater system, which is consistent with the observation by Surdam and Stanley (1979) of bioturbated, mollusk and ostracode-bearing mudstone with freshwater deposits of the upper Laney Member of the GRF, as well as the observation of Cohen (1989) of abundant gastropod infauna within the littoral to sub-littoral zones of modern Lake Tanganyika.

Fossiliferous siltstone Fossil-bearing siltstone is found in both profundal and marginal deposits. It is medium grey or tan in color and is either laminated or massive. Laminated intervals display mm- to cm-scale laminations of varied shades of brown silt and mudstone. Contacts among laminations occur as planar-parallel, wavy-parallel, and wavy non-parallel. Mollusc and ostracode fossils are most commonly associated with planar-parallel and massive interbeds. Where thicker than approximately 0.5 m in outcrop, this lithofacies typically constitutes low-angle, vegetated slopes that require trenching (<0.25 m) for stratigraphic observation. Exposure quality of thin interbeds of this lithofacies (<0.5 m) is highly variable and largely dependent upon the resistance of overlying lithologies.

Interpretation: This lithofacies is found within a variety of depositional and hydrodynamic environments. Where siltstone contains abundant gastropods that are continuously distributed throughout the bed, this lithofacies is interpreted to represent littoral deposition. Similarly dense gastropod concentrations are observed in the littoral margins of Lake Tanganika (Cohen 1989). Where this lithofacies occurs as thin, fining-upward interbeds within mudstone lithofacies, it is interpreted as turbidite deposits. In association with stacked, coarsening upward successions of sandstone and mudstone, the siltstone lithofacies is interpreted as pro-delta and distal bar deposits. Similar pro-delta deposits are observed in the Laney Member of the GRF (Stanley and Surdam 1978), in Late Pleistocene Lake Bonneville (Lemons and Chan 1999), and in Jurassic deposits within the East Gobi Basin, Mongolia (Johnson and Graham 2004).

Delta foreset sandstone Within this study area, steeply dipping delta foreset lithofacies are limited to the Farson Sandstone Member at the WMP and WC (Pietras 2003) field sections. At WMP this lithofacies constitutes approximately 4.5 m of vertical section. Foresets dip 28 degrees (Fig. 3.3e) and are composed of micaceous, biotite-rich, vF-F, sub-angular sandstone that is well-cemented by calcite. Relatively large (up to 4 cm) rip-ups of underlying tan siltstone are observed along foreset planes, while twig and reed impressions are found less frequently. Irregular, 10–20 cm loading features typify the contact of this facies with underlying, convoluted siltstone. The upper portion of the steeply dipping foreset lithofacies is typically abruptly overlain by mudstone.

Interpretation: The steeply dipping foresets of this lithofacies are interpreted as delta front deposits. A high flow regime, capable of transporting terrigenous plant material basin-ward and eroding cohesive mud and siltstone, is thought to have existed during deposition. Soft-sediment deformation within underlying units suggests this lithofacies was deposited rapidly across a soft

substrate, while bed thickness indicates water depth was at least 4.5 m. Accounting for compaction effects, foreset height and interpreted water depth may have been greater. Larger (25 m) Gilbert-type foreset beds are observed in Eocene Fossil Lake (Buchheim and Eugster 1998) and within Upper Laney Member of the Green River Formation (Stanley and Surdam 1978). Modern analogues include deltaic deposits in freshwater lakes Constance (Müller 1966), Pyramid (Born 1972) and Malawi (Scholz et al. 1993).

Trough cross-bedded sandstone This lithofacies is a dominant component of the Farson Sandstone and is observed in both field and core sections. Beds are 10 cm–4 m thick and are composed of vertically aggraded sets that range between 5 cm and 25 cm in thickness and approximately 15–40 cm in width. Individual mm- to cm-scale bedding planes consist of grain-supported, angular to sub-angular, vF to M sand. Bounding surfaces between sets curve approximately 25 degrees at their steepest, and are tangential to underlying erosion surfaces. Laminae are often highlighted by concentrations of biotite and muscovite. No visibly identifiable floral or faunal remnants are preserved. Outcrop relief of this lithofacies is highly variable and dependent upon localized weathering effects.

Interpretation: Trough cross-beds occur in a variety of depositional environments, where flow is sufficient for the down-flow migration of dune structures (Allen 1962; Harms and Fahnestock 1965). In association with stacked sequences of laminated mudstone, siltstone and sandstone, this lithofacies is interpreted to represent delta slope and channel deposits. Similar trough cross-bedded deposits are documented in the Bitter Creek deltaic complex of the Laney Member (Stanley and Surdam 1978), as well in Jurassic-Cretaceous lacustrine deltas in the East Gobi Basin, Mongolia (Johnson and Graham 2004).

Horizontally-bedded sandstone Horizontally bedded sand is exclusive to the Farson Sandstone and is observed in both core and field sections. Packages are between 20 cm and 2 m thick, and are composed of 2–5 mm thick, horizontal to near horizontal (less than 2 degree dip), vertically aggregated beds of vF sand, which are distinguished by muscovite- and biotite-rich interlaminations. Infrequently, vertical burrow structures, reed and twig imprints, and cm-scale interbedded tuffs are observed.

Interpretation: Horizontally laminated sandstone within the Farson Sandstone suggests deposition within high flow regimes (Harms and Fahnestock 1965; Bridge 1978; Paola et al. 1989; Arnott and Southard 1990; Cheel 1990; Arnott 1993). Typically found at the top of coarsening-upward packages of littoral mudstone, siltstone and sandstone, we study interprets horizontal laminations to have been deposited by shallow, high energy unidirectional flow and/or bidirectional wave-generated currents in a swash zone along upper delta-front and delta margins.

Hummocky cross-stratified sandstone Micro-hummocky cross-bedded, vF sand is limited to Farson Sandstone deposits and is observed in both core (BR) and field (WMP) sections. Individual laminations are approximately 1–3 mm and dip approximately 15 degrees. Distinguished by mica-rich laminations, bed sets range between 3 and 6 cm thick, while aggregated packages of bed sets range between 10 and 25 cm in thickness. In the WMP field section, hummocks entrain abundant phosphatic fish "debris" composed of broken ribs, scales, platelets and vertebrae. Outcrop exposure of this lithofacies is highly variable and largely dependent upon the resistance of overlying lithofacies.

Interpretation: Hummocks result from a combination of oscillatory and weak unidirectional flow (Nøttvedt and Kreisa 1987; Leckie and Krystinik 1989; Arnott and Southard 1990; Dumas et al. 2005) in an environment where sedimentation rates are high and water depth low enough to facilitate large, fast waves, yet deep enough to maintain the oscillatory waves and unidirectional currents (Dumas and Arnott 2006). In association with stacked successions of mudstone, siltstone and sandstone lithofacies, hummocks are interpreted to have formed in the littoral zone under combined-flow between fairweather and storm wave base, likely in upper delta-front and lower delta-platform environments.

Climbing-rippled sandstone This lithofacies is exclusive to the Farson Sandstone and is observed in both core and field section. Beds are between 0.3 and 1.5 m thick, and are composed of 2 mm to 4 cm thick vertically aggraded, variably undulating laminations of vF sand that are made distinct by intermittent silt-, muscovite- and biotite-rich laminations (Fig. 3.3f). Ripple limbs exhibit irregular sinuosity, dipping between 15 and 30 degrees on either side of the ripple crest. Unlike the planar parallel and hummocky sand lithofacies with which this lithofacies is commonly associated, organic matter and fossils are not observed. Outcrop expression is highly variable and largely dependent upon the resistance of overlying lithofacies.

Interpretation: Preservation of both the lee and stoss limbs of each ripple crest indicate deposition in an area having high rates of sedimentation from suspension and bed load (Jopling and Walker 1968; Allen 1982). Variability of inclination among the ripple limbs of this lithofacies is thought to be a function of small changes in the hydrodynamic environment and/or variable sediment discharge. As part of the Farson Sandstone, this lithofacies is interpreted to represent deposition along the delta-front, an area known for high-rates of sedimentation and wave-action modification thereof (McLane 1995).

Massive sandstone The massive sandstone lithofacies is exclusive to the Farson Sandstone, and is observed in both core and field sections observed as beds of vF to mL, grain-supported sandstone that occur in 10 cm–4 m intervals. Silt and mud rip-ups, fish debris, burrows preserved by differential cementation, and terrestrial plant material such as reeds and root casts are commonly observed throughout the beds. Internal architecture, however, is absent. Underlying siltstone frequently exhibits scour and convolute bedding due to loading of overlying sandstone. Grain-size within the sandstone beds is variable, ranging from vF to mL. Transitions between sandstone grain-size are often, but not always, abrupt. Where contacts are sharp, load-induced injection, or flame structures, are observed (Fig. 3.3g).

Interpretation: Lack of internal architecture within this lithofacies is interpreted to result from either liquefaction related to delta slump processes or bioturbation along the delta-top or delta shore-face. Where underlying sediments exhibit deformation, slumping is thought to have occurred, while burrows, though limitedly preserved, indicate bioturbation along shore-face or delta top environments. Stanley and Surdam (1978) observed similar massive units along the shore-face of the Bitter Creek deltaic complex in the Laney Member.

Stromatolite Though algal stromatolites are present in both the Rife and Scheggs beds, distinct morphological properties and depositional environments differentiate the two occurrences. Stromatolite beds within the Rife bed are 10–30 cm thick, weather orange-brown by concentric spalling (Fig. 3.3h), and are laterally extensive across several kilometers. Here, stromatolite beds are associated with a transition from organic-rich calcareous mudstone to green, mud-cracked, evaporite mineral-bearing siltstone. As such, this facies is interpreted as the base of the Tipton-Wilkins Peak contact. The stromatolite lithofacies in the Scheggs bed is exclusive to the Spring Mound (SM) field section and is laterally bound approximately 20 m to the north and south by two large (12 m high × 20 m wide) spring deposits with which it inter-fingers. The stromatolite package itself constitutes 40 cm of vertical section. The upper 30 cm of this is a breccia consisting of pebble- to gravel-sized clasts of broken algal material, shale and silt rip-ups (Fig. 3.3i).

Interpretation: Modern lacustrine stromatolite beds are observed along many lake margins and adjacent fluvial systems, such as Green Lake (Eggleston and Dean 1976), the Great Salt Lake (Halley 1976), and Lake Tanganyika (Cohen and Thouin 1987; Cassanova and Hillaire-Marcel 1992). Within the Rife bed, stromatolite beds are inferred to have formed near the shore, similar to those found in the Laney Member (Wolfbauer and Surdam 1974; Roehler 1993; Rhodes 2002). However, in the absence of an observable shore-parallel transect within the GGRB, neither this

study nor Laney Member studies can confirm whether stromatolite beds are linear, shore-parallel features. Previous studies have not reported stromatolite beds in the Scheggs bed. It is likely that the high rates of hydrologic influx, corresponding shoreline transgressions and the chemical parameters of an overfilled lacustrine system prevented extensive growth. The structural high and local calcium ion-rich geochemistry of the spring mounds are interpreted to have enabled stromatolite growth and preservation at the Spring Mound field section. From the morphology and preservation characteristics, we infer that stromatolite beds within the Scheggs bed were initially protected by adjacent mound structures, but increased wave action resulting from lake expansion re-worked and brecciated the algal mats.

Ostracode and ooid grainstone Ostracode and oolitic grainstone lithofacies are found in both the Scheggs and Rife beds. Medium to coarse grain-sized, undeformed ostracodes and oolites are preserved as horizontal laminations (2 mm–7 cm) and within vertical burrows. In both occurrences, ostracodes and oolites are associated with fossil-bearing siltstone, cm-laminated mudstone, and massive sandstone facies. Entrained within the grainstones are small (mm- to sub-mm) silt rip-ups and phosphatic fish debris, including scales, ribs, vertebrae and articulated jaws. The lithologic texture of the grainstone is generally friable in outcrop and loosely consolidated in core.

Interpretation: Though ostracodes are found throughout many lacustrine sub-environments (Cohen 2003), accumulation and formation of skeletal debris into a grainstone requires hydrologic sorting and/or minimal clastic dilution, suggestive of wave agitation along shorelines far from fluvial deltas. Oolites are similarly observed along wave-agitated lake margins (Cohen and Thouin 1987; Talbot and Allen 1996; Balch et al. 2005) where groundwater and lake water mixing leads to precipitation of inorganic carbonate (Wolfbauer and Surdam 1974; Kelts and Hsü 1978).

3.4 Lithofacies Assemblages and Associations

Two distinct lithofacies assemblages comprise the Tipton Member: fluvial-lacustrine and fluctuating profundal, both of which have distinct basin-ward and shoreward associations (Table 3.2; Fig. 3.4). Together, these lithofacies assemblages define four stratigraphic zones within the Tipton Member. The fluvial-lacustrine lithofacies assemblage defines the Scheggs bed (Zone A), while both fluctuating-profundal (Zones B and D) and fluvial-lacustrine assemblages (Zone C) characterize the overlying Rife bed (Fig. 3.2). These stratigraphic zones correspond to distinct zones of carbonate mineralogy as determined by XRD analysis. Profundal mudstone of fluvial-lacustrine Zones A and C is dominantly calcitic (69 % and 80 % calcite, respectively), while profundal mudstone of fluctuating-profundal Zones B and D is dominantly dolomitic (30 % and 12 % calcite, respectively).

3.4.1 Fluvial-Lacustrine Lithofacies Assemblage

Basin-ward association The dominant component of this association is the massive mudstone lithofacies, which bears abundant bivalves and gastropods (Fig. 3.5a). Interlaminations of fining upward beds (3–60 cm thick) of fossil-bearing siltstone lithofacies, which also preserve broken freshwater taxa, are frequent. Within the bottom-most cored meters of the CCR core, both massive and laminated organic-rich mudstone lithofacies contain interbeds of coquina. These interbeds range between 1 and 75 cm thick and contain bivalve and gastropod shell fragments within an organic-rich mudstone matrix. While the majority of these interbeds preserve primary aragonite, the largest interbed (75 cm) is has noticeably less mudstone matrix and is calcified throughout.

The basin-ward association of this assemblage reflects sustained water and sediment input into a hydrologically open, non-stratified lake system.

Table 3.2 Tipton Member Lithofacies Associations

Association	Dominant lithofacies	Occurrences	Interpretation
Fluvial lacustrine assemblage			
Basin-ward	Massive mudstone; fossiliferous siltstone (gastropods and bivalves); isolated occurrence of laminated mudstone containing bivalves.	Zone A (CCR, WM, VL, and upper portion in SM) and Zone C (CCR, WM).	Sustained high-stand conditions within a well-oxygenated, open lake system.
Shoreward	Coarsening-upward successions of massive sandstone; delta foreset sandstone; trough cross-bedded sandstone; horizontally-laminated sandstone; climbing-rippled sandstone; hummocky cross-stratified sandstone; gastropod coqina; fossil-bearing silstone (gastropods and bivalves).	Zone A (BR, SM, WMP, BT and WC) and Zone D (WM, VL, BR, SM, WMP, and BT).	Laterally migrating delta fan complex indicating sustained water and sediment influx into the lake.
Fluctuating profundal assemblage			
Basin-ward	Microlaminated kerogen-rich mudstone; massive kerogen-rich mudstone; fossil- bearing siltstone (fish); common tuff interlaminations.	Zone B (CCR, WM, VL, BR, SM, WM, and WMP) and Zone D (CCR, FC, WM, VL).	Continuous profundal deposition within a repeatedly oscillating closed, stratified lake system.
Shoreward	Thin beds of massive sandstone; fossiliferous siltstone; stromatolites, and ostracode and ooid grainstones.	Zone B (BT and WC) and Zone D (BR, SM, WMP, BT, and WC).	Littoral environments on the edge of a rapidly oscillating saline lake.

Abundantly preserved salt-sensitive fauna (e.g. bivalves) indicate well-oxygenated, freshwater conditions within the lake, while the absence of mudstone lamination and tuff interbeds suggest a combination of bioturbation, continuous sedimentation, and mixing within the suspended sediment column during deposition. Decreased Fischer Assay oil yield within fine-grained sediments is also evidence of sustained water and sediment input. Where fluvial systems enter a lacustrine basin, the concentration of particulate organics is reduced by clastic dilution, chemical degradation due to well oxygenated source waters, biologic consumption, or a combination thereof (Huc et al. 1990; Horsfield et al. 1994; Bohacs 1998). The effects of these processes are assumed to be greater in areas more proximal to source water input. The lateral expanse (>50 km of the study area) to which fine-grained profundal sediments of this association are depleted of kerogen is interpreted to reflect basinwide oxygenation and increased water and sediment input to the basin. Moreover, stacked 10–100 cm alternations between organic-rich and organic-depleted mudstone are not observed in this assemblage, which we interpret to reflect sustained hydrologic input and corresponding lake-level high-stand (Bohacs et al. 2000). Horsfield et al. (1994) observe similar lack of thin parasequences within fluvial-lacustrine deposits of the underlying Luman Tongue.

Organic-rich mudstone in Zone A of the CCR core is thought to reflect deeper, less-oxygenated waters beyond the effects of clastic dilution. At this location, Fischer Assay oil yield is greater (10.8 gal./ton) than that observed among fine-grained lithofacies located more proximal to the deltaic complex of the Farson Sandstone (e.g. 4.5 gal./ton at WM). Roehler (1992) for example interprets the CCR core location as one of the deepest areas of Lake Gosiute. Because the organic-rich mudstone lithofacies suggests anoxic or low-oxygenated bottom waters, interbeds of broken aerobic fauna are interpreted as

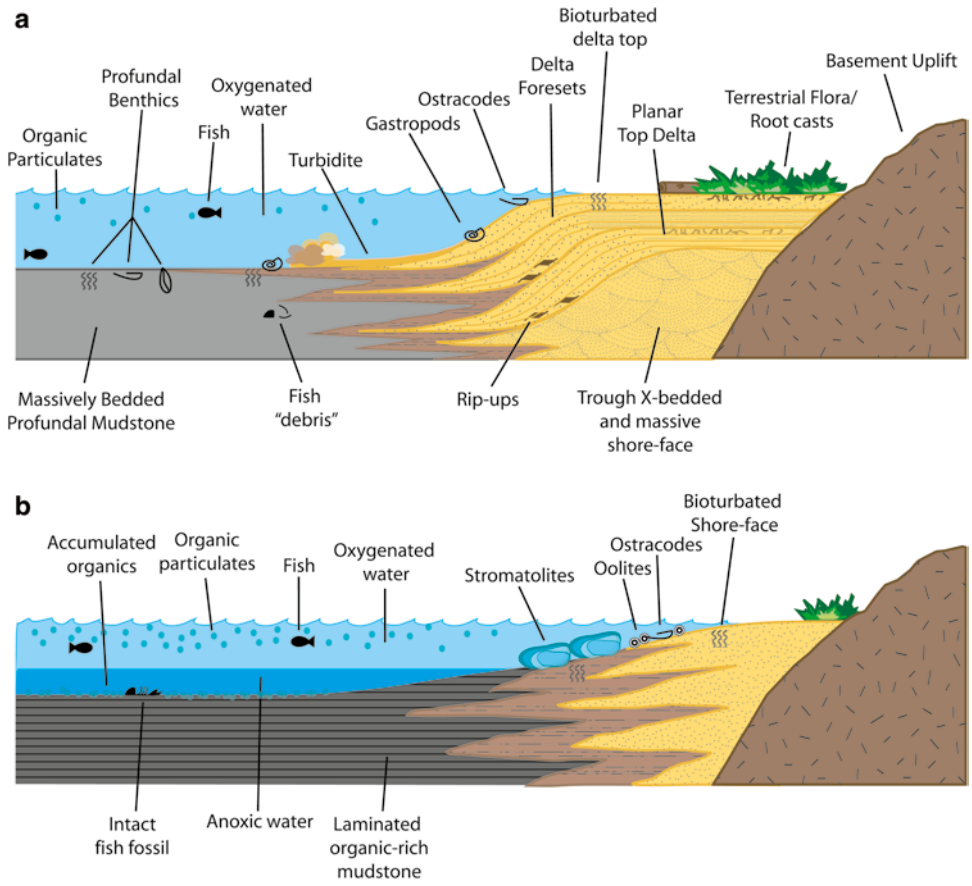

Fig. 3.4 Schematic interpretive cross-section of Lake Gosiute during (**a**) fluvial-lacustrine and (**b**) fluctuating profundal deposition

turbidite deposits. Gravity currents, similar to those described in Kneller and Buckee (2000), are thought to have transported these fauna basinward from shoreline and littoral habitats. In this manner, finer-grained sediment entrained in the current, such as silt and littoral mud, would have been deposited further basin-ward. Up-section within CCR core, small beds (5–15 cm) of fining-upward silt are interpreted as distal deposits of gravity currents.

Shoreward association Coarse-clastic deposits of the Farson Sandstone typify the shoreward association of the fluvial-lacustrine assemblage. Concentrated to the northern-most portion of the basin, stacked, coarsening-upwards successions of laminated mudstone, siltstone and sandstone lithofacies (Fig. 3.5b) are interpreted to represent a broad deltaic sequence, which grades basinward to laminated profundal mudstone. Mudstone lithofacies represent pro-delta deposits, siltstone lithofacies the distal bar, and sand lithofacies delta front and delta top deposits. Overall thickness of these successions decreases basin-ward, while the number of sequences and ratio of fine-grained sediments to sand increases. Load-induced contacts (e.g. Fig. 3.3g) are found between the gastropod-bearing siltstone and overlying trough cross-bedded, massive and Gilbert-type foreset lithofacies. Contacts between siltstone and high-flow regime planar parallel and wavy parallel lithofacies, however, are conformable. Similar lacustrine deltaic sequences have been described in the Laney Member (Stanley

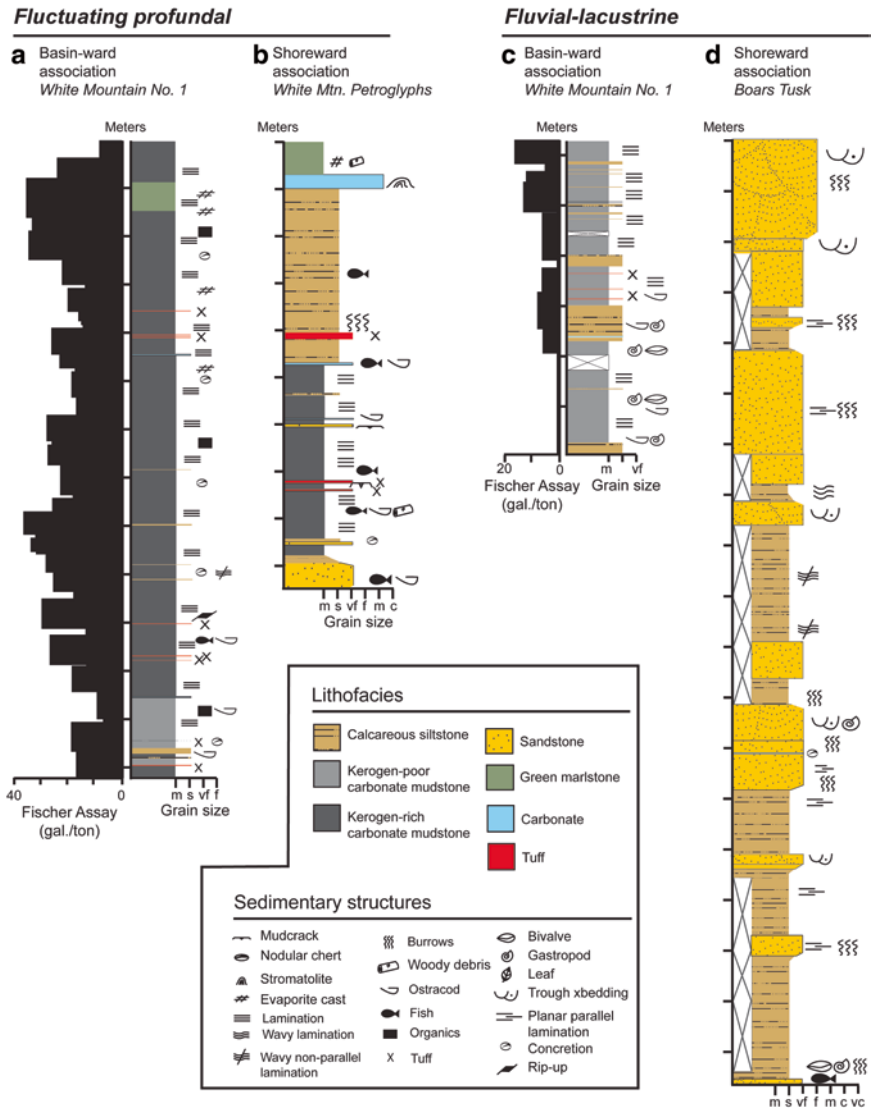

Fig. 3.5 Representative stratigraphic sections from the four principle lithofacies associations: The fluvial-lacustrine lithofacies assemblage has distinct (**a**) basin-ward and (**b**) shoreward associations. The basin-ward association is typified by the massive mudstone lithofacies and punctuated by fining upward interbeds of fossil-bearing siltstone lithofacies. Freshwater fauna, such as gastropods and bivalves are abundant throughout. The shoreward association is typified by stacked, coarsening upwards sequences of siltstone and sandstone lithofacies. The fluctuating profundal lithofacies assemblage also has distinct (**c**) basin-ward and (**d**) shoreward associations. The basin-ward association is typified by oscillations between thinly laminated, organic rich mudstone and variably laminated mudstone lithofacies. These oscillations are also apparent in Fischer Assay. The shoreward association is typified by a diverse array of fine-clastic, coarse-clastic, and biogenic lithofacies. Mud-cracked horizons are also observed. Well-preserved fish are common throughout both associations

and Surdam 1978), Lake Bonneville (Lemons and Chan 1999) and in the East Gobi Basin (Johnson and Graham 2004). The progradational and aggradational geometries of the sandstones suggest sustained sediment influx, while rip-ups and irregular lithofacies contacts indicate infrequent storm generated high-flow and erosive hydrologic conditions.

3.4.2 Fluctuating Profundal Lithofacies Assemblage

Basin-ward association The association is characterized predominantly by kerogen-rich, commonly fish fossil-bearing mudstone lithofacies (Fig. 3.5c), with minor interlaminations of fossiliferous siltstone and, less commonly, ostracode and ooid grainstone. The increased preservation of intact fish fossils and absence of benthos within this assemblage relative to that observed within the fluvial-lacustrine assemblage indicates increased chemical and thermal stratification and the presence of anoxic water bottoms. Moreover, the absence of bivalves suggests lake waters of this assemblage were more saline than those of the fluvial-lacustrine assemblage, where bivalves were abundant.

In detail, basin-ward association of the fluctuating profundal assemblage is characterized by alternating intervals of both massive and microlaminated kerogen-rich mudstone and less organic-rich mudstone lithofacies (Fig. 3.5c). These facies alternations are apparent in Fischer Assay logs of oil yield, and are interpreted to represent oscillations between low- and high-stand conditions within a hydrologically closed lake system. Specifically, laminated, organic-rich and massive organic-rich mudstone correspond to high-stand lake conditions, when lake level was at a maximum and clastic dilution at a minimum. During these conditions, cold, freshwater input flows over denser, more saline resident lake waters amplified the chemical and thermal stratification within the lake system. The corresponding increase in oxygenation and nutrient delivery results in increased production of particulate organics, which were preserved in the anoxic bottom waters. Less organic-rich mudstone intervals in turn correspond to low-stand lake conditions, when water input is decreased relative to high-stand conditions. Stratification, as well as oxygen and nutrient delivery was correspondingly suppressed by a reduction of freshwater input, resulting in a decrease in both the production and ultimate preservation of particulate organics.

Shoreward association A diverse array of successive, interbedded fine- and coarse-clastic sediments within the Rife bed typifies the shoreward association of the fluctuating profundal assemblage (Fig. 3.5d). Laminated organic-rich mudstone, massive organic-rich mudstone and, to a lesser extent, variably laminated mudstone lithofacies are interlaminated by thin (<20 cm) packages of ostracode and oolitic grainstone, stromatolite, and massive sandstone lithofacies. Meter-scale intervals of massive sandstone and fossil-bearing siltstone are observed in the north central to northern-most field sections and are thought to represent closer proximity to lake margins. In both the WMP and BT field sections, stromatolites overlie large packages of fish and ostracode-bearing fossiliferous siltstone. At BT these stromatolites constitute a 2 m interval. Woody debris, burrows, ostracode molds, and fish debris are common throughout all facies within this association.

Like the basin-ward expression of this assemblage, the absence of freshwater fauna and progradational geometries suggests a relative reduction in sediment and water input when compared to the fluvial-lacustrine assemblage. Facies diversity among this association is also thought to reflect periods of high- and low-stands within the lake system, with fine-grained and bio-clastic sediments reflecting low-stand deposits and pulses of coarse-grained clastics representative of shifts towards high-stand conditions. These oscillations indicate rapid, basin-wide alteration in sediment deposition, organic production, and stratification within the lake-system

3.5 Basin-Scale Stratigraphy

Figure 3.6 illustrates the basin-scale packaging of the Tipton Member, which records three vertical oscillations between fluvial-lacustrine and fluctuating profundal lithofacies. Deltaic sandstone bodies (Farson Sandstone) accumulated at the northern edge of the basin during fluvial-lacustrine intervals, but are largely absent within fluctuating profundal intervals. Within the Tipton

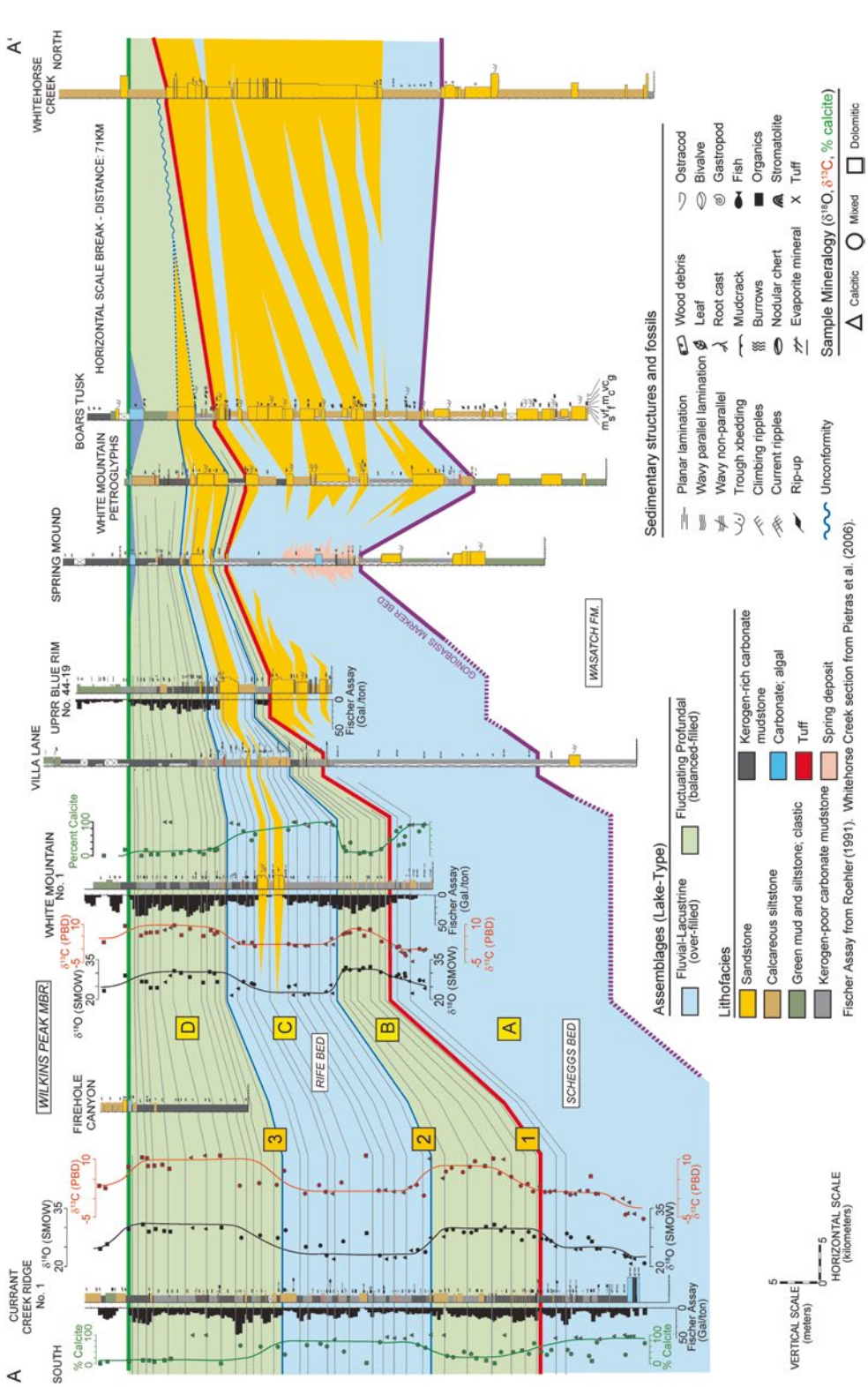

Fig. 3.6 Basin-scale cross-section of the Tipton Member west of the Rock Springs Uplift in the Green River Basin, Wyoming. From south (A) to north (A'), these sections are Currant Creek Ridge Core No. 1 (CCR), Firehole Canyon (FC), White Mountain (WM) field section modified from Pietras (2003)]. See Walker (2008) for complete Core No. 1 (WM1), Villa Lane (VL), UPRR Blue Rim 44-19 core (BR), Spring Mound (SM), White Mountain Petroglyphs (WMP), Boar's Tusk (BT), and Whitehorse Creek (WC). [Fischer Assay data modified from Roehler (1991a), and Whitehorse Creek stratigraphic dataset

Member, transitions between lithofacies assemblages are gradational, particularly in basin-ward locations. Because the basin-ward expressions of both assemblages share multiple lithofacies, transitions lack distinct lithologic contrast. Basin-ward transitions are, therefore, constrained primarily on the basis of relative organic-content (fluctuating profundal lithofacies exhibit higher Fischer Assay oil yield) and the presence or absence of freshwater bivalves. The appearance of fossil fish at the base of the Laney Member indicates the transition from a hydrologically closed lake system to a partly open system with fresh surface water (Carroll and Bohacs 1999; Rhodes 2002). Fish remains are preserved within all lake-type assemblages of the Tipton Member, and similarly indicate that conditions, at least the uppermost lake water, were fresh. It should be noted, however, that intact fossils are more common in the fluctuating profundal assemblage, while fish "debris", a slurry of bones, scales, and fins, is most common, though not restricted to, the fluvial-lacustrine assemblage. Though lithologic transitions also appear gradational at basin margins, they are marked by stronger lithologic contrasts. The contact from fluvial-lacustrine to fluctuating profundal assemblage, for example, is placed at the top of large bodies of prograding, coarse-clastic lithofacies and the initiation of profundal mudstone deposition.

3.5.1 Correlations

Correlation of the upper and lower limits of the Tipton Member was established using lithofacies assemblages, and is supported by Fischer Assay (Roehler 1991a), geochemical, and XRD analyses of CCR and WM cores (Fig. 3.6). Due to limited core and outcrop in the southern area of the basin, direct observation of the Wasatch Formation-Tipton Member contact was limited to field sections in the northern part of the basin (VL, SM, WMP, BT, and WC). Where observed, the contact is defined where oxidized (red) and reduced (green) fluvial plain siltstone and mudstone of the Wasatch Formation transition to gastropod-bearing mudstone and siltstone lithofacies of the Scheggs bed. This fossiliferous horizon is often referred to in literature as the *Goniobasis* Marker bed, as the horizon contains abundant *Goniobasis tenera* gastropods (Hanley 1976).

Previous analysis of the Tipton Member (Roehler 1991b) defined the Scheggs-Rife contact at the transition from freshwater, calcitic deposits to saline, dolomitic deposits. This study adheres to that previous terminology, placing the Scheggs-Rife contact at the first transition from a fluvial-lacustrine lithofacies assemblage (freshwater) to a fluctuating-profundal assemblage (more saline). This stratigraphic placement of the Scheggs-Rife contact coincides with a 56 % average decrease in calcite content and a gradual increase in $\delta^{18}O$ and $\delta^{13}C$ values (Fig. 3.6).

In the northern part of the basin (Fig. 3.6), the top of the Rife bed is characterized by stromatolite lithofacies (.25–1.5 m thick). These beds are conformably overlain by green, marcesite- and pyrite-bearing, mud-cracked mudstone and siltstone lithofacies of the Wilkins Peak Member. In the central and southern part of the GGRB, the Tipton Member-Wilkins Peak Member contact is defined where mm- and cm-laminated mudstone lithofacies of the Rife bed gradually transition to evaporative lithofacies of the Wilkins Peak Member. Within this study, the basin-ward and shore-ward expressions of the Tipton Member-Wilkins Peak Member contact are conformable, and coincide with a subtle isotopic trend towards lighter $\delta^{18}O$ and $\delta^{13}C$ values, as well as a sharp reduction in Fischer Assay oil yield, which is sustained at 0 gal./ton over a 1 m interval (Roehler 1991a). The conformable interpretation of the Tipton Member-Wilkins Peak Member contact presented by this study is somewhat discordant with that presented by Pietras et al. (2003), who propose that a major sequence boundary defines the contact. We argue instead that the Tipton-Wilkins Peak contact records a sharp change in water chemistry and brief subaeriel exposure of the edges of the basin, but not necessarily a basin-wide major lacuna.

3.6 Stable Isotope Analysis

Oxygen isotopes Stable isotopic analysis of profundal mudstone from two cores, CCR and WM, distinguish four distinct $\delta^{18}O$ zones within the Tipton Member (Table 3.3). These intervals directly correlate with zones defined by lithofacies assemblages. Fluvial-lacustrine Zones A and C have light $\delta^{18}O$ values (25.3‰ and 23.0‰, respectively), while fluctuating profundal Zones B and D exhibit the heaviest $\delta^{18}O$ signature within the Tipton Member (29.7‰ and 29.8‰, respectively). The $\delta^{18}O$ transition from Zone A to Zone B (Shift 1) occurs gradually over 4 m within both CCR and WM cores. The transition from Zone B to Zone C (Shift 2), however, is abrupt, occurring over a 2 m interval. Because Zones C and D are under-sampled in both CCR and WM cores, the transition interval of Shift 3 cannot accurately be assessed.

Carbon isotopes The $\delta^{13}C$ signature of the Tipton Member exhibits four distinct zones, all of which are coincident and directly correlative with those observed within the $\delta^{18}O$ profiles of the same cores (Fig. 3.6; Table 3.3). Like the $\delta^{18}O$ profile of the Tipton Member, $\delta^{13}C$ is heaviest in fluctuating profundal Zones B and D (5.3‰ and 8.5‰, respectively). Fluvial-lacustrine Zones A and C have relatively lighter $\delta^{13}C$ values at 0.6‰ and 1.9‰, respectively. Because carbon isotopic data was obtained from the same samples as $\delta^{18}O$ values, the isotopic transition intervals and trends of the $\delta^{13}C$ signature within the Tipton Member is the same as that of the $\delta^{18}O$ profile.

$\delta^{18}O$ and $\delta^{13}C$ covariance Among profundal mudstone samples of the Tipton Member, correlation between $\delta^{18}O$ and $\delta^{13}C$ is generally moderate. Correlation is notably stronger within all samples of the CCR core ($R^2 = 0.7292$, $n = 26$) than it is among those within the WM core (Fig. 3.7a). $\delta^{18}O$ and $\delta^{13}C$ correlation among samples sharing distinct carbonate mineralogy is also strongest in the CCR core (Fig. 3.7b). Dolomitic samples within the CCR core, for example, exhibit a stronger correlation ($R^2 = 0.9062$, $n = 6$) than dolomitic samples within the WM core ($R^2 = 0.0250$, $n = 10$). Moreover, while dolomitic samples have the strongest $\delta^{18}O$ and $\delta^{13}C$ correlation compared to other carbonate mineralogies within CCR core, calcitic samples are the most strongly correlated within the WM core ($R^2 = 0.3122$, $n = 8$). This suggests that carbonate mineralogy does not influence $\delta^{18}O$ and $\delta^{13}C$ correlation in a predictable way across the basin. Among both core, fluctuating profundal zones exhibit stronger overall $\delta^{18}O$ and $\delta^{13}C$ correlation ($R^2 = 0.2392$, $n = 18$) than do fluvial-lacustrine zones ($R^2 = 0.0835$, $n = 33$) (Fig. 3.7c).

3.7 Discussion

3.7.1 Stratigraphic Evolution

Major changes in Tipton Member lacustrine lithofacies were closely associated with initiations and cessations of Farson Sandstone deposition, suggesting that changes of fluvial influx into the basin were a primary driver. Within

Table 3.3 Average Zonal Tipton Member Geochemistry, mineralogy and oil yield

Zone	n	$\delta^{18}O^a$ (VSMOW)	±1σ	$\delta^{13}C^a$ (VPDB)	±1σ	% calcite[a]	±1σ	Oil yield (Gal./ton)[b]
D	5	29.8	1.7	8.5	1.9	12.0	5.3	19.2
C	*5*	*23.0*	*1.6*	*1.9*	*0.3*	*80.1*	*12.5*	*9.7*
B	13	29.7	1.6	5.3	2.2	30.4	18.4	17.6
A	*25*	*25.3*	*2.4*	*0.6*	*2.4*	*69.1*	*27.3*	*7.6*

Notes: Italicized rows represent fluvial-lacustrine lithofacies assemblages, non-italicized rows represent fluctuating profundal lithofacies assemblages

[a]Average among CCR and WM cores

[b]Thickness-weighted average oil yield from Fischer Assay of CCR and WM cores (Roehler 1991a)

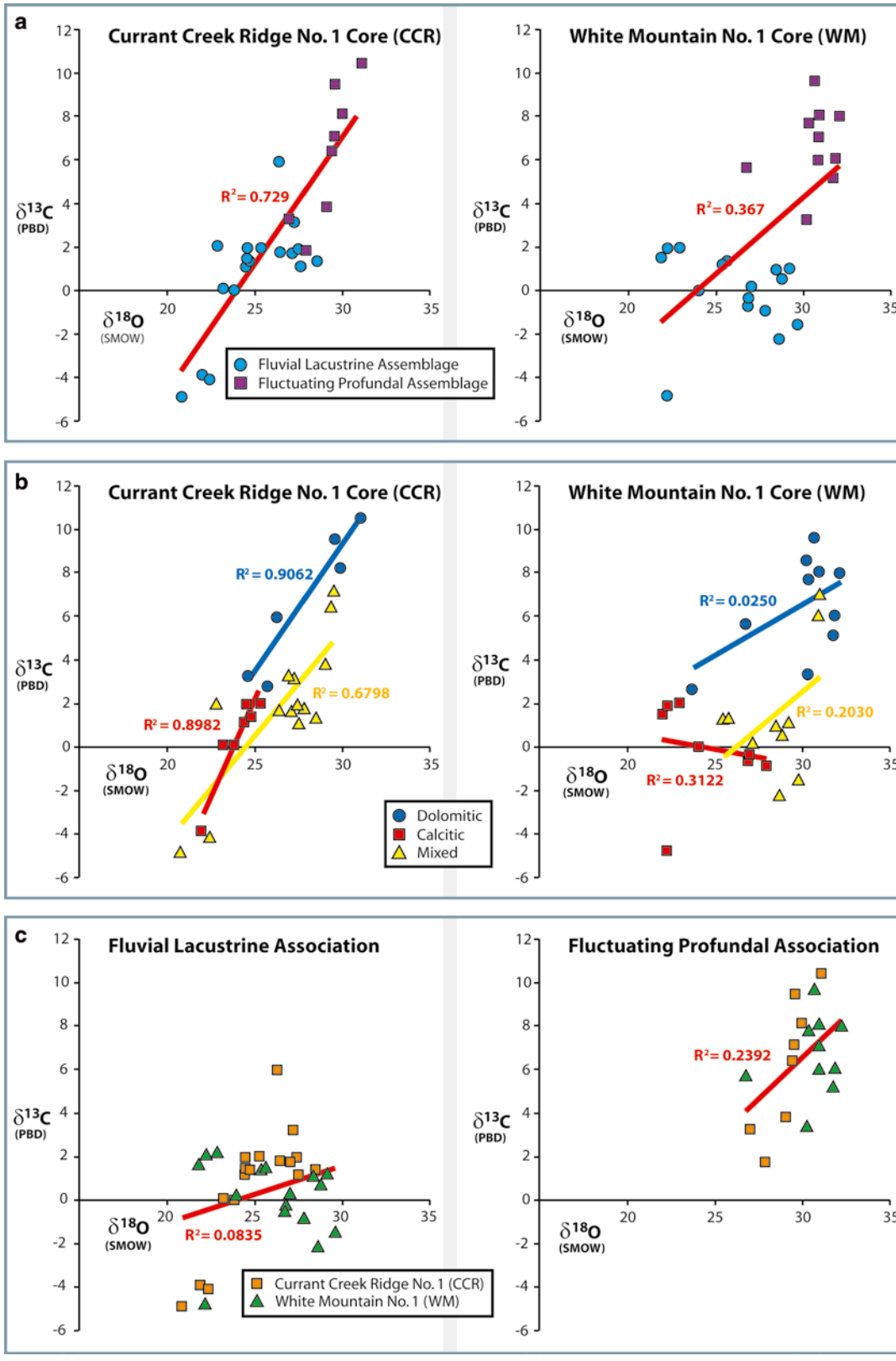

Fig. 3.7 The $\delta^{18}O$ and $\delta^{13}C$ covariance among litho-stratigraphic intervals of (**a**) CCR and WM cores, (**b**) carbonate mineralogy of samples within CCR and WM cores, and (**c**) within each litho-stratigraphic zone

fluvial-lacustrine Zones A and C, progradational geometries along the lake margin indicate significant sediment and, thus, fluvial input into a hydrologically open (i.e. overflowing) lake basin. The Farson Sandstone is not observed within Zones B and D, indicating a relative reduction in sediment/fluvial input during fluctuating profundal deposition. With continuing tectonic subsidence in the basin and the absence of the high sediment input, accommodation was increased in fluctuating profundal Zones B and D. Reflecting this, lake margins transgressed and reach their maximum extent (Fig. 3.6). Additionally, prograding stratal geometries of fluvial-lacustrine intervals are replaced by aggradation of sediment in Zones B and D, indicating a transition to a hydrologically closed (i.e. impounded) lake basin. Carroll and Bohacs (1999) define three lake types, overfilled, balanced-filled, and underfilled, that are controlled by the amount of water and sediment input relative to basin accommodation. Using this lake-type characterization, fluvial-lacustrine intervals of the Tipton Member are classified as overfilled, while fluctuating profundal intervals are balanced-filled.

Distinct zones of carbonate mineralogy and Fischer Assay oil yield coincide with the lithologically defined intervals. Fluvial-lacustrine intervals A and C are relatively calcitic, exhibiting 75 % calcite on average. These intervals are generally poor in organic matter, with a weighted average Fischer Assay oil yield of 8.7 gal./ton, suggesting that well-oxygenated, unstratified lake conditions were present during deposition. Low oil yields can result from clastic dilution resulting from sustained fluvial input of siliciclastic detritus into an open lake system (Bohacs et al. 2000; Carroll and Bohacs 2001).

In contrast, fluctuating profundal intervals are relatively dolomitic, exhibiting 21 % calcite on average. The presence of dolomite within the Tipton Member can be explained via the biogenic model of Desborough (1978), whereby Mg is preferentially concentrated along lake bottoms as blue-green algae anaerobically decompose. Supporting this model is relatively high Fischer Assay oil yield (18 gal./ton) among profundal deposits of fluctuating profundal intervals. Alternatively, the playa lake model is commonly applied to the GRF to explain dolomite generation and distribution (Eugster and Surdam 1973; Mason and Surdam 1992). However, its application to the Tipton Member is inappropriate due to a lack of playa indicators (e.g. evaporite mineral casts, large scale desiccation features).

3.7.2 Isotopic Evolution

Diagenesis Though post-lithification diagenesis can alter stable isotopic composition (Morrill and Koch 2002), our study observes several characteristics in both the lithology and geography of the study area that suggest the isotopic signature of the Tipton Member reflects the composition of Lake Gosiute during deposition.

Because aragonite is highly susceptible to diagenic alteration, its presence or absence can be used as a proxy for diagenic evaluation. Aragonitic bivalves were recovered from Zone A in the CCR core. Preserved growth bands within these shells, which would have been destroyed by diagenic alteration, suggest diagenesis had not occurred within surrounding sediments. Moreover, the mean $\delta^{18}O$ and $\delta^{13}C$ values of these bivalves (21.98‰ and −3.86‰, respectively) are lower than other light values recorded throughout the Tipton Member. Because aragonitic samples are interpreted to have been unaltered, similarly light $\delta^{18}O$ and $\delta^{13}C$ values within the Tipton Member are believed to reflect primary depositional conditions.

Profundal mudstone of the Tipton Member is relatively fine-grained and impermeable, a characteristic which inhibits the pervasiveness of diagenic solutions. Coquina interbeds within the CCR core best exhibit this impermeability. Preservation of primary aragonite is limited to matrix-supported interbeds, whereas clast- (i.e. shell-) supported interbeds are calcified. This suggests profundal mudstone is an effective shield against diagenic solutions.

The spatial distribution of isotopic trends themselves also suggests that alteration of $\delta^{18}O$ and $\delta^{13}C$ values is unlikely. Specifically, the same isotopic pattern is observed in CCR and WM

cores, which are separated by over 65 km, a distance unlikely to be transversed by a homogenous diagenic solution. In order to create four, isotopically distinct zones, diagenic solutions would have had to occur with variable intensities along multiple, vertically spaced horizons. Furthermore, if diagenesis were responsible for each zone, the shift from isotopically heavy Zone B to isotopically light Zone C (Shift 2) would indicate more intense diagenic alteration up-section, an event that is highly unlikely.

Mineralogical effects on $\delta^{18}O$ Because carbonate minerals exhibit differential fractionation at surface temperatures (Sharma and Clayton 1965; Fritz and Smith 1970; Rosenbaum and Sheppard 1986), sample mineralogy can also compromise $\delta^{18}O$ analysis. Dolomite, for example, is inferred to have a 3‰ heavier $\delta^{18}O$ value than calcite precipitated from the same water (Fritz and Smith 1970). The isotopic shifts within the Tipton Member involve calcitic, mixed, and dolomitic mineralogy. As such it is possible that differential fractionation among distinct carbonate mineralogies may influence the $\delta^{18}O$ signatures within the Tipton Member. However, in several shifts (i.e. Shift 1, Shift 2), the trends towards heavier or lighter isotopic values are preserved within the individual trend of each carbonate classification (e.g. calcite, mixed, and dolomitic). Therefore, while mineralogy may influence the magnitude of each isotopic shift, this observation suggests that shifts within the Tipton Member reflect major changes in lake water chemistry during deposition. Furthermore, covariance among mineralogy and $\delta^{18}O$ results is insignificant among all carbonate mineralogies, with R^2 correlation values of 0.1043 (dominantly dolomitic samples), 0.2146 (dominantly calcitic samples), and 0.4263 (mixed samples) (Fig. 3.8).

Effects on $\delta^{18}O$ and $\delta^{13}C$ and their implications The variable $\delta^{18}O$ signature observed within the Tipton Member is likely related to the combined effects of continued evaporation and variable residence time of lake waters. Evaporation preferentially removes $\delta^{16}O$ from surface waters, thereby concentrating $\delta^{18}O$ within a lake system. Increased residence time of lake waters within a lake basin compounds these evaporative effects, resulting in heavier $\delta^{18}O$ values. Because lake water within a hydrologically closed lake system experiences longer residence time and, thus, exhibits heavier $\delta^{18}O$ values, the

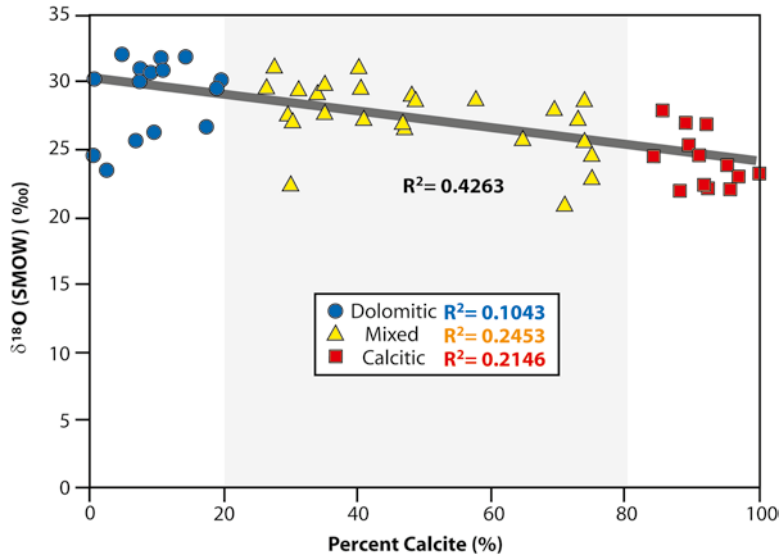

Fig. 3.8 Comparison of mineralogy and $\delta^{18}O$ composition within the Tipton Member. Calcitic samples exhibit the lowest $\delta^{18}O$ values, while dolomitic samples exhibit the highest $\delta^{18}O$ values

heavy isotopic signature of fluctuating profundal zones B and D of the Tipton Member are interpreted to reflect closed lake conditions. Lighter $\delta^{18}O$ values of Zones A and C indicate open lake conditions during fluvial-lacustrine deposition.

The $\delta^{13}C$ signature of lacustrine deposits is generally more complex, as it is related to the rate of primary productivity (Kirby et al. 2002), the rate of organic decomposition within the lake system (Pitman 1996), and dissolved inorganic carbon (DIC) input from Phanerozoic limestone in Lake Gosiute's catchment ($\delta^{13}C \approx 0$). Photosynthetic algae preferentially remove $\delta^{12}C$ throughout their lifetime, thereby enriching lake waters in $\delta^{13}C$ if they are buried prior to decomposition. In this way, higher inorganic $\delta^{13}C$ values reflect periods of abundant productivity, while lower $\delta^{13}C$ values indicate depositional periods that are less conducive to organic production. Deposits within fluctuating profundal Zones B and D have higher $\delta^{13}C$ (5.33‰ and 8.5‰, respectively) compared to fluvial-lacustrine Zones A and B (0.648 and 1.88‰) and are, therefore, interpreted to have supported higher rates of primary productivity.

Fischer Assay of balanced-filled and overfilled zones supports a primary productivity interpretation of $\delta^{13}C$ results. In those zones having higher concentrations of $\delta^{13}C$, increased Fischer Assay values correspond. Zones B and D have an average Fischer Assay value of 17.6 Gal./ton and 19.2 Gal./ton, respectively. Comparatively, Zones A and C, which have lower $\delta^{13}C$ values, exhibit significantly lower Fischer Assay measures of organic content at 7.6 Gal./ton and 9.7 Gal./ton, respectively.

Another possible influence on the $\delta^{13}C$ profile across the Tipton Member is the rate at which particulate organics decompose within the lake system. As organic material decomposes, $\delta^{12}C$ is released into the lake waters by methanogenesis, thereby decreasing the $\delta^{13}C$ values recorded by sediments (Pitman 1996). Consequently, low $\delta^{13}C$ may be used as a proxy to evaluate the extent to which lake waters were chemically and thermally stratified. Decomposition of organic matter is reduced if not stopped entirely within a stratified lake system. Within anoxic conditions of a stratified lake system, less $\delta^{12}C$ would be available to dilute $\delta^{13}C$ concentrations within the stratified lake. In this way, fluctuating profundal Zones B and D reflect periods of well-stratified lake waters. Low $\delta^{13}C$ values within fluvial-lacustrine Zones A and C contrarily reflect less-stratified lake waters.

Carbon inputs from limestone bedrock ($\delta^{13}C \approx 0$) can also lower the $\delta^{13}C$ value of lake sediments. Lower Phanerozoic sections surrounding the GGRB are carbonate, and marginal conglomerates include limestone and dolostone clasts. Though these may have influenced the $\delta^{13}C$ signature of the Tipton Member, the modeling of profundal deposits of the Laney Member (Doebbert 2006; Doebbert et al. 2010) indicates such an effect could not produce $\delta^{13}C$ shifts observed in the GGRB.

Correlation between $\delta^{18}O$ and $\delta^{13}C$ values is often interpreted as a reflection of hydrologically closed lakes because of increased residence time of lake waters (Talbot 1990; Pitman et al. 1996) and successive, rapid lake volume oscillations (Li and Ku 1997). These observations coincide with correlation trends observed among intervals of the Tipton Member, where balanced-filled (i.e. closed lake-basin) deposits of fluctuating profundal intervals (Zones B and D) have a stronger correlation ($R^2 = 0.2392$) than overfilled (i.e. open lake-basin) deposits of fluvial-lacustrine Zones A and C ($R^2 = 0.0835$) (Fig. 3.7c).

3.7.3 Possible Origins of Isotopic and Lake Type Variation

Long-term variation in the rates of precipitation and evaporation are one possible explanation for variation in $\delta^{18}O$ values of lake sediments, and would likely have varied following orbital changes to summer insolation (Morrill et al. 2001). The pace and magnitude of isotopic variation within the Tipton Member is difficult to relate to climate oscillations. In order to produce the dramatic $\delta^{18}O$ shifts observed within the Tipton Member, temperatures would have had to have oscillated between extreme values during the Eocene. The Paleocene-Eocene Thermal

Maximum (PETM) in the Bighorn Basin for example is marked by a 2‰ shift in $\delta^{18}O$ (Koch et al. 2003), and has been associated with a 4–6 °C temperature increase within the western United States (Fricke et al. 1999; Fricke and Wing 2004), as well as a global sea surface warming of 8 °C (Zachos et al. 2001, 2008). To produce the 4.46‰, 6.68‰, and 7.64‰ $\delta^{18}O$ shifts recorded within the Tipton Member (Shifts 1, 2, and 3, respectively), temperature change during Tipton deposition would have been pronounced, rapid in onset, and persistent, and have no clear corollary, in the marine record Westerhold and Röhl (2009). Existing geochronology (Smith et al. 2008, 2010) constrains Rife bed deposition to 0.60 ± 0.31 m.y. (2σ). Assuming all three lithostratigraphic zones within the Rife bed (zones B, C, and D) were deposited in approximately the same amount of time, each would represent ca. 200 k.y., and may potentially coincide with orbital eccentricity variations.

The lithofacies, aerial extent, and $\delta^{18}O$ characteristics of the two different lake types make is difficult, however to relate isotopic changes to climate parameters. Following the evaporation-driven hypothesis, during increased periods of evaporation, lake level should have diminished, subaerially exposing broad areas of the lake margin, which would have in turn led to evaporative concentration of ^{18}O in lake waters, which is inconsistent with lithofacies-based observations of high lake level during deposition of $\delta^{18}O$-heavy zones B and D (Figs. 3.6 and 3.9). These fluctuating profundal zones consist largely of deep lake deposits that lack evidence for systematic desiccation and consistently overlie shallower-water lithofacies of underlying fluvial-lacustrine zones A and C.

Diversions of upstream drainage provides an appealing solution to the apparent paradox of high lake level and high $\delta^{18}O$ composition observed in the Tipton Member. In such a scenario, abrupt changes to regional hydrology and isotopic composition would have been triggered by the inclusion or exclusion of a source of light $\delta^{18}O$-depleted waters and sediment delivered from an upland source (e.g., Carroll et al 2008). In our preferred model for the lake-type shifts observed within the Tipton Member (Fig. 3.9),

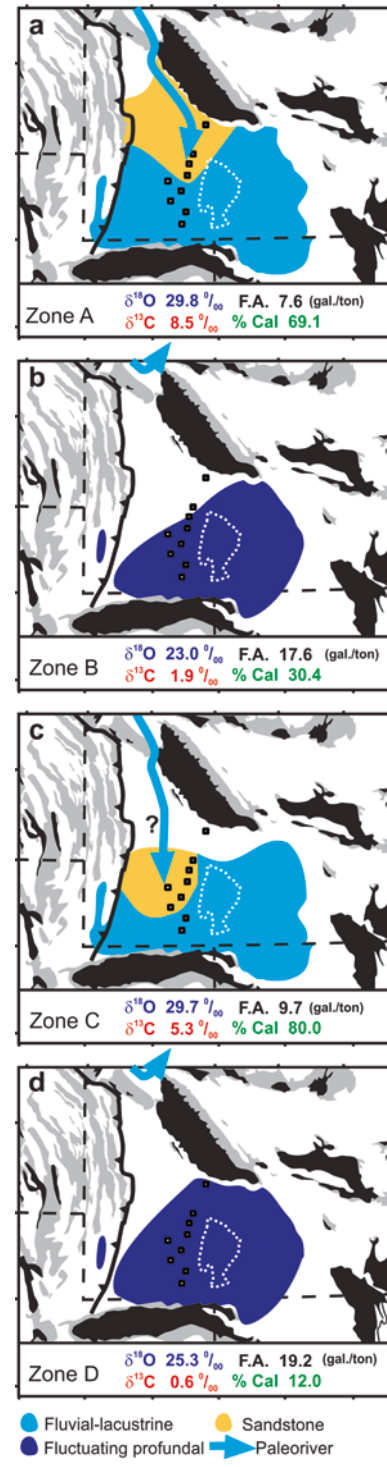

Fig. 3.9 Interpreted four part synoptic lake type evolution of the Tipton Member. A major water and sediment source entered the GGRB during fluvial lacustrine deposition (zones A and C), and was diverted away from the basin during fluctuating profundal deposition (zones B and D)

Shift 1 is attributed to diversion of such a stream, followed by its recapture (Shift 2) and ultimate diversion (Shift 3). With each drainage diversion event, deposition of the Farson Sandstone ceased, accommodation increased in the absence of sediment input within the basin center, and lake margins correspondingly transgressed. Removal of a low $\delta^{18}O$ hydrologic source and the associated increase in lake water residence time due to the lowered hydrologic throughput would both have acted to elevate the $\delta^{18}O$ composition of Lake Gosiute. Doebbert et al. (2010) interpreted a similar magnitude $\delta^{18}O$ and provenance shift in the Laney Member of the Green River Formation to have been triggered by the capture of a hinterland sourced stream. They interpreted it to be the terminus of a series of paleovalleys mapped by Janecke et al. (2000), the "Idaho River". Though precise paleotopography of the upstream fluvial network(s) that triggered Tipton Member lake-type reorganizations is not certain, the location of its entry point in the northwest corner of the Greater Green River Basin, the areal distribution and progradation direction of the Farson Sandstone, and the presence of hinterland-sourced quartzite cobbles to the alluvial Pass Peak Formation (Smith et al. 2008) suggest strong similarities between the stream the fed Gosiute during zones A and C of the Tipton and the aforementioned Idaho River. The river in question would have likely have utilized a narrow pathway between the Wind River and Teton-Gros Ventre uplifts in the northern part of the GGRB, but would have delivered far less volcaniclastic detritus to Lake Gosiute because it predated the main phase of Challis volcanism (Smith et al. 2008). The ultimate cause for particular avulsions and captures remains enigmatic. Some could have been triggered by episodic faulting at upstream pathways between growing geologic structures within the drainage network or alternatively some could have occurred in an entirely autogenic fashion due to stream processes. In either case, any successful paleogeomorphic model for Tipton Member must account for the avulsion, return, and subsequent avulsion of this (or another) fluvial source to the basin during its deposition.

3.8 Conclusions

1. Thirteen distinct lithofacies occur within the Tipton Member and comprise two lithofacies assemblages: fluvial-lacustrine and fluctuating profundal, both of which have distinct basin-ward and shoreward expressions.
2. The Scheggs-Rife contact coincides with the first transition from fluvial-lacustrine (overfilled) to fluctuating profundal (balanced-filled) deposits.
3. Though lithostratigraphic transitions between profundal assemblages are subtle, distinct mineralogical, stable isotopic, and Fischer Assay oil yield values delineate abrupt lake system transitions.
4. Fluvial-lacustrine (overfilled) intervals exhibit prograding stratal geometries, dominantly calcitic carbonate mineralogy, low Fischer Assay oil yield, and light $\delta^{18}O$ and $\delta^{13}C$ values. Deposition is interpreted to have occurred within an open lake basin.
5. Fluctuating profundal (balanced-filled) intervals are defined by vertically aggrading stratigraphic geometries, dominantly dolomitic carbonate mineralogy, high Fischer Assay oil yield, and heavy $\delta^{18}O$ and $\delta^{13}C$ values. Deposition is interpreted to have occurred within an intermittently-closed lake basin.
6. Contrary to previous interpretations, the Rife bed contains both fluvial-lacustrine and fluctuating profundal intervals. The lower Rife bed is characterized by fluctuating profundal deposits, the middle Rife bed by fluvial-lacustrine deposits, while the upper Rife bed exhibits fluctuating profundal deposits.
7. In the northern GGRB, the Farson Sandstone is a lateral equivalent of both the Scheggs bed and zone C of the overlying Rife bed, and is thus constrained to fluvial-lacustrine intervals.
8. Oscillating lithologic and stable isotopic signatures within the Tipton Member are thought to reflect paleohydrologic reorganizations of the Farson Sandstone-sourcing fluvial system. Specifically, a diversion, recapture and ultimate diversion of this source are thought to have resulted in Shifts 1, 2 and 3.

9. Two possible mechanisms for paleohydrologic reorganization are proposed: episodic faulting or uplift upstream of the basin; and dynamic geomorphology of the Farson Sandstone-sourcing river itself. In both instances, a major fluvial source is diverted outside of the GGRB.

Acknowledgments This study was assisted by discussions with Shanan Peters, Amalia Doebbert, Eric Williams. Lisa Lesar was a courageous assistant in the field. We thank the staff at the U.S.G.S. Core Repository in Denver, Colorado for use of their facility and intimate knowledge of available core. Jason Huberty assisted acquisition of XRD analyses. We thank the American Association of Petroleum Geologists, ConocoPhillips and the Department of Geology and Geophysics at the University of Wisconsin-Madison for their financial support.

References

Allen JRL (1962) Asymmetrical ripple marks and the origin of cross-stratification. Nature 194:84–115

Allen JRL (1982) Sedimentary structures: their character and physical basis, vol 30, Developments in sedimentology. Elsevier, Amsterdam

Arnott RW (1993) Quasi-planar-laminated sandstone beds of the Lower Cretaceous Bootlegger Member, north-central Montana; evidence of combined-flow sedimentation. J Sediment Petrol 63:488–494

Arnott RW, Southard JB (1990) Exploratory flow-duct experiments on combined-flow bed configurations, and some implications for interpreting storm-event stratification. J Sediment Petrol 60:211–219

Balch DP, Cohen AS, Schnurrenberger DW, Haskell BJ, Valero Garces BL, Beck JW, Cheng H, Edwards RL (2005) Ecosystem and paleohydrological response to Quaternary climate change in the Bonneville Basin, Utah. Palaeogeogr Palaeoclimatol Palaeoecol 221:99–122

Bohacs KM (1998) Contrasting expressions of depositional sequences in mudrocks from marine to nonmarine environs. In: Schieber J, Zimmerlie W, Sethi P (eds) Mudstones and shales, vol 1, Characteristics at the basin scale. Schweizerbart'sche Verlagsbuchhandlung, Stuttgart, pp 32–77

Bohacs KM, Carroll AR, Neal JE, Mankiewicz PJ (2000) Lake-basin type, source potential, and hydrocarbon character: an integrated sequence-stratigraphic-geochemical framework. In: Gierlowski-Kordesch EH, Kelts KR (eds) Lake basins through space and time, vol 46, American Association of Petroleum Geologists studies in geology. American Association of Petroleum Geologists, Tulsa, pp 3–34

Born SM (1972) Late Quaternary history, deltaic sedimentation, and mud lump formation at Pyramid Lake, Nevada. Center for Water Resources Research, Desert Research Institute, University of Nevada, Reno, p 97

Bradley WH (1929) The varves and climate of the Green River epoch, U.S. Geological Survey professional paper 158-E. U.S. Government Printing Office, Washington, DC, p 110

Bradley WH (1931) Origin and microfossils of the oil shale of the Green River Formation of Colorado and Utah, vol 168, U.S. Geological Survey professional paper. U.S. Government Printing Office, Washington, DC, p 58

Bridge JS (1978) Origin of horizontal lamination under turbulent boundary layers. Sediment Geol 20:1–16

Buchheim HP, Eugster HP (1998) Eocene Fossil Lake: the Green River Formation of Fossil Basin, southwestern Wyoming. In: Pitman JK, Carroll AR (eds) Modern & ancient lake systems; new problems and perspectives, vol 26, Utah Geological Association publication. Utah Geological Association, Salt Lake City, pp 191–208

Buchheim HP, Surdam RC (1977) Fossil catfish and the depositional environment of the Green River Formation, Wyoming. Geology 5:196–198

Carroll AR (1998) Upper Permian lacustrine organic facies evolution, Southern Junggar Basin, NW China. Org Geochem 28:649–667

Carroll AR, Bohacs KM (1999) Stratigraphic classification of ancient lakes: balancing tectonic and climatic controls. Geology 27:99–102

Carroll AR, Bohacs KM (2001) Lake-type controls on petroleum source rock potential in nonmarine basins. Am Assoc Pet Geol Bull 85:1033–1053

Carroll AR, Doebbert AC, Booth AL, Chamberlain CP, Rhodes-Carson MK, Smith ME, Johnson CM, Beard BL (2008) Capture of high-altitude precipitation by a low-altitude Eocene lake, western U.S. Geology 36:791–794

Cassanova J, Hillaire-Marcel C (1992) Late Holocene hydrological history of Lake Tanganyika, East Africa, from isotopic data on fossil stramatolites. Palaeogeogr Palaeoclimatol Palaeoecol 91:35–48

Castro EJ (1962) A subsurface study of the Tipton Member of the Green River Formation west of the Rock Springs Uplift University of Wyoming. M.Sc. thesis, University of Wyoming, 66 p

Cheel RJ (1990) Horizontal lamination and the sequence of bed phases and stratification under upper flow-regime conditions. Sedimentology 37:517–529

Cohen AS (1989) The taphonomy of gastropod shell accumulations in large lakes: an example from Lake Tanganyika, Africa. Paleobiology 15:26–45

Cohen AS (2003) Paleolimnology: the history and evolution of lake systems. Oxford University Press, New York

Cohen AS, Thouin C (1987) Near-shore carbonate deposits in Lake Tanganyika. Geology 15:414–418

Culbertson WC, Smith JW, Trudell LG (1980) Oil shale resources and geology of the Green River Formation in the Green River Basin, Wyoming, vol RI-80/6. U.S. Department of Energy, Laramie Energy Technology Center, Laramie, WY.

Dana GF, Smith JW (1972) Oil yields and stratigraphy of the Green River Formation's Tipton Member at Bureau of Mines sites near Green River, Wyoming. U.S. Department of the Interior, Bureau of Mines report of investigation no. 7681

DeCelles PG (1994) Late Cretaceous-Paleocene synorogenic sedimentation and kinematic history of the Sevier thrust belt, northeast Utah and southwest Wyoming. Geol Soc Am Bull 106:32–56

Demaison DJ, Moore GT (1980) Anoxic environments and oil source bed genesis. AAPG Bull 64:1179–1209

Desborough GA (1978) A biogenic-chemical stratified lake model for the origin of oil shale of the Green River Formation: An alternative to the playa-lake model. Geol Soc Am Bull 89:961–971

Dickinson WR, Klute MA, Hayes MJ, Janecke SU, Lundin ER, McKittrick MA, Olivares MD (1988) Paleogeographic and paleotectonic setting of Laramide sedimentary basins in the central Rocky Mountain region. Geol Soc Am Bull 100:1023–1039

Doebbert AC (2006) Geomorphic controls on lacustrine isotopic compositions: evidence from the Laney Member, Green River Formation (Wyoming). M.Sc. thesis, University of Wisconsin-Madison, 255 p

Doebbert AC, Carroll AR, Mulch A, Chetel LM, Chamberlain CP (2010) Geomorphic controls on lacustrine isotopic compositions: evidence from the Laney Member, Green River Formation, Wyoming. Geol Soc Am Bull 122:236–252

Dumas S, Arnott RWC (2006) Origin of hummocky and swaley cross-stratification: the controlling influence of unidirectional current strength and aggradation rate. Geology 34:1073–1076

Dumas S, Arnott RWC, Southard JB (2005) Experiments on oscillatory flow and combined flow bed forms: implications for interpreting parts of the shallow marine sedimentary record. J Sediment Res 72:501–513

Eggleston JR, Dean WE (1976) Freshwater stromatolitic biotherms in Green Lake, New York. In: Walker MR (ed) Stromatolites. Elsevier, Amsterdam, pp 479–488

Eugster HP, Surdam RC (1973) Depositional environment of the Green River Formation of Wyoming: a preliminary report. Geol Soc Am Bull 84:1115–1120

Fischer AG, Roberts LT (1991) Cyclicity in the Green River Formation (lacustrine Eocene) of Wyoming. J Sediment Petrol 61:1146–1154

Fricke HC, Wing SL (2004) Oxygen isotope and paleobotanical estimates of temperature and $d^{18}O$-latitude gradient over North America during the Early Eocene. Am J Sci 304:612–635

Fricke HC, Clyde WC, O'Neil JR, Gingerich PD (1999) Evidence for rapid climate change in North America during the latest Palaeocene thermal maximum: Oxygen isotope compositions of biogenic phosphate from the Bighorn Basin (Wyoming). Earth Planet Sci Lett 160:193–208

Fritz P, Smith DGW (1970) The isotopic composition of secondary dolomites. Geochim Cosmochim Acta 34:1161–1173

Halley RB (1976) Textural variation within Great Salt Lake algal mounds. In: Walker MR (ed) Stromatolites. Elsevier, Amsterdam, pp 435–445

Hanley JH (1976) Paleosynecology of nonmarine mollusca from the Green River and Wasatch Formations (Eocene), southwestern Wyoming and northwestern Colorado. In: Scott RW, West RR (eds) Structure and classification of paleocommunities. Dowden, Hutchinson & Ross, Inc, Stroudsburg, pp 235–261

Harms JC, Fahnestock RK (1965) Stratification, bed forms, and flow phenomena (with an example from the Rio Grande). In: Primary sedimentary structures and their hydrodynamic interpretation – a symposium, vol 12, Society of Economic Paleontologists and Mineralogists special publication. Society of Paleontologists and Mineralogists, Tulsa, pp 84–115

Horsfield B, Curry DJ, Bohacs KM, Littke R, Rullkötter J, Schenk HJ, Radke M, Schaefer RG, Carroll AR, Isaksen G, Witte EG (1994) Organic geochemistry of freshwater and alkaline lacustrine sediments in the Green River Formation of the Washakie Basin, Wyoming, U.S.A. Org Geochem 22:415–440

Huc AY, Le Fournier J, Vandenbrouke M, Bessereau G (1990) Northern Lake Tanganyika – an example of organic sedimentation in an anoxic rift lake. In: Katz BJ (ed) Lacustrine basin exploration: case studies and modern analogs, vol 50, American Association of Petroleum Geologists memoir. American Association of Petroleum Geologists, Tulsa, pp 169–185

Janecke SU, VanDenburg CJ, Blankenau JJ, M'Gonigle JW (2000) Long-distance longitudinal transport of gravel across the Cordilleran thrust belt of Montana and Idaho. Geology 28:439–442

Johnson CL, Graham SA (2004) Sedimentology and reservoir architecture of a synrift lacustrine delta, southeastern Mongolia. J Sediment Res 74:770–785

Jopling AV, Walker RG (1968) Morphology and origin of ripple-drift cross-lamination, with examples from the Pleistocene of Massachusetts. J Sediment Petrol 38:971–984

Kelts KR, Hsü KJ (1978) Freshwater carbonate sedimentation. In: Lerman A (ed) Lakes: chemistry, geology, and physics. Springer, Berlin, pp 295–323

Kirby ME, Mullins HT, Patterson WP (2002) Late glacial-Holocene atmospheric circulation and precipitation in the northeast United States inferred from modern calibrated stable oxygen and carbon isotopes. Geol Soc Am Bull 114:1326–1340

Kneller B, Buckee C (2000) The structure and fluid mechanics of turbidity currents: a review of some recent studies and their geological implications. Sedimentology 47:62–94

Koch PL, Clyde WC, Hepple RP, Fogel ML, Wing SL, Zachos JC (2003) Carbon and oxygen isotope records from paleosols spanning the Paleocene-Eocene boundary, Bighorn Basin, Wyoming. In: Wing SL, Gingerich PD, Schmitz B, Thomas E (eds) Causes and consequences of globally warm climates in the early paleogene, vol 369, Geological Society of America special paper. Geological Society of America, Boulder, pp 49–64

Leckie DA, Krystinik LF (1989) Is there evidence for geostrophic current preserved in the sedimentary record of inner to middle-shelf deposits? J Sediment Res 59:862–870

Lemons DR, Chan MA (1999) Facies architecture and sequence stratigraphy of fine-grained lacustrine deltas along the eastern margin of Lake Pleistocene Lake Bonneville, northern Utah and southern Idaho. Am Assoc Pet Geol Bull 83:635–665

Li HC, Ku TL (1997) $\delta^{13}C$-$\delta^{18}O$ covariance as a paleohydrological indicator for closed-basin lakes. Palaeogeogr Palaeoclimatol Palaeoecol 133:69–80

Mason GM, Surdam RC (1992) Carbonate mineral distribution and isotope fractionation: an approach to depositional environment interpretation, Green River Formation, Wyoming, U.S.A. Chem Geol 101:311–321

McLane M (1995) Sedimentology. Oxford University Press, New York

Morrill C, Koch PL (2002) Elevation or alteration? Evaluation of isotopic constraints on paleoaltitudes surrounding the Eocene Green River Basin. Geology 30:151–154

Morrill C, Small EE, Sloan LC (2001) Modeling orbital forcing of lake level change: Lake Gosiute (Eocene), North America. Global Planet Change 29:57–76

Müller G (1966) The new Rhine delta in Lake Constance. In: Shirley L (ed) Deltas in their geologic framework. Houston Geological Society, Houston, pp 10–124

Nøttvedt A, Kreisa RD (1987) Model for the combined-flow origin of hummocky cross-stratification. Geology 15:357–361

Oriel SS (1961) Tongues of the Wasatch and Green River Formations, Fort Hill area, Wyoming. U.S. Geological Survey professional paper 424-B, U.S. Government Printing Office, Washington, DC, pp 151–152

Paola C, Wiele SM, Reinhart MA (1989) Upper-regime parallel lamination as the result of turbulent sediment transport and low-amplitude bedforms. Sedimentology 36:47–60

Pasierbiewicz KW, Kotlarczyk J (1997) Flume experiments with fine-grained suspensions, with implications for the origin of mud laminites. J Sediment Res 677:510–513

Pietras JT (2003) High-resolution sequence stratigraphy and strontium isotope geochemistry of the lacustrine Wilkins Peak Member, Eocene Green River Formation, Wyoming, U.S.A. Ph.D. thesis, University of Wisconsin-Madison, 372 p

Pietras JT, Carroll AR, Rhodes MK (2003) Lake basin response to tectonic drainage diversion: Eocene Green River Formation, Wyoming. J Paleolimnol 30:115–125

Pipiringos GN (1955) Tertiary rocks in the central part of the Great Divide Basin, Sweetwater County, Wyoming. In: Anderman GG (ed) Green river basin, 10th annual field conference guidebook. Wyoming Geological Association, Casper, pp 100–104

Pitman JK (1996) Origin of primary and diagenetic carbonates in the lacustrine Green River Formation (Eocene), Colorado and Utah. US Geol Surv Bull 2157:17

Pitman JK, Norris RD, Jones LS, Corfield RM (1996) Effects of water-residence time on the isotopic evolution of an Eocene closed-basin lake complex. American Association of Petroleum Geologists and Society of Economic Paleontologists and Mineralogists annual meeting abstracts 5, p 113

Renaut RW, Gierlowski-Kordesch EH (2010) Lakes. In: James NP, Dalrymple RW (eds) Facies models 4, vol 6, Geotext. Geological Association of Canada, St. John's, pp 541–575

Rhodes MK (2002) Lacustrine stratigraphy and strontium isotope geochemistry of the Laney member, Green River Formation, southwestern Wyoming. Ph.D. thesis, University of Wisconsin-Madison, 367 p

Roehler HW (1991a) Correlation and depositional analysis of oil shale and associated rocks in the Eocene Green River Formation, Greater Green River Basin, southwest Wyoming. U.S. Geological Survey Miscellaneous investigations series Map I-2226

Roehler HW (1991b) Revised stratigraphic nomenclature for the Wasatch and Green River Formations of Eocene age, Wyoming, Utah, and Colorado, U.S. Geological Survey professional paper 1506-B. U.S. Government Printing Office, Washington, DC, p 38

Roehler HW (1992) Correlation, composition, areal distribution, and thickness of Eocene stratigraphic units, greater Green River basin, Wyoming, Utah, and Colorado, U.S. Geological Survey professional paper 1506-E. U.S. Dept. of the Interior, U.S. Geological Survey, Reston, p 49

Roehler HW (1993) Eocene climates, depositional environments, and geography, Greater Green River Basin, Wyoming, Utah, and Colorado, U.S. Geological Survey professional paper 1506-F. U.S. Government Printing Office, Washington, DC, p 74

Rosenbaum J, Sheppard SMF (1986) An isotopic study of siderites, dolomites, and ankerites at high temperatures. Geochim Cosmochim Acta 50:1147–1150

Scholz CA, Johnson TC, McGill JW (1993) Deltaic sedimentation in a rift valley lake; new seismic reflection data from Lake Malawi (Nyasa), East Africa. Geology 21:395–398

Schultz AR (1920) Oil possibilities in and around Baxter Basin, in the Rock Springs Uplift, Sweetwater County, Wyoming. US Geol Surv Bull 702:107

Sharma T, Clayton RN (1965) Measurement of O^{18}/O^{16} of total oxygen of carbonates. Geochim Cosmochim Acta 29:1347–1353

Smith ME, Carroll AR, Singer BS (2008) Synoptic reconstruction of a major ancient lake system: Eocene Green River Formation, Western United States. Geol Soc Am Bull 120:54–84

Smith ME, Chamberlain KR, Singer BS, Carroll AR (2010) Eocene clocks agree: coeval $^{40}Ar/^{39}Ar$, U-Pb, and astronomical ages from the Green River Formation. Geology 38:527–530

Stanley KO, Surdam RC (1978) Sedimentation on the front of Eocene Gilbert-type deltas, Washakie Basin, Wyoming. J Sediment Petrol 48:557–573

Steidtmann JR (1969) Stratigraphy of the early Eocene Pass Peak Formation, central-western Wyoming. In:

Barlow JA (ed) Symposium on tertiary rocks of Wyoming, 21st annual field conference guidebook. Wyoming Geological Association, Casper, pp 55–63

Surdam RC, Stanley KO (1979) Lacustrine sedimentation during the culminating phase of Eocene Lake Gosiute, Wyoming (Green River Formation). Geol Soc Am Bull 90:93–110

Talbot MR (1990) A review of the palaeohydrological interpretation of carbon and oxygen isotopic ratios in primary lacustrine carbonates. Chem Geol 80:261–279

Talbot MR, Allen PA (1996) Lakes, 3. In: Reading HG (ed) Sedimentary environments; processes, facies and stratigraphy. Blackwell, Oxford, pp 83–124

Tissot BP, Vandenbroucke M (1983) Geochemistry and pyrolysis of oil shales. ACS Symp Ser 230:1–11

Walker JC (2008) Lacustrine stratigraphic and stable isotopic expression of overfilled and balanced-filled transitions within the Tipton Member of the Green River Formation. M.Sc. thesis, University of Wisconsin-Madison, 166 p

Westerhold T, Röhl U (2009) High resolution cyclostratigraphy of the early Eocene – new insights into the origin of the Cenozoic cooling trend. Clim Past 5:309–327

Witkind IJ, Grose LT (1972) Areal geologic map of the Rocky Mountain region and environs. In: Mallory WW (ed) Geologic Atlas of the Rocky Mountain Region. Rocky Mountain Association of Geologists, Denver, p 34

Wolfbauer CA, Surdam RC (1974) Origin of nonmarine dolomite in Eocene Lake Gosiute, Green River Basin, Wyoming. Geol Soc Am Bull 85:1733–1740

Zachos J, Pagani M, Sloan L, Thomas E, Billups K (2001) Trends, rhythms, and aberrations in global climate 65 Ma to present. Science 292:685–693

Zachos JC, Dickens GR, Zeebe RE (2008) An early Cenozoic perspective on greenhouse warming and carbon-cycle dynamics. Nature 451:279–283

4 Stratigraphic Expression of Climate, Tectonism, and Geomorphic Forcing in an Underfilled Lake Basin: Wilkins Peak Member of the Green River Formation

Michael Elliot Smith, Alan R. Carroll, and Jennifer Jane Scott

Abstract

The Wilkins Peak Member of the Green River Formation is a complex amalgam of lacustrine and alluvial lithofacies deposited in a closed basin at the center of the Laramide broken foreland during the Early Eocene (51.6–49.8 Ma). Facies analysis and correlation of surface sections and core document remarkable lateral continuity of depositional cycles within the Wilkins Peak Member. New mapping and facies analysis this stratigraphic framework into Wilkins Peak Member-equivalent strata adjacent to the Uinta Uplift, where a peripheral facies belt contains lacustrine and fluvial facies that are compositionally distinct from basin interior facies. Peripheral belt lithofacies are composed of limestone and quartzose siliciclastic detritus, whereas basin interior strata are largely dolomite and fine-grained arkosic detritus. Strata at both peripheral and interior facies belts contains a clear oscillation between two modes: (1) a lacustrine mode, associated with rapid lake expansion and contraction with precipitation of carbonate and evaporites from saline lake waters; and (2) an alluvial mode, associated with low lake level and lower lake salinity and a basin-ward shift in alluvial depositional environments. Radioisotopic geochronology suggests that lacustrine-alluvial cycles strongly follow 100 k.y. eccentricity, with lacustrine modes occurring during eccentricity maxima, and alluvial modes coinciding with eccentricity minima. Alluvial fans were built into the Bridger subbasin over 2–4 million year timescales, with their coarsest-

The online version of this chapter (doi:10.1007/978-94-017-9906-5_4) contains supplementary material, which is available to authorized users.

M.E. Smith (✉)
School of Earth Science and Environmental Sustainability, Northern Arizona University, 602 S. Humphreys, Flagstaff, AZ 86011, USA
e-mail: michael.e.smith@nau.edu

A.R. Carroll
Department of Geoscience, University of Wisconsin-Madison, 1215 W. Dayton St., Madison, WI 53706, USA

J.J. Scott
Department of Earth Sciences, Mount Royal University, Mount Royal Gate 4825, T3E 6K6 Calgary, AB, Canada

M.E. Smith, A.R. Carroll (eds.), *Stratigraphy and Paleolimnology of the Green River Formation, Western USA*, Syntheses in Limnogeology 1, DOI 10.1007/978-94-017-9906-5_4

grained portions corresponding to unroofing of durable Paleozoic strata from the Uinta Uplift. From 56 to 47 Ma, successive fans propagated westward as unroofing expanded away from a structural culmination in the Uinta Uplift. Calcite-rich lithofacies including spring deposits are concentrated near faults and alluvial fan toes, and likely were promoted by the mixing of Ca-rich meteoric and/or hydrothermal waters with bicarbonate-rich lake waters. Accounting for the absence of basin interior-focused lithofacies in the Tipton Member of the Green River Formation, tectonic accommodation appears to have been continuous rather than episodic from the late Paleocene to the Early Eocene.

4.1 Introduction

Lacustrine basins contain some of the most complete and detailed regional records of continental faulting, uplift and climate (Platt 1992; Gawthorpe and Leeder 2000; Carroll et al. 2006; Carroll et al. 2010), but these signals are preserved via nonlinear geomorphic processes that leave a distinct imprint of their own. Lacustrine and fluvial records in non-marine basins are often incompletely understood due to the lateral and vertical complexity of their strata, incomplete exposure, and an absence of marine biostratigraphic control. As a result, past studies (e.g., Hayden 1869; Verges et al. 1998; Brozovich and Burbank 2000) have tended to lump non-marine deposits into thick stratigraphic packages, often based on incomplete exposures or coreholes within a particular tectonic basin (Olsen 1986; Crews and Ethridge 1993; Blair and Raynolds 1999). Conversely, geomorphic and sedimentologic analyses of modern lake basins provide highly detailed views of the spatial distribution of processes and facies environments (Rosen 1991; Renaut and Tiercelin 1994), but provide only a geologic "snapshot" of the present and recent past. Although valuable for reconstructing ancient depositional environments, these studies provide only limited insights for understanding long term sedimentologic responses to changes in climate, tectonically driven accommodation, and sediment supply. Truly detailed multidimensional stratigraphic studies of lacustrine and alluvial deposits at the basin scale remain rare.

Excellent surface exposure of the Eocene Green River Formation (GRF, Hayden 1869), numerous drill cores (Burnside and Culbertson 1979; Mason 1987; Roehler 1992c; Wiig et al. 1995), and high-resolution $^{40}Ar/^{39}Ar$ age control (Smith et al. 2008b; Smith et al. 2010) together provide an unique opportunity to observe nonmarine strata over million-year timescales at a spatial and temporal resolution typical of Quaternary deposits. The Wilkins Peak Member (WPM) of the GRF represents one of the most robust records for reconstructing changes in terrestrial environments during the warmest interval of the Cenozoic Era, the Early Eocene Climatic Optimum (EECO, ~52.6–50.3 Ma; cf. Zachos et al. 2001). Here we present a basin-scale integration of: (1) stratigraphic correlation of lacustrine strata across the Bridger subbasin of the Greater Green River Basin (GGRB); (2) new detailed stratigraphic mapping and facies analysis of previously-unrecognized lake-margin fluvial and lacustrine strata proximal to the Uinta Uplift; (3) reconstruction of the exhumation of the Uinta Uplift provenance analysis of conglomerates; and (4) $^{40}Ar/^{39}Ar$-based analysis of sedimentary cyclicity and alluvial fan growth and migration. We discuss: (1) the character and depositional history of uplift-proximal lithofacies in an underfilled basin; (2) the temporal relationship between climate cycles and the changes to the ancient landscape; (3) the temporal relationship between tectonism of the Uinta Uplift and basin fill; and (4) clastic and chemical sediment fluxes and storage across the landscape during the EECO.

4.2 Geologic Setting

Hundreds of meters in thickness of lacustrine GRF and equivalent alluvial strata were deposited during the Eocene epoch within the Greater Green River Basin (GGRB), a broad, low relief basin bounded by the Cordilleran fold and thrust belt to the west and anticlinal Laramide basement uplifts to the north, east, and south (Figs. 4.1 and 4.2; Dickinson et al. 1988; DeCelles 2004). Conglomerate deposits and growth strata indicate ongoing Cretaceous through Eocene uplift and denudation of basement structures across the Laramide foreland province (Love 1960; DeCelles 2004; Carroll et al. 2006). The first appearances of Precambrian conglomerate clasts derived from structures surrounding the GGRB occurred during the Paleocene (Berg 1962; Crews and Ethridge 1993; DeCelles 1994). From the Paleocene to the Eocene, stratal thicknesses (Fig. 4.2b) indicate that flexural accommodation in the GGRB shifted from a northern depocenter adjacent to the Wind River Uplift to a southern depocenter adjacent to the Uinta Uplift at ca. 53 Ma (Beck et al. 1988; Roehler 1992a). This shift coincided with the initiation of a ~5 Ma

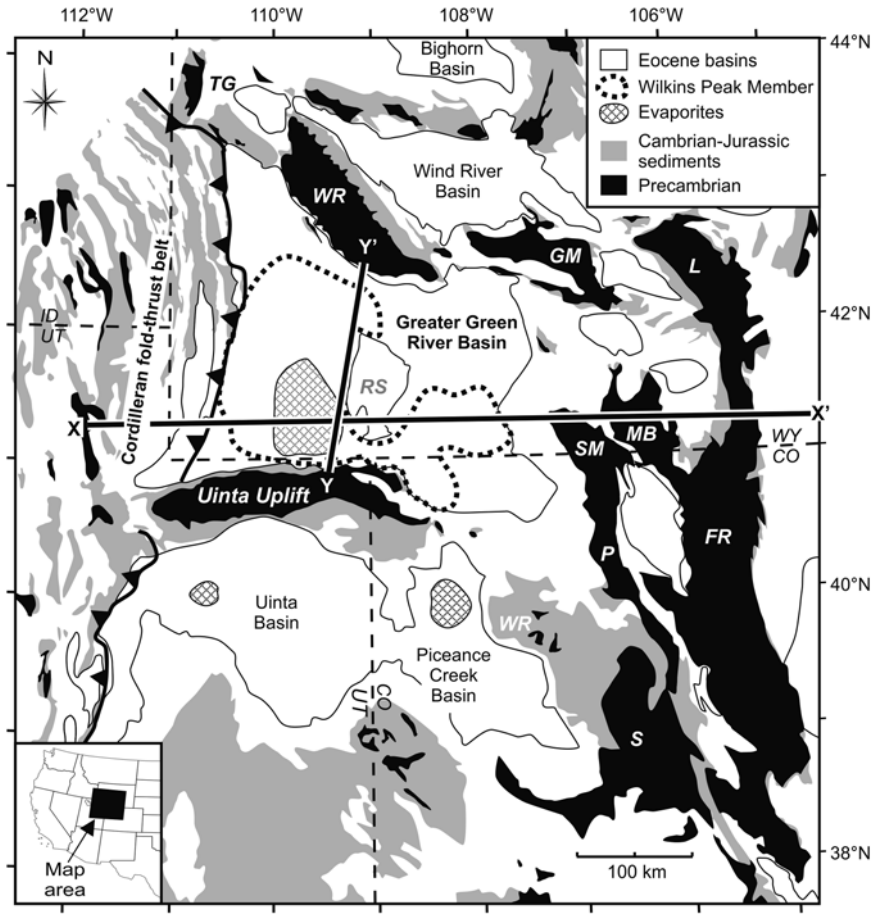

Fig. 4.1 Map of the Laramide broken foreland province showing principle uplifts and basins, Eocene paleocatchments for the Greater Green River Basin, and areas of alluvial, lacustrine, and evaporite accumulation within it (Modified from Smith et al. 2008a, b; cf. references therein). Abbreviations for Laramide uplifts: *TG* Teton-Gros Ventre, *WR* Wind River, *RS* Rock Springs, *GM* Granite Mountains, *L* Laramie, *FR* Front Range, *MB* Medicine Bow, *SM* Sierra Madre, *P* Park, *S* Sawatch, *WR* White River

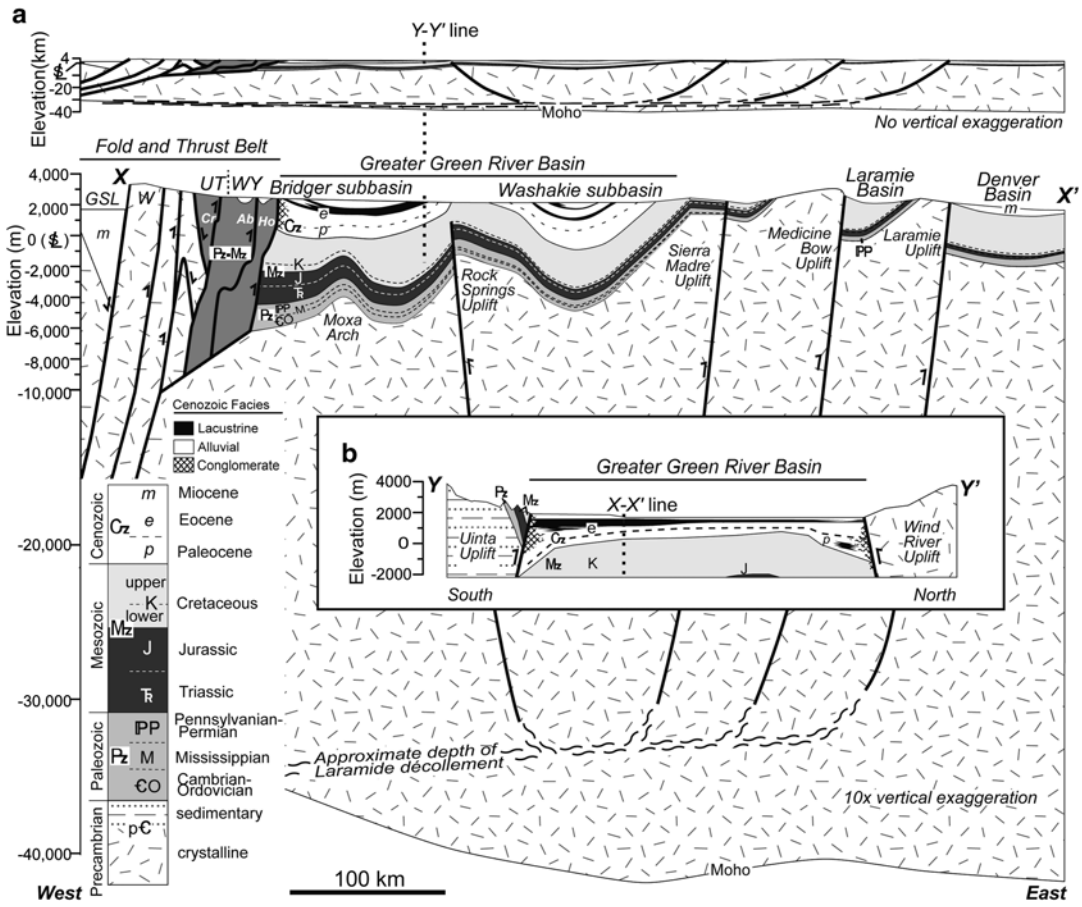

Fig. 4.2 Crustal-scale cross sections of the Greater Green River Basin (GGRB) and surrounding Laramide province (see Fig. 4.1 for locations): (**a**) East-west (X-X') cross section illustrating lithospheric buckling (Erslev 1993; Tikoff and Maxson 2001), large-scale wedge-top position of the GGRB in the Cordilleran-Laramide deformation region above proposed Laramide décollement in the lower crust (Erslev 1993; McClelland and Oldow 2004). Thicknesses of Phanerozoic strata from Mallory (1972), and depth of Mohorovičić discontinuity from Das and Nolet (1998). Abbreviations for structures in the Cordilleran fold and thrust belt (Royse 1993; DeCelles 1994): *W* Wasatch Culmination, *Cr* Crawford Thrust, *Ab* Absaroka Thrust, *Ho* Hogsback Thrust, *G* Great Salt Lake Basin. (**b**) North-south (Y-Y') cross section illustrating complementary Paleocene and Eocene synorogenic wedges that accumulated within the GGRB in foredeeps adjacent to the Wind River and Uinta uplifts (Beck et al. 1988; Roehler 1992a)

episode of GRF lacustrine deposition in the southern GGRB that lasted until ca. 48 Ma.

4.2.1 Stratigraphic Relationships

The Wilkins Peak Member (WPM) is the evaporative middle unit of the GRF in the GGRB, and it represents a ~1.7 Ma interval of the Early Eocene (51.6–49.9 Ma) during which Lake Gosiute was hydrologically closed, periodically hypersaline, and largely confined to the Bridger subbasin of the GGRB (Figs. 4.3 and 4.4; Sullivan 1985; Roehler 1992a; Smith et al. 2008b). The WPM is thickest (~500 m) in a local foredeep to the north of the Uinta and Henrys Fork thrusts in the Bridger subbasin (Figs. 4.4a and 4.5). It is bounded below and above by the more freshwater lake strata of the Tipton and Laney Members, respectively

(Fig. 4.5), and is laterally equivalent to alluvial facies of the Cathedral Bluffs Member of the Wasatch Formation (Roehler 1992a). Lithofacies within the Cathedral Bluffs Member vary from coarse-grained fanglomerates along its southern periphery derived from Paleogene denudation of the Proterozoic-Mesozoic bedrock of the Uinta Uplift (Fig. 4.6; Hansen 1965; Crews and Ethridge 1993) to fine-grained, pedogenically-modified fluvial and overbank deposits that fill the Great Divide, Washakie, and Sand Wash subbasins to the east of the Rock Springs Uplift and the western Bridger subbasin (Figs. 4.4 and 4.7; Bradley 1964; Sullivan 1985; Roehler 1992b, 1993).

4.2.2 Geochronology and Paleoclimatic Setting

A suite of 12 ash beds provide radioisotopic age control for Eocene strata in the GGRB (Smith et al. 2008b; Smith et al. 2010). All existing GRF $^{40}Ar/^{39}Ar$ ages and their uncertainties (Fig. 4.3) have been recalibrated here to the 28.201 Ma age for the Fish Canyon Tuff sanidine standard (Kuiper et al. 2008) using the ^{40}K decay constant value of Min et al. (2000). The resulting fully-propagated uncertainties of ca. ±200 ky (2σ) permit the GRF to be compared with astronomical solutions for insolation (Laskar et al. 2004; Laskar et al. 2011), magnetostratigraphy (Cande and Kent 1992, 1995), and marine-based global climate proxies (Zachos et al. 2001). $^{40}Ar/^{39}Ar$ and U-Pb geochronology indicate that the WPM was deposited between 51.6 and 49.9 Ma, near the end of the Early Eocene Climatic Optimum (Smith et al. 2008b; Smith et al. 2010), an ice-free period of global warmth (Zachos et al. 1994; Burgess et al. 2008; Huber and Caballero 2011). Despite its apparent continentality and orographic isolation, crocodile and palm fossils from GRF deposits indicate an equable subhumid climate in the Laramide foreland with temperatures that remained above freezing year-round (Markwick 1994; Wilf 2000). Land mammal-based biostratigraphy and magnetostratigraphy indicate that the WPM coincides both the Wasatchian-Bridgerian land mammal age boundary and paleomagnetic chron C23 (Fig. 4.3; cf. Smith et al. 2008b).

The WPM contains several scales of repetitively stacked lithofacies, discussed in detail below, that have been interpreted to result from orbital climatic forcing (Bradley 1929; Fischer and Roberts 1991; Roehler 1993; Machlus et al. 2008; Meyers 2008; Smith et al. 2010; Aswasereelert et al. 2013; Smith et al. 2014). The WPM accumulated during a particularly isolated hydrologic phase for the GGRB, which began when a river that drained an extrabasinal catchment(s) extending to near or at the Cordilleran crest in Idaho was diverted northward away from the GGRB into the Bighorn Basin (Fig. 4.8, Kraus 1985; Janecke et al. 2000; Carroll et al. 2008; Smith et al. 2008b; Chetel and Carroll 2010). Numerical models of local Early Eocene climate indicate that the same structural uplifts that were responsible for hydrologically isolating the GGRB also acted as barriers to the lateral advection of atmospheric moisture (Fig. 4.8; Sewall and Sloan 2006). Climate modeling by Sewall and Sloan (2006) suggests that the GGRB was largely isolated from Pacific moisture and received a majority of its precipitation via cyclonal semi-monsoonal airflow that originated from an expanded Mississippi embayment of the Gulf of Mexico. This model is based on evidence that the Cordilleran crest was apparently high enough to support an actively deforming critical wedge (DeCelles 2004) and supported subalpine fir-hemlock forests (Axelrod 1968, 1997) and snow (Seal and Rye 1993; Carroll et al. 2008). Similar to the present day, moisture derived from the east appears to have been topographically impeded by the Front Range uplift. Plant fossils in the GGRB and the Denver Basin of Colorado indicate that annual rainfall increased two-fold from the interior of the GGRB to its eastern edge (Wilf 2000; Johnson and Ellis 2002).

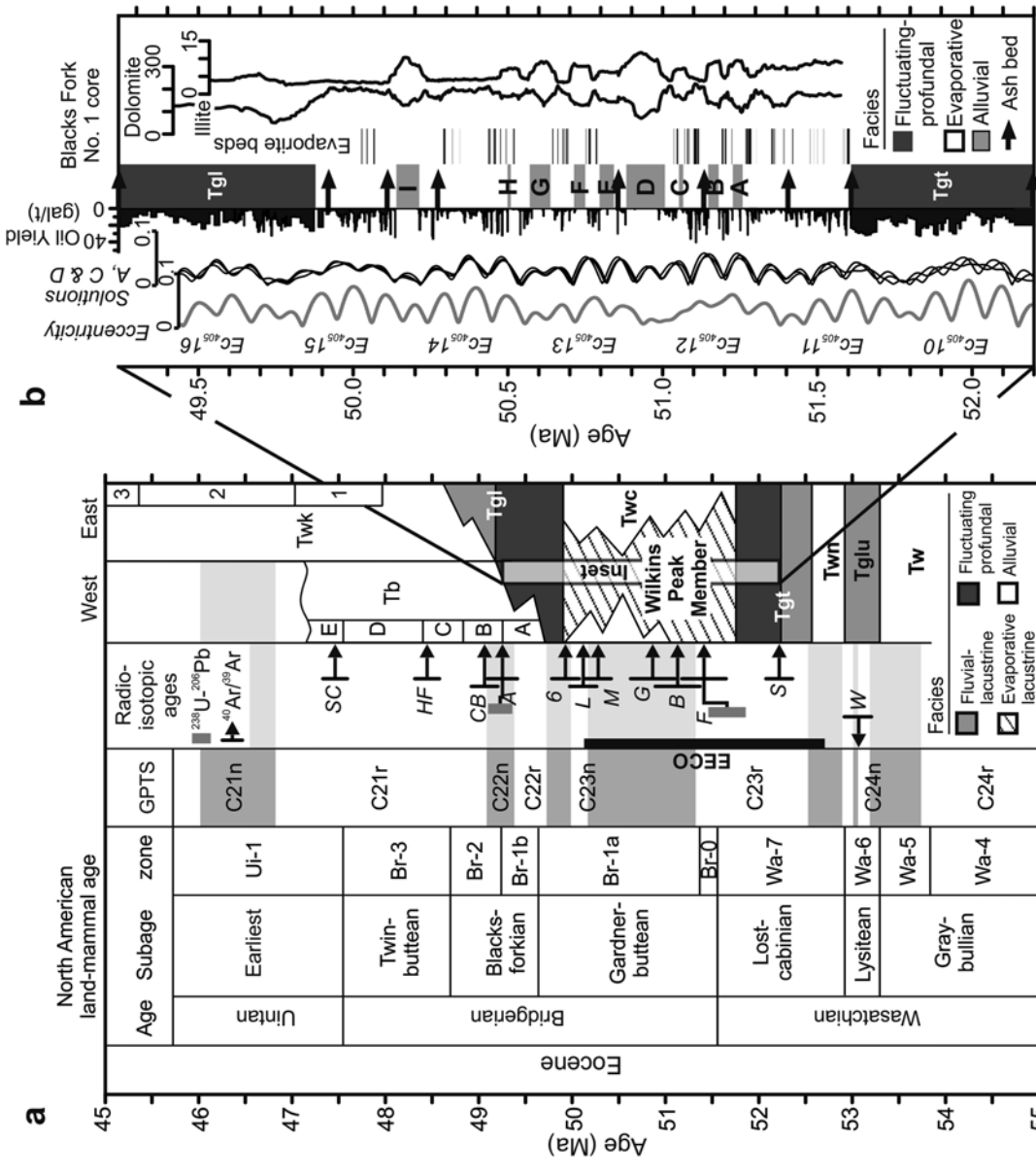
a
b
North American land-mammal age
Age
Subage
zone
GPTS
Radio-isotopic ages
Facies
Eocene
Uintan
Bridgerian
Wasatchian
Earliest
Twin-buttean
Blacks-forkian
Gardner-buttean
Lost-cabinian
Lysitean
Gray-bullian
Ui-1
Br-3
Br-2
Br-1b
Br-1a
Br-0
Wa-7
Wa-6
Wa-5
Wa-4
C21n
C21r
C22n
C22r
C23n
EECO
C23r
C24n
C24r
West
East
Twk
Tb
Tgl
Twc
Inset
Wilkins Peak Member
Tgt
Twn
Tglu
Tw
Fluvial-lacustrine
Evaporative lacustrine
Fluctuating profundal
Alluvial
Age (Ma)
Blacks Fork No. 1 core
Dolomite
Illite
Evaporite beds
Oil Yield (gal/t)
Solutions A, C & D
Eccentricity
Facies
Fluctuating-profundal
Evaporative
Alluvial
Ash bed

Fig. 4.3 (**a**) Chronostratigraphic diagram for Eocene strata in the Greater Green River Basin illustrating depositional timing of the Green River Formation and surrounding alluvial strata, paleomagnetic chrons, and terrestrial biostratigraphy (cf. Smith et al. 2014). Abbreviations for lithostratigraphic units: Green River Formation: *Tglu* Luman Member, *Tgt* Tipton Member, *Tgl* Laney Member; Wasatch Formation: Tw ("main body"), *Twn* Niland Tongue, *Twc* Cathedral Bluffs Member, *Tb* Bridger Formation, *Twk* Washakie Formation. Abbreviations for tuff beds: *W* Willwood, *S* Scheggs, *R* Rife, F Firehole, *B* Boar, *G* Grey, *M* Main, *L* Layered, *6* Sixth, *A* Analcite, *CB* Church Butte, *HF* Henrys Fork, *SC* Sage Creek. All ages (Smith et al. 2008b, 2010) shown with full 2σ uncertainties relative to the 28.201 Ma age for Fish Canyon rhyolite sanidine (Kuiper et al. 2008) using the ^{40}K λ values of Min et al. (2000), see Chap. 1 of this book for the complete data set for the Green River Formation. Lake type categorizations follow Carroll and Bohacs (1999) and Smith et al. (2008b). (**b**) Detailed time-stratigraphy of the Green River Formation within the basin center Blacks Fork core #1 constructed using the tiered interpolation method (Smith et al. 2011), and is shown relative to the most recently calculated values for insolation (Laskar et al. 2004, 2011). Note that the solutions become increasingly non-unique for periods preceding ~51 Ma. Shown are alluvial units A-I (Culbertson 1961), evaporite beds (Burnside and Culbertson 1979), organic content (from Fischer assay; Roehler 1991a), and select XRD peak heights for dolomite and illite (Mason 1987), which track lacustrine and alluvial modes, respectively

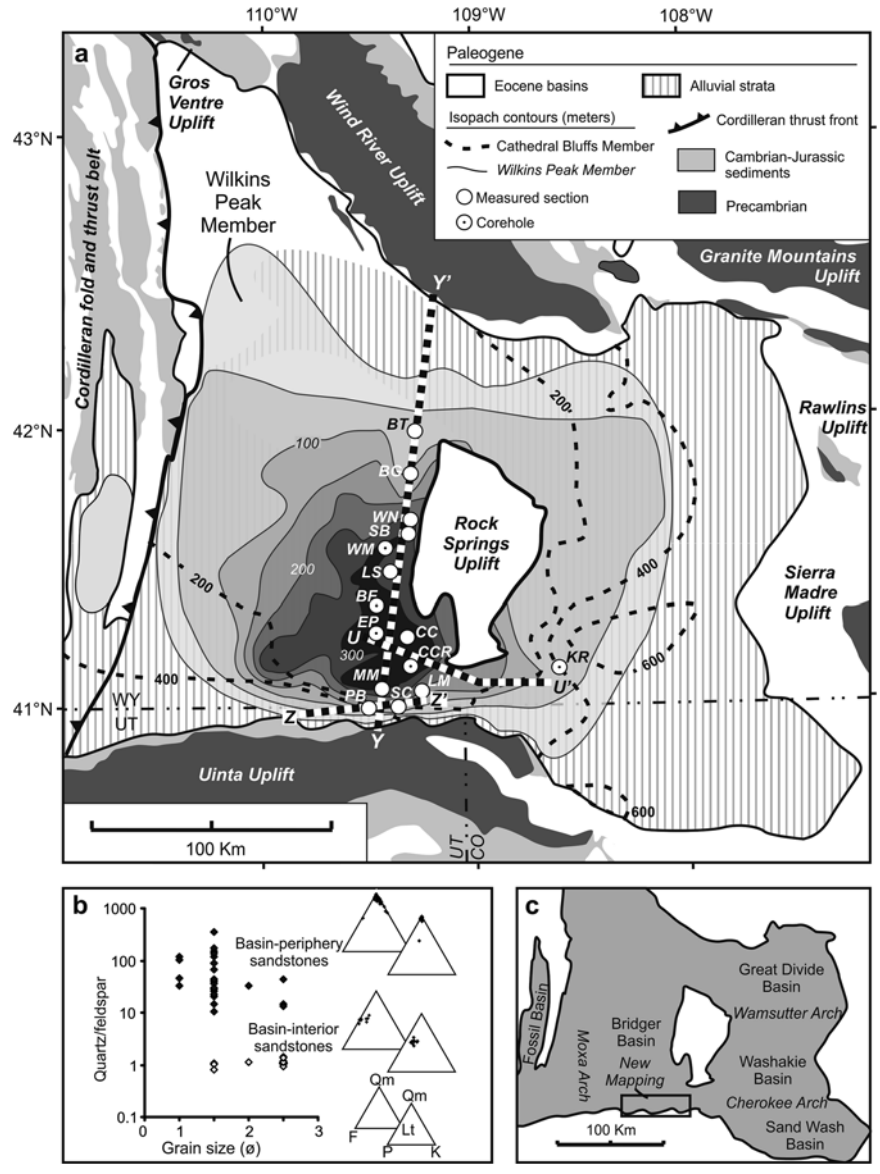

Fig. 4.4 Alluvial and lacustrine strata of the Wilkins Peak interval in the Greater Green River Basin: (**a**) Map showing isopachs of the Wilkins Peak Member and equivalent strata, locations of measured stratigraphic sections, paleoflow direction measurements (taken from basin interior alluvial units B and D, see Fig. 4.3). Section abbreviations: *BT* Boars Tusk, *BG* Breathing Gulch, *WN* White Mountain North, *SB* Stagecoach Boulevard, *WM* U.S. ERDA White Mountain #1 core, *LS* Lauder Slide, BF U.S. ERDA Blacks Fork no. 1 core, *EP* Union Pacific El Paso 44–3 core (Mason 1987), *CC* Currant Creek, *CCR* Currant Creek Ridge CCR-1 core (Mason 1987), *KR* Kinney Rim core (Mason 1987; Rhodes et al. 2002; Doebbert et al. 2010), *LM* Little Mountain, *SC* Spring Creek, *MM* Middle Marsh Creek, *PB* Pipeline Bridge (See Supplementary Fig. S4.2, accessed at http://extras.springer.com, for 1:100,000 scale geologic map showing section locations); (**b**) Plot of grain size versus quartz/feldspar ratios in the WPM sandstones, illustrating grain-size independence of sandstone compositional modes; (**c**) Map showing Eocene subbasins and intrabasinal uplifts of the GGRB and area of new geologic mapping adjacent to the Uinta Uplift (Supplementary Fig. S4.2)

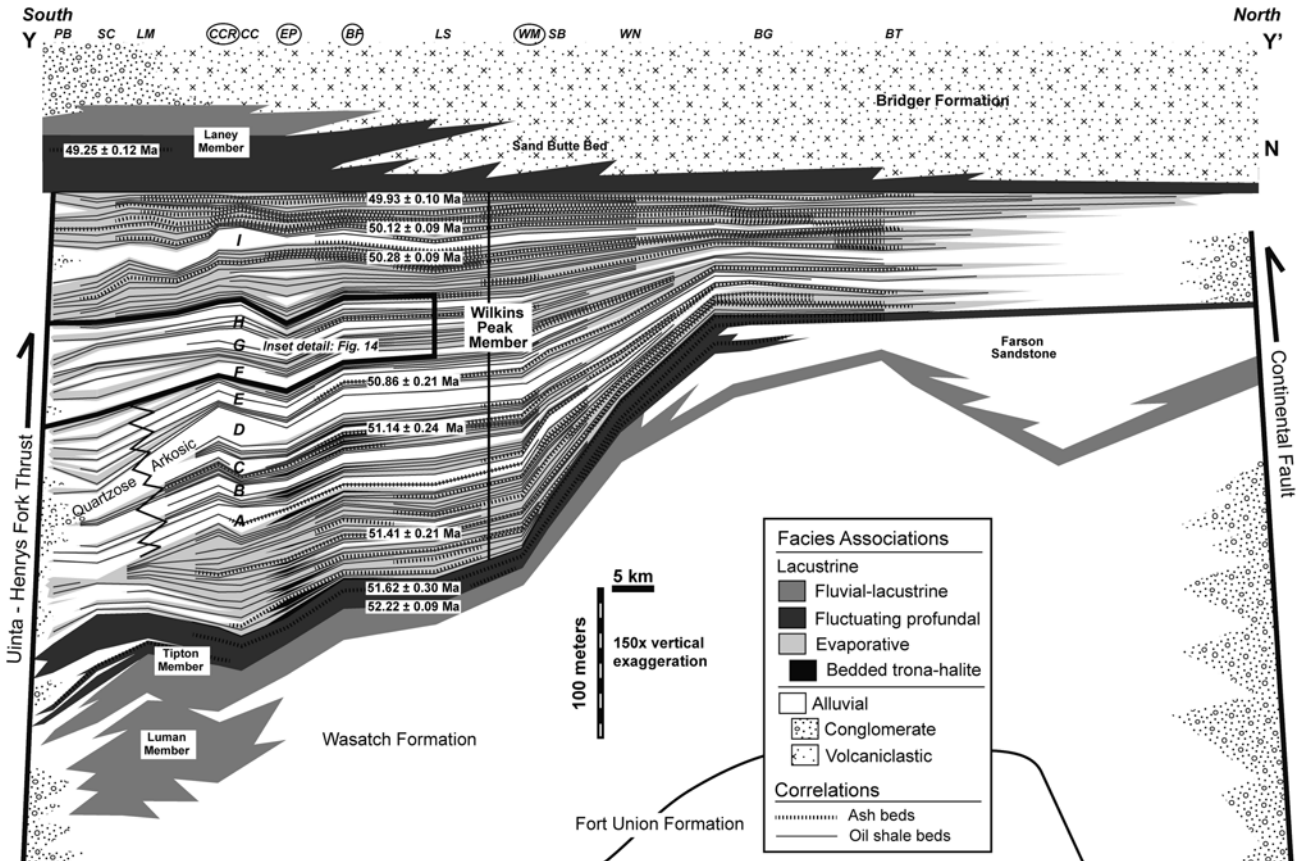

Fig. 4.5 Detailed north-south correlation (*Y-Y'*, Fig. 4.4a) of measured Paleogene strata in the Greater Green River Basin (see text for correlation methodology). The base of the Laney Member of the Green River Formation is the datum. Correlation is a simplified version of Supplementary Fig. S4.1, which can be accessed at http://extras.springer.com. Letters *A*–*I* indicate named alluvial horizons of Culbertson (1961). Section location symbols as in Fig. 4.4a. *Circled section labels* indicate coreholes. Supplementary Fig. S4.2 (http://extras.springer.com) contains a detailed map of section locations. Sections *WM*, *SB*, *WN*, *BG*, and *BT* modified from Pietras and Carroll (2006). Thicknesses north of BT are from Roehler (1992a). $^{40}Ar/^{39}Ar$ ages are shown with 2σ analytical uncertainties

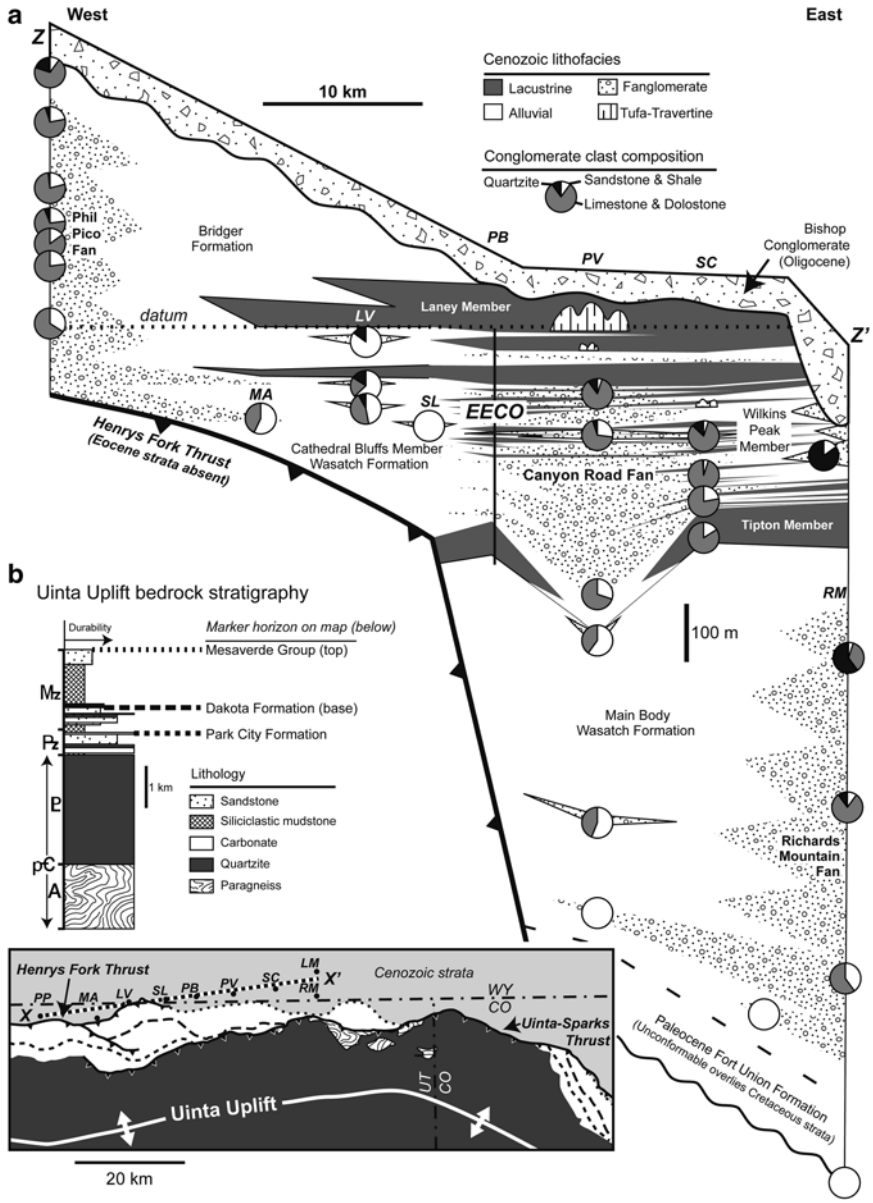

Fig. 4.6 (**a**) Along-strike cross-section (Z-Z') through measured Paleogene alluvial and lacustrine strata directly adjacent to the Uinta Uplift in the southernmost Bridger subbasin, illustrating the evolution of clast compositions within three discrete fanglomerate units. Each clast count represents >100 grid-sampled conglomerate clasts. Datum is the base of the Laney Member of the Green River Formation. Section abbreviations not shown in caption for Fig. 4.4: *PP* Phil Pico Mountain, *MA* Manila, *LV* Luverne, *SL* State Line, *PV* Pipeline Valley, *RM* Richards Mountain. (**b**) Map and generalized stratigraphic column of the lithology and modern structure of the pre-Eocene bedrock of the Uinta Uplift, modified from Hansen (1965) and Rowley et al. (1985)

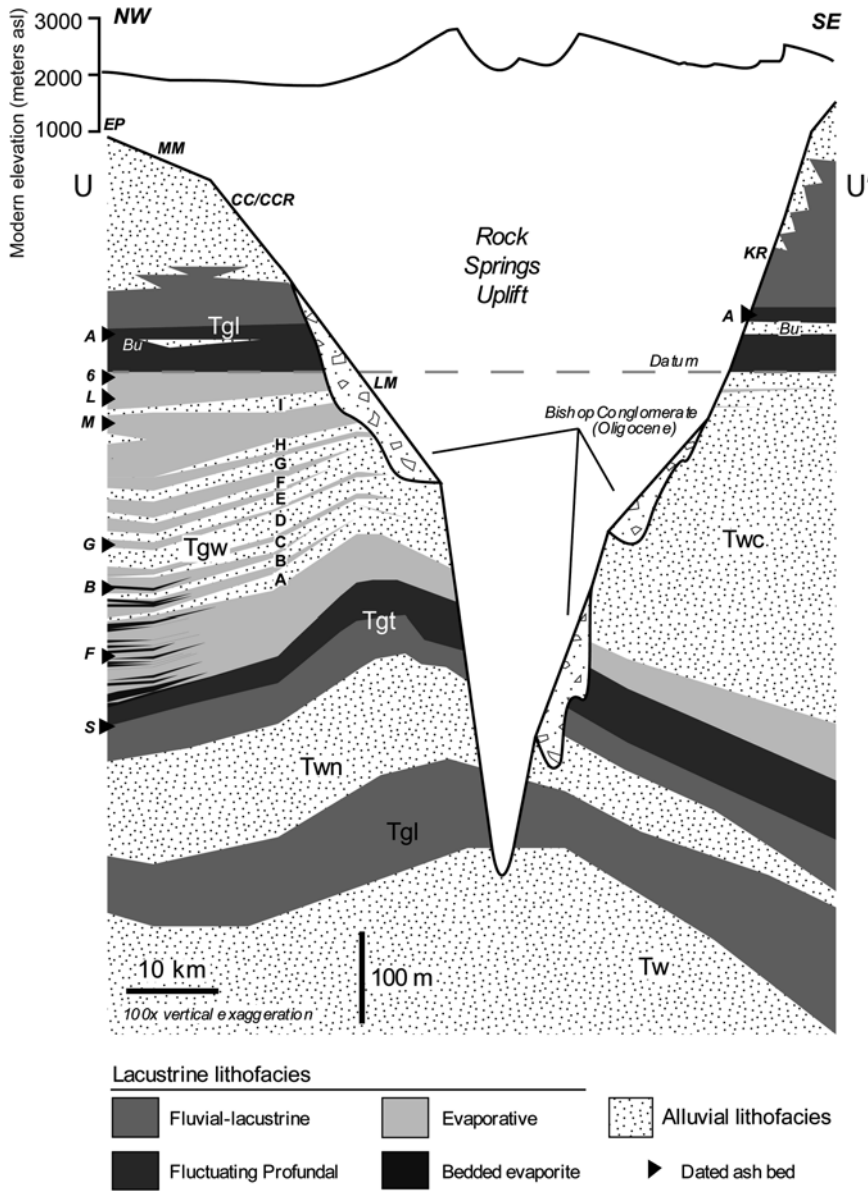

Fig. 4.7 E-W cross-section through the Uinta foredeep along the axis of the Aspen River (Modified from Smith et al. 2014). Stratal thicknesses from measured surface section and core, and from published stratigraphy (Roehler 1993; Johnson and Anderson 2009). Letters *A–I* indicate named alluvial horizons of Culbertson (1961). Lithostratigraphic and ash bed abbreviations as in Fig. 4.3. Section abbreviations are the same as shown in Fig. 4.4 caption

4.3 Methods

Over 2 km of core and outcrop stratigraphic sections were measured through Eocene strata at 12 locations in the GGRB. These sections have facilitated the construction of three cross-sections: (1) N-S across the Bridger subbasin (Y-Y'; Fig. 4.5 and Supplementary Fig. S4.1, which can be accessed at http://extras.springer.com); (2) E-W adjacent to the Uinta Uplift (Z-Z'; Fig. 4.6a); and (3) SE-NW across the GGRB (U-U'; Fig. 4.7). Assays of U, Th, and K concen-

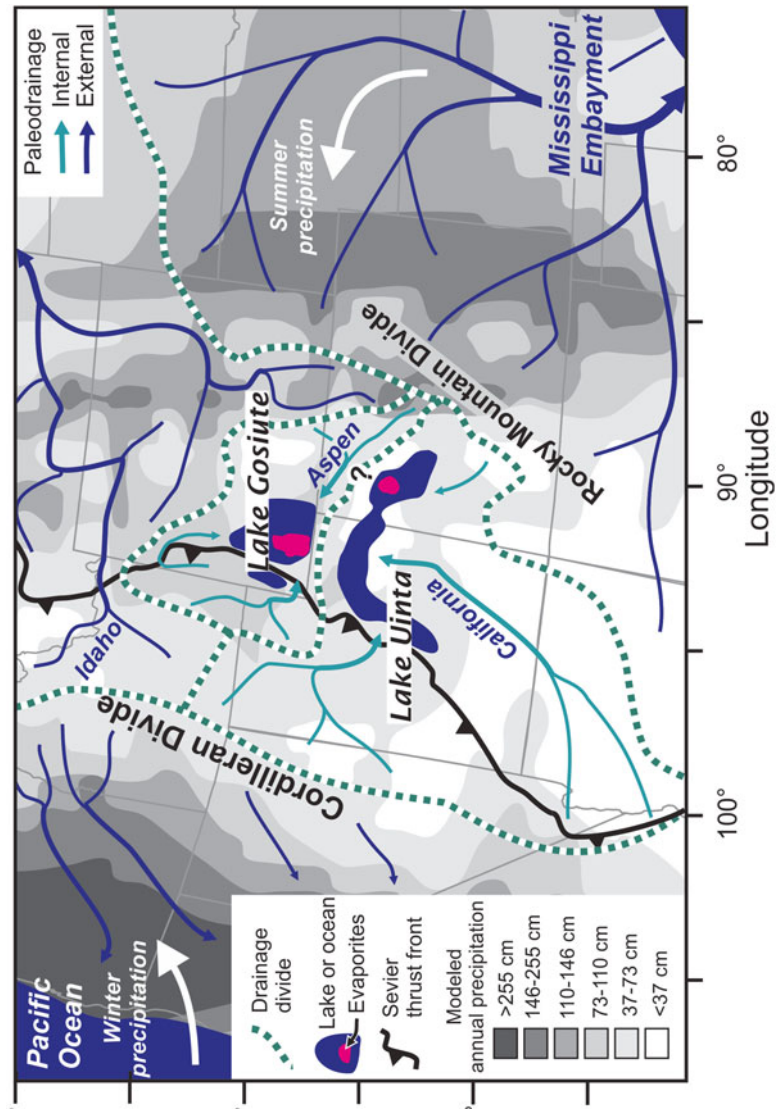

Fig. 4.8 Synthesis of Early Eocene palinspastic paleogeography and paleoclimatology of the Laramide province, showing modeled precipitation and snowfall (Sewall and Sloan 2006), position of significant orogenic barriers, and interpreted paleohydrology (from Smith et al. 2014). References for depicted paleorivers: Wilcox (Gregory and Chase 1994; Galloway et al. 2011; Mackey et al. 2012), Tyee (Heller et al. 1985; Dickinson et al. 1988), California (Davis et al. 2009; Davis et al. 2010; Wernicke 2011), Idaho (Kraus 1985; Janecke et al. 2000; Kent-Corson et al. 2006; Carroll et al. 2008), and Paleo-Missouri (Keefer 1965; Seeland 1978, 1992; Fan and Dettman 2009). Position of Cordilleran and Rocky Mountain divides from Cassel and Graham (2011), Henry et al. (2012), Lawton et al. (2009), and Mackey et al. (2012). Major Laramide uplifts: *BT* Beartooth, *B* Bighorn, *WR* Wind River, *U* Uinta, *FR* Front Range, *S* Sawatch

trations via gamma ray emissions were taken at 0.5 meter intervals of all surface sections using an Exploranium GR-320 enviSpec hand-held spectrometer (Supplementary Fig. S4.1, which can be accessed at http://extras.springer.com). New detailed (1:100,000 scale) mapping of Paleogene strata in a previously unmapped region between Little Mountain, WY and the town of Manila, UT was required to document the complex transition between lacustrine and alluvial facies near the Uinta Uplift (Figs. 4.6 and Supplementary Fig. S4.2, which can be accessed at http://extras.springer.com). The clast composition of selected sandstone beds were point-counted from thin sections using a petrographic microscope (Fig. 4.4b), and conglomerate clast compositions were determined in situ at 28 horizons adjacent to the Uinta Uplift using a 10 cm grid (Fig. 4.6a). Paleoflow orientations within trough cross-stratified sandstone beds were determined using trough limbs and axes (Fig. 4.4a).

4.4 Results

4.4.1 Sedimentary Facies

The WPM and laterally equivalent Cathedral Bluffs Member of the Wasatch Formation encompass a wide variety of non-marine facies (Bradley 1964; Smoot 1983; Sullivan 1985; Roehler 1993). We document two spatially and compositionally unique facies belts within the Bridger subbasin of the GGRB that each contain both lacustrine and alluvial lithofacies: (*I*) the basin interior (Fig. 4.9), which represents the bulk of WPM strata and is synonymous with much of the classic literature (e.g., Eugster and Hardie 1975; Smoot 1983); and (*II*) the basin periphery (Fig. 4.10), which is confined to within ~5 km of the southern edge of the Bridger subbasin (Fig. 4.4c), and was largely undocumented due to a lack of detailed geologic mapping of the GRF adjacent to the Uinta Uplift (Bradley 1964; Love and Christiansen 1985). Table 4.1 summarizes the 24 distinct lithofacies which comprise the Wilkins Peak Member and time-equivalent alluvial strata.

I. Basin Interior Facies Belt

The basin interior facies belt occupies all but the southernmost and westernmost Bridger subbasin, and consists of alternating intervals of predominantly carbonate lacustrine strata and predominantly siliciclastic alluvial-deltaic strata (Fig. 4.9).

L. *Lacustrine Macroassociation*

Basin interior lacustrine facies of the WPM have been well documented and interpreted by previous workers (Eugster and Hardie 1975; Smoot 1983; Pietras and Carroll 2006). Here we briefly summarize the classification scheme and interpretations of Pietras and Carroll (2006), who divide lacustrine strata into four lithofacies associations: (*i*) palustrine, (*ii*) littoral, (*iii*) salt-pan, and (*iv*) profundal-sublittoral. We also add to these findings new data concerning of pedogenic structures and ichnofossils.

(i) *Palustrine Association:* The palustrine association consists of two fine-grained carbonate lithofacies: (*1*) *Wavy-bedded calcareous siltstone-sandstone*; and (2) *Brecciated calcareous mudstone-siltstone*. Both lithofacies are composed of varying proportions of dolomitic micrite and calcareous silt- and sand-sized clasts. Calcareous silt horizons contain sedimentary structures indicative of unidirectional currents and/or wave-influenced subaqueous deposition (e.g., cross-bedding, wavy bedding, lenticular bedding). These beds are commonly disrupted and sometimes brecciated by desiccation cracks and/or authigenic evaporite crystal blades (Eugster and Hardie 1975; Smoot 1983). Biogenic structures associated with these facies include poorly preserved mammal footprints, larval insect trails, iron-stained root-marks, and insect tunnels on bedding planes (Scott 2010; Scott and Smith 2015). Palustrine association lithofacies are interpreted to represent deposition on eulittoral lake-fringing mudflats surrounding Lake Gosiute (Smoot 1983; Pietras and Carroll 2006), where fine-grained, crystalline carbonate sediments

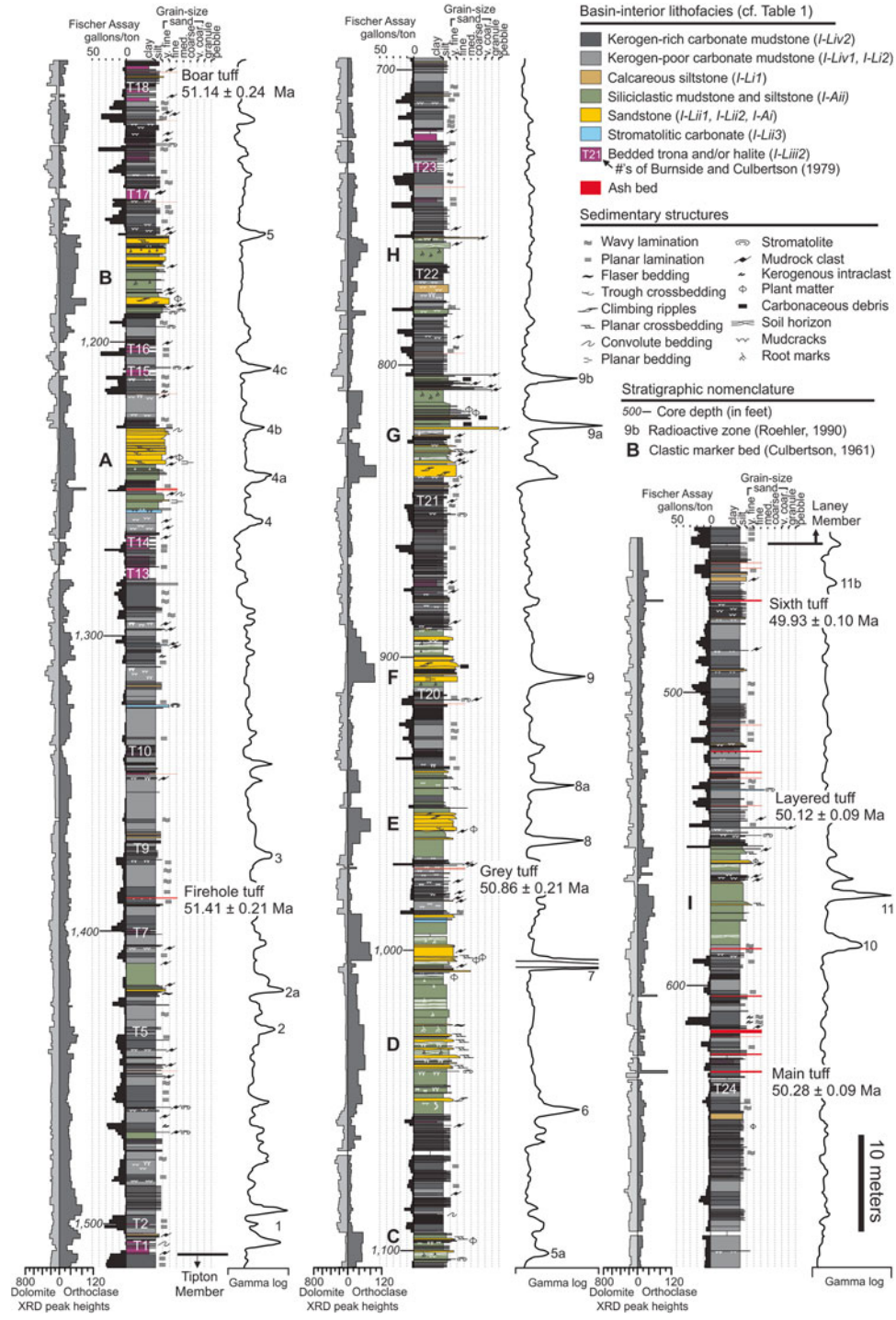

Fig. 4.9 Basin interior reference section of the Wilkins Peak Member in U.S. Energy Research and Development Administration Blacks Fork no. 1 corehole (location *BF* on Fig. 4.4a) measured at the U.S.G.S. core repository in Denver, CO, showing detailed lithology, total gamma ray (Roehler 1991b), and Fisher assay and XRD measurements (Mason 1987). Oil shale and trona bed labels follow the numbering schemes of Burnside and Culbertson (1979) and Roehler (1991a). Radioactive zones within the Wilkins Peak Member (Love 1964) follow numbering scheme of Roehler (1991b). $^{40}Ar/^{39}Ar$ ages (Smith et al. 2008b, 2010) are shown with 2σ analytical uncertainties relative to the 28.201 Ma age for Fish Canyon rhyolite sanidine (Kuiper et al. 2008) using the ^{40}K λ values of Min et al. (2000)

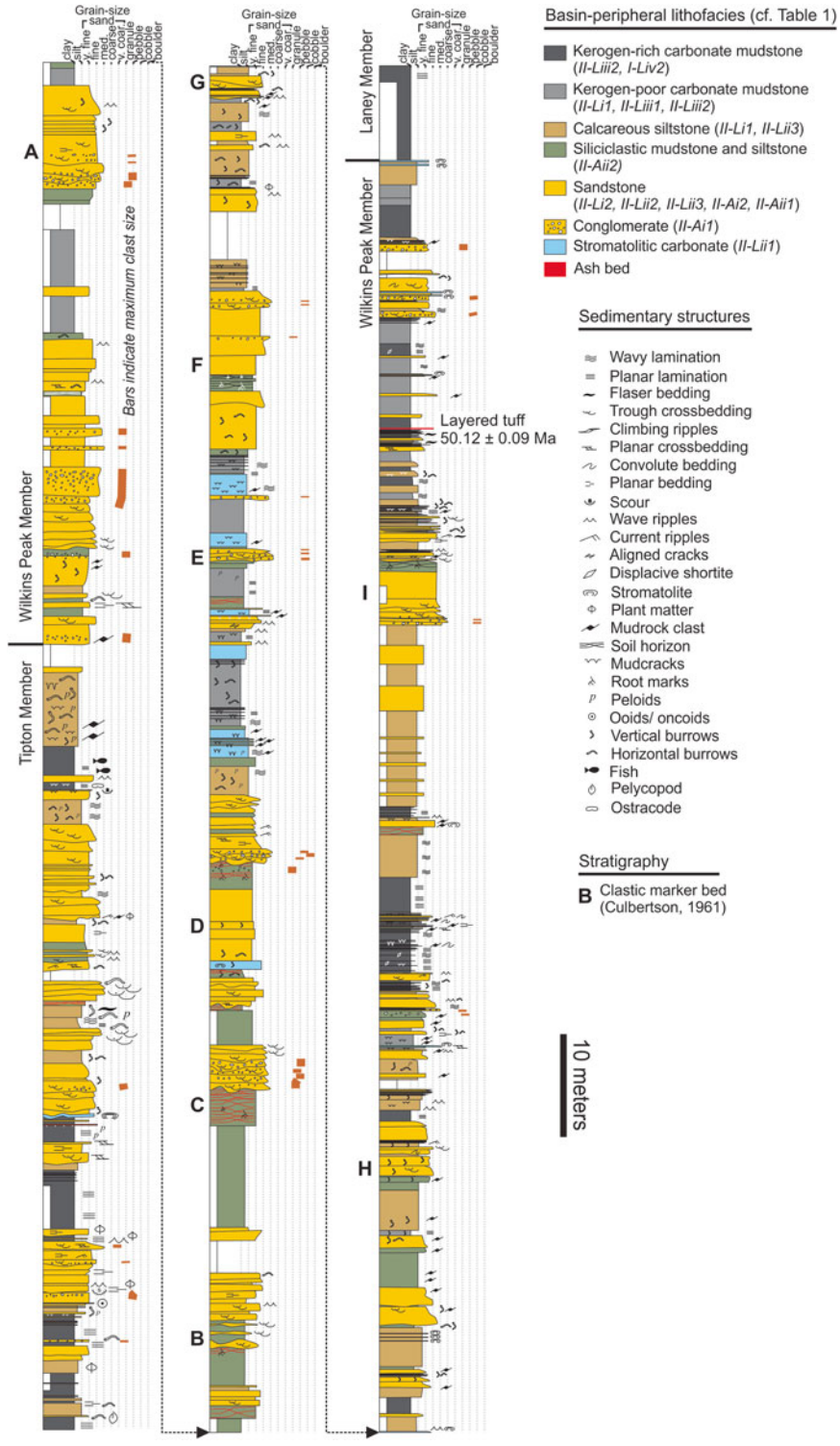

Fig. 4.10 Basin periphery reference section of the intercalated Cathedral Bluffs and Wilkins Peak Members at the Pipeline Bridge locale (Location *PB* in Fig. 4.4a), showing detailed lithologic and spectral gamma ray readings. Facies and sedimentary structures follow key for Fig. 4.9. *Orange lines* to the right of stratigraphic column indicate maximum clast size

Table 4.1 Lithofacies of the Wilkins Peak Member and equivalent strata

I. Interior facies belt		
L.	***Lacustrine Macroassociation***	
(i)	***Palustrine Association***	Mudstone Facies of Eugster and Hardie (1975), *follows* Pietras and Carroll (2006)
	1. *Wavy-bedded carbonate siltstone-sandstone*	Subfacies DM1-2 and EL-1 of Smoot (1983), *follows* Pietras and Carroll (2006)
	2. *Brecciated to massive carbonate mudstone-siltstone*	Subfacies DM3 and EL1-2 of Smoot (1983), Brecciated Carbonate Mudstone–Siltstone of Pietras and Carroll (2006)
(ii)	***Littoral Association***	
	1. *Calcareous intraclastic conglomerate*	Flat-Pebble Conglomerate Facies of Eugster and Hardie (1975), Subfacies SF5 of Smoot (1983), Intraclastic Conglomerate of Pietras and Carroll (2006)
	2. *Calcareous sandstone*	Lime Sandstone Facies of Eugster and Hardie (1975), Subfacies SF1-4 of Smoot (1983), *follows* Pietras and Carroll (2006)
	3. *Stromatolitic, laminated carbonate mudstone*	Facies SF (*part*) of Smoot (1983), *This study*
(iii)	***Salt-Pan Association***	*Follows* Pietras et al. (2006)
	1. *Displacive evaporites*	Subfacies SM2 of Smoot (1983)
	2. *Bedded evaporites*	Trona-Halite Facies of Eugster and Hardie (1975), Subfacies SM1 of Smoot (1983)
(iv)	***Profundal-Sublittoral Association***	*Follows* Pietras et al. (2006)
	1. *Massive carbonate mudstone and marlstone*	Subfacies PL2 of Smoot (1983)
	2. *Laminated kerogen-rich carbonate mudstone and marlstone*	Oil Shale Facies of Eugster and Hardie (1975), Subfacies PL1 of Smoot (1983)
A.	***Alluvial Macroassociation***	Siliciclastic Sandstone Facies of Eugster and Hardie (1975)
(i)	***Axial Fluvial Association***	Facies AS (*part*) of Smoot (1983), Siliciclastic Sandstone (*part*) of Pietras and Carroll (2006)
	1. *Trough cross-stratified and planar- to ripple-laminated sandstone*	*This study*
	2. *Drape-bedded sandstone.*	*This study*
(ii)	***Distal-Overbank Association***	Facies AS (*part*) of Smoot (1983)
	1. *Climbing-rippled and planar-bedded sandstone and siltstone*	Siliciclastic Sandstone (*part*) of Pietras and Carroll (2006), *This study*
	2. *Massive to faintly-bedded siltstone and mudstone*	Green-Brown Mudstone Siltstone of Pietras and Carroll (2006), *This study*
II. Peripheral facies belt		
L.	***Lacustrine Macroassociation***	
(i)	***Palustrine Association***	
	1. *Silty, mudcracked and/or bioturbated carbonate mudstone*	*This study*
	2. *Cross-stratified calcareous aolian sandstone*	*This study*
(ii)	***Littoral Association***	
	1. *Tufa-travertine and massive carbonate*	*This study*
	2. Planar-bedded and oscillation-rippled sandstone	*This study*

(continued)

Table 4.1 (continued)

	3. Massive fine-grained sandstone	*This study*
(iii)	***Sublittoral Association***	
	1. *Massive carbonate mudstone and marlstone*	*This study*
	2. *Laminated carbonate mudstone and marlstone*	*This study*
A.	***Alluvial Macroassociation***	
(i)	***Fan Delta Association***	
	1. Conglomerate	Subfacies AF1-2 of Smoot (1983), Facies 1 of Crews and Ethridge (1993), *This study*
	2. Trough cross-stratified sandstone	Subfacies AF2-3 of Smoot (1983), Facies 2, 4 and 5 of Crews and Ethridge (1993), *This study*
(ii)	***Floodplain Association***	Subfacies AF4 of Smoot (1983), Facies 3 of Crews and Ethridge (1993)
	1. Massive to planar bedded sandstone	*This study*
	2. Pedogenically-altered siliciclastic mudstone-sandstone	*This study*

were precipitated, frequently subaerially exposed and/or reworked by waves or sheetfloods.

(ii) *Littoral Association:* The littoral association consists of three predominantly carbonate lithofacies: (*1*). *Calcareous intraclastic conglomerate*; (*2*) *Ripple-laminated and massive calcareous sandstone*; and (*3*) *Non-columnar stromatolitic carbonate mudstone*. Lithofacies *1* and *2* are interpreted to reflect rapid deposition of reworked carbonate peloids and intraclasts in moderate to high energy littoral environments by unidirectional currents arising from storm-generated sheet floods and/or by oscillatory flow subsequent to rapid transgression (Smoot 1983; Pietras and Carroll 2006). Low-amplitude oscillatory ripple bedforms are sometimes present on bedding planes of calcareous sandstones, as are trace fossils dominated by high-density simple trails probably produced by insect larvae (Scott 2010; Scott and Smith 2015). Lithofacies *3* consists of flat-laminated to cumulate-laminated micrite, and was likely deposited in the photic zone or formed as a subaerial microbial/evaporitic crust. Reworked stromatolitic and palustrine association lithofacies are a probable source for silt- and sand-sized peloids that comprise lithofacies *1* and *2*.

(iii) *Salt-Pan Association*: This association is restricted to the south-central Bridger subbasin (Fig. 4.1; Burnside and Culbertson 1979; Wiig et al. 1995) and consists of two distinct lithofacies: (*1*) *Displacive evaporites*; and (*2*) *Bedded evaporites*, which consist predominantly of trona and halite and a host of other secondary evaporite minerals (Fahey 1962; Culbertson 1966; Deardorff and Mannion 1971; Wiig et al. 1995). Both lithofacies are preserved in the subsurface, and as recrystallized carbonate pseudomorphs in outcrop. Displacive evaporites cut across bedding, typically within carbonate mudstone, and include 2–8 mm diameter shortite rhombs and <10 cm diameter acicular trona fans and macrocrystalline vein fillings, which are interpreted to have precipitated post-depositionally from pore waters (Bradley and Eugster 1969; Roehler 1993; Pietras and Carroll 2006). Bedded evaporites preserve a range of textures, including primary anhedral to euhedral precipitates (e.g., blades, needles), mm-scale laminations, and rounded, 1–3 cm evaporite intraclasts (Bradley and Eugster 1969; Deardorff and Mannion 1971; Birnbaum and Radlick 1982). Together, these features are consistent with the precipitation of evaporite minerals from standing alkaline

bicarbonate brines during periods of intense evaporation, tractive reworking by occasional sheetflood events, and subsequent post depositional recrystallization.

(iv) *Profundal-Sublittoral Association:* This association consists of two fine-grained, predominantly carbonate lithofacies: (*1*) *Massive carbonate mudstone and marlstone*; and (*2*) *Laminated kerogen-rich carbonate mudstone and marlstone*. These facies reflect subaqueous deposition of primary micritic dolomite and calcite precipitated from the water column, mixed to varying degrees with organic matter, intraclastic carbonate silt, and terrigenous clays. Only rarely are very low-density, simple, small burrows preserved in mudstones of lithofacies *1* or *2* (Scott 2010; Scott and Smith 2015), and therefore the lack of lamination in lithofacies *1* appears unlikely to reflect bioturbation. Instead, we suggest that massive mudstone beds were deposited by hypopycnal plumes basinward of sites of fluvial input or in regions of entrainment during storm events (cf. Renaut and Gierlowski-Kordesch 2010). Primary productivity, clastic-dilution, and oxidation were likely the primary parameters controlling the concentration of organic matter and degree of lamination preserved within particular beds, all of which have long been hypothesized to relate to water depth and the degree of meromixis (Bradley 1970; Smoot 1983; Horsfield et al. 1994; Carroll and Bohacs 2001; Pietras and Carroll 2006). Organic-rich beds may however in some cases represent highly productive shallow water settings with negligible wave energy such as modern Lake Bogoria (Renaut and Tiercelin 1994), particularly where interbedded with evaporites. Several discrete, continuous horizons of profundal-sublittoral association lithofacies contain enriched U and Th concentrations, and can be correlated across the Bridger subbasin (Fig. 4.9 and Supplementary Fig. S4.1; Love 1964). Geochemical modeling by Mott and Drever (1983) suggests that these horizons were created via subaqueous replacement of calcite by uraniferous minerals precipitated from U-hypersaturated lake waters near the sediment-water interface during short periods of lowered pH due to freshwater input.

A. *Alluvial Macroassociation*

Fine-grained siliciclastic facies of the basin-center alluvial macroassociation occur within discrete 3–30 meter-thick intervals of the WPM in the interior of the Bridger subbasin. These intervals contain laterally discontinuous packages of channelized and cross-stratified arkosic sandstone and finer-grained planar-bedded to ripple-laminated to convolute-bedded, sometimes pedogenically-altered arkosic sandstone and siliciclastic mudstone. These horizons were first mapped as "sandstone siltstone mudstone" units A-I by Culbertson (1961), and subsequently briefly described by Love (1964), Smoot (1983, "Facies AS"), and Pietras and Carroll (2006, "Fluvial Association"). Alluvial macroassociation lithofacies contain sedimentary structures documented within inter-lacustrine fluvial horizons in the eastern GGRB (Rhodes et al. 2007) and the Uinta Basin (Remy 1992). Alluvial intervals are thicker and more heterolithic in the study area than they are in previously described areas of the Bridger subbasin (Pietras and Carroll 2006). Here we define six individual lithofacies that are broadly interpreted to have been deposited within a low-gradient distributary network of fluvial channels flowing across a broad, sometimes vegetated, and periodically inundated low-gradient floodplain into Lake Gosiute.

(i) *Axial Fluvial Association:* The axial fluvial association consists of two distinct sandy lithofacies which are interpreted to have been deposited within active stream channels: (*1*) *Trough cross-stratified and planar- to ripple-laminated sandstone*; and (*2*) *Drape-bedded sandstone*. Lithofacies *1* occurs as 1–10 m high channel forms, and consists of medium-grained sandstone arranged in shingled epsilon cross-sets (Fig. 4.11a), meter- to decimeter-scale trough

cross-stratification, and planar bedded horizons containing parting lineation on bedding planes. The lower portions of channel sets often exhibit multiple incision surfaces (Fig. 4.11a). Pebble-sized intraclasts of poorly-lithified mudstone and sandstone are often present at channel bases, and sometimes contain large fragments of reed stems and/or bone fragments (Fig. 4.11d), and are interpreted to be the products of cutbank erosion into floodplain deposits and channel levees. Simple trails and small vertical burrows (mm-diameter), probably produced by insect larvae, are occasionally preserved on the muddy upper bedding planes of rippled fining-upwards bedsets within channels (Scott 2010; Scott and Smith 2015). Lithofacies *1* is interpreted to have been deposited mainly by high-energy unidirectional currents within axial alluvial channels, with some periods of waning flow evidenced by trace fossils and mud-drapes on ripple bedforms. Lithofacies *2* consists of fine-grained sandstone that is often wave-rippled and arranged in 1–5 cm-thick normally graded beds. These beds are in turn often arranged in broad 2–10 m wide, ~1 m high hummocks that cap alluvial bedsets and are commonly directly overlain by overlying horizontally-bedded lacustrine mudstone (Fig. 4.11b). Drape-bedded sandstone lithofacies are here attributed to deposition under combined oscillatory and unidirectional flow resulting from rapid inundation and wave reworking of axial distributary channels by rising lake waters during transgressive events.

(ii) *Distal-Overbank Association*: This association encompasses two broad siliciclastic lithofacies: (*1*) *Climbing-rippled and planar-bedded sandstone and siltstone*; and (*2*) *Massive to faintly-bedded siltstone and mudstone*. These lithofacies are composed predominantly of green to brown siliciclastic sand, silt, and clay. Ubiquitous climbing-ripple cross-lamination (Fig. 4.11c) and convolute bedding within lithofacies *1* are indicative of rapid sedimentation by sediment-rich, decelerating currents (cf. Allen 1970) and subsequent dewatering-generated penecontemporaneous deformation. Bedding within lithofacies *2* ranges from mm-scale horizontal laminations to completely structureless and massive (Fig. 4.11f). Biogenic structures in distal-overbank association lithofacies include mammal footprints, bird footprints, carbonaceous rhizoliths, and insect burrows, tunnels and trails that indicate subaerial exposure of the substrate (Fig. 4.12k; Scott 2010; Scott and Smith 2015). Weakly developed paleosols within lithofacies *2* preserve mm-scale iron-stained root marks, internal brecciation (Fig. 4.11e), and desiccation cracks (Bohacs et al. 2007; Scott 2010). The distal-overbank association is attributed to overbank sedimentation onto broad low-gradient plains, with sediment accumulation distal to distributary networks feeding into shallow bodies of standing water (including Lake Gosiute), crevasse splays from trunk channels onto floodplains, and deposition via suspension fall-out in abandoned distributary channels.

II. Basin Peripheral Facies Belt

The basin peripheral facies belt extends ~5 km basin into the southern Bridger subbasin adjacent to the Uinta Uplift. It comprises a suite of lithofacies that are compositionally-distinct from those observed in the basin interior.

L. *Lacustrine Macroassociation*

Basin peripheral lacustrine facies are calcite-rich and lacking in dolomite, which presumably may be related to the input of Ca-rich waters from Uinta Uplift streams. These lacustrine deposits contain a diverse trace fossil assemblage that suggests the lake was fresh and oxygenated near to where these streams entered it.

(i) *Palustrine Association:* The palustrine association consists of two lithofacies interpreted to have been deposited near or slightly above lake level: (*1*) *Silty mudcracked and/or bioturbated carbonate mudstone*; and (*2*) *Calcareous aeolian sandstone*

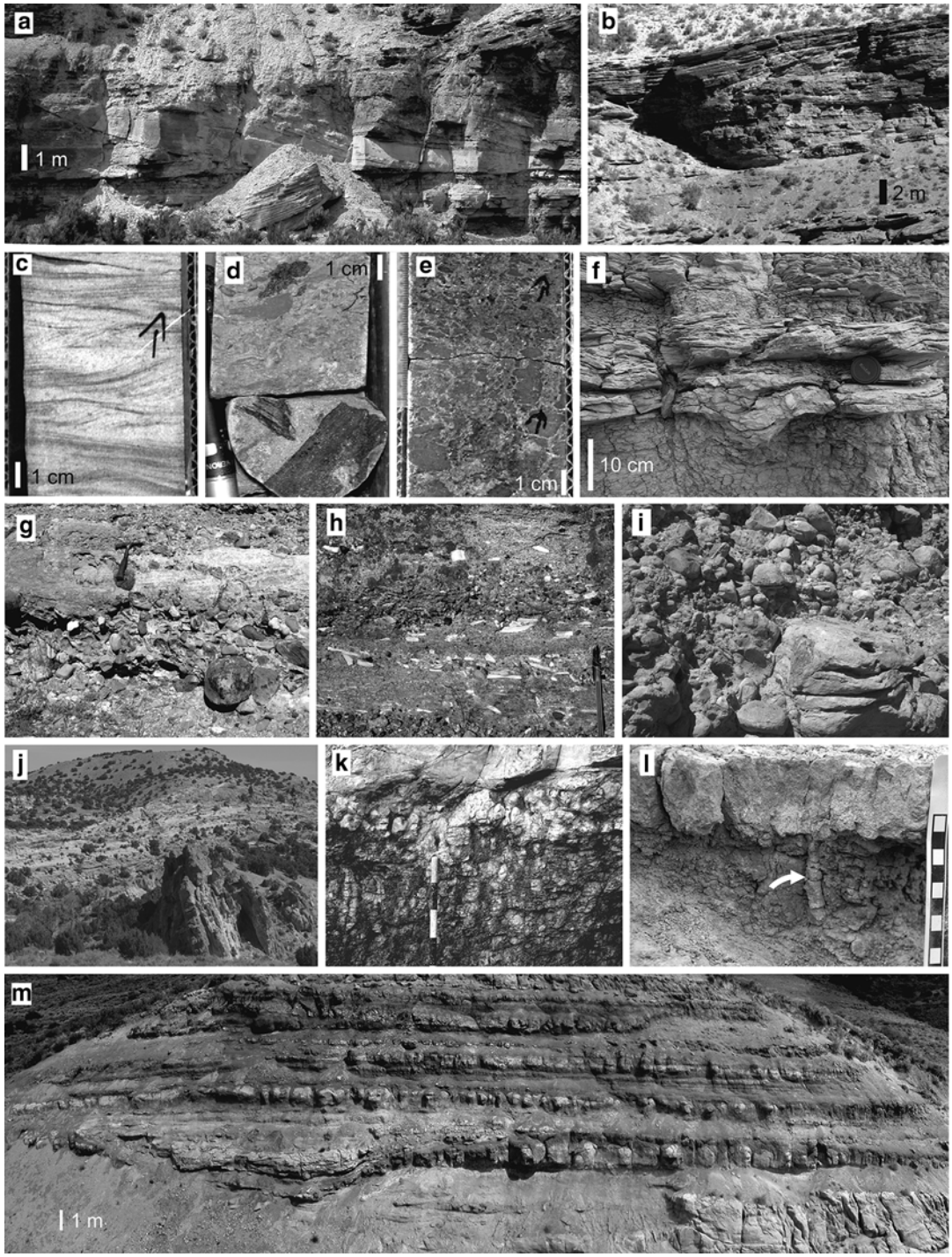
a
1 m
b
2 m
c
1 cm
d
1 cm
e
1 cm
f
10 cm
g
h
i
j
k
l
m
1 m

and siltstone. Lithofacies *1* is differentiated from its basin interior palustrine counterpart (lithofacies *I-Li*) primarily by the absence of dolomite and the increased density and diversity of trace fossils (Fig. 4.12h–j). The silty micritic carbonates exhibit both polygonal shrinkage cracks and bladed, disconnected syneresis cracks (Fig. 4.12e, g). Lithofacies *1* strata are interpreted to have been deposited in a frequently exposed oxygenated nearshore environment that experienced a high influx of fine-grained carbonate and/or autochthonous production of fine crystalline $CaCO_3$ (Freytet and Verrecchia 2002). The sediments were populated by arthropods (e.g., insects) and vermiform animals (e.g., oligochaetes and/or insect larvae). Rare syneresis cracks record the occasional local inundation by saline lake waters of Lake Gosiute. Lithofacies *2* consists of well-sorted peloids and sub-angular to sub-rounded fine-grained quartz clasts arranged in 5–10 cm-thick high-angle cross sets. Occasional 1–3 cm-diameter rhizoliths occur within. Lithofacies *2* is interpreted to reflect deposition by occasionally vegetated aeolian dunes in lake marginal areas (cf. Magee and Miller 1998).

(ii) *Littoral Association:* The littoral association consists of three lithofacies: (*1*) *Tufa-travertine and massive carbonate*; (*2*) *Oscillation-rippled sandstone*; and (*3*) *Massive fine-grained sandstone*. These facies reflect physical and chemical sedimentation of materials derived from the Uinta Uplift that were deposited in a broad array of shallow subaqueous to subaerial sedimentary environments. Carbonate production was likely enhanced by wave agitation and the influx of dissolved Ca^{2+} in streams waters flowing into the bicarbonate-oversaturated Lake Gosiute. Deposits of lithofacies *1* occur as geographically isolated 10 cm to 30 m high buildups, mounds, or biostromes composed of calcite and/or silica (Fig. 4.13a, b). Fabrics within these structures include laminated stromatolitic travertine (Fig. 4.13c, d) and massive or brecciated mounds of porous tufa. Tetrapod and insect trackways within associated sediments indicate at least occasional subaerial exposure of these units (Scott 2010; Scott and Smith 2015). At the southern basin periphery, the mounds within the WPM are largest and laterally widespread in the vicinity of the Canyon Road Fan (Fig. 4.6), and are most abundant just below the stratigraphic contact with the overlying Laney Member (Fig. 4.13). Lithofacies *1* deposits may reflect the rapid precipitation of calcite via mixing of Ca^{2+}-rich meteoric waters and/or fault-derived

Fig. 4.11 Photographs of alluvial lithofacies of the Wilkins Peak Member. Basin interior lithofacies: (**a**) epsilon cross stratification within channelized sandstone (lithofacies *I-Ai1*) within Basin interior alluvial unit C, Sage Creek Canyon; (**b**) drape bedding (lithofacies *I-Ai2*) capping alluvial unit D, Firehole Canyon; (**c**) climbing rippled fine-grained sandstone (lithofacies *I-Aii1*), *BF* core; (**d**) fossilized reeds within intraclastic conglomerate (lithofacies *I-Ai1*), *BF* core; (**e**) brecciated silty siliciclastic mudstone (lithofacies *I-Aii2*) in *BF* core; (**f**) finely bedded silty siliciclastic mudstone (lithofacies *I-Aii2*) intercalated with climbing-ripple cross-laminated sandstone (lithofacies *I-Aii1*) within alluvial unit B, note scour at base of sandstone bed. Basin peripheral lithofacies: (**g**) conglomerate (lithofacies *II-Ai1*) composed of limestone and sandstone clasts of Paleozoic strata interbedded with quartzose, trough cross-stratified sandstone (lithofacies *II-Ai2*), *PP* section, note hammer for scale; (**h**) Late Paleocene basal pebble conglomerate containing angular chips of Cretaceous shale, angularly overlies Lower Cretaceous Dakota Formation north of Goslin Mountain (base of the *RM* section); (**i**) crudely stratified conglomerate (lithofacies *II-Ai1*), *PP* section, note lens cap atop largest boulder; (**j**) onlap of upper WPM-equivalent alluvial strata onto vertical, E-W-striking beds of Paleocene strata, *LV* section; (**k**) paleosol horizon (lithofacies *II-Aii2*) overlain by massive sandstone bed (lithofacies *II-Aii1*) in *SC* section, illustrating blocky vertically-oriented peds and concretions; (**l**) vertical, sand filled burrow extending into pedogenically altered horizon (lithofacies *IIBii2*) from overlying sand bed, *SC* section, scale in cm; (**m**) roadcut of Cathedral Bluffs Member near *LM* section showing nested alluvial channels filled with trough cross-laminated pebbly quartzose sandstone (lithofacies *II-Ai12*) and overlain by fine overbank sandstones and paleosols (lithofacies association *II-Aii*)

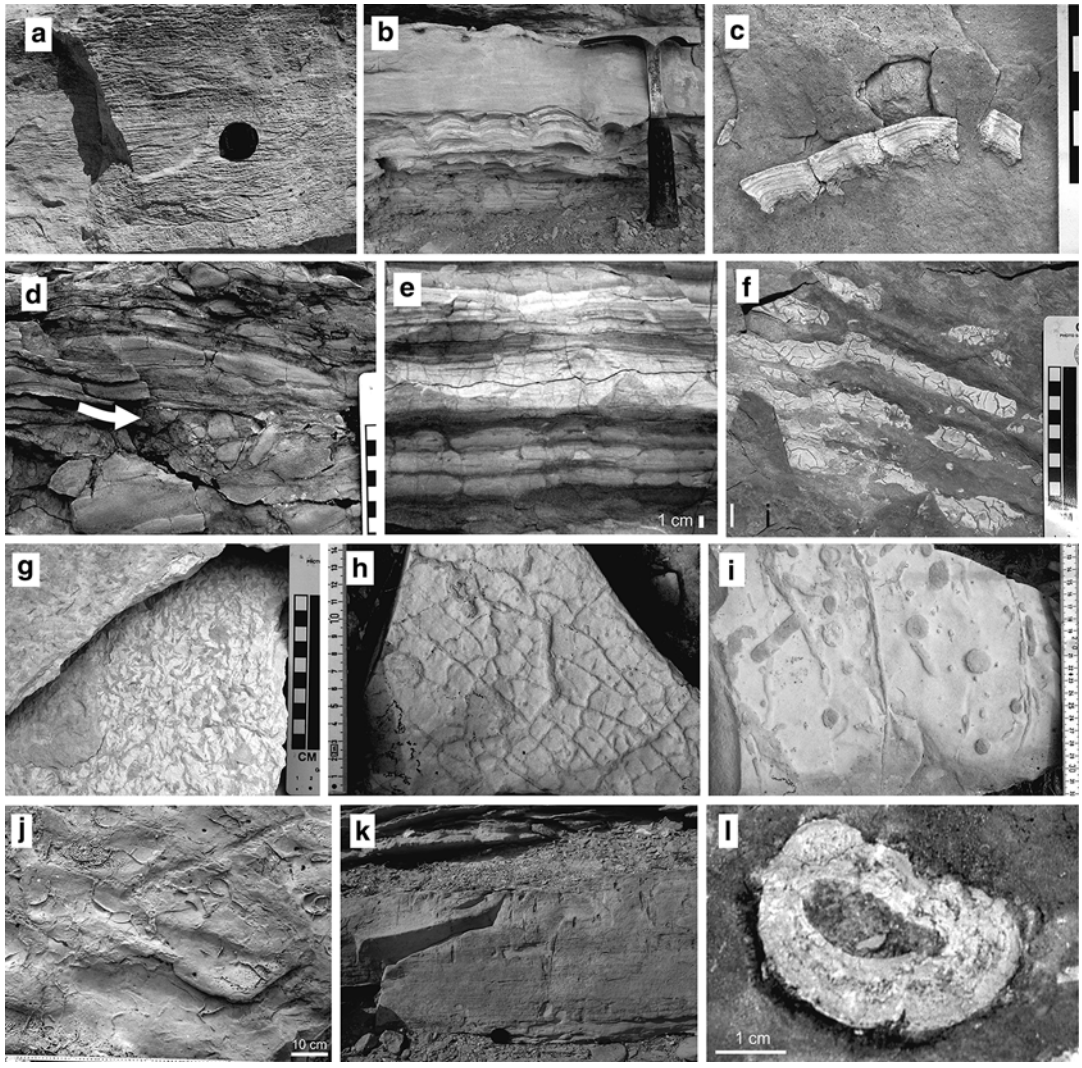

Fig. 4.12 Photographs of basin peripheral lacustrine lithofacies: (**a**) oscillation ripples in fine-grained quartzose sandstone (lithofacies *II-Lii2*), *PB* section; (**b**) stromatolitic laminations (lithofacies *II-Lii1*) atop silty mudstone (lithofacies *II-Li1*) overlain by fine-grained calcareous sandstone (lithofacies *II-Lii3*), *SC* section; (**c**) travertine intraclast within massive peloid and quartz sandstone (lithofacies *II-Lii3*), *PB* section; (**d**) intraclastic conglomerate containing carbonate mudstone clasts overlain by laminated silty micritic carbonate (lithofacies *II-Liii2*), *PB* section; (**e**) mudcracks in cm-bedded silty micrite (lithofacies *II-Li1*), *PB* section; (**f**) mudcracks in mud drapes in troughs between symmetric ripples (lithofacies *II-Lii2*), *PB* section; (**g**) mudcracked micritic carbonate (lithofacies *II-Li1*), *PB* section, note crude alignment of blade-shaped cracks; (**h**) complex network of 2–8 mm wide vertical and horizontal burrows and mudcracks in silty carbonate mudstone (lithofacies *II-Li1*), *PB* section; (**i**) ~1 cm wide vertical and horizontal burrows in carbonate mudstone (lithofacies *II-Li1*), *PB* section; (**j**) surface traces and/or mudcracks atop rippled bedding plane, *PB* section; (**k**) vertical ~1/2 cm burrows through massive to wave-ripple cross laminated sandstone (lithofacies *II-Lii3*), *PB* section, lens cap for scale; (**l**) mudchip-filled root cast with stromatolitic coating, *PB* section; surrounding material is massive fine calcareous sandstone

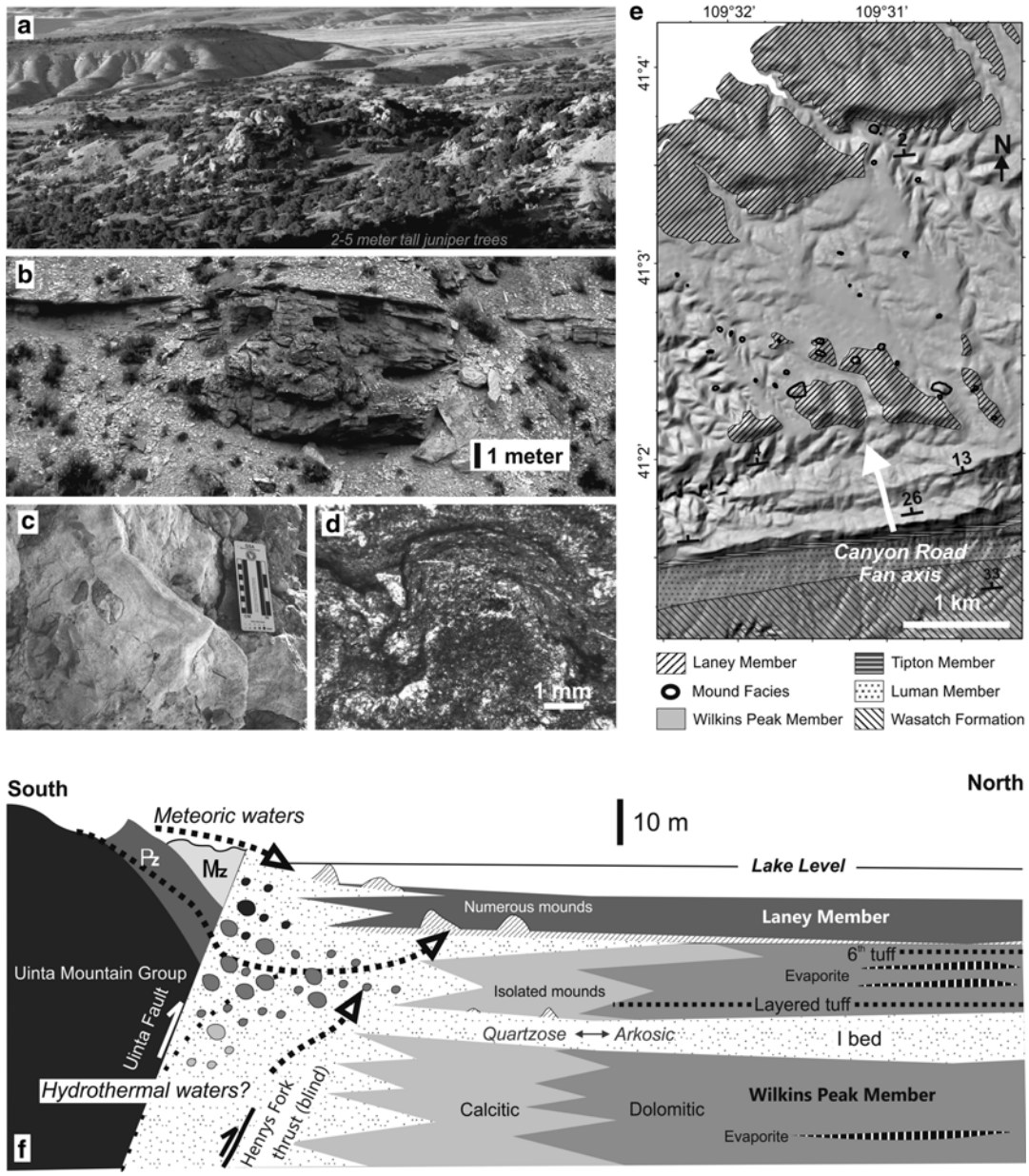

Fig. 4.13 Carbonate mounds adjacent to the Uinta Uplift (lithofacies *II-Lii1*): (**a**) 10–20 m high carbonate mounds near the base of the Laney Member north of the Canyon Road Fan, north of Canyon Road Fan; (**b**) meter-scale carbonate buildup and laterally equivalent finely-bedded silty carbonate; (**c**) travertine filling intergranular porosity within conglomerate bed, *SC* section; (**d**) photomicrograph of microbially-laminated carbonate from WPM spring mound; (**e**) map showing areal distribution of carbonate mounds to the north of the Canyon Road Fan and their relation to axis of Canyon Road Fan; (**f**) interpretive N-S cross section of canyon road fan showing carbonate in relation to clastic and lacustrine units and onlap of Laney Member, and hypothesized pathways for solute-bearing waters to mound sites (cf. Jones and Deocampo 2003)

hydrothermal waters with bicarbonate-supersaturated lake waters and/or CO_2 degassing at the surface (Fig. 4.13f; cf. Jones and Deocampo 2003). Similar deposits within the WPM are located near site *BG* (Fig. 4.4; Mayry 2007) and in the NW corner of the Bridger subbasin (Leggitt and Cushman 2001).

Intraclasts of stromatolite or travertine observed in lithofacies *2* and *3* (Fig. 4.12c) support the hypothesis of Smoot (1983) that peloids, which comprise the bulk of these lithofacies, were derived via reworking of lake-fringing carbonate crusts during storms events. Lithofacies *2* consists of well cemented peloidal calcareous and quartzose sandstones and siltstones that are typically present in 2–40 cm-thick normally graded beds, or in wavy- to flaser-bedded units containing wave ripples with mud drapes (Fig. 4.12f). Lithofacies *2* is interpreted to represent deposition in storm- and/or wave-influenced shoreface to backshore environments at the toes of fan deltas. Massive sandstones of lithofacies *3* is compositionally similar to lithofacies *2*, but are massive to faintly-bedded, likely due to disruption by bioturbation. Trace fossils common in lithofacies *2* and *3* were apparently produced in oxygenated shallow lacustrine substrates (Fig. 4.12g–k).

(iii) *Sublittoral Association*: The sublittoral association consists of two fine-grained lithofacies: (*1*) *Massive carbonate mudstone and marlstone*; and (*2*) *Laminated carbonate mudstone and marlstone*. Both facies contain silt- to clay-sized calcite and siliciclastic grains in varying proportions, and differ from basin interior profundal-sublittoral lithofacies by their calcitic composition and relative paucity of organic matter. Lithofacies *1* consists mainly of structureless to crudely horizontally bedded silty carbonate mudstone, and is commonly found laterally adjacent to tufa-travertine lithofacies (*II-Lii1*). Lithofacies *1* may have resulted from either the fallout deposition from hypopycnal flows during storm events and/or the rapid deposition of interlaminated micritic $CaCO_3$ surrounding springs of Ca^{2+}-rich water. Lithofacies *2* deposits contain 1–2 mm-thick laminae of carbonate and/or siliciclastic mud that are largely devoid of organic matter. These shaley mudstones are similar to laminated kerogen-poor micrite lithofacies present in Fossil Basin (Buchheim and Eugster 1998). Laminae in lithofacies *2* are typically ~10 times thicker than typical laminae in basin center profundal deposits (0.1 mm; Bradley 1929; Ripepe et al. 1991). Some strata representing lithofacies *2* contain bedding-plane assemblages of plant and insect fossils (lower Little Mountain site; Wilf 2000; Smith et al. 2008b). The preservation of fine laminae and fossil leaves, as well as the rarity of trace fossils suggests fallout deposition of fine carbonate mud in anoxic bottom waters with little post-depositional disturbance by waves, plants, or animals.

A. *Alluvial Macroassociation*

Basin peripheral alluvial lithofacies are quartzose, coarse-grained, and often pedogenically altered. They are interpreted to have been deposited by streams flowing atop alluvial fans that extended basinwards from the Uinta Uplift and were infrequently inundated by lake water.

(i) *Fan Delta Association:* The fan delta association consists of: *(1) Conglomerate*, containing granule- to boulder-sized clasts of Mesozoic, Paleozoic and Proterozoic sandstone, carbonate and quartzite; and (*2*) *Trough cross-stratified sandstone*, consisting of medium- to very coarse-grained quartzose to sub-lithic sandstone (Fig. 4.4a). Lithofacies *1* predominantly consists of well-sorted, matrix-supported, commonly imbricated conglomerate beds (Fig. 4.11g, i). The conglomerates are often interbedded with trough cross-stratified sandstone of lithofacies *2* (Fig. 4.11g, h, m). Facies 1 and 2 together likely represent deposition by

downstream-accreting dunes and sandy gravel sheets within alluvial fan distributary channels (cf. Miall 1978; DeCelles et al. 1991a; Crews and Ethridge 1993). Isolated, matrix-supported, poorly-sorted, sometimes coarsening-upwards conglomerate beds suggest occasional deposition by debris flows, or alternatively reflect fine sediment supply limitation during the waning stages of flood events (i.e., Topping et al. 2000). Lithofacies *2* sandstones commonly contain granule- to pebble-sized clasts in their D_{95} size fraction, and are arranged in meter-scale trough cross-stratified units. The coarsest deposits of lithofacies *1* and *2* at any particular location are confined to laterally shingled 10–100 m-wide channel forms incised into underlying strata (Fig. 4.11m). These channel forms reflect multiple avulsion events that led to incision and infill of steeply sided trenches in the fan surface (cf. DeCelles et al. 1991a; Crews and Ethridge 1993). Within the southern Bridger subbasin, the fan delta association is confined to three 0.5–1 km-thick, 3–6 km wide macro-scale deposits distributed E-W along the strike of the Uinta and Henrys Fork thrusts, and are laterally surrounded by finer-grained alluvial and/or lacustrine deposits (Fig. 4.6a; Anderman 1955; Wiegman 1964; Crews and Ethridge 1993; Roehler 1993). The axes of macro-scale fan-delta deposits presumably mark the sites where steep-gradient gravel-bed trunk streams that drained the north flank of the Uinta Uplift emptied into the GGRB.

(ii) *Floodplain Association*: The floodplain association consists of two lithofacies: (*1*) *Massive to planar-bedded sandstone*; and (*2*) *Pedogenically altered siliciclastic sandstone and siltstone*. Lithofacies *1* consists of massive to planar-bedded fine- to very coarse-grained quartzose to sub-lithic sandstone. Normal grading is apparent in some individual beds, as is rare trough cross-lamination. Lithofacies *2* consists primarily of brightly colored red, purple and green horizons of siliciclastic mudstone and sandstone. In many sandstone beds, detrital quartz grains are contained within a matrix of authigenic clay derived from former framework grains. These horizons are often discontinuous due to multiple incision surfaces that occur within strata of the basin peripheral alluvial macroassociation (Fig. 4.11m). These facies contain post-depositional features suggestive of a wide range of soil conditions (pH, redox). Pedogenic features include rhizoliths, carbonate concretions and calcic horizons (Fig. 4.11k), clay-lined aggregates arranged in regularly spaced bowl-shaped structures (Fig. 4.11m), and vertical burrows likely produced by crustaceans and/or insects (Fig. 4.11l). Paleo-vertisols of lithofacies *2* likely formed on the medial to distal toes of lake-marginal alluvial fans during extended periods of subaerial exposure, with the growth of vegetation into sediments deposited during episodic flood events (cf. Braunagel and Stanley 1977; Kraus and Brown 1988; Retallack 1988; Kraus and Aslan 1993).

4.4.2 Stratigraphic Correlation

Ash horizons, gamma ray logs, Fischer Assay oil shale records, and alluvial marker beds were used to correlate time-equivalent interior and peripheral strata (Fig. 4.14). The stratigraphic cross sections of the WPM between the Uinta and Wind River uplifts shown in Figs. 4.5, 4.6, 4.7 and Supplementary Fig. S4.1 (at http://extras.springer.com) represent a synthesis of new stratigraphic observations and published stratigraphy (Stuart 1965; Smoot 1983; Pietras and Carroll 2006).

4.4.2.1 Ash Beds

Ash horizons are the primary basis for correlation within the Bridger subbasin (Figs. 4.3, 4.5, and S1). These are present mainly within fine-grained intervals of lake strata (*I-Liv*) (Smith et al. 2003) and are commonly clearly differentiated from surrounding strata by their gray to orange color in outcrop and white color in core. Green River Formation ash beds typically con-

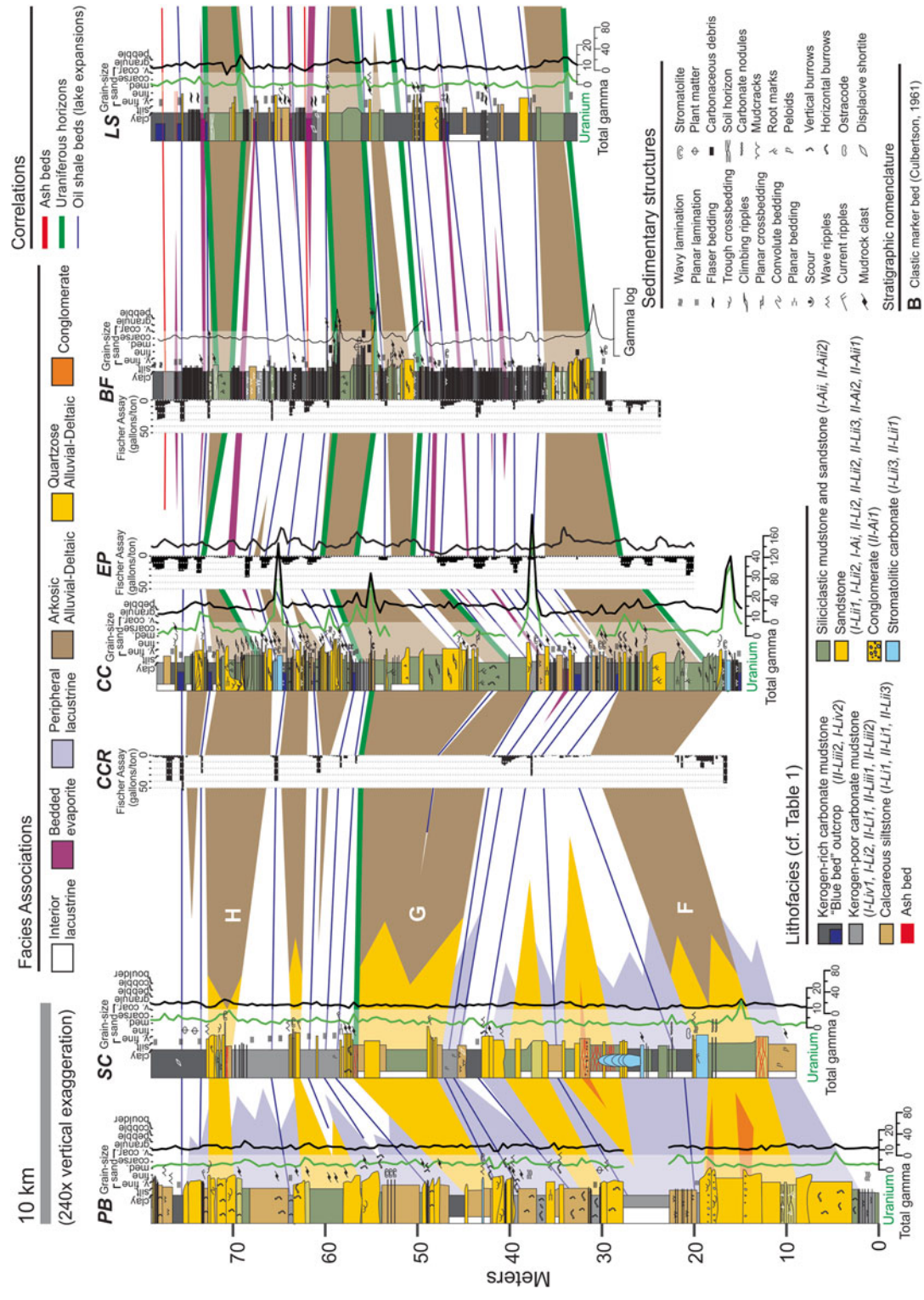

Fig. 4.14 Detailed cross section of the F through H marker bed interval showing correlation of intertongued alluvial and lacustrine basin interior and basin peripheral facies of the Wilkins Peak Member. Fischer assay for the *CCR* and *EP* cores from Mason (1987). Section labels follow key to Fig. 4.4

tain an assortment of phenocrysts encased in a matrix of zeolite minerals and/or authigenic feldpar formed via the alteration of primary volcanic glass ash (Goodwin and Surdam 1967; Smith et al. 2003). In several cases (e.g., the Firehole and Layered tuff beds), mm-scale fallout horizons within ash beds can be correlated basin-wide, and thin to the south away from likely volcanic sources in the Challis and Absaroka volcanic centers (cf. Smith et al. 2008b).

4.4.2.2 Gamma Ray Spectrometry

Laterally continuous radioactive zones containing uranium-rich phosphates within basin interior WPM strata were first recognized by Love (1964) and are used as a secondary correlation tool. These zones occur primarily within fine-grained marlstone intervals (*I-Liv*), and are most prominent within or adjacent to basin interior alluvial beds (Fig. 4.9 and Supplementary Fig. S4.1, which can be accessed at http://extras.springer.com). These radioactive zones cross-cut lateral facies changes in basin interior strata but do not all extend to the basin periphery. Geochemical modeling by Mott and Drever (1983) suggests that U-rich zones record basin-wide geochemical events associated with the lowering of the pH of otherwise highly alkaline, U-soluble lake waters, which is consistent with their basin-wide distribution and apparent isochroneity.

4.4.2.3 Lithostratigraphy

Two distinct types of marker beds occur within the WPM, and are here used as tertiary correlation tools: (1) nine olive-brown alluvial beds (beds A-I of Culbertson 1961) can be traced in outcrop and aerial photography for tens of kilometers across the Bridger subbasin (Culbertson 1961; Love 1964; Stuart 1965; Smoot 1983; Pietras and Carroll 2006); and (2) lacustrine expansion-contraction cycles occur within lacustrine intervals, and can often be correlated using highstand deposits or "oil shale beds" (lithofacies *I-Liv2*), which correspond to discrete (0.1–2 meter-thick) intervals of elevated kerogen content in Fischer assays logs (>20 L/t, up to 160 L/t) that can be correlated across much of the Bridger subbasin (Fig. 4.5 and Supplementary Fig. S4.1, which can be accessed at http://extras.springer.com). Expansion-contraction cycles have been assigned by previous workers to 70+ named beds (Burnside and Culbertson 1979; Roehler 1991b, 1992c, 1993; Culbertson 1998) based on Fischer assay logs (Fig. 4.9).

4.4.3 Lithofacies Stacking Patterns

Repetitive stacking of lithofacies occurs at two characteristic scales within both the interior and peripheral belts of the WPM (Fig. 4.14): (1) 0.1–6.0 meter-thick lacustrine expansion-contraction cycles bounded by flooding surfaces (Eugster and Hardie 1975; Smoot 1983; Fischer and Roberts 1991; Roehler 1993; Pietras et al. 2003b); and (2) 3–30 meter-thick oscillation between lacustrine and alluvial lithofacies (Culbertson 1961; Aswasereelert et al. 2013; Smith et al. 2014). The Green River Formation has long been suspected of recording orbital periodicities (Bradley 1929; Fischer and Roberts 1991; Roehler 1993), but the causal links between lithofacies stacking patterns and specific orbital changes to insolation have remained elusive. Based on $^{40}Ar/^{39}Ar$ geochronology and macrostratigraphy-based spectral analysis (Machlus et al. 2008; Meyers 2008; Smith et al. 2008b; Smith et al. 2010; Aswasereelert et al. 2013), the vertical stratigraphic oscillation between lacustrine and alluvial facies is the most prominent variation and likely coincides with the 100 k.y. eccentricity (Fig. 4.3). Lacustrine expansion-contraction cycles, which have been hypothesized to reflect precession cycles (Fischer and Roberts 1991; Roehler 1993), were of shorter apparent duration (5–30 ka; Pietras et al. 2003b), and exhibit a less well-defined spectral signature (Machlus et al. 2008; Aswasereelert et al. 2013).

4.4.3.1 Lacustrine Expansion-Contraction Cycles

Lacustrine expansion-contraction cycles within the WPM are expressed differently at interior versus peripheral locations, presumably due to differences in sediment type(s) and basin hypsometry. In the basin interior (Fig. 4.9), 0.1–6.0

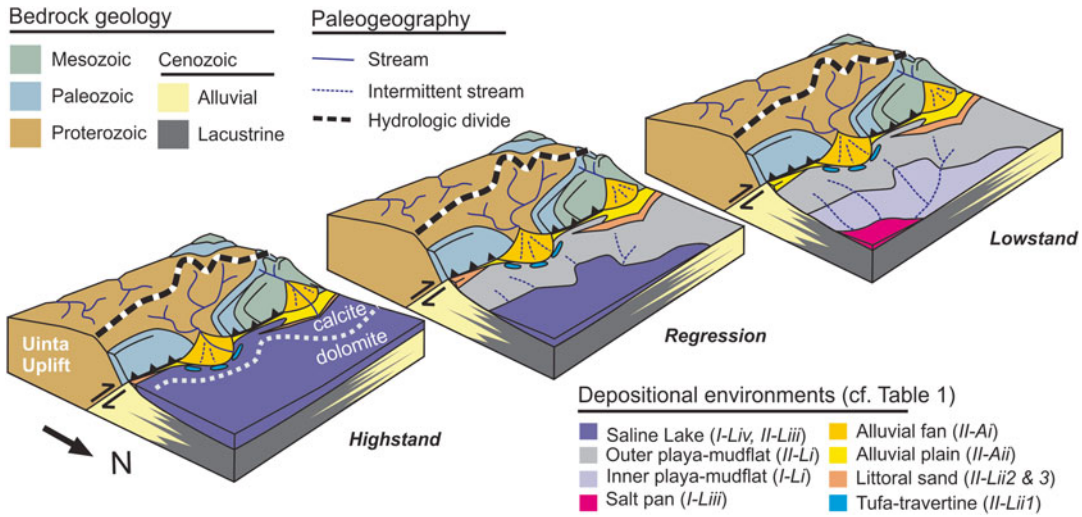

Fig. 4.15 Lithofacies interpretation diagrams illustrating characteristic depositional environments in the southern Bridger subbasin during ca. 5–30 ky-duration lacustrine expansion-contraction cycles. Note that arkosic bedload from the Aspen River was prevented from entering the Bridger subbasin during lacustrine modes. During alluvial modes (not depicted), alluvial environments would have filled the basin

meter-thick expansion-contraction cycles occur within lacustrine intervals. These typically consist of a thin transgressive basal lag of intraclastic conglomerate (lithofacies *I-Lii1*) and/or calcareous sandstone (lithofacies *I-Lii2*) that is overlain by organic-rich carbonate mudstone (lithofacies *I-Liv2*), and capped by mudcracked carbonate mudstones and siltstones of lithofacies *I-Li2* (Eugster and Hardie 1975; Pietras and Carroll 2006). In the subsurface depocenter of the Bridger subbasin ~10 km west of the Rock Spring Uplift, expansion-contraction cycles often culminate in evaporites (lithofacies *I-Liii1* and *2*). Strata at the basin periphery contain similarly-scaled lacustrine expansion-contraction cycles to those in the basin interior (Fig. 4.10), but are notably lacking in dolomite and evaporate minerals. A simple three step model that accounts for the observed differences between basin interior and basin peripheral lacustrine cycles as expressed across the Bridger subbasin is shown in Fig. 4.15. Oscillation-rippled sandstone (lithofacies *II-Lii2*) and isolated tufa-travertine deposits (lithofacies *II-Lii1*) comprise the expanded transgressive portion of the cycle. Thin intervals of sublittoral mudstones (lithofacies *II-Liii1*) deposited during highstands of Lake Gosiute typically overlie transgressive facies, and are in turn overlain by palustrine (*II-Li*), littoral (*II-Lii*), or alluvial (*II-A*) lithofacies deposited during recession and lowstand.

4.4.3.2 Lacustrine-Alluvial Cycles

Although not featured prominently in previous investigations of GRF cyclicity, macrostratigraphy-based spectral analysis of the WPM by Aswasereelert et al. (2013) indicated that the most prominent and regular repeating arrangement of facies within the WPM is the oscillations between the lacustrine and alluvial macroassociations. Sedimentology, $\delta^{13}C$ geochemistry and $^{40}Ar/^{39}Ar$-based cyclostratigraphy led Smith et al. (2014) to conclude that lacustrine intervals represent high eccentricity while alluvial phases represent low eccentricity (Fig. 4.16). Lacustrine intervals are composed of strata arranged in lacustrine expansion-contraction cycles which can themselves often be correlated basin-wide (Fig. 4.5). Within alluvial intervals, beds of particular lithofacies are much less con-

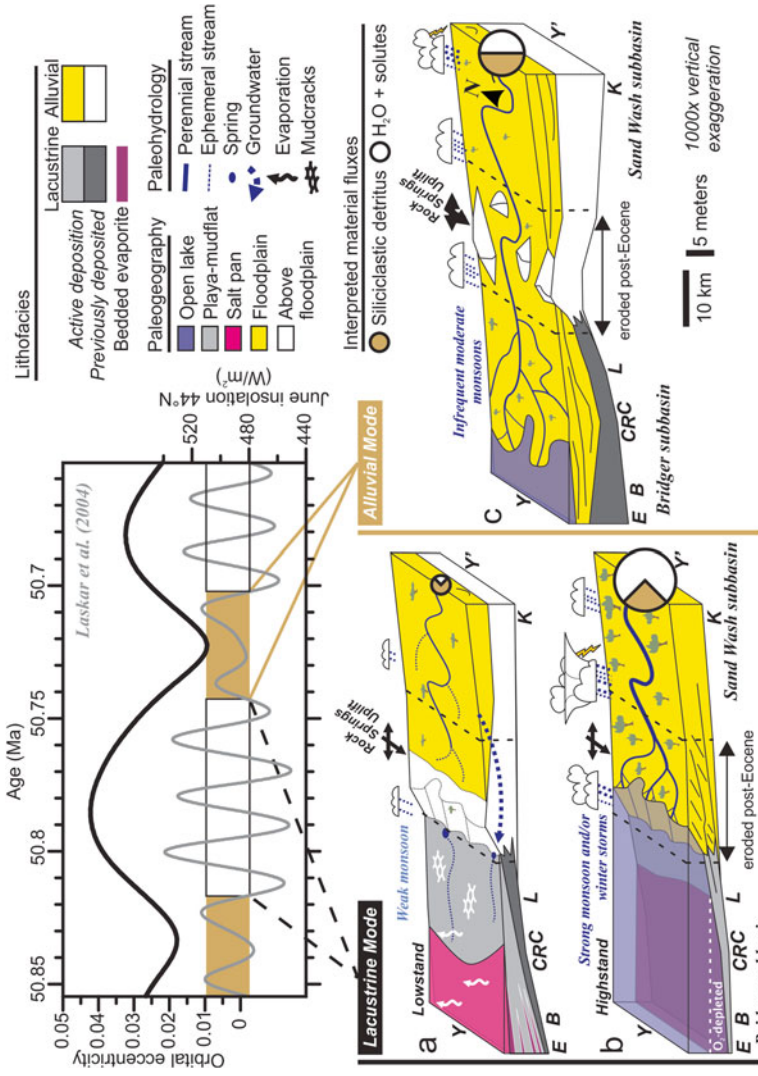

Fig. 4.16 Depositional environments along the axis of the Aspen River within the Uinta trough (cross section U-U', Fig. 4.4) during oscillations between (**a**) lacustrine highstand; (**b**) lacustrine lowstand, and (**c**) alluvial modes. *RSU* indicates the plunging southern terminus of the Rock Springs Uplift

tinuous due to the migration of fluvial channels and distributary networks.

The gradiational versus abruptness of transitions between lacustrine to alluvial lithofacies and alluvial to lacustrine lithofacies differ at peripheral versus interior locales. Alluvial to lacustrine transitions in the basin interior are often marked by abrupt transitions from drape-bedded sandstone (lithofacies *I-Ai2*) to microlaminated profundal micrites (lithofacies *I-Liv2*, Fig. 4.11b). Basin interior lacustrine to alluvial transitions are more gradational (Fig. 4.9). Cycle asymmetry is reversed at the basin periphery relative to cycles in the basin center. Alluvial to lacustrine transitions at the basin periphery are typically gradational, whereas lacustrine to alluvial transitions are abrupt and marked by incision of fluvial channels into subaerially exposed lacustrine facies (Fig. 4.11).

4.4.4 Basin-Scale Accumulation Patterns

Accumulation rates calculated using $^{40}Ar/^{39}Ar$ ages indicate that accommodation remained relatively stable over multi-million year intervals (Fig. 4.17). Maximum accumulation shifted from a Paleocene foredeep outboard of the Wind River Uplift to an Early Eocene foredeep adjacent to the Uinta Uplift (Beck et al. 1988). The most rapid accumulation in the Uinta Uplift foredeep (490 m/m.y.) occurred during deposition of the 'main body' of the Wasatch Formation, with rates diminishing to less than 200 m/Ma during the subsequent deposition of the Green River Formation. A roughly 2:1 asymmetry of basin fill between the Uinta Uplift foredeep in the southern Bridger subbasin (site EP: Fig. 4.17) and center of the GGRB (site Y: Fig. 4.17) was maintained throughout Paleogene deposition.

Strata of the WPM are remarkably laterally continuous north to south across the Bridger subbasin (Fig. 4.5). Internally, the WPM thickens from north to south by a factor of 3 into its depocenter in the Uinta Uplift foredeep due to both to the updip pinching out of lacustrine expansion-contraction cycles (Pietras and

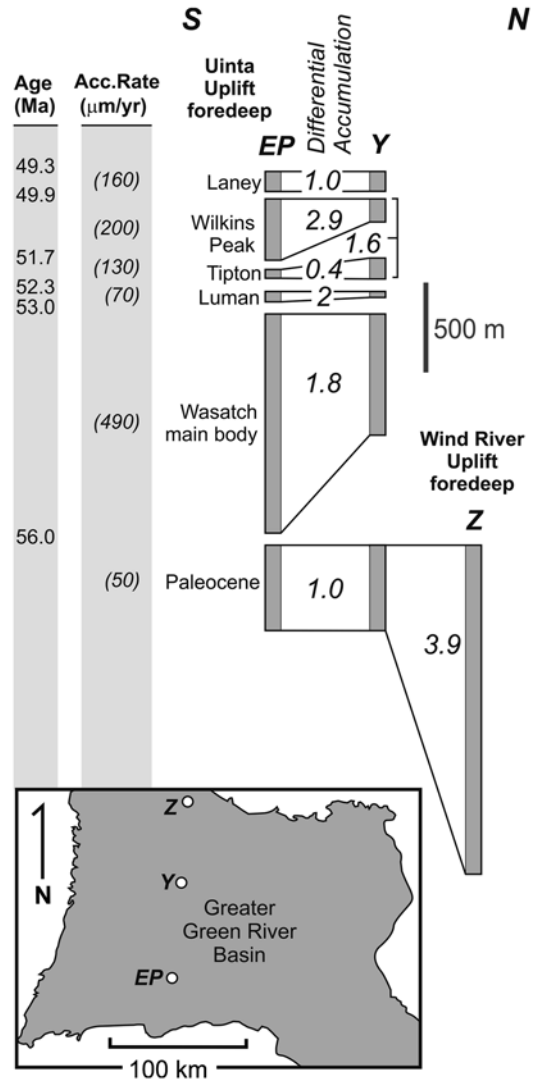

Fig. 4.17 Radioisotopically calibrated accumulation rate variations across the GGRB, illustrating the shift from a northern to southern depocenter during deposition of the main body of the Wasatch Formation and accumulation variations within the Green River Formation

Carroll 2006) and the presence of basin interior alluvial and evaporite lithofacies in the depocenter (Fig. 4.5). Within the WPM depocenter, alluvial beds are thickest and coarsest along the southeastern edge of the Bridger subbasin, near the apparent entry point for the Sand Wash River (Fig. 4.7). Bedded evaporates are by contrast confined to a depocenter in the west-central portion of Bridger subbasin (Fig. 4.1; Burnside and

Culbertson 1979; Wiig et al. 1995). Lacustrine intervals become thickest adjacent to the Uinta Uplift, where enhanced carbonate production by Ca-rich streams draining Paleozoic carbonates entered the bicarbonate-oversaturated but Ca-undersaturated waters of Lake Gosiute (cf. Church and Buchheim 2002; Smith et al. 2008b). Enhanced carbonate precipitation is consistent with spring deposits adjacent to the Uinta Uplift (Fig. 4.15) and with a tenfold increase in typical laminae thicknesses at the basin periphery relative to basin interior.

4.4.5 Clastic Provenance

The WPM and equivalent alluvial strata are geographically segregated into distinct arkosic and quartzose compositions (Fig. 4.4b). These each reflect a distinctly different sediment source composition, transport path, and drainage basin gradient. Sandstones deposited within 5 km of the Uinta Uplift along the southern periphery of the Bridger subbasin have quartzose to sub-lithic compositions (Fig. 4.4a). Uinta Uplift-derived sandstones often contain quartz grains with quartz-cemented rims, and are commonly interbedded with granule- to boulder-sized clasts of pre-Cenozoic bedrock derived from the Uinta Uplift. Paleocurrent indicators within these quartzose sandstones and conglomerates (trough orientations, pebble imbrication) are consistently north-directed. In contrast, channelized sandstone facies (*I-Ai1*) in basin interior alluvial units are relatively fine-grained and arkosic (~50 % feldspar; Fig. 4.4b). Basin interior sandstones contain biotite, muscovite, green amphibole, and metamorphic lithic grains, and they exhibit widely scattered west- and southwest-directed paleoflow indicators (Fig. 4.4a). Based on the differences listed above, we concur with Smoot (1983) that the basin interior sandstones were derived from crystalline basement uplifts east of the Bridger subbasin rather than from the Uinta Uplift.

4.4.5.1 Unroofing of the Uinta Uplift

J.W. Powell (1876) was first to note the sequential appearance of Cretaceous mudstone, Paleozoic carbonate, and Precambrian quartzite in Cenozoic conglomerates deposits adjacent to the Uinta Uplift, and subsequent studies have documented similar sequences within Paleogene strata along its flanks (Hansen and Bonilla 1954; Wiegman 1964; Crews and Ethridge 1993). Phanerozoic bedrock of the Uinta Uplift (Fig. 4.6b) consists of a thin interval (~500 m) of Cambrian through Mississippian carbonate strata overlain by ~2 km of Pennsylvanian through Cretaceous sandstone and siliciclastic mudstone (Hansen 1965; Love and Christiansen 1985; Rowley et al. 1985). Below Phanerozoic strata lies 2–3 km of quartzite and mudstone assigned to the Proterozoic Uinta Mountain Group, which was deposited atop gneissic Archean basement of the Red Creek Quartzite. In the studied area of Uinta Uplift-proximal strata between Richards Mountain and Phil Pico Mountain, conglomerates are concentrated within three 0.5–1 km-thick, ~15 km-wide composite alluvial fan bodies, each of which exhibit similar unroofing sequences (Fig. 4.6a). The ca. 56–52 Ma succession of conglomerates at Richard Mountain (Crews and Ethridge 1993) provides a useful example: the Late Paleocene-age basal conglomerate just north of Goslin Mountain contains mudstone and chert pebbles, and lies in angular unconformity atop vertically oriented to overturned Cretaceous Mesaverde Group (Fig. 4.11h; Wiegman 1964; Colson 1969; Bradley 1988). Overlying Early Eocene strata of the Wasatch Formation contain cobble- to boulder-sized clasts of Paleozoic sandstones and carbonates, which are replaced up-section by quartzite clasts derived from the Proterozoic Uinta Mountain Group (Fig. 4.11i, g). This Mesozoic-Paleozoic-Proterozoic unroofing sequence is repeated in younger fan deposits to the west: (1) first the WPM-equivalent Canyon Road fan (52–50 Ma), and (2) second the Phil Pico fan (50–47 Ma), which interfingers with the Laney Member of the GRF and overlying Bridger Formation (Fig. 4.6a). The earliest fans appeared adjacent to the "East Dome" structural culmination in the Uinta Uplift (Hansen 1965; Rowley et al. 1985) at approximately the Utah-Colorado border, and subsequent fans migrated

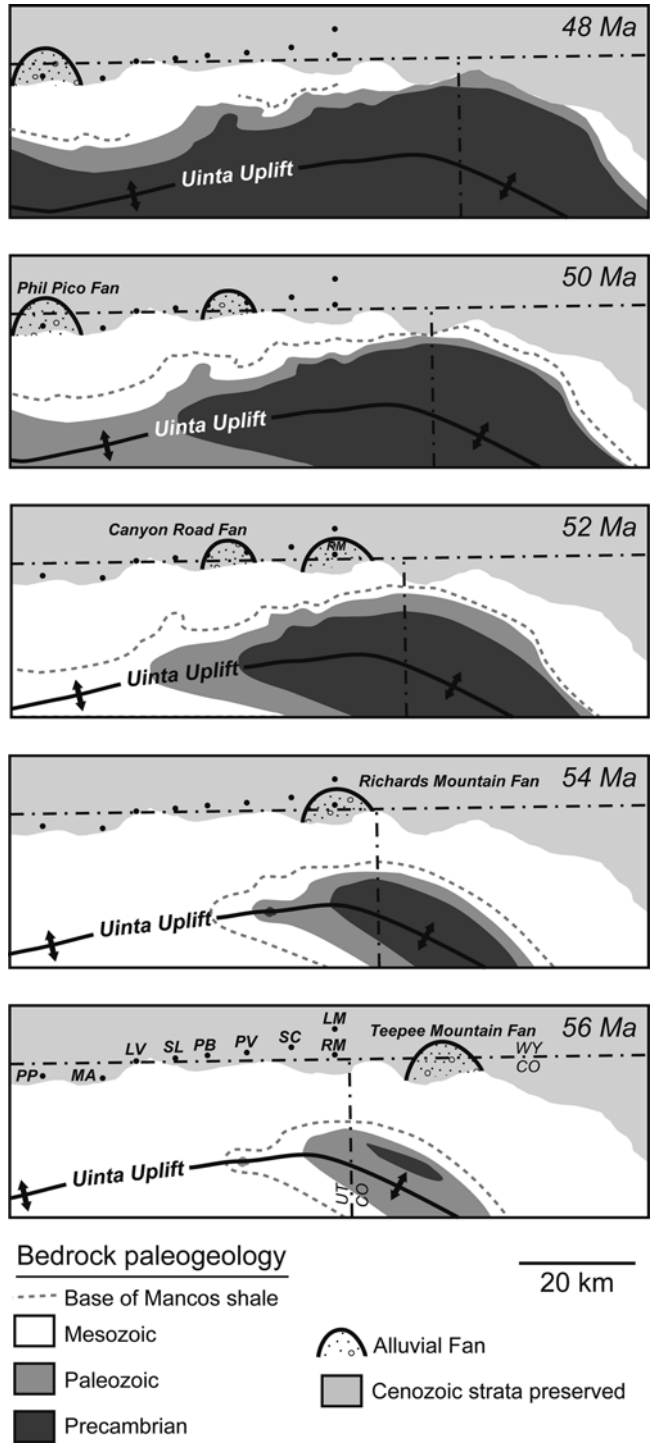

Fig. 4.18 Interpreted Paleocene through Early Eocene paleogeology of the Uinta Uplift showing asymmetric removal of Phanerozoic bedrock and coincident west-stepping development of fanglomerate deposits. Areas of earliest uplift delineated using conglomerate compositions (Fig. 4.6a). Broad outline of unroofing based on simple removal of strata from structurally highest areas following bedding orientations mapped within the Proterozoic Uinta Mountain Group mapped by Hansen (1965). Palinspastically-adjusted to reflect interpreted ~20 km of left-lateral translation along the Uinta Thrust (Johnston and Yin 2001)

to the west as the unroofed region expanded along its crest (Fig. 4.18).

4.5 Discussion

The scale of stratigraphic patterns in the WPM is useful to consider when attempting to resolve the forcing mechanisms responsible for its accumulation and stratigraphic stacking. Geochronology and cyclostratigraphy suggest the regularity of ca. 1–30 meter-scale vertical facies variability within WPM is likely climatic and/or stochastic rather than tectonic in origin. A strong apparent ca. 100 k.y. oscillation between lacustrine and alluvial modes suggests these lithofacies changes to have been driven by short eccentricity (Aswasereelert et al. 2013; Smith et al. 2014). In contrast, Uinta Uplift tectonism appears to have affected the basin on significantly longer timescales which include the 1–3 million year growth and abandonment of alluvial fans and 6 million years of continuous flexural subsidence in the southern GGRB (56–50 Ma). In the following discussion we first address the origin of fine-scale lithofacies variations, and then focus on the role of longer-term, tectonically driven processes.

4.5.1 Depositional Modes

The Wilkins Peak Member illustrates that the vertical juxtaposition of facies of underfilled lacustrine basins often violate Walther's "Law"; i.e., they were deposited from sedimentary environments that never coexisted at any one time, yet they are intercalated in a regular repetitive manner (Aswasereelert et al. 2013; Smith et al. 2014). Such stacking of genetically unrelated facies in the WPM reflects the repeated wholesale rearrangement of the hydrology and sediment transport between three basic paleogeographic and paleolimnologic configurations, or modes: (1) a lacustrine highstand mode; (2) a lacustrine lowstand mode; and (3) an alluvial mode (Smith et al. 2014). During lacustrine highstand modes (Fig. 4.16a), laterally extensive and isopachous beds of predominantly carbonate strata (Fig. 4.5) indicate that Lake Gosiute inundated a large portion of the Bridger subbasin and some parts of adjacent subbasins (Fig. 4.7). Due to remnant brines, its waters were likely salinity-stratified, dysoxic to anoxic and lacking in multicellular life. This promoted the preservation of very thin laminae and organic matter, particularly in the basin interior away from meteoric inflow where lake waters were also probably deepest. Arkosic detritus was largely confined to subbasins to the east of the Rock Springs Uplift during highstand lacustrine modes, whereas carbonate lacustrine sediment accumulated in the Bridger subbasin. During lacustrine lowstands (Fig. 4.16b), Lake Gosiute was restricted to the central Bridger subbasin, surrounded by a vast playa of mudflats and marshy areas, and was prone to evaporite deposition from its alkaline, hypersaline brine. Although lake level was low during lacustrine lowstands, little arkosic alluvium appears to have been transported into the Bridger subbasin during these evaporitic phases. The partitioning of siliciclastic detritus within the eastern subbasins is particularly apparent in the diminished orthoclase peak heights observed in XRD measurements of lacustrine intervals in basin interior coreholes (Fig. 4.9; Mason 1987). During alluvial modes (Fig. 4.16c), a broad, low-gradient alluvial plain extended into the Bridger subbasin from the east, with the Aspen River routed through relatively narrow gateways at the southern end of the Rock Springs Uplift. Concurrently, fan-deltas that had been restricted to the southern basin edge adjacent to the Uinta Uplift during lacustrine highstands extended several kilometers into the Bridger subbasin and merged with the alluvial surface constructed by eastern-derived arkosic alluvium between the measured outcrop sections *LM* and *CC* (Fig. 4.7). Although Lake Gosiute appears to have been aerially restricted during alluvial modes, perhaps counter-intuitively, the trace fossil assemblage, uraniferous horizons (Mott and Drever 1983), and absence of evaporite minerals or carbonate lacustrine facies within alluvial-deltaic intervals suggests diminished salinity and alkalinity during their deposition (Fig. 4.9).

4.5.2 Unroofing of the Uinta Uplift

The appearance of conglomerates in the stratal record has often been interpreted to reflect the creation of tectonically induced relief (Powell 1876; Knight 1937; Graham et al. 1986; DeCelles et al. 1991b; Carrapa and DeCelles 2008). Conglomerates proximal to the Uinta Uplift offer a unique temporally resolved view of its uplift and denudation over 8 million years and illustrate several under-recognized complexities in the temporal relationship between tectonism, the appearance of coarse-grained alluvium and lake-basin formation (Fig. 4.18). The appearance of coarse-grained conglomerates in Paleogene strata adjacent to the Uinta Uplift appear to have been delayed by at least 3 Ma after its initial upwarping, having been masked by the lack of coarse clasts produced during unroofing of the thick, fine-grained, poorly-cemented and non-durable Mesozoic strata (cf. Carroll et al. 2006). Conglomerates containing cobble- to boulder-sized clasts only appeared in Uinta Uplift-proximal strata after the subsequent emergence of the durable core of the Uinta Uplift. Individual fans along the north edge of the Uinta Uplift appear to have formed concurrently with the localized removal of its ~500 meter-thick Paleozoic carapace of durable sandstone and limestone (Fig. 4.6b). The removal of the Paleozoic occurred initially near Goslin Mountain, and spread laterally to the west with time. The typical duration between exposure and removal of the ~500 m of Paleozoic strata from catchments along the crest of the uplift was approximately 1–2 Ma. Applying the initial exposure gate provenance modeling concept of DeCelles (1988) yields a net denudation rate between 250 and 500 m/Ma, which exceeds recent estimates for landscape denudation calculated from the preserved volume of arkosic alluvium in the eastern GGRB and sodium in basin interior evaporites (Smith et al. 2008a). Based on all available geochronology and the along-strike stratigraphic correlation shown in Fig. 4.6a, this unroofing sequence migrated westward away from the eastern of dome of the Uinta Uplift, propagating successive fans every 1–3 Ma (Fig. 4.18). Though the west-stepping progression of fan deposits makes it is difficult to accurately interpret a discrete age for the initiation of uplift from a single fan deposit (Fig. 4.6), taken as a whole, the conglomerate record suggests continuous upward motion of the Uinta Uplift from the Paleogene through the Early Eocene.

4.5.3 Influence of Lithofacies-Dependent Sedimentation on Apparent Accommodation Patterns

Differential accumulation in tectonic basins is often attributed to asymmetric accommodation due to crustal flexure adjacent to actively forming geologic structures (i.e., Barbeau 2003). The areal distribution and thickness of lacustrine and alluvial deposits of the WPM, for example, is asymmetrical (Figs. 4.2 and 4.4a), thickening by a factor of ~3 towards the southern Bridger subbasin where accommodation was apparently greatest (Figs. 4.4a, 4.5 and 4.17). This stratal geometry has been cited to indicate a two discrete pulses of Uinta Uplift tectonism and flexurally-induced subsidence in the southern Bridger subbasin during the Early Eocene. The first would have resulted in differential accumulation of the "main body" of the Wasatch Formation, followed by a lull during deposition of the Tipton Member of the GRF, then a second pulse of flexure during WPM deposition (Gries 1983; Roehler 1993; Pietras et al. 2003a). However, this two-phase model is inconsistent with regional kinematic models (i.e., Bird 1998), which depict continuous Early Eocene contraction.

Considering geochronology-based accumulation rates (Fig. 4.17) and the sediment accumulation habits of lacustrine highstand facies within the GRF, it may not, however, be possible to distinguish two-phase from continuous tectonism by tracking differential accumulation. This is because laminated organic-rich mudstone of the ca. 52.5–51.6 Ma Tipton Member accumulated during consistently high lake levels and almost entirely lack basin interior-focused facies (Roehler 1993; Graf et al. 2015). Because

sediment couldn't accumulate rapidly in center of the basin, a lull in differential accumulation would have occurred even if flexure was ongoing. When juxtaposed against the pronounced asymmetry in basin fill within underlying and overlying strata of the "main body" of the Wasatch Formation and WPM, respectively, this ~0.9 million year hiatus in basin interior accumulation could be misinterpreted to indicate hiatus in flexural subsidence. Facies-based bias in accumulation patterns can also be observed at a finer scale within the WPM, where profundal facies within lacustrine intervals are also largely isopachus whereas alluvial and evaporate beds are concentrated in the southern Bridger subbasin (Figs. 4.4a and 4.5). When considered together with ongoing unroofing of the Uinta Uplift from the Paleocene through the Early Eocene indicated by the conglomerate record (Fig. 4.7 and 4.18), the balance of the evidence favors continuous rather than two-phase tectonism.

4.5.4 Fluvial Paleogeography

Due to the closed paleohydrology of the GGRB during WPM deposition, the WPM represents the integrated bedload, suspended load, and dissolved load of all of the streams draining its catchment area (Smith et al. 2008a). Closed to extrabasinal input from the Cordilleran divide (Fig. 4.8, Smith et al. 2008b; Doebbert et al. 2010), intrabasinal rivers would have provided the bulk of the water, solutes, and sediment. Two well-distinguished catchment types were responsible for delivering clastic detritus to the study area during WPM deposition (Fig. 4.1): (1) small, high-relief basins on the north flank of the Uinta Uplift; and (2) a large alluvial basin draining Precambrian-cored Laramide uplifts to the south and east that fed the Aspen River (Smith et al. 2014). During alluvial modes, these Uinta Uplift-derived streams would have converged with the Aspen River approximately 5 km from the southern margin of the GGRB before flowing out into the Bridger subbasin.

4.5.4.1 Uinta Uplift Mountain Streams

Coarse-grained fanglomerate deposits containing tractive and mass-flow-derived textures adjacent to the Uinta Uplift attest to steep gradients within the streams that drained small catchments along its north flanks. Although the clastic deposits of basin peripheral streams are of limited aerial extent, the input of Ca^{2+} rich waters appears to have played an important role in triggering the precipitation of carbonate from Ca-undersaturated, bicarbonate-rich lake waters along the southern edge of the basin (Fig. 4.13e). Interparticle travertine coatings within basin periphery conglomerates and the large volume of calcareous intraclasts and peloids within peripheral lacustrine deposits attest to this Ca^{2+} input (Fig. 4.13c).

4.5.4.2 The Aspen River Megafan

The composition, texture and stratigraphic packaging of basin interior alluvial units suggests they that they repeatedly prograded westward into the Bridger subbasin during alluvial modes (Fig. 4.7, Smith et al. 2014). The vast thickness of arkosic Cathedral Bluffs Member alluvium in subbasins to the east of the Rock Springs Uplift was also derived from uplifts to the southeast (Figs. 4.4a and 4.7). In addition to being the site of sediment accumulation, these subbasin may have served as short term reservoirs of clastic detritus during periods of elevated lacustrine base level (Sullivan 1985; Roehler 1993; Smith et al. 2008a). Individual alluvial units in the WPM represent basinward expansions of the distal terminus of a vast, low-gradient inland delta, or fluvial megafan (cf. Leier et al. 2005) that deposited alluvium eroded from the west side of the Rocky Mountains in Colorado (Fig. 4.1). The Aspen River catchment extended into Laramide highlands along the Rocky Mountain divide, and consequently the advection of siliciclastic detritus was likely sensitive to changes in summer monsoon intensity, which has been modelled to have been focused on the eastern slope of the Rocky Mountain divide (Fig. 4.8; Sewall and Sloan 2006; Huber and Goldner 2012).

4.5.5 Compositional Partitioning by Interbasinal Structures

The WPM and time-equivalent strata are compositionally segregated both laterally (i.e., between subbasins of the GGRB) and vertically (i.e., between alluvial and lacustrine intervals within the Bridger subbasin). Precipitated solutes (carbonates and evaporites) comprise the bulk of material within the Bridger subbasin, whereas a larger volume of siliciclastic alluvium comprises the WPM-equivalent basin-fill in the Great Divide, Washakie, and Sand Wash basins (Fig. 4.4). Partitioning between subbasins is here interpreted to have been accomplished by a sill formed at or near the Rock Springs Uplift (Fig. 4.16). This sill appears to have only been effective during lacustrine phases, and interestingly, even during lowstands. During alluvial modes, water and sediment were routed around the Rock Springs Uplift, spilling into the southeast corner of the Bridger subbasin unimpeded. The effectiveness of compositional partitioning between subbasins during lacustrine modes is strikingly illustrated in the basin interior XRD logs for dolomite and orthoclase (Fig. 4.9), and appears to have reached its peak effectiveness during deposition of middle portion of the WPM.

Smith et al. (2014) proposed a model in which the compositional partitioning of siliciclastic detritus is attributed to the coupled geomorphic and depositional response of the Aspen River to lake level changes and ongoing growth of the Rock Springs Uplift (Fig. 4.16). According to this model, the Aspen River entered Lake Gosiute east of the Rock Springs Uplift during lacustrine highstand modes, and built deltas of arkosic detritus at or near the Rock Springs Uplift saddle (Fig. 4.16a). Although no strata remain in the saddle between the Uinta and Rock Springs uplifts due to post-Eocene erosion (Fig. 4.7), the Aspen River would presumably have debauched in this ~20 km wide area. Subsequently, during lacustrine lowstand modes, the recently deposited and permeable sandy deltaic deposits prevented the overland surface flow of a diminished Aspen River from crossing the Rock Springs Uplift saddle, but allowed water and solutes to percolate through the delta and possibly emerge at down-gradient springs (Fig. 4.16b). Only during alluvial phases did siliciclastic material enter the Bridger subbasin, with some sediment derived via the reworking of lacustrine highstand delta deposits that had accumulated near the southern end of the Rock Springs Uplift (Fig. 4.16c).

4.6 Conclusions

1. A unique suite of alluvial and lacustrine facies occur in the WPM adjacent to the Uinta Uplift and can be correlated to basin interior lacustrine and alluvial strata at high resolution.
2. Conglomerate clast compositions in the southern Bridger subbasin indicate that unroofing of the Uinta Uplift occurred continuously from the Paleocene through the Early Eocene. Stratigraphic packaging and conglomerate compositions indicate progressive westward-migrating removal of its Phanerozoic carapace over a period from ca. 56–47 Ma, with growth and abandonment of individual alluvial fans occurring over 2–4 m.y. intervals.
3. The expression of tectonic accommodation via differential accumulation within the Green River Formation is highly dependent on the presence or absence of basin interior-focused lithofacies. Basinal accommodation potential is masked during intervals of consistently high lake level due to the absence of thick accumulation of bedded evaporites and basin interior alluvial strata. Accounting for the resulting bias in accumulation patterns, load induced flexural differential subsidence caused by uplift of the Uinta Mountains was likely continuous throughout the Early Eocene.
4. The most strongly expressed climate signal contained within the Wilkins Peak Member and equivalent deposits is an alternation between lacustrine carbonate and alluvial clastic deposition, which was recently related to 100 k.y. eccentricity. The repeated appearance of conglomerate horizons at the basin periphery concurrently with alluvial intervals suggests that individual conglomerate beds

reflect changes in base level rather than pulses of uplift.

5. In addition to climatically governed fluctuations in lake level, changes in the lateral advection of weathering products from the Lake Gosiute watershed strongly influences the character of the Wilkins Peak Member. This "geomorphic amplification" of the climate signal is accomplished by the compartmentalization of alluvium within subbasins of the eastern GGRB during lacustrine modes and episodic westward over-spilling of the Aspen River and other rivers from the Great Divide/Washakie/Sand Wash subbasins into the Bridger subbasin during alluvial depositional modes.

Acknowledgments This manuscript benefited from discussions with Robin Renaut, Meredith Rhodes-Carson, Jeff Pietras, Paul Buchheim, Leroy Leggitt, Joe Smoot, Cynthia Stiles, Tim Lowenstein, and field assistance from Rachel Simpson, Lincoln Freimund, Brooke Norsted, and Terri Graham. National Science Foundation grants EAR-0230123, EAR-0114055 and EAR-0516760, the Donors of the Petroleum Research Fund of the American Chemical Society, Chevron, ConocoPhillips, summer research grants from GSA, AAPG, and Sigma Xi, and the Bailey Distinguished Graduate Research Fellowship provided funding for M.E. Smith and A.R. Carroll. Funding for J.J. Scott was provided by the Natural Sciences and Engineering Research Council (NSERC) grants to Robin Renaut (RG629-03) and Luis Buatois (Discovery Grant 311726–05 and −08), and J.J.S. (PGS-D scholarship, Post-Doctoral Fellowship), and summer research grants from GSA, AAPG, and IAS.

References

Allen JRL (1970) A quantitative model of climbing ripples and their cross-laminated deposits. Sedimentology 14:5–26

Anderman GG (1955) Tertiary deformational history of a portion of the north flank of the Uinta Mountains in the vicinity of Manila, Utah. In: Anderman GG (ed) Green River Basin, 10th annual field trip conference guidebook. Wyoming Geological Association, Casper, pp 130–134

Aswasereelert W, Meyers SR, Carroll AR, Peters SE, Smith ME, Feigl KL (2013) Basin-scale cyclostratigraphy of the Green River Formation, Wyoming. Geol Soc Am Bull 125:216–228

Axelrod DI (1968) Tertiary floras and topographic history of the Snake River Basin, Idaho. Geol Soc Am Bull 79:713–734

Axelrod DI (1997) Paleoelevation estimated from Tertiary floras. Int Geol Rev 39:1124–1133

Barbeau DL (2003) A flexural model for the Paradox Basin: implications for the tectonics of the Ancestral Rocky Mountains. Basin Res 15:97–115

Beck RA, Vondra CF, Filkins JE, Olander JD (1988) Syntectonic sedimentation and Laramide basement thrusting, Cordilleran foreland; timing of deformation. In: Schmidt CJ, Perry WJ Jr (eds) Interaction of the Rocky mountain foreland and the Cordilleran thrust belt, Geological Society of America Memoir, 171. Geological Society of America, Boulder, pp 465–487

Berg RR (1962) Laramide sediments along the Wind River Thrust, Wyoming. Am Assoc Pet Geol Bull 46:220–230

Bird P (1998) Kinematic history of the Laramide orogeny in latitudes 35°-45°N, western United States. Tectonics 17:780–801

Birnbaum SJ, Radlick TM (1982) A textural analysis of trona and associated lithologies, Wilkins Peak Member, Eocene Green River Formation, southwestern Wyoming. In: Handford CR, Loucks RG, Davies GR (eds) Depositional and diagenetic spectra of evaporites – a core workshop, Calgary, 26–27 June. Core Workshop no. 3, Society of Economic Paleontologists and Mineralogists, Tulsa, pp 75–99

Blair TC, Raynolds RG (1999) Sedimentology and tectonic implications of the Neogene synrift hole in the wall and wall front members, Furnace Creek basin, Death Valley, California. In: Wright LA, Troxel BW (eds) Cenozoic basins of the Death Valley region, Geological Society of America Special Paper 333. Geological Society of America, Boulder, pp 127–168

Bohacs KM, Hasiotis ST, Demko TM (2007) Continental ichnofossils of the Green River and Wasatch Formations, Wyoming: a preliminary survey, proposed relation to lake-basin type, and application to integrated paleo-environmental interpretation. Mountain Geol 44:79–108

Bradley MD (1988) Structural interactions between the Uinta arch and the overthrust belt, north-central Utah; Implications of strain trajectories and displacement modeling. In: Schmidt CJ, Perry WJ Jr (eds) Interaction of the Rocky Mountain foreland and the Cordilleran thrust belt, Geological Society of America Memoir 171. Geological Society of America, Boulder, pp 431–445

Bradley WH (1929) The varves and climate of the Green River epoch. U.S. Geological Survey Professional Paper 158-E. U.S. Govt Print Off, Washington, 110 p

Bradley WH (1964) The geology of the Green River Formation and associated Eocene rocks in southwestern Wyoming and adjacent parts of Colorado and

Utah. U.S. Geological Survey Professional Paper 496-A. U.S. Govt Print Off, Washington, 86 p
Bradley WH (1970) Green River oil shale-concept of origin extended. Geol Soc Am Bull 81:985–1000
Bradley WH, Eugster HP (1969) Geochemistry and paleolimnology of the trona deposits and associated authigenic minerals of the Green River Formation of Wyoming. U.S. Geological Survey Professional Paper 496-B. U.S. Govt Print Off, Washington, 71 p
Braunagel LH, Stanley KO (1977) Origin of variegated redbeds in the Cathedral Bluffs Tongue of the Wasatch Formation (Eocene), Wyoming. J Sediment Petrol 47:1201–1219
Brozovich N, Burbank DW (2000) Dynamic fluvial systems and gravel progradation in the Himalayan foreland. Geol Soc Am Bull 112:394–412
Buchheim HP, Eugster HP (1998) Eocene Fossil Lake: the Green River Formation of Fossil Basin, southwestern Wyoming. In: Pitman JK, Carroll AR (eds) Modern and ancient lake systems; new problems and perspectives, Utah Geological Association Publication 26. Utah Geological Association, Salt Lake City, pp 191–208
Burgess CE, Pearson PN, Lear CH, Morgans HEG, Handley L, Pancost RD, Schouten S (2008) Middle Eocene climate cyclicity in the southern Pacific: implications for global ice volume. Geology 36:651–654
Burnside MJ, Culbertson WC (1979) Trona deposits in the Green River Formation, Sweetwater, Uinta, and Lincoln Counties, Wyoming. U.S. Geological Survey Open-File Report 79–737. 10 p
Cande SC, Kent DV (1992) A new geomagnetic polarity timescale for the Late Cretaceous and Cenozoic. J Geophys Res 100:13917–13951
Cande SC, Kent DV (1995) Revised calibration of the geomagnetic polarity timescale for the Late Cretaceous and Cenozoic. J Geophys Res 100:6093–6095
Carrapa B, DeCelles PG (2008) Eocene exhumation and basin development in the Puna of northwestern Argentina. Tectonics 27:1–19
Carroll AR, Bohacs KM (1999) Stratigraphic classification of ancient lakes: balancing tectonic and climatic controls. Geology 27:99–102
Carroll AR, Bohacs KM (2001) Lake-type controls on petroleum source rock potential in nonmarine basins. Am Assoc Pet Geol Bull 85:1033–1053
Carroll AR, Chetel LM, Smith ME (2006) Feast to famine: sediment supply control on Laramide basin fill. Geology 34:197–200
Carroll AR, Doebbert AC, Booth AL, Chamberlain CP, Rhodes-Carson MK, Smith ME, Johnson CM, Beard BL (2008) Capture of high-altitude precipitation by a low-altitude Eocene lake, western U.S. Geology 36:791–794
Carroll AR, Graham SA, Smith ME (2010) Walled sedimentary basins of China. Basin Res 222:17–32
Cassel EJ, Graham SA (2011) Oligocene sediments ("auriferous gravels"), northern Sierra Nevada, California: implications for climate, tectonics, and topography. Geol Soc Am Bull 123:1699–1719
Chetel LM, Carroll AR (2010) Terminal infill of Eocene Lake Gosiute, Wyoming, USA. J Sediment Res 80:492–514
Church M, Buchheim HP (2002) Varves and varve-derived climate cycles? Evidence from Eocene Green River Formation. Geol Soc Am Abs Pro 34(6):555
Colson CT (1969) Stratigraphy and production of the Tertiary formations in the Sand Wash and Washakie Basins. In: Barlow JA (ed) Symposium on Tertiary rocks of Wyoming. 21st annual field conference guidebook, Wyoming. Geological Association, Casper, pp 121–128
Crews SG, Ethridge FG (1993) Laramide tectonics and humid alluvial fan sedimentation, NE Uinta Uplift, Utah and Wyoming. J Sediment Petrol 63:420–436
Culbertson WC (1961) Stratigraphy of the Wilkins Peak Member of the Green River Formation, Firehole Basin quadrangle, Wyoming. U.S. Geol Surv Prof Pap 424-D:170–173
Culbertson WC (1966) Trona in the Wilkins Peak Member of the Green River Formation, southwestern Wyoming. U.S. Geol Surv Prof Pap 550-B:159–164
Culbertson WC (1998) Road log for the geology field trip of June 13, 1997, Geology and outcrops of the trona-bearing rocks of the Green River Formation. Wyoming State Geological Survey Public Information Circular 40. pp 205–211
Das T, Nolet G (1998) Crustal thickness map of the western United States by partitioned waveform inversion. J Geophys Res 103:30021–30038
Davis SJ, Mulch A, Carroll AR, Horton TW, Chamberlain CP (2009) Paleogene landscape evolution of the central North American Cordillera: developing topography and hydrology in the Laramide foreland. Geol Soc Am Bull 121:100–116
Davis SJ, Dickinson WR, Gehrels GE, Spencer JE, Lawton TF, Carroll AR (2010) The Paleogene California River: evidence of Mojave-Uinta paleodrainage from U-Pb ages of detrital zircons. Geology 38:931–934
Deardorff DL, Mannion LE (1971) Wyoming trona deposits. Univ Wy Cont Geol 10:25–37
DeCelles PG (1988) Lithologic provenance modeling applied to the Late Cretaceous synorogenic Echo Canyon Conglomerate, Utah: a case for multiple source areas. Geology 16:1039–1043
DeCelles PG (1994) Late Cretaceous-Paleocene synorogenic sedimentation and kinematic history of the Sevier thrust belt, northeast Utah and southwest Wyoming. Geol Soc Am Bull 106:32–56
DeCelles PG (2004) Late Jurassic to Eocene evolution of the Cordilleran thrust belt and foreland basin system, western U.S.A. Am J Sci 304:105–168
DeCelles PG, Gray MB, Ridgeway KD, Cole RB, Pivnik DA, Pequera N, Srivastava P (1991a) Controls on synorogenic alluvial-fan architecture, Beartooth

Conglomerate (Palaeocene), Wyoming and Montana. Sedimentology 38:567–590

DeCelles PG, Gray MB, Ridgeway KD, Cole RB, Srivastava P, Pequera N, Pivnik DA (1991b) Kinematic history of a foreland uplift from Paleocene synorogenic conglomerate, Beartooth Range, Wyoming and Montana. Geol Soc Am Bull 103:1458–1475

Dickinson WR, Klute MA, Hayes MJ, Janecke SU, Lundin ER, McKittrick MA, Olivares MD (1988) Paleogeographic and paleotectonic setting of Laramide sedimentary basins in the central Rocky Mountain region. Geol Soc Am Bull 100:1023–1039

Doebbert AC, Carroll AR, Mulch A, Chetel LM, Chamberlain CP (2010) Geomorphic controls on lacustrine isotopic compositions: evidence from the Laney Member, Green River Formation, Wyoming. Geol Soc Am Bull 122:236–252

Erslev EA (1993) Thrusts, back-thrusts, and detachment of Rocky mountain foreland arches. In: Schmidt CJ, Chase RB, Erslev EA (eds) Laramide Basement Deformation in the Rocky Mountain Foreland of the Western United States, Geological Society of America Special Paper 280. Geological Society of America, Boulder, pp 339–358

Eugster HP, Hardie LA (1975) Sedimentation in an ancient playa-lake complex: the Wilkins Peak Member of the Green River Formation of Wyoming. Geol Soc Am Bull 86:319–334

Fahey JJ (1962) Saline minerals of the Green River Formation. U.S. Geological Survey Professional Paper 405. United States Government Printing Office, Washington, 50 p

Fan M, Dettman DL (2009) Late Paleocene high Laramide ranges in northeast Wyoming: oxygen isotope study of ancient river water. Earth Planet Sci Lett 286:110–121

Fischer AG, Roberts LT (1991) Cyclicity in the Green River Formation (lacustrine Eocene) of Wyoming. J Sediment Petrol 61:1146–1154

Freytet P, Verrecchia EP (2002) Lacustrine and palustrine carbonate petrography: an overview. J Paleolimnol 21:221–237

Galloway WE, Whiteaker TL, Ganey-Curry P (2011) History of Cenozoic North American drainage evolution, sediment yield, and accumulation in the Gulf of Mexico basin. Geosphere 7:938–973

Gawthorpe RL, Leeder MR (2000) Tectono-sedimentary evolution of active extensional basins. Basin Res 12:195–218

Goodwin JT, Surdam RC (1967) Zeoloitization of tuffaceous rocks of the Green River Formation, Wyoming. Science 157:307–308

Graf JW, Carroll, AR, Smith ME (2015) Lacustrine sedimentology, stratigraphy and stable isotope geochemistry of the Tipton Member of the Green River Formation: In: Smith ME, Carroll AR (eds) Stratigraphy and paleolimnology of the Green River formation, Western U.S.. Springer, Dordrecht

Graham SA, Tolson RB, DeCelles PG, Ingersoll RV, Bargar E, Caldwell M, Cavazza W, Edwards DP, Follo WF, Handschy JW, Lemke L, Moxon I, Rice R, Smith GA, White J (1986) Provenance modelling as a technique for analysing source terrane evolution and controls on foreland sedimentation. In: Allen PA, Homewood P (eds) Foreland basins, Special Publication 8. International Association of Sedimentologists, Blackwell Publishing Ltd., Oxford, pp 425–436

Gregory KM, Chase CG (1994) Tectonic and climatic significance of a late Eocene low-relief, high-level geomorphic surface, Colorado. J Geophys Res 99:20141–20160

Gries R (1983) North–south compression of Rocky Mountain foreland structures. In: Lowell JD, Gries R (eds) Rocky Mountain foreland basins and uplifts, 34th annual field conference guidebook. Rocky Mountain Association of Geologists, Denver, pp 9–32

Hansen WR (1965) Geology of the Flaming Gorge area Utah-Colorado-Wyoming. U.S. Geological Survey Professional Paper 490. U.S. Govt Print Off, Washington, 196 p

Hansen WR, Bonilla MG (1954) Laramide faulting and folding on the north flank of the Uinta Mountains in eastern Daggett County, Utah. Colorado Sci Soc Proc 17:29

Hayden FV (1869) Preliminary field report of the United States Geological Survey of Colorado and New Mexico. Third Annual Report, U.S. Geological Survey of the Territories. U.S. Govt Print Off, Washington, 155 p

Heller PL, Peterman ZE, O'Neil JR, Shafiqullah M (1985) Isotopic provenance of sandstones from the Eocene Tyee Formation, Oregon Coast Range. Geol Soc Am Bull 96:770–780

Henry CD, Hinz NH, Faulds JE, Colgan JP, John DA, Brooks ER, Cassel EJ, Garside LJ, Davis DA, Castor SB (2012) Eocene-Early Miocene paleotopography of the Sierra Nevada-Great Basin-Nevadaplano based on widespread ash-flow tuffs and paleovalleys. Geosphere 8:1–27

Horsfield B, Curry DJ, Bohacs KM, Littke R, Rullkoetter J, Schenk HJ, Radke M, Schafer RG, Carroll AR (1994) Organic geochemistry of freshwater and alkaline lacustrine sediments in the Green River Formation of the Washakie Basin, Wyoming, U.S.A. Org Geochem 22(3–5):415–440

Huber M, Caballero R (2011) The early Eocene equable climate problem revisited. Clim Past 7:603–633

Huber M, Goldner A (2012) Eocene monsoons. J Asian Earth Sci 44:3–23

Janecke SU, VanDenburg CJ, Blankenau JJ, M'Gonigle JW (2000) Long-distance longitudinal transport of gravel across the Cordilleran thrust belt of Montana and Idaho. Geology 28:439–442

Johnson PL, Anderson DW (2009) Concurrent growth of uplifts with dissimilar orientations in the southern

Green River Basin, Wyoming: implications for Paleocene–Eocene patterns of foreland shortening. Rocky Moun Geol 44:1–16

Johnson KR, Ellis B (2002) A tropical rainforest in Colorado 1.4 million years after the Cretaceous-Tertiary boundary. Science 296:2379–2383

Johnston RE, Yin A (2001) Kinematics of the Uinta fault system (southern Wyoming and northern Utah) during the Laramide Orogeny. Int Geol Rev 43:52–68

Jones BF, Deocampo DM (2003) Geochemistry of saline lakes. In: Drever JI (ed) Surface and ground water, weathering, and soils. Elsevier, Amsterdam, pp 393–424

Keefer WR (1965) Stratigraphy and geologic history of the Cretaceous, Paleocene, and Lower Eocene rocks in the Wind River Basin, Wyoming. U.S. Geological Survey Professional Paper 495-A. U.S. Govt Print Off, Washington, 77 p

Kent-Corson ML, Sherman LS, Mulch A, Chamberlain CP (2006) Cenozoic topographic and climatic response to changing tectonic boundary conditions in western North America. Earth Planet Sci Lett 252:453–466

Knight SH (1937) Origin of the giant conglomerates of Green Mountain and Crook's Mountain, central Wyoming. Proc Geol Soc Am 1936:84

Kraus MJ (1985) Early Tertiary quartzite conglomerates of the Bighorn Basin and their significance for paleogeographic reconstruction of northwest Wyoming. In: Flores RM, Kaplan SS (eds) Cenozoic paleogeography of the West Central United States, Rocky Mountain Paleogeography Symposium 3. Rocky Mountain Section, SEPM (Society for Sedimentary Geology), Tulsa, pp 71–91

Kraus MJ, Aslan A (1993) Eocene hydromorphic paleosols: significance for interpreting ancient floodplain processes. J Sediment Res 63:453–463

Kraus MJ, Brown TM (1988) Pedofacies analysis; A new approach to reconstructing ancient fluvial sequences. In: Reinhardt J, Sigleo WR (eds) Paleosols and Weathering Through Geologic Time: Principles and Applications, Geological Society of America Special Paper 216. Geological Society of America, Boulder, pp 143–152

Kuiper KF, Deino A, Hilgen FJ, Krijgsman W, Renne PR, Wijbrans JR (2008) Synchonizing rock clocks of Earth history. Science 320:500–504

Laskar J, Robutel P, Joutel F, Gastineau M, Correia ACM, Levrard B (2004) A long term numerical solution for the insolation quantities of the Earth. Astron Astrophys 428:261–285

Laskar J, Fienga A, Gastineau M, Manche H (2011) La10: a new orbital solution for the long-term motion of the Earth. Astron Astrophys 532(A89):1–15

Lawton TF, Bradford IA, Vega FJ, Gehrels GE, Amato JM (2009) Provenance of Upper Cretaceous–Paleogene sandstones in the foreland basin system of the Sierra Madre Oriental, northeastern Mexico, and its bearing on fluvial dispersal systems of the Mexican Laramide Province. Geol Soc Am Bull 121:820–836

Leggitt VL, Cushman RA Jr (2001) Complex caddisfly-dominated bioherms from the Eocene Green River Formation. Sediment Geol 145:377–396

Leier AL, DeCelles PG, Pelletier JD (2005) Mountains, monsoons, and megafans. Geology 33:289–292

Love JD (1960) Cenozoic sedimentation and crustal movement in Wyoming. Am J Sci 258-A:204–214

Love JD (1964) Uraniferous phosphatic lake beds of Eocene age in intermontane basins of Wyoming and Utah, U.S. Geological Survey Professional Paper 474-E. U.S. Govt Print Off, Washington, 66 p.

Love JD, Christiansen AC, compilers (1985) Geologic map of Wyoming. U.S. Geological Survey, Washington, 1:500 000 scale

Machlus ML, Olsen PE, Christie-Blick N, Hemming SR (2008) Spectral analysis of the lower Eocene Wilkins Peak Member, Green River Formation, Wyoming: support for Milankovitch cyclicity. Earth Planet Sci Lett 268:64–75

Mackey GN, Horton BK, Milliken KL (2012) Provenance of the Paleogene-Eocene Wilcox Group, western Gulf of Mexico basin: evidence for integrated drainage of the southern Laramide Rocky Mountains and Cordilleran arc. Geol Soc Am Bull 124:1007–1024

Magee JW, Miller GH (1998) Lake Eyre paleohydrology from 60 ka to the present: beach ridges and glacial maximum aridity. Palaeogeogr Palaeoclimatol Palaeoecol 144:307–329

Mallory WW (1972) Geologic atlas of the Rocky Mountain Region. Rocky Mountain Association of Geologists, Denver, 331 p

Markwick PJ (1994) "Equability", continentality, and Tertiary "climate": The crocodilian perspective. Geology 22:613–616

Mason GM (1987) Mineralogic aspects of stratigraphy and geochemistry of the Green River Formation, Wyoming. PhD thesis, University of Wyoming, Laramie, 377 p

Mayry MS (2007) Geochemistry and sedimentology of spring mounds: Eocene Green River Formation. MSc thesis, Loma Linda University, 232 p

McClelland WC, Oldow JS (2004) Displacement transfer between thick- and thin-skinned décollement systems in the central North American Cordillera. In: Grocott J, McCaffrey KJW, Taylor G, Tikoff B (eds) Vertical Coupling and Decoupling in the Lithosphere, Special Publication 227. Geological Society, London, pp 177–195

Meyers SR (2008) Resolving Milankovitchian controversies: the Triassic Latemar Limestone and the Eocene Green River Formation. Geology 36:319–322

Miall AD (1978) Lithofacies type and vertical profile models in braided river deposits, a summary. In:

Miall AD (ed) Fluvial sedimentology, Memoir 5. Canadian Society of Petroleum Geologists, Calgary, pp 597–604

Min K, Mundil R, Renne PR, Ludwig KR (2000) A test for systematic errors in $^{40}Ar/^{39}Ar$ geochronology through comparison with U-Pb analysis of a 1.1 Ga rhyolite. Geochim Cosmochim Acta 64:73–98

Mott LV, Drever JI (1983) Origin of uraniferous phosphatic beds in Wilkins Peak Member of the Green River Formation. Am Assoc Pet Geol Bull 67:70–82

Olsen PE (1986) A 40-million-year lake record of early Mesozoic orbital climatic forcing. Science 234:842–848

Pietras JT, Carroll AR (2006) High-resolution stratigraphy of an underfilled lake basin: Wilkins Peak Member, Eocene Green River Formation, Wyoming, USA. J Sediment Res 76:1197–1214

Pietras JT, Carroll AR, Rhodes MK (2003a) Lake basin response to tectonic drainage diversion: Eocene Green River Formation, Wyoming. J Paleolimnol 30:115–125

Pietras JT, Carroll AR, Singer BS, Smith ME (2003b) 10 k.y. depositional cyclicity in the Early Eocene: Stratigraphic and $^{40}Ar/^{39}Ar$ evidence from the lacustrine Green River Formation. Geology 31:593–597

Platt NH (1992) Fresh-water carbonates from the Lower Freshwater Molasse (Oligocene, western Switzerland); sedimentology and stable isotopes. Sediment Geol 78:81–99

Powell JW (1876) Report of the geology of the eastern portion of the Uinta Mountains and region of country adjacent thereto. U.S. Geological and Geographical Survey of the Territories, Second Division. U.S. Govt Print Off, Washington, 218 p

Remy RR (1992) Stratigraphy of the Eocene part of the Green River Formation in the south-central part of the Uinta Basin, Utah. U.S. Geological Survey Bulletin 1787-BB. U.S. Govt Print Off, Washington, 79 p

Renaut RW, Gierlowski-Kordesch EH (2010) Lakes. In: James NP, Dalrymple RW (eds) Facies Models 4, Geological Association of Canada GEOtext 6, St. John's, pp 541–575

Renaut RW, Tiercelin J-J (1994) Lake Bogoria, Kenya rift valley-A sedimentological overview. In: Renaut RW, Last WM (eds) Sedimentology and geochemistry of modern and ancient saline lakes, Special Publication 50, SEPM (Society for Sedimentary Geology), Tulsa, pp 101–123

Retallack GJ (1988) Field recognition of paleosols. In: Reinhardt J, Sigleo WR (eds) Paleosols and weathering through geologic time: principles and applications, Special Paper 216. Geological Society of America, Boulder pp 1–20

Rhodes MK, Carroll AR, Pietras JT, Beard BL, Johnson CM (2002) Strontium isotope record of paleohydrology and continental weathering, Eocene Green River Formation, Wyoming. Geology 30(2):167–170

Rhodes MK, Malone DH, Carroll AR, Smith ME (2007) Sudden desiccation of Lake Gosiute at ~49 Ma: downstream record of Heart Mountain Faulting? Mt Geol 44:1–10

Ripepe M, Roberts LT, Fischer AG (1991) ENSO and sunspot cycles in varved Eocene oil shales from image analysis. J Sediment Petrol 61:1155–1163

Roehler HW (1991a) Correlation and depositional analysis of oil shale and associated rocks in the Eocene Green River Formation, Greater Green River Basin, southwest Wyoming. U.S. Geological Survey Miscellaneous Investigations Series Map I-2226

Roehler HW (1991b) Identification of oil-shale and trona beds and their geophysical log responses in the Energy Research and Development Administration Blacks Fork no. 1 corehole, Eocene Green River Formation, southwest Wyoming. U.S. Geological Survey Miscellaneous Field Studies Map MF-2158

Roehler HW (1992a) Correlation, composition, areal distribution, and thickness of Eocene stratigraphic units, greater Green River basin, Wyoming, Utah, and Colorado, U.S. Geological Survey Professional Paper 1506-E. 49 p

Roehler HW (1992b) Description and correlation of Eocene rocks in stratigraphic reference sections for the Green River and Washakie Basins, southwest Wyoming. U.S. Geological Survey Professional Paper 1506-D. 83 p

Roehler HW (1992c) North–south correlation of oil-shale and trona beds in the Eocene Green River Formation, Green River Basin, southwest Wyoming. U.S. Geological Survey Miscellaneous Field Studies Map MF-2192

Roehler HW (1993) Eocene climates, depositional environments, and geography, Greater Green River Basin, Wyoming, Utah, and Colorado. U.S. Geological Survey Professional Paper 1506-F. 74 p

Rosen MR (1991) Sedimentologic and geochemical constraints on the evolution of Bristol Dry Lake Basin, California, USA. Palaeogeogr Palaeoclimatol Palaeoecol 84:229–257

Rowley PD, Hansen WR, Tweto O, Carrara PE (1985) Geologic map of the Vernal 1° x 2° quadrangle, Colorado, Utah, and Wyoming. U.S. Geological Survey Miscellaneous Investigations Series Map I-1526

Royse F Jr (1993) An overview of the geologic structure of the thrust belt in Wyoming, northern Utah, and eastern Idaho. In: Snoke AW, Steidtmann JR, Roberts SM (eds) Geology of Wyoming, Memoir 5. Geological Survey of Wyoming, Laramie, pp 272–311

Scott JJ (2010) Saline lake ichnology: composition and distribution of Cenozoic traces in the saline, alkaline lakes of the Kenya Rift Valley and Eocene Green River Formation. University of Saskatchewan, Saskatoon, 526 p

Scott JJ, Smith ME (2015) Trace fossils of the Eocene Green River lake basins, Wyoming, Utah, and Colorado. In: Smith ME, Carroll AR (eds) Stratigraphy

and paleolimnology of the Green River Formation, Western U.S.. Springer, Dordrecht

Seal RRI, Rye R (1993) Stable isotope study of fluid inclusions in fluorite from Idaho; implications for continental climates during the Eocene. Geology 21(3):219–222

Seeland DA (1978) Eocene fluvial drainage patterns and their implications for uranium and hydrocarbon exploration in the Wind River Basin, Wyoming. U.S. Geological Survey Bulletin 1446. 21 p

Seeland DA (1992) Depositional systems of a synorogenic continental deposit-The upper Paleocene and lower Eocene Wasatch Formation of the Powder River Basin. U.S. Geological Survey Bulletin 1917-H. 20 p

Sewall JO, Sloan LC (2006) Come a little bit closer: a high-resolution climate study of the early Paleogene Laramide foreland. Geology 34:81–84

Smith ME, Singer B, Carroll A (2003) $^{40}Ar/^{39}Ar$ geochronology of the Eocene Green River Formation, Wyoming. Geol Soc Am Bull 115:549–565

Smith ME, Carroll AR, Mueller ER (2008a) Elevated weathering rates in the Rocky Mountains during the Early Eocene Climatic Optimum. Nat Geosci 1:370–374

Smith ME, Carroll AR, Singer BS (2008b) Synoptic reconstruction of a major ancient lake system: Eocene Green River Formation, Western United States. Geol Soc Am Bull 120:54–84

Smith ME, Chamberlain KR, Singer BS, Carroll AR (2010) Eocene clocks agree: Coeval $^{40}Ar/^{39}Ar$, U-Pb, and astronomical ages from the Green River Formation. Geology 38:527–530

Smith ME, Singer BS, Simo JA (2011) A time like our own? Radioisotopic calibration of the Ordovician greenhouse to icehouse transition. Earth Planet Sci Lett 311:364–374

Smith ME, Carroll AR, Scott JJ, Singer BS (2014) Early Eocene carbon isotope excursions and landscape destabilization at eccentricity minima: Green River Formation of Wyoming. Earth Planet Sci Lett 403:393–406

Smoot JP (1983) Depositional subenvironments in an arid closed basin; the Wilkins Peak Member of the Green River Formation (Eocene), Wyoming, U.S.A. Sedimentology 30:801–827

Stuart WJ Jr (1965) Stratigraphy of the Green River Formation, west of the Rock Springs Uplift. In: De Voto RH, Bitter RK (eds) Sedimentation of late Cretaceous and Tertiary outcrops, Rock Springs uplift, 19th annual field conference guidebook. Wyoming Geological Association, Casper, pp 159–166

Sullivan R (1985) Origin of lacustrine rocks of the Wilkins Peak Member, Wyoming. Am Assoc Pet Geol Bull 69:913–922

Tikoff B, Maxson J (2001) Lithospheric buckling of the Laramide foreland during Late Cretaceous and Paleogene, western United States. Rocky Moun Geol 36:13–35

Topping DJ, Rubin DM, Vierra LE Jr (2000) Colorado River sediment transport 1. Natural sediment supply limitation and the influence of Glen Canyon Dam. Water Resour Res 36:515–542

Verges J, Marzo M, Santaeularia T, Serra-Kiel J, Burbank DW, Munoz JA, Gimenez-Montsant J (1998) Quantified vertical motions and tectonic evolution of the SE Pyrenean foreland basin. In: Mascle A, Puigdefabregas C, Luterbacher HP, Fernandez M (eds) Cenozoic foreland basins of Western Europe, Geological Society Special Publication 134, London, pp 107–134

Wernicke B (2011) The California River and its role in carving Grand Canyon. Geol Soc Am Bull 123:1288–1306

Wiegman RW (1964) Late Cretaceous and early Tertiary stratigraphy of the Little Mountain area, Sweetwater County, Wyoming. MSc thesis, University of Wyoming, Laramie, 53 p

Wiig SV, Grundy WD, Dyni JR (1995) Trona resources in the Green River Basin, southwest Wyoming. U.S. Geological Survey Open-File Report OF 95–476. 91 p

Wilf P (2000) Late Paleocene-early Eocene climate changes in southwestern Wyoming: Paleobotanical analysis. Geol Soc Am Bull 112:292–307

Zachos JC, Stott LD, Lohmann KC (1994) Evolution of early Cenozoic marine temperatures. Paleoceanography 9:353–387

Zachos J, Pagani M, Sloan L, Thomas E, Billups K (2001) Trends, rhythms, and aberrations in global climate 65 Ma to present. Science 292:685–693

5 Lake Type Transition from Balanced-Fill to Overfilled: Laney Member, Green River Formation, Washakie Basin, Wyoming

Meredith K. Rhodes and Alan R. Carroll

Abstract

Outcrops of the Laney Member of the Green River formation that rim the Washakie basin provide a well exposed ~60 km stratigraphic transect that records the final stages of Eocene Lake Gosiute. The Laney Member comprises two main facies associations: fluctuating profundal facies of the lower LaClede Bed; and fluvial-lacustrine facies of the upper LaClede and Sand Butte Beds. The lower LaClede Bed consists of repetitive, 1–5 m scale facies successions that record episodes of lake expansion and contraction that occurred over time scales in the range of 10–50 ky. These deposits are also punctuated by a ~12 m interval of dolomitic siltstone and siliciclastic siltstone and sandstone (the "buff marker bed"), that has previously been interpreted to record a unique event of basinwide desiccation due to temporary blockage of a major influent stream. The maximum extent of lower LaClede Bed lakes progressively increased though time, as recorded by northeastward advance of successive shorelines within the study transect. The upper LaClede Bed in contrast lacks clearly defined parasequences, and instead consists of continuous mudstone deposits that grade upward into deltaic volcaniclastic facies of the Sand Butte Bed. The latter includes well-developed foresets reaching up to 25 m in relief, that record progressive infill of Lake Gosiute from the northwest to southeast.

We interpret the lower LaClede Bed to record deposition in a balanced-fill lake basin, in which lakes of varying salinity expanded and contracted across a low-relief basin floor. The preservation of shoreline and alluvial facies in the northeastern part of the transect suggest maximum lake depths

The online version of this chapter (doi:10.1007/978-94-017-9906-5_5) contains supplementary material, which is available to authorized users.

M.K. Rhodes
Geofuels, LLC, 1406 Seminole Hwy, Madison, WI 53711, USA

A.R. Carroll (✉)
Department of Geoscience, University of Wisconsin – Madison, 1215 W. Dayton St., Madison, WI 53706, USA
e-mail: carroll@geology.wisc.edu

M.E. Smith, A.R. Carroll (eds.), *Stratigraphy and Paleolimnology of the Green River Formation, Western USA*, Syntheses in Limnogeology 1, DOI 10.1007/978-94-017-9906-5_5

of ~50 m or less, based on analogy to the modern Bear River Delta in Utah. We interpret the upper LaClede Bed to record deposition in an overfilled lake basin, that was continuously occupied by a relatively stable, freshwater lake with an outlet to the south.

Previous studies concluded that the transition to overfilled conditions resulted from capture of the Idaho River. The results of this study suggest a more complex process of continuous watershed expansion that occurred throughout Laney Member deposition. Based on $^{87S}r/^{86}Sr$ ratios, the base of the Laney Member in the Bridger basin appears to be slightly older than in the Washakie basin. Capture of the Idaho River did trigger the shift to overfilled conditions however, and southward spillage of Lake Gosiute caused lakes in the Piceance Creek and Uinta basins to merge and deposit the highly organic-rich Mahogany zone. Detritus from the Challis volcanic field eventually filled in Lake Gosiute, and was then carried downstream to partly fill Lake Uinta.

5.1 Introduction

Interest in lacustrine basins has grown dramatically in recent decades, due to their highly detailed records of past climatic conditions on the continents, their sensitivity to tectonically-driven deformation and dynamic topography, and their extensive commercial resources. The Green River Formation represents one of the best known and most economically important intervals of lacustrine strata in the world, In recent years, it has also become a focal point for the development of high resolution radioisotopic and astrochronologic timescales. Many aspects of its geologic evolution have been documented by previous studies, but due to its extraordinary stratigraphic complexity and the evolving nature of scientific questions that it can help address, a daunting amount of work remains to be done.

Herein we examine the detailed stratigraphy and genetic evolution of one unit of the Green River Formation, the Laney Member in southwest Wyoming. The Laney Member was proposed by Carroll and Bohacs (1999) and Bohacs et al. (2000) to record a genetic transition from a balanced-fill to overfilled lake basin, prior to the final infill of Eocene Lake Gosiute. In this paper we examine the stratigraphic relations exposed in outcrop along the Delaney and Kinney Rims of the Washakie basin to provide the first detailed documentation of this lake-type transition.

5.2 Geologic Setting

The Green River Formation was deposited between approximately 54 and 44 Ma by a series of lakes that ranged from freshwater to hypersaline, within the broken foreland associated with the western U.S. cordilleran orogenic zone (Bradley 1964; Dickinson et al. 1988; Roehler 1993; Smith et al. 2008; Fig. 5.1). Eocene Lake Gosiute occupied the Greater Green River basin, which includes the Bridger, Great Divide, and Washakie basins in southwestern Wyoming and the Sand Wash basin in northwestern Colorado. The present study focuses on Laney Member outcrops and proximal drill cores along two continuous cuestas known as the Delaney and Kinney Rims, which bound the northern and western edges of the Washakie basin (Fig. 5.2).

The Laney Member of the Green River Formation marks the final transition from a saline lake to a freshwater lake, that was progressively filled in by volcaniclastic sediment. The Laney Member encompasses three sub-units: the LaClede Bed, dominated by oil shale, the Sand Butte Bed, composed of volcaniclastic siltstone and sandstone, and the Hartt Cabin Bed, composed of heterolithic, shallow freshwater lake deposits (Roehler 1973). The LaClede Bed may be subdivided into upper and lower intervals that correspond overfilled and balanced-fill lake basin conditions, respectively (Rhodes et al. 2007;

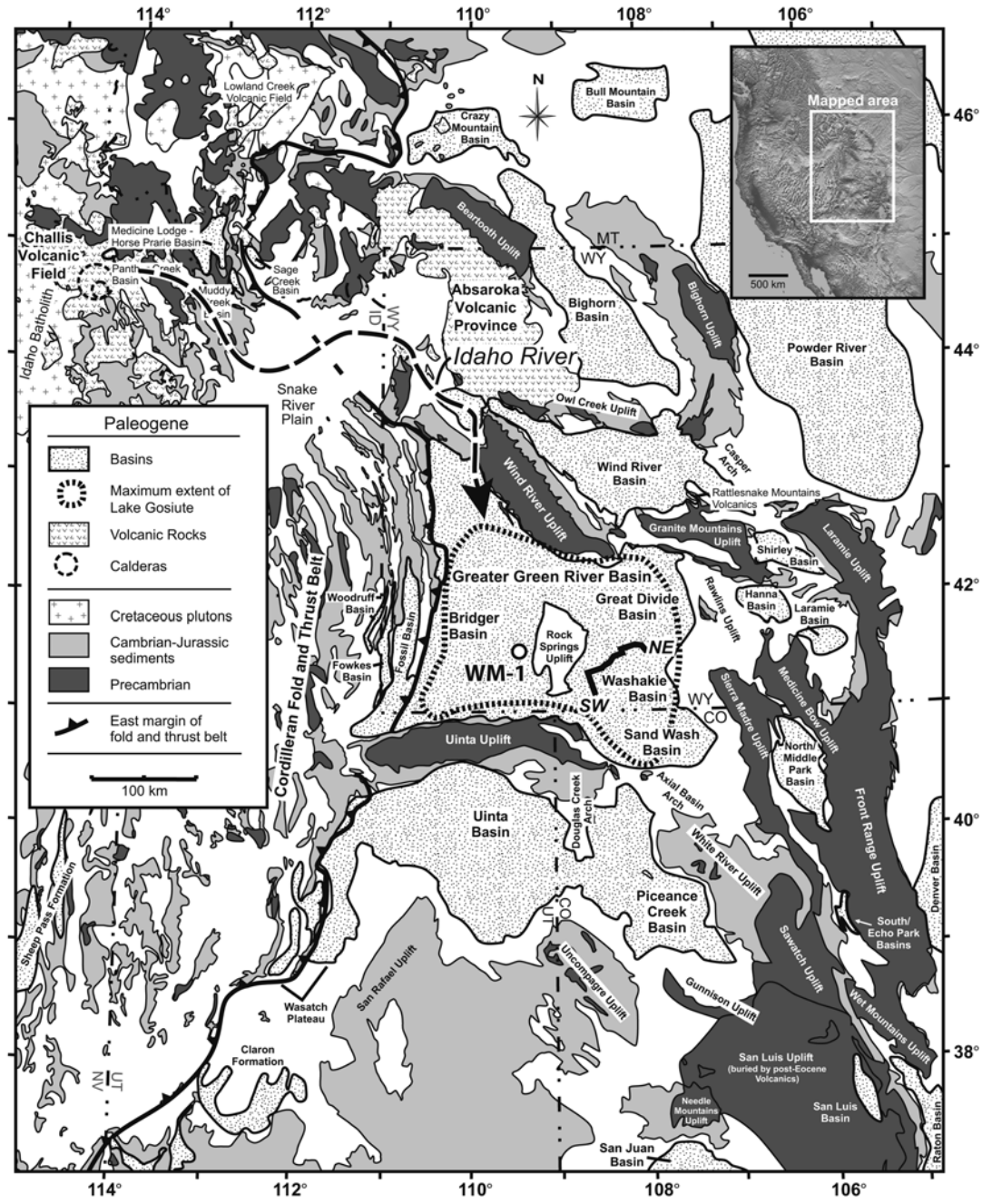

Fig. 5.1 The geology of the Greater Green River Basin, southwestern Wyoming (Modified from Smith et al. 2008). The *SW-NE line* indicates the location of the cross section shown in Fig. 5.2. *WM-1* is the location of the *WM-1* drill core

Smith et al. 2008). The LaClede Bed grades upward into time-transgressive, volcaniclastic deltaic deposits of the Sand Butte Bed (Roehler 1973; Surdam and Stanley 1980). Stratigraphic relationships and paleocurrent analyses indicate that these deltas generally prograded across the basin from the north to the south. It was originally inferred that the volcaniclastic sediment derived from the Absaroka volcanic volcanic field, located in northwest Wyoming (Roehler

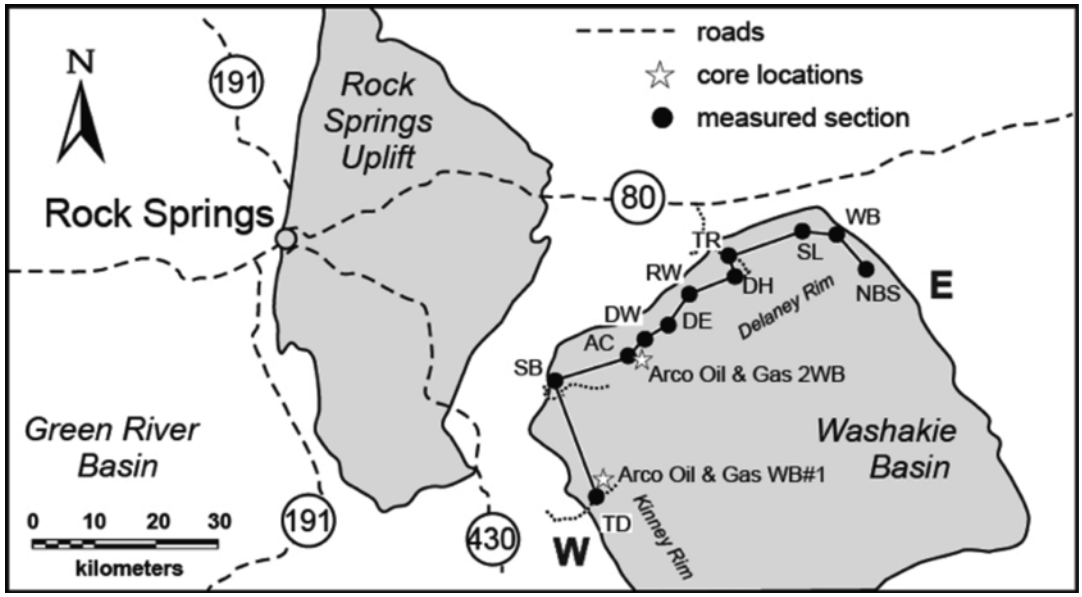

Fig. 5.2 Detailed location map of the measured sections and core along the Delaney and Kinney Rims, Washakie Basin, Green River Basin

1973; Surdam and Stanley 1980; Smith et al. 2008). However, a more recent radioisotopic provenance analysis demonstrated that this sediment was in fact sourced from the higher-elevation Challis volcanic field in central Idaho (Chetel et al. 2011).

5.3 Field Locations and Data Collection

Description of strata along the Delaney and Kinney Rims of the Washakie Basin in the Green River Basin was completed for ten stratigraphic sections and two drill cores obtained from near the outcrop exposures (Supplementary Fig. S5.1, Stratigraphic Cross Section of the Laney Member, Green River Formation, Washakie Basin, Wyoming which can be accessed at http://extras.springer.com). Two of the outcrop sections (DH and SL) are poorly exposed but were measured in an attempt to extend the upper LaClede correlation northward along the Delaney Rim. The two cores that were logged and correlated to outcrop sections (Arco Oil and Gas WB1 and Arco Oil and Gas WB2) were described at the USGS Core Research Center in Denver, CO.

Outcrop correlation was facilitated by measuring the ppm U, ppm Th, %K, and total gamma radiation at 50-cm intervals within seven measured sections with a hand held gamma ray scintillometer (GR-320 enviSPEC portable gamma ray spectrometer, manufactured by Exploranium). Each interval was measured for a total of 60 s. Gamma ray calculations were processed using *Explore* software (Exploranium Radiation Detection Systems, Software Version 3V02). The natural gamma ray spectrum of lacustrine strata reflects changes in volcanic input (K, Th) and detrital heavy minerals (U; Bohacs 1998), and has proven to be an excellent correlation tool for Laney Member strata.

5.4 Sedimentary Facies

Several past studies have documented details of the Laney Member sedimentary facies (Bradley 1964; Buchheim 1978; Stanley and Surdam 1978; Surdam and Stanley 1979, 1980; and Kornegay and Surdam 1980; Roehler 1992). The organization of sedimentary facies presented here builds on those reports, and provides the basis for the basin-scale stratigraphic

Table 5.1 Facies and environmental interpretations

Surdam and Stanley (1979)	This study	Description	Environmental interpretation
Laminated carbonate	**Laminated micritic mudstone**	Brown to blue-gray planar to wavy millimeter-scale organic and carbonate laminations, abundant ostracode and fish fossils	Profundal
Laminated carbonate	**Laminated dolomicritic mudstone**	Brown to blue-gray mm-scale laminated mudstone, ostracode and fish fossils common	Profundal
Evaporite (?)	**Massive dolomicritic mudstone**	Massive tan dolomicritic mudstone, evaporites and mudcracks are common near the top of massive beds	Littoral to sublittoral Dolomite from exposed mudflats through evaporative pumping and washed into the lake during contraction and lowstand
Laminated carbonate	**Stromatolite**		
	algal mats	Laterally continuous thin (cm-scale) algal mats, associated with rip-up clasts, oolites, and ostracodes	Littoral, low relief lake floor
	elongate	Individual elongate (~40-cm long) stromatolites associated with lithic sandstone	Littoral, delta front
	domal	Individual domal (~50–60-cm diameter) stromatolites weather by concentric delamination	Littoral, delta front
Laminated carbonate, *or* molluscan ostracodal calcareous mudstone	**Ostracode, oolitic, and intraclastic grainstone**	Massive white-tan med-coarse grained ostracode, oolitic, and intraclastic grainstone, silicified to very friable in outcrop, rare gastropods	Littoral shoal or foreshore
Evaporite (?)	**Massive dolomicritic silty mudstone**	Massive tan to pink silty dolomicritic mudstone with chert nodules, root casts	Lake plain (paleosol)
Evaporite	**Dolomitic siltstone and sandstone ("buff marker")**	Silt to medium sized sand, beds coarsen and thicken upward, then fine and thin upward. Rip-up clasts occur in discrete horizons before the unit thins upward. Dolomite rhombs make up >50 %.	Low-relief delta front to delta plain
Sandstone and mudstone	**Volcaniclastic sandstone**	Gray brown silty mudstone with plant fragments, gray siltstone, and very fine gray brown volcaniclastic sandstone	High-relief pro-delta to delta front
Variegated red bed, thick-bedded mud rock	**Variegated silty mudstone**	Variegated silty mudstone with claystone, and fine sand to pebble sized clasts	Flood plain
Sandstone	**Lithic to arkosic sandstone**	Fine to coarse grained micaceous lenticular to laterally continuous sandstone with trough cross beds, asymmetrical ripples, burrows, and iron nodules.	Fluvial

interpretations that follow. We subdivide the strata exposed along the Delaney and Kinney Rims into nine lithofacies that are interpreted to represent depositional environments ranging from profundal lacustrine to fluvial (Fig. 5.2). Table 5.1 summarizes these facies and compares them to the "lithologic elements" identified by Surdam and Stanley (1979).

5.4.1 Laminated Micritic Mudstone

Laminated micritic mudstone is the dominant facies in the LaClede Bed of the Laney Member (Fig. 5.3a). It is characterized by tan to gray-brown organic-rich micritic mudstone (oil shale) that contains sub-mm parallel to wavy lamination, abundant ostracode and fish fossils, and numerous mm- to dm-scale analcimated tuff horizons. Mm- to cm-scale volcanic tuff horizons are common, and sometimes exhibit grain-size grading with coarser phenocrysts occurring near their bases (Smith et al. 2003). The bases of some tuffs are marked by compacted, cm-scale tuff-filled cracks that formed in the underlying laminated micrite (Fig. 5.3b). These mud cracks appear polygonal in plan view, and are exclusively associated with tuffs containing analcime. This facies also contains thin (<10 cm), dark brown beds of highly organic-rich dolomicritic mudstone (oil shale) known as "blue beds" because they weather to a light gray/blue color. Blue beds may contain up to 22 % total organic carbon by weight (Fig. 5.3a; Horsfield et al. 1994).

This facies is interpreted to represent a profundal lacustrine environment, based on the preservation fine lamina that are often less than 100 μm thick and the presence of fish fossils (Bradley 1929; Buchheim and Surdam 1977). Anoxic bottom waters likely prevented disruption of lamina by burrowing organisms (c.f. Demaison and Moore 1980). It has been argued previously that the Lake Gosiute was permanently stratified, with anoxic and possibly euxinic bottom waters (c.f. Bradley 1929; Ludlam 1969; Kelts and Hsü 1978). However, Buchheim and Surdam (1977) noted that fossil catfish commonly occur within laminated facies of the Laney Member. Assuming that they were not washed in from rivers flowing into the lake, the presence of these bottom-feeding and dwelling fish argues against permanent lake stratification and suggest that hypolimnetic waters have been at least intermittently dysoxic or oxic with low levels of hydrogen sulfide.

The continuity of lamination and lack of tractive sedimentary structures in this facies suggests that the lake bottom was largely unaffected by waves or currents. Alternatively, sediment cohesion or microbial binding may have inhibited scouring and re-deposition. Some tuff intervals do contain low-angle cross stratification that suggest limited reworking by waves or currents. Tuffs with mudcracks at their base are generally found fully encased within profundal laminated micrite, which appears to preclude an origin via subaerial desiccation. Instead, we propose that they formed subaqueously in response to analcimation of primary volcanic glass shards. Mineral reactions that produce analcime from volcanic glass within alkaline brines include an early hydration reaction (Surdam and Parker 1972), and may have dehydrated underlying, recently-deposited mud.

Horsfield et al. (1994) noted that kerogen in blue beds is dominated by alginate but also includes subsidiary quantities of vitrinite and intertinite, which they proposed was related to increased advection of terrestrial organic matter into the lake. They conclude that enhanced surface runoff may have triggered increased primary productivity, resulting in greater organic matter flux to the sediment. More speculatively, increased runoff may have promoted water column stratification and bottom water anoxia due to temporary ectogenic meromixis. The cause of these episodes of enhanced runoff are not clear. The presence of interinite suggests the possibility that they could record the aftermath of major fires which removed stabilizing vegetation and led to temporarily increased erosion within the lake's watershed.

5.4.2 Laminated Dolomicritic Mudstone

Laminated dolomicritic mudstone is generally tan or brown in color and characterized by alternating mm- to sub-mm-scale laminae of organic matter and dolomicrite. Ostracodes and fish fossils are common in this facies. Laterally extensive, mm- to dm-scale tuff horizons similar to those in the laminated micritic mudstone facies are abundant throughout.

Fig. 5.3 Outcrop photos of Laney Member sedimentary facies (see Fig. 5.2 for locations). (**a**) Laminated micritic mudstone on the Kinney Rim; exposure height is ~2 m. Note thin resistant "blue bed" just above center in the photo. (**b**) Detail of laminated micritic mudstone showing fine lamination and a cm-scale tuff with compacted mud-cracks at its base. (**c**) Algal stromatolite mat at AC, viewed on bedding surface. (**d**) Elongate stromatolite facies at TR. (**e**) Stacked succession of stromatolite heads (location unknown). (**f**) Solitary stromatolite at SB. (**g**) Domal stromatolite at NBS

This facies is interpreted to represent profundal deposition during evaporative concentration of a shrinking lake. Most studies have inferred a penecontemporaneous origin of dolomite in the Green River Formation, but the actual genetic mechanism (or mechanisms) responsible for its formation remains incompletely understood. Wolfbauer and Surdam (1974) and Surdam and Stanley (1979) argued that dolomitization of recently deposited sediment occurred on lake-fringing mudflats due to evaporative concentration of subsurface Mg-rich brine. In contrast, Desborough (1978) proposed that cyanobacteria preferentially concentrated Mg in their tissues with respect to Ca, and that when these tissues degraded at the lake bottom they released Mg that promoted precipitation of authigenic dolomite. Baker and Kastner (1981) suggested that the low sulfate concentration of alkaline Lake Gosiute may have helped promote dolomitzation. In addition to these abiotic mechanisms, Ma (2006) proposed on the basis of elevated $\delta^{13}C$ values that dolomite formed as a result of methanogenesis.

5.4.3 Massive Dolomicritic Mudstone

The massive dolomicritic mudstone contains tan to dark brown, massive dolomicritic mudstone with ostracodes, evaporite casts, algal laminations, and abundant mudcracks. This facies is interpreted to record the transition from sublittoral to supralittoral lacustrine environments that occurs during lake contraction. The lack of lamination could have resulted from bioturbation or brecciation of original lamination by multiple generations of mud cracks, or may reflect storm reworking of fringing mudflats.

5.4.4 Algal Stromatolite

The algal stromatolite facies contains several different stromatolite morphologies, including laterally extensive algal mats, individual elongate stromatolite bodies, and solitary domal stromatolite bodies. Laterally extensive algal mats are found within the Antelope Creek (AC) section (Fig. 5.3c–f). These units are 10–30 cm thick and weather dark gray and tan in outcrop. They are typically underlain by platy dolomicritic intraclasts, and commonly interbedded with ostracode, oolitic, and intraclastic grainstone. Individual elongate stromatolite bodies occur in the Table Rock (TR) section, nearer to the inferred lake margin than the algal mats at Antelope Creek. The Table Rock stromatolite bodies formed over a scoured surface and are closely associated with lithic sandstone and ostracode and oolite grainstone facies. Solitary domal stromatolite bodies in the North Barrel Springs (NBS) section are 0.5- to 1.0-m in diameter, and occur in association with lithic sandstone and associated variegated silty mudstone facies (Fig. 5.3g).

Modern lacustrine stromatolites have been reported in a number of locales, including Green Lake of Fayetteville, New York (Eggleston and Dean 1976), Great Salt Lake (Halley 1976), and Lake Tanganyika (Cohen and Thouin 1987; Casanova and Hillaire-Marcel 1992). These algal buildups have been documented to occur in both lake marginal and fluvial environments. Stromatolite in the Laney Member has been interpreted to form in relatively shallow (littoral) waters during the early phase of lake expansions (Buchheim 1978). Individual stromatolite layers can be correlated over distances exceeding 20 km based on their consistent stratigraphic relationship to distinctive volcanic tuffs, implying contemporaneous growth across large areas of a low-gradient lake margin (Schultz et al. 2004). The shape of elongate and domal stromatolite bodies in Laney strata may have been influenced by unidirectional currents within fluvial environments, or by increasing wave scour closer to the lake margin (Platt and Wright 1991).

5.4.5 Ostracode, Oolite, and Intraclastic Grainstone

The ostracode and intraclastic grainstone lithofacies contains medium sand-sized ostracode and intraclast grains that are very poorly cemented and often poorly exposed (Fig. 5.4a, b).

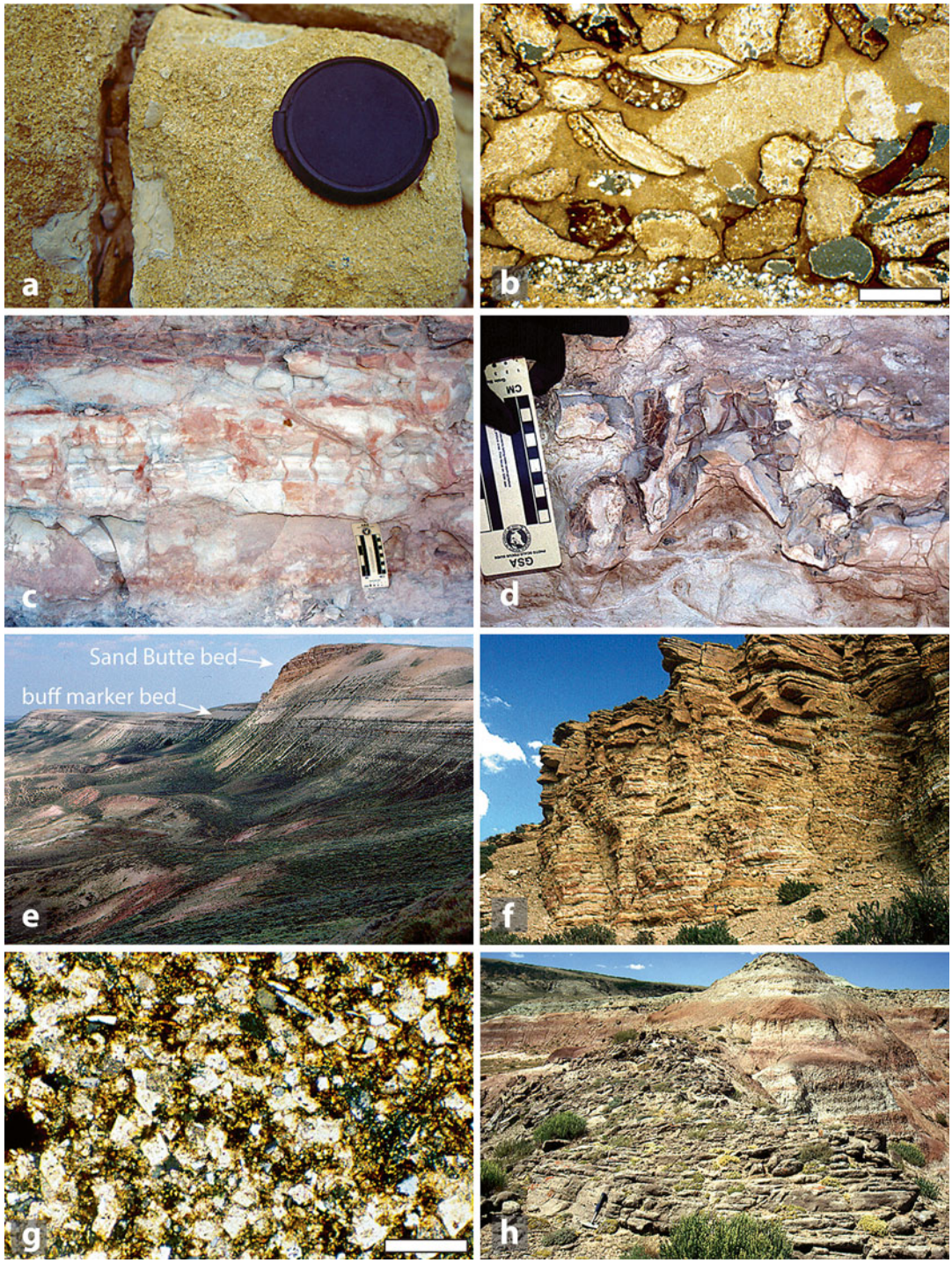

Fig. 5.4 Outcrop photos of Laney Member sedimentary facies (see Fig. 5.2 for locations). (**a**) Ostracode, ooid, and intraclast bed at SB (view of bedding surface). (**b**) Photomicrograph of sample from bed in Fig. 5.4a (scale bar = 1 mm). (**c**) Massive dolomicritic silty mudstone at AC. (**d**) Partially silicified massive dolomicritic silty mudstone with at AC. (**e**) Overview of Cathedral Bluffs Tongue (*red* and *green* slumped beds at base of succession) and Laney Member at SB (overall thickness of Laney ~220 m). (**f**) Siltstone and sandstone facies at TD (buff marker; thickness is ~12.5 m). (**g**) Photomicrograph from within the buff marker bed, note abundance of dolomite rhombs (scale bar = 1 mm). (**h**) Sandstone facies interbedded with variegated silty mudstone facies at NBS

Consequently, sedimentary structures within this facies are difficult to discern. These poorly lithified sediments are commonly associated with thin lignite beds, wispy laminated green mudstone, gastropod fossils, tufa, and algal stromatolite. Larger intraclasts commonly contain stromatolitic lamination and together with ostracodes are often lithified as grapestone (cf. Winland and Matthews 1974).

Similar to marine oolite, lacustrine oolite is interpreted to record shallow, wave-agitated lake marginal areas (Talbot and Allen 1996). Inorganic carbonate can precipitate in lacustrine environments when chemically different water masses are mixed (such as groundwater and lake water) or as a result of photosynthetic activity (Kelts and Hsü 1978).

The ostracode, oolitic, and intraclastic grainstone in the Laney Member are interpreted to represent beach sands and littoral shoals. Similar facies have been observed along modern lacustrine shorelines that lack clastic input, as is the case for stretches of the shoreline of Lake Tanganyika (Cohen and Thouin 1987).

5.4.6 Massive Dolomicritic Silty Mudstone

The massive dolomicritic silty mudstone lithofacies weathers spheroidally and is commonly pink to tan in color (Fig. 5.4c, d). Beds are typically 0.5–2.0 m thick, and are commonly associated with cm-scale chert nodules and root traces. Mudcracks and incipient brecciation are common, as are interbeds of subhorizontally laminated siltstone. Lacustrine fossils are absent.

The presence of root traces is interpreted to reflect colonization of an exposed lake-plain by land plants, and the lack of lacustrine fossils and presence of mudcracks further indicate that the sediment was subaerially exposed. The chert nodules have been previously interpreted to be Magadi-type chert, diagenetically altered from magadiite, a hydrous sodium silicate deposited from strongly alkaline lake waters (Eugster 1967, 1969; Surdam and Stanley 1979). More recent work on lake Magadi concluded that chert formation occurred due to decomposition of pyroclastic deposits by alkaline groundwater, and that chert precipitation was strongly influenced by biogenic CO_2 (Behr 2002). However, the Magadi basin lies within an area of active volcanism and is underpinned by trachyte, and thus differs substantially from the setting of the Green River basin.

Overall this facies is interpreted to record incipient pedogenic modification of an originally deposited silty mudstone, but well-developed soil structures are absent.

5.4.7 Dolomitic Siltstone and Sandstone

This facies is restricted to one stratigraphic interval that is informally known as the "buff marker bed" (Roehler 1973). This unit is roughly 12.5 m thick at its best exposure in the Trail Dugway (TD) section where it is composed of silt to medium grained micaceous sand, and dolomite, interbedded with mudstone (Fig. 5.4e, f). The interval near the base of the buff marker bed consist of siltstone to fine sandstone, and is parallel to sub-parallel bedded with wavy mudstone laminations. The beds coarsen and thicken upward in the section and are composed of wavy-bedded, fine- to medium-grained sand and mudcracked mudstone. Sandstone units contain ripple cross lamination, trough cross beds, and some massive laterally discontinuous beds. The beds fine- and thin-upward and are composed of thin dolomitic siltstone and mudstone beds with intraclasts 3–4-cm in length. Overall dolomite content reaches as much as 50 % (Fig. 5.4g). The only fossils that have been recovered from this facies include crocodile and insects (Buchheim 1978).

Surdam and Stanley (1979) interpreted this facies as an "evaporite" facies and reported that it contained "beds and nodules of saline minerals". We did not observe such features in outcrop or core however, and did not find any clear evidence that they were originally present (such as pseudomorphs or collapsed beds). We agree however with previous interpretations that this facies records a major drop in the level of Lake Gosiute, and that it represents deposition in playa to shal-

low lake (littoral) settings which received siliciclastic input from intrabasinal streams draining the Laramide ranges to the east and south of the Greater Green River Basin (Fig. 5.1).

5.4.8 Volcaniclastic Sandstone

The Sand Butte Bed of the Laney Member is characterized by volcaniclastic detritus generally ranging in size from siltstone to medium-grained sandstone, interbedded with gray brown silty mudstone containing plant fragments. It outcrops along the Delaney Rim from the Delaney East section to the Antelope Creek section, along the entire Kinney Rim. Surdam and Stanley (1980) documented basaltic and andesitic rock fragments within the Sand Butte Bed, with an increasing component of pyroclastic material toward its southern extent in the Green River Basin. The uppermost sandstone bed in the Antelope Creek section is a very-fine-grained, purple, cross-bedded sandstone that contains bone fragments and carbonaceous material.

Bradley (1964), Roehler (1973), and Stanley and Surdam (1978) interpreted the Sand Butte Bed as a Gilbert-type fluvial/deltaic deposit with individual bottomset, foreset, and topset strata that can be mapped in outcrops along the Delaney Rim. The thickness and bedding within the deltaic foresets suggests progradation into a shallow lacustrine environment (Stanley and Surdam 1978). The presence of 10 m-scale soft sediment deformation at the base of the deltas suggests that this facies was rapidly deposited across a soft substrate, and may have been destabilized by seismic activity. The Sand Butte deltas have been compared to the late Quaternary Truckee River deltaic deposits in Pyramid Lake, Nevada (Stanley and Surdam 1978). Surdam and Stanley (1980) inferred that the source of volcaniclastic detritus lay within the Absaroka volcanic field, located approximately 100 km to the north of the Green River basin. However, more recent geochemical provenance studies by Chetel et al. (2011) demonstrate that this material was instead derived from the Challis volcanic field, located approximately 500 km to the northwest in central Idaho.

5.4.9 Variegated Silty Mudstone

Variegated silty mudstone crops out along most of the Delaney Rim, and along the base of Kinney Rim. It is characterized by red, purple, green, and white laterally continuous mottled bands of claystone to mudstone with varying amounts of silt and sand (Fig. 5.4h).

This facies represents the alluvial Wasatch Formation that intertongues with the lacustrine members of the Green River Formation along the margins of the basin. The variegated beds have been described in detail by Braunagel and Stanley (1977) to represent sedimentary couplets that fine upward and are interpreted to have been deposited between channels during flooding events.

5.4.10 Lithic to Arkosic Sandstone

The lithic sandstone facies is characterized by gray-tan to purple-red medium to coarse-grained sandstone with cm-scale iron concretions, low and high angle planar cross beds, 0.5- to 1-m scale trough cross beds, plant fragments, lignite, ripple marks and surfaces that have been scoured to ~1 m. Resistant sandstones are more calcareous and often interbedded with green, bluish, and/or brown mudstone.

The predominantly fluvial characteristics and mineral composition of the lithic to arkosic sandstone lithofacies are interpreted to indicate deposition from streams originating in the Laramide uplands to the east and south of the Greater Green River Basin.

5.5 Facies Associations

The above facies form three major associations that approximately coincide with established stratigraphic subdivisions. The Laney Member encompasses the fluctuating profundal and fluvial-lacustrine facies associations (c.f. Carroll and Bohacs 1999), whereas the Cathedral Bluffs Tongue of the Wasatch Formation represents the alluvial facies association. The detailed expression of each of these facies associations also varies laterally within the study area (Fig. 5.5).

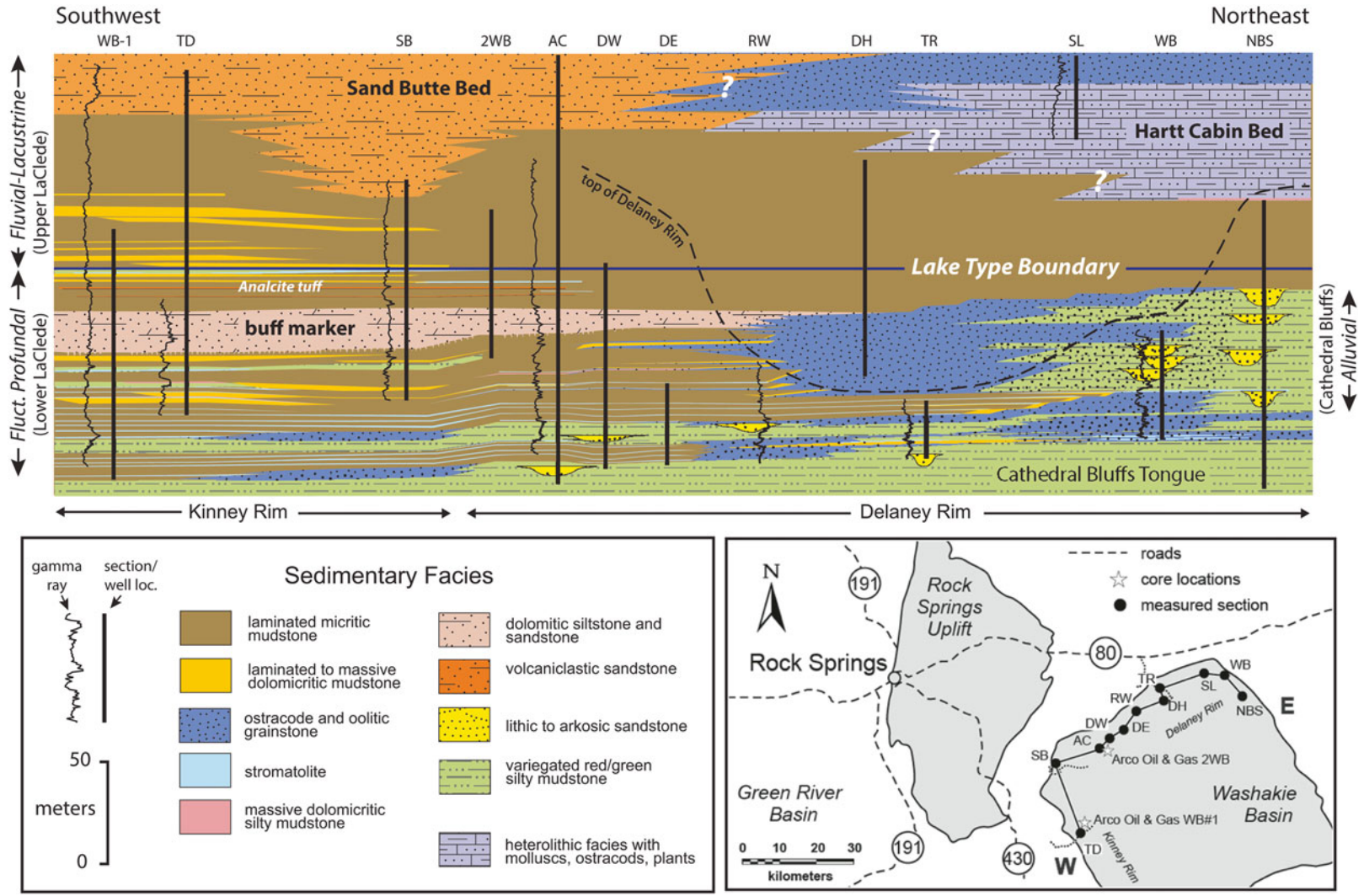

Fig. 5.5 Stratigraphic cross section of the Laney Member along the Kinney and Delaney Rims

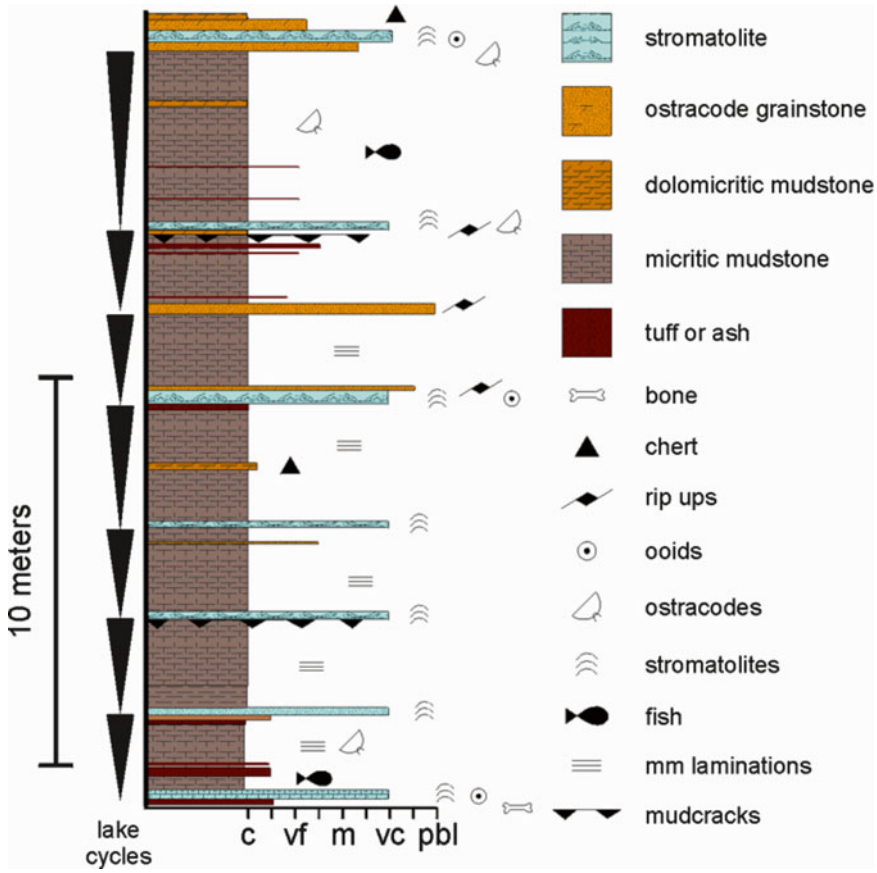

Fig. 5.6 Detailed measured section of the fluctuating profundal facies from the DW section (see Fig. 5.2 for location)

Stratigraphic correlations within the study area were based primarily on distinctive stratal surfaces and lithologic markers that can often be traced visually across tens of km. These include exposure surfaces interpreted to record episodes of lake desiccation, flat pebble conglomerate and stromatolite horizons interpreted to represent lake transgression, and highly organic-rich profundal facies (oil shale) interpreted to record maximum lake expansion. Distinctive volcanic tuff horizons and gamma-ray spectroscopy profiles were used to support correlations.

5.5.1 Fluctuating Profundal Facies Association (Lower LaClede Bed)

The fluctuating profundal facies association coincides with the lower LaClede Member. In the southwestern part of the study area (Localities WB-1 to DE in Fig. 5.5), this association is typically dominated by repetitive facies successions ~1–5 m thick. These successions typically start with flat pebble conglomerate, which is overlain by ostracod or ooid grainstone and/or stromatolite (Figs. 5.6, 5.7; locally one or more of these facies may be missing). They then grade abruptly into laminated micritic and dolomicritic mudstone, in varying proportions. Massive dolomicritic mudstone containing mudcracks predominates near the top of the succession. The massive dolomicritic silty mudstone facies forms a minor component of this association, and is located stratigraphically above massive dolomicritic mudstone when present.

The lower LaClede bed at the TD through DE localities contains at least 14 of these repetitive successions, which correspond to the "depositional cycles" of Surdam and Stanley (1979;

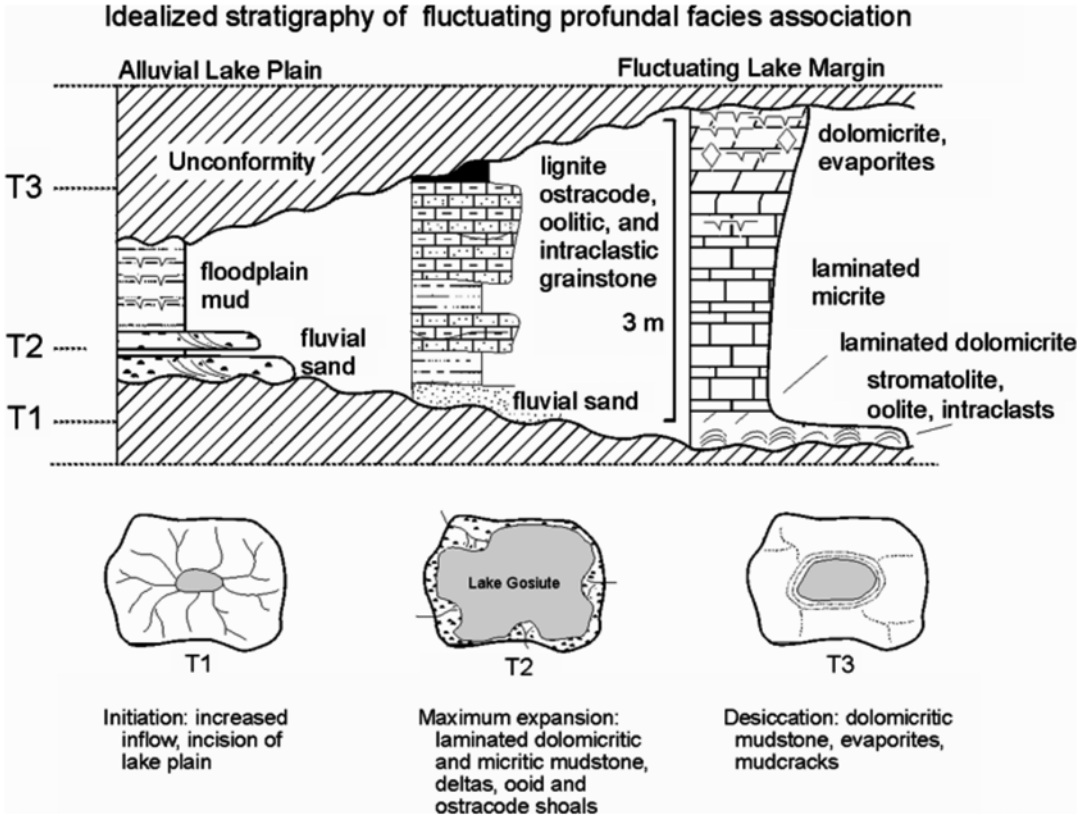

Fig. 5.7 Idealized chronostratigraphy of the fluctuating profundal facies association (Modified from Surdam and Stanley 1979; Rhodes et al. 2002)

Fig. 5.5). These successions meet the definition of parasequences (Van Wagoner et al. 1988), in which lacustrine flooding surfaces substitute for marine flooding surfaces (Bohacs 1998). Three to four of these parasequences are preserved above the alluvial Cathedral Bluffs Tongue and below a ~10-m interval of lithic sandstone and variegated silty mudstone facies. An additional 9–10 parasequences lie above that. These are overlain in turn by an interval of recessive dolomitic siltstone and sandstone facies known informally as the "buff marker bed". The base of the buff marker bed is abrupt, possibly scoured, and has compacted mud cracks at its base that penetrate downward ~2–3 m into the underlying profundal mudstone. The cracks are spaced 15–20 m apart, are typically filled with dolomitic siltstone and sandstone similar to the buff marker facies, and also contain algal intraclasts. Dm-scale beds within the buff marker initially coarsen and thicken upward for ~6.5 m, then thin and fine upward for its remaining ~6 m (Fig. 5.8). An additional 2–3 fluctuating profundal parasequences lie above the buff marker. Above these last parasequences the LaClede Bed transitions into the fluvial-lacustrine facies association. This transition is informally designated herein to mark the boundary between the "lower LaClede Bed" and "upper LaClede Bed".

Ostracod and oolitic grainstone, lignite, sandstone, carbonaceous mudstone, and lignite become gradually more abundant toward the northeast part of study area (Localities RW through SL in Figs 5.5, 5.9). The buff marker bed simultaneously thins in the same direction, and was either never deposited or was eroded from localities from DH through NBS. The upper part of the lower LaClede bed does not crop out along the Delaney Rim between localities RW and WB; the sections at localities DH

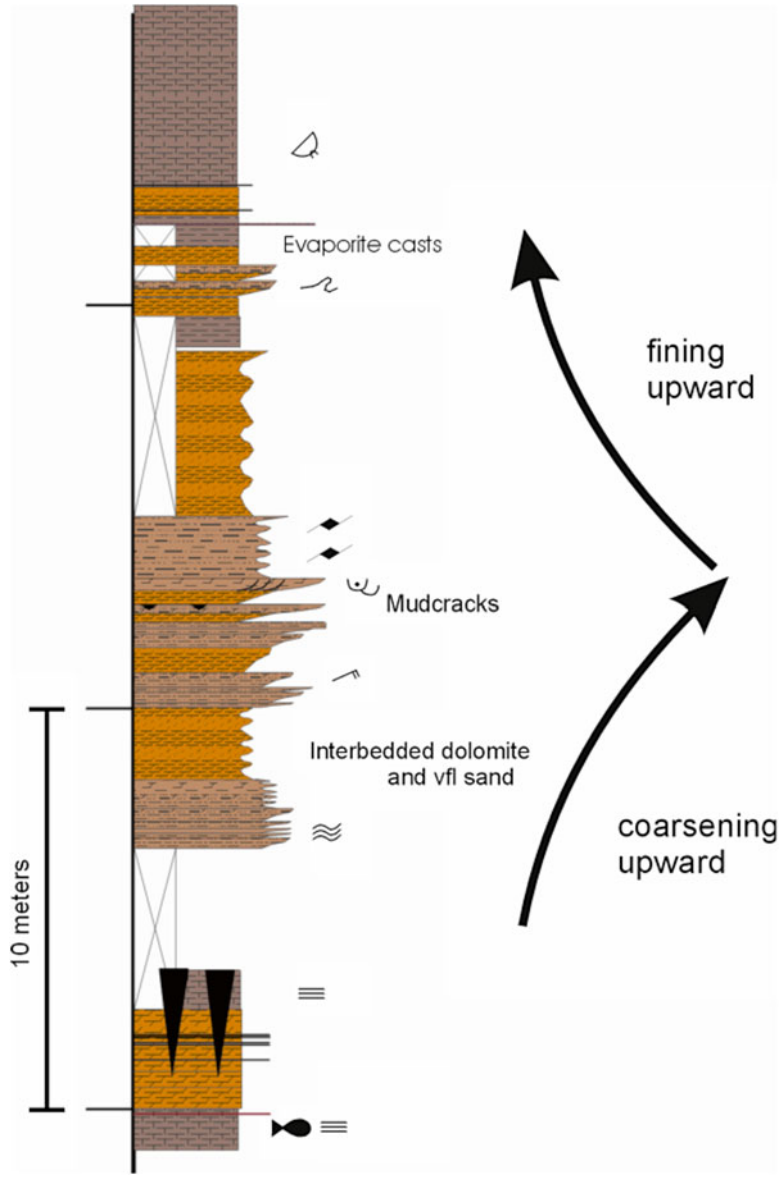

Fig. 5.8 Stratigraphic section through the buff marker bed at TD, illustrating transition from coarsening- and thickening-upward to fining- and thinning-upward beds (see Fig. 5.2 for location)

and SL were therefore described using poorer-quality exposures located to the southeast of the Delaney Rim itself. At the easternmost localities the fluctuating profundal association grades laterally into the alluvial association (WB and NBS in Fig. 5.5)

Buchheim (1978) and Surdam and Stanley (1979) interpreted cycles (parasequences) in the lower LaClede Bed to record the episodic rise and fall of Lake Gosiute. The basal stromatolite and associated facies were deposited during lake transgression, laminated dolomicritic mudstone and laminated micritic mudstone as the lake expanded, and dolomicritic mudstone was deposited as the lake contracted. Ostracode and ooid grainstone facies are interpreted to represent carbonate shoals that formed during lake transgressions.

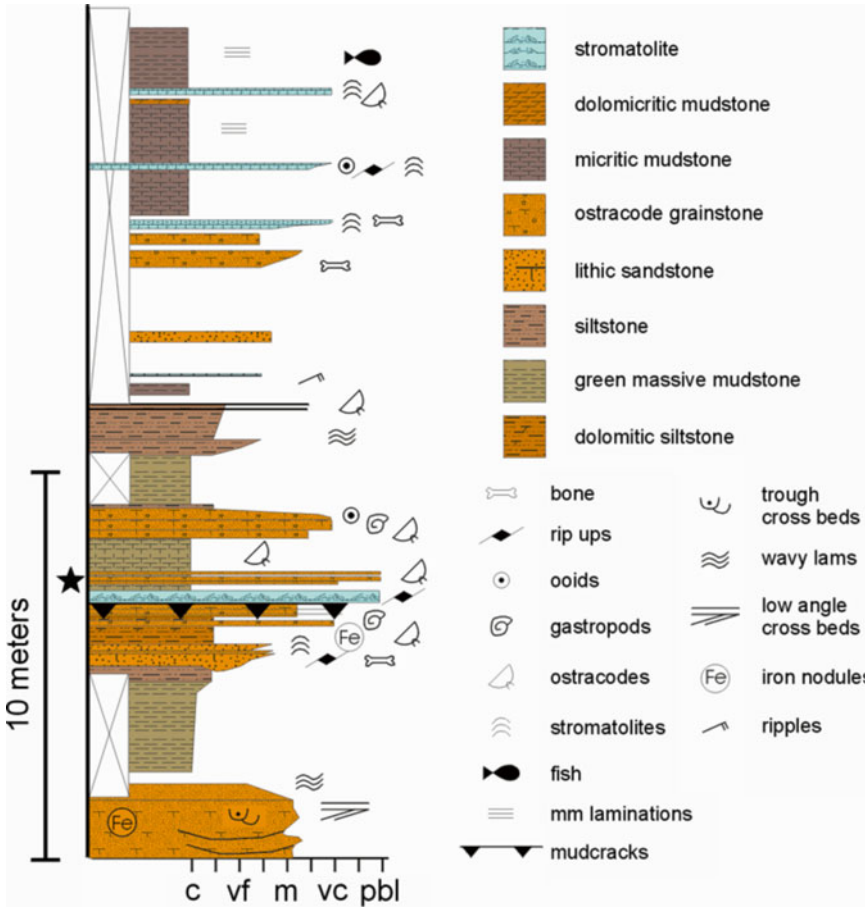

Fig. 5.9 The lake marginal expression of the fluctuating profundal facies association at the TR section (see Fig. 5.2 for location)

The exposures along the Kinney and Delaney Rims are interpreted to represent an approximate transect from the basin margin (northeast) to basin center (southwest), though the true basin hypsometry cannot be fully determined from the data in this study. Overall the lower LaClede Bed consists of a series retrogradational parasequences, which record a progressive northeastward expansion of the maximum extent of lacustrine facies through time (Fig. 5.5). Individual parasequences generally thicken upward within the Lower LaClede Bed overall, with the thickest parasequences occurring above the buff marker.

The buff marker bed stands out as unique within this interval, and has been interpreted to represent sudden desiccation of Lake Gosiute, followed by fluvial-deltaic deposition of a mixture of fine-grained volcaniclastic sediment and dolomite on a playa or in a shallow lake (Rhodes et al. 2007). The large mudcracks represent giant mudcrack polygons that formed during desiccation. The vertical succession in sedimentary structures, bed thickness, and grainsize suggest initial progradation of these materials across an exposed basin floor, followed by retrogradation of fluvial-deltaic in response to a rising lake. Rhodes et al. (2007) proposed that these events resulted from upstream volcanic blockage and subsequent reestablishment of a major stream that drained into Lake Gosiute. The buff marker bed also contains abundant

mica grains however, which are difficult to reconcile with a purely volcanic source. It may alternatively record landslide blockage of an influent river that drained crystalline basement rocks. It could conceivably also reflect an unusually abrupt and intense episode of climatic aridity (c.f. Surdam and Stanley 1979), but if such an episode did occur it appears to have been unique during the deposition of the Laney Member. The profundal facies directly underlying the buff marker contain no precursor evidence of such a change, and giant mudcracks formed directly on laminated micritic mudstone. The overlying profundal facies likewise show no evidence of a permanent climate shift. It is also worth noting that a similarly distinctive deposit has not been reliably identified within the Laney Member in the Bridger basin (c.f. Murphy et al. 2014).

5.5.2 Fluvial-Lacustrine Facies Association (Upper LaClede Bed)

The fluvial-lacustrine facies association occurs within the upper part of the LaClede bed, and extends upward to include the Sand Butte and Hartt Cabin Beds. The transition between the lower vs. upper LaClede Bed is marked by a partially silicified intraclast, oolite and stromatolite horizon that forms a well-defined topographic bench at the SB locality (Fig. 5.5). Overlying strata consist of alternating beds of laminated micritic and laminated to massive dolomicritic mudstone. Micritic mudstone dominates the fluvial-lacustrine facies association along the Delaney and Kinney Rims (Fig. 5.10). Unlike the fluctuating profundal facies association below, the fluvial-lacustrine facies association lacks evidence for episodic salinity fluctuations or lake desiccation. Distinct parasequences are difficult to define, partly due to the dominance of uninterrupted mudstone facies and partly due to incomplete outcrop exposure. Stromatolite horizons, which serve as resistant marker beds in the lower LaClede Bed, are absent in the upper LaClede, but freshwater molluscs are relatively common. The contact between the upper LaClede Bed and the overlying Sand Butte Bed is gradational, and marked by interbeds of mudstone and sandstone (Fig. 5.10).

Detailed lateral correlation of strata of the fluvial lacustrine facies association is hampered by its generally poor outcrop exposure. However, the contact between the LaClede and Sand Butte Beds is clearly diachronous, generally younging from northwest to southeast (described in detail by Surdam and Stanley 1980; Chetel and Carroll 2010, and Doebbert et al. 2010; Fig. 5.11). We interpret the upper LaClede Bed to represent the profundal to sublittoral deposits of a relatively stable, freshwater lake that was progressively infilled by volcanic detritus. Due to this infilling, its stratigraphic architecture is likely dominated by shoreline progradation, however, outcrop quality is insufficient to fully test this hypothesis. The contact between the upper LaClede Bed and the Hartt Cabin Bed is also poorly exposed, and is presumably gradational. The base of the Hartt Cabin bed is marked locally at the NBS and WB localities by a ~10 cm silicified coquina or packstone containing *Elimia tenera* allochems which is known informally as the "turretella agate".

5.5.3 Alluvial Facies Association (Cathedral Bluffs Tongue)

The alluvial Wasatch Formation, characterized by sandstone and variegated silty mudstone, underlies and interfingers with the fluctuating profundal facies of the lower LaClede bed. Laterally discontinuous, medium to thick-bedded lithic sandstone beds punctuate the variegated silty mudstone facies and cap sinuous outcrop ridges. These sinuous sand-capped ridges appear to represent paleo-channel fill and therefore appear to represent exhumed Eocene inlets to Lake Gosiute. The variegated silty mudstone that surrounds the sandstone is interpreted to be the result of alluvial flood plain deposition (Braunagel and Stanley 1977).

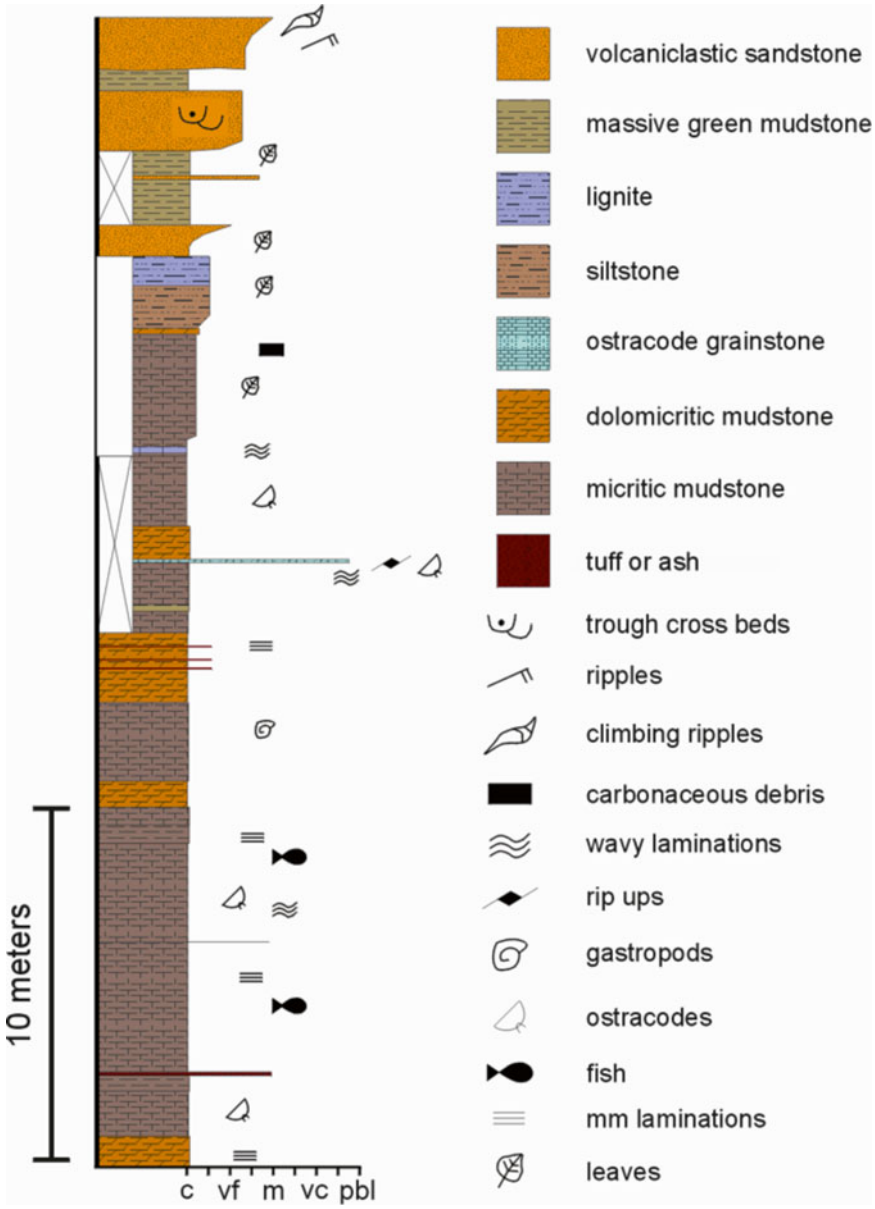

Fig. 5.10 Detailed measured section showing fluvial-lacustrine facies association within the SB section (see Fig. 5.2 for location)

5.6 Discussion and Conclusions

Overall the Laney Member records a stepwise shift from a balanced-fill to overfilled lake basin. During deposition of the lower LaClede Bed, Lake Gosiute experienced continuous and dramatic fluctuations in hydrology, during which the Washakie basin shifted from an exposed lake plain to a relatively deep lake and back again. The timing of these fluctuations is presently unknown, but similarly-scaled parasequences elsewhere in the Green River Formation have been interpreted to reflect precessional-scale climate changes (e.g., Bradley 1929; Fischer and Roberts 1991; Roehler 1993; Machlus et al. 2008; Meyers 2008; Aswasereelert et al. 2013;

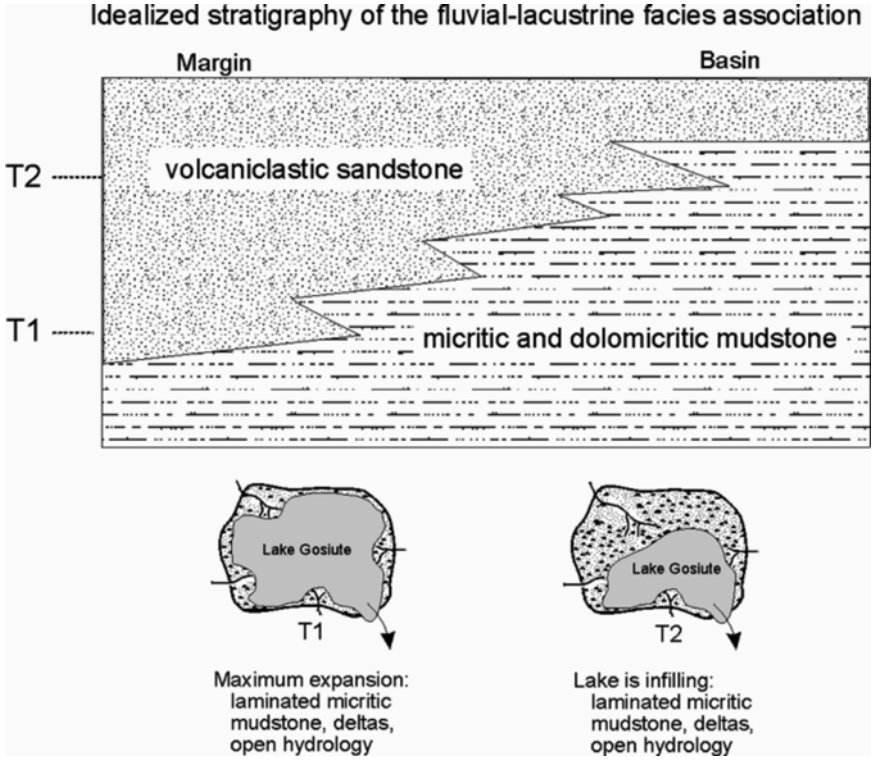

Fig. 5.11 Idealized cross section through the fluvial-lacustrine facies association, illustrating the time-transgressive nature of the basal contact of the Sand Butte Bed (volcaniclastic sandstone)

Machlus et al. 2015). Smith et al. (2008) estimated average net accumulation rates on the order of 100 μm per year for fluctuating profundal facies of the Laney Member, based on interpolation between dated tuffs. Parasequence thickness in the lower LaClede Bed ranging from 1 to 5 m in thickness would represent 10–50 ky based on this assumption. This age range is permissive of forcing by either precession or obliquity.

The transition from the Wilkins Peak Member to Laney Member in the Bridger basin (Fig. 5.1) resulted from capture of a stream draining areas east of Lake Gosiute, based on the occurrence of anomalously high $^{87}Sr/^{86}Sr$ ratios in the lowermost Laney Member in the Bridger basin (Doebbert et al. 2014; Smith et al. 2014; Fig. 5.12). A similar spike in $^{87}Sr/^{86}Sr$ was not observed in the Washakie basin however (Rhodes et al. 2002; Carroll et al. 2008), suggesting that the base of the Laney Member is slightly older in the Bridger basin than in the Washakie basin. The lowermost Laney Member beds in the Bridger basin therefore appear to be time-equivalent to alluvial facies of the Cathedral Bluffs Tongue in the Washakie basin. Lake Gosiute subsequently expanded eastward across the Rock Springs Arch, due to ongoing capture of streams with lower $^{87}Sr/^{86}Sr$. The changing spatial relationships between lacustrine and alluvial facies in the Washakie basin indicate that the maximum extent of Lake Gosiute continued to gradually expand northeastward after this time (Fig. 5.5). $^{87}Sr/^{86}Sr$ in the lower LaClede Bed slowly shifted toward lower values throughout this time (Fig. 5.12), suggesting the continued expansion of drainage from less radiogenic source lithologies. These could potentially include Eocene volcanic rocks located north of the basin, or marine carbonate facies in the Sevier fold and thrust belt to the west.

The maximum water depth of the lake during deposition of the lower LaClede Bed is unknown.

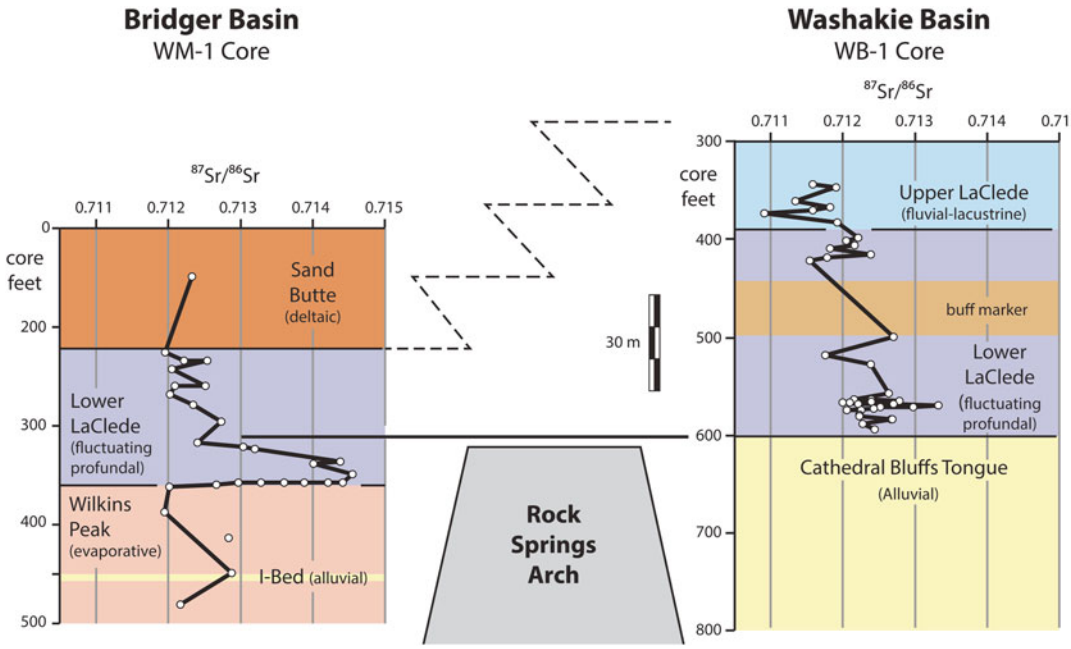

Fig. 5.12 Chemostratigraphic correlation of the Laney Member between the Bridger and Washakie basins based on $^{87}Sr/^{86}Sr$ (see Fig. 5.1 for location of the WM-1 drill core, and Fig. 5.2 for location of the WB-1 drill core; Sr isotopic data reported by Rhodes et al. 2002; Doebbert et al. 2014). The *solid horizontal line* joining the two sections indicates our interpreted chronostratigraphic correlation of the LaClede Bed between the two localities. The *dashed zig-zag line* indicates the time-transgressive gradational contact between the Sand Butte and LaClede Beds

It may be constrained however by the lateral relationship between profundal facies preserved in the southwestern part of the study area vs. alluvial facies preserved to the northeast. The rapidity of vertical facies changes within individual parasequences and the gradual nature of lateral transitions across the study transect are consistent with a relatively low-relief basin floor. Assuming that the study transect is oriented in the maximum dip direction of the lake floor, maximum water depth can be estimated based on analogy to modern depositional systems. For example, the modern Bear River delta in Utah loses elevation at an average rate of approximately 1 m per km as it flows toward Great Salt Lake. This comparison may be reasonable considering that the lower LaClede Bed is underlain by alluvial facies (Fig. 5.5), which may have been deposited on alluvial plains associated with low-relief deltas. Based on these assumptions, the maximum lake depth would be about 50 m. However, the true gradient of the Lake Gosiute basin floor may have been less than the Bear River Delta, based on the preservation of stromatolite horizons that continue uninterrupted for distances of 20 km or more. If so then the lake may have been considerably less than 50 m deep at its maximum.

The fluvial-lacustrine facies of the upper LaClede Bed record a markedly different basin hydrology in which lake level fluctuations were minimal. We infer that from this point onward the basin was generally filled to its spill point, and that an outlet existed to the Piceance Creek basin to the south (c.f. Smith et al. 2008). Minimum water depths during deposition of the upper LaClede Bed are constrained by the preserved relief on the Sand Butte Member delta foresets. The largest of these reach about 25 m in relief, although most are less than 10 m (Surdam and Stanley 1979, 1980; Chetel and Carroll 2010). Delta foresets only indicate relief at the lake margin however, and do not take into account the slope of the lake floor between the toe of the

foresets and the deepest point of the basin. Post-depositional compaction has also not been accounted for in depth estimates based on preserved height of foresets. The maximum lake depth during deposition of the upper LaClede Bed was therefore likely greater than indicated by foreset relief. The average size of foresets appears to change little across the basin, consistent with a low-relief basin floor and modest water depths.

The transition between the lower and upper LaClede Bed may be considered a "fill to spill" surface, based on the change in paleohydrology of Lake Gosiute that occurred at this time (~49 Ma; Smith et al. 2003, 2008, 2010). This timing coincides with the expansion of the Mahogany Zone across the Piceance and Uinta basins, implying that spillover of Lake Gosiute imposed a first-order control on the hydrology of Lake Uinta. Carroll et al. (2008) and Doebbert et al. (2010) proposed on the basis of oxygen and strontium isotopic studies that these changes occurred in response to capture of a river draining high-elevation volcanic topography within the Challis volcanic field in central Idaho. Rather than corresponding to a discrete surface, however, this observed shift toward lower $\delta^{18}O$ and $^{87}Sr/^{86}Sr$ values occurs over an interval of up to ~20 m. Instead of a discrete drainage capture event, this gradual shift suggests a more complex process of drainage expansion (or construction of volcanic topography) that may have spanned as much as 200 ky. Chetel et al. (2011) demonstrated based on Pb isotopic data and detrital ages that the Sand Butte Bed volcaniclastic material originated in the Challis volcanic field. Its appearance in the Washakie basin well after the transition to fluvial-lacustrine facies reflects the time required for this material to reach the Greater Green River basin and then progressively infill the lake.

Much remains to be learned about the Laney Member. For example, stratigraphic relationships to the Rock Springs Arch and to the Laney Member in the Bridger basin to the west remain uncertain, as does the origin and significance of the buff marker. The relationship of the Laney Member to the detailed structural evolution of the margins of the Greater Green River basin also remains poorly understood. Some of the most glaring gaps in our knowledge concern the origin of the mudstone facies themselves, which comprise a complex mixture of carbonate and silicate mineralogies and possess extraordinarily complex sedimentary structure down to the micron level. We look forward to future studies that will investigate some of these problems in greater depth.

Acknowledgments We thank B.L. Beard, K.M. Bohacs, H.P. Buchheim, G. Grabowski, C.M. Johnson, J.T. Pietras, and M.E. Smith for their helpful assistance, advice, and discussions concerning the Laney Member. E. Drew, E. Parcher-Wartes, and J. Van Alstine served as tireless field assistants during this project, and A. DeVaughn assisted with laboratory analyses. We are grateful for funding received from Conoco, Texaco, the U.S. National Science Foundation (EAR-9406684 and EAR-9628549 to C.M. Johnson), the Donors of the Petroleum Research Fund of the American Chemical Society, the J. David Love Wyoming Field Geology Fellowship, and the University of Wisconsin-Madison Department of Geoscience, and the Morgridge Distinguished Graduate Fellowship. We also thank M.E. Smith for thoughtfully reviewing the manuscript.

References

Aswasereelert W, Meyers SR, Carroll AR, Peters SE, Smith ME, Feigl KL (2013) Basin-scale cyclostratigraphy of the Green River Formation, Wyoming. Geol Soc Am Bull 125:216–228

Baker PA, Kastner M (1981) Constraints on the formation of sedimentary dolomite. Science 213:214–216

Behr H (2002) Magaiite and Magadi chert; a critical analysis of the silica sediments in the Lake Magadi Basin, Kenya. In: Renaut RW, Ashley G (eds) Sedimentation in continental rifts, vol 73, Society for Sedimentary Geology (SEPM) Special Publication. SEPM (Society for Sedimentary Geology), Tulsa, pp 257–273

Bohacs KM (1998) Contrasting expressions of depositional sequences in mudrocks from marine to nonmarine environs. In: Schieber J, Zimmerlie W, Sethi P (eds) Mudstones and shales, v. 1, characteristics at the basin scale. Schweizerbart'sche Verlagsbuchhandlung, Stuttgart, pp 32–77

Bohacs KM, Carroll AR, Neal JE, Mankiewicz PJ (2000) Lake-basin type, source potential, and hydrocarbon character: an integrated sequence-stratigraphic-geochemical framework. In: Gierlowski-Kordesch EH, Kelts KR (eds) Lake Basins through space and time, vol 46, American Association of Petroleum Geologists Studies in Geology. American Association of Petroleum Geologists, Tulsa, pp 3–34

Bradley WH (1929) The varves and climate of the Green River epoch. U.S. Geological Survey professional paper 158-E. U.S. Government Printing Office, Washington DC, 110 p

Bradley WH (1964) The geology of the Green River Formation and associated Eocene rocks in southwestern Wyoming and adjacent parts of Colorado and Utah. U.S. Geological Survey professional paper 496-A. U.S. Government Printing Office, Washington DC, 86 p

Braunagel LH, Stanley KO (1977) Origin of variegated redbeds in the Cathedral Bluffs Tongue of the Wasatch Formation (Eocene), Wyoming. J Sediment Petrol 47:1201–1219

Buchheim HP (1978) Paleolimnology of the Laney Member of the Eocene Green River Formation. PhD thesis, University of Wyoming, Laramie, 101 p

Buchheim HP, Surdam RC (1977) Fossil catfish and the depositional environment of the Green River Formation, Wyoming. Geology 5:196–198

Carroll AR, Bohacs KM (1999) Stratigraphic classification of ancient lakes: balancing tectonic and climatic controls. Geology 27:99–102

Carroll AR, Doebbert AC, Booth AL, Chamberlain CP, Rhodes-Carson MK, Smith ME, Johnson CM, Beard BL (2008) Capture of high-altitude precipitation by a low-altitude Eocene lake, western U.S. Geology 36:791–794

Casanova J, Hillaire-Marcel C (1992) Late Holocene hydrological history of Lake Tanganyika, East Africa, from isotopic data on fossil stromatolites. Palaeogeogr Palaeoclimatol Palaeoecol 91:35–48

Chetel LM, Carroll AR (2010) Terminal infill of Eocene Lake Gosiute, Wyoming, USA. J Sediment Res 80:492–514

Chetel L, Janecke SU, Carroll AR, Beard BL, Johnson CM, Singer BS (2011) Paleographic reconstruction of the Eocene Idaho River, North American Cordillera. Geol Soc Am Bull 123:71–88

Cohen AS, Thouin C (1987) Near-shore carbonate deposits in Lake Tanganyika. Geology 15:414–418

Demaison DJ, Moore GT (1980) Anoxic environments and oil source bed genesis. AAPG Bull 64:1179–1209

Desborough GA (1978) A biogenic-chemical stratified lake model for the origin of oil shale of the Green River Formation: an alternative to the playa-lake model. Geol Soc Am Bull 89:961–971

Dickinson WR, Klute MA, Hayes MJ, Janecke SU, Lundin ER, McKittrick MA, Olivares MD (1988) Paleogeographic and paleotectonic setting of Laramide sedimentary basins in the central Rocky Mountain region. Geol Soc Am Bull 100:1023–1039

Doebbert AC, Carroll AR, Mulch A, Chetel LM, Chamberlain CP (2010) Geomorphic controls on lacustrine isotopic compositions: evidence from the Laney Member, Green River Formation, Wyoming. Geol Soc Am Bull 122:236–252

Doebbert AC, Johnson CM, Carroll AR, Beard BL, Pietras JT, Rhodes-Carson MK, Norsted B, Throckmorton LA (2014) Controls on Sr isotopic evolution in lacustrine systems: Eocene Green River Formation, Wyoming. Chem Geol 380:172–179

Eggleston JR, Dean WE (1976) Freshwater stromatolitic biotherms in Green Lake, New York. In: Walker MR (ed) Stromatolites. Elsevier, Amsterdam, pp 479–488

Eugster HP (1967) Hydrous sodium silicates from Lake Magadi, Kenya; precursors of bedded chert. Science 157:1177–1180

Eugster HP (1969) Inorganic bedded cherts from the Magadi area. Contrib Mineral Petrol 22:2–31

Exploranium Radiation Detection Systems Portable gamma ray spectrometer GR-320 users manual, software version 3V02, 73 p

Fischer AG, Roberts LT (1991) Cyclicity in the Green River Formation (lacustrine Eocene) of Wyoming. J Sediment Petrol 61:1146–1154

Halley RB (1976) Textural variation within Great Salt Lake algal mounds. In: Walker MR (ed) Stromotolites. Elsevier, Amsterdam, pp 435–445

Horsfield B, Curry DJ, Bohacs KM, Littke R, Rullkötter J, Schenk HJ, Radke M, Schaefer RG, Carroll AR, Isaksen G, Witte EG (1994) Organic geochemistry of freshwater and alkaline lacustrine sediments in the Green River Formation of the Washakie Basin, Wyoming, U.S.A. Org Geochem 22:415–440

Kelts KR, Hsü KJ (1978) Freshwater carbonate sedimentation. In: Lerman A (ed) Lakes: chemistry, geology, and physics. Springer, Berlin, pp 295–323

Kornegay GL, Surdam RC (1980) The Laney Member of the Green River Formation, Sand Wash Basin, Colorado, and its relationship to Wyoming. In: Hollis S (ed) Stratigraphy of Wyoming. Wyoming Geological Association 31st annual field conference guidebook, pp 191–204

Ludlam SD (1969) Fayetteville Green Lake, New York; 3. The laminated sediments. Limnol Oceanogr 14:848–857

Ma L (2006) Origin of dolomite in the Green River Formation. University of Houston Ph.D. dissertation, 336 p

Machlus ML, Olsen PE, Christie-Blick N, Hemming SR (2008) Spectral analysis of the lower Eocene Wilkins Peak Member, Green River Formation, Wyoming: support for Milankovitch cyclicity. Earth Planet Sci Lett 268:64–75

Machlus ML, Ramezani J, Bowring SA, Hemming SR, Tsukui K, Clyde WC (2015) A strategy for cross-calibrating U–Pb chronology and astrochronology of sedimentary sequences: an example from the Green River Formation, Wyoming, USA. Earth Planet Sci Lett 413:70–78

Meyers SR (2008) Resolving Milankovitchian controversies: the Triassic Latemar Limestone and the Eocene Green River Formation. Geology 36:319–322

Murphy JT, Lowenstein TK, Pietras JT (2014) Preservation of primary lake signatures in alkaline earth carbonates of the Eocene Green River Wilkins Peak-Laney Member transition zone. Sediment Geol 314:75–91

Platt NH, Wright VP (1991) Lacustrine carbonates: facies models, facies distributions and hydrocarbon aspects. In: Anadón P, Cabrera L, Kelts K (eds) Lacustrine facies analysis, vol 13, International Association of

Sedimentologists Special Publication. Blackwell Scientific Publications, Oxford/Boston, pp 57–74

Rhodes MK, Carroll AR, Pietras JT, Beard BL, Johnson CM (2002) Strontium isotope record of paleohydrology and continental weathering, Eocene Green River Formation, Wyoming. Geology 30(2):167–170

Rhodes MK, Malone DH, Carroll AR, Smith ME (2007) Sudden desiccation of Lake Gosiute at ~49 Ma: downstream record of heart mountain faulting? Mt Geol 44:1–10

Roehler HW (1973) Stratigraphic divisions and geologic history of the Laney member of the Green River Formation in the Washakie Basin in southwestern Wyoming. U.S. Geological Survey Bulletin 1372-E. U.S. Government Printing Office, Washington DC, 28 p

Roehler HW (1992) Correlation, composition, areal distribution, and thickness of Eocene stratigraphic units, greater Green River basin, Wyoming, Utah, and Colorado. U.S. Geological Survey professional paper 1506-E. U.S. Government Printing Office, Washington DC, 49 p

Roehler HW (1993) Eocene climates, depositional environments, and geography, Greater Green River Basin, Wyoming, Utah, and Colorado. U.S. Geological Survey professional paper 1506-F. U.S. Government Printing Office, Washington DC, 74 p

Schultz C, Buchheim HP, Awramik S (2004) A high resolution archive of lake dynamics preserved in the stromatolites of the Laney Member of the Green River Formation (Eocene). Geol Soc Am Abstr Progr 36:285

Smith ME, Singer B, Carroll A (2003) $^{40}Ar/^{39}Ar$ geochronology of the Eocene Green River Formation, Wyoming. Geol Soc Am Bull 115:549–565

Smith ME, Carroll AR, Singer BS (2008) Synoptic reconstruction of a major ancient lake system: Eocene Green River Formation, Western United States. Geol Soc Am Bull 120:54–84

Smith ME, Chamberlain KR, Singer BS, Carroll AR (2010) Eocene clocks agree: coeval $^{40}Ar/^{39}Ar$, U-Pb, and astronomical ages from the Green River Formation. Geology 38:527–530

Smith ME, Jicha BR, Carroll AR, Cassel EJ, Scott JJ (2014) Paleogeographic record of Eocene Farallon slab rollback beneath western North America. Geology 42:1039–1042

Stanley KO, Surdam RC (1978) Sedimentation on the front of Eocene Gilbert-type deltas, Washakie basin, Wyoming. J Sediment Petrol 48:557–573

Surdam RC, Stanley KO (1979) Lacustrine sedimentation during the culminating phase of Eocene Lake Gosiute, Wyoming (Green River Formation). Geol Soc Am Bull 90:93–110

Surdam RC, Stanley KO (1980) Effects of changes in drainage-basin boundaries on sedimentation in Eocene Lakes Gosiute and Uinta of Wyoming, Utah, and Colorado. Geology 8:135–139

Talbot MR, Allen PA (1996) Lakes, 3. In: Reading HG (ed) Sedimentary environments; processes, facies and stratigraphy. Blackwell, Oxford, pp 83–124

Van Wagoner JC, Posamentier HW, Mitchum RM, Vail PR, Sarg JF, Loutit TS, Hardenbol J (1988) An overview of sequence stratigraphy and key definitions. In: Wilgus CW et al (eds) Sea level changes: an integrated approach, vol 42, SEPM special publication. Society of Economic Paleontologists and Mineralogists, Tulsa, pp 39–45

Winland HD, Matthews RK (1974) Origin and significance of grapestone, Bahama Islands. J Sediment Petrol 44:921–927

Wolfbauer CA, Surdam RC (1974) Origin of nonmarine dolomite in Eocene Lake Gosiute, Green River Basin, Wyoming. Geol Soc Am Bull 85:1733–1740

Stratigraphy and Interbasinal Correlations Between Fossil and the Green River Basin, Wyoming

6

H. Paul Buchheim, Roberto E. Biaggi, and Robert A. Cushman Jr.

Abstract

Recent attempts to temporally connect the various Green River Formation lake systems have benefited from newer dating methods that allow for high-resolution radiometric dates with small error ranges. However, lithostratigraphic correlations of coeval sedimentary units have not been previously successful. Correlations based on mapping of coeval units that can be physically traced from one basin into another would allow for more precise temporal comparisons between depositional basins. However; in most interbasinal areas, erosion appears to have removed deposits that would allow tracing of coeval tuff beds or other sedimentary units. For many years, various investigators postulated a possible hydrologic connection between Fossil Lake and Lake Gosiute. Until now, none have succeeded in actually making the connection, although a number of workers suggested that a connection might be possible in the southern part of Fossil Basin. This investigation applies lithostratigraphic correlations to demonstrate that Fossil Lake and Lake Gosiute were hydrologically connected during two different periods of Fossil Butte Member deposition.

6.1 Introduction

Recent attempts (Smith et al. 2008) to temporally connect the various Green River Formation lake systems have benefited from newer dating methods that allow for high-resolution radiometric dates with small error ranges. The K-spar tuff near the top of the Fossil Butte Member dated at 51.97 Ma has an error range of ±0.09 Ma (Smith et al. 2010). However, lithostratigraphic correlations of coeval sedimentary units have not been successful to date.

H.P. Buchheim (✉)
Department of Earth and Biological Sciences, Loma Linda University, Loma Linda, CA 92350, USA
e-mail: pbuchheim@llu.edu

R.E. Biaggi
Ciencias Naturales, Universidad Adventista del Plata, Libertador San Martin, Entre Rios 03103, Argentina

R.A. Cushman Jr.
Department of Biological Sciences, Walla Walla University, College Place, WA 99324, USA

M.E. Smith, A.R. Carroll (eds.), *Stratigraphy and Paleolimnology of the Green River Formation, Western USA*, Syntheses in Limnogeology 1, DOI 10.1007/978-94-017-9906-5_6

Correlations based on mapping of coeval units that can be physically traced from one basin into another would allow for more precise temporal comparisons between depositional basins. However, in most interbasinal areas, erosion appears to have removed deposits that would allow tracing of coeval tuff beds or other sedimentary units. For many years, various investigators postulated a possible hydrologic connection between Fossil Lake and Lake Gosiute. Until now, none have succeeded in actually making the connection. Oriel and Tracey (1970) suggested that a connection might be possible, although they never identified one. McGrew and Casilliano (1975) stated that it was not known if Fossil Lake was connected with Lake Gosiute at any time. However, they suggested that if the lakes were connected, the connection would probably be near the southern end of Fossil Lake. Buchheim et al. (2011) predicted a connection in the southern part of Fossil Basin in the area of I-80. The primary objective of this paper is to document, with lithostratigraphic correlations, that Fossil Lake and Lake Gosiute were hydrologically connected during two different periods of Fossil Butte Member deposition.

The significance of hydrologic connections and the identification of marker beds that can be physically traced between two previously unconnected basins is more than simply the discovery of the connection; there are greater implications. Physically connecting the basins opens the door to many exciting future studies including:

1. What are the consequences of this hydrologic connection to lake fauna, such as migrations of fish species between the basins? Population and diversity changes should be evident in both lakes.
2. Fossil Lake is a wedge-top lake within the foreland basin and represents the upstream system. What kind of geochemical similarities and differences occur before and after the connection, including stable isotopes of carbon, oxygen, and strontium? Do the carbonates in Fossil Lake reflect a fresher lake chemistry than those deposited in Lake Gosiute? This situation may be similar to that observed for the modern Utah Lake (fresh) and Great Salt Lake (hypersaline).
3. Is the climate signal the same in both lakes during the connection? How does it diverge prior to, and subsequent to, the connection? One might compare carbon-oxygen isotopic signals. Fossil Lake and Lake Gosiute were likely overfilled-lakes during this period, as pointed out by Smith et al. (2008).
4. Does the connection say anything about basinal tectonics and landscape evolution of the basins? Clearly subsidence in both basins exceeded sedimentation rates and input of clastic detritus.

6.2 Geologic Setting

Fossil Lake was deposited in a wedge-top basin within the Wyoming thrust belt and foreland basin area. Fossil Basin is a structural basin created by a series of thrust-faulted ridges of north-south trending Paleozoic through Mesozoic rocks (Oriel and Tracey 1970). It is bounded (Fig. 6.1) on the east by Oyster Ridge that separates it from the Green River Basin. The Tunp Range forms the northwest boundary, and the Wasatch Mountains form the far western boundary. The Crawford Mountains formed an island in the western portion of the main lake. The basin extends southward to the Uinta Mountains.

The Green River Formation in Fossil Basin gently dips a few degrees to the southwest and forms a northeast trending, asymmetrical syncline. On the west side of the basin, the Green River Formation is heavily faulted by the Rock Creek Fault and associated normal faults and has dropped down 300 m along Rock Creek, 6 km west of Fossil Butte National Monument. Further to the southwest, normal faulting dropped the Green River Formation less than 100 m and has created isolated outliers in a heavily faulted terrain. See Oriel and Tracey (1970), Rubey et al. (1975), and Hurst (1984) for further details of the structural geology of Fossil Basin.

Fossil Lake originated as a small floodplain lake and evolved into a relatively large lake sys-

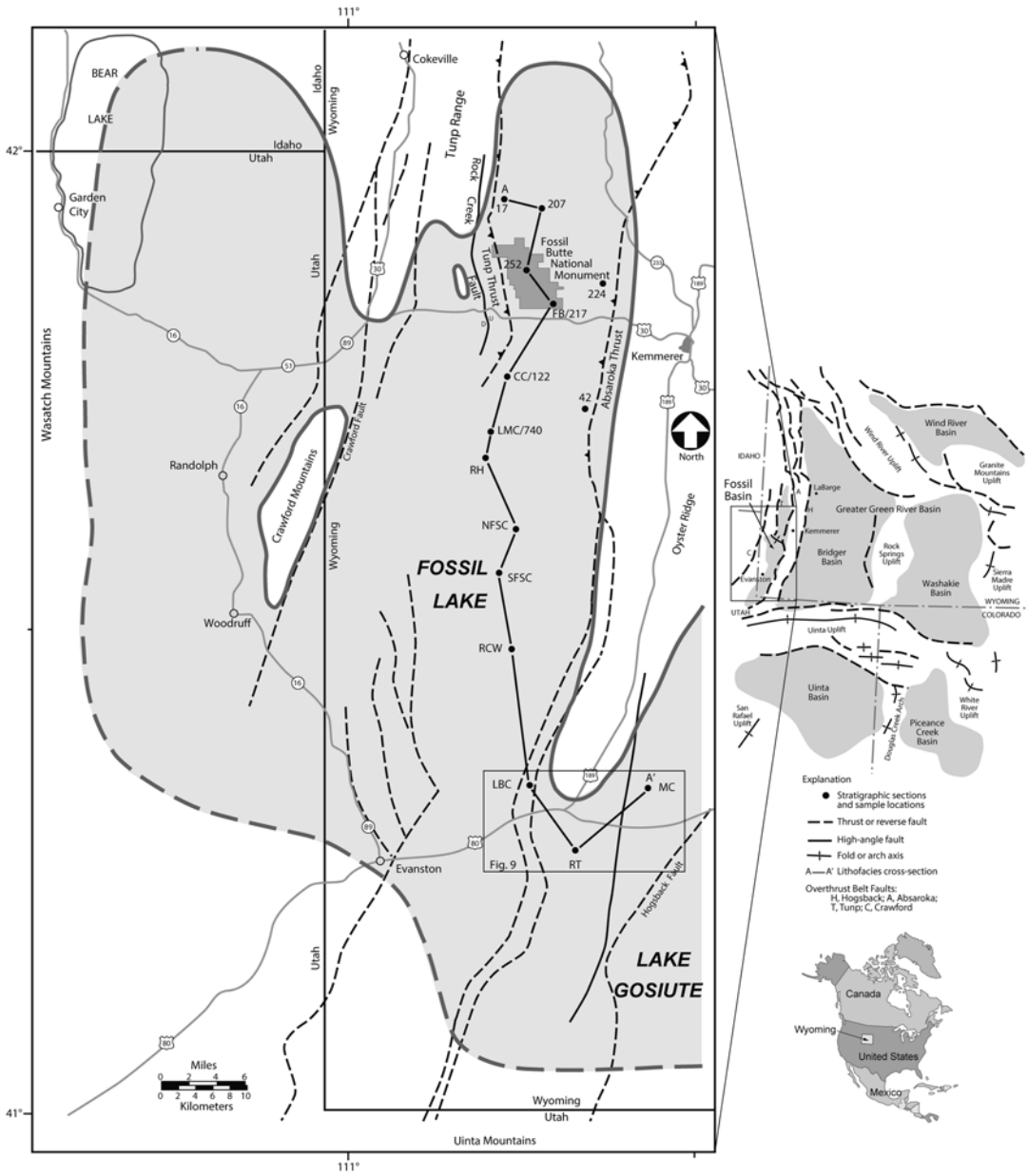

Fig. 6.1 Location of measured sections, as well as the maximum extent of Fossil Lake during deposition of the Fossil Butte Member. Structural and geologic map information after Rubey et al. (1975) and Lamerson (1982)

tem. It became increasingly saline-alkaline through time, culminating in a hypersaline stage during deposition of the Angelo Member (Buchheim 1994a). Lithofacies development varied with sedimentation rates, distance from shore, and water depth. Profundal kerogen-rich laminated micrite was deposited near the basin center where algal productivity was not highly diluted by carbonate or clastic sedimentation. A shoreward increase of bed thickness, number of laminae, and carbonate lamina thickness support the conclusion that calcium-rich inflows mixed with alkaline lake water to deposit carbonate laminae (Buchheim and Eugster 1998).

6.3 Previous Geologic and Stratigraphic Work

The Eocene Green River Formation in Fossil Basin, Wyoming, is one of the world's most famous lake and fossil deposits. Much of the research in Fossil Basin has been motivated by the abundant and well-preserved fossil fish, first described by the pioneer paleontologist Edward Drinker Cope (1877, 1884). Peale (1879, p. 535) described the geology of Fossil Butte and its fossil fish. The first general geologic map of Fossil Basin was by Veatch (1907). Schultz (1914) first delineated the general structure. Oriel and Tracey (1970) published a comprehensive stratigraphic study of Fossil Basin, including both Tertiary and older geologic formations, focusing on the Green River Formation with inclusion of type sections of the Fossil Butte and Angelo Members. Rubey et al. (1975) published two geologic maps of the northern half of Fossil Basin (Kemmerer and Sage 15-min quadrangles). More recently M'Gonigle and Dover (1992) published the Kemmerer quadrangle geologic map followed shortly by the Evanston quadrangle (Dover and M'Gonigle 1993).

Buchheim et al. (2011) provide the most recent revision and analysis of the stratigraphy of the Green River Formation in Fossil Basin, retaining some and adjusting other boundaries of the Fossil Butte and Angelo Members, and adding the Road Hollow Member. They also completed detailed 1:24,000 scale mapping of 1,500 km^2 of Fossil Basin. The maps are not yet published but the Arcview GIS dataset is available at the IRMA Portal of the National Park Service (https://irma.nps.gov/App/Reference/Profile?Code=1044844). This mapping project provided the geologic correlations for connecting Fossil Lake with Lake Gosiute.

6.4 Stratigraphy

6.4.1 Lithology

The modified lithology terminology of Buchheim and Eugster (1998) was used for fine-grained carbonates rather than that of Dunham because most of the carbonates in Fossil Basin would be "mudstone" in the Dunham classification scheme. Dunham's classification provides no resolution in terms of facies differences. The sections would all be characterized as "mudstone" with some siliciclastics interbeds and coarser carbonates in near-shore facies, etc. The Buchheim-Eugster classification scheme provides a much higher resolution of facies variations. It characterizes lithologic units based on organic richness, sedimentary structure, mineralogy, and grain size. For example, kerogen-rich laminated micrite (KRLM) provides all of this information while characterizing lithofacies variations.

6.4.2 Green River Formation Members in Fossil Basin

The Green River Formation in Fossil Basin (Figs. 6.2 and 6.3) is composed of a 160 m thick lens, composed primarily of calcimicrite and dolomicrite, that grades laterally and vertically into fluvial siliciclastics of the Wasatch Formation. The evolution of the stratigraphic nomenclature in Fossil Basin is summarized in Fig. 6.4. Stratigraphic and lithologic details concerning the Wasatch Formation have been previously described by Oriel and Tracey (1970) as being composed of more than 500 m of variegated red, purple, brown, yellow, and gray colored mudstone, claystone, siltstone, sandstone, and conglomerate. The sandstone tongue of the Wasatch Formation is a prominent ledge or cliff former that provides a useful stratigraphic marker throughout much of Fossil Basin (Buchheim et al. 2011).

Table 6.1 provides lithofacies descriptions, contacts, and other pertinent data for the members of the Green River Formation in Fossil Basin (from Buchheim et al. 2011). The Green River Formation in Fossil Basin is composed of three members (Fig. 6.2), recently redefined and described by Buchheim et al. (2011). The revised stratigraphic nomenclature now includes the basal Road Hollow Member (fluvial-lacustrine facies), the Fossil Butte Member (fluctuating profundal facies), and the uppermost Angelo Member (evaporative facies). This

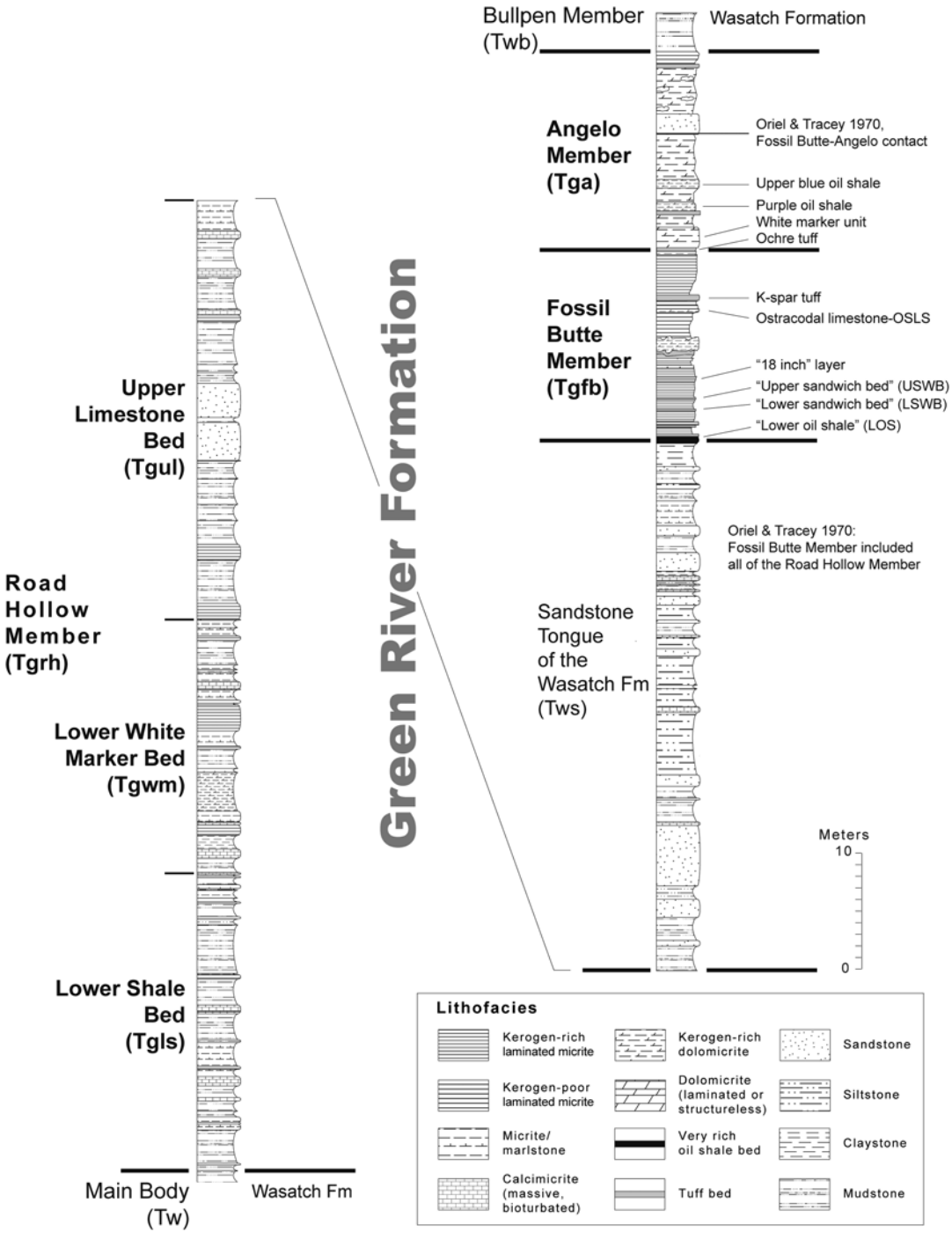

Fig. 6.2 Stratigraphic section of the Green River and sandstone tongue of the Wasatch Formation. This is a composite section assembled from the type sections of each of the members (for type sections see Buchheim et al. 2011; and Oriel and Tracey 1970)

sequence was interpreted by Buchheim (1994a) as deposited in a hydrologically closed basin, evolving from an overfilled lake to an underfilled lake with an overall increase in lake salinity and alkalinity in the late stages of lake evolution.

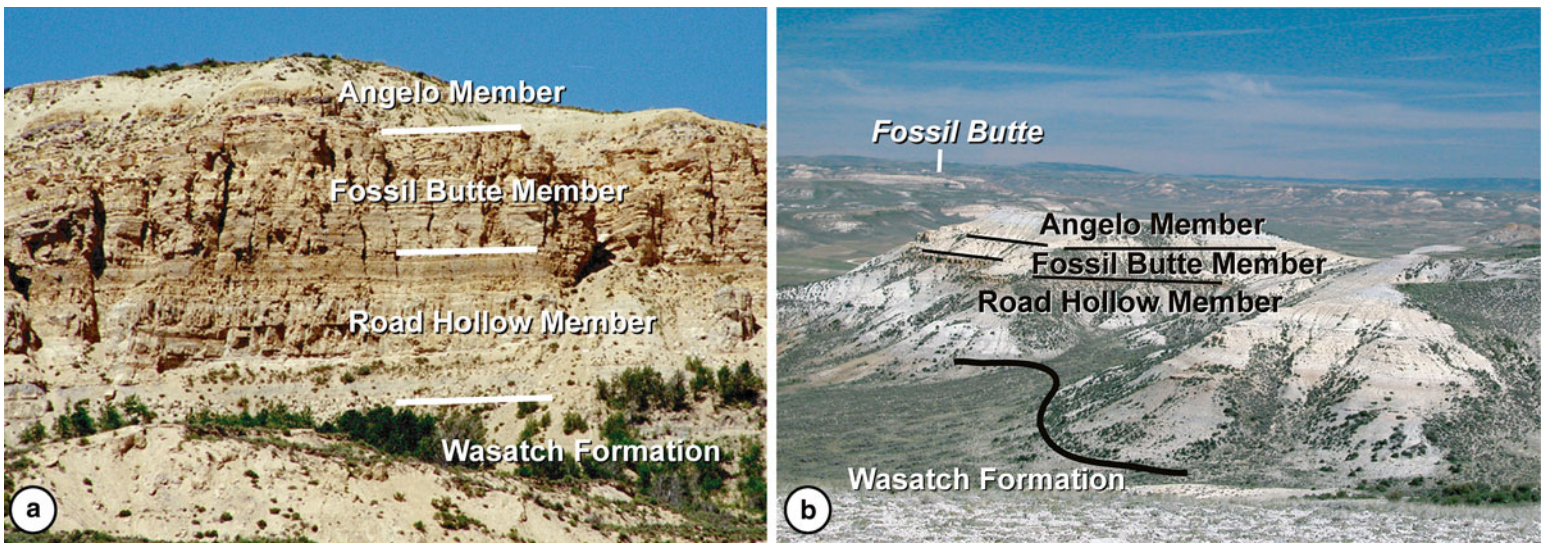

Fig. 6.3 (**a**) Contacts between the various Green River Formation Members and the Wasatch Formation at Fossil Butte, location FB 217; (**b**) contacts near the type section of the Angelo Member at location 42

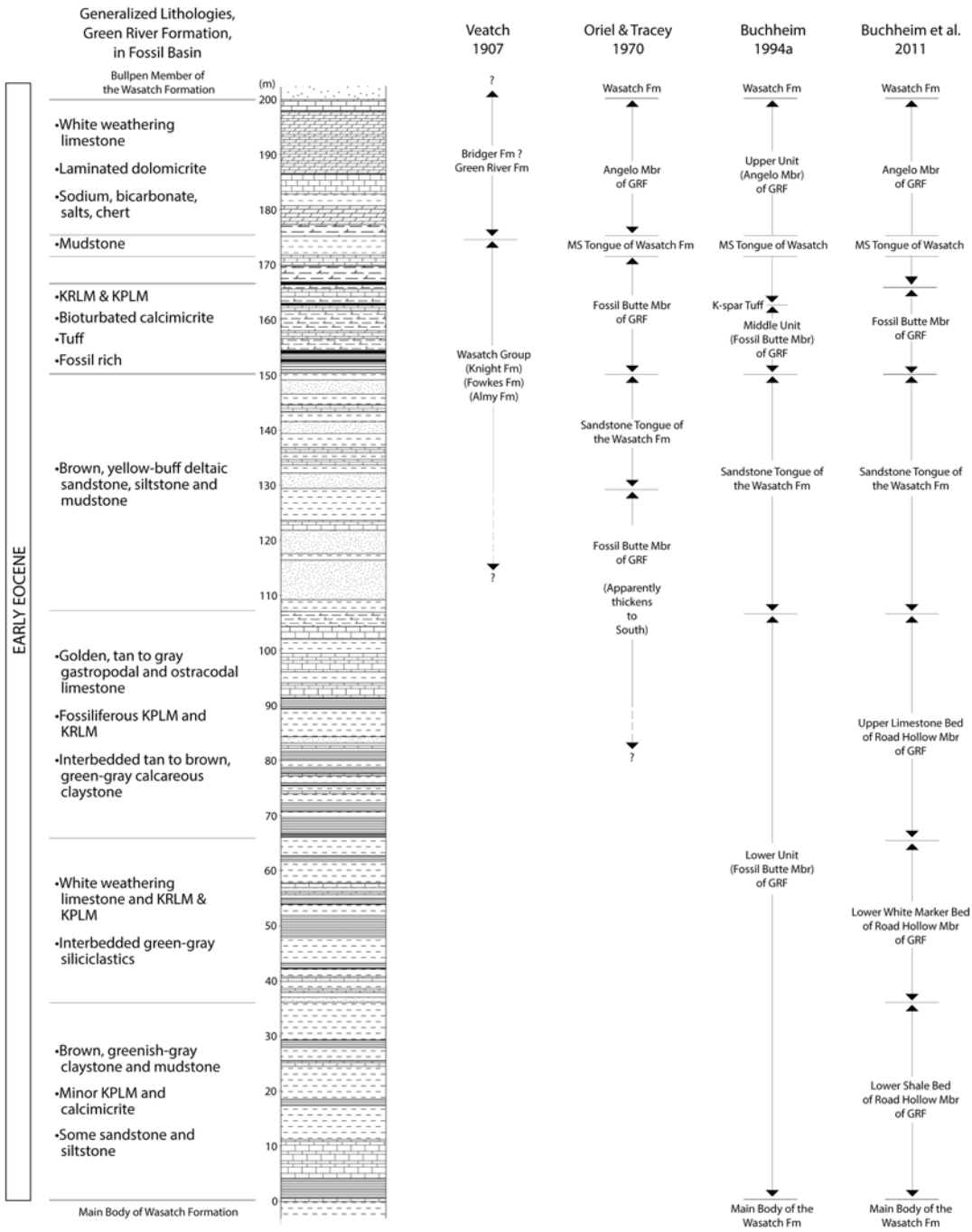

Fig. 6.4 Published revisions to the stratigraphic nomenclature of the Green River Formation. Generalized lithology of the various units is depicted on the *left side*

6.4.2.1 Road Hollow Member

The Road Hollow Member represents the earliest stage of Fossil Lake evolution (Buchheim et al. 2002). The lake first formed in the southern part of Fossil Basin and expanded northward as the lake developed as can be readily seen in Fig. 6.5

Table 6.1 Green River Formation Members in Fossil Basin, WY

	Road Hollow Member	Fossil Butte Member	Angelo Member
Lithofacies	Sandstone, siltstone, mudstone, and claystone, and carbonate units composed of KRLM, KPLM, BM, KRLD, and KPLD, ostracodal or gastropodal limestone, and tufa.	At loc. 217, 85 % KRLM and KPLM; 13 % dolomicrite; KRLM and KPLM decreases to <20 % micrite near basin margins and is replaced by bioturbated micrite (e.g., loc. 740).	Dolomicrite and silty dolomicrite with calcite pseudomorphs after saline minerals. Quartz and feldspar form a high percentage of some of the dolomicrite beds.
Thickness	At least 22 m at loc. 217; up to 125 m in southern part of basin.	11 m measured at loc. 217.	27 m measured at loc. 217.
Contacts	Top: includes a limestone ledge at the base of the Sandstone Tongue of the Wasatch Formation. The Sandstone Tongue forms massive outcrops and cliffs or a slope with outcroppings or ledges of dark brown sandstone	Top: ochre tuff 3–4 m above the "kspar tuff"; at basin center locations the tuff forms a slope of ochre colored mudstone with a very distinctive "white marker" bed 2–3 m thick above it.	Top Marker: top of limestones at a sandstone ledge; tufa "logs" occur commonly below the contact; Bullpen Member forms gentle slopes above ledge forming Angelo; Bottom marker: ochre tuff 3–4 m above the "kspar tuff".
	Base: red, gray, and brown slopes and ledges of siltstone and sandstone; contact is gradational and moves up section toward the south.	Base: the "lower oil shale" 1–2 m below the "lower sandwich bed". Also marked in the central and southern half of the basin by the top of the Sandstone Tongue of the Wasatch Formation	
Age	No age constraints	51.97 M.Y. ±0.09 (Smith et al. 2010)	No age constraints
Paleontology	Fossil fish include the herring *Knightia* and *Diplomystus*, the percoid *Priscacara*, and the osteoglossid *Phareodus* in laminated micrites. Fish coprolites abundant in some beds. Gastropods common in bioturbated micrites, bivalves in some units, and ostracods very common in limestones and laminated micrites. Rare crocodile teeth observed in Road Hollow sandstones south of Little Muddy Creek. Bird, turtle and mammal bones occur in one sandstone unit. Plant leaves and fragments in several shale units.	Abundant fossil fish including *Knightia* and *Diplomystus*. At least 13 other fish genera are present (Grande 1984). Other vertebrates include turtles, crocodiles, and birds. Ostracods and gastropods are common and shrimp and crayfishes occur in basin margin carbonates. Insect and plant fossils are common. Stromatolites and associated caddisfly larval cases and insect boring ichnofossils.	A few units contain most of the fossil fish common to the middle unit. Ostracods occur in several units; plant remains occur in two units. Bird bones occur in one limestone unit. Bird tracks occur in one sandstone unit. Stromatolites and associated caddisfly larval cases occur in some units. Avian egg-shell fragments occur in some beds.
Geographic Expression	Forms slopes at most locations; sandstone tongue forms ledges and low cliffs.	Forms cliff and bluff exposures, but forms mostly slopes south of T 21 N as softer siltstones and mudstones dominate the section.	Forms outcrops and steep slopes in the northern half of the basin; forms poorly exposed slopes south of loc. 217.
Lake Basin Phase	Overfilled	Balanced-fill/Overfilled	Underfilled

KRLM kerogen-rich laminated micrite, *KPLM* kerogen-poor laminated micrite, *PBLM* partly burrowed laminated micrite, *BM* bioturbated micrite, *KRLD* kerogen-rich laminated dolomicrite, and *KPLD* kerogen-poor laminated dolomicrite

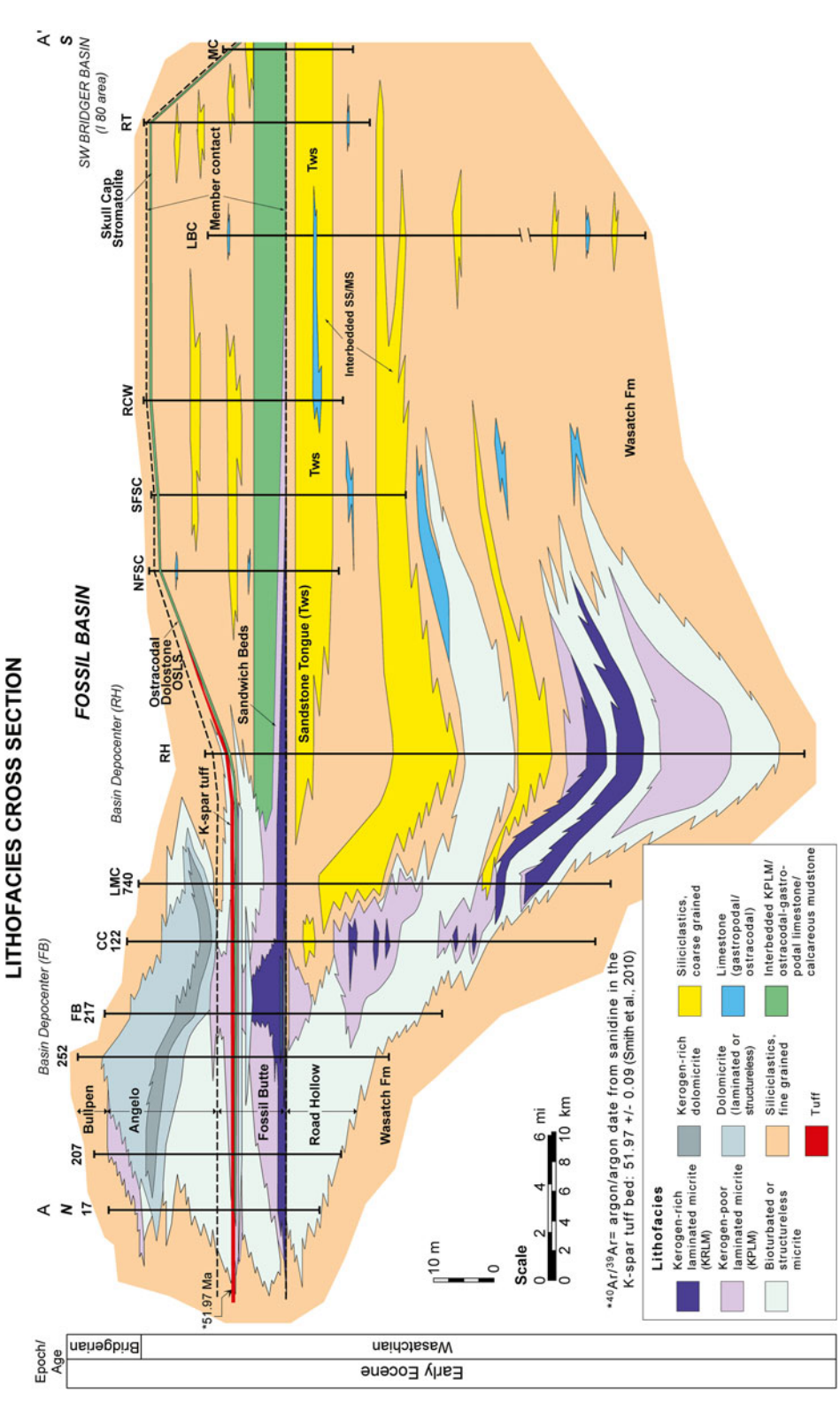

Fig. 6.5 Lithofacies cross section illustrating the correlation of facies in Fossil Basin and into the Green River Basin. In particular, note the base of the Fossil Butte Member (sandwich beds) that were deposited during the greatest expansion of Fossil Lake and can be traced into the Green River Basin. The ostracodal limestone (OSLS) is also a basin wide marker that becomes the 'skull cap' stromatolite bed (SCS), the most important marker bed in terms of basin to basin correlations (See text for details)

depicting a cross section of the lithofacies and their stratigraphic architecture, as modified from Buchheim et al. (2011). Buchheim (1994a) divided the Fossil Butte Member into "lower" and "middle" subunits, which were subsequently revised and elevated to member status (Buchheim et al. 2011). Oriel and Tracey (1970) did not realize that a very thick section of the Green River Formation existed south of their mapping area (mapped by Rubey et al. 1975). The "lower unit" of Buchheim (1994a, b) was elevated to the Road Hollow Member. The Road Hollow Member is named after the canyon where the Road Hollow type section (41.676408° N, −110.856822° W) was described (Buchheim et al. 2011).

The Road Hollow Member was described in detail by Buchheim et al. (2011), and is characterized by siliciclastic units composed of sandstone, siltstone, mudstone, and claystone, and carbonate units that are composed of KRLM, KPLM, bioturbated micrite (BM), KRLD, KPLD, ostracodal and gastropodal limestone, and tufa. Volcanic tuff, bioturbated micrite, and dolomicrite units occur in the Road Hollow Member but are less common than in the Fossil Butte and Angelo Members. Buchheim et al. (2011) described the Road Hollow Member as a shallow, fluvial–lacustrine depositional system. It consists of numerous fluvial to deltaic siliciclastic units interbedded with various lacustrine carbonate units. The profundal lacustrine carbonates (KRLM and KPLM) grade laterally into shallow lacustrine limestone and fluvial to deltaic sandstone and siltstone. A typical lithofacies succession in the Road Hollow Member consists of sandstone, siltstone, mudstone, and micrite (KPLM and KRLM) or limestone (Biaggi 1989). This represents a deepening upward, transgressive sequence in the Road Hollow Member. In the southern part of Fossil Basin, a major siliciclastic sequence overlies the Road Hollow Member. Oriel and Tracey (1970) identified this sequence as the sandstone tongue of the Wasatch Formation. Petersen (1987) suggested that this major siliciclastic sequence was deposited by a lacustrine, Gilbert-type delta. The Gilbert-type delta in Fossil Basin is similar to the Gilbert-type delta described by Surdam and Stanley (1980) in the Green River Basin. Siliciclastic/carbonate ratios indicate increasing siliciclastic input in the southern part of Fossil Basin (Biaggi 1989). Sandstone lithologies range from very fine to coarse grained, homogeneous to thinly and thickly bedded, and vary from light tan to gray. Sedimentary structures in the sandstone units include ripple and trough cross-bedding, current lineation, and small and large-scale planar cross-bedding. Several Road Hollow Member units are fossiliferous, containing gastropods, ostracods, fish, leaves, and other plant debris. KPLM units contain the most fossils, but some limestone units contain gastropods and ostracods. Ostracods are the most abundant fossil in the Road Hollow Member. Fish are less abundant than in the Fossil Butte Member and include *Knightia* and *Diplomystus* (herring), *Priscacara* (percoid), and *Phareodus* (osteoglossid).

Biaggi (1989) and Buchheim et al. (2011) divided the Road Hollow Member into three beds (Fig. 6.2). Although Road Hollow Member units were correlated and mapped at least 30 km south of the type section (nearly to Interstate 80), they still require additional detailed sedimentological study to clearly understand the nature of this early stage of Fossil Lake.

The Road Hollow Member deposition ranges in age from late Graybullian time, through Lysitean time, and into early Lostcabinian time (Fig. 6.6). This includes parts of land mammal zones Wa-5 and Wa-7 and all of land mammal zone Wa-6.

6.4.2.2 Fossil Butte Member

Oriel and Tracey (1970) first defined the type section for the Fossil Butte Member at Fossil Butte (41.827776° N, −110.725354° W) and Buchheim and Eugster's (1998) location 217. Although the thinnest of the Green River Formation members in Fossil Basin, it is one of the most famous lacustrine deposits because of the abundant fossils preserved within. It contains a well described fish fauna, numerous fossil plants, some rare snakes, bats, mammals, insects, and more (Grande and Buchheim 1994).

Much of the research in Fossil Basin has been motivated by the abundant and well-preserved

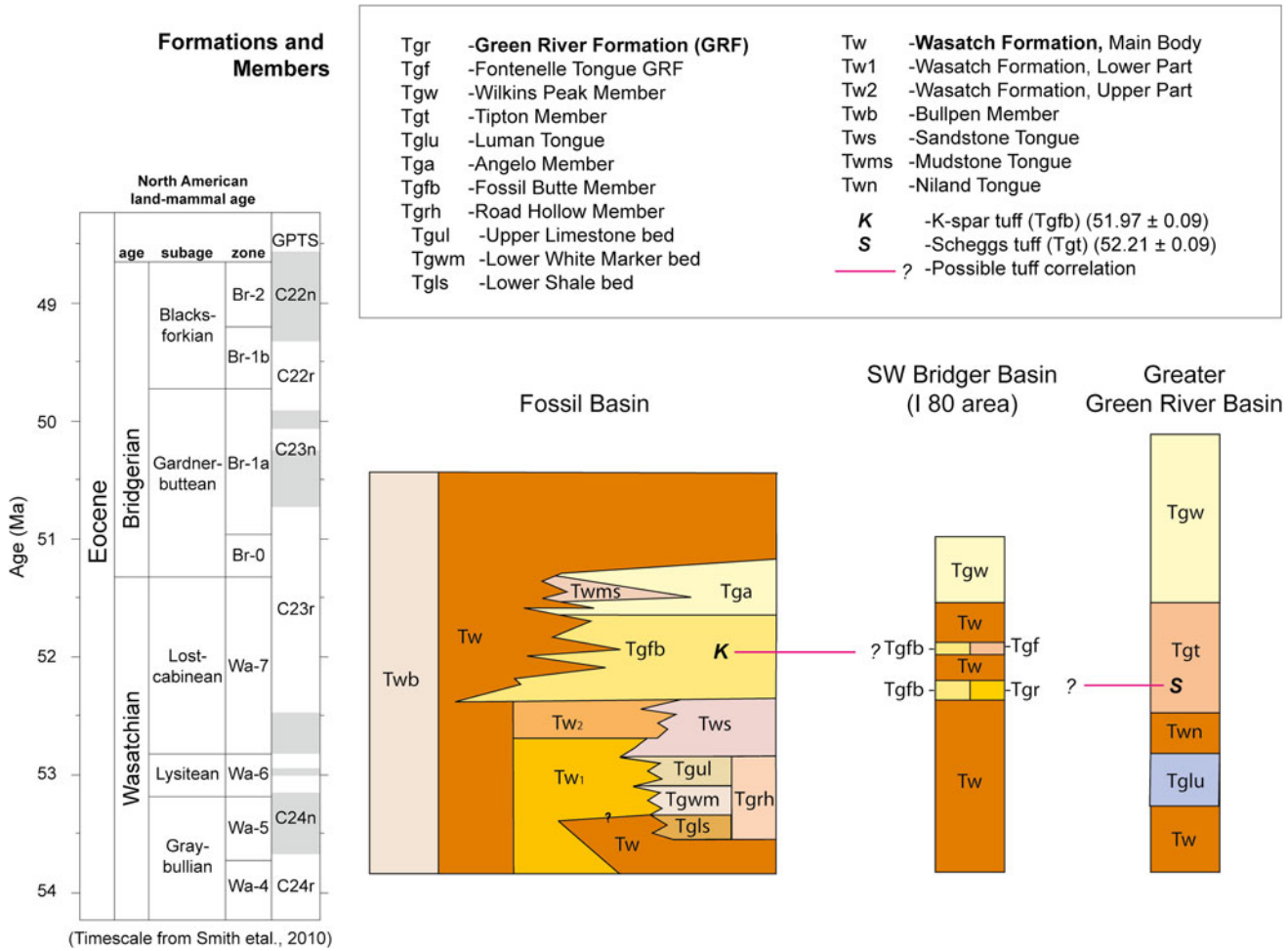

Fig. 6.6 The stratigraphic relationships between the various stratigraphic units associated with the Green River Formation (Buchheim et al. 2011) in Fossil Basin and the extreme SW corner of the Green River Basin are illustrated along with the bio and magnetostratigraphy (From Smith et al. 2008). Correlation of map units modified from Dover and M'Gonigle 1993. The unpublished geologic map GIS database files are available at the IRMA Portal of the National Park Service site: (https://irma.nps.gov/App/Reference/Profile?Code=1044844); the map can be viewed at the ESRI site: http://www.arcgis.com/home/webmap/viewer.html?webmap=b9042f1da9d3482ba8c5a43e93a1bc18

fossil fishes. The geologic history, with an emphasis on paleontology, was summarized by McGrew and Casilliano (1975). A review of the paleontology of the entire Green River Formation (Grande 1984) also provides a comprehensive list of the fossils preserved in the Green River Formation. Buchheim (1986) and Grande and Buchheim (1994) addressed taphonomic aspects of the fossil fish. Leggitt (1996) and Leggitt and Buchheim (1996) described fossil bird sites. Cushman (1999) characterized the implications of the plant microfossils for the depositional environment and climate history. Grande (1985, 1989, 1994) investigated the historical biogeography. Grande (1994) also addressed faunal indicators of freshwater conditions, tropical climate, and biogeographic origins.

The Fossil Butte Member is the most widespread lacustrine member in Fossil Basin and represents profundal sedimentation. Buchheim (1994a, b) recognized that the Fossil Butte Member was deposited in response to the largest lacustrine transgression in the history of Fossil Lake. This was followed by a major regression and a subsequent, second major transgression (Fig. 6.5). Recognizing major transgressions in a lacustrine system becomes extremely important when correlating units near the basin margins, where only the most extensive transgressions are preserved in the rock record. Recognizing these "events" provides a critical tool to understanding large scale basinal stratigraphic events.

Lithologic and stratigraphic characterizations of the Fossil Butte Member are shown in Table 6.1 and Fig. 6.5. The Fossil Butte Member is dominated by kerogen-rich laminated calcimicrite (KRLM) and represents primarily a fluctuating profundal lithofacies association. The basal 6 m contains some of the most paleontologically-rich beds in the world. Most of the commercial collection of fossils comes from the "sandwich beds" and the "18 inch" unit. Abundant tuff beds, that range in thickness from only a few mm to over 25 cm, provide dependable marker beds for correlation and spatial analysis studies. Buchheim and Biaggi (1988) and Buchheim (1994b) conducted a spatial analysis of laminae number between the two tuff beds ("lower sandwich bed") to determine the nature and origin of the laminae described as varves in the Green River Formation (Bradley 1929, 1948,1963; Crowley et al. 1986; Ripepe et al. 1991; Fischer and Roberts 1991). Bradley's 1948 paper specifically discusses the origin of varves in Fossil Basin. The Buchheim and Biaggi (1988) and Buchheim (1994b) study determined that laminae number between the tuff beds varied progressively, from about 800 laminae near the lake center gradually increased to approximately 1,600 laminae nearer the lake margins. This discovery led to a new model (Buchheim 1994b) that explained the deposition of laminated carbonates by the mixing of calcium-rich inflow waters with bicarbonate-rich lake-water and explained the origin of the lithofacies, lithofacies assemblages, bioturbation, kerogen content, and the increase in number of laminae and thickness toward the basin margins (Fig. 6.7).

Buchheim (1994a) proposed that lithofacies depended on rates of deposition, distance from shore, and water depth. Kerogen-rich laminated micrite was deposited in the basin center where lake-generated organics (algae) were least affected by carbonate or clastic sedimentation. Bottom waters were seasonally low in

Fig. 6.7 Fossil Basin lake model (**a**) describing the origin of observed trends, such as thinning of the lower sandwich bed towards lake center (After Buchheim 1994b). The increase in laminae number and thickness towards the basin margin is explained by the Fossil Basin lake model. Calcium-rich inflow first mixes with the bicarbonate dominated lake water at the shore, causing greater carbonate deposition shoreward. Weather fluctuations may cause variations in inflow, resulting in laminae deposition only shoreward, or at times over the entire lake. Annual laminae are deposited as well, but are masked; Lower Sandwich bed from the Fossil Butte Member, correlated and compared from lake center (**b**) to lake margin (**c**). The upper and lower tuffs are excellent markers and can be accurately traced basin wide. Bed thickness increases dramatically from center to margin, while kerogen content decreases due to dilution by mineral content (After Church 2003). Thin sections from lake center (**d**) and margin (**e**) localities. Note that laminae increase in thickness and decrease in kerogen content towards the margin (From Church 2003)

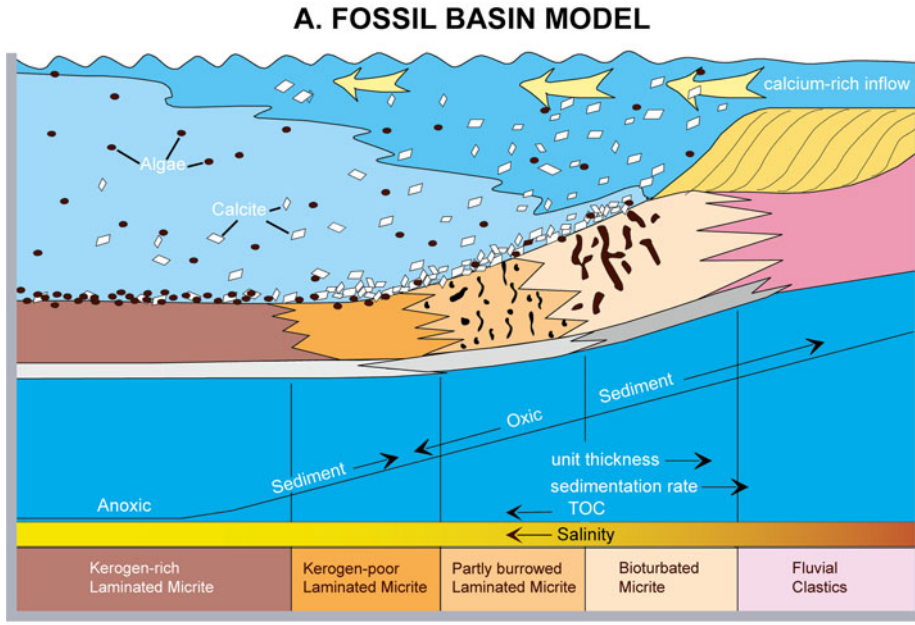
A. FOSSIL BASIN MODEL
calcium-rich inflow
Algae
Calcite
Sediment
Oxic
Sediment
unit thickness
sedimentation rate
TOC
Anoxic
Salinity
Kerogen-rich Laminated Micrite
Kerogen-poor Laminated Micrite
Partly burrowed Laminated Micrite
Bioturbated Micrite
Fluvial Clastics

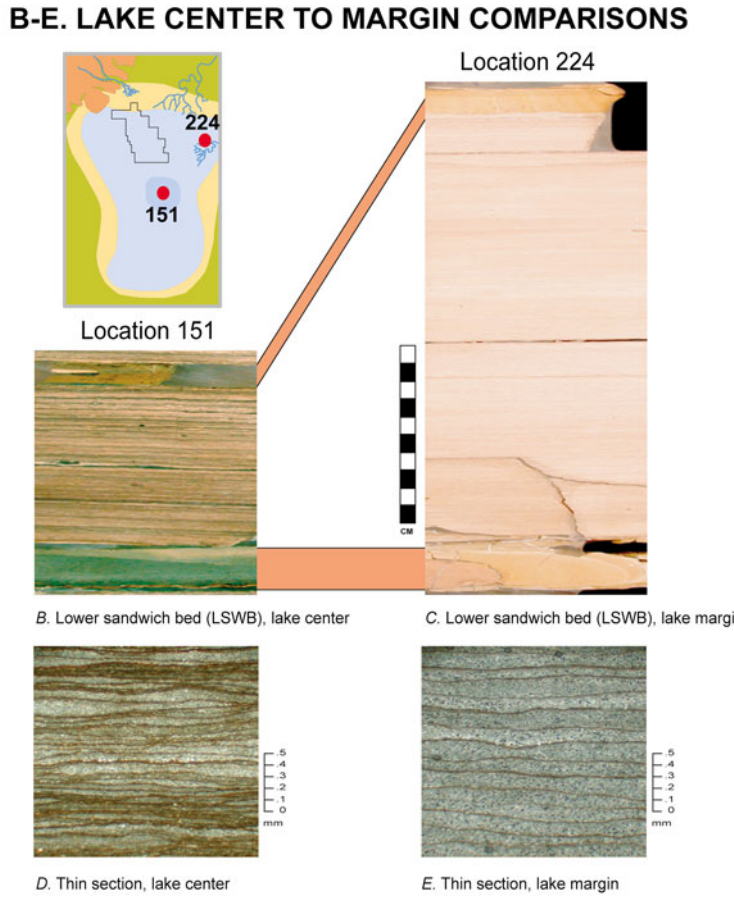
B-E. LAKE CENTER TO MARGIN COMPARISONS
224
151
Location 224
Location 151
CM
B. Lower sandwich bed (LSWB), lake center
C. Lower sandwich bed (LSWB), lake margin
mm
D. Thin section, lake center
E. Thin section, lake margin

oxygen, enhancing preservation. Organic-rich sediments provided reducing environments that, increased the preservation potential for fish and other organisms. Organic content decreases shoreward where it was diluted by carbonate precipitation. The more oxygenated nearshore areas allowed habitation by burrowing organisms. Bed thickness, number of laminae, and carbonate lamina thickness increase shoreward reflecting initial mixing of calcium-rich inflows with the more alkaline lake water. Episodic fluctuations in runoff may have resulted in nearshore lamina deposition, whereas seasonal or large inflow events may have resulted in basin-wide lamina deposition. This is suggested by the greater number of laminae and thicker laminae observed in coeval units near the lake margin.

Key to interbasinal correlation and stratigraphic basin analysis are several marker beds, including the "lower oil shale", "sandwich beds", "ostracodal limestone (OSLS)", and k-spar tuff. The ostracodal limestone (OSLS) and associated tuff beds can be traced over much of Fossil Basin. The k-spar tuff is traceable over about 400 km^2 of Fossil Basin. However, the associated ostracodal limestone (OSLS) occurs over 1,000 km^2 and is critical to connecting Fossil Lake with Lake Gosiute. This will be discussed in more detail in the "interbasinal correlation" section.

The Fossil Butte Member was entirely deposited during the Lostcabinian stage and within land mammal zone Wa-7 (Fig. 6.6).

6.4.2.3 Angelo Member

The Angelo Member (Figs. 6.2, 6.3, and 6.5) represents evaporative facies composed of laminated dolomicrite containing abundant calcite pseudomorphs after trona. It was the most evaporative phase of Fossil Lake's history (Buchheim 1994a). It contains several 1 m thick beds of laminated calcimicrite with fossil fish (Buchheim et al. 2011). The Angelo Member is the least widespread member and is best developed in the northern part of the basin (Fig. 6.5). It grades laterally into bioturbated calcimicrite, and is the most dolomitic, evaporative facies dominated member. The type section, as measured and described by Oriel and Tracey (1970), is located at 41.712274° N, −110.688892° W near the eastern margin of Fossil Lake. A more accessible location (Fig. 6.1, location 42) occurs about 1.5 km NE of the type section and can be partly accessed from the top of the mesa (at 41.723234°N, −110.679289°W). However, the unit is also well exposed on Fossil Butte. Excellent exposures also occur in the northern part of the Fossil Basin in Schuster Basin (Buchheim and Eugster 1998) location 242 (41.903576°N, −110.692500°W) and location 207 (41.922219°N, −110.736665°W).

Numerous tuff and other marker beds (many coined by Buchheim 1994a) within this member allow precise correlation throughout the depositional basin (Buchheim 1994a; Buchheim and Biaggi 1988). The ochre tuff marks the basal contact with the Fossil Butte Member. The upper k-spar tuff is also prominent. In addition, several other beds of significance provide opportunity for basinal spatial analysis studies including the "white marker bed", "purple oil shale", "upper blue oil shale", "chert horizon" and the Mudstone Tongue of the Wasatch Formation (Oriel and Tracey 1970). The Mudstone Tongue was used by Oriel and Tracey (1970) to define the contact between the Fossil Butte Member and the Angelo Member. However, the contact was redefined recently by Buchheim et al. (2011).

Loewen (1999) correlated and analyzed facies from lake center to margin based on one 1 cm thick tuff bed. He was able to document salinity gradients from saline to relatively fresh at the lake margin (Loewen 1999). The evidence for these gradients included: (1) lake- center laminated dolomicrite grades laterally into lake margin laminated calcimicrite, (2) calcite pseudomorphs after saline minerals are associated with the dolomicrite and absent from the calcimicrite, (3) fossil fish are absent from dolomicrite, but present in calcimicrite, and (4) gastropods are absent in dolomicrite, but present in calcimicrite.

Angelo Member deposition ranges in age from middle Lostcabinian to early Gardnerbuttean (Fig. 6.6). This correlates with parts of land mammal zones Wa-7 and Br-0.

6.5 Lithofacies Associations and Spatial Distribution

The basic lithofacies association in Fossil Basin (Fig. 6.5) is characterized by a basal flooding surface facies of KRLM, overlain by a shallowing upward sequence including KPLM (kerogen-poor laminated micrite), PBLM (partly bioturbated laminated micrite), BM (bioturbated micrite) or wackestone composed of calcimicrite. The BM facies contains one or more of the following: ostracods, mollusks, oolites, oncolites or stromatolites. This sequence is interpreted to represent a flooding event, and is overlain by shallowing-upward facies. Major transgressive facies within Fossil Basin are represented by the deepest water facies within any given section at more marginal locations. Figure 6.9 provides a spatial view of facies distribution during the maximum flooding phase of the Fossil Butte Member.

6.6 Interbasinal Correlation

Documenting the hydrologic and temporal connections between Fossil Lake and Lake Gosiute has long been a goal of various Fossil Basin investigators, but has proved elusive until now. The apparent lack of tuff and other marker beds, faulting in the Muddy Creek area (MC location on Fig. 6.1), and the total erosion of the Green River Formation along highway 189 west of Oyster Ridge in the area of I-80 (where many thought a connection might be possible), presented a daunting task to anyone attempting a connection. Most of this area is composed of the fluvial Wasatch Formation and lacks well-exposed outcrops. However, this situation changed when detailed 1:24,000 scale mapping was funded by the National Park Service (to the primary author) in an effort to map the Green River Formation in detail in the area of Fossil Butte National Monument and southward as far as possible. In addition, years of detailed stratigraphic work (by Buchheim et al. 2011 and others) provided evidence that the relatively thin limestone units in the vicinity of I-80 in the southern part of Fossil Basin were the product of two major transgressions during deposition of the Fossil Butte Member. During the mapping project, detailed stratigraphic sections were measured to allow geologic mapping to proceed southward. These sections, and the identification of the major flooding surfaces that deposited the basal units of the transgressions finally provided evidence to successfully make the ultimate correlations into the Green River Basin.

Figure 6.8 documents the correlation of stratigraphic units within Fossil Basin and into the Green River Basin. The stratigraphic sections provide the primary database for the correlation, but in addition, the following points are important to the confidence level in the correlations:

1. The major flooding surface at the base of the Fossil Butte Member can be readily identified and traced, including the "sandwich beds" (two sets of tuff beds 1 m apart) at the base of the Fossil Butte Member. The tuff beds can be traced as far south as Ryckman Creek and their associated laminated micrite facies as far south as the Radio Tower. This sequence overlies the sandstone tongue of the Wasatch Formation that forms prominent sandstone outcrops throughout Fossil Basin. This observation provides the foundation of our interbasinal correlation.
2. A second major flooding surface within the Fossil Butte Member is represented by the k-spar tuff and "ostracodal limestone (OSLS)." The regression subsequent to the sandwich beds flooding surface can be traced southward into a thick slope-forming series of Wasatch Formation siltstone, sandstone, and mudstone. This represents the fluvial floodplain that prograded northward into the lake as it regressed.
3. A vertical facies sequence composed of KRLM followed by KPLM, bioturbated limestone and/or ostracodal limestone, represents major lake expansion, followed by lake contraction and shallowing. This sequence was recognized initially by Buchheim (1994a) and modeled in more detail by Buchheim and Eugster (1998). Correlation of profundal KRLM to more marginal localities in the

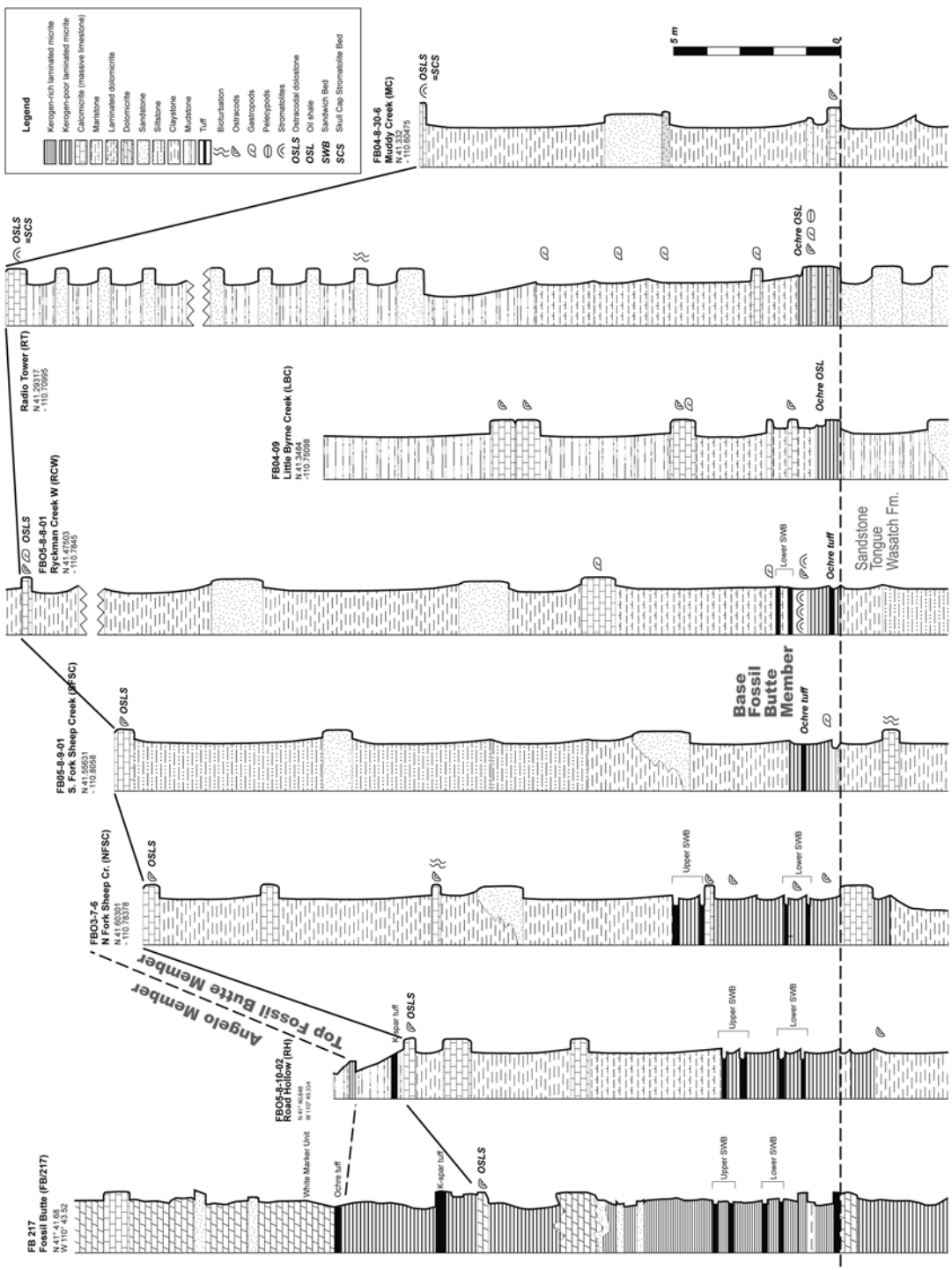

Fig. 6.8 Correlation of stratigraphic sections from Fossil and Green River Basins. The datum is the base of the "sandwich beds" in the Fossil Butte Member, that are the first kerogen-rich laminated micrite above the sandstone tongue of the Wasatch Formation and are associated with two sets of tuff beds that are significant geochronological marker beds. Distance between sections is not to scale; see location map, Fig. 6.1 for location information

southern part of Fossil Basin demonstrated that the facies association may be topped by ostracodal grainstone and/or mollusk coquinas and associated stromatolites in some areas. The "skull cap" stromatolite (SCS) at the top of the Fossil Butte Member is a good example of a stromatolite associated with the uppermost, shallow-water phase of the facies association. This provided evidence that the flooding surfaces at most marginal locations are represented as ostracodal grainstone/mollusk wackestone/stromatolite beds.

4. The most difficult challenge that impeded correlation into the Green River Basin was poor outcrop exposure and major faulting that down-faulted the Green River Formation. However, once the sandwich horizon was identified at the "Radio Tower" location south of I-80 and the ostracodal limestone (OSLS) was correlated with the "skullcap" stromatolite unit (SCS), we were able to continue mapping and tracing these units into the Green River Basin.
5. An ochre colored, ostracodal limestone occurs within the sandwich bed on the Fossil Basin side of the correlation at Little Byrne Creek that can be traced across the highway 189 gap to the Radio Tower section that straddles Fossil Basin and the Green River Basin. This provided an additional verification for the connection. The ochre color may be staining from one of the sandwich tuff beds, although the actual sandwich bed tuffs cannot be verified.
6. Recently acquired Sr isotopic data reported by Doebbert et al. (Chemical Geology, in press) support the chemostratigraphic correlation between the Tipton and Fossil Butte Members. Doebbert's data indicate an average Tipton Member $^{87}Sr/^{86}Sr$ ratio of 0.71402, ±0.00086 (1 std. dev., n = 22). This can be compared to results from a fish fossil and enclosing micrite from the 18″ layer, which were provided by Arvid Aase and analyzed by Jeff Pietras. The micrite $^{87}Sr/^{86}Sr$ ratio was 0.71388, and the fish bones measured 0.71396 (J.T. Pietras, personal communication). These ratios are statistically indistinguishable from each other and from the Tipton average, and therefore consistent with a connection between the two lakes.

The correlations demonstrate that the Fossil Butte Member of the Green River Formation correlates lithostratigraphically with the Tipton Member (Fontenelle Tongue) of the Green River Formation in the Green River Basin (see Fig. 6.9). This supports previous interpretations that the Fossil Butte Member is equivalent to the Tipton Member in the Green River Basin (Smith et al. 2008). This correlation is also supported by the age dates of Smith et al. (2010) for the k-spar tuff, which was dated at 51.97 ± 0.09 Ma**.** The k-spar tuff occurs near the top of the Fossil Butte Member. Smith's date from the Scheggs tuff in the Tipton Member is 52.21 ± 0.09 Ma (Smith et al. 2010). There are no published dates from the Fontenelle Tongue of the Tipton Member in the vicinity of our proposed lake connection. Both the Fossil Butte and Tipton Members were deposited during maximum expansions of their respective lakes. Both are overlain by evaporative facies of the Angelo (Fossil Basin) and Wilkins Peak members (Green River Basin), respectively. Consequently, the correlation is supported by regional sequence stratigraphy, chronostratigraphy, climatic interpretations, lithostratigraphy, and facies types.

6.7 Stratigraphic Architecture and Sequence Stratigraphic Models

ST1 Figure 6.10 illustrates the development of the stratigraphic architecture and systems tracts in Fossil Basin beginning with the onset of lacustrine deposition during Road Hollow Member time. ST1 is a fluvial-lacustrine systems tract deposited when rates of water and sediment fill were relatively high compared to rates of basin accommodation (c.f., Carroll and Bohacs 1999; Bohacs et al. 2000). Rates of accommodation increased at this time, allowing the development of shallow lakes that were frequently filled by meandering river systems. Depositional sequences are characterized by interbedded fluvial sandstone, overbank claystone, calcareous mudstone, micrite (massive limestone), and laminated micrite. It is the thickest member of the Green River Formation in Fossil Basin.

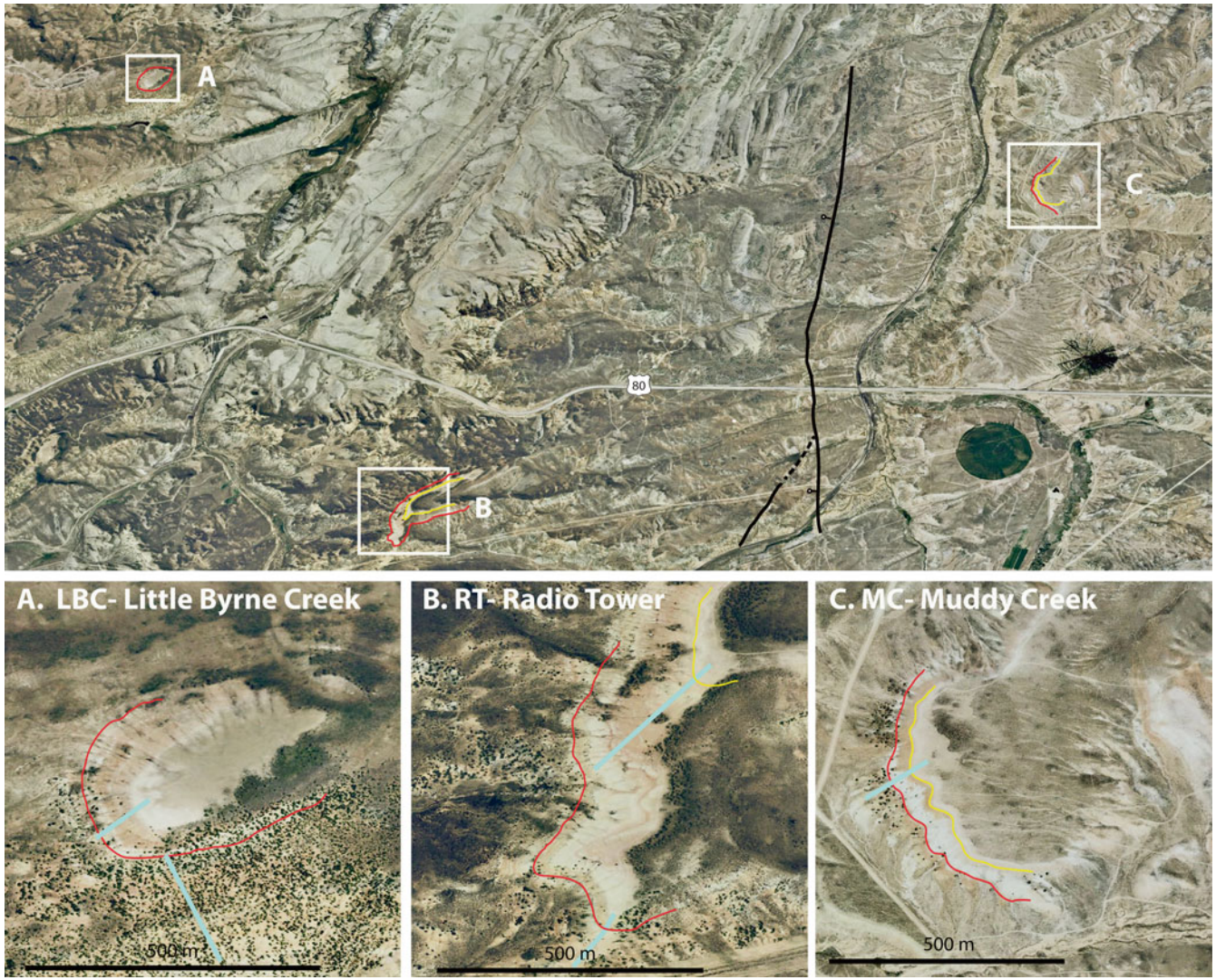

Fig. 6.9 Location of measured sections at the juncture of Fossil and Green River Basin (also see Fig. 6.1 for general location map; Fig. 6.8 for correlation of sections). *Red* is contact line depicts the base of the Fossil Butte Member (location of sandwich beds); *yellow* contact line depicts ostracodal limestone (OSLS)/skull cap stromatolite (SCS), which is the approximate upper contact of the Fossil Butte Member, equivalent to the Fontenelle Tongue of the Tipton Member in the Green River Basin. *Blue lines* represent approximate line of measured section. Aerial photographs from Google Earth

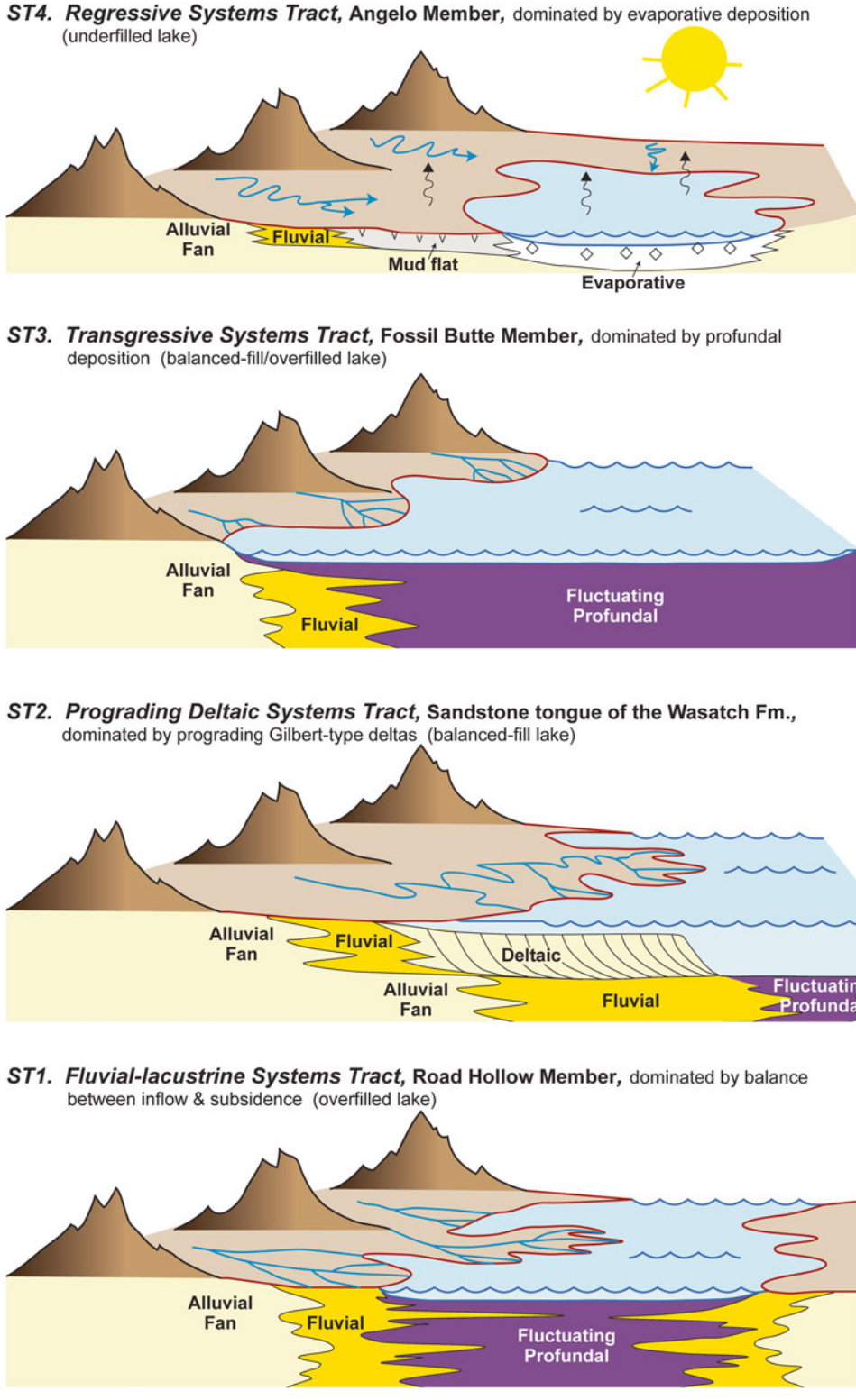

Fig. 6.10 The development of systems tracts in Fossil Basin related to lake transgressions, regressions, and progradations. ST1, the fluvial-lacustrine system tract was deposited during Road Hollow Member time as the depositional regime alternated between fluvial and lacustrine. ST2 was deposited during deposition of the sandstone tongue of the Wasatch time period. Fossil Lake was well established and a generally balanced between subsidence and sedimentation rates. ST3 illustrates the most dramatic flooding event in Fossil Basin, as Fossil Lake transgressed nearly the entire basin floor and hydrologically connected with Lake Gosiute. ST4 is a regressive system tract deposited during Angelo Member time. Evaporative facies dominated the system as the climate phased into a long dry period

Sedimentation was probably more rapid than deposition of the subsequent members, as the unit is thick and dominated by siliciclastics. The basin was tectonically active with rapid uplift and subsidence. This set up a delivery system for abundant clastic input from high erosion rates periodically balanced by subsidence rates. This process produced thin, alternating fluvial and lacustrine units. During this phase, Fossil Lake was an over-filled lake and probably overflowed into the Green River Basin via an exit that must have existed in the southeast corner of the basin at the southernmost extremity of Oyster Ridge. Figure 6.11 depicts the basin and lake configuration during this period. Figure 6.5 illustrates the overall stratigraphic architecture and facies relationships of the Road Hollow Member with subsequent members.

ST2 The Sandstone Tongue of the Wasatch (separates the Road Hollow from the Fossil Butte Member) was deposited in a prograding deltaic systems tract dominated by a large prograding Gilbert-type delta system (Petersen 1987) first recognized by Oriel and Tracey (1970) who mapped the sandstone unit. Accommodation space perfectly matched sediment infill during this time period. This unit can be traced into the lake-center at Fossil Butte where it is characterized by alternating turbiditic, silty-claystone and laminated micrite beds.

ST3 The basal kerogen-rich laminated micrite (sandwich beds) of the Fossil Butte Member marks a rather dramatic expansion of Fossil Lake to its largest expanse. Figure 6.5 illustrates the expansive nature of the basal facies, which flooded nearly the entire basin, and represents a flooding surface of a transgressive system tract (Fig. 6.10) dominated by profundal deposition in an over-filled lake basin. This supports the correlation of the Fossil Butte Member in Fossil Basin with the Tipton Member (Fontenelle Tongue) in the Green River Basin. Both members were deposited during one of the most expansive transgressive events in the Green River lakes system. The Fossil Lake expansion was mirrored by an equivalent expansion in the Green River Basin of Lake Gosiute, thus allowing both lakes to converge. Although Fossil Lake experienced it's largest expansion (to an over-filled lake) during Fossil Butte Member time, it also retracted (to a balanced-fill lake) and then expanded again just prior to Angelo Member time (k-spar tuff horizon). Tipton as mapped by Roehler (1993) appears to contain both lake types (based on Smith et al. 2008 interpretation). More recently the M.S. thesis of Jen Walker (this volume) shows that the Tipton oscillates back and forth between balanced and overfilled.

So why was this event so abrupt? The flooding was not diachronous, but a synchronous event as evidenced by the parallel relationship between the "sandwich tuff beds" and the base of the unit, at least as far south as Ryckman Creek West section (Fig. 6.8). Evidence of these tuffs further south is indicated by ochre staining of ostracodal limestone with apparent tuff material mixed in. The limestone beds that are equivalent to the basal sandwich beds occur on top of the Sandstone Tongue of the Wasatch, as do the sandwich beds. We suggest that a major climatic shift toward a much wetter climate took place at this time. This interpretation is also supported by palynological evidence (Cushman 1999). Fossil Lake subsequently underwent a regression with another significant expansion marked by the k-spar tuff and associated "ostracodal limestone (OSLS)" (Fig. 6.5) that can be traced southward (Fig. 6.8), along with the sandwich beds, into the Green River Basin. This apparently was short lived, as the unit is rather thin.

ST4 Another major climatic shift takes place at the conclusion of Fossil Butte Member time in the deposition of the Angelo Member. This can be readily observed in the restricted lateral stratigraphic dimensions of the Angelo Member (Fig. 6.5)**.** In addition, the Angelo Member is dominated by dolomite, evaporative minerals, and a general lacks fish fossils. This climatic shift is also supported by the plant microfossil evidence (Cushman 1999). The stratigraphic and facies relationships also mirror the Green River Basin in the deposition of the Wilkins Peak Member, which is also characterized by many of these fea-

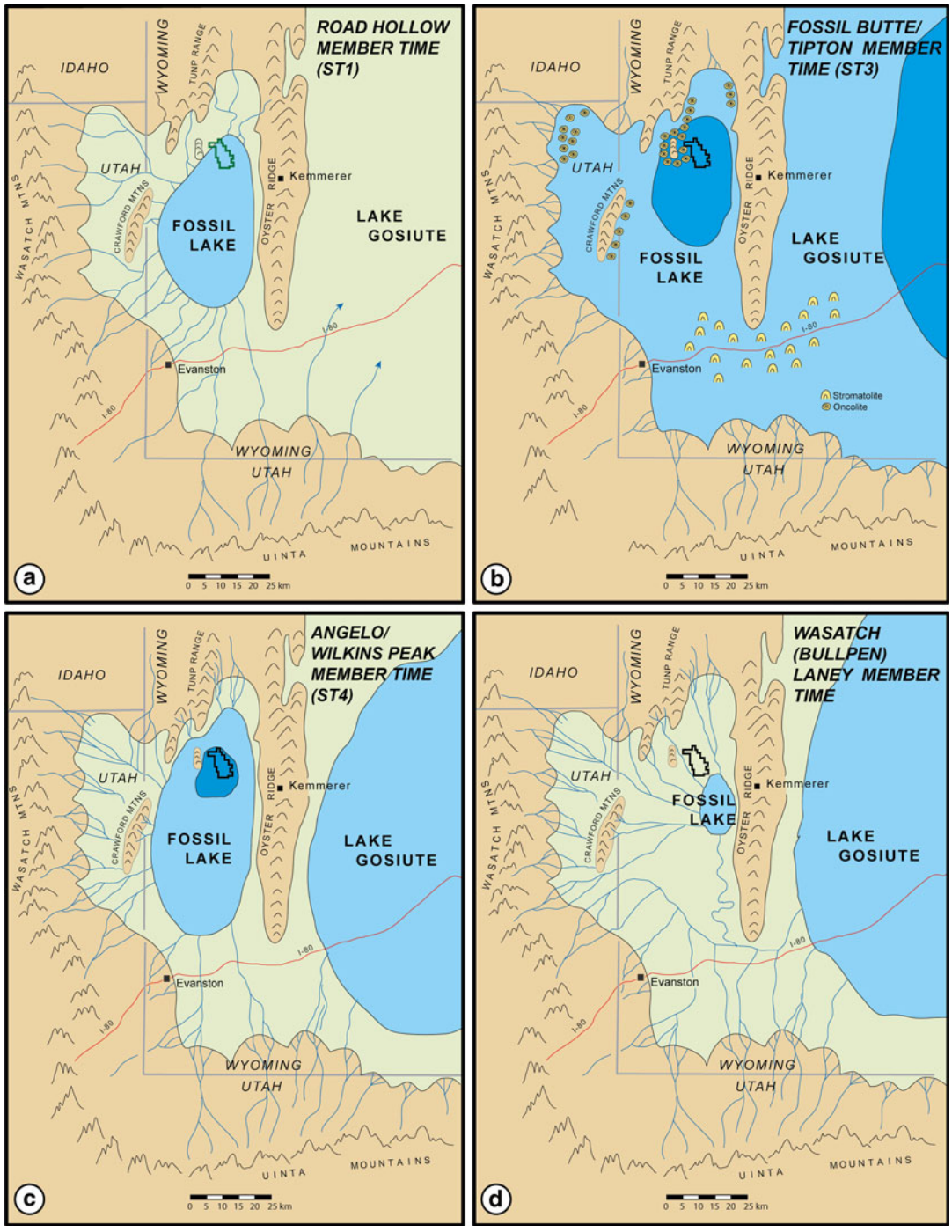

Fig. 6.11 Landscape Evolution during deposition of the Green River Formation in Fossil Basin. *Dark blue* indicates center and deepest portion of the lake. Note the skull cap stromatolite that makes an excellent marker bed through the area. Oncolites were deposited adjacent to islands and steep shorelines (frequently flooding surfaces on top of alluvial fans)

tures. This is characterized as a regressive systems tract, dominated by evaporative deposition, in an under-filled lake system (Fig. 6.5).

6.8 Landscape Evolution and Paleogeographic Reconstructions

The detailed mapping and successful correlation of the connection between Fossil Lake and Lake Gosiute also provided evidence for interpreting landscape evolution in Fossil Basin (Fig. 6.11). Landscape evolution in Fossil Basin is apparent in the stratigraphic architecture of lacustrine sedimentation and facies development. The thick, fluvial-lacustrine Road Hollow Member was deposited during the early phases of basin development when subsidence and sedimentation rates were in equilibrium. The onset of Fossil Butte Member deposition was marked by a basinwide transgression that resulted in an over-filled lake before again contracting to a balanced-fill lake; this occurred several times during Fossil Butte Member time. Relatively high wave energy along the lake shoreline produced abundant oncolites. Several islands emerged in the western and northern areas of Fossil Lake. Deposition of the Angelo Member occurred during the late stages of deposition in Fossil Lake. At this time, the lake was surrounded by broad mudflats and basin subsidence slowed. Base level equilibrium was attained allowing Fossil Lake to form a shallow, hypersaline lake in a hydrologically-closed and under-filled lake. Near the end of Fossil Lake deposition, an abrupt freshening occurred (as represented by a meter-thick KPLM at the top of the Angelo Member at Fossil Butte, loc. 217). This unit is a laminated calcimicrite signals a climatic shift or a shift to over-filled basin conditions due to rapid sedimentation evidenced by the deposition of the Bullpen Member of the Wasatch Formation overlying the Green River Formation. The Bullpen Member deposition is probably associated with the onset of renewed tectonism in the Wyoming Thrust Belt (Fig. 6.12).

6.9 Conclusions

Detailed stratigraphic studies over three decades and extensive geologic mapping of the Green River Formation in Fossil Basin has provided the foundation for making temporal and lithostratigraphic correlations between Fossil Basin and the Green River Basin. The basal "sandwich beds" and the ostracodal limestone (OSLS) near the top of the Fossil Butte Member were mapped and correlated across the highway 189 "gap" into the Green River Basin. The ostracodal limestone (OSLS) correlates with the "skull cap" stromatolite unit (SCS) in the Green River Basin. The "skull cap" (SCS) stromatolite is in the Fontenelle Tongue of the Tipton Member. The correlation of the Fossil Butte and Tipton Members is consistent with the interpretation that both of these members represent major expansions in the Green River lake system, and they both are subsequently followed by evaporative facies of the Angelo and Wilkins Peak members, respectively.

This breakthrough provides impetus for future significant investigations, including questions concerning how climatic, tectonic, and landscape changes affected the sedimentological and paleontological records in adjacent basins that were, for most of their existence, hydrologically disconnected. How did they differ when they were not connected? What fish fauna changes and exchange took place after the connection? There are fossil fish preserved in the Tipton Member (Bradley 1964), but little work has been done to compare or contrast the populations. On the other hand, the Fossil Butte and Tipton members are very different in many respects, especially in terms of lithology. The Tipton is largely composed of illitic clays (Bradley 1964), whereas the Fossil Butte Member is primarily carbonate (micritic mudstone or laminated micrite). Why are they different? This also provides the basis for numerous other exciting studies and maybe even an encouragement to attempt to temporally connect Lake Gosiute with Lake Uinta. We think it can be done.

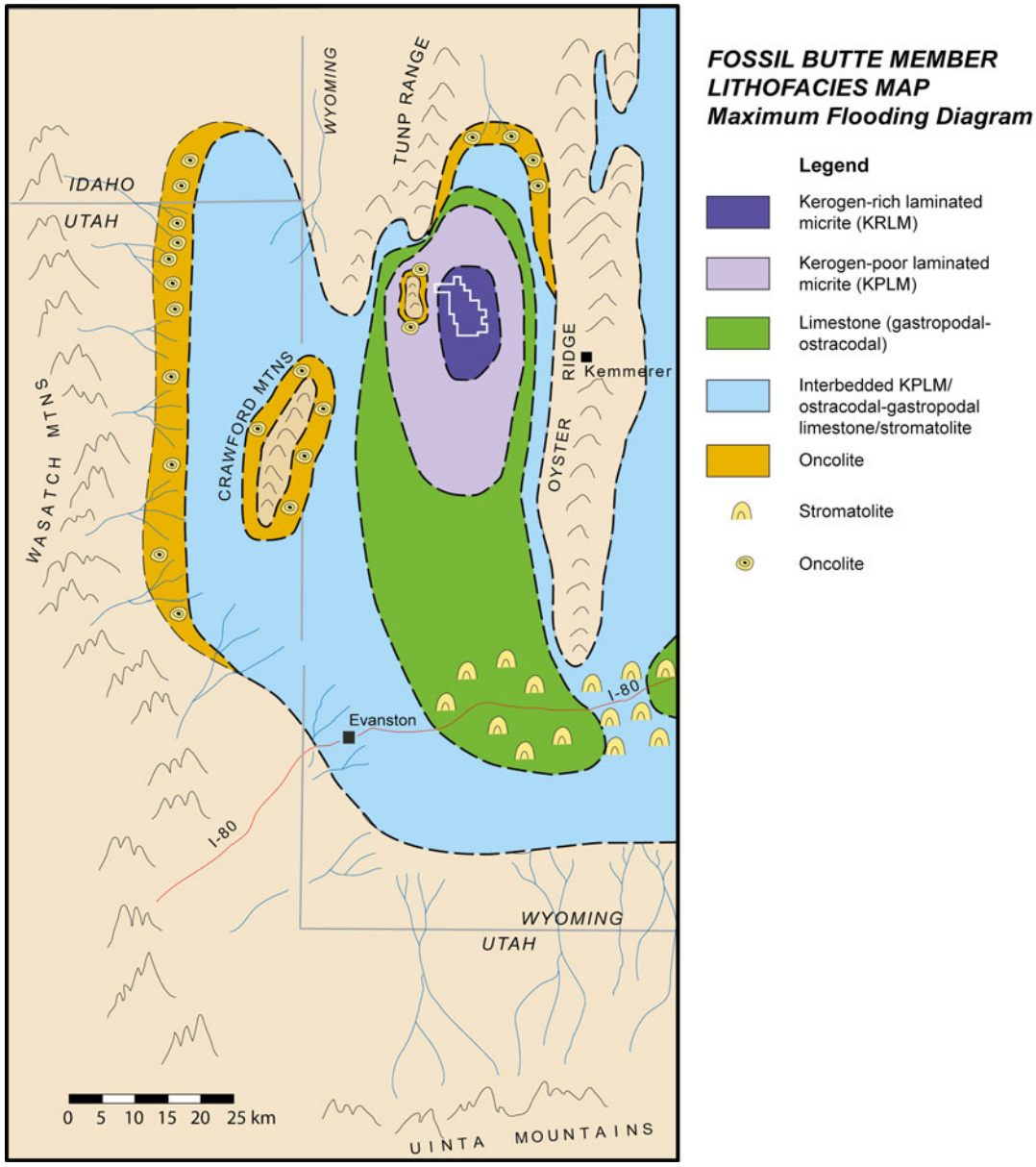

Fig. 6.12 Lithofacies distribution during Fossil Butte Member time when maximum flooding dominated deposition in Fossil Basin (and probably Green River Basin). This was the first of two time periods when Fossil Lake and Lake Gosiute were hydrologically connected; the second was near the close of Fossil Butte Member time when the k-spar tuff was deposited

Acknowledgments We thank the National Park Service and Fossil Butte National Monument for their generous financial support of a basin-wide mapping project that allowed the stratigraphic understanding critical to the interbasinal correlations, and in particular Arvid Aase, the Fossil Butte National Monument paleontologist, who was the park liaison for the mapping project. His assistance was critical to successful completion of that project. We thank the Department of Earth and Biological Sciences at Loma Linda University for their support of summer field assistants and additional financial support in the stratigraphic correlation and other field projects. We greatly appreciated the timely assistance of T. Joe Willey and Bob Wonderly with their personal 4-wheel drive vehicles when

our primary field vehicle was in the shop for several weeks. Our lives were happier in camp with the wonderful camp cooking of my wife, Carole Buchheim as well as support from Judy Cushman. Student field assistants and graduate students that participated in mapping, stratigraphy, or thesis fieldwork included Tom Amato, Doug Britton, Hans Buchheim, Cody Carter, Meredith Church, Jamey Cooper, Allen Cooper, Matthew Cushman, Angela Forgey, Heather Futcher, Daniel Gonzalez, Maria Kim, Mark Loewen, Matt Mayry, Chip McHenry, Holly Moon, Matthew Niemeyer, Gail Outhwaite, Rick Peters, Steve Peterson, Curtis Rehling, Jason Scott, Carol Shultz, Bethania Siviero, Craig Sipes, Nathan Stanton, Heather Stearman, Ryan Thompson, Ester Trivino, Georgiana Tutu, Desiree Wentland, Jimmy Wilhelm, Wendy Worthy, and Aimee Wyrick. We especially appreciate the access provided us by local private fossil quarriers including: Dick Dayvault, Bob and Bonnie Finney, Rick Hebdon, Thomas Lindgren, Tony Lindgren, Jerome Montgomery, Charlie Nunn, Pete Severns, and Jimmy Tynsky. We appreciate the access local ranchers generously provided us with including: Don and Kathy Failoni, Josephine Julian, Truman Julian, and Don Lewis.

References

Biaggi RE (1989) Paleogeography and paleoenvironments of the lower unit, Fossil Butte Member, Eocene Green River Formation, southwestern Wyoming [M.S. thesis], Loma Linda University, Loma Linda, CA, 134 p

Bohacs KM, Carroll AR, Neal JE, Mankiewicz PJ (2000) Lake-basin type, source potential, and hydrocarbon character: an integrated sequence-stratigraphic-geochemical framework. In: Gierlowski-Kordesch E, Kelts K (eds) Lake basins through space and time, vol 46, American Association of Petroleum Geologists Studies in Geology. American Association of Petroleum Geologists, Tulsa, pp 3–37

Bradley WH (1929) The varves and climate of the Green River Epoch: U.S. Geological Survey professional paper 158-E. U.S. Government Printing Office, Washington, DC, pp 87–110

Bradley WH (1948) Limnology and the Eocene lakes of the Rocky Mountain Region. Geol Soc Am Bull 59:635–648

Bradley WH (1963) Paleolimnology. In: Frey DG (ed) Limnology in North America. University of Wisconsin Press, Madison, pp 621–652

Bradley WH (1964) Geology of the Green River Formation and associated Eocene rocks in southwestern Wyoming and adjacent parts of Colorado and Utah, United States Geological Survey professional paper 496-A. U.S. Government Printing Office, Washington, DC, p 57

Buchheim HP (1986) Paleoenvironments and sediment fossil fish relationships: a case study from the Eocene Green River Formation, Wyoming [abstract]. In: Proceedings fourth North American paleontological convention, p A7

Buchheim HP (1994a) Eocene Fossil Lake, Green River Formation, Wyoming: a history of fluctuating salinity. In: Renaut RW, Last WM (eds) Sedimentology and geochemistry of modern and ancient saline lakes, vol 50, SEPM Special Publication. SEPM (Society for Sedimentary Geology), Tulsa, pp 239–247

Buchheim HP (1994b) Paleoenvironments, lithofacies and varves of the Fossil Butte Member of the Eocene Green River Formation, southwestern Wyoming: University of Wyoming. Contrib Geol 30:3–14

Buchheim HP, Biaggi RE (1988) Laminae counts within a synchronous oil shale unit: a challenge to the "varve" concept [abstract]. Abstr Progr Geol Soc Am 20(7):317

Buchheim HP, Eugster HP (1998) Eocene Fossil Lake: the Green River Formation of Fossil Basin, southwestern Wyoming. In: Pitman JK, Carroll AR (eds) Modern and ancient lake systems, vol 26, Utah Geological Association guidebook. Utah Geological Association, Salt Lake City, pp 191–207

Buchheim HP, Loewen MA, Cushman RA Jr, Biaggi RE (2002) Stratigraphic revision of the Green River Formation in Fossil Basin, Wyoming: three distinct phases of Fossil Lake [abstract]. Geol Soc Am Abstr Progr 34(6):479

Buchheim HP, Cushman RA, Biaggi RE (2011) Stratigraphic revision of the Green River Formation in Fossil Basin, Wyoming: overfilled to underfilled lake evolution. Rocky Mt Geol 46(2):165–181

Carroll AR, Bohacs KM (1999) Stratigraphic classification of ancient lakes; balancing tectonic and climatic controls. Geology 27:99–102

Church M (2003) Deposition of laminated sediments in Eocene Fossil Lake: a function of episodic inflow processes. [M.S. thesis], Loma Linda University, Loma Linda, CA, 83 p

Cope ED (1877) A contribution to the knowledge of the ichthyological fauna of the Green River shales. US Geol Geogr Surv Bull 3:807–819

Cope ED (1884) The vertebrata of the tertiary formations of the West: U.S. Geological and Geographical Survey of the Territories. Annual report no. 3, 1009 p

Crowley KD, Duchan CE, Rhi J (1986) Climate record in varved sediments in Eocene Green River Formation. J Geophys Res 91:8637–8648

Cushman RA Jr (1999) Vegetational history and climatic transition in an Eocene intermontane basin: plant microfossil evidence from the Green River Formation, Wyoming. In: Santucci VL, McClelland L (eds), National park service paleontological research: geologic resources division technical report, vol 4. NPS/NRGRD/GRDTR-99/03, pp 66–71

Dover JH, M'Gonigle JW (1993) Geologic map of the Evanston 30′×60′ Quadrangle, Uinta and sweetwater counties, Wyoming: U.S. Geological Survey, Miscellaneous investigations series, Map I-2168, scale 1:100,000

Fischer AG, Roberts LT (1991) Cyclicity in the Green River Formation (lacustrine Eocene) of Wyoming. J Sediment Petrol 61:1146–1154

Grande L (1984) Paleontology of the Green River Formation, with a review of the fish fauna. Geol Surv Wyoming Bull 63:333

Grande L (1985) The use of paleontology in systematics and biogeography, and a time control refinement for historical biogeography. Paleobiology 11(2):234–243

Grande L (1989) The Eocene Green River Lake system, Fossil Lake, and the history of the North American fish fauna. In: Flynn J (ed) Mesozoic/Cenozoic vertebrate paleontology: classic localities, contemporary approaches, 28th international geological congress field trip guidebook T322. American Geophysical Union, Washington, DC, pp 18–28

Grande L (1994) Studies of paleoenvironments and historical biogeography in the Fossil Butte and Laney Members of the Green River Formation: University of Wyoming. Contrib Geol 30(1):15–32

Grande L, Buchheim HP (1994) Paleontological and sedimentological variation in Early Eocene Fossil Lake. Contrib Geol 30(2):33–56

Hurst DJ (1984) Depositional environment and tectonic significance of the Tunp Member of the Wasatch Formation, southwest Wyoming [M.S. thesis], University of Wyoming, 115 p

Lamerson PR (1982) The Fossil Basin and its relationship to the Absaroka thrust system, Wyoming and Utah. In: Powers RB (ed) Geologic studies of the Cordilleran thrust belt, vol 3. Rocky Mountain Association of Geologists, Denver, pp 279–340

Leggitt VL (1996) An avian botulism epizootic affecting a nesting site population of *Presbyornis* on a carbonate mudflat shoreline of Eocene Fossil Lake [M.S. thesis], Lorna Linda University, 114 p

Leggitt VL, Buchheim HP (1996) An avian botulism epizootic affecting a nesting site population of *Presbyornis* on a carbonate mudflat shoreline of Eocene Fossil Lake [abstract]. The Paleontological Society Special Publication Number 8, p 234

Loewen MA (1999) Lateral salinity gradients during hypersaline lake stages of Eocene Fossil Lake, Wyoming [M.S. thesis], Loma Linda University, Loma Linda, CA, 58 p

McGrew PO, Casilliano M (1975) The geological history of Fossil Butte National Monument and Fossil Basin, National Park Service occasional paper, no. 3. National Park Service, Washington, DC, p 37

M'Gonigle JW, Dover JH (1992) Geologic map of the Kemmerer 30′×60′ quadrangle, Lincoln, Uinta, and sweetwater counties, Wyoming: U.S. Geological Survey Miscellaneous investigations series Map I-2079, scale 1:100,000

Oriel SS, Tracey JI (1970) Uppermost cretaceous and tertiary stratigraphy of Fossil Basin, Southwestern Wyoming, vol 635, U.S. Geological Survey professional paper. U.S. Government Printing Office, Washington, DC, p 53

Peale AC (1879) Report on the geology of the Green River district: 11th annual report, U.S. Geological Survey of the territories, p 509–646

Petersen FS (1987) Lacustrine deltaic deposits of the Sandstone Tongue of the Wasatch Formation, Fossil Basin, Wyoming [M.S. thesis], Loma Linda University, Loma Linda, CA, 217 p

Ripepe M, Roberts LT, Fischer AG (1991) ENSO and sunspot cycles in varved Eocene oil shales from image analysis. J Sediment Petrol 61:1155–1163

Roehler HW (1993) Eocene climates, depositional environments, and geography, greater Green River basin, Wyoming, Utah, and Colorado: U.S. Geological Survey professional paper 1506-F. U.S. Government Printing Office, Washington, DC, 74 p

Rubey WW, Oriel SS, Tracey JI (1975) Geology of the Sage and Kemmerer 15-minute quadrangles, Lincoln County, Wyoming, vol 855, U.S. Geological Survey professional paper. U.S. Government Printing Office, Washington, DC, p 18

Schultz AR (1914) Geology and geography of a portion of Lincoln County, Wyoming. US Geol Surv Bull 543:141

Smith ME, Carroll AR, Singer BS (2008) Synoptic reconstruction of a major ancient lake system: Eocene Green River Formation, western United States. Geol Soc Am Bull 120(1&2):54–84

Smith ME, Chamberlain KR, Singer BS, Carroll AR (2010) Eocene clocks agree: coeval $^{40}Ar/^{39}Ar$, U-Pb, and astronomical ages from the Green River Formation. Geology 38:527–530

Surdam RC, Stanley KO (1980) Effects of changes in drainage-basin boundaries on sedimentation in Eocene Lakes Gosiute and Uinta of Wyoming, Utah, and Colorado. Geology 8:135–139

Veatch AC (1907) Geography and geology of a part of south-western Wyoming, with special reference to coal and oil: U.S. Geological Survey professional paper 56, 178 p

Sedimentology of the World Class Organic-Rich Lacustrine System, Piceance Basin, Colorado

7

Kati Tänavsuu-Milkeviciene and J. Frederick Sarg

Abstract

The Piceance lake basin formed between *ca* 54–48 Ma years ago, during the early to middle Eocene, and it contains the largest known oil shale resources in the world today (~1.5 trillion bbls in place). Based on the detailed facies and facies association study three small-scale (decimetre to metre) depositional cycles have been separated that characterize deposition along the basin margin and in the deeper part of the basin. Stacked depositional cycles form large-scale depositional sequences (metre to 10's of metres). Depositional sequences characterize significant changes in lake regime and are divided into periods of low, rising, and high lake. During low lake level, main accumulation of deposits occurred in the deeper part of the basin where organically lean deposits formed. Following rising and high lake levels brought thick accumulations of siliciclastic and carbonate deposits along lake margin that were later, during high lake level capped by littoral to sublittoral siltstones and mudstones, and lean oil shales. In the deeper part of the lake thick organically rich deposits formed. The overall lake evolution is characterized by lake stages that reflect long-term changes in the basin controlled by both, climate and tectonics. Lake Stage 1, Fresh to Mesosaline lake was deposited during decreasing tectonic activity and increasing climate control. Lake Stages 2 and 3, Transitional and Highly Fluctuating lake are interpreted to be dominated by an increasingly warm and arid climate and characterized by laterally discontinuous and very rich oil shale deposits. The following Stages 4 and 5, Rising and High lake record the change to a wetter climate and increasing tectonic

K. Tänavsuu-Milkeviciene (✉)
Department of Geology and Geological Engineering,
Colorado School of Mines, Golden, CO 80401, USA

Statoil ASA, Research Centre Rotvoll,
Trondheim NO-7005, Norway
e-mail: KTAN@statoil.com

J.F. Sarg
Department of Geology and Geological Engineering,
Colorado School of Mines,
Golden, CO 80401, USA

M.E. Smith, A.R. Carroll (eds.), *Stratigraphy and Paleolimnology of the Green River Formation, Western USA*, Syntheses in Limnogeology 1, DOI 10.1007/978-94-017-9906-5_7

activity, resulting in increased runoff, development of a widespread deep lake that extended across the Piceance basin, and are marked by the laterally continuous rich oil shale deposits. Stage 6, Closing lake marks high siliciclastic input, the beginning of the closing of the Piceance basin, and progressively decreasing organic richness.

7.1 Introduction

The Piceance basin is one of the three Green River Formation lake basins that formed during the early to middle Eocene and contain a vast amount of oil shale resources. The Piceance basin is estimated to be one of the largest depositories of oil shale in the world known today (~1.5 trillion bbls in place) (Johnson et al. 2010) and is a classic example of a deep organic-rich lake with a mixed carbonate-siliciclastic and evaporite-rich lacustrine depositional system. The Piceance lacustrine basin formed over a period of *ca* 5–6 Myr (Smith et al. 2008, 2010), during which time continuous deposition occurred in the lake. This has led to the formation of thick lacustrine deposits, up to 1,000 m in thickness, in the lake depocenter, in the northern portion of the basin, representing the entire section of the lake evolution.

Because of its high organic content and well-defined organic-rich and organic-poor intervals, rich oil shale zones and lean oil shale zones have been separated in the deeper part of the basin (Cashion and Donnell 1972, 1974). This has also led to the usage of two stratigraphic schemes, one that uses lithofacies, and another that uses these rich and lean zones (e.g., Cole and Daub 1991; Pitman 1996; Dyni 2006; Johnson et al. 2010; Self et al. 2010b). The latter has been important from the industry point of view to identify the organic-rich intervals, whereas the lithologic units give the overview of the lithotypes. Several assessments of the oil shale deposits have been made previously and the distribution of the rich and lean zones within the deeper part of the basin area is well known (Pitman and Johnson 1978; Pitman et al. 1989; Mercier et al. 2009; Johnson et al. 2010). However, rich and lean zones are not well defined along the basin margins and in the southern portion of the basin, and it has been problematic to correlate the basin margin deposits with the deeper basinal deposits (see also Johnson et al. 2010; Johnson 2012).

This paper presents an overview of the main facies and facies associations in the Piceance basin area, describes lateral and vertical variation of facies associations and their depositional relationships. We will also describe sequence stratigraphic units and surfaces, how they form and how they are connected to the formation of the rich and lean oil shale zones. Finally, this work will give an overview of the evolution of the Piceance lake basin and how it responded to the climate and tectonic changes during the early and middle Eocene. Defining the sequence stratigraphic framework, the formation of rich and lean oil shale zones, and the evolution of the Piceance basin could be useful for interpreting other lake basins, especially for understanding the short-term and long-term alternations caused by climate and tectonic changes and how they change throughout lake evolution and for predicting the distribution of facies associations and organic-rich deposits throughout the lake basin.

7.2 Geology and Stratigraphy

During the Laramide Orogeny a series of continental basins, the Piceance basin, the Uinta basin and the Greater Green River basin formed in the Colorado, Utah, and Wyoming, respectively (Dickinson et al. 1988) (Fig. 7.1). Lacustrine deposits formed in mid-latitude warm-temperate to subtropical climate (Sewall and Sloan 2006; Clementz and Sewall 2011). The deposition in lakes was initiated and terminated by tectonic and landscape evolution events convolved with climate effects (Carroll et al. 2006; Davis et al. 2009; Chetel et al. 2011; Tänavsuu-Milkeviciene and Sarg 2012).

For most of their history these non-marine basins were separated from one another by

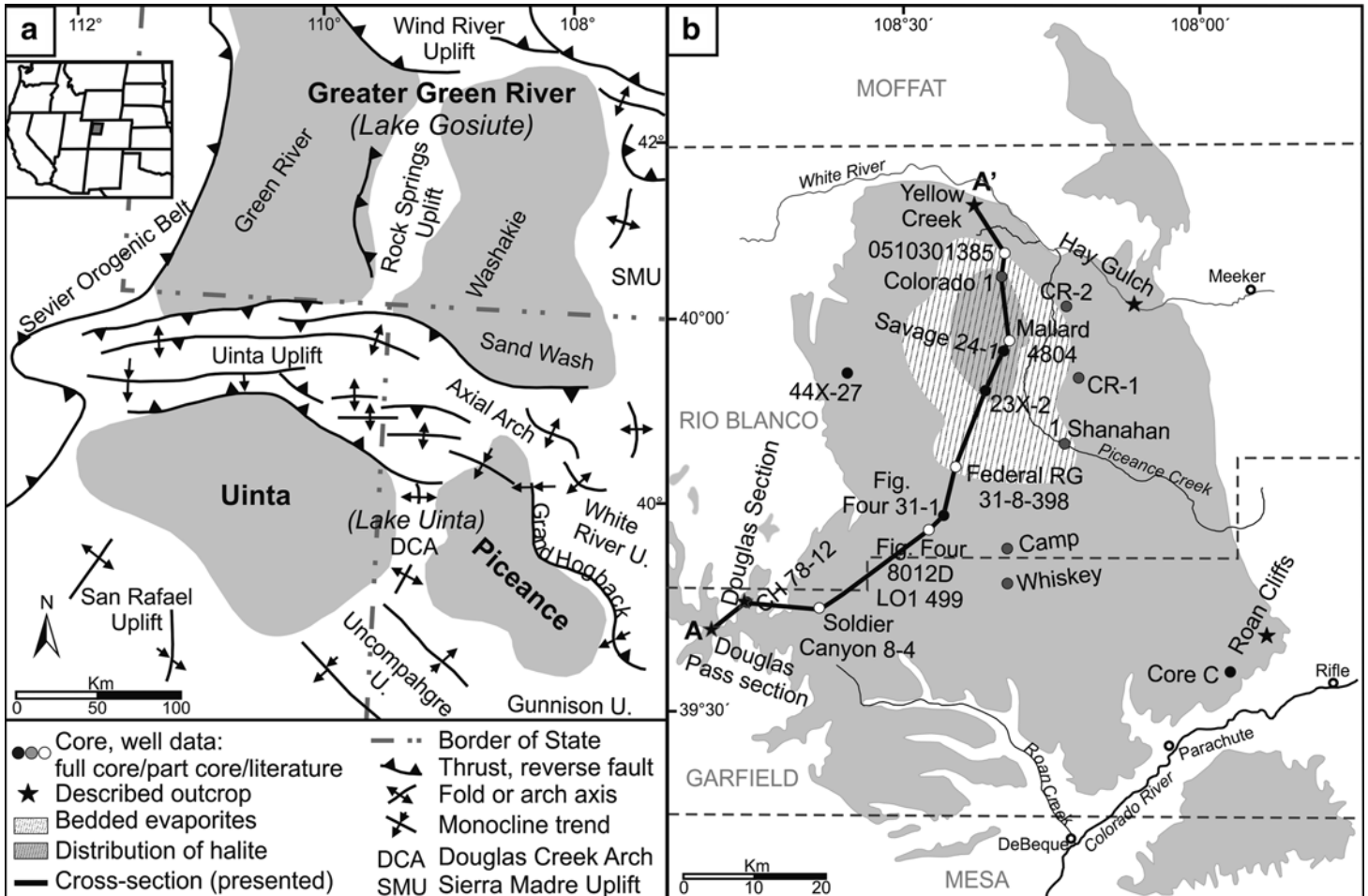

Fig. 7.1 (**a**) Eocene intermountain basins and basin bounding uplifts of the western USA (Modified after Dickinson et al. 1988). The Uinta basin and the Piceance basin form Lake Uinta. (**b**) Close-up map of the Piceance basin with described cores and outcrops from the study area, and the representative cross-section (A-A'). Black circles mark cores, where the entire interval of the Green River Formation was described. *Gray circles* mark cores, where only part of the Green River Formation interval was described. *White circles* mark wells from literature that are used on presented cross-section (A-A'). *Shaded area* in the northern part of the basin indicates distribution of the thick-bedded evaporites, as well as the basin depocenter (After Dyni 1981; Dyni and Hawkins 1981). Cross-section A-A' is shown in Fig. 7.3

anticlinal basement-cored uplifts, and developed as separate lakes, but were at times, connected (Surdam and Stanley 1980; Smith et al. 2008; Davis et al. 2009). The Piceance basin is separated from the Greater Green River basin by the Uinta Mountains to the north and northwest, and from the Uinta basin by the Douglas Creek Arch to the west (Fig. 7.1). When the Piceance basin and Uinta basin were connected they formed a vast lake named Lake Uinta (Fig. 7.1). At times Lake Uinta was connected with the Greater Green River basin (known also as Lake Gosiute) to the north through the Sand Wash basin (Smith et al. 2008; Davis et al. 2009) (see also Fig. 7.1).

The Piceance lake basin covers a portion of northwestern and western Colorado (see Fig. 7.1). Three erosional remnants of previous lake deposits are exposed: the southernmost Grand Mesa *ca* 648 sq km, the middle Battlement Mesa *ca* 285 sq km, and the largest remnant, located north of the Colorado River, and the Piceance Creek covering the northern part of the basin *ca* 4,403 sq km (Young 1995; Johnson 2012, personal communication) and comprising the Roan Plateau. This work focuses on the northern part of the basin. The overall thickness of the Green River Formation varies, and is up to 1,100 m thick in the northern-central part of the Piceance basin.

Deposition of the Green River Formation lacustrine sediments occurred over a period of 5–6 Myr, between *ca* 53 to *ca* 48 Ma (Smith et al. 2008, 2010). The Green River Formation in the study area is subdivided into (1) five members, based on lithology and (2) 17 rich and lean zones, based on kerogen content (Fig. 7.2). The oldest member, the freshwater mollusc-bearing Cow Ridge Member interfingers with the alluvial Wasatch Formation (Fig. 7.2). The base of the Formation is marked by a major transgression of lake deposits and is marked by a distinctive ostracod, oolite, and mollusc-rich bed i.e., Long Point Bed (Fig. 7.2) (Johnson 1984).

The Cow Ridge Member is overlain by mixture of lake-margin fluvial-dominated siliciclastic deposits and microbial and non-microbial carbonates of the Douglas Creek Member in the western and southern parts of the study area. In the eastern and northern parts of the study area marginal wave-dominated siliciclastic deposits with some

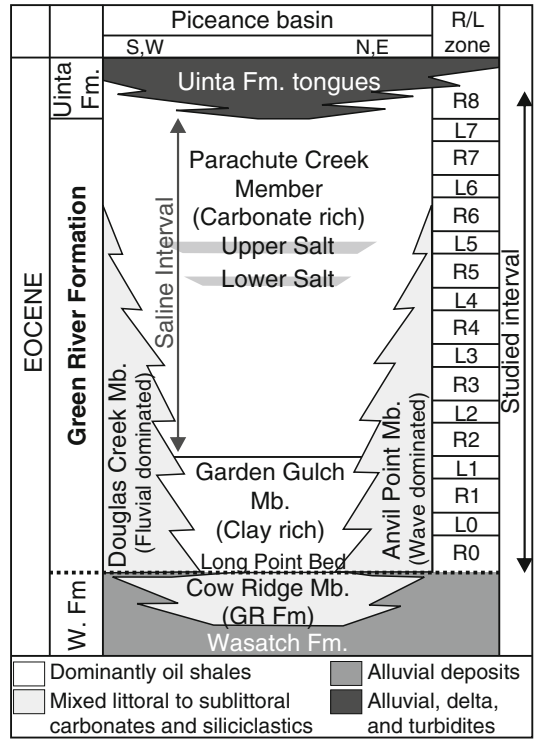

Fig. 7.2 Lithostratigraphic subdivision of the lower and middle Eocene deposits and correlation with kerogen-rich (*R*) and kerogen-poor (*L*) zones in the Piceance basin (Modified after Pitman 1996; Dyni 2006; Johnson et al. 2010; Self et al. 2010b; Rich and lean zones after Cashion and Donnell 1972, 1974). Upper salt and lower salt zones mark the thickest, bedded halite intervals in the basin. The saline interval marks the range of evaporite deposition. Note that the subdivision of the Green River Formation interval into rich and lean zones applies only for the deep, profundal deposits in the basin area

thin microbial carbonate deposits of the Anvil Point Member overlie the Cow Ridge Member (Fig. 7.2). In the central part of the Piceance basin, illitic (clay-rich) oil shale deposits of the Garden Gulch Member overlie the Cow Ridge Member. The thickest and most wide spread part of the Green River Formation, the Parachute Creek Member (Fig. 7.2), consists of calcite and dolomite-rich mudstones. In places, bedded and disseminated evaporites (halite, nahcolite, dawsonite) occur in the Parachute Creek Member (Fig. 7.2). The upper part of the Parachute Creek Member interfingers with the alluvial, deltaic and turbidite deposits of the Uinta Formation (Fig. 7.2). Based on kerogen content, deposits of the Piceance basin are subdivided into nine oil-rich zones (R) and

eight oil-lean zones (L) (Cashion and Donnell 1972, 1974) (Fig. 7.2). The interval of the Green River Formation studied in this work represents the interval between the Long Point Bed and the Uinta Formation sandstones.

7.3 Methods

This study is based on centimeter-scale descriptions of outcrop and core sections, and integrated Fischer assay and gamma ray log data. Data we employed included, (1) six core sections covering the entire Green River Formation interval, (2) six core sections from the Parachute Creek Member, (3) five outcrop sections from the Douglas Creek and Parachute Creek Members, for a total of 13 measured sections, and (4) over 900 Fischer assay and gamma ray well-log data from the Green River Formation (after Mercier et al. 2009; Self et al. 2010a, b) (see Fig. 7.1). This data set allowed interpretation of lateral and vertical facies association relationships, stacking patterns, basin architecture, and changes in depositional processes. Additional published material was used to clarify the depositional environments (Johnson et al. 1988; Johnson 2012).

Integration of facies associations, gamma ray character, and Fischer assay logs were used to correlate main surfaces such as lake stage boundaries, sequence boundaries, transgressive surfaces, and distribution of the sedimentary units in the study area (Fig. 7.3). Tops for rich and lean oil shale zones are after Mercier et al. (2009) and Self et al. (2010a, b) and lake stage intervals are after Tänavsuu-Milkeviciene and Sarg (2012). Described core and outcrop sections were used to identify lateral and vertical variation of facies associations. The cross-section from the southwestern Douglas Creek Arch part of the basin, up to northern part of Piceance basin was chosen to represent the facies associations in whole study area (Figs. 7.1 and 7.3, A-A') because it best displays those relationships. The cross-section is flattened on the Mahogany bed that displays the best laterally continuous oil shale interval, and can be correlated across the entire basin (Fig. 7.3).

7.4 Facies Associations

Deposition in the Piceance basin is characterized by complex depositional system that ranges from alluvial deposits to deep lake deposits (Fig. 7.4).

Twenty-four sedimentary facies (F) were defined by sedimentary structures, textures, and composition (Table 7.1). Sedimentary facies are grouped into 13 facies associations (FA) based on the lateral and vertical association of facies. Facies and facies association descriptions are updated and modified after Tänavsuu-Milkeviciene and Sarg (2012). Facies associations are divided from alluvial to lake deposits. Lake deposits are grouped into lacustrine environments or zones, based on energy level and relative water depth (Fig. 7.4). Lacustrine zones defined by energy levels are: (1) the littoral zone, above fair-weather wave base, (2) the sublittoral zone, between fair-weather wave base and storm wave base, and (3) the profundal zone, below the storm wave base (after Reading and Collinson 1996; Cohen 2003; Renaut and Gierlowski-Kordesch 2010).

7.4.1 Alluvial Facies Association

7.4.1.1 Facies Association 1: Alluvial Deposits

Facies Association 1 (FA1) occurs in the western portion of the basin area, along the Douglas Creek Arch and is characterized by plane-parallel deposits of interbedded mottled (F1), homogeneous (F2), and laminated (F3) mudstones and siltstones, and plane-parallel (F7) or structureless (F10) sandstones (Fig. 7.5a–c: Table 7.1). Mottled, grey to reddish colored mudstones and siltstones (F1) with plant remains and subtle erosional boundaries (Fig. 7.5c) suggest *in situ* early palaeosol development or presence of reworked pedogenic mud aggregates (Wright and Marriott 2007; Müller et al. 2004). Planar-bedded units of plane-parallel (F7) and structureless (F10) siltstones and sandstones interbedded with mudstones indicate sheet-flow deposits (Fig. 7.5a, b), formed as shallow flows spread out across the floodplain (Wakelin-King and Webb 2007). Interbedded siltstones and sandstones are intersected by concave-up, erosionally based

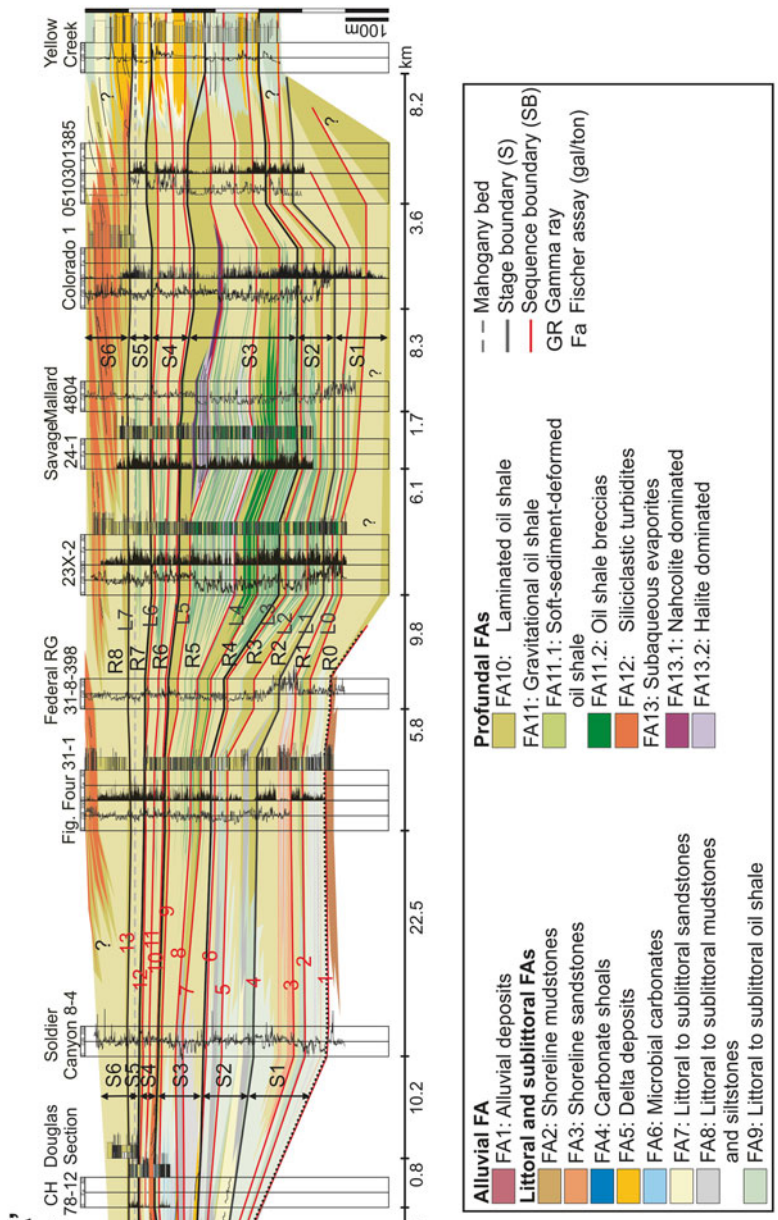

Fig. 7.3 Well-outcrop ross-section of the Green River Formation in the Piceance basin that shows the distribution of the facies associations from the western part of the basin northwards through the deepest part of the basin up to northern margin of the basin (Rich (*R*) and lean (*L*) zones after Cashion and Donnell 1972, 1974; Self et al. 2010b)

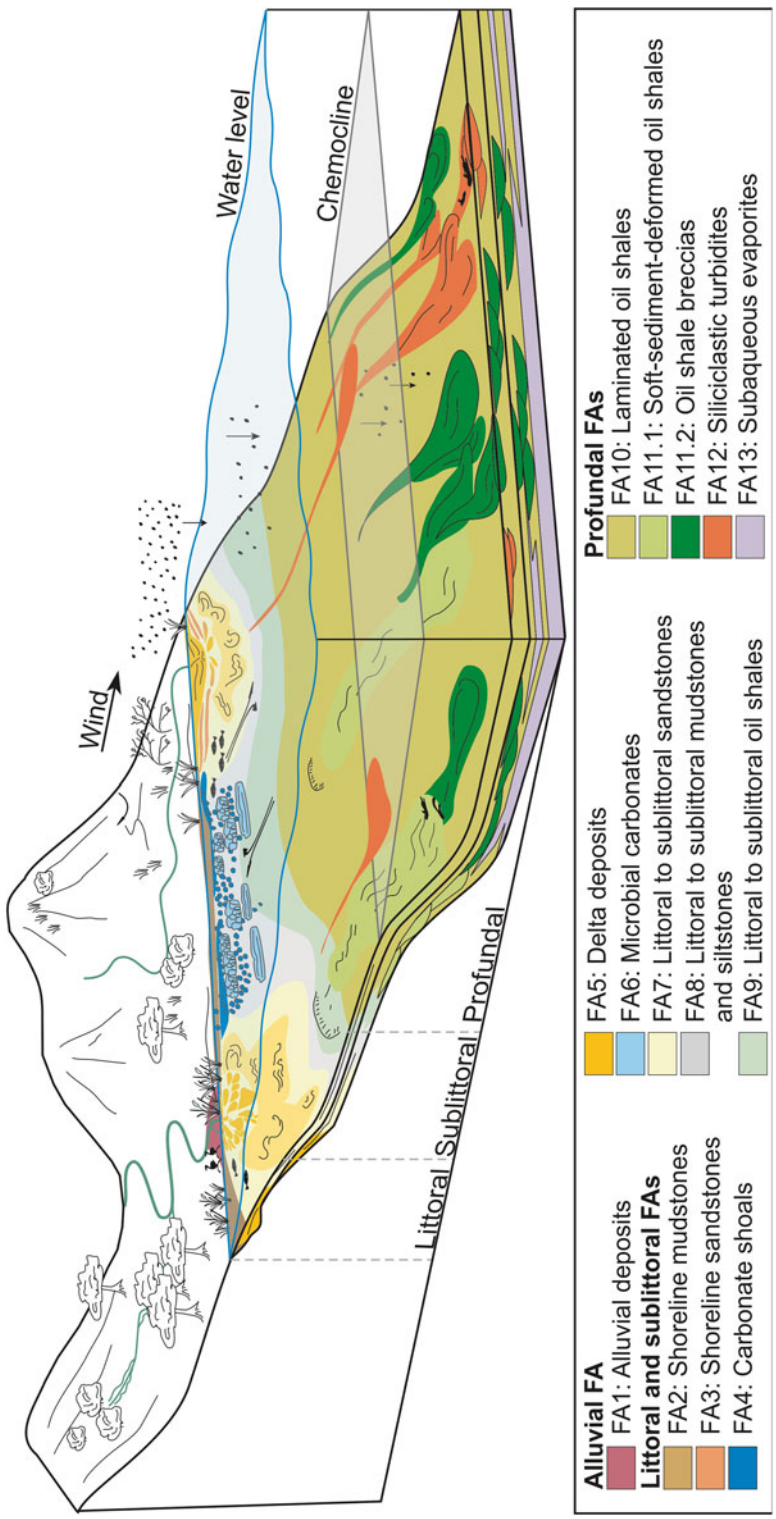

Fig. 7.4 Illustrative depositional model of the Green River Piceance lake basin (Modified after Tänavsuu-Milkeviciene and Sarg 2012) that describes approximate position of facies associations found in the lake basin. Along margin on right is wave-dominated and on left fluvial-dominated deposits. Note, carbonate deposits form at the same time as silicialstic deposits and the occurrence of evaporite deposits within oil shale deposits in the profundal zone

Table 7.1 Facies and their relation to the Facies Associations, Green River Formation, Piceance basin

	Facies	Texture/lithology	Structure	FA
1	Mottled mudstone	Siliciclastic mud and silt	Structureless, red to greenish colored, mottled	1
2	Homogeneous mudstone	Siliciclastic mud and silt	Homogeneous, massive	1, 2, 7, 8
3	Laminated mudstone	Siliciclastic mud, silt, with very fine, fine sand layers	Parallel-laminated	1, 2, 5, 7, 8, 12
4	Wave ripple cross-laminated sandstone	Silt to fine sand	Wave ripple cross-lamination	3, 5.1, 7, 8, 9
5	Current ripple cross-laminated sandstone	Silt to fine sand	Current ripple cross-lamination	5.1, 5.3, 7, 8, 9
6	Climbing ripple cross-laminated sandstone	Silt to fine sand	Climbing ripple cross-lamination	5
7	Plane-parallel sandstone	Silt to medium sand	Sub-horizontal lamination	5.1, 5.2, 7, 12
8	Cross-stratified sandstone	Silt to medium sand	Planar and trough cross-stratification	3, 5
9	Hummocky, swaley cross-stratified sandstone	Silt to fine sand	Low angle, hummocky, swaley cross-stratification	3
10	Structureless sandstone	Fine sand to gravel	Structureless, amalgamated, normally graded, ungraded. Occur rip-up clasts	3, 5.1, 5.3, 12
11	Conglomerate	Granule to pebble	Massive, intraformational rip-up clast conglomerate	3, 5.1, 5.3
12	Microbial carbonates	Lime mudstone to grain-rich bindstone	Finely-laminated, domal stromatolites, thrombolites, shrub-like features, intraclasts	2, 6
13	Nonskeletal limestone	Calcitic mixed packstone to grainstone	Oolites, pisolites, carbonate intraclasts, minor bioclasts; massive, plane-parallel, cross-stratified	4, 6
14	Molluscan limestone	Calcitic coquina	Gastropods, bivalves, structureless or plane-parallel	4
15	Intraclastic mudstone	Carbonate mudstone clasts in a siliciclastic mud matrix		2
16	Finely-laminated oil shale	Dominantly dolomitic kerogen-rich mudstone	Parallel-laminated	10
17	Illitic oil shale	Kerogen-rich mudstone, clay-rich	Parallel-laminated, in places also ostracod-rich	9, 10
18	Laminated silt-rich oil shale	Kerogen-rich mudstone, dominantly carbonate-rich, with silt to very fine sand	Parallel-laminated, minor silt to sand layers and lenses	9
19	Wavy-laminated oil shale	Kerogen-rich mudstone, clay-rich or carbonate-rich	Wavy to disrupted lamination	9, 10, 11.1
20	Soft-sediment-disturbed oil shale	Dominantly dolomitic kerogen-rich carbonate	Overturned lamina, microfaulted, incipient brecciation	11.1
21	Oil shale breccia	Matrix-supported breccias, dominantly dolomitic kerogen-rich mudstone with clasts (clasts mm to cm in scale)	Organic, carbonate, and siliciclastic clasts. In places, nahcolite clast. Carbonate clasts are homogeneous or finely laminated. Occur graded bedding	11.2

(continued)

Table 7.1 (continued)

	Facies	Texture/lithology	Structure	FA
22	Nahcolite		Nodules and/or crystals to crystal accumulations form mm-dm thick beds	10, 11.2, 13
23	Halite		Hopper crystals and bottom growth crystals form mm-cm thick beds	13
24	Dawsonite		Fine crystals	13

Updated and modified after Tänavsuu-Milkeviciene and Sarg (2012)

decimeter to meters thick and several meter wide sandstone units that continue as thin, decimeters thick single very fine to fine-grained sandstone beds (Fig. 7.5a). These erosionally based sandstones are described as flood channel and levee deposits (Müller et al. 2004; Wakelin-King and Webb 2007). Additionally, decimeter thick, up to several meters wide siltstone to very fine-grained sandstone bodies with erosional lower bounding surfaces that contain coarser grained sandstone lenses and beds are observed in places, and load into underlying finer-grained deposits. These suggest separate flood channels (Fig. 7.5a–c). Overall, the dominance of planar beds, scours and mud layers, as well as the occurrence of possibly reworked pedogenic deposits and the association FA1 with deltaic deposits (FA5) and microbial carbonates (FA6) suggest deposits formed in a dryland river system, in floodplain or as overbank deposits in the vicinity of the lake (Wakelin-King and Webb 2007; Wright and Marriott 2007).

7.4.2 Littoral and Sublittoral Facies Associations

7.4.2.1 Facies Association 2: Shoreline Mudstones

Facies Association 2 (FA2) occurs within the lake margin (Fig. 7.4) and in places, can be traced laterally hundreds of meters along the outcrop (Fig. 7.5e). FA2 consists of homogeneous (F2) or laminated (F3) mudstone and siltstones in association with microbial carbonate (F12) and intraclastic mudstone (F15) (Table 7.1).

7.4.2.2 Facies Association 3: Shoreline Sandstones

Facies Association 3 (FA3) occurs at the margins of the lake, dominantly in the eastern and northern parts of the basin, in association with delta (FA5) deposits and littoral to sublittoral sandstones (FA7) (Figs. 7.3, 7.4 and 7.6, Section 1). This FA consists of gradationally based or sharp based fine-grained to medium-grained quartz sandstones with wave rippled cross-lamination (F4), climbing ripple cross-lamination (F6), low-angle cross-stratification (F8), and hummocky and swaley cross-bedding (F9), or sharp based fine-grained to coarse-grained amalgamated, normally graded or ungraded (F10) sandstones and sub-horizontal or parallel-laminated gravel beds (F11) (Fig. 7.6a and Section 1; Table 7.1). Medium to coarse-grained sandstones with gravel beds, occurrence of graded bedding, amalgamation, and hummocky and swaley cross-stratification suggests storm wave activity and deposition in the lake shore area (Renaut and Owen 1991; Bray and Carter 1992; Ilgara and Nemec 2005). These deposits are interpreted to have formed due to longshore transport in a shoreline setting (Fig. 7.4). Alternatively, they could have been formed as wave reworked deposits in wave-dominated delta deposits (see Fig. 7.6, Section 1). However, deposits brought in by river discharge and reworked into shoreface deposits makes the distinction between delta and shore deposits difficult (see also Bhattacharya and Giosan 2003; Smith et al. 2005) (see Figs. 7.4 and 7.6, Section 1).

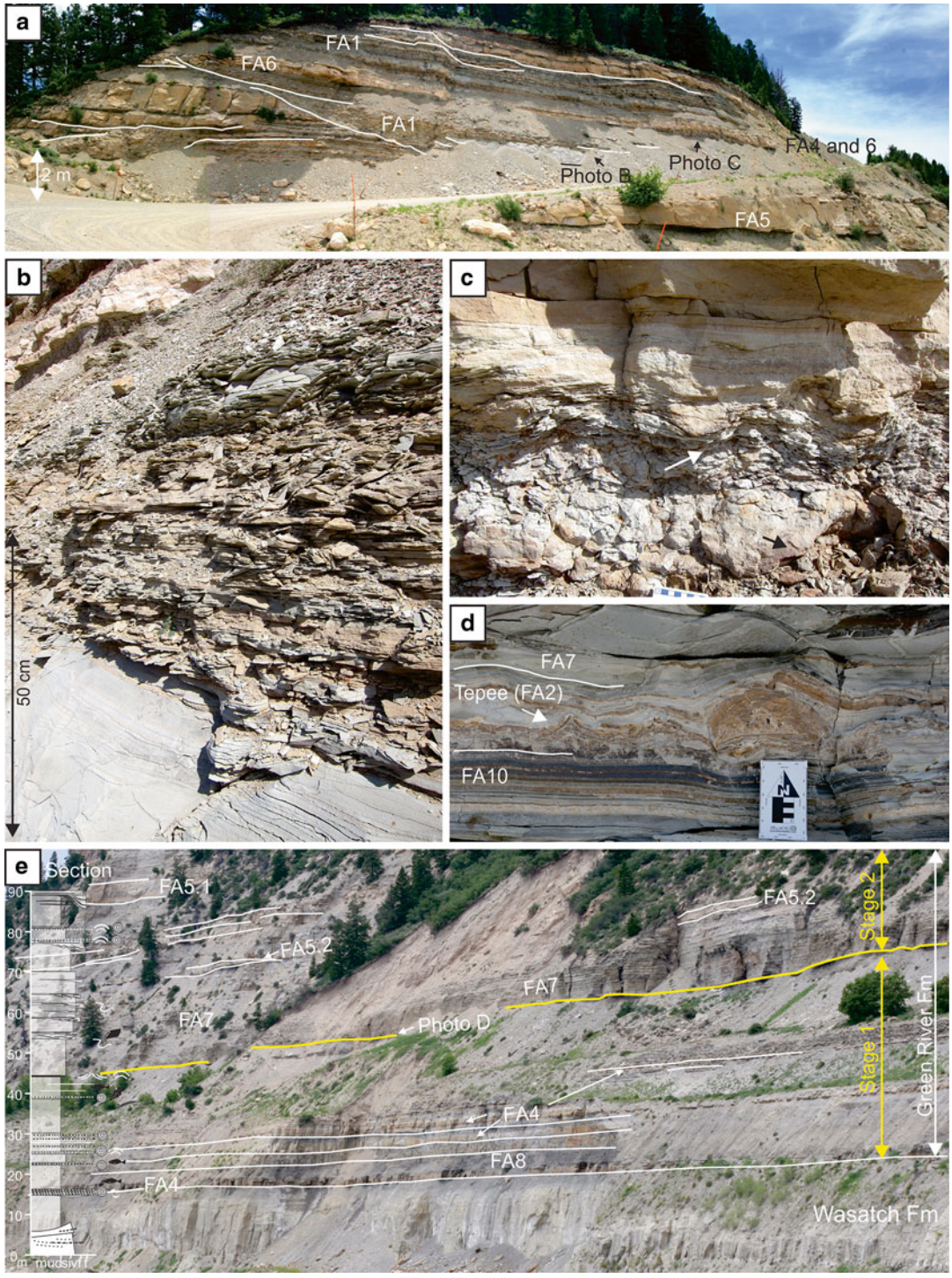
a
FA1
FA6
FA1
2 m
Photo B
Photo C
FA4 and 6
FA5
b
50 cm
c
d
FA7
Tepee (FA2)
FA10
e
Section
FA5.1
FA5.2
FA7
Photo D
FA4
FA8
FA4
FA5.2
FA7
Stage 2
Stage 1
Green River Fm
Wasatch Fm
m mudstone

7.4.2.3 Facies Association 4: Carbonate Shoals

Facies Association 4 (FA4) occurs in the marginal areas, dominantly in the western and southern parts of the basin, is laterally equivalent to shoreline sandstones (FA3), and occurs in association with microbial carbonates (FA6), littoral and sublittoral mudstones (FA8), and littoral to sublittoral oil shales (FA9) (Figs. 7.3, 7.4, 7.5e, and 7.6b). This FA is composed of sharply based, massive or plane-parallel, non-skeletal coated carbonate grainstones and packstones (F13), and coquina (F14) beds of moderately to very well sorted oolites, with ostracode or quartz grain cores, pisoids and peloids, and siliciclastic to microbial carbonate rip-up intraclasts (Figs. 7.5e and 7.6b; Table 7.1) (Sarg et al. 2013). This indicates the deposition in high-energy carbonate shoals parallel to the lakeshore (Milroy and Wright 2002; McGlue et al. 2010). Alternately, deposits of FA4 could indicate shallow littoral deposits (Milroy and Wright 2002), or they could have been redistributed by wind activity and shoreline currents into deeper, lower energy sublittoral environments (Milroy and Wright 2002; McGlue et al. 2010) (see Fig. 7.4). In places, carbonate grainstones display reverse grading where the coarser grained oolites or pisolites occur in the upper portion of the bed, suggesting episodic reworking in variable energy environment.

7.4.2.4 Facies Association 5: Delta Deposits

Facies Association 5 (FA5) occurs across the basin margins and it consists of depositional packages, where sandstone and mudstone deposits are separated by littoral to sublittoral mudstone to sandstone deposits of FA7 and 8 (Figs. 7.3, 7.4, and 7.6c, d). In a few places, mudstones from FA2 separate sandstone units. Three types of depositional packages are classified here. Type 1 (FA5.1) is formed from laterally continuous sandstone bodies that are separated by laminated mudstone and siltstone (F3) beds, a few centimeters to tens of centimetrers thick. No desiccation cracks or root structures have been found in these interfingered mudstone or siltstone deposits. Two types of depositional units occur within Type 1 sandstone package. The first type of depositional unit is characterized dominantly by sharp-based very fine-grained to fine-grained sandstones that coarsen upward or have no particular grain-size trend and consists of climbing ripple cross-lamination (F6), plane parallel (F7), and low angle cross-stratification (F8) (Fig. 7.6c). Locally, current ripple cross-lamination (F5), structureless (F10), or wave-modified deposits occur. Intraformational clasts (F11) of mudstone or siltstone, plant remains and fish remains occur on the erosional lower bounding surfaces (Fig. 7.6e, f). The second type of depositional unit is characterized by gradationally based upward-coarsening deposits that are composed of wave ripple cross-laminated (F4) and low angle cross-stratified (F8), very fine-grained to fine-grained sandstone deposits (Fig. 7.6d) and are associated with coarser-grained sandstones of shoreline mudstones (FA3).

These laterally extensive depositional units are interpreted as mouth bar deposits, where dominantly sharp-based deposits that consist of climbing ripple and plane-parallel sandstones are interpreted as river-dominated delta-front deposits (Fig. 7.6c). Gradationally based

Fig. 7.5 Representative photographs of the lake margin deposits. (**a**) Highly fluctuating cycles of marginal lake deposits that display close relationship between alluvial plane-bedded dry river deposits (*FA1*) and are interbedded with carbonate shoal (*FA4*), microbial carbonates (*FA6*), and delta deposits (*FA5*). (**b**) Planar-bedded overbank or floodplain deposits with silty and sandy sheet flow deposits (*FA1*). (**c**) Mottled, inclined mudstone with organic rip ups (*black arrow*), formed as plaeosol or as reworked pedogenic mud aggregates (*FA1*) overlain by sandstones with load structures (*white arrow*). (**d**) Tepee structures (FA2) followed by microbial carbonates (*FA6*), the base of the tepee structures marks SB4, and boundary between Stage 1 and 2. The stratigraphic position of the bed is shown on Fig. 7.5e. (**e**) Mixed siliciclastic and carbonate facies associations formed in the western part of the basin that characterize deposits formed in the lower Green River Formation, Stage 1 and 2. Note the alternation between carbonate shoal (FA4) and sublittoral to profundal oil shale (*FA9* and *FA10*) deposits in Stage 1, and the high siliciclastic input in the beginning of Stage 2

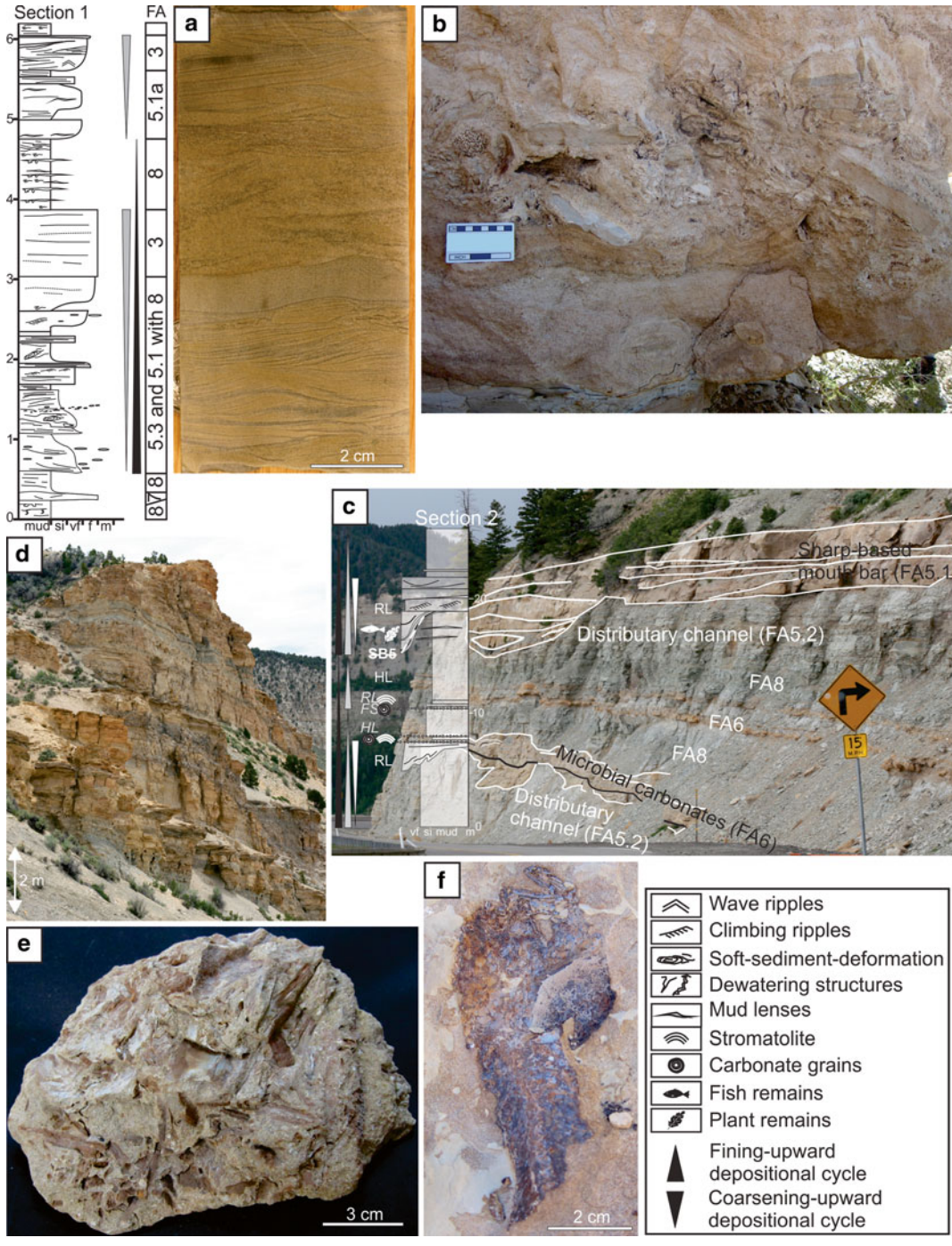

Fig. 7.6 Representative photographs of the lake margin deposits. Section 1 marks wave-dominated deposits and relationship between FA3 and FA5. (**a**) Bundled upbuilding wave ripple cross-laminated shoreline deposits (FA3). (**b**) Storm-generated intraclastic carbonate shoal (FA4) with rip-up microbial carbonates, oncolites, oolites, and siliciclastic mudstone clasts. (**c**) Lake margin deposits that form upward-fining depositional cycles from distributary channels (5.2) and bars (5.1) upwards into microbial carbonates (FA6) that are covered by littoral to sublittoral siltstones (FA8). (**d**) Wave-dominated delta (FA5) to shoreline (FA3) deposits. (**e**) Organic rip-up clasts, wood pieces on the lower bounding surface of the mouth bar. (**f**) Fish fossil found on the lower portion of the mouth bar deposits

deposits, with wave-dominated structures in association with FA3 are interpreted as wave-dominated delta-front deposits (Renaut and Tiercelin 1994; Buatois and Mangano 1995; Schomacker et al. 2010) (Figs. 7.3, 7.4, and 7.6d). Likewise, some wave ripple dominated deposits could indicate wave-reworked shoreline sandstones formed in the wave-dominated delta setting (see also FA3 and Fig. 7.4) (Bhattacharya and Giosan 2003; Smith et al. 2005).

The second type of depositional package, Type 2 (FA5.2), is composed of laterally discontinuous sandstones of low angle and trough cross-stratified (F8), plane-parallel (F7) and climbing ripple (F6) cross-laminated deposits with concave-up basal scour and near horizontal upper surfaces. In places, heterolithic successions of parallel-laminated (F3) mudstones and siltstones and interbedded sandstones fill the scours (Fig. 7.6c; Table 7.1). Locally, the basal surface is undulating and contains large-scale soft-sediment deformation, comprised of small-scale (centimeters in size) and large-scale (decimeters and meters in size) slump and load structures (Fig. 7.6c). These erosionally based structures with no subaerial features suggesting channel deposits that formed in a delta front area as distributary channels to mouth bars (Olariu and Bhattacharya 2006; Schomacker et al. 2010). Sandstone-dominated channel fills are interpreted to have formed in the proximal delta front area. Heterogeneous channels fills, as well as channels with undulating scour boundaries, and load deposits are interpreted to have accumulated in a more distal position of the delta front.

Type 3 depositional packages in this facies association (FA5.3) are composed of very fine to fine-grained cross-stratified (F8) and climbing (F6) to current (F5) ripple cross-laminated sandstones, or medium to coarse-grained structureless sandstones (F10) that pass upwards into parallel-laminated (F3) mudstones and siltstones (Fig. 7.6, Section 1; Table 7.1). The sandstone to mudstone stacked depositional units in Type 3 (FA5.3) are interpreted as turbidites formed dominantly during hyperpycnal density flows in the distal part of the delta front (see also Renaut and Tiercelin 1994) (Fig. 7.4). This is also supported by the aggradational pattern of depositional packages and the vertical relationship with Type 1 (FA5.1) mouth bar deposits (Fig. 7.6, Section 1).

7.4.2.5 Facies Association 6: Microbial Carbonates

Facies Association 6 (FA6) consists of millimeter to centimeter-scale, thinly laminated limestones interbedded with boundstones displaying small vertically oriented shrub-like features, and massive limestones displaying clotted fabric (Fig. 7.7a) that are interpreted as microbial carbonate deposits: stromatolites and thrombolites formed in the marginal areas of the lake (Rainey and Jones 2009; Gierlowski-Kordesch 2010; Wright 2012) (see Figs. 7.3 and 7.4). Laminated carbonates (F12) occur as laterally continuous, millimeter to centimeter-thick horizontal carbonate layers, and as beds and laterally linked or discontinuous columns, tens of centimeters to 1 m thick, with well-developed domal heads (Fig. 7.7a, b). Different desiccation features such as mudcracks or large-scale sheet cracks have not been observed. The lack of desiccation features suggests that these carbonates formed dominantly in a subaqueous setting in the lake, in the littoral and sublittoral zones (see also Cohen et al. 1997). Intraclastic carbonate and nonskeletal lime packstones/grainstones (F13) containing oolites and pisolites occur as thin layers or beds and in pockets between microbialite mounds.

These mixed microbialite and nonskeletal deposits probably formed in the shallower, higher energy littoral zone to upper sublittoral zone, whereas laterally continuous laminated deposits with less distinctly developed domal heads are interpreted to have been deposited in the deeper, sublittoral zone (Platt and Wright 1991; Cohen et al. 1997; Renaut and Gierlowski-Kordesch 2010; Sarg et al. 2013) (see Fig. 7.7a, b). Thin, millimetre-thick laminated carbonates in association with sublittoral to profundal oil shales, FA9 and 10 (see Fig. 7.7b) are interpreted to be microbialites formed in the deepest, sublittoral zone.

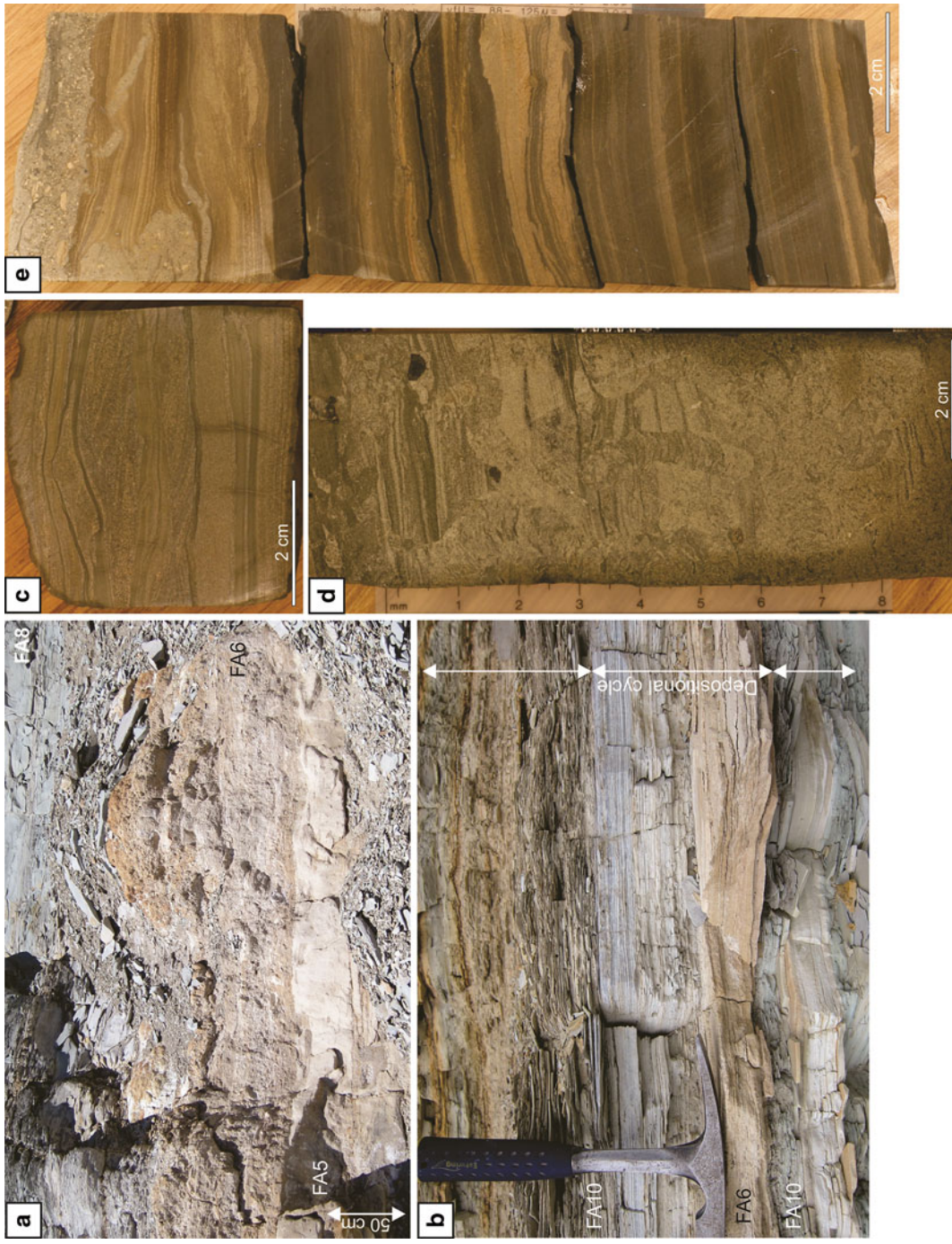

Fig. 7.7 Representative photographs of the littoral to sublittoral lake deposits. (**a**) Microbial carbonates (FA6) that lay sharply on delta sandstones (FA5). Lower portion of the carbonate unit consist of brecciated carbonate beds that are stabilized by stromatolites and continue upwards into thrombolites. Microbial carbonates are overlain by littoral to sublittoral siltstones (FA8). (**b**) Deeper microbial carbonates (FA6) formed in the lower sublittoral or in the most upper portion of profundal part of lake, interbedded with profundal, organic-rich, laminated oil shale (FA10) deposits. (**c**) Mud draped thin sand layers and bidirectional wave ripples in the littoral and sublittoral sandstones (FA7). (**d**) Possible burrows in the littoral to sublittoral sandstones (FA7). (**e**) Sublittoral oil shale (FA9) with thin siltstone and sandstone layers

7.4.2.6 Facies Association 7: Littoral to Sublittoral Sandstones

Facies Association 7 (FA7) consists of very fine- to fine-grained plane-parallel (F7), thinly bedded sandstones. In places, wave ripple cross-lamination (F4), wave-modified deposits, or less commonly, current ripple cross-lamination (F5) occur (Fig. 7.7c; Table 7.1). This facies association is interpreted to have been deposited basinward from delta (FA5) sandstones and forms in places in the prodelta part of the deltaic deposits (FA5) (see Figs. 7.3, 7.4 and 7.5e, Section). However, FA7 also occurs basinward from shoreline sandstones (FA3) (Figs. 7.3 and 7.4), and is therefore recognized as a separate facies association and is interpreted to have formed in the distal part of areas subject to higher siliciclastic input, filling interdistributary areas. Soft-sediment-deformation features, such as small-scale (centimeter-thick) load casts, slumps, ball and pillow structures, and large-scale (meter-thick) slump structures are abundant. Abundant soft-sediment deformations indicate post-depositional processes like rapid deposition or loading by landslides or waves (Sabato 2007; Bridge and Demicco 2008). Vertical to sub-vertical, lenticular, deformed cracks, a few millimeters to centimeters in length and filled with sand size deposits occur in mudstones and siltstones below the sandstones. These features are connected with the overlying sand and in places show lateral and vertical linkage with other sand intervals, and are therefore interpreted as interstratal dewatering structures, formed due to the compaction of mudstones layers during burial (Tanner 1998). In places, cm-scale vertical features cross-cut deposits that suggest bioturbation (Fig. 7.7d).

7.4.2.7 Facies Association 8: Littoral to Sublittoral Mudstones to Siltstones

Facies Association 8 (FA8) consists of interfingering parallel-laminated (F3) or massive (F2) mudstones to siltstones with up to fine-grained wave ripple cross-laminated (F4) or less commonly, current ripple cross-laminated (F5) sandstone lenses, lamina, and beds several centimeters thick (Figs. 7.6c and 7.7a, e; Table 7.1). Interfingering of mudstones with ripple cross-laminated sandstones indicates deposition above storm wave base. These dominantly fine-grained sediments are interpreted to be deposited in the areas with limited siliciclastic input (Figs. 7.3 and 7.4), in lower littoral to sublittoral zones (Smith et al. 2005; Keighley 2008). Small-scale soft-sediment deformation features (centimeter-thick), such as load casts, slumps, ball and pillow structures occur in these deposits and indicate post-depositional processes suggesting rapid deposition or loading by landslides or waves (Sabato 2007; Bridge and Demicco 2008). Horizontally oriented triangular features that resemble cracks, a few millimeters to centimeters in length, and filled with sand size deposits occur in mudstones and siltstones. These features are interpreted here as syneresis cracks as they are not connected vertically with any other bed or layer and have been interpreted to be formed due to the swelling or shrinking of clays caused by the salinity changes (Plummer and Gostin 1981).

7.4.2.8 Facies Association 9: Littoral to Sublittoral Oil Shale

Facies Association 9 (FA9) consists dominantly of laminated silt-rich oil shale (F18) and undulating, wavy-structured oil shale (F19) deposits that indicate a low-energy environment (Table 7.1). In the lower part of the Green River Formation these deposits are illite-rich (F17). Oil shale deposits interfinger with thin, millimeter to centimeter-thick, structureless, normally graded or wave ripple cross-laminated (F4) and current ripple cross-laminated (F5) very fine- to fine-grained sandstone layers and lenses (Fig. 7.7e). An association of mudstones with siltstones and sandstones suggest deposition in the nearshore lower littoral to sublittoral zones, above storm wave base (Renaut and Tiercelin 1994; Smith et al. 2005), in the distal portions of carbonate shoals (FA4), microbial carbonates (FA6), and littoral to sublittoral mudstones (FA8) (Figs. 7.3 and 7.4).

7.4.3 Profundal Facies Associations

7.4.3.1 Facies Association 10: Laminated Oil Shale

Facies Association 10 (FA10) occurs as laterally relatively continuous units across the lake basin

and is composed of rhythmically millimeter laminated, light brown to dark brown, black or gray kerogen-rich (dark) and kerogen-poor (light) mudstone i.e., oil shale couplets (F16) (Fig. 7.8a). The top and the base of each lamina are generally distinct and sharp. In the lower part of the Green River Formation, oil shale is illite-rich (F17) and in the middle and upper part of the formation it is carbonate-rich (F16). Dominantly mud-sized deposits suggest deposition below the storm wave base in a profundal environment. The dark to light lamina may be related to short-term variation in sediment supply, periodic algal blooms, or individual floods (Renaut and Gierlowski-Kordesch 2010; Ghadeer and Macquaker 2012). Undulating, wavy, disrupted oil shale (F19) and in places, millimeter-thick siltstone to very fine-grained sandstone lamina and lenses occur in deposits suggesting deposition due to current and mass flows caused by storms or sediment gravity flows (Schieber 2011; Ghadeer and Macquaker 2012) (Fig. 7.8a). In places, bedding is sharply constricted giving a morphology resembling loops or links of a chain, i.e., loop bedding (Fig. 7.8a). Nahcolite crystals and nodules (F22) of variable size, from a few centimeters to tens of centimetrers in diameter, occur within this facies association (Fig. 7.8b). Pyrite occurs as small crystals within the deposits or as rinds around the nahcolite nodules. No trace fossils were found. Relatively continuous units, finely laminated with some disturbed sedimentary features, occurrence of pyrite, and lack of trace fossils indicate deposition in meromictic conditions in a deep-lake environment (Demaison and Moore 1980; Kelts 1988; Johnson and Graham 2004; Scholz et al. 2011) (Figs. 7.3 and 7.4).

7.4.3.2 Facies Association 11: Gravitational Oil Shale

Facies Association 11 (FA11) occurs as laterally discontinuous units of contorted, soft-sediment-deformed, kerogen-rich or kerogen-poor deposits in which the original texture and stratification have been obliterated (Fig. 7.8c–f). Deposits of FA11 occur as stacked packages or single beds from centimeter to several meters in thickness in association with laminated oil shales (FA10), siliciclastic turbidites (FA12), and subaqueous evaporites (FA13) (Figs. 7.3 and 7.4). The thickness and frequency of FA11 decrease towards the lake margins (Fig. 7.3, compare 23X-2 and Fig. Four 31-1). No desiccation cracks, bioturbation, ripple cross-lamination or algal structures have been observed from these deposits. Deposits of FA11 are divided into two types, based on texture and structure. Type 1 (FA11.1) is composed of soft-sediment folds, overturned strata (F20), and disrupted (F19) deposits (Fig. 7.8d; Table 7.1) that formed as slide and slump deposits that were transported for a short distance. The scale of deformed deposits varies greatly from millimeters to metres.

Type 2 (FA11.2) consists of blebby appearing and matrix-supported oil shale deposits containing angular, sub-angular, and sub-rounded clasts ripped up from the surrounding environment (F21), including carbonate clast, siliciclastic clasts, organic rip-ups and evaporite clasts (Fig. 7.8c, f; Table 7.1). The amount and occurrence of clasts in these deposits is variable and they form normally graded beds or are randomly distributed. The upper and lower bounding surfaces can be sharp, erosional or gradational. In places, nahcolite nodules (F22) have formed in deposits. Thick units of FA11.2 are interpreted as amalgamated slump and debris-flow deposits formed due to higher energy turbulent currents (Shanmugam 2000; Arnott 2010) (Figs. 7.3 and 7.4).

The occurrence of contorted, soft-sediment-deformed, and blebby deposits in association with finely laminated deposits of FA10, and the lack of shallow water indicators suggests that deposits of FA11 formed as gravitational deposits in the profundal areas (see also Dyni and Hawkins 1981; Gierlowski-Kordesch and Rust 1994; Keighley 2008) (Figs. 7.3 and 7.4).

7.4.3.3 Facies Association 12: Siliciclastic Turbidites

Facies Association 12 (FA12) consists dominantly of well to very well sorted siltstones to sandstones that form sharp-based centimeter to a few meters thick normally graded or ungraded depositional cycles separated by laminated and

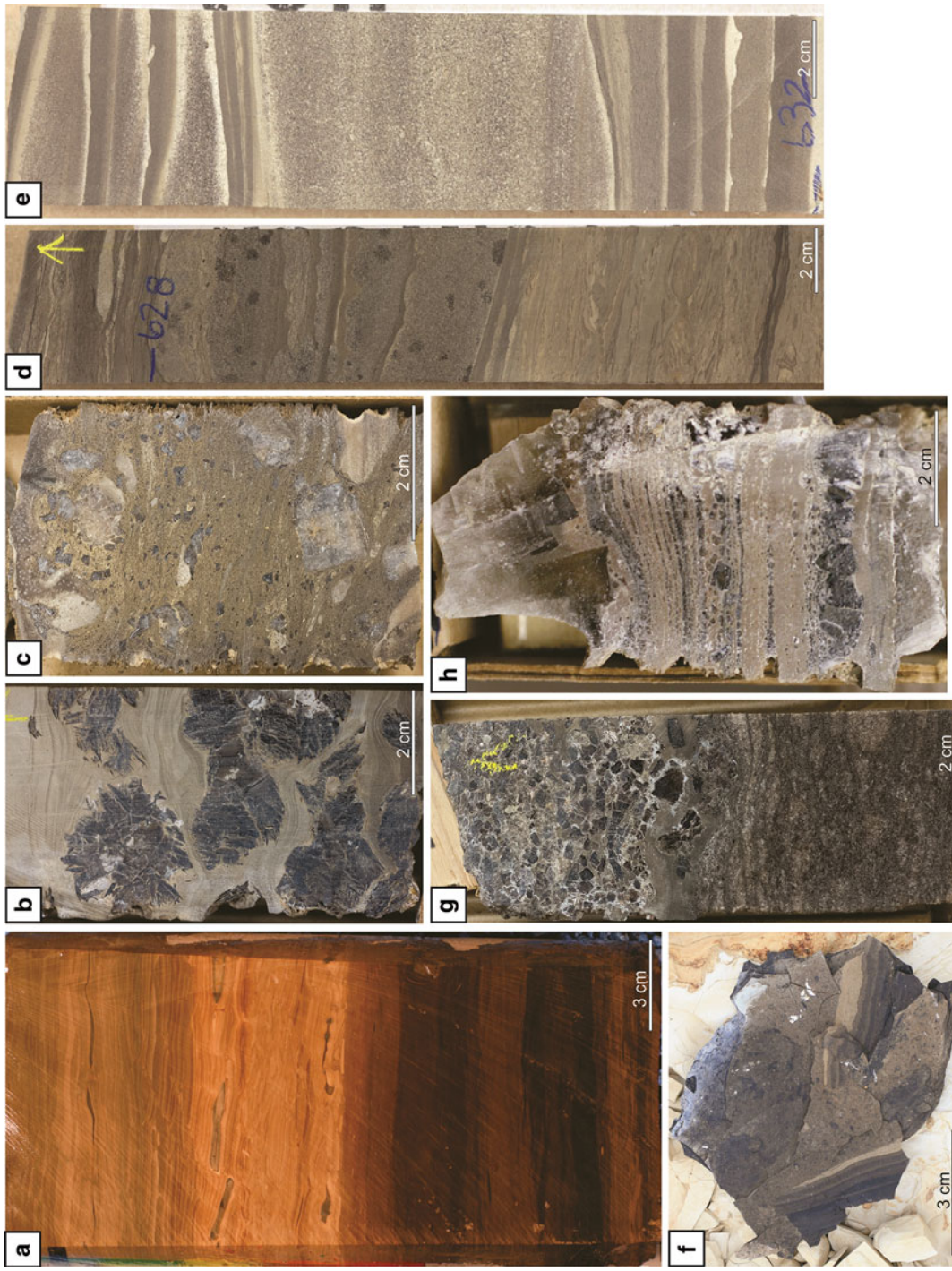

Fig. 7.8 Representative photographs of the profundal lake deposits. (**a**) Disrupted oil shale (FA10). Sharp difference in color marks the difference in organic-richness of deposits, the lower darker portion is richer and the upper portion of the core interval is leaner. (**b**) Laminated oil shale (FA10) with nahcolite nodules. Note the deformation features greater by the nodule growth. (**c**) Oil shale breccia (FA11.2) with evaporite rip-ups. (**d**) Soft-sediment-deformed oil shale (FA11.1) overlied by siliciclastic turbidites (**e**) Upward-fining medium-grained sandstone to mudstone siliciclastic turbidite (FA12) units. (**f**) Bedding-plane view of oil shale breccia (FA11.2), with organic clasts. (**g**) Nahcolite mush and crystal growth (FA13.1). (**h**) Halite bottom growth (FA13.2) and halite to nahcolite laminites (FA13)

soft-sediment deformed mudstones of FA10 and FA11.1, respectively (Fig. 7.8d, e). Load and flame structures occur on bedding planes that suggest rapid depositional rates (Fig. 7.8d). Normally graded depositional units start with coarse to fine-grained structureless (F10) sandstones and grade upwards into parallel-laminated fine to very fine-grained sandstones (F7) or parallel-laminated siltstones (F3) (Fig. 7.8e). Angular to subangular rip-up clasts, as oil shale rip-ups and plant fragments are common, and occur distributed within the sandstone bed or follow bedding planes (Fig. 7.8d). Deposits form stacked packages where the thickness of sandstone to siltstone units decreases upwards and continue into fine-grained sandstones with oil shale rip-ups (Fig. 7.8d). In places, vertical, deformed features, filled with sandstones and connected with overlying sandstones, i.e., water escape structures, occur in the underlying facies associations. These sedimentary structures indicate sediment-gravity flows, principally turbidity currents probably triggered by high intensity storms or river floods (Buatois and Mangano 1995; Johnson and Graham 2004; Osleger et al. 2009) (Figs. 7.3 and 7.4), where upward-fining depositional units are interpreted to indicate Bouma division (after Bouma 1962): structureless, normally graded or ungraded sandstones equate to the Ta, planar-laminated sandstones to the Tb, and planar-laminated siltstones to the Td division (Fig. 7.8e). The association of FA12 with FA10 and FA11.1 suggest deposition in the deep-water, profundal area (see Figs. 7.3 and 7.4).

7.4.3.4 Facies Association 13: Subaqueous Evaporites

Facies Association 13 (FA13) is composed of a few to tens of centimeters thick beds and scattered crystals of nahcolite (F22), halite (F23), and dawsonite (F24) (Fig. 7.8g, h) that occur in association with laminated and gravitational oil shales of FA10 and 11 (Figs. 7.3 and 7.4; Table 7.1). No dissolution surfaces have been found within these deposits. Because dawsonite occurs only as minute crystals, disseminated throughout the oil shale and can be digenetic in origin (Boak and Sheven 2015), it's visual detection usually is difficult or impossible, it is not described future in this work (for additional information see Smith and Milton 1966; Brownfield et al. 2010). Deposits of this facies association are divided into two types. Type 1 (FA13.1) consists dominantly of nahcolite (F22) that occurs as tan to light brown closely to loosely packed crystal accumulations and dark-brown to black fine-grained nodules and radiating nodular aggregates, occasionally rimmed with pyrite (Fig. 7.8b, g, h). Nahcolite crystal accumulations form in many places, upward-fining beds, where the frequency and amount of crystals decrease upwards, and in the upper part, deposits transition gradually into laminated oil shales (FA10). Nahcolite nodules are a few to tens of centimeters in diameter, and appear scattered throughout the deposits or in parallel-bedded zones in association with FA10 and FA11 (Fig. 7.8b). In places, they are rimmed with pyrite. Type 2, (FA13.2) halite (F23) is present as clear to gray crystal cubes, hopper crystals, intra-sediment crystals, and bottom growths within nahcolite deposits and carbonate muds (Fig. 7.8h). Commonly, halite forms couplets with nahcolite, with thicknesses that range from a few millimeters to centimeters (Fig. 7.8h).

FA13 is interpreted to have formed in water saturated with bicarbonate, and periodically with sodium chloride. Laminated, coupled deposits suggest cyclic and perhaps seasonal precipitation. Because depositional rates can be very rapid, there is no evident correlation between crystal size and water depth (Cohen 2003). The occurrence of halite and nahcolite crystals, beds, couplets, bottom growths, and the lack of dissolution features in evaporites and desiccation features in over and underlying deposits of FA10 and FA11, suggest evaporite growth in a standing body of water, in a meromictic lake (Hardie et al. 1978; Last and Vance 1997; Schubel and Lowenstein 1997; LaClair and Lowenstein 2009) (see Fig. 7.3).

7.5 Stratigraphic Architecture

7.5.1 Basin Evolution and Lake Stages

The Green River paleo-lake underwent a long-term evolution that can be described in a series of lake stage units that are tens to hundreds of meters thick (Tänavsuu-Milkeviciene and Sarg 2012). This long-term evolution over a period of about 6 My occurred in response to tectonic and climate changes during early to middle Eocene time. Lake stage depositional packages that characterize lake evolution reflect variation in facies association distribution, richness of oil shale, water chemistry, degrees of lake restriction and salinity, and siliciclastic sediment input (Tänavsuu-Milkeviciene and Sarg 2012) (Table 7.2). Six lake stages have been separated, based on large-scale changes in sedimentological patterns and depositional trends (Table 7.2). Stages do not follow lithological units, i.e., members of the Green River Formation. Broadly, lake stages characterize genetically related units that occur at a particular period during the lake evolution. Lake stages are composed of groups of sequences, but they do not form larger sequences or sequence sets (Figs. 7.3 and 7.10). Boundaries of lake stages are marked by erosional and correlative surfaces, and are characterized by gamma ray marker peaks and long-term changes in Fischer assay logs i.e., oil shale richness (Fig. 7.3, Stage boundaries).

The evolution and progression of lake stages in the Piceance basin are consistent with the global Eocene climate trend. Additionally, lake stages also record a deepening-upward trend followed by a late siliciclastic fill that reflect larger-scale changes in the basin caused by tectonics and climate (Fig. 7.9; Table 7.2). Lake stages represent the main Green River Formation lake interval in the Piceance basin. However, the exact timing and the length of each lake stage is not well established because of incomplete age control. There are only three tuff beds that have been dated and correlated into the Piceance basin (after Smith et al. 2008, 2010) (Fig. 7.9). To estimate the chronology of the Green River Formation study interval and the position of lake stages, rich and lean zones, sequence boundaries, available age dates and stratigraphic studies done by Smith et al. (2008, 2010) and Davis et al. (2009) were used (see Fig. 7.9).

The initial Stage 1 (Fresh to mesosaline lake) marks the beginning of a large, single lake basin, formed before the Eocene climate optimum, and characterized by fresh to mesosaline (i.e., higher salinity, but below the level for precipitation of dawsonite, nahcolite, or gypsum) water conditions. This stage includes from the molluscan-rich Long Point Bed at the base of the Green River up through the organic-rich illite shale of the R1 zone (Figs. 7.3 and 7.9). The beginning of Stage 2 (Transitional lake) marks the beginning of important mineralogical and depositional changes in the lake and occurred during the beginning of the Eocene climate optimum. The deposition along the basin margin is characterized by relatively high siliciclastic input and formation of the first thick microbial carbonate deposits. Basinward, the clay-rich oil shale was replaced by the carbonate-rich oil shale and the first evaporite deposition occurred (dawsonite followed by nahcolite). Stage 2 encompasses the L1 through L3 interval of the Green River (Figs. 7.3 and 7.9). The R2 and R3 rich zones are on average less rich then the underlying fresh-lake R1 or the overlying R4 zone (see Fig. 7.3 and Feng 2011). Lake stages 1 and 2 fall under the balanced fill lake of Bohacs et al. (2000). Following Stage 3 (Highly fluctuating lake) represents an underfilled lake (Bohacs et al. 2000) and formed during the peak of the Eocene climate optimum. It is characterized by thick evaporite intervals and highly fluctuating cycles from shallow to deeper lake environments, indicating rapid fluctuation between dry and wet times during the hot house of the optimum. This stage includes from the R4 through the L5 zones (Figs. 7.3 and 7.9). Both the R4 and R5 can be very rich, although they are generally diluted by increased nahcolite precipitation within these intervals (Feng 2011). The following stage, Stage

Table 7.2 Overview and short descriptions of lake stages (S) in the Piceance basin

Lake stage	Description
S1	Beginning of stage marks lake-wide transgression and beginning of large lake system. Laterally continuous, progradational to aggradational depositional units dominate. Along the margins carbonate shoals (FA4) and channelized delta (FA5) deposits formed. In the deeper basin area Type 2 depositional units and clay-rich oil shale (FA10 and FA11) deposits formed. Deposits are rich in fish remains and ostracods, especially in the earlier part of the stage. Organic-rich deposits resulted in high runoff and high nutrient input (R0 and R1). The richest deposits formed in the upper part of the stage (R1)
S2	Beginning of stage marks rapid increase in siliciclastic input at the marginal areas, dominance of laterally discontinuous progradational to aggradational highly cyclic deposits, changes in mineralogy, and first appearance of thick microbial carbonates (FA6). Thick sandstone units (FAs3, 5, and 7) capped with thick carbonate shoals (FA4) and microbial carbonates (FA6) formed along the basin margins. In the deeper lake areas, clay-rich oil shales where replaced with carbonate-rich oil shales (FA10 and FA11) and evaporite (FA13) deposition increased upwards within stage. In the deepest part of the basin, Type 3 depositional units formed that changed to Type 2 depositional units towards margins. Richest organic-rich deposits formed as oil shale breccias (FA11.2) in the deepest portion of the lake. Richest deposits formed during the beginning of the stage (R2), whereas increased lake restriction and salinity lead to higher dilution of organics upwards (during R3)
S3	Deposition of aggradational to retrogradational highly cyclic, laterally discontinuous depositional units. Thick sandstone units (FAs3, 5, and 7) capped with thick microbial carbonates (FA6) formed along the basin margins. Clastic input and deposits into the marginal areas decreased upwards within stage. In the profundal area, Type 3 depositional units, with thick evaporite (FA13) deposits dominate. The richest oil shale deposits occur dominantly as discontinuous oil shale breccia (FA11.2) deposits that form very thick stacked depositional packages in the deeper part of the basin and thin towards the basin margins. Especially thick and very rich oil shale breccia deposits formed during the first part of the stage (R4). In the upper part, extensive evaporite deposition led to the higher dilution of organic material and to somewhat leaner deposits
S4	Lateral increase of profundal FAs (FAs10 to 12) and laterally continuous depositional units. Previous marginal deposits (FAs1 to 8) were covered by the profundal deposits (FAs10 to 12). Increase in fluvial input caused decrease in salinity and evaporites and increase in nutrient supply. Type 2 depositional units dominate in the profundal part
S5	High runoff resulted in high lake level. Profundal, laterally continuous FAs dominate (FAs10 to 12), with Type 2 depositional units occur over most of the deep basin area. Some evaporite deposition (early diagenetic nahcolite nodules, FA13.1) occurred in the southern and western parts of the basin. Rich oil shales formed as laminated oil shales (FA10) and as oil shale breccias (FA11.2)
S6	Progradation of siliciclastics from north to south, and closing of the basin. Evaporites, as nahcolite nodules and in places crystals (FA13.1), occur in deposits in the southern part of the basin. Laminated oil shale (FA10) and soft-sediment-deformed oil shale (FA11.1) deposits interfinger with Uinta Formation sandstones. Some rich oil shale occurs in the southern part of the lake

4 (Rising lake) includes the R6 rich zone and formed after the Eocene climate optimum. It is characterize by the increasingly deeper profundal oil shale deposits, indicating an overall increase in runoff and lake level rise (Figs. 7.3 and 7.9). Stage 5 (High lake) marks the time period of the high lake level, when profundal, rich oil shale deposits of the Mahogany zone (R7) can be correlated over much of the basin area (Figs. 7.3 and 7.9). Lake stages 4 and 5 would be classified as balanced fill lakes (Bohacs et al. 2000). Stage 6 (Closing lake) marks the beginning of the closing of the lake and is an overfilled lake (Bohacs et al. 2000). Siliciclastic deposits from the north prograded southwards and finally filled in the Piceance lake basin (Figs. 7.3 and 7.9). The final fill with

Fig. 7.9 (continued) hypothermals. Lake stages after Tänavsuu-Milkeviciene and Sarg (2012), age data and related correlation after Smith et al. (2008, 2010), rich and lean zones after Cashion and Donnell (1972, 1974), Mercier et al. (2009), Johnson et al. (2010), geomagnetic polarity timescale, Eocene boundaries, negative carbon isotope excursions, and hyperthermals after Zachos et al. (2001, 2008, 2010), Sexton et al. (2006, 2011), Dutton et al. (2005), Lourens et al. (2005), Nicolo et al. (2007), Bijl et al. (2009)

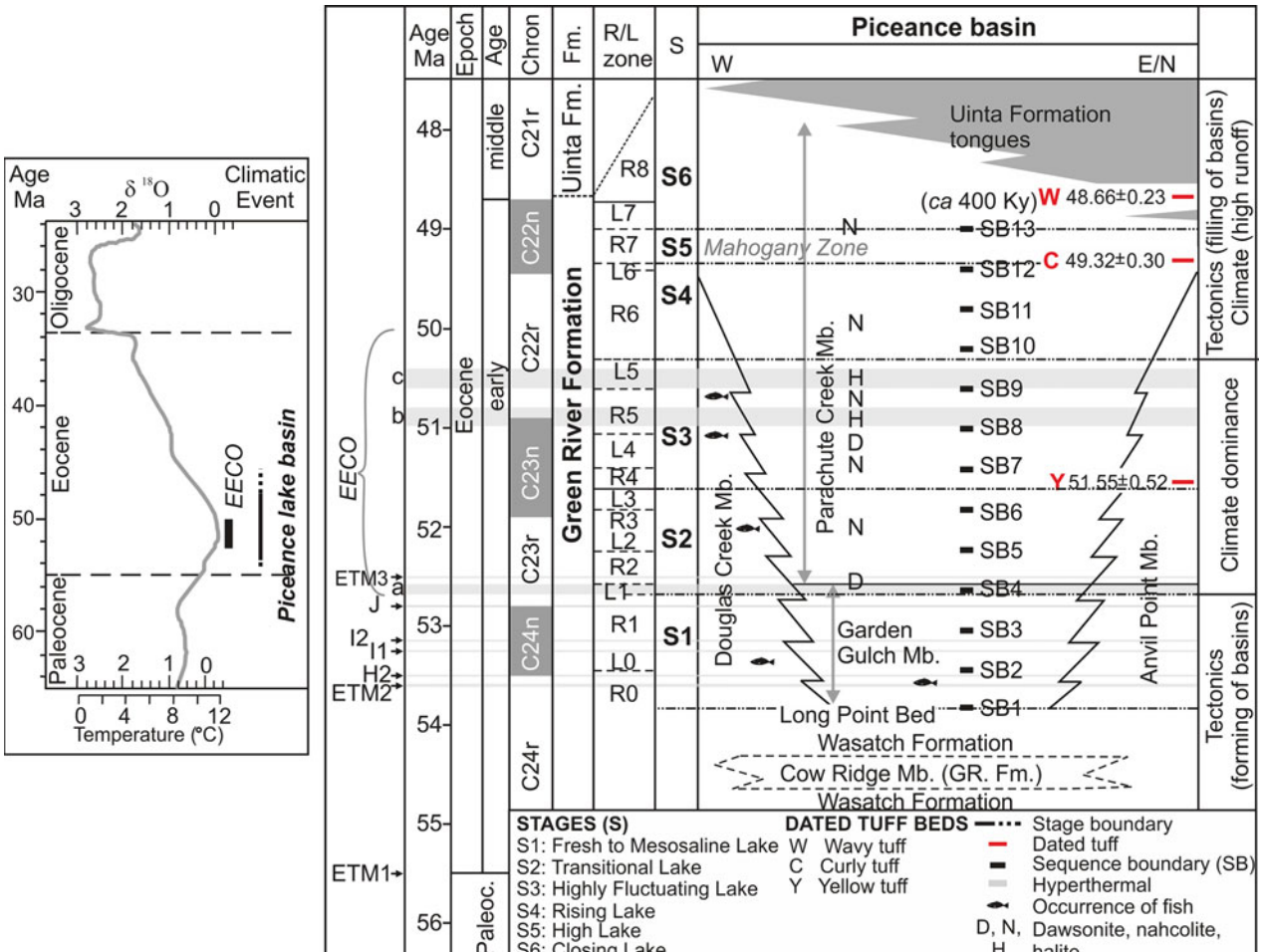

Fig. 7.9 Piceance basin stratigraphy and age model (After Smith et al. 2008, 2010) in correlation with Eocene climate curve and Early Eocene Climate Optimum (EECO) (After Zachos et al. 2001), and position of stages (*S*), rich (*R*) and lean (*L*) zones, and sequence boundaries (*SB*). Lake stages were separated based on the depositional trends of the facies associations in the Piceance basin. Position of rich and lean oil shale zones is based on the correlation between lake stages and rich and lean zones. Position of large-scale sequences (*ca* 400 Ky) is marked by major facies association changes, major changes in oil shale richness, gamma ray signals, Fischer assay logs, and

siliciclastics was probably the result of the combination of increased tectonic activity, weathering, erosion, and inflow (Carroll et al. 2006; Smith et al. 2008; Davis et al. 2009; Chetel et al. 2011; Tänavsuu-Milkeviciene and Sarg 2012).

7.5.2 Depositional Architecture

Based on vertical and lateral variation of facies associations three idealized depositional cycles have been recognized that characterize depositional pattern in the lake from littoral lake margin to deeper sublittoral and finally profundal environments (Fig. 7.10a).

Type 1 depositional cycles occur along basin margins and in the photic zone of the lake. Type 1 depositional cycles are bounded by erosional boundaries. These cycles starts either by erosionally based structureless alluvial (FA1) or delta (FA5) deposits or by littoral to sublittoral siliciclastic (FA7) deposits. In places, shoreline sandstones occur. Littoral to sublittoral undefined silicicilastic (FA7) deposits most probably present distal part of delta front. On log data, the beginning of depositional cycle is marked by gamma-ray peak that occurs just below the erosion-based sandstones (Fig. 7.3). Siliciclastic deposits that mark the lower boundary of sequences contain abundant load structures and dewatering structures that suggest rapid deposition. In vertical section siliciclastic deposits display overall upward-coarsening and upward-shallowing trends (Fig. 7.5b). This is supported by vertical changes from littoral and sublittoral siliciclastics (FA7) upwards into delta (FA5) or shoreline (FA3) deposits. Progradational siliciclastic deposits are overlain by sharp based carbonate deposits, composed of interbedded carbonate shoal (FA3) and microbial carbonate (FA6) deposits. Carbonate deposits change vertically from intraclastic breccia, intraclastic rudstone, coated grains, or with a mixture of different carbonate grains and clasts into microbial carbonates that pass from agglutinated, dendrolitic stromatolites and thrombolites to fine-grained laminated stromatolites indicating an overall upward-deepening trend (Sarg et al. 2013). Carbonate deposits are abruptly covered by clay- or carbonate-rich mudstones or siltstones (FA8). In places lean, sublittoral oil shale (FA9) formed in the upper part of these sequences (Fig. 7.10a).

In the profundal zone, cycle boundaries are conformable, and are marked by sharp changes in organic richness of deposits. Type 2 depositional cycle character occurs basinward from the Type 1 depositional cycle. Type 2 depositional cycle begin either with lean laminated oil shale (FAs 9, 10) or with sublittoral mudstones and siltstones (FA8). Thin layers and beds of silt and very fine-grained sandstones occur in these deposits. Lean oil shale (FAs 9, 10) deposits or sublittoral mudstone and siltstone (FA8) deposits are followed by meter to decimeter thick siliciclastic turbidite intervals (FA12). Turbidites (FA12) form normally graded or soft-sediment-deformed, sharp-based sandstone units interbedded with sublittoral mudstones and siltstones. Organically lean deposits are sharply overlain by organic rich laminated oil shale (FA10) and gravitational oil shale (FA11) deposits (Fig. 7.10a). Sharp boundaries between organic rich and organic lean deposits is well seen on Fischer assay logs (Fig. 7.3, L and R zones), and are marked by gamma ray peaks.

Deposits of Type 3 depositional cycle occur in the most basinward position from Type 1 and Type 2 depositional cycles. The beginning of Type 3 depositional cycles are marked by evaporite deposits, halite and nahcolite crystal accumulations and nodules or by lean oil shale deposits that contain large amounts of disseminated nahcolite crystals. No silt or sandstone beds have been found in Type 3 cycles. The lower portion of these depositional cycles is comprised of lean oil shale that is sharply overlain by organic-rich laminated oil shale (FA10) or gravitational oil shale (FA11) deposits (Fig. 7.10a). This turnaround in organic richness is similarly to Type 2 and is very well marked on Fischer assay logs (see also Fig. 7.3, L and R zones) and are represented as peaks on gamma ray logs (Fig. 7.3).

Depositional cycles vary greatly in thickness and in lateral extension and can be followed in outcrops. Type 1 depositional cycle vary laterally over relatively short distances, from meters to

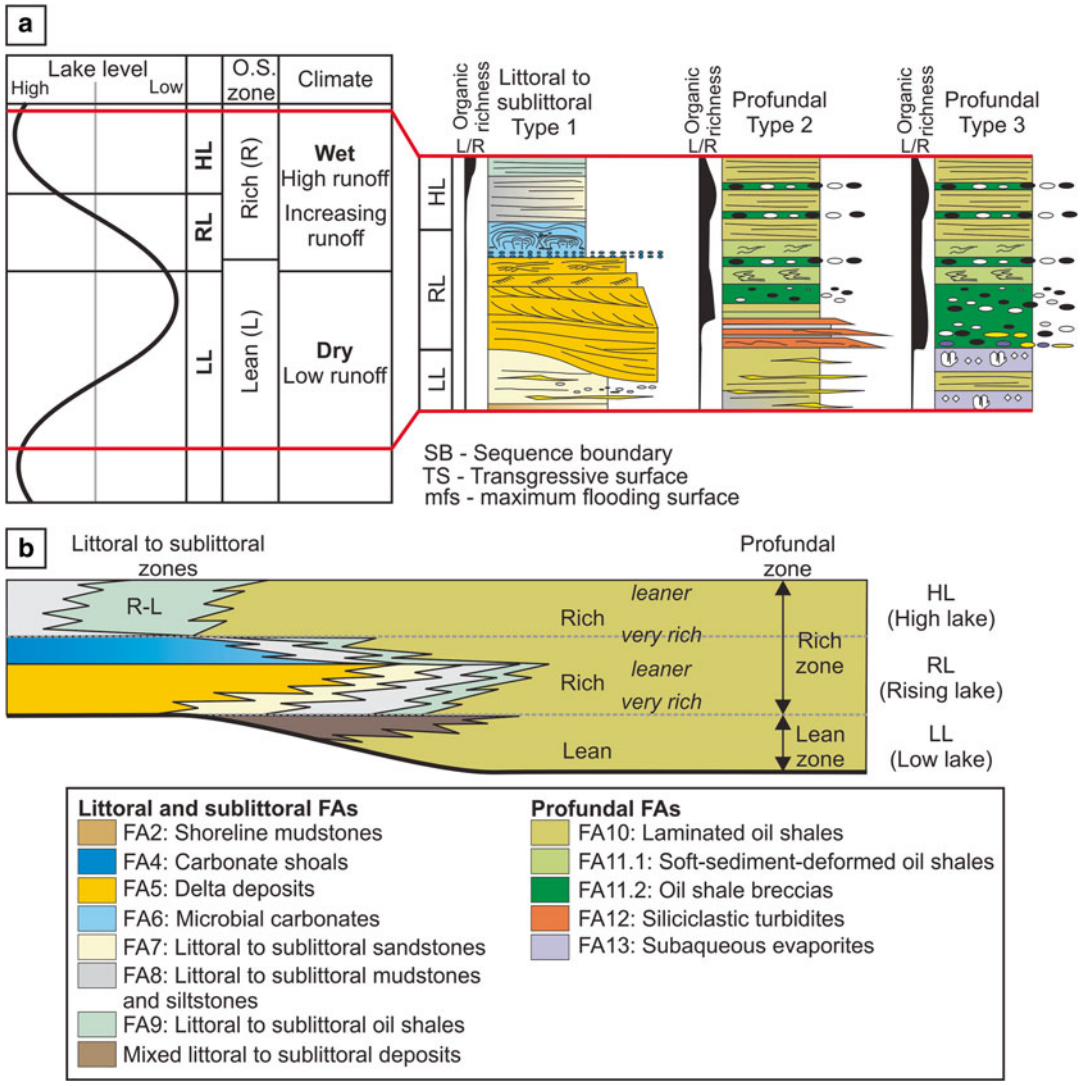

Fig. 7.10 Idealized depositional cycles and depositional sequences of the Piceance basin lake deposits. Based on this model deposition was dominantly controlled by the climate changes from dry to humid. (**a**) Three idealized depositional cycles for the littoral to sublittoral and profundal lake zones. (**b**) Composite depositional model for the large-scale depositional sequences in the lake system that shows the lateral and vertical variation of facies associations and distribution of organic-rich material across the basin (Modified from Tänavsuu-Milkeviciene et al. 2012)

hundreds of meters (Fig. 7.5a, e and 7.6c). Type 2 and Type 3 depositional cycles are usually more stable and can be followed over longer distances over hundreds of meters. However, single cycles vary too greatly to be followed in subsurface.

Stacked depositional cycles described above form depositional sequences, metres to 10s of metres thick correlative units that are bounded by surfaces that can be recognized regionally; are characterized by erosional surfaces, strong shifts in facies associations basinward, show rapid decline in oil shale richness, and prominent peaks on well logs (Fig. 7.3). Depositional sequences are at the scale of the well correlated rich and lean oil shale zones and large scale facies association shifts. Altogether, 13 depositional sequences have been recognized (see Fig. 7.3).

7.6 Discussion and Depositional Model

Deposition in the littoral to sublittoral zones is characterized by overall upward-fining cycles. However, single sandstone rich facies associations (FAs3, 5, 7) within the cycle form dominantly progradational, upward-coarsening deposits. Facies association changes within cycles are marked by sharp, in part erosional boundaries, from mudstones to sandstones, and from sandstones to carbonates suggesting abrupt changes in lake conditions. Mudstones and oil shale abruptly overlie carbonates due to drowning. In addition, regional metre-scale depositional sequences appear to be correlative across the lake basin, suggesting allocyclic control on the large scale stratigraphy.

Deposition in lacustrine settings is cyclic in nature and it is not controlled by global sea/level changes but by changes climate and tectonics. These may include changes in fresh water runoff from the catchment area and the intensity of evaporation. The tectonic regime of the area has direct impact on local climate, and changes in local lake basin morphology. Tectonically induced changes generally have timespans on the order of 100's of thousands to millions of years. They will affect the whole lake basin by either increasing or decreasing subsidence, changing provenance terrains, and/or changing catchment area relief. The Green River Formation fill of the Piceance basin suggests early moderate subsidence that resulted in thicker early Green River fill in Stage 1, subsequently slowed, than increased again in Stage 3, and then slowed during Stages 4 and 5 (see Fig. 7.3). Subsidence then increased again during the closing Stage 6. This periodicity occurred over 2 my time periods (Fig. 7.9)

Climate changes can occur on over a range of frequencies from very short on the scale of decadal wet and dry cycles to 100,000 year plus climatic changes related to global warm/cool temperature cycles (i.e., solar forcing Milankovitch cyclicity). Because lakes are closed systems, climate has very strong influence on deposition. Therefore, switches in regional climate system from more humid to more arid control variation in runoff and vegetation, as well as intensity of chemical and physical weathering and this in turn affects inflow of siliciclastics and nutrients into the lake. The depositional cycles identified in this study appear to be at a higher frequency than the tectonic changes suggested by accommodation cycles. Therefore, based on an understanding of climate influence on deposition in lakes, a climate based depositional model is proposed below to explain formation depositional sequences in the Piceance Lake. The periodicity of the 13 depositional sequences identified here is suggested to be on the 400 Kyr Milankovitch eccentricity cycles, based on correlation to the absolute age dates documented in the greater Green River system (Smith et al. 2008, 2010) (Fig. 7.9).

During times of low precipitation rates and dry climate period overall hydrologic input decreases (Fig. 7.10a). Main inflow into the lake was by groundwater inflow and/or flash-flood runoff (Sewall and Sloan 2006; Lyons et al. 2011). Sporadic and limited runoff and lower inflow led to lowering of lake level. Decreased precipitation also resulted in limited nutrient inflow into the lake and led to a decline in algal production. Deposition along lake margins was dominated by overbank and dryland river deposits (FA1) and marginal mudstones (FA2) (see example Fig. 7.5a–d). At times, strong, but intermittent flash-flood deposits could form. Low lake level deposits along the basin margins are not well preserved, however. This could be caused by the erosion and reworking of possibly relatively thin deposits during following rising lake. In places, low lake level deposits are preserved basinward. The thickest deposits preserved in the profundal zone as lean oil shale deposits, or lean oil shale deposits interbedded with nahcolite and halite beds (see example Fig. 7.8b, g, h) (Fig. 7.10).

During the change to a wetter period, increased precipitation and runoff resulted in stronger erosion and higher physical weathering of the surrounding areas. Higher inflow and as a consequence, increased sediment and nutrient input into the lake led to lake level rise. Along

basin margins lake level rise is well marked by erosionally-based channel or carbonate lag and shoal deposits (Figs. 7.5c and 7.10). Rip-up siliciclastic and carbonate clasts, mudstone clasts, tree branches, fish scales and fragments occur at erosional boundaries (Fig. 7.6e, f). Soft-sediment deformations are abundant on the base of siliciclastic deposits.

Increased runoff increased erosion of surrounding areas and was followed by transport of nutrients into the lake. Due to increased nutrient input algal and bacterial colonies bloomed and the beginning of the rising lake is marked by sharp increase in organic-richness of profundal lake deposits (Fig. 7.10) (Feng 2011). In places, in deeper sublittoral areas the beginning of the rising lake was also marked by sharply based siliciclastic turbidites (FA12) (Fig. 7.10a). Similar observations have been described by other studies (Harris et al. 2005; Lyons et al. 2011).

During the ensuing humid climate period, inflow into the lake remained high due to high river and groundwater inflow, resulting in high lake levels (Fig. 7.10a). Higher inflow into the lake resulted in the most widespread and deepest lake condition (Fig. 7.10). High nutrient input enhanced productivity and in cases of anoxic bottom conditions preservation potential of organic matter increased hugely. This resulted in formation of the most widespread rich oil shale deposits (Fig. 7.10).

The organic-rich and organic-lean mudrocks within the Piceance basin can be related in distribution to their position within depositional sequences. Low lake deposits form lean oil shale deposits that can be separated in the deeper part of the basin, but thin out towards the basin margins. Along the basin margins, thick siliciclastic and carbonate deposits formed during rising lake and are followed by littoral to sublittoral mudstones and oil shale deposits formed during high lake. These deposits are equivalent to the rich oil shale deposits formed during the rising and high lake in the deeper part of the basin. Richness decreases from the profundal areas to the basin margin within these mud rocks (see also Feng 2011).

7.7 Conclusions

The Piceance basin formed as a mixed carbonate-siliciclastic and evaporite-rich deep, stratified organic-rich lake basin in the early to middle Eocene age. Altogether, 24 facies and 13 facies association have been described from the basin area. Most of the deposits formed in the profundal zone as laminated oil shale, gravitational oil shale, siliciclastic turbidites, or subaqueous evaporites. Along the lake margin, alluvial and littoral to sublittoral deposits, shoreline mudstones, shoreline sandstones, carbonate shoals, microbial carbonates, delta, and littoral to sublittoral mudstones to sandstones, and oil shale deposits formed.

Long-term changes in lake are reflected by lake stages (tens to hundreds of meters). Lake stages are controlled by a combination of climate and tectonics that regulate variation in sedimentological patterns, depositional trends, and organic-richness throughout the basin evolution. Stage 1, Fresh to mesosaline lake, was deposited during decreasing tectonic activity and increasing climate control. Lake Stages 2 and 3, Transitional and Highly fluctuating lake periods are interpreted to have been dominated by an increasingly warm and arid climate during the Early Eocene Climate Optimum. Following Stages 4, 5, and 6, Rising, High, and Closing lake periods record the change to a wetter climate and increasing tectonic activity, resulting in a widespread deep lake and increased siliciclastic input that extended across the Piceance basin.

Three depositional cycles have been described, one from the littoral and sublittoral zone and two from the profundal zone, Type 1, Type 2 and Type 3 respectively. Depositional cycles combine into larger-scale depositional sequences that display similar depositional patterns. Altogether 13 depositional sequences (10s of metres thick) have been defined within the Green River Formation in the Piceance basin. They display significant changes in lake regime and are divided into periods of low, rising, and high lake that are separated by erosional surfaces, prominent facies association shifts, and drastic changes in richness of deposits.

A climate model is proposed for formation of the depositional sequences and is suggested to control the formation of organic rich and lean deposits. Facies within sequences and organic-rich mudrocks are controlled by variations in run-off and vegetation that influence the inflow of siliciclastics and nutrients, and the formation and distribution of organic-rich deposits. Organic richness of deposits varies vertically and laterally within depositional sequences. The richest deposits form dominantly in the beginning or latter part of the rich units in early rising and late high lake level times. During low lake, organic lean deposits formed in the deeper part of the basin and thin out towards the basin margins. The rising lake is marked by thick siliciclastic and carbonate deposits along the basin margin, and rich oil shale deposits in the deeper part of the basin. During the following high lake, littoral to sublittoral deposits formed along the basin margins, whereas in the profundal zone rich oil shale deposits were deposited.

Acknowledgments This work is part of the Colorado School of Mines COSTAR oil shale project, financed by ExxonMobil, Total and Shell. We thank the USGS Core Research Center in Denver for providing the core data. We also thank Martynas Milkevičius and Suriamin for help with fieldwork and photography.

References

Arnott RWC (2010) Deep-marine sediments and sedimentary systems. In: James NP, Dalrymple RW (eds) Facies models, vol 6, Geological Association of Canada IV Series. GEOtext, St. John's, pp 295–322

Bhattacharya JP, Giosan L (2003) Wave-influenced deltas: geomorphological implications for facies reconstruction. Sedimentology 50:187–201

Bijl PK, Schouten S, Sluijs A, Reichart G-J, Zachos JC, Brinkhuis H (2009) Early Palaeogene temperature evolution of the southwest Pacific Ocean. Nature 461:776–779

Boak J, Sheven P (2015) Mineralogy of the Green River Formation in the Piceance Creek Basin, Colorado. In: Smith ME, Carroll AR (eds) Limnogeology of the Eocene Green River Formation: synthesis in limnogeology. Springer, Dordrecht, pp 183–209

Bohacs KM, Carroll AR, Neal JE, Mankiewicz PJ (2000) Lake-basin type, source potential, and hydrocarbon character: an integrated sequence-stratigraphic-geochemical framework. In: Gierlowski-Kordesch EH, Kelts KR (eds) Lake basins through space and time, vol 46, AAPG studies in geology. American Association of Petroleum Geologists, Tulsa, pp 3–34

Bouma AH (1962) Sedimentology of some Flysch deposits. Elsevier, Amsterdam, 168 p

Bray TF Jr, Carter CH (1992) Physical processes and sedimentary record of a modern, transgressive, lacustrine barrier island. Mar Geol 105:155–168

Bridge JS, Demicco RV (2008) Earth surface processes, landforms and sediment deposits. Cambridge University Press, Cambridge, p 815

Brownfield ME, Mercier TJ, Johnson RC, Self JG (2010) Nahcolite resources in the Green River Formation, Piceance Basin, Colorado. U.S. Geological Survey, Reston Digital Data Series, DDS-69-Y, Chp. 2. 51 p

Buatois LA, Mangano MG (1995) Sedimentary dynamics and evolutionary history of a Late Carboniferous Gondwanic lake in north-western Argentina. Sedimentology 42:415–436

Carroll A, Chetel LM, Smith ME (2006) Feast to famine: sediment supply control on Laramide basin fill. Geology 34:197–200

Cashion WB, Donnell JR (1972) Chart showing correlation of selected key units in the organic-rich sequence of the Green River Formation, Piceance Creek Basin, Colorado, and Uinta Basin, Utah. U.S. Geological Survey, Reston Oil and Gas Investigations, Chart OC-65

Cashion WB, Donnell JR (1974) Revision of nomenclature of the upper part of the Green River Formation, Piceance Creek Basin, Colorado, and Eastern Uinta Basin, Utah. U.S. Geological Survey, Bulletin, 1394-G, 9 p

Chetel LM, Janecke SU, Carroll AR, Beard BL, Johnson CM, Singer BS (2011) Paleogeographic reconstruction of the Eocene Idaho River, North American Cordillera. Geol Soc Am Bull 123:71–88

Clementz MT, Sewall JO (2011) Latitudinal gradients in greenhouse seawater $\delta^{18}O$: evidence from Eocene sirenian tooth enamel. Science 332:455–458

Cohen AS (2003) Paleolimnology: the history and evolution of lake systems. Oxford University Press, Oxford, 528 p

Cohen AS, Talbot MR, Awramik SM, Dettman DL, Abell P (1997) Lake level and paleoenvironmental history of Lake Tanganyika, Africa, as inferred from late Holocene and modern stromatolites. Geol Soc Am Bull 109:444–460

Cole RD, Daub GJ (1991) Methane occurrences and potential resources in the lower Parachute Creek Member of Green River Formation, Piceance Creek Basin, Colorado. In: 24th Oil Shale symposium proceedings: Colorado School of Mines Quarterly, vol 83, Golden, pp 1–7

Davis SJ, Mulch A, Carroll AR, Horton TW, Chamberlain CP (2009) Paleogene landscape evolution of the

central North American Cordillera: developing topography and hydrology in the Laramide foreland. Geol Soc Am Bull 121:100–116

Demaison GJ, Moore GT (1980) Anoxic environments and oil source bed genesis. Am Assoc Pet Geol Bull 64:1179–1209

Dickinson WR, Klute MA, Hayes MJ, Janecke SU, Lundin ER, McKittrick MA, Livares MD (1988) Paleogeographic and paleotectonic setting of Laramide sedimentary basins in the central Rocky Mountain region. Geol Soc Am Bull 100:1023–1039

Dutton A, Lohmann KC, Leckie RM (2005) Insights from the Paleogene tropical Pacific: foraminiferal stable isotope and elemental results from Site 1209, Shatsky Rise. Paleoceanography 20:16p

Dyni JR (1981) Geology of the nahcolite deposits and associated oil shales of the Green River Formation in the Piceance Creek Basin, Colorado. PhD thesis, University of Colorado, Boulder, 144 p

Dyni JR (2006) Geology and resources of some world oil-shale deposits. U.S. Geological Survey, Reston Scientific Investigation Report, 2005–5294, 42 p

Dyni JR, Hawkins JE (1981) Lacustrine turbidites in the Green River Formation, northwestern Colorado. Geology 9:235–238

Feng J (2011) Source rock characterization of the Green River Oil Shale, Piceance Creek Basin, Colorado. MSc thesis, Colorado School of Mines, Golden, 84 p

Ghadeer SG, Macquaker JHS (2012) The role of event beds in the preservation of organic carbon in fine-grained sediments: analyses of the sedimentological processes operating during deposition of the Whitby Mudstone Formation (Toarcian, Lower Jurassic) preserved in northeast England. Mar Pet Geol 35:309–320

Gierlowski-Kordesch EH (2010) Lacustrine carbonates. In: Alonso-Zarza AM, Tanner LH (eds) Carbonates in continental settings: facies, environments, and processes, vol 61, Developments in sedimentology. Elsevier, Amsterdam/London, pp 1–101

Gierlowski-Kordesch EH, Rust BR (1994) The Jurassic East Berlin Formation, Hartford basin, Newark Supergroup (Connecticut and Massachusetts): a saline lake-playa-alluvial plain system. In: Renaut RW, Last WM (eds) Sedimentology and geochemistry of modern and ancient saline lakes, vol 50, SEPM Special Publications. SEPM, Tulsa, pp 249–265

Hardie LA, Smoot JP, Eugster HP (1978) Saline lakes and their deposits: a sedimentological approach. In: Matter A, Tucker ME (eds) Modern and ancient lake sediments, vol 2, International Association of Sedimentologists, Special Publication. Blackwell Scientific, Oxford, pp 1–6

Harris NB, Freeman KH, Pancost RD, Mitchell GD, White TS, Bate RH (2005) Patterns of organic-carbon enrichment in a lacustrine source rock in relation to paleo-lake level, Congo Basin, West Africa. In: Harris NB (ed) The deposition of organic-carbon-rich sediments: models, mechanisms, and consequences, vol 82, SEPM Special Publications. SEPM, Tulsa, pp 103–123

Ilgara A, Nemec W (2005) Early Miocene lacustrine deposits and sequence stratigraphy of the Ermenek Basin, Central Taurides, Turkey. Sediment Geol 173:233–275

Johnson RC (1984) New names for units in the lower part of the Green River Formation, Piceance Creek Basin, Colorado. U.S. Geological Survey, Bulletin, 1529-I, 20 p

Johnson RC (2012) The systematic geologic mapping program and a quadrangle-by-quadrangle analysis of time-stratigraphic relations within oil shale-bearing rocks of the Piceance Basin, western Colorado. U.S. Geological Survey, Scientific Investigations Report 2012–5041, 28 p

Johnson CL, Graham SA (2004) Cycles in perilacustrine facies of late Mesozoic rift basin, southeastern Mongolia. J Sediment Res 74:786–804

Johnson RC, Nichols DJ, Hanley JH (1988) Stratigraphic sections of Lower Tertiary strata and charts showing palynomorph and mollusk assemblages, Douglas Creek Arch area, Colorado and Utah, U.S. Geological Survey, Miscellaneous field studies map. The Survey, Reston

Johnson RC, Mercier TJ, Brownfield ME, Pantea MP, Self JG (2010) An assessment of in-place oil shale resources in the Green River Formation, Piceance Basin, Colorado. U.S. Geological Survey, Reston Digital Data Series DDS–69–Y, Chp. 1, 187 p

Keighley D (2008) A lacustrine shoreface succession in the Albert Formation, Moncton Basin, New Brunswick. Bull Can Petrol Geol 56:235–258

Kelts K (1988) Environments of deposition of lacustrine petroleum source rocks: an introduction. In: Fleet AJ, Kelts K, Talbot MR (eds) Lacustrine petroleum source rocks, vol 40, Geological society special publications. Published for the Geological Society by Blackwell Scientific Publications, Oxford/Boston/Edinburgh/Palo Alto/Melbourne, pp 3–26

LaClair D, Lowenstein TK (2009) Fluid inclusion microthermometry from halite in the Eocene Green River Formation, Piceance Creek basin, Colorado, USA: evidence for a perennial stratified saline lake. Geological Society of America, annual meeting, abstracts with programs, Portland, 41, p 512

Last WM, Vance RE (1997) Bedding characteristics of Holocene sediments from salt lakes of northern Great Plains, Western Canada. J Paleolimnol 17:297–318

Lourens LJ, Sluijs A, Kroon D, Zachos JC, Thomas E, Röhl U, Bowles J, Raffi I (2005) Astronomical pacing of late Palaeocene to early Eocene global warming events. Nature 435:1083–1087

Lyons RP, Scholz CA, Buoniconti MR, Martin MR (2011) Late Quaternary stratigraphic analysis of the Lake Malawi Rift, East Africa: an integration of drill-core and seismic-reflection data. Palaeogeogr Palaeoclimatol Palaeoecol 303:20–37

McGlue MM, Soreghan MJ, Michel E, Todd JA, Cohen AS, Mischler J, O'Connell CS, Castañeda OS, Hartwell

RJ, Lezzar KE, Nkotagu HH (2010) Environmental controls on shell-rich facies in tropical lacustrine rifts: a view from Lake Tanganyika's littoral. Palaios 25:426–438

Mercier TJ, Brownfield ME, Johnson RC, Self JG (2009) Fischer assays of oil shale drill cores and rotary cuttings from the Piceance Basin, Colorado–2009 Update. U.S. Geological Survey, Reston Open-File Report 98–483, Version 2.0, 16 p

Milroy PG, Wright VP (2002) Fabrics, facies control and diagenesis of lacustrine ooids and associated grains from the Upper Triassic, southwest England. Geol J 37:35–53

Müller R, Nystuen JP, Wright VP (2004) Pedogenic mud aggregates and paleosol development in ancient dryland river systems; criteria for interpreting alluvial mudrock origin and floodplain dynamics. J Sediment Res 74:537–551

Nicolo MJ, Dickens GR, Hollis CJ, Zachos JC (2007) Multiple early Eocene hyperthermals: their sedimentary expression on the New Zealand continental margin and in the deep sea. Geology 35:699–702

Olariu C, Bhattacharya JP (2006) Terminal distributary channels and delta front architecture of river-dominated delta systems. J Sediment Res 76:212–233

Osleger DA, Heyvaert AC, Stoner JS, Verosub KL (2009) Lacustrine turbidites as indicators of Holocene storminess and climate: Lake Tahoe, California and Nevada. J Paleolimnol 42:103–122

Pitman JK (1996) Origin of primary and diagenetic carbonates in the lacustrine Green River Formation (Eocene), Colorado and Utah. U.S. Geological Survey, Bulletin, 2157, 17 p

Pitman JK, Johnson RC (1978) Isopach, structure contour, and resource maps of the Mahogany oil-shale zone, Green River Formation, Piceance Creek Basin, Colorado. U.S. Geological Survey Miscellaneous Field Investigations Map MF-958, scale 1:126,720. The Survey, Reston

Pitman JK, Pierce FW, Grundy WD (1989) Thickness, oil-yield, and kriged resource estimates for the Eocene Green River Formation, Piceance Creek Basin, Colorado. U.S. Geological Survey Oil and Gas Investigations Chart OC-132. The Survey, Reston

Platt NH, Wright VP (1991) Lacustrine carbonate facies models, facies distributions and hydrocarbon aspects. In: Anadon P, Cabrera L, Kelts K (eds) Lacustrine facies analysis, international association of sedimentologists, vol 13, Special publication. Blackwell Scientific Publications, Oxford, pp 57–74

Plummer PS, Gostin VA (1981) Shrinkage cracks; desiccation or synaeresis? J Sediment Petrol 51:1147–1156

Rainey DK, Jones B (2009) Abiotic versus biotic controls on the development of the Fairmont Hot Springs carbonate deposit, British Columbia, Canada. Sedimentology 56:1832–1857

Reading HG, Collinson JD (1996) Clastic coasts. In: Reading HG (ed) Sedimentary environments: processes, facies and stratigraphy, 3rd edn. Blackwell Science, Oxford, pp 154–231

Renaut RW, Gierlowski-Kordesch EH (2010) Lakes. In: James NP, Dalrymple RW (eds) Facies models, vol 6, Geological Association of Canada IV Series. GEOtext. St. John's, pp 541–575

Renaut RW, Owen RB (1991) Shore-zone sedimentation and facies in a closed rift lake: the Holocene beach deposits of Lake Bogoria, Kenya. In: Anadón P, Cabrera L, Kelts K (eds) Lacustrine facies analysis, vol 13, Special Publication, International Association of Sedimentologists. Blackwell Scientific, Oxford, pp 175–195

Renaut RW, Tiercelin J-J (1994) Lake Bogoria, Kenya rift valley – a sedimentological overview. In: Renaut RW, Last WM (eds) Sedimentology and geochemistry of modern and ancient saline lakes, vol 50, SEPM Special Publications. SEPM, Tulsa, pp 101–123

Sabato MM (2007) Recognition of trigger mechanisms for soft-sediment deformation in the Pleistocene lacustrine deposits of the Sant'Arcangelo Basin (Southern Italy): Seismic shock vs. Overloading. Sediment Geol 196:31–45

Sarg JF, Suriamin, Tänavsuu-Milkeviciene K, Humphrey JD (2013) Lithofacies, stable isotopic composition, and stratigraphic evolution of microbial and associated carbonates, Green River Formation (Eocene), Piceance basin. Am Assoc Pet Geol Bull 97:1937–1966

Schieber J (2011) Reverse engineering mother nature – Shale sedimentology from an experimental perspective. Sediment Geol 238:1–22

Scholz CA, Talbot MR, Brown ET, Lyons RP (2011) Lithostratigraphy, physical properties and organic matter variability in Lake Malawi Drillcore sediments over past 145,000 years. Palaeogeogr Palaeoclimatol Palaeoecol 303:38–50

Schomacker ER, Kjemperud AV, Nystuen JP, Jahren JS (2010) Recognition and significance of sharp-based mouth-bar deposits in the Eocene Green River Formation, Uinta Basin, Utah. Sedimentology 57:1069–1087

Schubel KA, Lowenstein TK (1997) Criteria for the recognition of shallow-perennial-saline-lake halites based on recent sediments from the Qaidam Basin, Wester China. J Sediment Res 67:74–87

Self JG, Brownfield ME, Johnson RC, Mercier TJ (2010a) Fischer assay histograms of oil shale drill cores and cuttings from the Piceance Basin, northwestern Colorado. U.S. Geological Survey, Reston Digital Data Series DDS–69–Y, chp. 7, 9 p

Self JG, Johnson RC, Brownfield ME, Mercier TJ (2010b) Stratigraphic cross sections of the Eocene Green River Formation in the Piceance Basin, Northwestern Colorado. U.S. Geological Survey, Reston Digital Data Series DDS–69–Y, chp. 5, 7 p

Sewall JO, Sloan LC (2006) Come a little bit closer: a high-resolution climate study of the early Paleogene Laramide foreland. Geology 34:81–84

Sexton PF, Wilson PA, Norris RD (2006) Testing the Cenozoic multisite composite $\delta^{18}O$ and $\delta^{13}C$ curves: new monospecific Eocene records from a single locality, Demerara Rise (Ocean Drilling Program Leg 207). Paleoceanography 21(PA2019):1–17

Sexton PF, Norris RD, Wilson PA, Pälike H, Westerhold T, Röhl U, Bolton CT, Gibbs S (2011) Eocene global warming events driven by ventilation of oceanic dissolved organic carbon. Nature 471:349–352

Shanmugam G (2000) 50 years of the turbidite paradigm (1950s-1990s): deep-water processes and facies models-a critical perspective: Marine. Pet Geol 17:285–342

Smith JW, Milton C (1966) Dawsonite in the Green River Formation of Colorado. Econ Geol 61:1029–1042

Smith DG, Jol HM, Smith ND, Kostaschuk RA, Pearce CM (2005) The wave-dominated Willial River Delta, Lake Athabasca, Canada: its morphology, radar stratigraphy, and history. In: Giosa L, Bhattacharya JP (eds) River deltas-concepts, models, and examples, vol 83, SEPM Special Publication. SEPM, Tulsa, pp 101–123

Smith ME, Carroll AR, Singer BS (2008) Synoptic reconstruction of a major ancient lake system: Eocene Green River Formation, western United States. Geol Soc Am Bull 120:54–84

Smith ME, Chamberlain KR, Singer BS, Carroll AR (2010) Eocene clocks agree: Coeval 40Ar/39Ar, U-Pb, and astronomical ages from the Green River Formation. Geology 38:527–530

Surdam RC, Stanley KO (1980) Effects of changes in drainage-basin boundaries on sedimentation in Eocene Lakes Gosiute and Uinta of Wyoming, Utah, and Colorado. Geology 8:135–139

Tänavsuu-Milkeviciene K, Sarg JF (2012) Evolution of an organic-rich lake basin – stratigraphy, climate, and tectonics: Piceance Creek basin, Eocene Green River Formation. Sedimentology 59:1735–1768

Tänavsuu-Milkeviciene K, Sarg JF, Bartov Y (2012) Climate control on sequence stratigraphy in organic-rich lake basin: green river formation, Greater Lake Uinta, Colorado and Utah. AAPG RMS, Grand Junction

Tanner PWG (1998) Interstratal dewatering origin for polygonal patterns of sand-filled cracks: a case study from late Proterozoic metasediments of Islay, Scotland. Sedimentology 45:71–89

Wakelin-King GA, Webb JA (2007) Upper-flow-regime mud floodplains, lower-flow-regime sand channels: sediment transport and deposition in a drylands mud-aggregate river. J Sediment Res 77:702–712

Wright VP (2012) Lacustrine carbonates in rift settings: the interaction of volcanic and microbial processes on carbonate deposition. In: Garland J, Neilson JE, Laubach SE, Whidden KJ (eds) Advances in carbonate exploration and reservoir analysis, vol 370, Special Publications. Geological Society, London

Wright VP, Marriott SB (2007) The dangers of taking mud for granted: lessons from Lower Old Red Sandstone dryland river systems of South Wales. Sediment Geol 195:91–100

Young RG (1995) Stratigraphy of green River Formation in Piceance Creek Basin, Colorado. In: Averett WR (ed) The Green River Formation in Piceance Creek and Eastern Uinta basins. Grand Junction Geological Society, Grand Junction, pp 1–13

Zachos JC, Pagani M, Sloan L, Thomas E, Billups K (2001) Trends, rhythms, and aberrations in global climate 65 Ma to present. Science 292:686–693

Zachos JC, Dickens GR, Zeebe RE (2008) An early Cenozoic perspective on green house warming and carbon-cycle dynamics. Nature 451:279–283

Zachos JP, McCarren H, Murphy B, Röhl U, Westerhold T (2010) Tempo and scale of late Paleocene and early Eocene carbon isotope cycles: implications for the origin of hyperthermals. Earth Planet Sci Lett 299:242–249

Mineralogy of the Green River Formation in the Piceance Creek Basin, Colorado

8

Jeremy Boak and Sheven Poole

Abstract

Quantitative X-Ray Diffraction (XRD) analysis was performed on 82 samples spanning the Green River Formation in the Piceance Creek Basin of Colorado. Samples represented basin *margin* (outcrop sections in Douglas Pass), and basin *center* (Savage 24-1 and Shell 23X-2 core) depositional environments. Bulk mineralogy is integrated into a stratigraphic framework of lake stages, incorporating variations in organic richness. Twenty-eight Douglas Pass samples consist of argillaceous, siliceous, feldspathic and dolomitic mudstone and siltstone composed predominantly of clay minerals, quartz, carbonate minerals, feldspar, and analcime. Fifteen Shell 23X-2 well samples cover the lower third of the basin center section. Data for 35 additional Shell 23-X2 samples from the U. S. Geological Survey core database were added to the dataset. The lower 24 Shell 23-X2 samples consist of argillaceous and siliceous mudstone and siltstone composed of clay minerals, carbonate minerals, quartz, feldspar and dawsonite. The upper 26 samples overlap the lower John Savage well section. Thirty-nine Savage 24-1 well samples cover the upper 2/3 of the basin center section. With the upper part of the Shell 23-X2 well samples, they consist of feldspathic and dolomitic mudstone and siltstone composed of feldspar, carbonate minerals, quartz, nahcolite [$NahCO_3$], dawsonite [$NaAl(OH)_2(CO_3)$], and clay minerals. Buddingtonite [$(NH_4)AlSi_3O_8 \bullet 0.5H_2O$] comprises a significant fraction of the feldspar.

Overall, basin center samples are clay-poor (6 %), and organic matter-rich (12 %), whereas basin margin samples are clay-rich (22 %), with

J. Boak (✉)
Department of Geology and Geological Engineering,
Colorado School of Mines, Berthoud Hall 311A,
1516 Illinois Street, Golden CO 80401, USA
e-mail: jboak@mines.edu

S. Poole
XTO Energy, Fort Worth, TX, USA

M.E. Smith, A.R. Carroll (eds.), *Stratigraphy and Paleolimnology of the Green River Formation, Western USA*, Syntheses in Limnogeology 1, DOI 10.1007/978-94-017-9906-5_8

more diverse clay types, and less organic matter (7 %). Divalent carbonates are dominantly dolomite-ankerite, with calcite essentially absent in the middle basin center, but commonly present in the basin margin section. Buddingtonite, nahcolite, dawsonite, and halite (NaCl) are common in the basin center, but sparse to absent in the basin margin, whereas analcime ($NaAlSi_2O_6•H_2O$) is abundant in the basin margin (max 37 %), and sparse in the basin center.

Changes in mineralogy are related to lake stages (as defined by Tanavsuu-Milkeviciene and Sarg 2012), including a sharp reduction in clay and increase in authigenic dawsonite and feldspar content during Stage 2 (transitional lake), and a fall in quartz and dawsonite near the end of Stage 3 (rapidly fluctuating lake) in the basin center. These changes are attributed to reactions controlled by variations in salinity, alkalinity, pH, and silica concentration. Halite and nahcolite reflect saturation in the deep lake center. Differences between basin margin and center likely reflect varying lake levels but persistent stratification of the lake throughout most of its history. Mineralogic variations in the Green River Formation have relevance to other organic-rich shale and mudstone formations in lacustrine and potentially even in marine environments where organic matter preservation is enhanced by water column stratification.

8.1 Introduction

The unusual mineralogy of the Eocene Green River Formation (GRF) has been described by a number of authors, beginning with Bradley (1925, 1929, 1964), and including Milton and Fahey (1960), Milton (1961), Smith and Robb (1966) and Brobst and Tucker (1973). Many of these papers focus on specific mineral relationships. Smith and Robb (1973) provide a comprehensive interpretation of the chemistry that produced the widely correlatable finely laminated oil shale of the basin center in the Piceance Creek and Uinta Basins with extensive discussion of the mineral constituents. Although these papers highlight the wide range of minerals present in the formation, relatively little discussion exists of the stratigraphic variation of mineral composition, and its relation to the evolution of lake chemistry and paleoenvironments through time. Robb and Smith (1974) discuss a mineralogic profile using semi-quantitative X-Ray Diffraction (XRD) data through Colorado Corehole No. 1. They highlight some trends in the stratigraphic variation, specifically the almost complete disappearance of clay minerals at the top of the Garden Gulch Member. Dean et al. (1981) presented a mineralogic profile through Well CR-2, also based on semi-quantitative XRD, but did not discuss the mineralogic trends in the Formation. Brobst and Tucker (1973) discussed semi-quantitative XRD mineralogic analysis of three outcrop sections mainly of the Parachute Creek Member, and suggested that dolomite formed as a primary precipitate, and that dawsonite formed by reaction of analcime, and possibly as a direct precipitate.

This study has attempted to update understanding of mineralogic variation through collection of a suite of samples of oil shale and related rock in two segments of an outcropping section at the margin of the Piceance Creek Basin at Douglas Pass, and in a reference section comprised of portions of two wells in the basin center. We have correlated the variation in mineralogy to variations in stratigraphy documented by Tanavsuu-Milkeviciene and Sarg (2012, 2015). Figure 8.1 shows the general stratigraphy of the GRF in the Piceance Creek Basin, showing major lithostratigraphic units, including the underlying (and to some extent interfingering) Wasatch Formation and the overlying (and also interfingering) Uinta Formation. Samples in this study

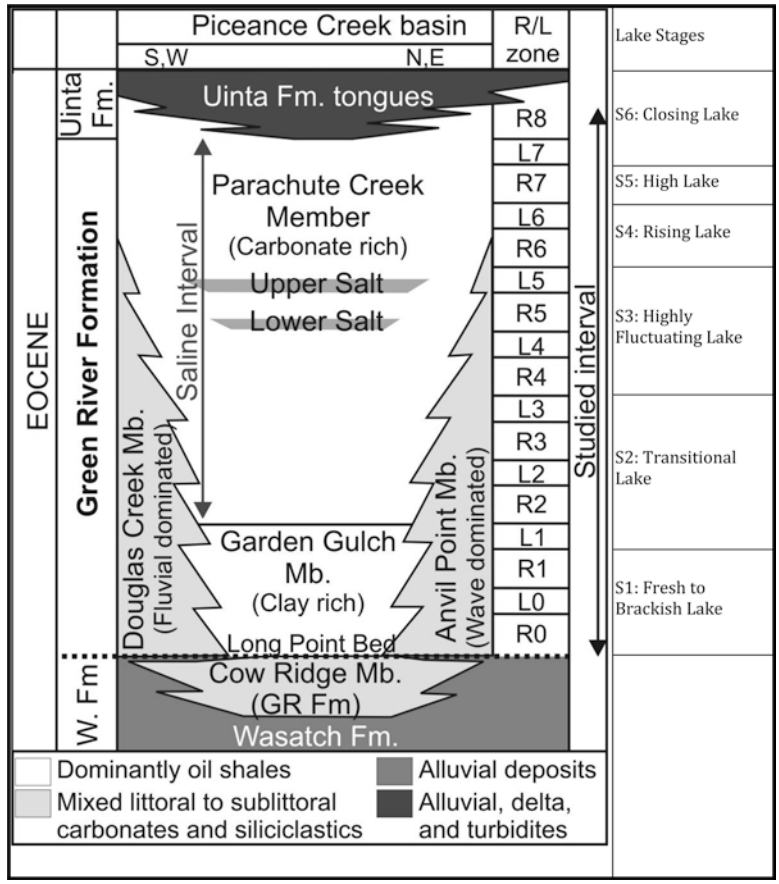

Fig. 8.1 Stratigraphy of the Green River Formation, with rich and lean zones and lake stages after Tänavsuu-Milkeviciene and Sarg (2012)

came from the Garden Gulch and Parachute Creek Members of the GRF. The figure also shows the subdivision of the GRF into alternating organically rich and lean (R&L) zones defined by Donnell and others (Donnell and Blair 1970; Cashion and Donnell 1972, 1974), and also the subdivisions into stages according to the scheme of Tanavsuu-Milkeviciene and Sarg (2012). As these latter authors state, these stages

> reflect variations in facies association distribution, richness of oil shale, water chemistry, degrees of lake restriction and salinity, and siliciclastic sediment input. Lake stages are characterized by large-scale changes in sedimentological patterns and depositional trends that are controlled by a combination of climate and tectonics. (Tanavsuu-Milkeviciene and Sarg 2012, p. 1756)

The focus of this study is on fine-grained mudstone and siltstone, although textures can be difficult to relate to original grain size distributions due to significant diagenetic alteration.

8.2 Sample Collection

We collected 238 samples from segments of two wells, the Savage 24-1 (Section 24, T1S, R98W, Rio Blanco County CO; 39.955° N latitude; 108.334° W longitude [NAD 27]) and Shell 23X-2 (Section 2, T2S, R98W, Rio Blanco County CO; 39.906° N latitude; 108.362° W longitude [NAD 27]) and from two segments of an outcrop section at Douglas Pass along and near State Route 139 in Garfield County, CO (between 39.597 and 39.635 N latitude and 108.763 and 108.818 W. longitude). Figure 8.2 shows the location of wells and measured sections evaluated in this study.

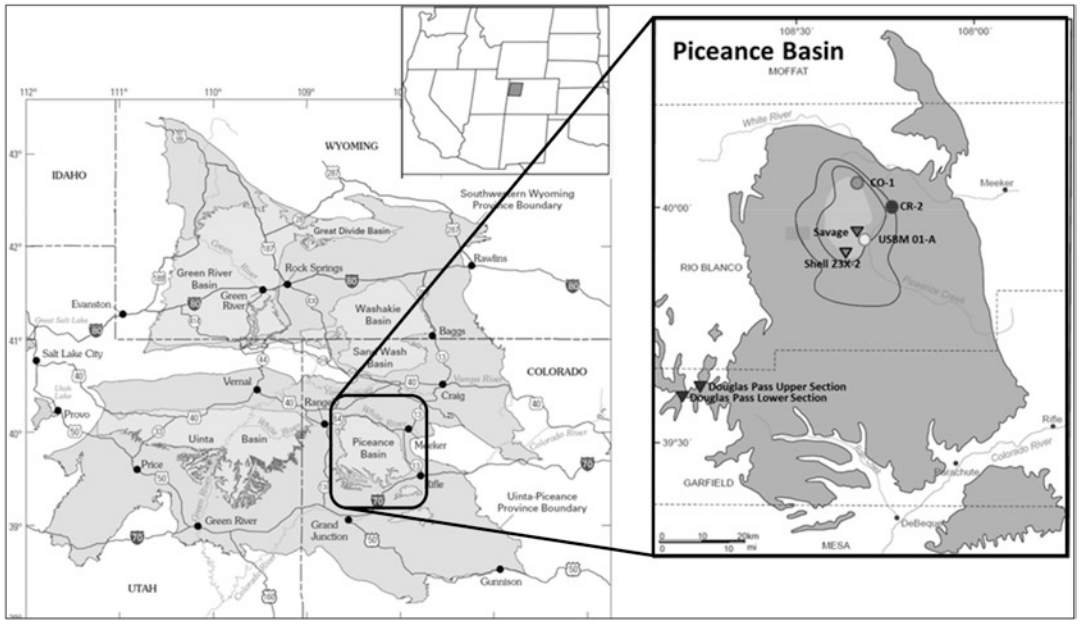

Fig. 8.2 Location of wells and measured sections evaluated in this study (Modified from Johnson et al. 2010)

Of these samples, 82 were selected for quantitative X-ray diffraction (XRD) analysis. The Savage 24-1 and Shell 23X-2 wells represent basin center deposition. The Douglas Pass outcrops are located along the Douglas Creek Arch, a structural feature that sometimes separated the Colorado and Utah portions of ancestral Lake Uinta (Murray and Haun 1974; Bader 2009). Thus, the sediment deposited there represents marginal environments of the lake, and the section includes numerous erosional intervals reflecting lake level fluctuations. Samples were taken throughout the section in all six stages of lake evolution. However, the sampling program was intended to sample representatives of individual sedimentary facies, and was not intended to provide a statistically representative sample of the full section, as the available resources were insufficient to analyze such a large number of samples. Samples were taken primarily in the lower part of the Shell 23X-2 well, representing the first two stages of lake evolution. The Savage 24-1 well terminated before reaching the lower part of the section, and samples from this well represent the upper part of the basin center section in Stages 3 through 6.

The samples consisted primarily of finer-grained sedimentary rock, as part of a joint mineralogic and organic geochemical study. The geochemistry is discussed in Feng (2011). Nahcolitic and halitic intervals were not intentionally sampled, although some mudstone samples turned out to consist largely of nahcolite. The samples collected consist primarily of mudstone, with a small number of siltstone and sandstone samples analyzed, particularly in the Douglas Pass section.

Quantitative X-ray Diffraction (XRD) patterns were gathered and analyzed on 28 samples from Douglas Pass, on 39 samples from the Savage 24-1 well, and on 15 samples from the Shell 23X-2 well. ExxonMobil had previously analyzed 35 samples from the Shell 23X-2 well for quantitative XRD mineralogy. These data were available through the database of the U. S. Geological Survey's Core Research Center (http://my.usgs.gov/crcwc/core/report/10109), and were incorporated in this evaluation of the mineralogy of the Green River Formation.

8.3 Methods

8.3.1 X-Ray Diffraction Mineralogy

Core and outcrop samples were crushed and homogenized for analysis, then riffle split into aliquots for XRD and inorganic chemical analysis. Care was taken to avoid use of aqueous solutions in sample processing to preserve water-soluble minerals (mainly halite and nahcolite) for all analyses. Shell 23X-2 and Savage 24-1 core pieces approximately 2 by 2 by 5 cm were hand crushed in a ceramic mortar and pestle using only impact forces (percussion as opposed to shearing) and sieved until all material passed through a 40 mesh screen. 22 of the 39 Savage 24-1 samples were taken from material processed for SRA organic geochemistry, which was ball-milled in steel chambers with steel ball bearings, and/or in a shatter box. Shearing effects, particularly of clay minerals, may be present in these samples, due to extended mechanical crushing times without intermittent sieving. Clay mineral levels are very low in the Savage 24-1 section. Mineral identification and quantification were not considered to be significantly affected for important phases.

All 28 Douglas Pass samples were crushed from hand specimen with a hammer, and then jaw crushed to coarse gravel. The gravel-sized material was mixed and divided using a large riffle splitter into aliquots representative of the entire specimen, at the U. S. Geological Survey in Denver, Colorado. Samples chosen for XRD were further divided using an 8-jar rotary splitter into ~20 g aliquots at the Chevron Energy Technology Center (ETC) laboratory. Selected fine-grained Douglas Pass samples were processed in the same manner as core samples by hand crushing with a ceramic mortar and pestle and sieving to 40-mesh. Most well-cemented Douglas Pass samples of sandstone or siltstone were alternately sieved and mechanically ground for less than 10 s at a time using an automatic mortar and pestle, until all material passed a 40 mesh screen.

Once samples were reduced to less than 0.4 mm grain size, they were divided using a small riffle splitter into aliquots. Next, zinc oxide was added at 10 weight percent (wt %) as an internal standard. Samples and internal standard were then wet-ground with hexane in a McCrone Mill using plastic chambers with agate beads, to less than ~2 μm to ensure a narrow particle size distribution. The 22 Savage 24–1 well samples from ball-milled material were McCrone milled for a much shorter period, just long enough to homogenize the grain sizes and mix in the internal standard, to avoid worsening of any shearing effects present. Samples were re-homogenized by hand after drying, and loosely packed into side-loading sample mounts against frosted plastic plates.

All 82 samples were characterized by XRD for quantitative bulk mineralogy at the ETC laboratory based on methods by Srodon (1999), and described in Omotoso et al. (2006). Samples were analyzed using a Thermo XTRA XB diffractometer with Cu K alpha radiation, configured with a K beta filter monochromator with fixed slit assembly and solid-state detector. Diffractometer operation settings were 40 kV and 40 mA total power. XRD scans ran 2 h per sample, from 5 to 65 degrees 2-theta, at 2 s per step, and 0.02-degree step size. Patterns were corrected for lateral shifts by aligning the pattern with the primary quartz peak at 26.6 degrees 2-theta, and primary zincite peak at 31.8 degrees 2-theta.

Sample XRD patterns were interpreted using proprietary Chevron software, which compares patterns with standard mineral patterns. Five samples with low totals and anomalous mineral compositions were also analyzed with the software JADE at the U. S. Geological Survey, to identify and quantify minerals for which standards were not available in the Chevron software. The two different programs identify and group different mineral species differently, and JADE does not quantify organic matter as the Chevron software does. Major mineral quantities agreed well between the analyses by both software programs, once they were normalized for OM and clay minerals. Chevron XRD methods have been shown to produce results that are accurate to ± 4 wt%. Samples evaluated by JADE software

showed zincite amounts up to 14 %, suggesting that internal standard addition might be a source of quantification error. The Chevron software reports clays in the following categories for bulk XRD analysis: Di 2:1 Clay (= dioctahedral 2:1 layer clay), illite, mixed-layer illite-smectite, smectite, Tri 2:1 Clay (= trioctahedral 2:1 layer clays), biotite, phlogopite, biotite/vermiculite, trioctahedral smectite; Tri 1:1 Clay (= trioctahedral 1:1 layer clay) serpentine minerals and berthierine.

Organic matter is also quantified by XRD analysis in this sample set, with a high uncertainty due to the broad undefined peak exhibited by amorphous matter. Feng (2011) analyzed the same sample set used in this study by Source Rock Analyzer (SRA) for total organic carbon (TOC) content. Organic carbon (C_{org}) was also measured by infrared spectroscopy during major and trace element analysis. The coefficient of determination for the comparison of organic matter (OM) by XRD to TOC obtained by SRA was good for the core sample sets ($r^2 = 0.84$ for Savage 24-1, and $r^2 = 0.95$ for Shell 23X-2), but less so for Douglas Pass samples ($r^2 = 0.68$), most likely a result of lower concentrations of organic matter in the basin margin than in the basin center. Correlation between C_{org} and TOC was very good ($r^2 = 0.99$). Correlation between Corg and OM by XRD is lower ($r^2 = 0.70$), suggesting that OM by XRD is the least reliable measure of organic content. The organic matter types are comparable across the sample suite, so that variations in hydrogen content (included in OM, but not in TOC or C_{org}) are unlikely to be responsible.

Buddingtonite, dawsonite and nahcolite present in the GRF are represented by only one standard in the Chevron software databases. The ability to test patterns against more than one standard can be important to accurate quantification, and may be a source of uncertainty in the results. Solid solution minerals also posed some problems for analysis. Buddingtonite, which has a very diagnostic peak at 20.5 degrees 2-theta, characteristically showed a shift probably explained by buddingtonite representing solid solution in potassium feldspar (as observed by Svensen et al. 2008, and Ramseyer, et al. 1993). The mineral is significant enough that it was reported separately, but quantification may be less accurate. Dolomite-ankerite series minerals were lumped in these analyses, as it appeared that a substantial compositional range existed. The nahcolite standard pattern in the Chevron software is missing peaks identified in all nahcolite-bearing samples at 55.3, 58.4, 60.8 degrees 2-theta. A standard pattern obtained with JADE from the International Centre for Diffraction Data® (ICDD®) database for comparison shows these peaks for nahcolite, suggesting that the nahcolite standard in the Chevron software may not have been scanned to the full 65 degrees.

8.3.2 Scanning Electron Microscopy – Energy Dispersive Spectrometry (SEM-EDS)

Four basin center Savage 24-1 core samples with high proportions of authigenic minerals according to XRD results were analyzed by SEM-EDS at the Colorado School of Mines. The selected thin sections were polished and sputter coated with gold. The instrument used was a JEOL 840A equipped with a Princeton Gamma Tech Avalon EDS system, run at 20 kV accelerating voltage. The beam voltage was turned down to 10 kV for samples containing saline minerals such as nahcolite, to attempt to obtain EDS spectra of minerals with less stable components.

8.4 Results

8.4.1 Minerals Present

Thirty-five mineral species were identified by XRD in the samples analyzed (See Table 8.1). Of these, sixteen minerals occurred with sufficient frequency and abundance in the sample population to be considered of primary importance. These minerals are highlighted in the table in boldface. Most of the others were trace constituents, or occurred in only one or two samples. Full mineralogic abundances are tabulated in Poole

Table 8.1 Minerals identified in the Green River Formation in this study, with representative formulas

Mineral	Formula[a]
Framework Silicates	
Quartz	SiO_2
Potassium Feldspar	$KAlSi_3O_8$
Albite	$NaAlSi_3O_8$
Buddingtonite	$NH_4AlSi_3O_8 \bullet 0.5H_2O$
Analcime	$NaAlSi_2O_6{\cdot}H_2O$ – $NaAlSi_3O_8{\cdot}H_2O$
Sheet Silicates	
Muscovite/sericite	$K_2Al_4\ (Al_2Si_6O_{20})(OH)_4$
Illite	$K_{1-1.5}Al_4(Si_{7-6.5}Al_{1-1.5}O_{20})(OH)_4$
Illite-smectite	$(K,Na,Ca_{0.5})_{0.6}(Al)_4[(Si,Al)_8O_{20}](OH_4)\bullet nH_2O$
Kaolinite	$Al_2Si_2O_5(OH)_4$
Chlorite	$(Mg,Al,Fe)_{12}[(Si,Al)_8O_{20}](OH)_{16}$
Trioctahedral Clay	$(K,Na,Ca_{0.5})_{0.6}(Mg,Fe)_4[(Si,Al)_8O_{20}](OH_4)\bullet nH_2O$
Divalent Carbonates	
Calcite	$CaCO_3$
Aragonite	$CaCO_3$
Mg-Calcite	$(Ca,Mg)CO_3$
Dolomite	$CaMg(CO_3)_2$
Ferroan Dolomite	$Ca(Mg,Fe)(CO_3)_2$
Siderite	$FeCO_3$
Magnesite	$MgCO_3$
Kutnohorite	$CaMn(CO_3)_2$
Sodium Carbonates and Salts	
Halite	NaCl
Nahcolite	$NaHCO_3$
Dawsonite	$NaAl(OH)_2CO_3$
Natrite	Na_3CO_3
Northupite	$Na_3Mg(CO_3)_2Cl$
Sulfides and Sulfates	
Pyrite	FeS_2
Marcasite	FeS_2
Gypsum	$CaSO_4{\cdot}2H_2O$
Anhydrite	$CaSO_4$
Barite	$BaSO_4$
Rare or trace minerals	
Amphibole	$Ca_2(Mg,Fe)_4Al(Si_7AlO_{22})(OH)_2$
Apatite	$Ca_5(PO_4)_3(OH,F,Cl)$
Woodhouseite	$CaAl_3(SO_4)(PO_4)_3(OH)_6$
Brucite	$Mg(OH)_2$
Gibbsite	$Al(OH)_3$
Anatase	TiO_2

Major phases are in boldface

[a]Formulas for solid solution minerals are nominal compositions and do not reflect the exact composition of the phase identified

(M. S. Thesis 2014). The list of significant minerals is substantial, as could be expected in a mixed carbonate-clastic environment in which evaporite formation occurred and diagenetic alteration is consequently high.

8.4.2 Stratigraphic Variation of Mineralogy

The variation of mineralogy with stratigraphic position is illustrated in Figs. 8.3, 8.4 and 8.5 for the basin center in the two well sections, and for the basin margin at Douglas Pass. A number of distinctive features of basin center mineralogy stand out in the figures, and provide important reference points for examining the variation of the chemistry of Lake Uinta. The summary stage descriptions paraphrase the descriptions in Tanavsuu-Milkeviciene and Sarg (2012, 2015).

Stage 1 (the fresh to brackish lake) is characterized by establishment of widespread lacustrine deposition in a relatively short stratigraphic interval, comprising organic-rich illitic oil shale and by relatively reducing conditions (Feng 2011). In the basin center, Stage 1 is characterized by the presence of abundant illitic clay, low abundance of feldspar and absence of dawsonite and nahcolite (Fig. 8.3). The feldspar contains a relatively high fraction of buddingtonite. Dolomite – ferroan dolomite –ankerite are the dominant carbonate minerals. Three samples in the Shell 23-X2 well contain significantly more calcite than dolomite. The Douglas Pass section shows a similar mineralogic character in Stage 1, although calcite/calcite + dolomite ratios are generally higher

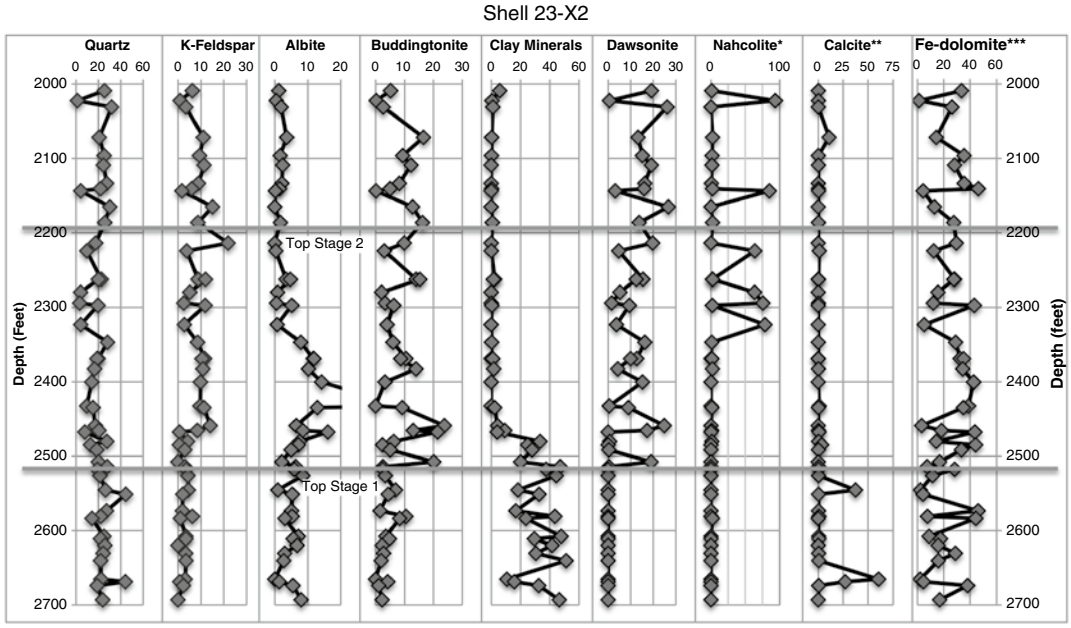

Fig. 8.3 Variation of significant minerals in the Shell 23X-2 well, in weight percent. Stage boundaries of Tanavsuu-Milkeviciene and Sarg (2012) are shown (* nahcolite includes natrite, northupite, halite; ** calcite includes Mg-calcite and aragonite; *** Fe-dolomite includes dolomite, Fe-dolomite and siderite)

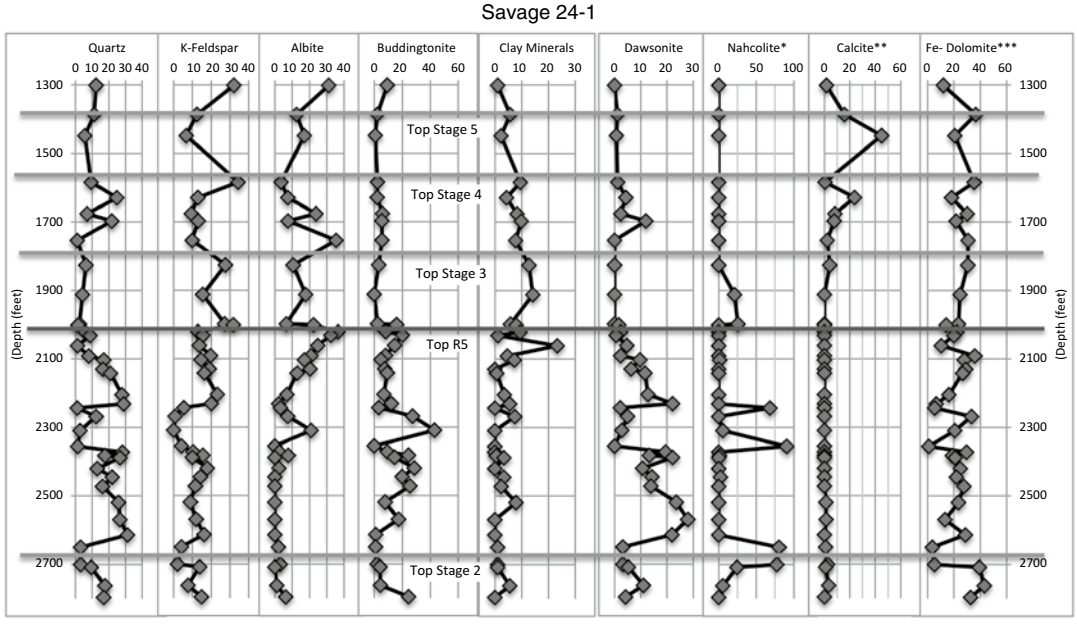

Fig. 8.4 Variation of significant minerals in the Savage 24-1 well, in weight percent. Stage boundaries of Tanavsuu-Milkeviciene and Sarg (2012) are shown (* nahcolite includes natrite, northupite, halite; ** calcite includes Mg-calcite and aragonite; *** Fe-dolomite includes dolomite, Fe-dolomite and siderite)

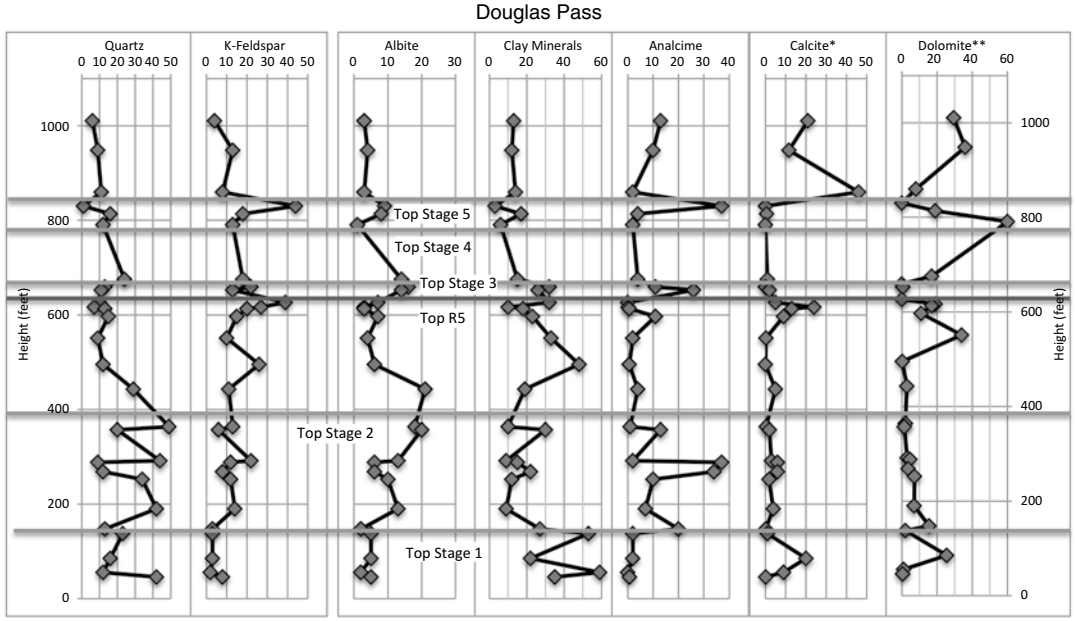

Fig. 8.5 Variation of significant minerals in the Douglas Pass Section, in weight percent. Stage boundaries of Tanavsuu-Milkeviciene and Sarg (2012) are shown (*calcite includes calcite and Mg-calcite and aragonite; **dolomite includes dolomite, Fe-dolomite and siderite)

in the basin margin than in the basin center throughout the section (Fig. 8.5).

Stage 2 (the transitional lake) is characterized by an influx of clastic sediment to the basin, possibly in response to flash floods during increasingly arid conditions. Lack of well-developed soil horizons in this interval suggests that this influx was only partially driven by basinward migration of clastic facies due to lower lake levels during arid times. One of the transitions in Stage 2 is a transition in the basin center section in which clay mineral content decreases to low values and dawsonite increases (Fig. 8.3). Still higher in the section, nahcolite appears. Although the sampling program chose to avoid nahcolite-rich samples in which the nahcolite was present as visible grains (commonly well-formed crystals), a number of samples contained very high levels of nahcolite. Thus, the distribution of nahcolite abundances is distinctly bimodal, although this may not reflect the actual distribution in the section. At the same time, potassium feldspar and buddingtonite increase in abundance with respect to Stage 1. Albite shows a slight increase, then a decrease through Stage 2. In the Douglas Pass section, there is a similar decline of clay mineral content, although the clay content does not decrease as markedly. Albite appears to increase throughout the section, and analcime appears as a prominent constituent of the mineralogy, especially later in the stage. Dolomite declines upward and carbonates are generally low in abundance.

Stage 3 (the fluctuating lake) is characterized by highly fluctuating lake levels and cyclic sedimentation on a scale of meters, with substantial thickness of laminated oil shale, oil shale breccia and evaporite mineral deposition, both of nahcolite and halite. In the basin center during Stage 3, the abundance of saline minerals (dawsonite, nahcolite) remains generally high through much of the unit until the R5 zone, where dawsonite and quartz both decline in abundance. Dawsonite declines to zero at the top of R5. Buddingtonite also drops sharply at about this interval. The abundance of albite increases toward this transition in parallel with the decrease in dawsonite and quartz. Potassium feldspar appears to increase across this transition as well. Clay content appears to increase at or near the top of R5

from below to above 10 wt%. Nahcolite is present above this level, but disappears before the end of the stage, probably due to dissolution during a well-documented later dissolution event (Hite and Dyni 1967). Dolomite appears to vary in abundance in cycles that reflect the fluctuating character of this stage. Calcite reappears just above R5. In the Douglas Pass section, this transition is more complicated. K-feldspar appears to increase up to the top of R5, then drop abruptly. Quartz and clay minerals appear to decline through the stage, but the clay minerals increase just at the top of the stage. Analcime, low through much of the stage, appears to increase in the vicinity of R5. It may be that sample density is not enough to define a consistent trend in the basin margin.

Stage 4 (the rising lake) is characterized by rising lake levels, more consistently laminated oil shale deposition, deeper lake deposits indicating flooding of the Douglas Creek Arch, and turbidite deposition. *Stage 5 (the high lake)* represents the widest expansion of Lake Uinta, and is characterized by widespread profundal laminated oil shale deposition, and less common oil shale breccia. Nahcolite continued to be deposited, primarily as nodules, and in lesser amounts, although in many places it has been subsequently removed by dissolution. *Stage 6 (the closing lake)* is characterized by steadily increasing volumes of siliciclastic sediment, prograding from the north, northeast, and northwest. In the remaining deeper sections of the lake, turbidite deposition is common. In the basin center, Stage 4, Stage 5 and Stage 6 are marked by a brief recurrence of dawsonite plus quartz (as well as buddingtonite) in stage 4, and a decline in feldspar abundance, particularly albite, although this trend is reversed at the top of Stage 5 and into Stage 6. The clay content continues a downward trend begun in stage three. Calcite generally increases in abundance upward through the three stages. In the Douglas Pass basin margin section, the three stages show a general decline in clastic minerals (quartz, feldspar, and clay minerals), and a rise in carbonate minerals, with widely varying calcite/calcite + dolomite ratios. Analcime is also highly variable in these stages.

8.4.3 Summary of Basin Center and Basin Margin Mineralogy

The mineralogic variations described above lead to the definition of three mineralogic units, Lower (Stage 1 and transition zone in Stage 2); Middle (remainder of Stage 2 and Stage 3 to the top of R5); and Upper (remainder of Stage 3 and Stages 4, 5, and 6). The boundaries separating the three units are drawn at the top of the two major transitions described in the previous section. The Lower unit ends at the top of the transition to clay-poorer compositions in both the basin margin and basin center. This is also near the first occurrence of dawsonite in the basin center. The Middle unit ends with the sharp reduction in dawsonite abundance at or near the top of the R5 zone in the basin center. The mean abundances of major minerals in the basin margin and basin center samples for the Lower, Middle and Upper mineralogic units are summarized in Table 8.2, and the average values are displayed in Fig. 8.6. The sample sizes are small for the basin margin section, and inferences of patterns may be uncertain in this part of the basin.

The four most abundant minerals in each unit are highlighted in bold in the table. Feldspar is the only mineral that is in this grouping in all three mineralogic units in both basin environments. It increases in abundance upward in the basin center section, and from the Lower to the Middle units in the basin margin. Buddingtonite occurs in only two samples in the basin margin section. In both basin areas, clay mineral content decreases and feldspar and dolomite content increase between the Lower and Upper units. However, in the basin margin, the Middle unit shows a slightly lower dolomite + siderite content, comparable to the Lower unit, whereas the feldspar content is more comparable to the Upper unit. Quartz shows a decline upward in the basin center section, and between the Middle and Upper units of the basin margin section.

Dawsonite and nahcolite are present in the Middle unit in the basin center, but absent or nearly so in the lower unit and in the entire basin margin section. Nahcolite is absent as a result of dissolution in much of the Upper unit in the basin center (Hite and Dyni 1967). However, we have

Table 8.2 Average and standard deviation of major mineral abundances and organic content in three mineralogically defined portions of the sampled sections

	Basin center (Shell 23-X2 & John Savage 24–1)			Basin margin (Douglas pass section)		
Mineral	Lower (24)	Middle (56)	Upper (12)	Lower (5)	Middle (14)	Upper (9)
Quartz	**24.3** ± 7.7	**16.4** ± 9.2	**9.0** ± 7.6	**21.2** ± 12.4	**21.8** ± 14.8	11.4 ± 6.4
Feldspar	**12.1** ± 4.7	**28.2** ± 16.0	**40.3** ± 16.6	**8.0** ± 3.2	**26.6** ± 8.7	**25.3** ± 14.7
K-Feldspar	2.6 ± 1.7	10.2 ± 5.7	19.4 ± 10.3	3.8 ± 2.4	16.8 ± 9.0	17.0 ± 11.5
Albite	4.9 ± 2.4	7.2 ± 9.4	16.3 ± 10.1	3.8 ± 1.6	9.8 ± 6.2	8.0 ± 5.6
Buddingtonite	4.6 ± 4.3	10.8 ± 8.8	4.6 ± 4.4	2[a]	ND	3[a]
Clay minerals	**28.9** ± 14.3	2.2 ± 3.9	7.4 ± 3.9	**39.2** ± 16.2	**20.7** ± 11.6	**15.3** ± 9.0
Dolomite/Siderite[b]	**19.5** ± 14.5	**24.0** ± 12.4	**25.0** ± 8.0	**8.9** ± 11.2	8.1 ± 9.5	**18.9** ± 20.2
Calcite/Aragonite[c]	6.4 ± 15.8	0.5 ± 1.5	**9.1** ± 13.5	6.1 ± 8.6	5.7 ± 6.4	9.1 ± 15.6
Dawsonite	1.0 ± 4.1	11.2 ± 8.0	1.9 ± 3.4	ND	ND	ND
Nahcolite[d]	0.2 ± 0.5	**14.8** ± 29.4	2.1 ± 7.4	5[a]	ND	ND
Analcime	0.3 ± 0.8	ND	1.2 ± 1.5	4.9 ± 8.5	**8.7** ± 12.2	**12.1** ± 12.0
Pyrite/Marcasite	2.6 ± 1.9	1.6 ± 1.6	1.7 ± 1.2	0.8 ± 0.7	1.1 ± 1.9	0.3 ± 0.4
Organic matter[e]	9.3 ± 3.7	12.6 ± 6.3	13.7 ± 8.8	8.8 ± 2.4	6.8 ± 3.1	6.6 ± 4.0

Number of samples in parentheses; top four mineral abundances in bold
ND not detected
[a]Single sample values
[b]Dolomite/siderite includes dolomite, ferroan dolomite and siderite
[c]Calcite/aragonite includes calcite, Mg-calcite, and aragonite
[d]Nahcolite includes nahcolite, natrite, northupite and halite
[e]Organic matter for basin center not measured in 35 samples from USGS database; mineral averages were normalized to 100 % without organic matter for these samples

not observed the dissolution features evident in basin center deposits (in core and outcrop) in any part of the section at the basin margin. Analcime is abundant only in the basin margin, and increases upward in the section. Carbonate minerals are more abundant in the basin center than in the basin margin. Calcite and aragonite are almost completely absent in the Middle unit of the basin center. Three samples in the Lower unit have high calcite content. The Upper unit of each section shows higher calcite + aragonite content.

Mineral constituents generally found as clastic sediment (quartz, feldspar, clay minerals) are consistently present at higher amounts than divalent carbonate minerals and nahcolite, reflecting the balance of clastic and chemical sedimentary constituents. The clastic minerals are only less than 50 % of the total in the basin center where diagenetic minerals such as dawsonite and analcime are significant constituents. The discussion section below considers the effect of diagenesis on the relationship of clastic and chemical constituents in these mineralogically complicated sedimentary rocks.

8.4.4 Mineralogic Variation of Major Constituents of Green River Formation

The mineralogy of the 117 analyzed samples is further summarized graphically in Fig. 8.7, which shows the relative proportions of major components of these fine-grained rocks. The base of the ternary plot in Fig. 8.7a shows the clastic constituents as clay minerals at one apex and the main framework silicates, quartz and feldspar, at the other. At the top of the figure is the chemical sedimentary component, the divalent carbonates. The figure leaves out the evaporative and diagenetic sodium bicarbonate and carbonate minerals (nahcolite and dawsonite), as well as analcime, also a diagenetic constituent. The average shale of Hillier (2006) is shown for comparison. The figure shows the diversity of composition, from argillaceous mudstone to siliceous and feldspathic mudstone to dolomitic mudstone. It is significant to note that, even in the portions of the section where clay content is minimal, many

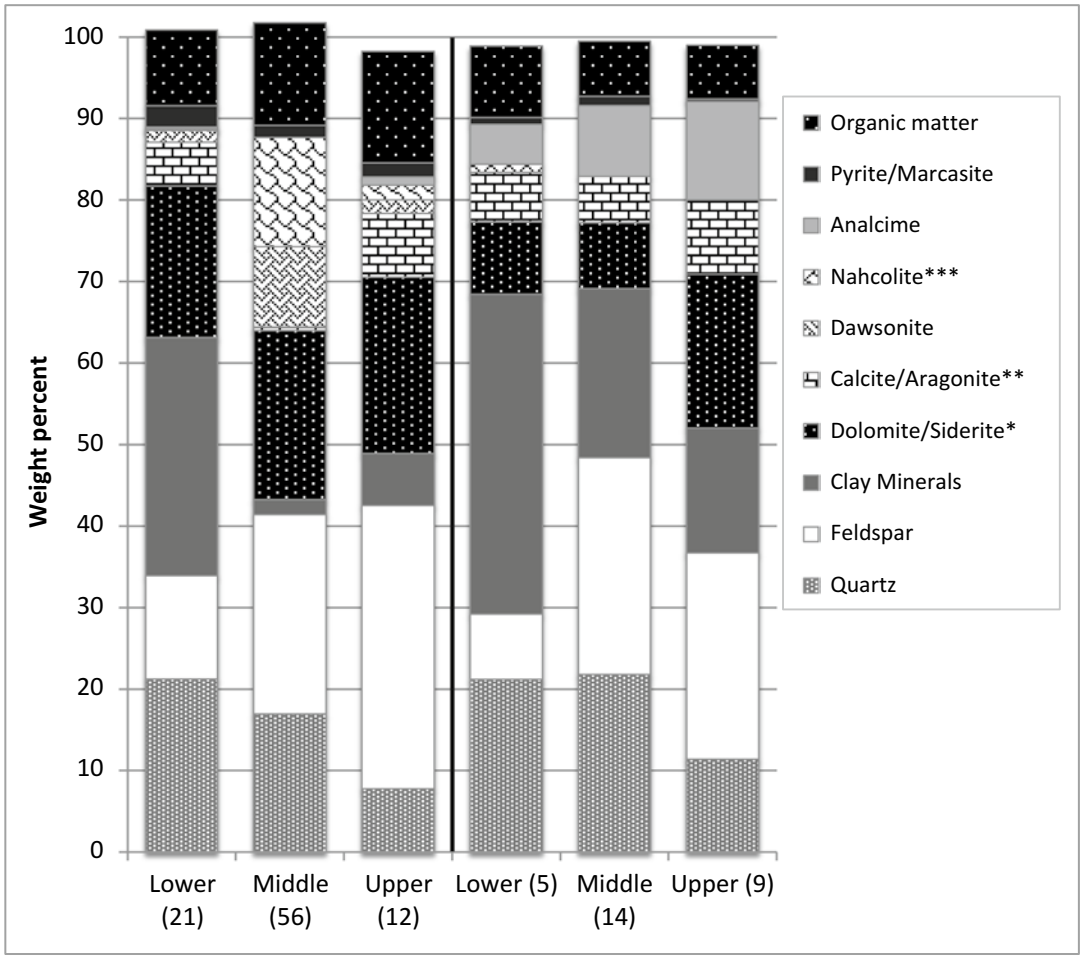

Fig. 8.6 Average mineralogy of mudstone and siltstone of Green River Formation in the Piceance Basin showing general compositional changes between three mineralogic units in the basin margin and basin center. Number of samples is shown in parentheses (***nahcolite includes natrite, northupite, and halite; **calcite/aragonite includes Mg-calcite; *Dolomite/siderite includes Fe-dolomite)

samples would be classified as feldspathic mudstones. These quantitative data counter a common assertion that oil shale is properly marlstone – a mix of clay and carbonate whose definition is vague (Brobst and Tucker 1973; Katz 1988, for example).

Figure 8.7b plots the major clastic silicate minerals on a second ternary diagram with quartz and feldspar along the base, and clay minerals at the apex. The chart indicates that a surprising number of the samples in both basin center and basin margin are highly feldspathic. The average shale of Hillier (2006) is shown for comparison. Possibly the most distinctive feature of the composition of fine-grained Green River Formation samples is the high feldspar content, not necessarily the high carbonate content. Note that the more clay-rich rocks of the lower sections are siliceous rather than feldspathic.

8.5 Comparison to Existing Mineralogic Data

Two substantial mineralogy datasets spanning much or all of the GRF in the Piceance Creek Basin exist. Both are from basin center wells, the CR-2 (Dean et al 1981) and the USBM/AEC Colorado Core Hole No. 1 (Robb and Smith 1974). Both present semi-quantitative mineralogy,

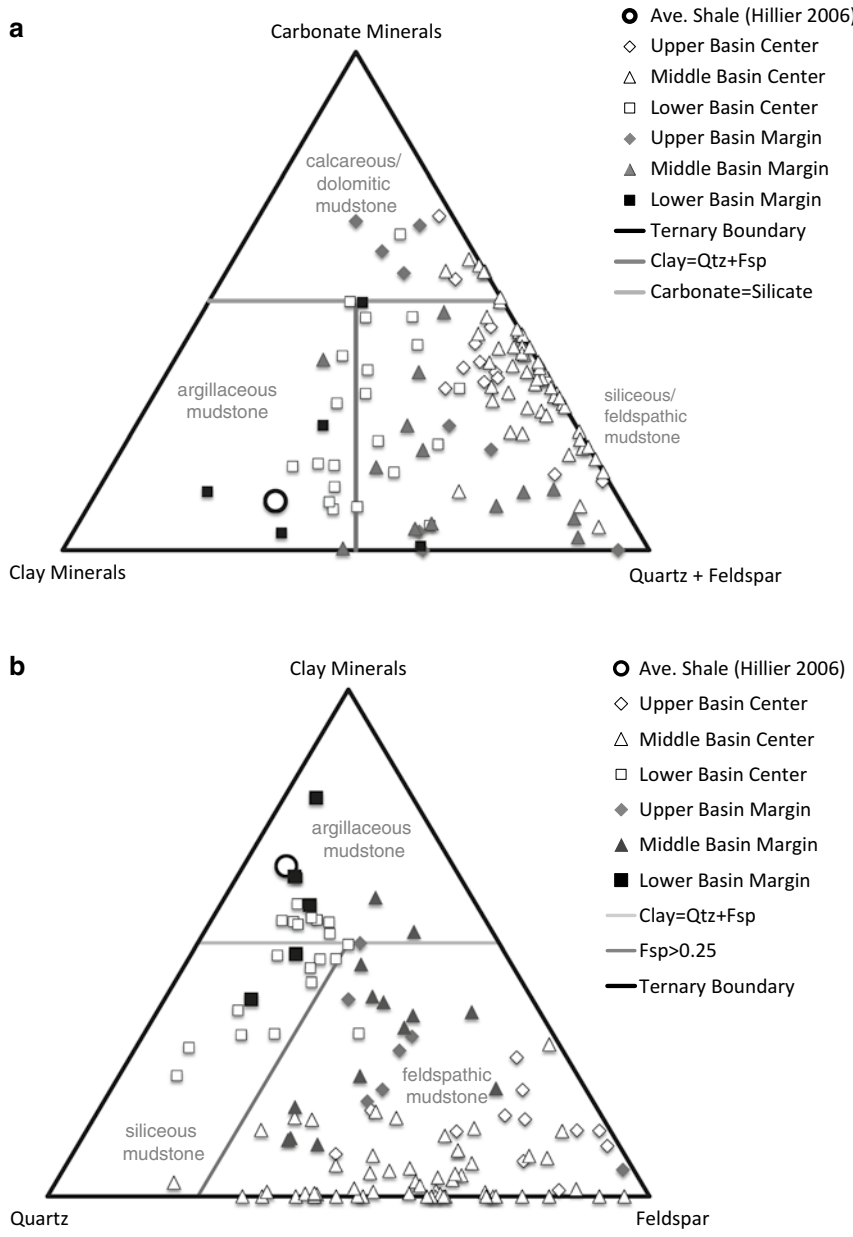

Fig. 8.7 Mineralogy of oil shale samples from three parts of the section in the basin margin and basin center. Average shale of Hillier (2006) is also shown. (**a**) Ternary plot of clay minerals – quartz + feldspar – carbonate minerals indicates the compositional diversity of Green River Formation mudstone and siltstone. (**b**) Ternary plot of clay minerals – quartz – feldspar indicates highly feldspathic character of mudstone and siltstone in both basin margin and center

as they were gathered at a time when quantification of X-Ray Diffraction data was in an early stage of development. Values reported are relative peak height amplitude, which is useful for sample-to-sample comparison for individual minerals, but less certain for mineral-to-mineral comparison within a given sample. However, both datasets involve very high density sampling of the section, so they provide valuable comparison datasets to the sparser sampling completed in this preliminary survey. Thanks to a data file transferred to us by John Dyni, U. S. Geological Survey [personal

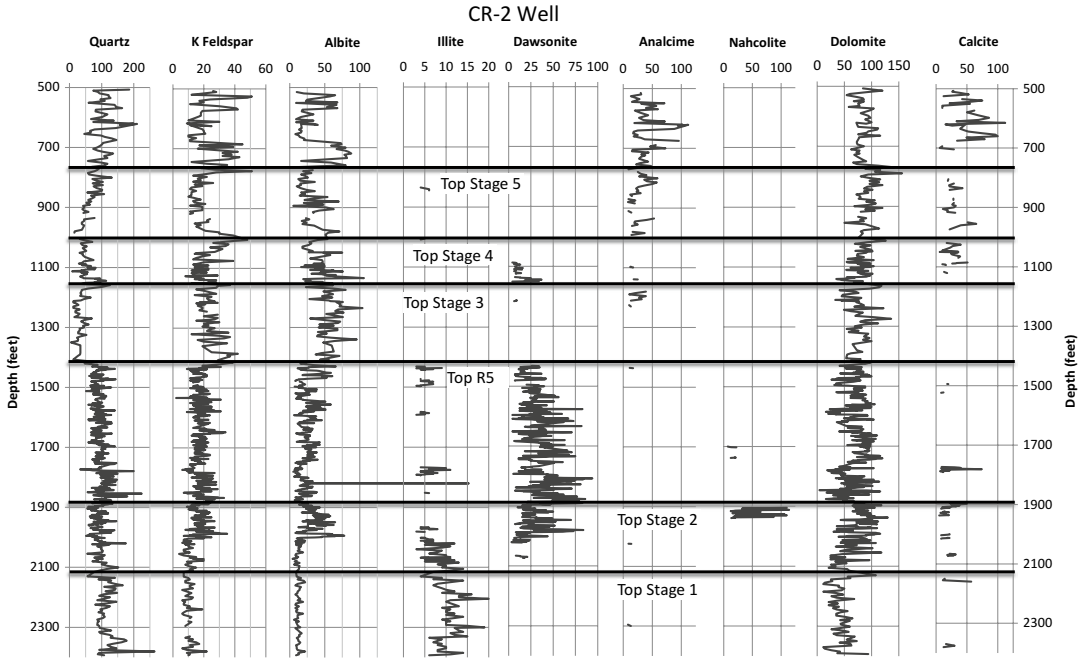

Fig. 8.8 X-ray Diffraction peak heights for samples from The U. S. Geological Survey CR-2 well, with stage boundaries and the top of the R5 zone added (Data tabulated from file from J. Dyni (Personal communication) containing data presented in Dean et al. 1981)

communication], we have been able to create digital files of the peak height intensity for the CR-2 dataset, which is summarized in Fig. 8.8. The profile from Robb and Smith is only available in printed form, and the image in Fig. 8.9 has been scanned from the Rocky Mountain Association of Geologists 1974 Field Guide in which it was published (Robb and Smith 1974).

The two major transitions identified in this paper are both prominently visible in the published profiles. The decline in clay mineral abundance and increase in dawsonite abundance in Stage 2 (the transitional lake) in well CR-2 parallels that in our basin center dataset. Unfortunately, clay minerals were not included in the data for the Colorado 1 well, although the text mentions the decrease in clay content in this interval. The boundary between clay-rich and clay poor composition has long been recognized (Brobst and Tucker 1973; Smith and Robb 1973; Trudell et al. 1970). The increase in feldspar content across this boundary is also evident in both wells. Dolomite content appears to increase in these two wells, starting slightly before this transition. This change is not clearly evident in our data, as high dolomite content occurs in several samples in Stage 1 in the Shell 23X-2 well. The average value is slightly lower for this zone, but the variance is large in both zones.

In addition, both profiles show the disappearance of dawsonite at the top of the R5 zone near the top of Stage 3 (the fluctuating lake), and its brief recurrence in Stage 4 (the rising lake). In both wells, as in our samples, the disappearance of dawsonite is accompanied by a decrease in quartz content. Robb and Smith (1974) argue that, in general, the visually observed inverse relationship between the dawsonite + quartz pair and albite was not statistically significant in the portions of the section where they completed a statistical evaluation of peak height. However, over the transition from R5 to L5, the trend is fairly clear in all three wells described here. The fact that albite and quartz are present as detrital minerals throughout the section may make correlation less likely throughout the well, or in any other interval, but it is hard to suggest the stratigraphic transition is not significant in this zone.

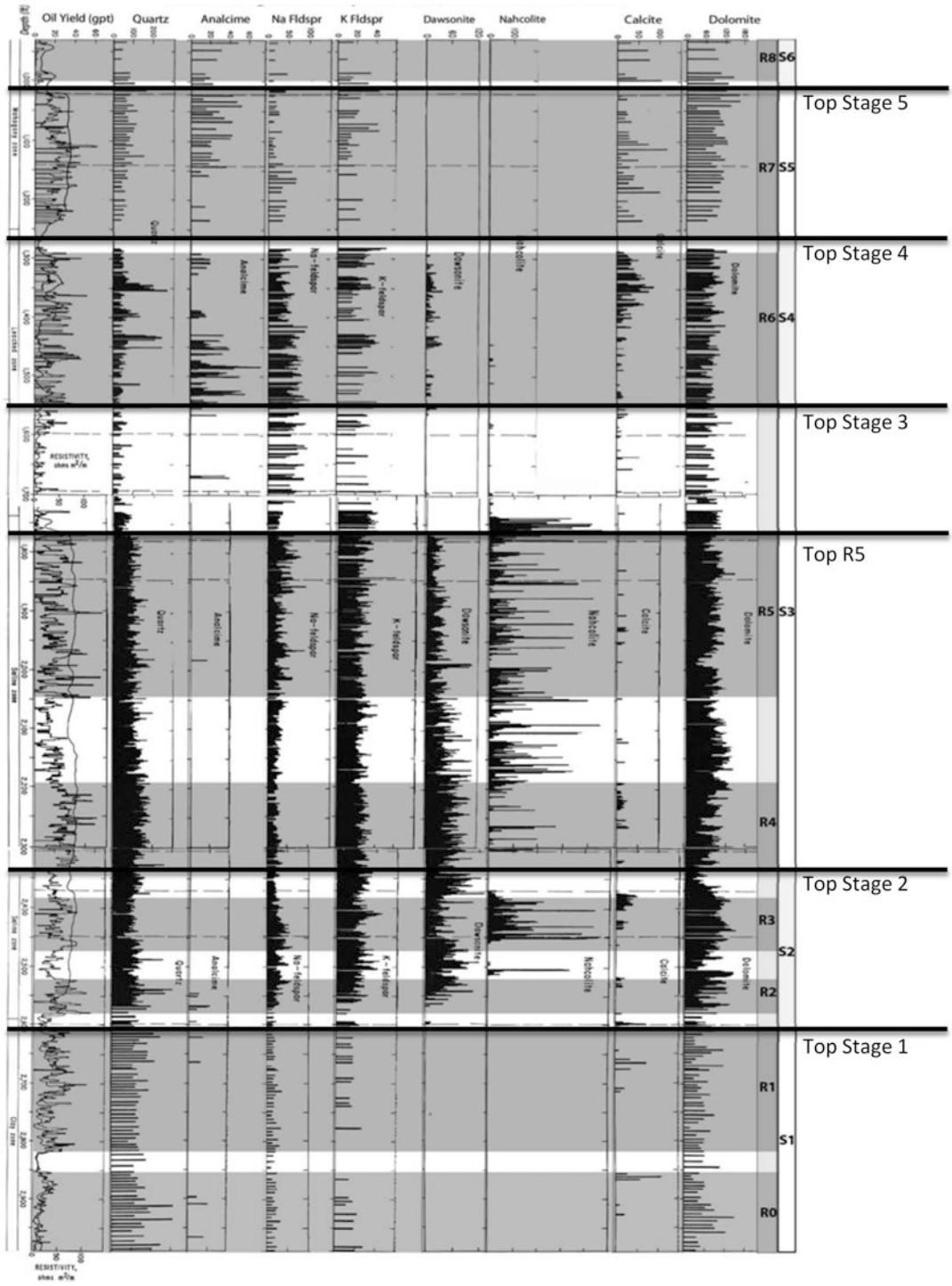

Fig. 8.9 Qualitative mineralogic profile through USBM/AEC Colorado Core Hole No. 1, with rich zones shaded and numbered, and stages numbered (Modified after Robb and Smith 1974)

The CR-2 well is distinctive in having only one very short segment of nahcolite-bearing rock with a few other limited occurrences. This well appears to be at the edge of the depositional area for nahcolite, which apparently does not extend as far out as the dawsonite zone. Much later dissolution has removed nahcolite (Hite and Dyni 1967), generally above the R5 section in numerous wells. The disappearance of nahcolite due to dissolution is evident in the Fischer Assay Gas + Loss values for many wells, and its disappearance in the Colorado-1 well is an example. Nahcolite is essentially absent from a level in the L5 zone not far above the top of R5. This dissolution event is evident in many cores, and especially in outcrop sections, which preserve nahcolite crystal forms in the walls of solution vugs. These features clearly indicate that high salinity of the lake water outlasted the disappearance of dawsonite.

The slight increase in clay content above R5 that was observed in our data is not evident in the CR-2 well. An increase in calcite abundance in stage 4 (rising lake) and stage 5 (high lake) is similar to the trend in the Savage 24-1 well. Small quantities of analcime are also present in the Savage 24-1 well in Stages 3 (above R5), 4, and 5. A similar trend appears in the CR-2 well, with the highest values in Stage 6 (closing lake), for which there is only one sample in the Savage 24-1 well dataset.

8.6 Discussion

The mineralogy of the GRF is complicated by the fact that it comprises three main mineral components – silicate minerals, divalent carbonate minerals, and sodic saline minerals. Some minerals in each group represent primary phases deposited as sedimentary particles (clastic or chemical), whereas others are authigenic, reflecting diagenetic alteration. Some minerals occur in both categories. It is also clear that some authigenic minerals reflect synsedimentary alteration, probably through pore fluids in communication with lake waters, whereas others may reflect burial diagenesis. Draping of sediment over nahcolite nodules (Jagniecki and Lowenstein 2015) is a common feature indicating formation prior to significant sediment compaction, whereas formation in veins or formation of minerals requiring elevated temperature (such as shortite [Jagniecki et al. (2013)]) are indicative of burial diagenesis. In general, the stratigraphic variations in abundance of most authigenic minerals in the sections we have sampled suggests that they are synsedimentary. However, diagnostic features separating synsedimentary from burial diagenetic formation in these very fine-grained sediments have not yet been identified.

Silicate minerals like quartz, feldspar and clay minerals, are commonly found as clastic minerals. However, each of these can form as authigenic minerals during sedimentation and lithification. Poole (2014) has identified clear examples of euhedral albite and potassium feldspar presumed to be authigenic in origin. She was not able to identify buddingtonite as a separate phase, and we interpret it as a diagenetic alteration mineral present as zones in potassium feldspar (Oh et al. 1993; Ramseyer et al. 1993; Svensen et al. 2008). It is also possible that the buddingtonite occurs in restricted zones not found on the thin section examined under the SEM. Because of mineral relationships discussed in this section, we interpret albite as occurring both as a detrital constituent and as an authigenic mineral. We do not have evidence for diagenetic clay mineral formation, and regard it as primarily clastic in origin, but have not yet examined it under the SEM. Quartz appears to be present as both a clastic and authigenic mineral. Although quartz and feldspar also appear to be present as authigenic minerals, they are in general forming from constituents likely to have been present as clastic minerals originally. Albite may have incorporated chemical constituents from the lake water, potentially biasing the average values reported above in favor of clastic minerals. At the same time, dawsonite and analcime, which we interpret as entirely authigenic, appear to have formed in part from clastic minerals (or possibly glassy volcanic tuff constituents), which would decrease the clastic total.

Divalent carbonates such as aragonite, calcite, dolomite (including ferroan dolomite), and sider-

ite might form by direct precipitation, although aragonite and calcite are the only two that are generally considered primary (biologically moderated) precipitates. The series dolomite-ankerite is commonly considered to be secondary in nature, forming after original calcite or aragonite in environments of elevated salinity (Holland 1978; Eugster and Hardie 1978). Eugster and Surdam (1973) suggested that dolomite in the Green River Formation was formed as a secondary mineral in shallow playa environments and was swept off into deeper parts of the lake by floodwaters, thus constituting a clastic mineral formed by diagenetic alteration of an original chemical precipitate. On the other hand, Desborough (1978) presents volumetric arguments that dolomite formed in place, probably with significant influence of algal organic matter that may have been enriched in magnesium. Iron, presumably carried into the lake as oxides and hydroxides as well as other minerals, is present only in pyrite and ferroan dolomite (± siderite) in these samples. The Fe has been reduced by the anoxic conditions of the deeper lake, and further enables the formation of dolomite-ankerite. Mason (2009) has likewise suggesting the derivation for iron in siderite from clastic sediment input, and its importance in forming ferroan dolomite and ankerite. He also highlights the potential for microbial action as critical in the formation of siderite. Mason and Surdam (1992) also highlight the likelihood of diagenetic processes in forming Fe-dolomite. In general, we interpret dolomite and ferroan dolomite found in both basin margin and basin center to be a diagenetic mineral formed at or near the sediment-water interface. There does seem to be a zonation similar to that observed by Mason and Surdam (1992) in that the shallowest water carbonates tend to be calcitic, the deeper carbonates in the basin margin dolomitic (including ferroan dolomite) and the basin center carbonates are relatively uniformly ferroan dolomite-ankerite. Much remains to be worked out in these very fine-grained rocks regarding the formation and alteration of carbonate minerals.

The dominant saline minerals in this sample suite are nahcolite, halite and dawsonite. Nahcolite and halite formed as chemical precipitates, both in the water column and as displacive crystals within sediment (LaClair and Lowenstein 2009, 2010; Jagniecki and Lowenstein 2015). Poole (2014) showed fine blades of dawsonite cutting across bedding in basin center mudstone, indicating that it is authigenic (see also Smith and Milton 1974). Brobst and Tucker (1973) suggested that dawsonite formed by alteration of analcime in turn formed from a zeolite precursor, which was itself formed from volcanic tuff. Their interpretation was based on occurrences of both minerals in sections near the margin of Lake Uinta in Colorado. The sparse occurrence of analcime even in the lower part of the basin center section, where saline minerals do not form, argues against this interpretation. On the other hand, Remy and Farrell (1989) suggests that analcime formed by alteration of clay minerals. The inverse relation noted between clay minerals and dawsonite at the top of the Lower mineralogic unit favors this mechanism of formation in the sections we examined.

The data presented here can be summarized by the following observations regarding the character of basin margin and basin center mineralogy:

1. Basin margin mudstone, siltstone, and fine sandstone samples are comprised of clastic sedimentary minerals – quartz, feldspar and clay minerals, with lesser carbonate content, although carbonate content increases substantially in the Upper mineralogic unit (the rising lake [4] and high lake [5] stages), due to flooding of the Douglas Creek Arch, which appears to have isolated this formerly marginal area from clastic sediment supply. The samples show a near absence of nahcolite, dawsonite, and buddingtonite that would be indicative of hypersalinity (nahcolite, dawsonite) and perhaps of reducing conditions (buddingtonite – see Ramseyer et al. 1993). Clay minerals are common throughout the section, although average amounts decrease upward in the section. In the Middle unit, this appears to reflect increased silt and fine sand contribution, whereas in the Upper unit, it reflects greater carbonate deposition. The basin margin clay mineral suite includes kaolinite, chlorite, and trioctahedral smectitic clay as well as abundant illite (and illite/smectite). Calcite + aragonite/total carbonate ratios are highly variable, but

generally higher than in the basin center. Analcime occurs throughout the section, and appears to be the main diagenetic silicate mineral, although the possibility exists that some feldspar is also diagenetic in origin. Authigenic minerals include analcime, ferroan dolomite and possibly feldspar.

2. Basin center mudstone is also generally high in silicate minerals presumed to reflect clastic constituents (quartz, feldspar, clay minerals). Clay minerals are abundant only in the Lower unit. Feldspar content increases throughout the section. Buddingtonite is a common constituent of the feldspar fraction, primarily in the Lower and Middle mineralogic units. With the exception of three samples, dolomite (including ferroan dolomite) is the dominant carbonate. Calcite abundance increases in the Upper unit. Dawsonite and nahcolite are present in the Middle unit. Authigenic minerals include three types of feldspar (albite, K-feldspar, and buddingtonite) as well as dolomite (including ferroan dolomite), dawsonite (in the Lower and Middle units) and minor analcime (in the Upper Unit). We have not observed information relevant to determining the history of dolomite formation.

The following observations relate to the three mineralogic units – Lower (Stage 1 and transition zone in Stage 2); Middle (remainder of Stage 2 and Stage 3 to the top of R5); and Upper (remainder of Stage 3 and Stages 4, 5, and 6):

1. The Lower unit is illitic, with lower abundances of quartz and feldspar. Clay mineral content in the basin center is commonly as high as, or higher than in the basin margin. Ferroan dolomite is the primary carbonate, but calcite rich samples occur. In Stage 2 (transitional lake) there is a transition involving a sharp reduction in clay content, an increase in feldspar content (both albite and K-feldspar), and the appearance of dawsonite. The feldspar and dawsonite are interpreted as authigenic minerals. The presence of authigenic buddingtonite and ferroan dolomite suggest early establishment of reducing conditions (as suggested by Feng 2011).
2. The Middle unit is feldspar- and carbonate-rich, and clay-poor. Dawsonite is common through most of the unit. At the middle or top of Stage 2, nahcolite appears in our samples as well as in the Colorado 1 well. This middle unit is the heart of the saline zone, with significant beds comprised almost entirely of nahcolite and/or halite. All three feldspar types are more abundant than in the Lower unit, but the ratio of buddingtonite to K-feldspar, although variable, is generally lower than in the Lower unit.
3. The Upper unit is feldspar and carbonate-rich, with increasing calcite + aragonite/total carbonate, and a slight increase of illite content. Dawsonite and buddingtonite occur only in the R6 zone in the Upper unit, although Brobst and Tucker show occurrences in the underlying L5 zone. Nevertheless, conditions continued to be hypersaline, although after a last major evaporite zone in L5, nahcolite is present only in nodules and distributed grains, and halite is absent. A large scale leaching of evaporitic minerals by ground water is documented across the basin (Hite and Dyni 1967). However, the presence of nahcolite in some wells and the common identification of solution cavities with pseudomorphs of nahcolite clearly indicate its original presence. Dawsonite does not appear to have been affected by the dissolution front. Analcime occurs in both the basin margin and basin center section in the Upper unit.

Smith (1983) and Smith and Robb (1973) provided a detailed description of a model for development of the mineralogic character primarily of the Mahogany zone of the GRF in which virtually all minerals are diagenetic in origin. This view leads them to suggest that, from very early in its history, Lake Uinta was chemically stratified, and the lower portion of the lake was highly saline and alkaline. The stratification also maintained the reducing conditions that enabled preservation of so much organic matter. They do not discuss evaporation as a primary mechanism in developing elevated salinity and chemical stratification. The organic matter itself drove the reducing conditions by consuming the oxygen and elevating the carbonate and bicarbonate concentration in the lower part of the lake, enabling formation of

exotic carbonate minerals like dawsonite and nahcolite. Even the illitic clay in the lower part of the formation is a reaction product of presumed feldspathic precursors in their model.

A critical tenet of their interpretation is that the very fine, repetitive and laterally correlative laminations of the GRF, which they interpret as varves, demand very little current action, and suggests to them very little clastic input via fluvial sedimentation. Rather they prefer a wind-blown and seasonal source for silicate minerals. The facies associations defined by Tanavsuu-Milkeviciene and Sarg (2012) clearly indicate that the laminated oil shale is only a part of the story, and that oil shale breccia and turbidite, as well as a wealth of marginal facies suggest substantial transport of clastic sediment into the deep lake by streams and lake currents. The generally fine-grained nature of the deeper facies of the basin center do reflect much quieter deposition, but do not eliminate clastic sediment as a major portion of the GRF. Indeed, Fig. 8.6 clearly indicates that quartz, feldspar and clay minerals constitute, on average, more than half of the rock in the units described here.

Our interpretation of the mineralogic evolution of the lake contains important similarities to that of Smith and Robb, but with a more traditional view of the formation of the main mineral constituents. The first conclusion drawn with respect to the evolution is that it appears to have developed chemical stratification very early in its development.

The organic richness of sediments deposited in Stage 1 suggests reducing conditions very early in lake history. Feng (2011) has also pointed out that V/Cr ratios in the USBM 01A well indicate dysoxic to anoxic conditions from the early stages (R1). In addition, the relatively high values of dolomite/dolomite+calcite suggests mesosaline conditions – brackish to moderate salinity (Holland 1978; Eugster and Hardie 1978), and the tendency for the dolomite to be Fe-bearing indicates significant Fe^{+2} present at least in the pore waters of the shallow part of the sedimentary column. Reduced iron in solution provides further support for the reducing conditions inferred. It is unclear whether the presence of Fe^{+2} would make it possible to form dolomite over calcite as a primary mineral, even at low salinities. However, the difficulty of making dolomite in general suggests that such an effect would be minor, and that elevated salinity would still be indicated. Calcite-rich zones may reflect temporary changes in these conditions, but dolomite is strongly predominant in the wells examined.

In the deep lake zone, stratification would support reducing conditions, as oxidation of organic matter would quickly deplete the oxygen, and elevate the CO_2 concentration. Another possible indicator of reducing conditions is the occurrence of the ammonium feldspar buddingtonite as a major constituent of the feldspars. Poole (2014) was unable to identify buddingtonite as a separate phase under the scanning electron microscope, suggesting that the mineral identified in XRD as buddingtonite is a solid solution with sufficient potassium to be difficult to distinguish in the spectrum from the Energy Dispersive Spectrometer. The buddingtonite is likely to be a diagenetic alteration product from substitution of NH_4^+ in detrital K-feldspar in the presence of ammonia derived from organic matter (Oh, et al. 1993; Ramseyer et al. 1993; Svensen et al. 2008). Conditions that favor elevated ammonia in bottom or pore waters would be likely to be reducing. GRF organic matter contains substantial nitrogen (Baughman 1978, p. 16). These lines of evidence all support the idea of early development of a relatively persistently chemically stratified lake with a reducing deeper zone This concept is in line with the conclusions of a wide range of workers, including Bradley (1929, 1931), Picard (1955), Smith and Robb (1973), Desborough and Pitman (1974), Roehler (1974), Smith (1974), Williamson and Picard (1974), Desborough (1978), and Cole and Picard (1978), and is in agreement with Jagniecki and Lowenstein (2015). However, conditions of hypersalinity, resulting in deposition of sodium minerals, did not occur until after Stage 1. As noted above, salinity may well have increased throughout the lower unit, reaching levels sufficient to support chemical stratification well before they reached the levels of hypersalinity required to produce first dawsonite, and then nahcolite. Although stratification is not necessary to cause anoxic conditions at the sediment-water interface, it would seem odd to have produced the most reducing conditions in an

unstratified lake, followed by less reducing conditions in a stratified one. Thus, the Piceance Creek Basin portion of Lake Uinta rapidly established mesosaline, stratified conditions with a reducing bottom zone during the first stages of its existence. Fresh to brackish water was limited to the upper part of the lake, and truly fresh water conditions may have been still more restricted.

In this model, the illite content of both margin and center is interpreted as representing the fine-grained fraction of clastic sediment provided to the lake from surrounding land. Detrital illite generally has a composition between that of muscovite [$KAl_3Si_3O_{10}(OH)_2$] and pyrophillite [$Al_2Si_4O_{10}(OH)_2$]. Breakdown of potassium feldspar to clay may be written as either:

$$2KAlSi_3O_8 + 2H^+ = Al_2Si_4O_{10}(OH)_2 + 2SiO_2 + 2K^+ \quad (8.1)$$

K - feldspar *pyrophyllite + quartz*

or

$$3KAlSi_3O_8 + 2H^+ = KAl_3Si_3O_{10}(OH)_2 + 6SiO_2 + 2K^+ \quad (8.2)$$

K - feldspar *muscovite + quartz*

Both reactions are favored by slightly acidic fresh water (rainwater, for example) and by low activity of silica. The reverse reactions would be favored by saline, alkaline waters such as those prevalent in the ocean or saline lakes, and by higher silica activity in the water.

A parallel set of reactions could be written for the albite component of plagioclase, involving paragonite [$NaAl_3Si_3O_{10}(OH)_2$] and pyrophyllite [$Al_2Si_4O_{10}(OH)_2$].

$$2NaAlSi_3O_8 + 2H^+ = Al_2Si_4O_{10}(OH)_2 + 2SiO_2 + 2Na^+ \quad (8.3)$$

Albite *= pyrophyllite + quartz*

or

$$3NaAlSi_3O_8 + 2H^+ = NaAl_3Si_3O_{10}(OH)_2 + 3SiO_2 + 2Na^+ \quad (8.4)$$

Albite *= paragonite + quartz*

However, paragonite and sodic clay minerals are relatively rare compared to illite. Similar relationships hold for calcic plagioclase. Calcium is also weathered out of mafic minerals like amphibole and pyroxene. So the reactions that occur in weathering tend to favor reactions (8.2) and (8.3), putting sodium (and calcium) into solution, and potassium into illite. Mudstone comprised of the fine-grained portion of the weathering products generally reflect this separation, with relatively low sodium and calcium content, and potassium/aluminum ratios less than the 1:3 ratio in muscovite. The atomic (K + Na + Ca/2)/Al ratio is not much greater.

Thus, it seems likely that the composition of the silicate minerals present in the lower part of the basin center section reasonably reflects the clastic sedimentary input to the lake, with a mix-

ture of quartz, feldspar, and clay minerals. The assemblage in the lower part of the Shell 23X-2 well is generally similar to that in the basin margin as displayed by the Douglas Pass section. The clay mineral assemblage is slightly more diverse in Douglas Pass, with minor amounts of kaolinite, illite/ smectite, chlorite and trioctahedral clay minerals present. However, illite dominates the assemblage. Although some portion of the illite might be authigenic, and reflect the initiation of more alkaline conditions to follow, it is reasonable to interpret it as representing the finest grained fraction of the clastic input to the lake.

During stage 2, the concentration of sodium in the water in the basin center increased to very high levels – a hypersaline lake. Dawsonite is the first saline mineral to appear stratigraphically, then nahcolite in the R2 zone (Figs. 8.3 and 8.4). This relationship is observed in both the CR-2 and Colorado 1 well data (Dean et al. 1981; Smith and Robb 1973 – Figs. 8.8 and 8.9). Albite content of the sediment increases in this interval, as does potassium feldspar content, whereas illite content drops to near zero. The albite content appears to decrease later in stage 2 in the Shell and CR-2 wells. In the Colorado 1 well, a decrease in albite appears to accompany the occurrence of nahcolite. These relationships are consistent with reactions like (8.2) and (8.3) operating in reverse to break down illite and make authigenic feldspar. Poole (2014) observed euhedral diagenetic albite and K-feldspar under the SEM, and Brobst and Tucker (1973) indicated that most of the albite in the sections they measured was of an ordered, low temperature type. The low clay content and substantially elevated feldspar content relative to the Lower mineralogic unit shown in Fig. 8.7b suggests that diagenetic feldspar predominates over original clastic feldspar in the middle and upper mineralogic units. Table 8.2 indicates that feldspar is twice as common in the Middle unit as in the lower unit, and still higher in the Upper unit in the basin center, and the basin margin shows an equally strong shift. Conversion of clay minerals to feldspar consumes significant quantities of silica, potentially depressing silica activity in the lake water. An additional reaction would account for the formation of dawsonite:

$$KAl_3Si_3O_{10}(OH)_2 + 2Na^+ + 2H_2O + 2CO_2 = KAlSi_3O_8 + 2NaAl(OH)_2CO_3 + 2H^+ \quad (8.5)$$

Muscovite — *K - feldspar + Dawsonite*

Dawsonite could also form by reaction of smectite clays by a parallel reaction:

$$Al_2Si_4O_{10}(OH)_2 + 2Na^+ + H_2O + CO_2 = NaAlSi_3O_8 + NaAl(OH)_2CO_3 + SiO_2 + 2H^+ \quad (8.6)$$

Pyrophyllite — *Albite + Dawsonite + Quartz*

Or without formation of albite:

$$Al_2Si_4O_{10}(OH)_2 + 2Na^+ + 2H_2O + 2CO_2 = 2NaAl(OH)_2CO_3 + 4SiO_2 + 2H^+ \quad (8.7)$$

Pyrophyllite — *Dawsonite + Quartz*

An additional reaction also governs the relationship of albite and dawsonite:

$$NaAl(OH)_2 CO_3 + 3SiO_2 = NaAlSi_3O_8 + H_2O + CO_2 \quad (8.8)$$

$$Dawsonite + Quartz = Albite$$

As silica activity increases, salinity increases (H_2O activity decreases), or CO_2 activity decreases, formation of albite would be favored. The ratio of albite to dawsonite might provide some indication of the activity of SiO_2 in the lake, or at least just below the sediment-water interface. However, as albite and quartz were deposited as clastic constituents prior to the evolution of lake conditions to hypersalinity, and may not have been entirely broken down, an exact reaction relationship might not be evident in the mineral abundances. The change taking place at the top of the Middle mineralogic unit may reflect a shift in the balance of clay diagenesis from favoring dawsonite-producing reactions to favoring albite-producing reactions.

Although clay mineral abundance declines in the basin margin early in Stage 2, the degree of reduction is far less than in the basin center. In addition, dawsonite, buddingtonite, and nahcolite are absent except for small amounts of nahcolite in one sample, and buddingtonite in two samples. Thus in the Douglas Pass area, the lake appears to have been less saline and less reducing than in the basin center, reflecting deposition primarily above the chemocline. It is possible that dawsonite is a key indicator mineral for the location of the boundary between the shallow, less saline water responsible for sedimentation in the basin margin, and the saline, reducing bottom water of the lake, at least during the interval where it formed. The presence of analcime in numerous samples also suggests that in the basin margin, sodium is generally found in silicate rather than saline phases. Ferroan dolomite is present, but calcite and aragonite are more abundant, suggesting less diagenetic alteration of carbonate. The carbonate-rich beds described by Suriamin (2010) were also relatively little dolomitized, further indicating less saline conditions. These marginal environments may have experienced relatively saline conditions at times, but were in general fresher than the basin center throughout the lake history. Dolomite appears to be most common in deeper water environments at the basin margin, suggesting a gradient with depth of salinity and possibly redox conditions.

An additional factor in the basin margin mineralogy may be that Stage 2 is a time of increased clastic sediment influx, and at the basin margin, this sediment appears to be more silty/sandy in character. This change may reflect in part the lowering of lake levels (and progradation of sedimentary facies) as aridity increased, as well as a transition to more flash flood deposition of clastic sediment, as commonly observed in arid environments. There is the additional possibility that the decrease in clay reflects increasing aridity and shutdown of the clay-forming reactions. However, if clay-forming reactions were reduced, it would be expected to result in some increase in K/Al ratio, as potassic feldspar (1:1) replaced illite ($\leq$1:3) in the sedimentary input. Only if all of the decrease in feldspar weathering consists of albite would the K/Al ratio remain essentially constant. The chemical relationships in USBM 01-A described by Feng (2011) appear to indicate that K/Al remains roughly constant, although the values are more variable above this transition.

Nahcolite precipitation begins late in stage 2. It forms both in the water column and as displacive crystals in the sediment (LaClair and Lowenstein 2009, 2010; Jagniecki and Lowenstein 2015). Nahcolite occurs later in the evolution of the lake than dawsonite, perhaps because the reactions creating dawsonite can occur at lower salinity or lower CO_2 content in the interstitial water, or because nucleation in the water requires supersaturation to create the new

phase. Formation of nahcolite from solution would follow the reaction:

$$Na^{+} + HCO_3^{-} = NaHCO_3 \tag{8.9}$$

which may also be written as:

$$Na^{+} + H_2O + CO_2 = NaHCO_3 + H + \tag{8.10}$$

This form indicates that the reaction will be favored by higher alkalinity and salinity. Decreased silica activity would favor dawsonite over nahcolite formation in the presence of smectite clay:

$$2NaHCO_3 + Al_2Si_4O_{10}(OH)_2 = 2NaAl(OH)_2CO_3 + 4SiO_2 \tag{8.11}$$

$$2NaHCO_3 + KAl_3Si_3O_{10}(OH)_2 = 2NaAl(OH)_2CO_3 + KAlSi_3O_8 \tag{8.12}$$

Diagenetic alteration of most of the clay minerals into feldspars could deplete the interstitial water of silica, thus favoring formation of dawsonite and delaying the formation of nahcolite.

Stage 3 is the main saline zone in the GRF. In general, nahcolite abundance in the Shell 23X-2 and Savage 24-1 core samples is bimodal, with a small numbers of samples with very high nahcolite content, and most having relatively little. This relationship suggests the possibility that nahcolite tended to be deposited in pulses, with much lower rates of subaqueous evaporite deposition in between. This is certainly so in some cores, where relatively pure nahcolitic and especially halitic zones occur. The more complete sampling of the Colorado 1 well does not look so strongly segregated into nahcolite-rich and nahcolite-poor layers, but the sampling approach for that well involved homogenization of approximately one-foot intervals, and might have masked such mineralogic contrasts. Mineral abundance relationships with nahcolite appear mainly to reflect dilution of other minerals by nahcolite deposition.

The second major transition in mineralogy occurs near the top of Stage 3, when dawsonite disappears at the top of the R5 zone in the basin center. Immediately above is a highly saline zone, so the disappearance may in part reflect the dilution effect of saline minerals (nahcolite and halite), but even above this zone, dawsonite is absent. Quartz declines in tandem with dawsonite through this transition. The transition most likely reflects a change in the bottom waters or interstitial waters in which the diagenetic minerals formed. The transition mimics reaction (8.8), with dawsonite + quartz decreasing through the transition, and albite increasing. Both albite and quartz occur above and below the transition, reflecting a probable original detrital component that is never completely broken down. Poole has observed both relict and authigenic feldspar grains under the SEM (Poole 2014). As noted above, reaction (8.6) would be favored by an increase in silica activity, by a decrease in dissolved CO_2, or an increase in salinity (decrease in activity of H_2O).

A large decrease in CO_2 may be unlikely at this time, as nahcolite deposition continued after cessation of dawsonite deposition, although apparently at a less substantial rate, as nodules and displacive crystals. The occurrence of a relatively thick saline bed above the dawsonite might suggest an increase in salinity, but dawsonite deposition does not resume afterward, although it makes a brief return in the R6 zone. Interestingly, the next stage is the rising lake stage (4), reflecting a substantial influx of water into the system following the saline bed deposition. This influx flooded marginal areas, and generally led to increasing carbonate content (especially calcite + aragonite) of basin margin and basin center sediment. Clay mineral content increases immediately above R5, but then declines as the carbonate increase takes effect. The sodium mineral assemblage changes from albite + dawsonite + nahcolite to albite + analcime + nahcolite (where not dissolved). With the exception of nah-

colite, the overlying assemblage appears enriched in silicate minerals, and resembles that of the basin margin throughout its history.

Generally, highly alkaline environments result in higher silica solubility in waters (Eugster and Jones 1979). The bottom waters of Lake Uinta, or at least the pore waters immediately beneath the lake bottom, are presumed to have been very saline and very alkaline, in order to create the mineral assemblage found in the basin center samples. Smith and Robb (1973) suggest that the pore waters were actually less alkaline than the water of the lake, citing work of Taft and Harbaugh (1964) on oceanic organic-bearing carbonate sediment. They also deduce a pH near nine for the interstitial water from the coexistence of ferroan dolomite with siderite and pyrite (citing Garrels and Christ 1965). An influx of less saline, presumably less alkaline water in the rising lake stage would be expected to reduce silica solubility, a tendency favorable to formation and preservation of dawsonite. Less saline water would not favor the continued formation of nahcolite either. On the other hand, if the presence of clay minerals in the assemblage indicates less destruction, it might mean that the consumption of silica decreased, raising overall silica activity. It is not clear exactly what combination of chemical changes resulted from the influx of water during the rising lake stage, but it is clear that it drives the convergence of the basin margin and basin center mineral assemblages.

8.7 Conclusions

Quantitative mineralogy of 82 samples from the Green River Formation identifies distinct mineralogic trends in both marginal and deep basin environments. Three mineralogic units have been identified, most distinctively in the basin center. The two boundaries between these units bear important relationships to, but are not coincident with, the stratigraphic stage boundaries defined by Tanavsuu-Milkeviciene and Sarg (2012, 2015) on the basis of a larger set of core and outcrop descriptions. The lower mineralogic boundary marks the end of a transition whose start marks the Stage 1-2 boundary. The upper mineralogic boundary may be a precursor to the end of the period of thick evaporite deposition. Preliminary work in the Wyoming Green River Formation suggests that, whereas the stratigraphic stages correlate well from lake to lake, the mineralogic changes show similar, but not directly correlative patterns.

The data suggest that the Piceance Creek Basin part of Lake Uinta evolved rapidly into a deep, chemically stratified lake, with a deep zone showing mesosaline and reducing conditions, and a fresher shallow and marginal zone (Lower unit). Later, the deep zone became hypersaline, with diagenetic dawsonite and authigenic nahcolite as successive markers of this evolution (Middle unit). A critical marker of this hypersaline zone appears to be high ratios of feldspar to quartz + clay minerals in mudstone due to diagenetic alteration.

In the last stage, a rising lake appears to reflect influx of more water (Upper unit). Evaporation appears to have been sufficient to ensure that the lake was still sometimes saline enough to precipitate moderate amounts of nahcolite, primarily within the sediment column, it no longer formed dawsonite due to increased silica activity near the sediment-water interface. This could reflect conditions in which diagenetic alteration of clays did not proceed as far as in the still more saline earlier periods. Slightly fresher and perhaps less reducing conditions also resulted in increased calcite + aragonite/total carbonate. Future geochemical work will attempt to identify more specifically the conditions in the multicomponent chemical space of pH – aCO_2 –$aSiO_2$ – aNa^+ – aK^+.

The exotic mineralogy of the GRF may provide interpretive insight into a wide variety of mesosaline environments that preserve organic rich mudstone. The elevated salinity in these environments may encourage chemical stratification, which in turn favors preservation of organic matter. Dysoxic to anoxic conditions result from exhaustion of free oxygen by oxidation of organic matter in the isolated deep zone of the lake. A decrease in clay minerals results from diagenetic alteration in the elevated alkalinity and salinity of

these environments. The ratio of quartz to feldspar may be of value in understanding the evolution of other organic-rich shale formations in restricted, stratified basins where conditions were not so extreme as to form saline minerals like dawsonite and nahcolite. Data from the Montney Formation of Canada suggest the possibility of reduction in clay minerals by alteration to diagenetic feldspar (Chalmers and Bustin 2012; Krause et al. 2011), although lack of original formation of clays in a very arid climate is an alternative explanation.

More importantly, these diagenetic reactions may be significant in determining rock properties of these mudstones (especially brittleness) critical to natural fracturing during genesis of hydrocarbons, and to enhanced fracturing for production of those hydrocarbons. Thus, the conditions of formation of these rocks in restricted marine and lacustrine environments may be responsible not only for their organic richness, but also for their susceptibility to hydraulic fracturing to produce hydrocarbons.

References

Bader JW (2009) Structural and tectonic evolution of the Douglas Creek arch, the Douglas Creek fault zone, and environs, northwestern Colorado and northeastern Utah: implications for petroleum accumulation in the Piceance and Uinta basins. Rocky Mt Geol 44(2):121–145

Baughman G (1978) Synthetic fuels data handbook. Cameron Engineers, Denver, 438 pp

Bradley WH (1925) A contribution to the origin of the Green River Formation and its oil shale. Am Assoc Pet Geol Bull 9:247–262

Bradley WH (1929) The varves and climate of the Green River epoch, U.S. Geological survey professional paper 158-E. U.S. Government Printing Office, Washington, DC, pp 87–110

Bradley WH (1931) Origin and microfossils of the oil shale of the Green River Formation of Colorado and Utah. U.S. Geological survey professional paper 168. U.S. Government Printing Office, Washington, DC, 58 p

Bradley WH (1964) Geology of Green River Formation and associated Eocene rocks in southwestern Wyoming and adjacent parts of Colorado and Utah, U.S. Geological Survey professional paper 496-A. U.S. Government Printing Office, Washington, DC, pp 1–86

Brobst DA, Tucker JD (1973) X-ray mineralogy of the Parachute Creek Member, Green River Formation, in the Northern Piceance Creek Basin, Colorado. U. S. Geological Survey professional paper 803. U.S. Government Printing Office, Washington, DC, 53 pp

Cashion WB, Donnell JR (1972) Chart showing correlation of selected key units in the organic-rich sequence of the Green River Formation, Piceance Creek Basin, Colorado, and Uinta Basin, Utah. U.S. Geological Survey, oil and gas investigations, Chart OC-65, U.S. Geological Survey, Washington, DC

Cashion WB, Donnell JR (1974) Revision of nomenclature of the upper part of the Green River Formation, Piceance Creek Basin, Colorado, and Eastern Uinta Basin, Utah. U.S. Geological Survey Bulletin, 1394-G. U.S. Government Printing Office**,** Washington, DC, 9 p

Chalmers GRL, Bustin RM (2012) Geological evaluation of Halfway – Doig – Montney hybrid gas shale – tight gas reservoir, northeastern British Columbia. Mar Pet Geol 38:53–72

Cole RD, Picard MD (1978) Comparative mineralogy of nearshore and offshore lacustrine lithofacies, Parachute Creek Member of the Green River Formation, Piceance Creek Basin, Colorado, and eastern Uinta Basin, Utah. Geol Soc Am Bull 89:1441–1454

Desborough GA (1978) A biogenic-chemical stratified lake model for the origin of oil shale of the Green River Formation: an alternative to the playa-lake model. Geol Soc Am Bull 89:961–971

Desborough GA, Pitman JK (1974) Significance of applied mineralogy to oil shale in the upper part of Parachute Creek Member of the Green River Formation, Piceance Creek Basin, Colorado. In Murray DK (ed) Energy resources of the Piceance Creek Basin, Colorado: Rocky Mountain Association of Geologists, 35th annual field conference guidebook, pp 81–89

Dean WE, Pitman JK, Harrach GH (1981) Geochemical and mineralogical analyses of U.S. Geologic Survey Oil Shale Core CR-2, Piceance Creek Basin, Colorado. U.S. Geological Survey open file report 81–596. The Survey, Reston

Donnell JR, Blair RW Jr (1970) Resource appraisal of three rich oil-shale zones in the Green River Formation, Piceance Creek basin, Colorado. In Gary JH (ed) Synthetic liquid fuels from oil shale, tar sands, and coal, A symposium. Colo Sch Mines Q 65(4):73–87

Eugster HP, Hardie LA (1978) Saline lakes. In: Lerman A (ed) Lakes: chemistry, geology, and physics. Springer, New York, pp 237–293

Eugster HP, Jones BF (1979) Behavior of major solutes during closed-basin brine evolution. Am J Sci 279:609–631

Eugster HP, Surdam RC (1973) Depositional environment of the Green River Formation of Wyoming: a preliminary report. Geol Soc Am Bull 84:1115–1120

Feng J (2011) Source rock characterization of the Green River oil shale, Piceance Creek Basin, Colorado. MSc thesis, Colorado School of Mines, Golden CO, 84 pp

Garrels RM, Christ CL (1965) Solutions, minerals, and equilibria. Harper and Row, New York, 450 pp

Hillier S (2006) Appendix A. Mineralogical and chemical data. In: Reeves GM, Sims I, Cripps JC (eds) Clay materials used in construction, vol 21, Geological society, engineering geology special publications. Geological Society of London, London, pp 449–459

Hite RJ, Dyni JR (1967) Potential resources of dawsonite and nahcolite in the Piceance Creek Basin, northwest Colorado. In Symposium on oil shale, 4th, Colo Sch Mines Q 62(3):25–38

Holland HD (1978) The chemistry of the atmosphere and oceans. Wiley, New York, p 170

Jagniecki EA, Jenkins DM, Lowenstein TK, Carroll AR (2013) Experimental study of shortite (Na2Ca2(CO3)3) formation and application to the burial history of the Wilkins Peak Member, Green River Basin, Wyoming, USA. Geochim Cosmochim Acta 115:31–45

Jagniecki EA, Lowenstein TK (2015) Evaporites of the Green River Formation, Bridger and Piceance Creek Basins: deposition, diagenesis, paleobrine chemistry, and eocene atmospheric CO2. In: Stratigraphy and paleolimnology of the Green River Formation, Western U.S. Springer, Dordrecht, pp 277–312

Johnson RC, Mercier TJ, Brownfield ME, Pantea MP, Self JG (2010) An assessment of in-place oil shale resources in the Green River Formation, Piceance Basin, Colorado. U.S. Geological Survey, Digital data series, DDS-69-Y(Chp. 1). U.S. Geological Survey, Reston, 187

Katz B (1988) Clastic and carbonate lacustrine systems: an organic geochemical comparison (Green River Formation and East African lake sediments). In: Fleet AJ, Kelts K, Talbot MR (eds) Lacustrine petroleum source rocks, Geological society special publication 40. Blackwell, London, pp 81–90

Krause FF, Wiseman AC, Williscroft KR, Solano N, Morris NJ, Meyer R, Marr R (2011) The Montney Formation: mineralogy, what shall it be? Canadian Society of Petroleum Geologists Convention. http://www.cspg.org/documents/Conventions/Archives/Annual/2011/232-The_Montney_Formation.pdf. Downloaded 6 Nov 2012

LaClair D, Lowenstein TK (2009) Fluid inclusion microthermometry from halite in the Eocene Green River Formation, Piceance Creek Basin, Colorado, USA: evidence for a perennial stratified Saline Lake. Geological Society of America Annual Meeting, Portland, OR, 18–21 Oct 2009, Abstracts with Programs, Vol. 41 no. 7

LaClair D, Lowenstein TK (2010) Using microthermometry and laser Raman Spectroscopy and evaporites to reconstruct the paleoclimate of the Eocene Green River Formation, Colorado, USA. 10th biennial pan-American current research on fluid inclusions conference, Las Vegas, Nevada, 7–10 June 2010

Mason GM (2009) Eocene age fossilized filamentous bacteria: new evidence suggesting a bacterial genesis of siderite in the Green River Formation, Wyoming. In: Proceedings of the 28th oil shale symposium, Colorado Energy Research Institute Document CERI-2009-2, Colorado School of Mines, Golden, Colorado

Mason GM, Surdam RC (1992) Carbonate mineral distribution and isotope fractionation: an approach to depositional environment interpretation, Green River Formation, Wyoming, U.S.A. Chem Geol 101:311–321

Milton C, Fahey J (1960) Classification and association of the carbonate minerals of the Green River Formation. Am J Sci (Bradley Volume) 258-A:242–246

Milton C (1961) Section of geological sciences: mineralogy and petrology of the Green River Formation of Wyoming, Utah, and Colorado. Trans N Y Acad Sci 23:561–567. doi:10.1111/j.2164-0947.1961.tb01388.x

Murray DK, Haun JD (1974) Introduction to the geology of the Piceance Creek Basin and vicinity, northwestern Colorado. In: Murray DK (ed) Energy resources of the Piceance Creek Basin, Colorado: Rocky Mountain Association Geologists, 25th annual field conference guidebook, pp 29–39

Oh MS, Foster KG, Alcaraz A, Crawford RW, Taylor RW, Coburn TT (1993) Thermal decomposition of buddingtonite in oil shales. Fuel 72(4):517–523

Omotoso O, Mccarty DK, Hillier S, Kleeberg R (2006) Some successful approaches to quantitative mineral analysis as revealed by the 3rd Reynolds Cup Contest. Clay Clay Miner 54(6):748–760

Picard MD (1955) Subsurface stratigraphy and lithology of the Green River Formation in the Uinta Basin, Utah. Am Assoc Pet Geol Bull 39:75–102

Poole S (2014) Mineralogy of the Green River Formation, Piceance Creek Basin, Colorado. MSc thesis, Colorado School of Mines, Golden CO

Ramseyer K, Diamond L, Boles JR (1993) Authigenic K-NH_4 feldspar in sandstones; a fingerprint of the diagenesis of organic matter. J Sediment Petrol 63:1092–1099

Remy RR, Ferrell RE (1989) Distribution and origin of analcime in marginal lacustrine mudstones of the Green River Formation, South-Central Uinta Basin, Utah. Clay Clay Miner 37(5):419–432

Robb WA, Smith JW (1974) Mineral profile of oil shales in Colorado Core Hole No. 1, Piceance Creek basin, Colorado. In Murray DK (ed) Energy Resources of the Piceance Creek Basin, Colorado; 25th Field Conference, Rocky Mountain Association of Geologists, Denver CO

Roehler HW (1974) Depositional environments of Eocene rocks in the Piceance Creek Basin, Colorado. In: Murray DK (ed) Energy resources of the Piceance Creek Basin, 25th annual field conference guidebook. Rocky Mountain Association of Geologists, Denver, pp 57–64

Smith JW (1974) Geochemistry of oil-shale genesis in Colorado's Piceance Creek Basin. In: Murray DK (ed) Energy resources of the Piceance Creek Basin, 25th annual field conference guidebook. Rocky Mountain Association of Geologists, Denver, pp 71–79

Smith JW (1983) The chemistry that formed the Green River Formation oil shale. In: Miknis FP, McKay JF (eds) Geochemistry of oil shales, American chemical society symposium series 230. American Chemical Society, Washington, DC, pp 225–248

Smith JW, Milton C (1966) Dawsonite in the Green River Formation of Colorado. Econ Geol 61: 1029–1042

Smith JW, Robb WA (1966) Ankerite in the Green River Formation's Mahogany zone. J Sediment Petrol 36(2):486–490

Smith JW, Robb WA (1973) Aragonite and the genesis of carbonates in Mahogany zone oil shales of Colorado's Green River Formation, U. S. Bureau of Mines Report of .Investigations 7727. U.S. Dept. of Interior, Bureau of Mines, Washington, DC, 21pp

Surdam RC, Stanley KO (1979) Lacustrine sedimentation during the culminating phase of Eocene Lake Gosiute, Wyoming (Green River Formation). Geol Soc Am Bull 90:93–110

Surdam RC, Stanley KO (1980) Effects of changes in drainage- basin boundaries on sedimentation in Eocene Lakes Gosiute and Uinta of Wyoming, Utah, and Colorado. Geology 8:135–139

Srodon J (1999) Nature of mixed-layer clays and mechanisms of their formation and alteration. Annu Rev Earth Planet Sci 27:19–53

Suriamin H (2010) Facies, diagenesis, and geochemistry of the Eocene Green River Formation carbonates in the Piceance Creek Basin, Colorado. MSc. Thesis, Colorado School of Mines, Golden, CO, 108 pp

Svensen H, Bebout G, Kronz A, Li L, Planke S, Chevallier L, Jamtveit B (2008) Nitrogen geochemistry as a tracer of fluid flow in a hydrothermal vent complex in the Karoo Basin, South Africa. Geochim Cosmochim Acta 72:4929–4947

Taft WH, Harbaugh JW (1964) Modern carbonate sediments of southern Florida, Bahamas, and Espiritu Santo Island: Baja, California, vol 8, Stanford university publications, geological sciences. School of Earth Sciences, Stanford University, Stanford, pp 1–133

Tanavsuu-Milkeviciene K, Sarg JF (2012) Evolution of an organic-rich lake basin – stratigraphy, climate and tectonics: Piceance Creek basin, Eocene Green River Formation. Sedimentology 59(6):1735–1768

Tanavsuu-Milkeviciene K, Sarg JF (2015) Sedimentology of the world class organic-rich lacustrine system, Piceance basin, Colorado. In: Stratigraphy and paleolimnology of the Green River Formation, Western U.S. Springer, Dordrecht, pp 153–181

Trudell LG, Beard TN, Smith JW (1970) Green River Formation lithology and oil shale correlations in the Piceance Creek Basin, Colorado, U.S. Bureau of Mines, RI 7357. U.S. Dept. of Interior, Bureau of Mines, Washington, DC, 226 pp

U.S. Geological Survey Core Research Center (2012) Core Library Number C042. http://my.usgs.gov/crcwc/core/report/10109. Viewed 30 Oct 2012

Williamson CR, Picard MD (1974) Petrology of carbonate rocks of the Green River Formation (Eocene). J Sediment Petrol 44:739–759

Facies, Stratigraphic Architecture, and Lake Evolution of the Oil Shale Bearing Green River Formation, Eastern Uinta Basin, Utah

9

Morgan J. Rosenberg, Lauren P. Birgenheier, and Michael D. Vanden Berg

Abstract

To better understand the evolution of Utah's Eocene Lake Uinta and to help facilitate prudent and economic development of its unconventional oil shale resource, a predictive genetic model of the basin's lacustrine strata has been refined here. This model provides a better understanding of facies distribution, stratigraphic architecture, and a precise history of depositional evolution of Lake Uinta in eastern Utah.

This study evaluates the upper Douglas Creek and Parachute Creek Members of the Green River Formation, exposed along the Evacuation Creek outcrop on the eastern flank of the Uinta Basin. In addition to the outcrop, the Asphalt Wash-1 core, located about 13.7 km (8.5 mi) to the northwest of Evacuation Creek, was described. Ten different facies are defined and grouped into four facies associations: siliciclastics, carbonates, saline deposits, and volcanic-derived deposits.

This research further defines a genetic framework that recognizes small-scale phases in lake evolution which are defined by the relationship between absolute lake level, accommodation, siliciclastic input, and salinity. The combination of short-term climatic changes and longer-term tectonics shaped the evolution of Lake Uinta from an overfilled basin with fluctuations in sediment supply and accommodation that vary in both frequency and length (lake phases 1a and 1b), to a balance-filled basin with

The online version of this chapter (doi:10.1007/978-94-017-9906-5_9) contains supplementary material, which is available to authorized users.

M.J. Rosenberg (✉) • L.P. Birgenheier
Geology and Geophysics Department, University of Utah, 115 South 1460 East, Room 383, Salt Lake City, UT 84112-0102, USA
e-mail: mjrprov1@gmail.com; lbirgenheier@egi.utah.edu

M.D. Vanden Berg
Energy and Minerals Program, Utah Geological Survey, 1594 W. North Temple, Suite 3110, Salt Lake City, UT 84114, USA

M.E. Smith, A.R. Carroll (eds.), *Stratigraphy and Paleolimnology of the Green River Formation, Western USA*, Syntheses in Limnogeology 1, DOI 10.1007/978-94-017-9906-5_9

little to no sediment input with a high lake level (lake phases 2a, 2b, and 3a), to an underfilled basin with abundant saline minerals (lake phase 3b). This research provides a key dataset towards developing a regional genetic framework for lake evolution in the eastern Uinta Basin.

9.1 Introduction

Increasing oil prices along with concerns of declining conventional oil reserves have led to an increased emphasis on unconventional petroleum research. The thermally immature lacustrine oil shale deposits of the Green River Formation in Utah, Colorado, and Wyoming provide a substantial unconventional resource. Oil shale contains an abundance of thermally-immature organic matter called kerogen, formed predominately by the deposition and preservation of algae found in lacustrine settings (Dyni 2006; Ruble and Philp 1998). Oil shale has the potential to be an important energy resource if economic and environmentally sound retorting technologies can be developed (Dyni 2006). The upper Green River Formation in the Uinta Basin hosts one of the largest deposits of oil shale in the world; estimated in-place resources total 1.32 trillion barrels of oil (USGS 2010) with approximately 77 billion barrels as a potential economic resource (Vanden Berg 2008; Cashion 1967). Within the Mahogany zone, the interval with the highest organic-richness, beds can surpass 70 gallons of oil per ton of rock (GPT) (Vanden Berg 2008). The Mahogany zone typically averages between 20 and 25 GPT, while other rich zones average between 5 and 15 GPT (Birgenheier and Vanden Berg 2011).

Despite decades of research, controls on the shorter-term cyclicity of organic-rich and lean zones, combined with longer-term changes in stratigraphy, are still lacking for the eastern Uinta Basin. Tänavsuu-Milkeviciene and Sarg (2012) performed a detailed study of the evolution of the Piceance Creek Basin and studies of Wyoming's Greater Green River Basin, in large part, formed the basis for Carroll and Bohacs' (1999, 2001) seminal model of lake facies and depositional controls that categorizes overfilled, balance filled and underfilled lake conditions relative to the balance of water and sediment input.

In the Uinta Basin, numerous studies have been completed in the south-central region, in the Sunnyside Delta interval (middle Green River Formation) of Nine Mile Canyon. Keighley et al. (2002, 2003), Schomacker et al. (2010), and Moore et al. (2012) focused on the sedimentology, stratigraphic architecture, and presented a high resolution sequence stratigraphic model of a discrete interval within the Sunnyside Delta Interval. Detailed comparative analysis of the Douglas Creek Member on the eastern side of the basin, which is largely correlative with the Sunnyside Delta Interval, is lacking. Taylor and Ritts (2004) performed a reservoir characterization study comparing and contrasting short intervals of fluvial-deltaic shoreline deposits from Nine Mile Canyon, as well as wave-modified shoreline deposits from Raven Ridge in the northeastern Uinta Basin. Morgan et al. (2003) has provided a detailed outcrop characterization and log correlation study of the lower to middle Green River Formation across the basin. Vanden Berg (2008) has conducted a resource evaluation of the organic-rich oil-shale zones within the Uinta Basin, but this excludes detailed facies descriptions and interpretations of the organic-rich and lean zones. Despite this research, there are no studies to date that highlight the detailed facies changes and stratigraphic architecture of the alternating rich and lean zones in the Parachute Creek Member that overlies the Douglas Creek Member. Specifically a predictable sequence stratigraphic model from a significant thickness of the formation on the eastern side of the basin is needed, with a focus on sedimentologic processes, lateral facies architecture, and controls on lake deposition. Existing studies reveal numerous stratigraphic and geographic knowledge gaps in the eastern side of the Uinta

Basin, which are essential for developing basin wide genetic models and interpretations.

The long-term evolution of Lake Uinta is thought to have been controlled by a combination of climatic and tectonic factors that resulted in different phases in lake evolution, due to changes in the balance between lake accommodation as well as sediment and water influx, resulting in basins that are either overfilled, balance filled, or underfilled with water and sediment relative to neighboring basins (Carroll and Bohacs 1999; Smith et al. 2008; Keighley et al. 2003; Fouch et al. 1992; Moncure and Surdam 1980; Morgan et al. 2003; Picard and High 1972; Ryder et al. 1976; Birgenheier and Vanden Berg 2011). This model accurately reflects the long term changes in the Green River Formation in the Uinta Basin, but does not appropriately explain the controls on the more detailed facies changes and architecture, as well as the stratigraphic packaging. Very recent studies in the Uinta Basin have established a relationship between fluvial sandstone system deposition and early Eocene abrupt global warming events (hyperthermals) (Birgenheier et al. 2013; Plink-Bjorklund and Birgenheier 2012; Foreman et al. 2012). During these global warming events, an overall arid climate is thought to produce highly seasonal, flashy discharge events such as monsoons. These events quickly deposit high volumes of siliciclastic material at high energy levels that resulted in deposition of the lean zones seen in outcrop (Birgenheier et al. 2013; Plink-Bjorklund and Birgenheier 2012; Birgenheier and Vanden Berg 2011).

The main objective of this study is to use a high quality, laterally extensive outcrop section to constrain the controls on rich and lean zone deposition in the eastern Uinta Basin. The nearby Asphalt Wash-1 core was used to examine the details of mud-rich lithologies that are poorly exposed in outcrop. This research aims to further define a genetic framework that recognizes small-scale phases in lake evolution that could be applied throughout the basin and used to better predict facies distribution as it relates to Utah's oil shale development. Specifically, the superb outcrop quality allows for a unique evaluation of lateral and stratigraphic changes in facies architecture in the oil shale bearing interval of the Green River Formation.

9.2 Geologic Background and Location

The Green River Formation is an Eocene lacustrine deposit that spans northeastern Utah (Uinta Basin), southwestern Wyoming (Green River and Washakie Basins), and northwestern Colorado (Piceance Creek Basin) (Fig. 9.1) (Blakey and Ranney 2008). These isolated intermontane basins are part of the Colorado Plateau province of the western United States and were formed by a combination of Sevier and Laramide orogenic events (Dickinson et al. 1988). Although formed by similar mechanisms, these basins have different attributes when compared to the Uinta Basin. The Piceance Creek Basin is smaller, deeper, and more organic-rich than the Uinta Basin, whereas the Green River Basin is shallower and has the highest fluvial siliciclastic sediment supply (Tänavsuu-Milkeviciene and Sarg 2012).

During the Late Cretaceous, Laramide deformation broke up the broad foreland province previously occupied by the Western Interior Seaway (east of the Sevier orogenic belt) into sedimentologically isolated basins. These isolated basins were separated and confined by basement-cored uplifts and primarily occupied by nonmarine environments such as lakes (Dickinson et al. 1988; Blackstone 1983; Hagen et al. 1985; Crews and Ethridge 1993; Osmond 1965; DeCelles 1994; Johnson 1985; Fouch 1975). Laramide deformation is attributed to continued subduction of the Farallon plate beneath the North American plate, but is distinguished by a series of basement-cored, thick-skinned contractional uplifts, which served as local sediment sources (Crews and Ethridge 1993; Blackstone 1983). The irregular distribution, shape and size of the uplifts across the central Rocky Mountain region cause many of the basins, like the Uinta Basin, to be asymmetric in cross-section (Abbott 1957; Cashion 1967; Dickinson et al. 1988). Subsidence of these basins is presumed to be in response to thrust-thickened loading along basin-margin uplifts (Crews and Ethridge 1993; Hagen et al. 1985). The Uinta Basin is an intermontane low that is constrained by the Uinta uplift to the north and San Rafael and Uncompahgre uplifts to the south (Fig. 9.1)

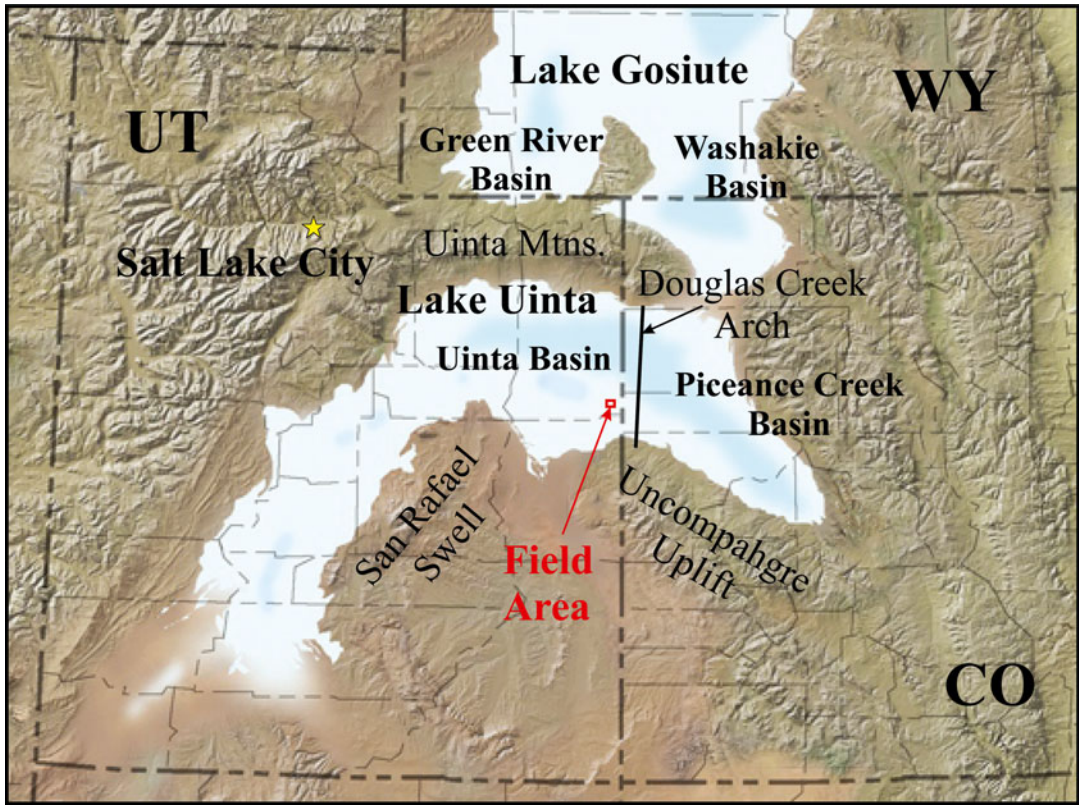

Fig. 9.1 Paleogeographic map of the Colorado Plateau during the Eocene Epoch. This map illustrates the regional extent of the Green River Formation with the field area marked in *red* (Modified from Blakey and Ranney 2008)

(Abbott 1957). Sevier orogenic events generated Jurassic through early Cenozoic thrusted uplifts that border the Uinta Basin to the west (Johnson 1985). The Douglas Creek arch is a structural high on the eastern flank of the Uinta Basin that periodically served as an emergent topographic high and acted as a sill separating the Uinta and Piceance Creek Basins. This faulted anticline extends approximately 75 km from north to south and is about 35 km wide (Bader 2009). At the end of the Cretaceous, the basins on either side of the arch began to subside, while the arch remained a positive structural feature (Osmond 1965). During the Eocene, the Uinta and Piceance Creek Basins were occupied by Lake Uinta (Fig. 9.1). During periods of high lake level, the Douglas Creek arch was submerged, and the Uinta and Piceance Creek lake basins were in water mass communication. In contrast, during periods of low lake level, these lake basins were isolated from one another (Carroll and Bohacs 1999; Ruble and Philp 1998; Birgenheier and Vanden Berg 2011; Keighley et al. 2003; Tänavsuu-Milkeviciene and Sarg 2012; Surdam and Stanley 1980; Smith et al. 2008).

The Green River Formation in the Uinta Basin is separated into the lower, middle, and upper members (Fig. 9.2) (Witkind). The lower member is characterized by regionally extensive lacustrine carbonate units and locally extensive fluvial-deltaic sandstone facies that commonly interfinger with the underlying Colton/Wasatch Formation (Ryder et al. 1976; Morgan et al. 2003; Birgenheier and Vanden Berg 2011; Abbott 1957). The carbonate marker bed, a regionally extensive dolomitic organic-rich unit, marks the top of the lower member. The middle and upper members of the Green River Formation in the eastern Uinta Basin, the focus of this study, are designated as the Douglas Creek Member

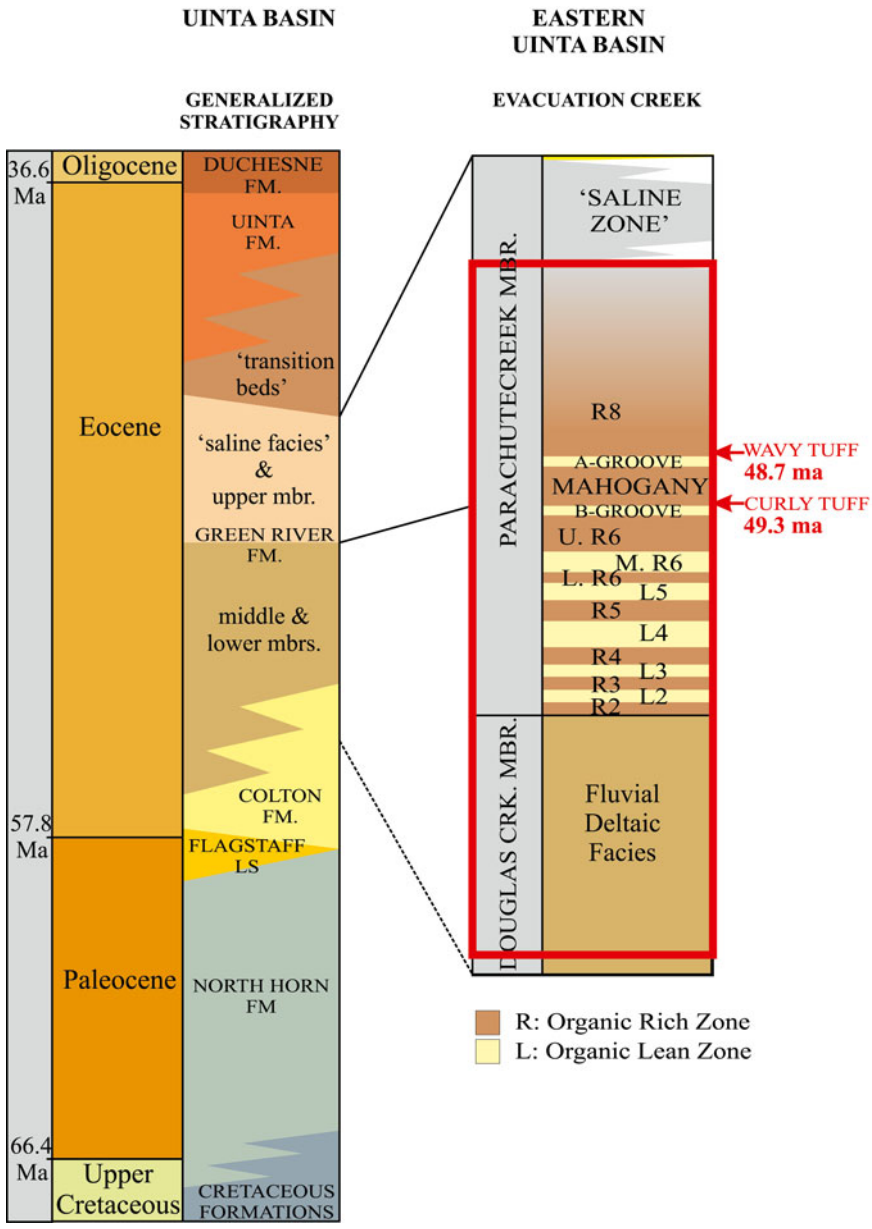

Fig. 9.2 Stratigraphy of the *middle* and *upper* Green River Formation. The studied interval is highlighted in *red*. Uinta Basin general stratigraphy from Keighley et al. (2002), based on map by Witkind (1995). Radiogenic dates from Smith and others (2010)

overlain by the Parachute Creek Member (Fig. 9.2). The Douglas Creek Member is characterized by fluvial-deltaic and carbonate facies, whereas the Parachute Creek Member is characterized by alternating rich (R) and lean (L) oil shale zones (R2–R8 in stratigraphic order), with the Mahogany zone (R7) being the most organic-rich, and a saline facies within the middle R8 (Fig. 9.2; Ryder et al. 1976; Birgenheier and Vanden Berg 2011).

The study area is located on the southeastern edge of the Uinta Basin, just west of the Douglas

Creek Arch. A 6.4 km (4 mi) laterally extensive northwest to southeast trending outcrop of the middle Douglas Creek Member to the lower R8 is well exposed at Evacuation Creek. The Asphalt Wash-1 core is located approximately 13.7 km (8.5 mi) to the northwest of the Evacuation Creek outcrop (T11S, R24E, Sec. 7; 39° 52′ 37.5″ N 109° 16′ 9.9″ W) (Fig. 9.3) and records the upper Douglas Creek Member through the basal portion of the saline zone within the middle R8.

9.3 Methods

Four detailed sections were measured along the Evacuation Creek outcrop (Fig. 9.3). This northwest to southeast trending outcrop is about 6.4 km (4 mi) long, with 4.4 km (2.7 mi) between all measured sections, informally named (from NW to SE): Condo, Flash Flood, Temple, and Gray Huts. Each section was described using a 1.5 m measuring ruler while noting lithology, sedimentary structures, organic-richness, presence of fossils, nature of contacts, and architecture at the centimeter to meter scale. The thickness of these sections ranges from 135 m (442.9 ft) to 209 m (685.7 ft) and averages about 180 m (590.6 ft). Additionally, high-resolution gigapan photographs were taken at each measured section location and used to highlight facies architecture, mainly sandstone bodies, laterally along the Evacuation Creek outcrop (Fig. 9.4). Key units were traced between measured sections to document lateral changes on the gigapans.

In addition to the Evacuation Creek outcrop descriptions; the Asphalt Wash-1 core was similarly described in terms of lithology, sedimentary structures, and level of detail. The Asphalt Wash-1 core spans two nonadjacent stratigraphic intervals from 636 to 612 m (2,088 to 2,007 ft) and 416 to 94 m (1,364 to 307 ft).

9.4 Results

9.4.1 Facies and Facies Associations

Detailed measured section and core descriptions are documented in Supplementary Appendix 9.1, which can be accessed at http://extras.springer.com. Ten facies were defined based on lithology, sedimentary structures, organic-richness, presence of fossils, and bed geometry (Table 9.1; Figs. 9.5, 9.6, and 9.7). These ten facies were grouped into four facies associations: siliciclastics, carbonates, saline deposits, and volcanic-derived deposits. The siliciclastic facies association is interpreted as a low-gradient deltaic complex composed of terminal distributary channels and fluvial mouthbars with evidence of wave influence. The carbonate facies association is typical of shallow lacustrine carbonate ramps ranging from littoral (high energy) to sublittoral to profundal (low energy) deposits (Renaut and Gierlowski-Kordesch 2010). Carbonate benches are characterized by a very gently sloping terrace, which subsequently have steeply sloping transitions into deeper water, resulting in abrupt facies changes. Carbonate ramps, as seen here, are characterized by a constant, gradual slope from the littoral zone, into deeper water, resulting in gradual facies transitions. The saline deposits are associated with a profundal hypersaline lacustrine environment with minimal siliciclastic input. Numerous tuff beds throughout the interval record volcanic activity in the form of both fallout tuffs and volcanic sediment sourced from the Absaroka Volcanic Province (Smith et al. 2008). The ten facies that make up the facies associations are described in detail below.

9.4.1.1 Facies Association 1: Siliciclastic Deposits

Facies 1.1 (F1.1)

Facies 1.1 consists of erosionally-based, fine to medium, lenticular sandstone bodies (Table 9.1; Fig. 9.5). Color ranges from light tan to yellow or orange. Rip-up clasts are common along the base of the downcutting, lenticular sandbodies. Parallel to low-angle laminations are common towards the bottom of the sandstones, whereas asymmetric ripples tend to be more common towards the upper half. Individual lenticular bodies average about 3–4 m thick, but range from less than a meter to 7 m in thickness. Sandbodies are on average 10–20 m wide, but range from about 5 to up to many tens of meters wide. These bodies can be single storied, or multistoried. Thickness of indi-

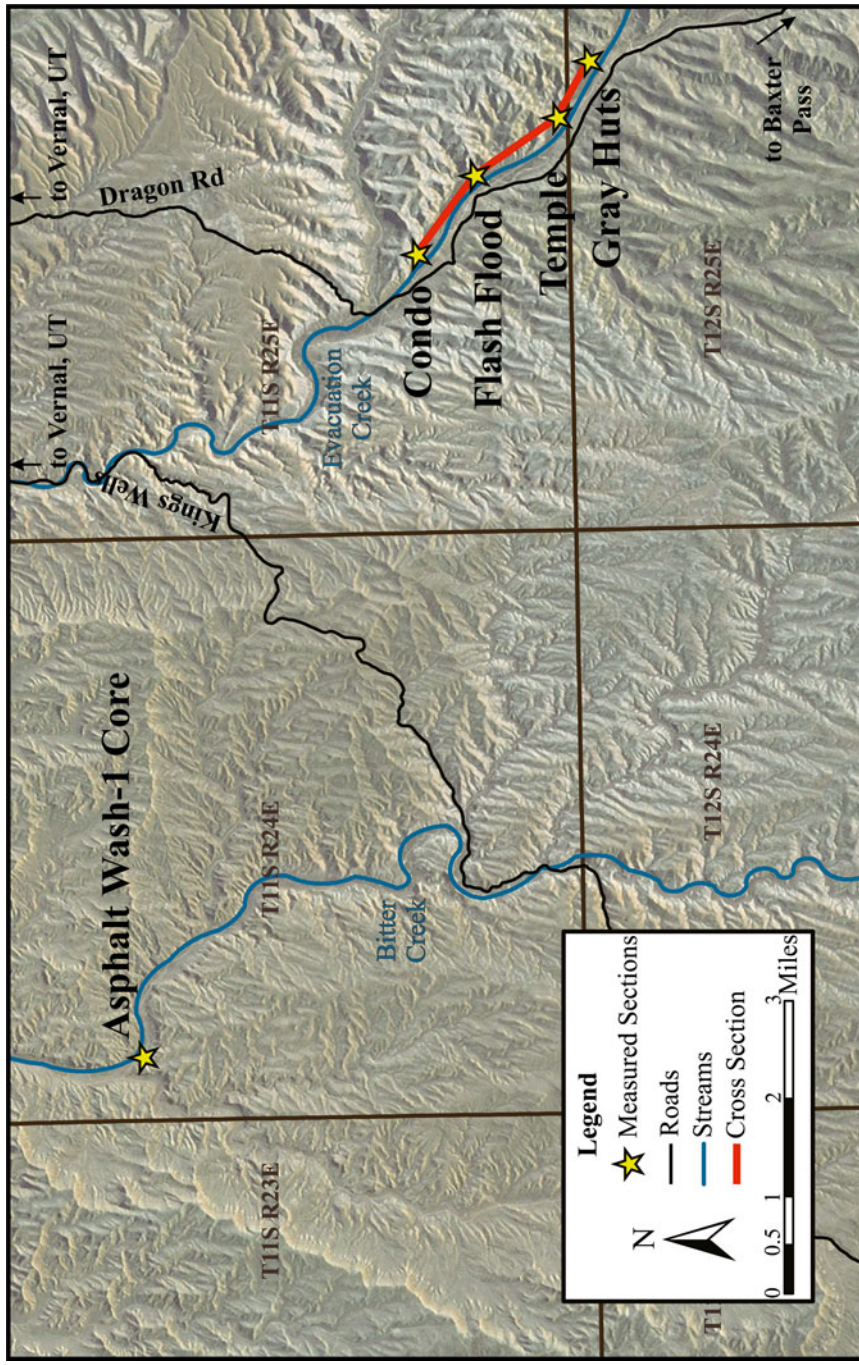

Fig. 9.3 Map showing the locations of measured sections along Evacuation Creek and the Asphalt Wash-1 core

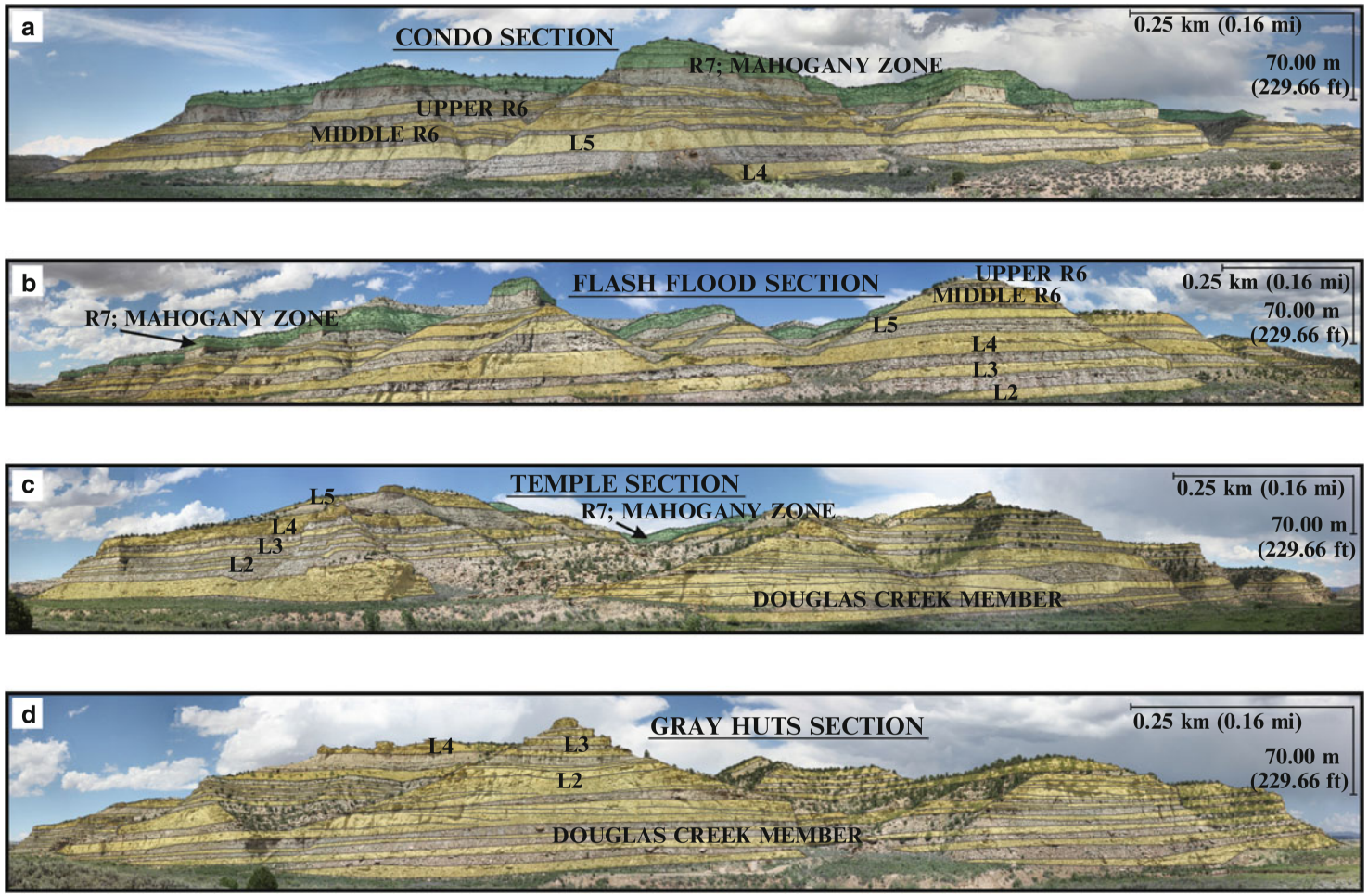

Fig. 9.4 Gigapan photographs of Evacuation Creek outcrop moving from NW (**a**) to SE (**d**). Sandstone bodies highlighted in *yellow* and Mahogany zone (R7) highlighted in *green*. (**a**) Condo section (**b**) Flash flood section (**c**) Temple section (**d**) Grey huts section. Vertical scales vary and were estimated from measured section locations

Table 9.1 Facies table

Facies	Description	Lake zonation	Depositional environment
F1.1	Erosionally based, channelized fine to medium grained sandstone, rip-up clasts common at base, low angle laminations to current ripples present	Littoral	Terminal distributary channel
F1.2	Massive, tabular, fine grained sandstone with some low angle laminations present	Littoral	Proximal fluvial mouthbar
F1.3	Organic poor claystone to siltstone, parallel laminated, some rip up clasts, few ripples	Sublittoral to Profundal	Distal fluvial mouthbar
F2.1	Carbonate grainstone, ooids to peloids to oncolites	Littoral	Carbonate ramp (high energy)
F2.2	Microbialites; ranging from stromatolites to thrombolites	Littoral	Carbonate ramp (high energy)
F2.3	Organic poor carbonate mudstone	Sublittoral	Carbonate ramp (low energy)
F2.4	Organic-rich carbonate mudstone, commonly associated with fish scales/bones	Profundal	Carbonate ramp (low energy)
F2.5	Organic-rich carbonate mudstone, very few fossils, parallel to wavy laminations	Profundal	Laminated, deep open water
F3.1	Organic-rich carbonate mudstone with abundant hypersaline precipitant minerals	Profundal	Laminated, deep open water
F4.1	Tuff	Volcanic ash	Volcanic ash deposit

Descriptions of the ten facies identified from the Evacuation Creek outcrop and Asphalt Wash-1 core. Facies association 1 is composed of siliciclastic deposits; facies association 2 is composed of carbonate deposits; facies association 3 is composed of saline deposits; facies association 4 is composed of volcanic-derived deposits

vidual stories ranges from 1 to ~12 m. Sandbodies are commonly amalgamated in both the vertical and horizontal direction with other sandstones. Some bodies contain evidence of lateral migration (Figs. 9.8 and 9.9). Dewatering structures and soft sediment deformation are also common, indicating rapid sedimentation rates. Paleocurrent data (n=25) indicate a prominent average flow direction to the northwest, with less prominent flow direction to the northeast (Supplementary Appendix 9.1, which can be accessed at http://extras.springer.com).

Facies 1.2 (F1.2)

Facies 1.2 is composed of massive, fine sandstone (Table 9.1; Fig. 9.5). Sandstone bodies are commonly tabular and sharp-based. Facies 1.2 consistently overlies facies 1.1 and commonly transitions into facies 1.1 laterally at sharp boundaries (Figs. 9.9 and 9.10). Colors range from light tan to yellow or orange. Bed thickness is commonly meter scale, and multiple beds are often stacked, forming tabular packages. These packages range in thicknesses from 1 to 7 m. Where sedimentary structures are visible, parallel to low-angle laminations are found locally (Fig. 9.5). Soft sediment deformation is also extensive in some beds.

Facies 1.3 (F1.3)

Facies 1.3 consists of finely laminated, organic-poor claystone to siltstone (Table 9.1; Fig. 9.5). The base of this facies is commonly gradational rather than sharp and overlies many other facies, including organic-rich carbonate mudstone (F2.5), microbialites (F2.2), and sandstones (F1.1 and F1.2). Color is usually light tan to light gray. Plane parallel laminations are common. Modified ripples are present in the siltstone, but are uncommon relative to plane parallel laminations. Few *Lithophypoderm sp.* fossils (commonly called "botfly" larvae) are present. Some dewatering structures and soft sediment deformation are also present. This facies also commonly contains thin (<5 mm), very fine sandstone interlaminations, which contain some asymmetric ripples that range from NNE to SW paleoflow directions.

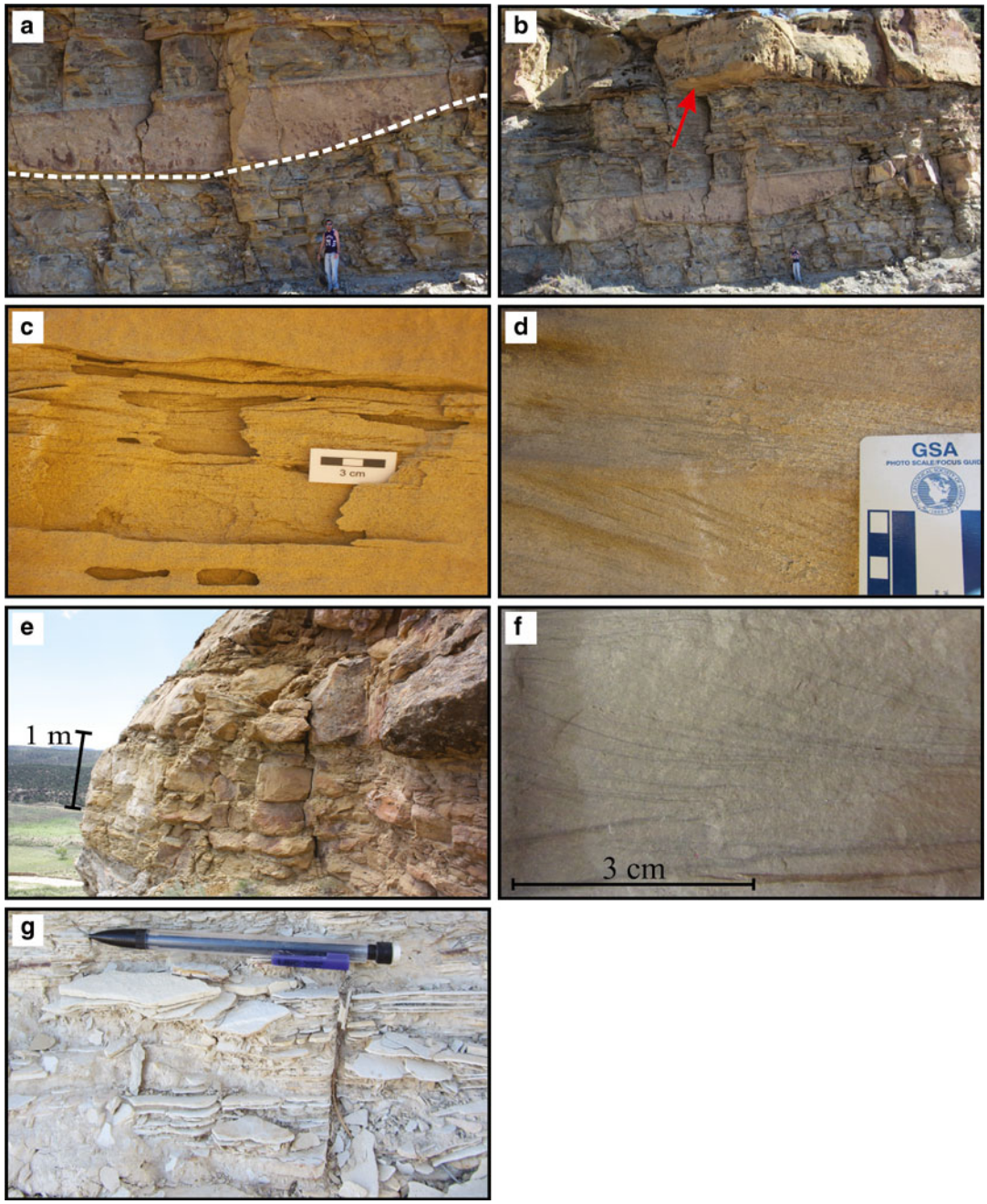

Fig. 9.5 Facies association 1; siliciclastic deposits. (**a**) Facies 1.1 from Gray Huts section; erosionally-based (highlighted by *white dotted line*), fine to medium grained sandstone channel, rip-up clasts common at base, low-angle laminations to current ripples common; interpreted as littoral, terminal distributary channel. (**b**) Facies 1.2 from Gray Huts section; massive, fine grained sandstone (*red arrow*) with few ripples, low angle laminations; interpreted as proximal, fluvial mouthbar. (**c**) Facies 1.1 from Flash Flood section; close up of medium grained sandstone. (**d**) Facies 1.1 from Flash Flood section; close up of medium grained sandstone with current ripples. (**e**) Facies 1.2 from Flash Flood section; massive, fine grained sandstone. (**f**) Facies 1.1 from Asphalt Wash-1 core; fine grained sandstone with abundant current ripples, from Asphalt Wash-1 core. (**g**) Facies 1.3 from Gray Huts section; organic poor claystone to siltstone, parallel laminations, some rip-up clasts, few ripples; interpreted as sublittoral to profundal, distal, fluvial mouthbar

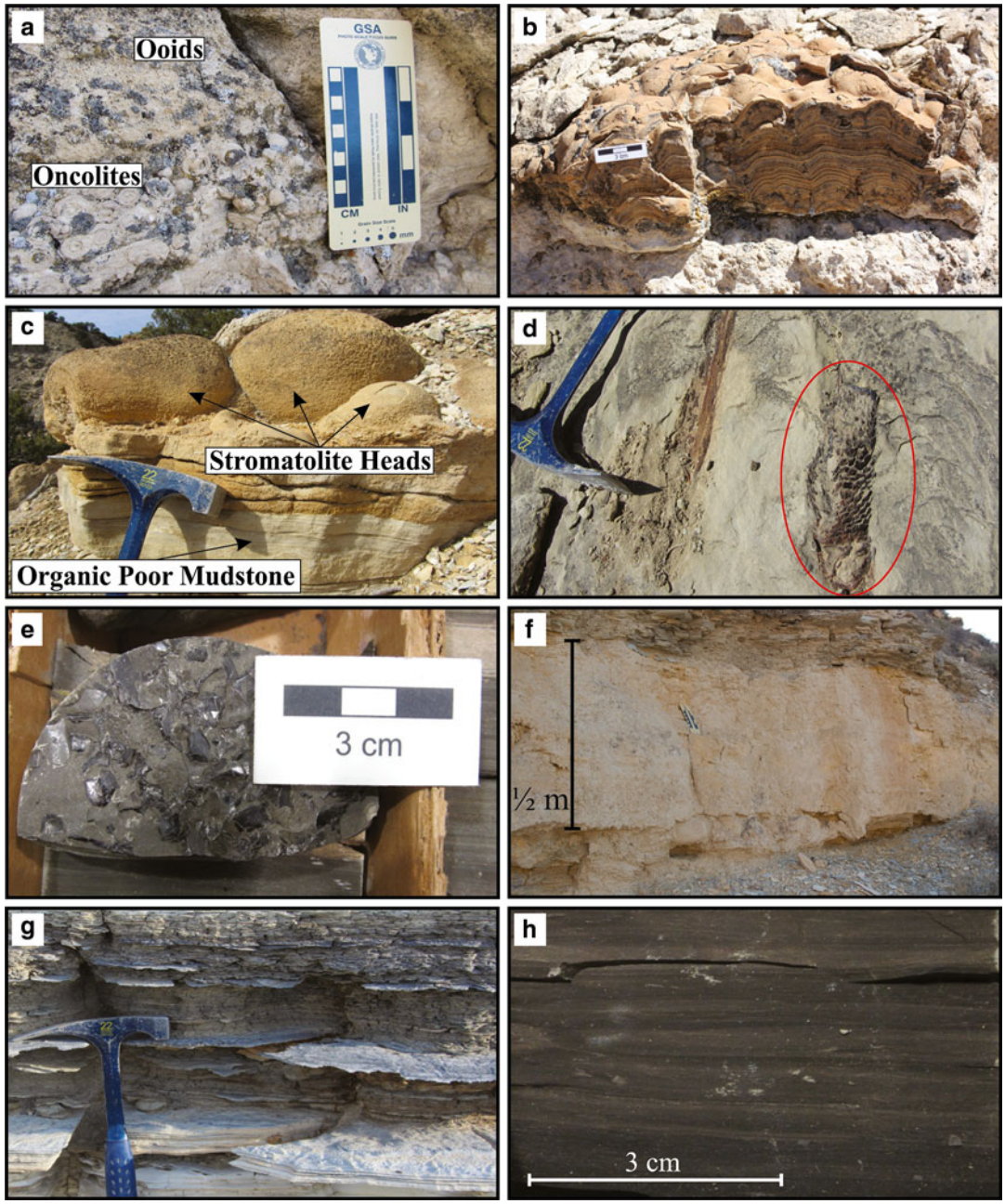

Fig. 9.6 Facies association 2; carbonate deposits. (**a**) Facies 2.1 from Gray Huts section; carbonate grainstone, ooids/peloids and oncolites in base of Gray Huts section; interpreted as littoral, high-energy carbonate ramp. (**b**) Facies 2.2 from Temple section; stromatolites; interpreted as littoral, high-energy carbonate ramp. (**c**) Facies 2.2 and 2.3 from Gray Huts section; stromatolite heads overlaying organic poor carbonate mudstone; interpreted as sublittoral, low-energy carbonate ramp. (**d**) Facies 2.4 from Gray Huts section; organic-rich carbonate mudstone with articulated fish scales (*circled*), plant debris common (right of hammer); interpreted as profundal, low-energy carbonate ramp. (**e**) Facies 2.4 from Asphalt Wash-1 core; organic-rich carbonate mudstone with abundant fish scales. (**f**) Facies 2.2 from Gray Huts section; thick (~1 m) thrombolite build-up which can be traced along the entire Evacuation Creek outcrop. (**g**) Facies 2.5 from Condo section; finely laminated, organic-rich carbonate mudstone, parallel to wavy laminations; interpreted as profundal, "deep" open water, found in Mahogany Zone. (**h**) Facies 2.5 from Asphalt Wash-1 core; finely laminated, organic-rich carbonate mudstone from the Mahogany zone

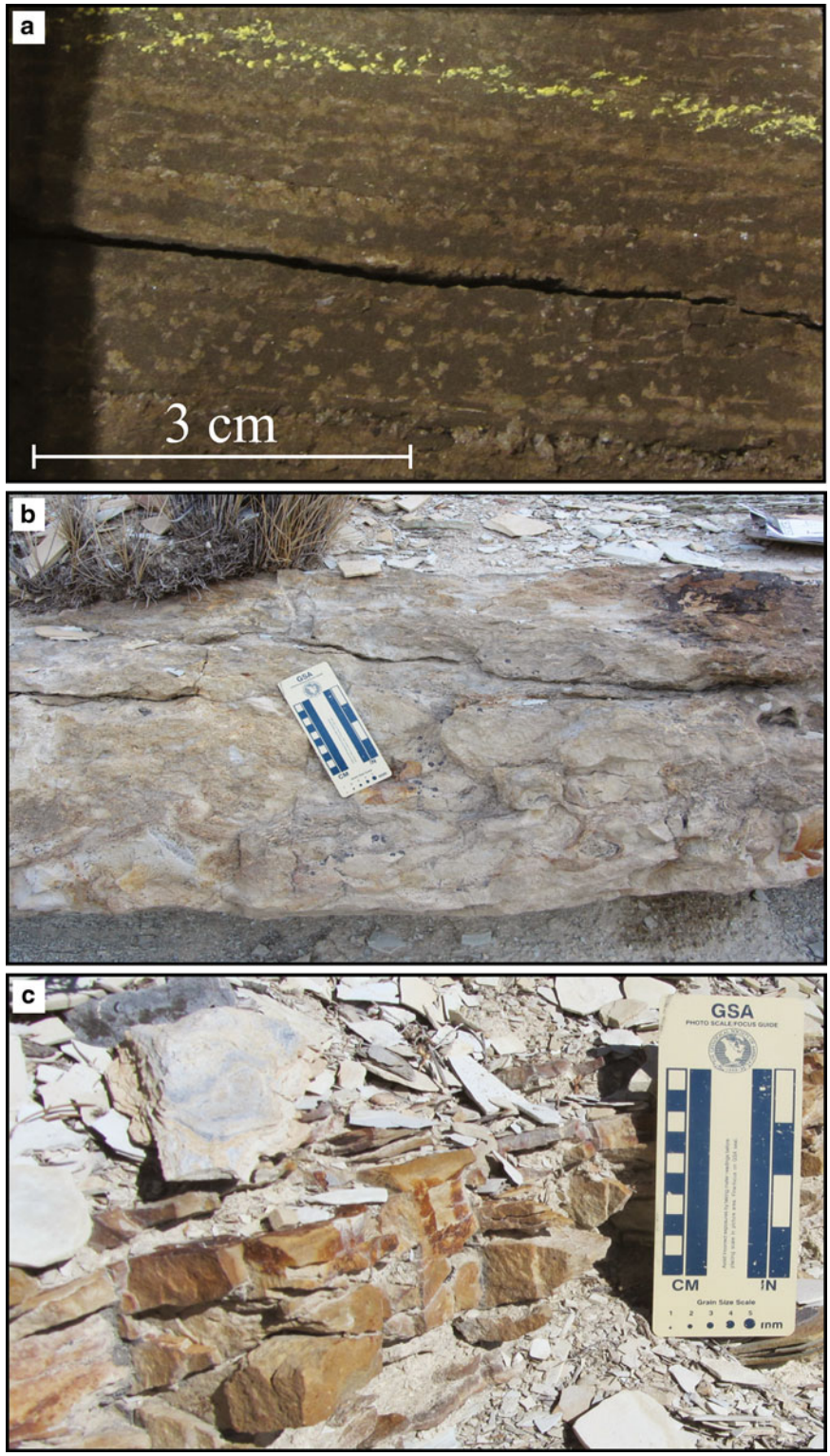

Fig. 9.7 Facies association 3 and 4; saline deposits and volcanic-derived deposits; (**a**) Facies 3.1 from Asphalt Wash-1 core; organic-rich carbonate mudstone with abundant disseminated saline mineral crystals; interpreted as profundal, laminated "deep" open hypersaline water. (**b**) Facies 4.1 from Condo section; Curly Tuff. (**c**) Facies 4.1 from Gray Huts section; fine to medium grained volcanic ash deposit

9.4.2 Facies Association 1 Interpretation

The three siliciclastic facies observed in this study have been interpreted to comprise different associated components of a fluvial-dominated deltaic complex that expresses some wave influence or modification. Facies 1.2 and 1.3 are interpreted as proximal and distal portions of fluvial mouthbar complexes, respectively, that were deposited slightly downdip of their updip counterparts, terminal distributary channels (F1.1).

Fluvial mouthbars are sediment bodies that form where a river (terminal distributary channel) meets a large standing water body, such as a lake (Schomacker et al. 2010). The sediment transport velocity of the river drops dramatically upon entering the body of water, causing deposition of coarser sand proximal to the shoreline of the lake and finer sediments in more distal settings (Olariu and Bhattacharya 2006; Moore et al. 2012). Sorting within the mouthbar deposits is very good, due to reworking by lacustrine and fluvial processes after initial deposition (Moore et al. 2012). The term "mouthbar" is used instead of "delta" because of the low gradient in which the fluvial system entered the shallow lake. Due to the interpreted low gradient and shallow lake level, full delta systems were not able to form, but instead a series of mouthbar complexes were deposited. These complex siliciclastic packages were predominantly sourced from the south of Lake Uinta (Cashion 1967; Picard and High 1972; Ryder et al. 1976; Dickinson et al. 1988; Moore et al. 2012). Paleocurrents indicate a prominent northwestern flow direction in the lower part of the sandstone packages, with an increasing northeastern to southwestern flow direction higher up in the sandstone packages (Supplementary Appendix 9.1, which can be accessed at http://extras.springer.com). This transition in paleoflow direction is an indication of both primarily fluvial and secondarily wave processes affecting sand deposition as the system prograded into the basin. The distal siliciclastic deposits have a greater influence from longshore wave action (as fluvial discharge energy decreases), generating flow indicators perpendicular to the fluvial onset direction (Bhattacharya and Giosan 2003).

Numerous fluvial channel splits, due to the formation of fluvial mouthbars, generate terminal distributary channels (Fig. 9.8) (Olariu and Bhattacharya 2006). These channels are the most distal features of a distributive system, so it is nearly impossible to count the number of channel splits (Olariu and Bhattacharya 2006). These lenticular sandstone channels are almost always observed incising into underlying tabular mouthbars (Figs. 9.8, 9.9, and 9.10). Figure 9.11 illustrates a simplified model of the association of siliciclastic deposits that are interpreted to comprise these deltaic complexes. Initially, the main river channel is bifurcated by a single mouthbar as it enters the lake system. The formation of the mouthbar diverts the main channel into two smaller channels, which are the terminal distributary channels. The terminal distributary channels represent the final splits of the main channel.

Facies 1.2 and 1.3 are distinguished by their difference in grain size. The proximity of the fluvial mouthbar to the lake margin can be interpreted by looking at the lower bounding surface, as well as the internal structure and grain size. Proximal mouthbar sandstone bodies (facies 1.2) are typically sharp and erosionally based. Similar to the interpretations by Moore et al. (2012) in Nine Mile Canyon, facies 1.2 is interpreted as fluvial mouthbars based on the lack of subaerial exposure indicators (especially in the lower portion of the Parachute Creek Member), lack of basal erosional surfaces, and abundant soft-sediment deformation.

In distal fluvial mouthbars (facies 1.3), the lower bounding surface is more depositional than erosional, so it appears slightly undulating and nearly horizontal (Schomacker et al. 2010). Distal mouthbars also show evidence of wave modification. This wave modification is observed in the upper portions of the sandstone packages, as they prograded into the basin. In the distal claystone and siltstone packages, there is no direct evidence of wave modification because these were deposited below wave base. Thin stratified and normally graded bedsets are observed in the interpreted distal mouthbar

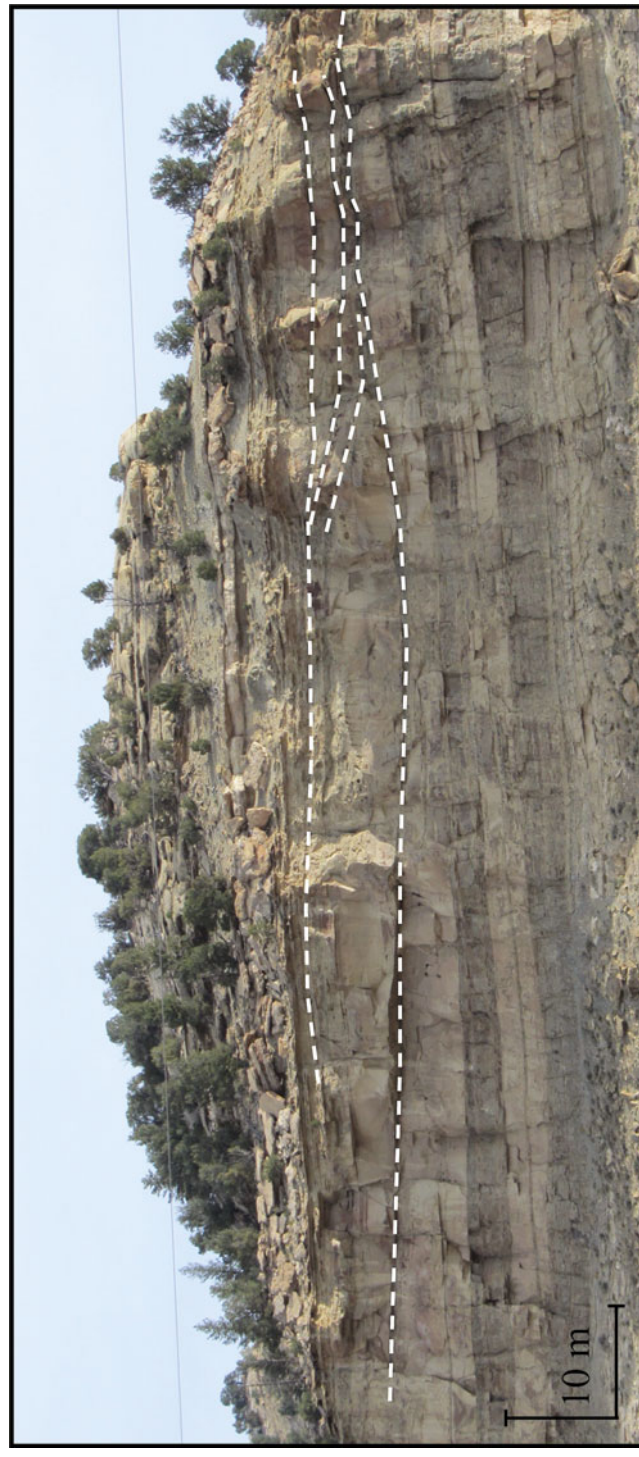

Fig. 9.8 Example of a terminal distributary channel (F1.1) from the Gray Huts section in the L2 zone

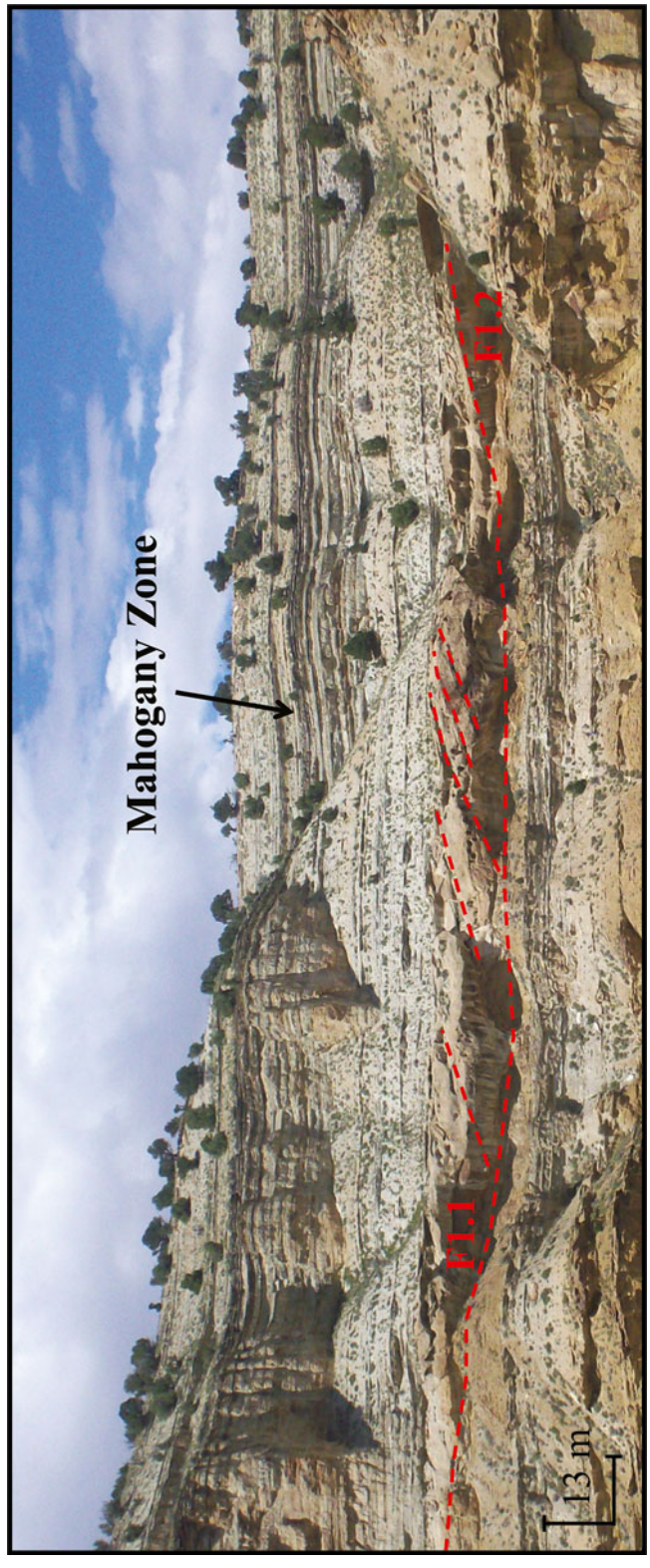

Fig. 9.9 Example of a terminal distributary channel (F1.1) and fluvial mouthbar (F1.2) from the Condo section in the upper R6 zone

Fig. 9.10 Example of a terminal distributary channel (F1.1) and fluvial mouthbar (F1.2) from the Gray Huts section in the Douglas Creek Member

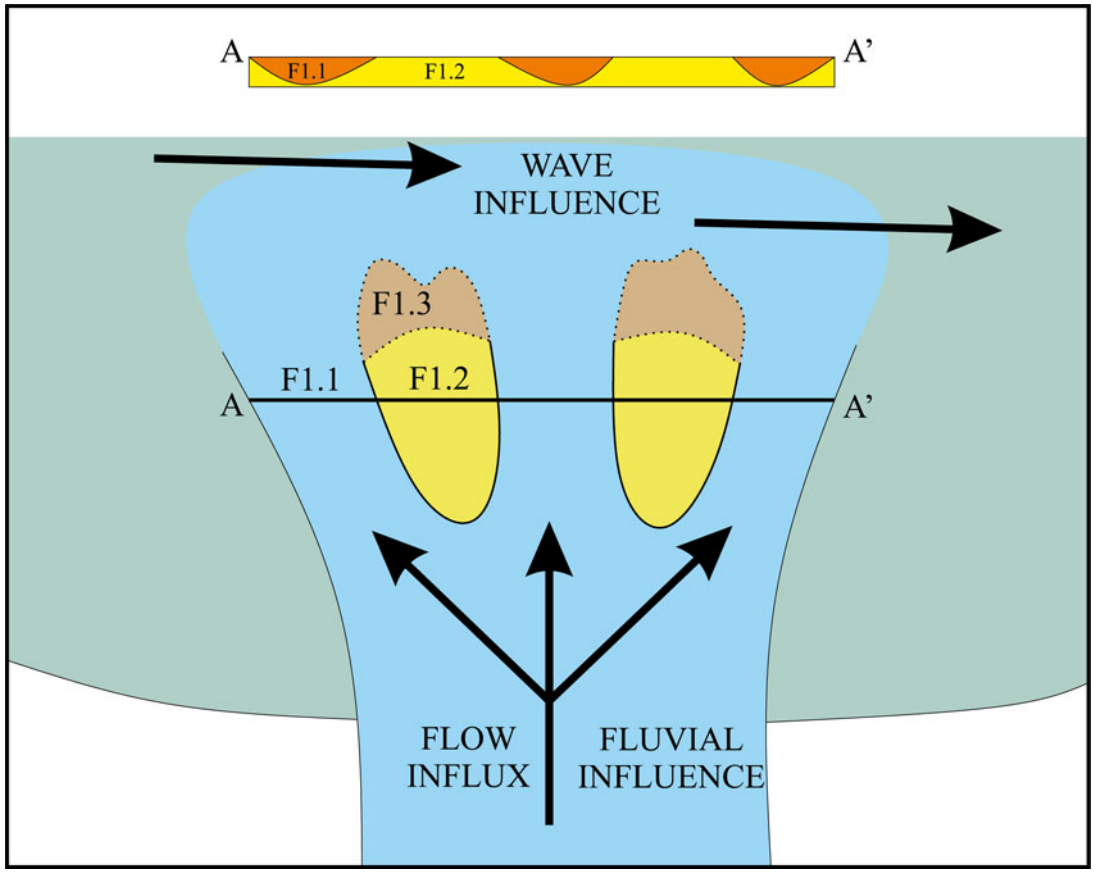

Fig. 9.11 Simplified cartoon of terminal distributary channel and fluvial mouthbar system (Modified from Schomacker et al. (2010), Bhattacharya and Giosan (2003), and Olariu and Bhattacharya (2006))

deposits in the Asphalt Wash-1 core. Ripples occur within very fine sandstones that rarely occur within normally graded bedsets. Therefore, the most distal siliciclastic input was probably deposited as hyperpycnal flows due to density differences between the incoming sediment-laden freshwater and lakewater.

Where the main distributary channel becomes terminal, there is a high degree of division within the channel that occurs, generating an intimate relationship between the channel and mouthbar deposits, as seen across Evacuation Creek. Numerous channel bodies alternating with mouthbar deposits represent many thin, migrating channels entering the lake system from the south. The orientation of these channels varies more in terminal distributary channels than in proximal distributary channels due to their extremely low gradients farther from the shoreline (Moore et al. 2012).

Across the Evacuation Creek outcrop, these facies relationships can be seen within the extensive sandstone bodies (Figs. 9.8, 9.9, and 9.10). Laterally, distributary channels (F1.1) and proximal mouthbars (F1.2) often transition back and forth, reflecting an instance where numerous mouthbars are dividing these channels and vice versa (Fig. 9.11). Vertically, mouthbars (F1.2) and channels (F1.1) always alternate, which is an indication of additional mouthbars being generated with channel movement. As progradation occurs in this siliciclastic setting, facies 1.1 will then overlie facies 1.2, creating an alternating vertical pattern between facies 1.1 and 1.2 (Fig. 9.12).

Taylor and Ritts (2004) surveyed lacustrine sandstone deposits by examining the depositional geometries and heterogeneity within both fluvial-deltaic and wave dominated shorelines. Datasets for their study were from outcrops within Nine

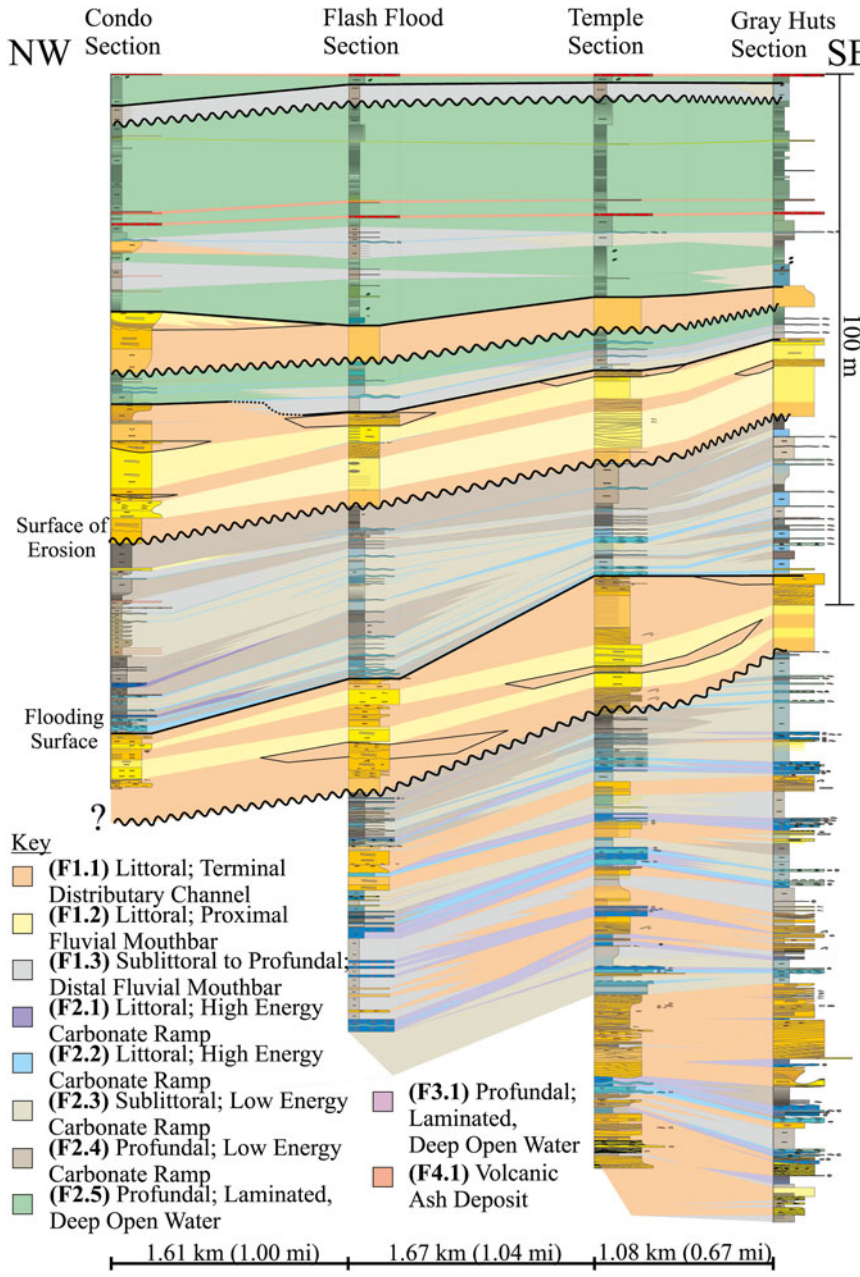

Fig. 9.12 Lithostratigraphic cross section of rocks exposed along Evacuation Creek outcrop

Mile Canyon in the south-central part of the Uinta Basin and Raven Ridge, located in the northeastern part of the basin. Generally, the fluvial-deltaic lacustrine shorelines are dominant in the gently-dipping southern margin of the basin, where there is less subsidence and more sediment influx. These shorelines are observed in the Nine Mile Canyon localities. The wave-modified shorelines are dominant at the steeper gradient, northern margin of the basin, where there are higher subsidence rates and lower sediment influx. These are observed at the Raven Ridge localities.

There are similarities from both types of lacustrine shorelines that are observed within the Evacuation Creek sandstone deposits, but overall there are more similarities with the fluvial deltaic shoreline, suggesting a dominance of fluvial deltaic processes with secondary wave influence characteristics. In the deltaic facies described from Nine Mile Canyon, amalgamated undulatory distributary channels have been described to have an intimate relationship with distributary mouthbar deposits similar to what is observed at Evacuation Creek (Taylor and Ritts 2004). These channels, as described by Taylor and Ritts (2004), typically truncate and amalgamate with distributary mouthbar deposits and can also be truncated themselves by additional distributary channels. The basal bounding surfaces are sharp and erosive when underlain by carbonates or mudstones. They describe the distributary mouthbars as tabular and laterally extensive across the outcrop. Their lower bounding surfaces are sharp, and erosive or nonerosive. These mouthbars, incised by the amalgamated undulatory distributary channels are very similar to what is observed in the Evacuation Creek lean zones.

In the wave-dominated facies described from Raven Ridge in the northeastern part of the Uinta Basin, shallow-lacustrine sheet sand deposits are described by Taylor and Ritts (2004) as extremely thin, tabular, laterally extensive sandstones with sharp bounding surfaces. Few of these thin sandstone beds are observed interbedded with lacustrine carbonate deposits at Evacuation Creek and interpreted as mouthbar complexes. These interpreted mouthbar complexes show additional wave modification in the form of broad symmetrical ripples, indicating current flow.

9.4.2.1 Facies Association 2: Carbonate Deposits

Facies 2.1 (F2.1)

Facies 2.1 is composed of carbonate grainstone ranging in "grain size" from ooids to oncolites (Table 9.1; Fig. 9.6). Oncolites are only found in the lower Gray Huts section in the Douglas Creek Member. The carbonate grains are light gray in color. Some units contain broad asymmetric ripples with a west to southwest paleocurrent direction (Fig. 9.13). Some ostracodal grainstones are also present. Many beds coarsen upward and are associated with microbialite layers that vary in thickness from millimeters to over one meter (F2.2).

Facies 2.1 is interpreted as being deposited in a high-energy carbonate ramp setting in the littoral zone of the lake, more specifically, ooid shoals. The geometry of the lake margin, as well as the energy level, is indicated by the carbonate facies present (Ryder et al. 1976). The abundance of ooids to oncolites suggests a high energy wave reworking of the carbonate grains during carbonate formation in relatively shallow water of the littoral zone (Ryder et al. 1976; Renaut and Gierlowski-Kordesch 2010). This facies is consistent with the Ryder et al. (1976) interpretation of lake margin carbonate flats in the Lower Green River Formation units. Shoal environments are characterized by relatively strong, consistent currents evidenced by lithologies that indicate agitation, this is supported by the presence of broad asymmetric ripples (Fig. 9.13) (Ryder et al. 1976). The absence of fluvial, siliciclastic material in this facies indicates that all paleocurrent indicators are from wave influence. Algal microbialites are often seen in association with shoal environments (Williamson and Picard 1974; Borer et al. 1998). This association helps to determine the shoreline geometry. Lakes with steep margins generate carbonate bench profiles and sharp facies transitions, whereas lakes with gentler-sloped margins generate carbonate ramp profiles and more gradual facies transitions. Facies 2.1 is interpreted as a high-energy carbonate ramp because of the common, gradational association with microbialites, as well as the presence of ooid shoals, indicating reworked ooids along the shoreline (Renaut and Gierlowski-Kordesch 2010). These shoals illustrate that the depositional environment was wave-influenced, as well as having a ramp-style geometry suitable for microbialites.

Facies 2.2 (F2.2)

Facies 2.2 consists of microbialites, forms ranging from stromatolites to thrombolites (Table 9.1; Fig. 9.6). Color is commonly light gray to tan. Bed thickness ranges from mm to over 1 m. This lithofacies commonly contains rip-up clasts of other microbialite fragments near the base of

Fig. 9.13 Ooid grainstone (F2.1) with ripples from the Flash Flood section in the R4 zone. The *dashed lines* highlight the ripple crests, and the *wavy line* follow the bedding plane topography

units. Well-preserved stromatolites in the form of low-relief domes or bioherms (commonly referred to as "heads") are found in some beds. These heads are commonly 10–15 cm in diameter. The growth of these heads was promoted by sufficient carbonate sediment supply and the amount of oxygen available based on proximity to the photic zone (Williamson and Picard 1974).

Facies 2.2 is also interpreted as deposited in a high-energy carbonate ramp setting in the littoral zone. Key features of this facies are carbonate bioherms that can be up to 1 m thick. The larger buildups are commonly interbedded stromatolites and thrombolites. Algal buildups of this nature are present as autochthonous growth structures (Williamson and Picard 1974). The necessity for a stable substrate for these buildups indicates a low-angle shoreline geometry during deposition (Renaut and Gierlowski-Kordesch 2010). The thick nature of some of the algal mats suggests a constant carbonate sediment flux, evident by a constant reworking in a high-energy environment. The energy level was thus high enough to provide a carbonate influx, but low enough to promote algal mat construction.

Facies 2.3 (F2.3)

Facies 2.3 consists of finely laminated, organic-poor carbonate mudstone (Table 9.1; Fig. 9.6). Color ranges from light tan to light gray. Plane parallel laminations are common in this lithofacies. Fossils found in this facies include few "bot-fly" larvae, fish scales/bones, plant debris, and rare bird feathers. This facies is often associated with thin microbialite layers (F2.2).

Facies 2.3 is interpreted as low energy carbonate ramp deposits found in the sublittoral lake zone. The interpretation of a low energy setting is due to the sublittoral nature of the deposits, where wave influence is more infrequent. Possible reasons for this facies' lack of preserved organic material include: low rates of plankton productivity, dilution by relatively high rates of carbonate production, conditions not conducive to organic matter preservation, or a combination of these factors (Renaut and Gierlowski-Kordesch 2010).

Facies 2.4 (F2.4)

Facies 2.4 consists of finely laminated, organic-rich carbonate mudstone, commonly known as "oil shale" (Table 9.1; Fig. 9.6). Color ranges from light gray in outcrop to black in core. Plane parallel laminations are very common in this lithofacies. Numerous fish scales and bones are found in this lithofacies and it is commonly associated with thin (0.1–0.3 m) microbialite layers (F2.2). Organic-richness is moderate to high, with beds ranging from 10 to 30 GPT across the basin (Vanden Berg 2008), but is likely lower in the study area on the eastern edge of the basin.

Facies 2.4 is interpreted as low energy carbonate ramp deposits, found in the distal sublittoral to profundal lake zones. Organic-rich carbonate muds can be deposited in a range of lake depth conditions. The low wave energy in this gently sloping environment allows for carbonate mud deposition (Renaut and Gierlowski-Kordesch 2010). Its association with thin microbialites (facies 2.2) indicates the transition on the ramp between high and low wave energy or littoral to sublittoral or profundal environments, respectively. The presence and size of these associated thin microbialites (F2.2) helps to define the lake zone of deposition. Due to the shallow-angle of carbonate ramp environments, a slight vertical change in lake level can result in a significant lateral shift in facies deposition from a littoral microbialite deposit, to a sublittoral or even profundal carbonate mudstone, which is recorded in a short stratigraphic thickness (Williamson and Picard 1974). The presence of thin interbedded microbialites is an indication of an episodically shallower environment of deposition in the deeper realm of the littoral or even shallow sublittoral zone. Increased organic material preservation in this facies is the result of increased biologic activity, with only minor dilution from detrital input.

Facies 2.5 (F2.5)

This facies consists of finely laminated, organic-rich carbonate mudstone (Table 9.1; Fig. 9.6). Color ranges from light gray to black, but is typically dark gray and similar to facies 2.4. It is also commonly termed "oil shale." Plane parallel to

wavy laminations are very common in this lithofacies. Fossil abundance varies by zone, but fossilized "botfly" larvae (found in specific stratigraphic intervals within the upper R6 and lower R8), insects, and plants are common, whereas fish fossils are very rare, as compared to facies 2.4. Soft sediment deformation is common, and some particularly organic-rich intervals are brecciated, containing oil shale rip-up intraclasts. Facies 2.5 is generally more organic-rich than facies 2.4, with individual beds reaching up to 70 GPT in the Mahogany zone (Vanden Berg 2008). Facies 2.4 and 2.5 are similar, but exhibit a clear geochemical difference. X-ray fluorescence data measured on the Asphalt Wash-1 core at approximately 1.5–4.6 m (5–15 ft.) intervals illustrates that facies 2.5 is more calcium rich than facies 2.4 (Fig. 9.14) (Birgenheier and Vanden Berg 2011).

Facies 2.5 is interpreted as the deepest, open water deposits found in the profundal lake zone (Ryder et al. 1976; Ruble and Philp 1998). These finely laminated carbonate mudstones are indicative of a deep lacustrine environment in which there was minimal siliclastic input, along with high plankton and algal production and preservation rates that outpaced carbonate production overall (Renaut and Gierlowski-Kordesch 2010). The soft sediment deformation and oil-shale breccia beds formed through

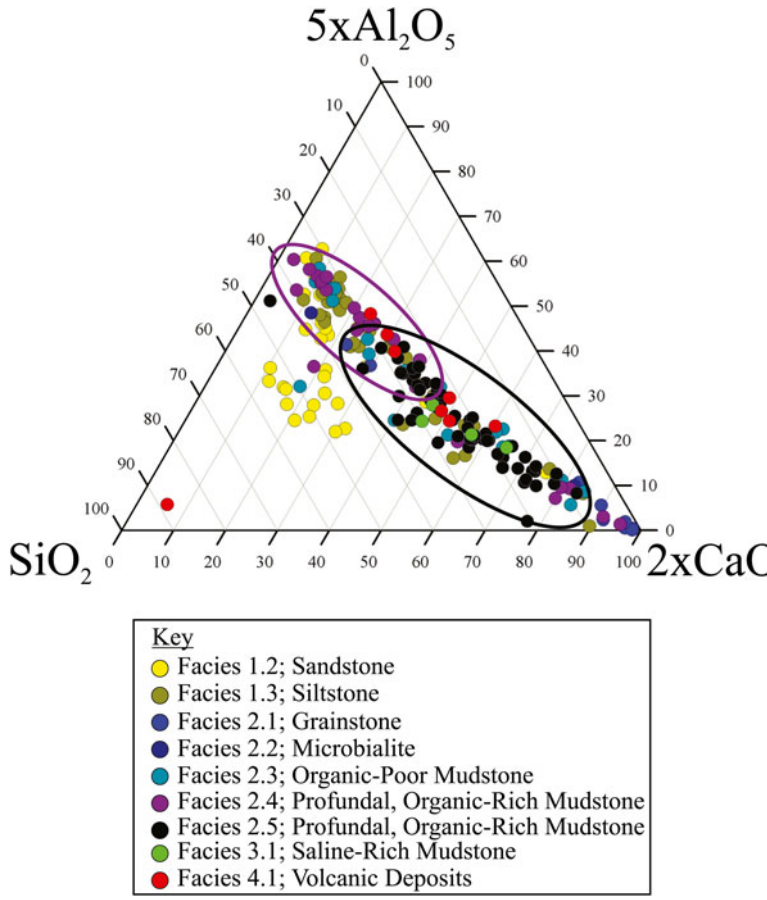

Fig. 9.14 Ternary diagram the illustrates the geochemical differences between facies. This diagram suggests a geochemical difference between F2.4 and 2.5 where 2.4 is more carbonate poor, whereas F2.5 is more carbonate rich

downslope migration and failure of the organic-rich material. The organic-rich carbonate sediment was saturated with water during deposition. As compaction occurred, the beds fail, promoting soft sediment deformation and downslope movement. The general absence of fish material relative to facies 2.4 suggests a chemically or biologically stressed environment, perhaps a density stratified saline and/or anoxic water column. The geochemical distinction between F2.4 and F2.5 seen in Fig. 9.14 suggests a transition from proximal to a more distal organic-rich environment within the profundal zone. Higher clay content would be expected in a more proximal location, closer to the source of detrital input, whereas higher carbonate production and less detrital input would be expected in more distal environments.

9.4.2.2 Facies Association 3: Saline Deposits

Facies 3.1 (F3.1)

Facies 3.1 is composed of finely laminated organic-rich carbonate mudstone, similar to facies 2.5, but with abundant saline minerals (Table 9.1; Fig. 9.7). The most common saline minerals found in the Green River Formation include shortite and nahcolite (Fahey 1962). These saline minerals occur in a variety of forms including small to large nodules, thin beds, or small-disseminated crystals along bedding planes. The nodules average a few centimeters in diameter, but can be more than a decimeter. The saline minerals themselves are white to clear to grey. The background sediment in this facies is medium to dark gray in color and consists of moderately organic-rich carbonate mudstone that is faintly laminated or massive. Facies 3.1 is eroded at Evacuation Creek, but exposed in outcrops nearby to the north and is captured at the top of the Asphalt Wash-1 core.

Facies 3.1 is interpreted as deep, open water deposits found in the profundal lake zone, with minimal siliciclastic disturbance. This facies is not the deepest interpreted lake zone (F2.5; Mahogany Zone), but is still relatively deep compared to the other facies present in the system. Overall, high lake salinity resulted in saline mineral precipitation at or near the sediment-water interface of the deep lake (Johnson 1985; Ruble and Philp 1998; Vanden Berg et al. 2012). Precipitation of saline minerals in solution resulted as the lake water became supersaturated due to a low freshwater input and relatively high evaporation rates. Stratification ensued and dense brines accumulated at the bottom of the lake (Fahey 1962). Relatively high lake levels precluded evaporite mineral deposition in this environment.

9.4.2.3 Facies Association 4: Volcanic-Derived Deposits

Facies 4.1 (F4.1)

Facies 4.1 is composed of fine to medium grained volcanic ash deposits (reworked and ash-falls) (Table 9.1; Fig. 9.7) (Smith et al. 2010). Colors range from light tan to light yellow. Most beds are less than 10 cm thick, but few are close to half a meter thick. This lithofacies contains abundant igneous crystals visible in hand specimen, such as biotite.

The two thickest and most prominent tuff beds present along Evacuation Creek, and the eastern Uinta Basin include the Curly and Wavy tuffs, which are also present regionally. The Curly tuff lies near the base of the Mahogany zone, whereas the Wavy tuff lies in the lower part of the R8 zone. These tuffs were sourced by the Absaroka Volcanic province to the north, beginning at about 49 million years ago (Ma) (Smith et al. 2008, 2010). Both of these beds are about a half-meter thick and are present in all measured sections (Fig. 9.12). The Curly and Wavy tuffs are probably reworked volcanic material brought into the lake by fluvial processes, as they contain bedding, lamination, and swirled textures. The thinner tuffs are massive and, hence, more likely to be ash fall deposits. The regionally-extensive Mahogany marker is a 15 cm thick tuff that is located 2–3 m above the Mahogany bed, the richest bed within the Mahogany zone (Cashion 1967). Age constraints on the Curly and Wavy tuffs, derived using $^{40}Ar/^{39}Ar$ methods indicate ages of 49.3 Ma and 48.7 Ma, respectively (Smith et al. 2008, 2010).

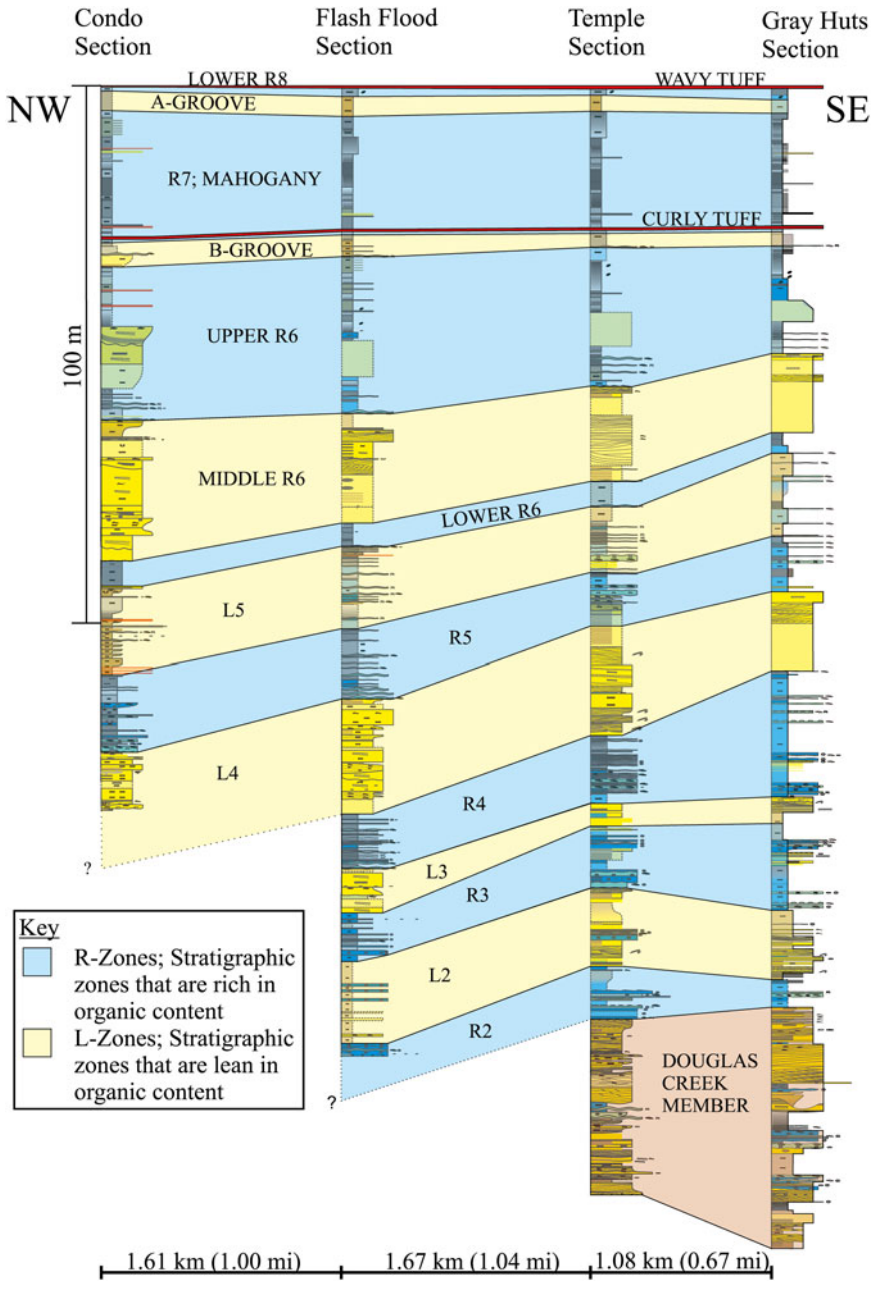

Fig. 9.15 Cross section of interpreted stratigraphic units present along Evacuation Creek outcrop

9.4.3 Stratigraphy and Facies Architecture

The lateral extent and geometry of facies architecture and stratigraphic units across the Evacuation Creek outcrop is shown in cross section in Figs. 9.12 and 9.15. These facies architectures and stratigraphic units were also correlated to the Asphalt Wash-1 core (Figs. 9.16 and 9.17). Tables 9.2a and 9.2b further summarize each stratigraphic unit by indicating which sections they are present, thickness ranges, facies type, and other key characteristics.

The Douglas Creek Member is the lowest stratigraphic unit present. High heterogeneity is

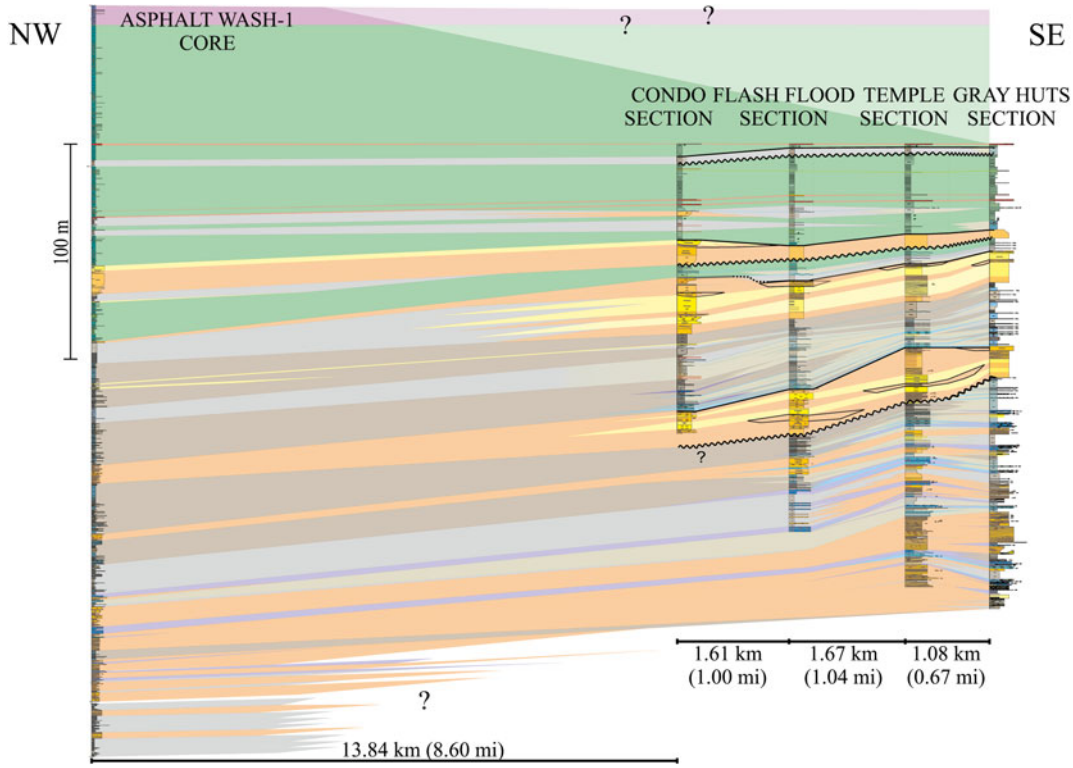

Fig. 9.16 Lithostratigraphic cross section of Evacuation Creek outcrop and Asphalt Wash-1 core

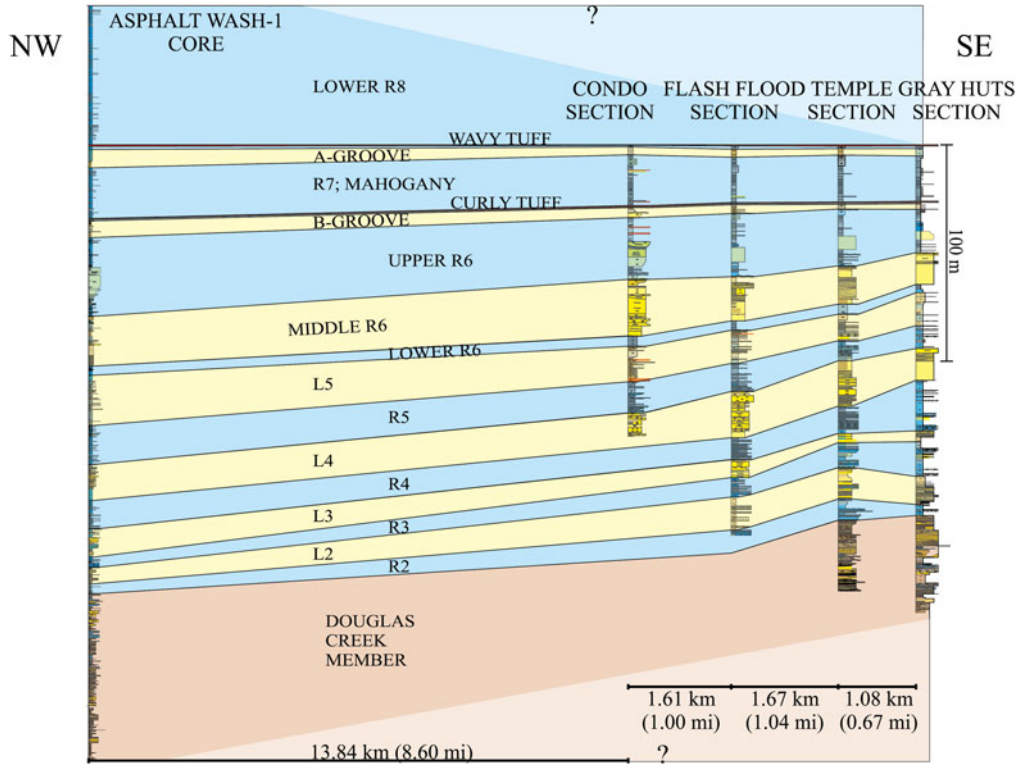

Fig. 9.17 Cross section of interpreted stratigraphic units present in Evacuation Creek outcrop and Asphalt Wash-1 core

Table 9.2a Summary of stratigraphic units

	Units present					Thickness				
Stratigraphic unit	AW	C	FF	T	GH	Min. (m)	Max. (m)	Avg. (m)	AW (m)	Facies present
R8	**x	**x	**x	**x	**x	–	–	–	L: 71.9 /M: **9.0	F2.5, F3.1, F4.1
A-Groove	x	x	x	x	x	3.0 (GH)	3.6 (C/FF)	3.2	3	F2.3
R7; Mahogany Zone	x	x	x	x	x	20.9 (GH)	28.0 (C)	23.5	23.8	F2.5, less F4.1
B-Groove	x	x	x	x	x	2.5 (T)	4.5 (C)	4.5	8.5	F1.1, F1.3, F2.3
Upper R6	x	x	x	x	x	20.2 (GH)	29.0 (FF)	27.7	35.4	F2.5, F1.1-F1.2, minor F1.3, F2.3
Middle R6	x	x	x	x	x	14.6 (GH)	24.8 (C)	20.2	23.5	F1.1 and F1.2
Lower R6	x	x	x	x	x	3.9 (GH)	4.9 (T)	4.4	4	F2.4, less F2.2-F2.3
L5	x	x	x	x	x	12.2 (T)	17.0 (C)	16.5	22.6	F1.3, less F2.2-F2.3
R5	x	x	x	x	x	9.8 (T)	14.0 (C)	13.1	18.6	F2.4, less F2.1-F2.2, minor F1.3
L4	x	*x	x	x	x	14.8 (GH)	21.0 (FF)	18	16.5	F1.1-F1.3
R4	x	–	x	x	x	10.5 (FF)	23.7 (GH)	15	12.8	F2.1-F2.4
L3	x	–	x	x	x	3.5 (T)	8.0 (FF)	7.4	13.1	F1.1, F1.3, minor F2.3
R3	x	–	x	x	x	9.5 (FF)	16.0 (GH)	10.6	4.3	F2.1-F2.4, minor F1.1, F1.3
L2	x	–	x	x	x	13.0 (GH)	15.0 (FF)	12.7	8.8	F1.1, F1.3, minor F2.1
R2	x	–	*x	x	x	5.0 (GH)	10.2 (T)	6.4	4	F2.1, F2.2, F2.4, minor F1.1, F1.3
Douglas Creek Mbr	*x	–	–	*x	*x	*33.0 (T)	*45.0 (GH)	*39.0	*76.0	F1.1-F1.3, F2.1-F2.5

This table summarizes the stratigraphic units that are found in the Evacuation Creek measured sections and Asphalt Wash-1 core. *AW* = Asphalt Wash-1 core, *C* = Condo section, *FF* = Flash Flood section, *T* = Temple section, *GH* = Gray Huts section, * = unit cut off. Average thickness for Evacuation Creek sections only

observed in the Douglas Creek Member throughout all Green River Formation depositional localities (Cashion 1967). Individual sandstone bodies of facies association 1 are laterally extensive, but individual carbonate units of facies association 2 are not. The Douglas Creek Member has the largest range of lithologies within the Evacuation Creek outcrops, reflecting a highly variable environment with periods and regions of fluvial input, but also periods and regions ideal for carbonate generation. The Douglas Creek Member in the Asphalt Wash-1 core contains the same lithologies identified in Evacuation Creek, but grades from siliciclastic-dominated at the base of the core (which is not the base of the Douglas Creek Member), with an increase in carbonate facies towards the top of the unit (Fig. 9.16). The Asphalt Wash-1 core contains a thin, rooted, paleosol bed near its base (0.5 m or 1.6 ft), which is below the exposed rocks at the Evacuation Creek outcrops.

The Parachute Creek Member, which overlies the Douglas Creek, is defined by a succession of alternating organic-rich (R) and lean (L) units with varying lithologies (Figs. 9.15 and 9.17). Generally, organic-rich zones are identified as facies association 2 (carbonate deposits), whereas lean zones contain mostly facies association 1 (siliciclastic deposits), except the A and B-Grooves,

Table 9.2b Summary of stratigraphic units continued

Stratigraphic unit	Key characteristics
R8	Wavy tuff 5–7 m above base, "botfly" larvae fossils above Wavy tuff; Lower: F2.5, only base exposed at Evacuation Creek; Middle: dominated by F3.1, only present in AW
A-Groove	Dolomitic in all sections
R7; Mahogany Zone	Curly tuff near base, additional thin tuff beds; most organic-rich carbonate mudstone
B-Groove	Thin lean unit
Upper R6	Composed of three units: lower and upper are dominantly carbonate mudstone, middle unit siliciclastics; "Botfly" larvae fossils near top
Middle R6	Blocky sandstone at Condo to thinner, poorly exposed sandstone at Gray Huts; mudcracks present near top across Evacuation Creek
Lower R6	Thin rich unit, very few fossils observed (plant)
L5	Finer grained siliciclastic facies than other lean zones, larger amount of carbonates
R5	Some fish and plant debris; contains few microbialite beds that can be traced through all Evacuation Creek sections
L4	Facies transition from Evacuation Creek to AW represents down-dip facies change within mouthbar complex
R4	Fish, plant, and shell (AW) debris; alternating rich and lean cycles, carbonate dominated, cycles from littoral to profundal, decreasing number of microbialites from Evacuation Creek to AW
L3	Transitions laterally from sandstone to siltstone to carbonate mudstone, demonstrating lateral relationship on local scale
R3	Some fish and plant debris; irregular thickness variations across Evacuation Creek possibly due to erosion from overlying unit deposition
L2	Lowermost organic-lean zone in Parachute Creek Member; 3 distinct grainstone beds in all sections
R2	Lowermost laterally extensive organic-rich zone; some fish and plant debris; defined here as base of Parachute Creek Member
Douglas Creek Mbr	High heterogeneity; sandstone bodies laterally extensive, some fish and plant debris, carbonates not; paleosol bed present in AW

This table summarizes the key characteristics of the stratigraphic units present at the Evacuation Creek measured sections and Asphalt Wash-1 core

which are mostly carbonate dominated. Units features are summarized in Table 9.2a and 9.2b.

9.5 Discussion

9.5.1 Genetic Stratigraphic Model

The nature of the surfaces that separate the rich and lean zones and the stacking patterns within are important for interpreting the genetic stratigraphy and lake evolution through time for the Parachute Creek Member of the Green River Formation (Table 9.3). Also important to this

Table 9.3 Summary of organic-rich and organic-lean zones

	Organic-rich zones	Organic-lean zones
Primary lithology	Carbonate facies	Siliciclastic facies
Stacking pattern	Aggradation or Retrogradation	Progradation
Basal surface	Flooding surface	Surface of erosion
Top surface	Surface of erosion	Flooding surface

Summary of the characteristics of the organic-rich and organic-lean zones observed in the study area. Features summarized include lithology, stacking patterns, and bounding surfaces typically observed

discussion is determining relative lake level changes that reflect accommodation as a result of tectonic subsidence, sediment supply, and absolute lake level changes. There are three major types of surfaces that are found in the Evacuation Creek outcrop. The first surface is a regional surface of erosion that is located at the base of the lean, siliciclastic units, at the top of the underlying organic-rich carbonate units. There are four main, laterally-extensive surfaces of erosion, found at the base of the L4, L5, middle R6, and upper R6 sandstone units (Figs. 9.12, 9.15, and 9.17). The extent of these erosional surfaces not only encompasses this field area, but are also observed on the basin and interbasin scale (Keighley et al. 2002, 2003; Birgenheier and Vanden Berg 2011; Tänavsuu-Milkeviciene and Sarg 2012).

Depositionally, these laterally extensive surfaces of erosion mark the base of mouthbar complexes and terminal distributary channels that comprise the lean zones. The architecture and depositional nature of these siliciclastic complexes are similar to those described by (Taylor and Ritts 2004). The inherent erosional nature of high flow rates prior to fluvial and mouthbar deposition does not necessitate an interpretation that includes a significant change in absolute lake level at these regional surfaces of erosion. This is further supported by an overall similarity in littoral to sublittoral lake depth recorded in the bounding carbonate units as compared to the littoral to sublittoral lake depth interpreted from the siliciclastic distributary channel and mouthbar units. Autocyclic deposition of channels and mouthbar facies throughout the succession would produce seemingly random and nonsystematic surfaces of erosion. Instead, the surfaces of erosion recorded here are regional in extent and stratigraphically systematic, suggesting an allocyclic control on siliciclastic deposition, mainly hinterland climate or tectonics. As such, the laterally extensive surfaces of erosion are interpreted to represent reduced accommodation (or a relative lake level fall) as a result of regional increased fluvial sediment supply and subsequent higher siliciclastic deposition rates, partially filling the available accommodation space in the lake basin (Fig. 9.19). These surfaces of erosion are rather consistent with Keighley and others (2003) Type A sequence boundaries (Exxon type 1), indicating a basinward shift in facies across a regionally mappable surface. Fluvial incision of varying degrees are associated with these surfaces and are consistent with studies in the south-central Uinta Basin (Keighley et al. 2003). These contacts are best developed where lacustrine successions are truncated by laterally extensive, amalgamated fluvial channels, and are commonly at the top of well-developed paleosols. The main discrepancy between the regional surfaces of erosion at Evacuation Creek and these Type A sequence boundaries is that at Evacuation Creek, there are no paleosol beds to mark these surfaces, indicating that the underlying strata had more of a lacustrine origin. Additionally, in Keighley and others (2003) sequence stratigraphic model, Type A sequence boundaries are more common up section, correlative to the lower section at Evacuation Creek.

Within the rich and lean depositional units, there are different types of stacking patterns that can be used to determine variations in sediment supply. The siliciclastic associations, or lean zones, are built of 3–5 m-scale parasequences that coarsen from very fine or fine to medium sandstone, indicating a vertical distal to proximal stacking trend within each parasequence. Parasequences stack repeatedly and exhibit an overall coarsening trend, indicating a progradational stacking pattern and an increase in sediment supply (or decrease in accommodation) upwards. Laterally, these progradational parasequences can be traced throughout the entirety of the Evacuation Creek outcrop, indicating a regional increase in sediment supply (or decrease in accommodation to sediment supply ratio) over the lean zone depositional events. Progradational stacking patterns are also identified in the lake-margin clastic parasequences in Nine Mile Canyon by Keighley and others (2003).

The next major type of genetic surface is a regional surface of subaerial exposure, which is only observed in one stratigraphic horizon. Near the top of one of the progradationally stacked zones (middle R6) in multiple locations

along the Evacuation Creek outcrop, there is an extensive mudcrack horizon indicating subaerial exposure (Fig. 9.18). The mudcracks are in a thin mudstone layer near the top of the middle R6 zone, and are underlain and overlain by sandstone units. On top of the underlying sandstone unit, there are bioherms that protrude up through the mudstone layer (Fig. 9.18e). These bioherms developed on the sandy substrate, and were surrounded during mud deposition. After bioherm growth, the mudstones were exposed for a period of time, stimulating crack formation.

The last major type of surface is a laterally extensive flooding surface, found at the base of the organic-rich carbonate units or rich zones (Figs. 9.12, 9.15, and 9.17). These surfaces represent an increase in accommodation to sediment supply ratio (or rise in relative lake level), following a basinward progradation of parasequences in the underlying mouthbar complexes and terminal distributary channels represented by lean zones. Following high rates of siliciclastic deposition, siliciclastic sediment supply waned, and through a combination of low siliciclastic deposition rates and continued subsidence, relative flooding ensued. With low siliciclastic input, carbonate deposition dominated, and the overlying organic-rich carbonate units were deposited, relatively free of siliciclastic dilution. Both organic preservation basinward and carbonate preservation on the shelf thrive in conditions of low siliciclastic sediment input. The flooding surfaces at the base of rich zones are laterally extensive (Figs. 9.12, 9.15, and 9.17).

Keighley and others (2003) have described similar major flooding surfaces in Nine Mile Canyon. They have identified these surfaces at the base of lacustrine-dominated intervals where carbonates abruptly overlie sandstone deposits. These surfaces are consistent with the flooding surfaces at Evacuation Creek that lie at the top of the lean zones and base of the rich zones.

The stacking patterns in the organic-rich carbonate units are composed of retrogradational or aggradational stacked parasequences. These parasequences are on the 3–5 m-scale and comprise organic-rich carbonate mudstone (F2.4) that transitions upwards to organic-lean carbonate mudstones (F2.3) to microbialites (F2.2). These shallowing-upward sequences are commonly capped by a carbonate grainstone (F2.1). Keighley and others (2003) identify ~10 m aggradational stacking patterns in their lacustrine parasequences. The facies transitions of the parasequences in these rich zones are often a result of the shallow-ramp geometry of the basin. Slight fluctuations in lake level resulted in significant facies changes from organic carbonate mudstone to microbialites or grainstones. The absence of siliciclastic material, in addition to these stacked carbonate parasequences, illustrate a decrease in sediment supply (or increase in accommodation), relative to the siliciclastic packages below and above. Aggradational or retrogradational stacking patterns that are preserved reflect a system in which subsidence outpaced carbonate sedimentation rates, allowing for relative lake level rise. Laterally, individual carbonate parasequences are difficult to trace across a continuous distance such as the Evacuation Creek outcrop, suggesting local lateral changes in carbonate facies deposition, but at any given location, similar retrogradational or aggradational patterns are always exhibited, reflecting overall relative lake level rise.

Keighley and others (2003) present a high-resolution sequence stratigraphic interpretation of the strata present in Nine Mile Canyon. Their interpretations use traditional sequence stratigraphic terminology, which is not used in this study. However some of Keighley concepts can be applied. They present lowstand systems tracts as occurring above Type A sequence boundaries and being capped by the first significant transgressive surface. These lowstand systems tract interpretations could be applied to some of the lower, well-defined lean zones such as L3 or L4. However, using traditional sequence stratigraphic terminology, these packages could similarly be described as highstand systems tracts due to their progradational stacking pattern. Transgressive and highstand systems tracts are also included in Keighley and others (2003) sequence stratigraphic model. Both of these systems tracts are bounded either at the base (TST) or top (HST) by maximum flooding surfaces,

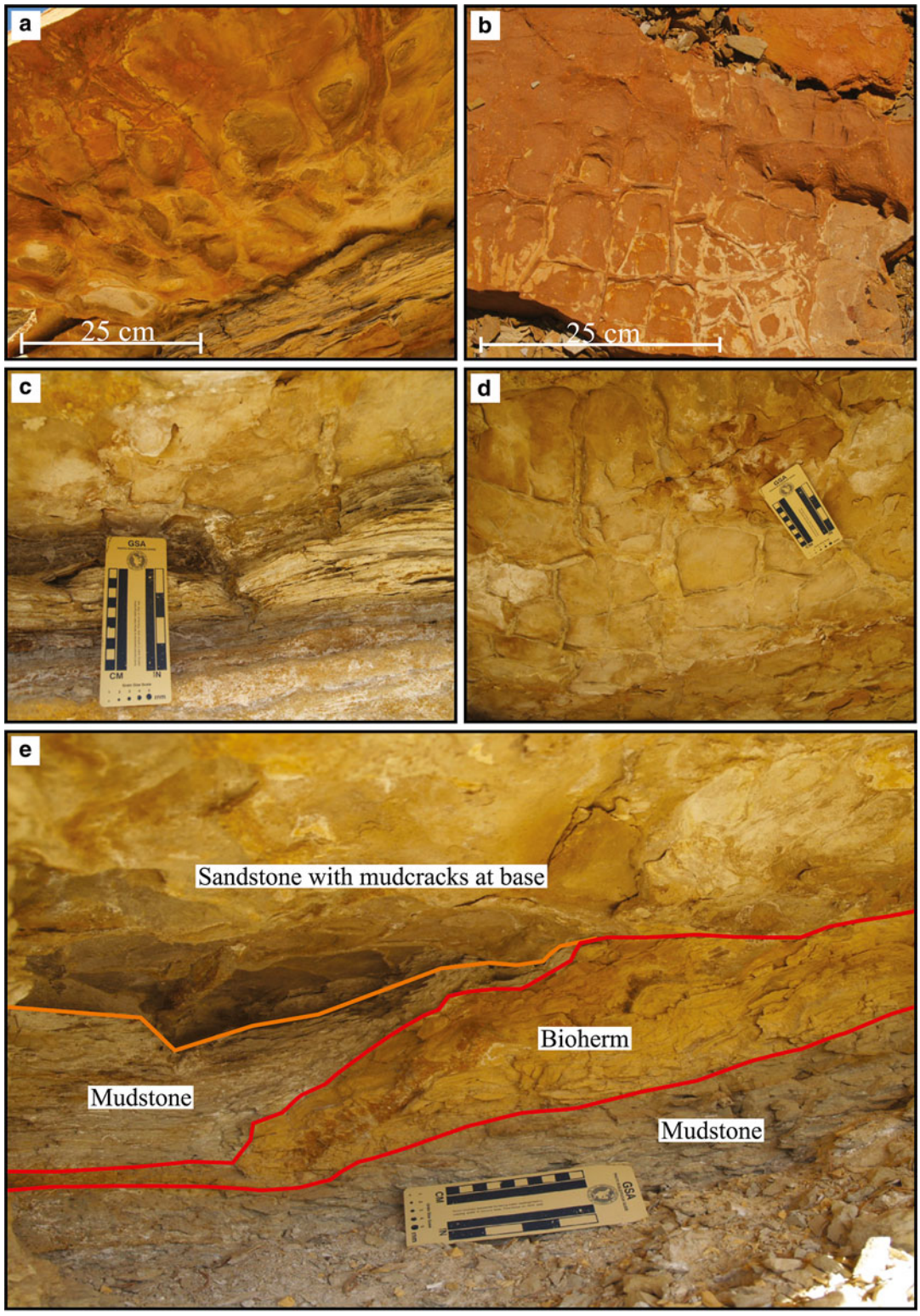

Fig. 9.18 Photographs of mudcracks present along the Evacuation Creek outcrop. (**a**) and (**b**). Mudcracks at the top of the middle R6 unit of the Condo section. (**c**), (**d**), and (**e**) Mudcracks at the top of the middle R6 unit of the Gray Huts section

which they define as being present within oil shale of profundal origin. In the Evacuation Creek section, any maximum flooding surface would be interpreted higher in section than what can be loosely correlated to Nine Mile Canyon. Alternately, Keighley and others' maximum flooding surface could be correlated to our laterally extensive flooding surfaces. Fundamentally, we view hinterland changes in siliciclastic sediment supply relative to accommodation rather than lake level or base level changes to be the main control on the aforementioned packages. Most of the traditional sequence stratigraphic terminology, including the model of Keighley and others (2003) implies significant lake level or base level change between alternating rich and lean units, for which we see no compelling evidence within one cycle of major key surfaces outlined above.

9.5.2 Stratigraphic Changes in Lake Level, Accommodation, and Sediment Supply

The upper Douglas Creek Member, is highly variable in terms of lithology, containing large amounts of siliciclastic material and lesser amounts of coarse carbonate material. Although there is a high degree of lithologic variability, most of the comprising facies reflect littoral deposition, so absolute lake level during Douglas Creek deposition is interpreted as the lowest during this study interval. There was minimal fluctuation in absolute lake level through the interval and more individual siliciclastic input events in comparison with overlying units (Fig. 9.19). The upper Douglas Creek Member represents a laterally variable environment with

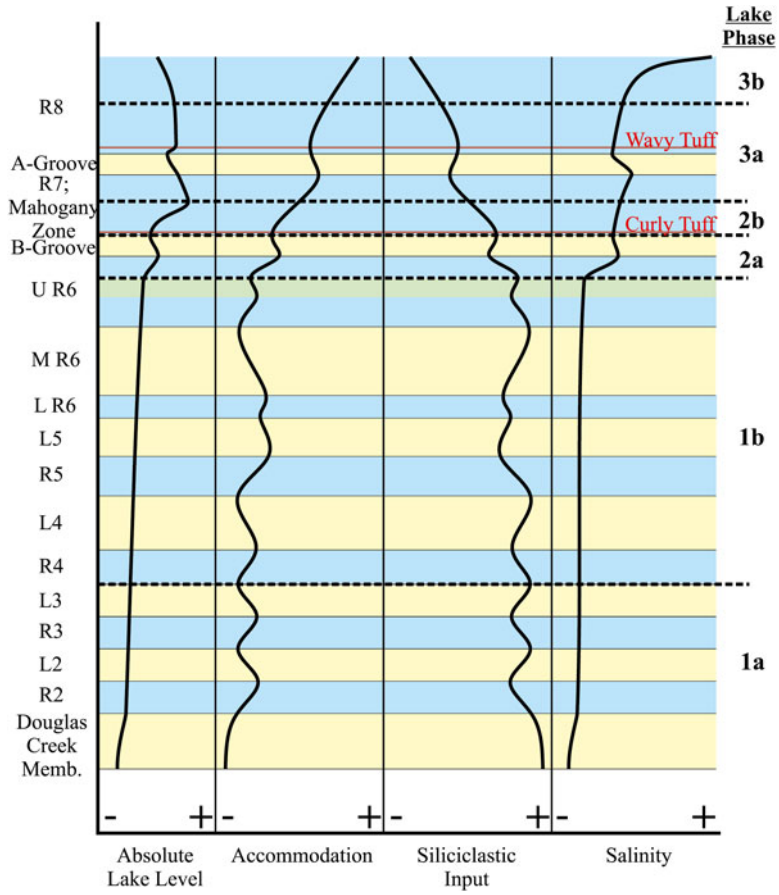

Fig. 9.19 Estimated stratigraphic changes in absolute lake level, accommodation, siliciclastic input, and salinity for the study area. Stratigraphic units are labeled to the left and lake phases are labeled to the *right*. The Curly and Wavy tuffs have age constraints of 49.3 Ma and 48.7 Ma, respectively (Smith et al. 2010)

multiple siliciclastic deposition events, separated by small-scale carbonate precipitation. The siliciclastic deposits have a high degree of fluvial influence that suggests a more proximal location to the source relative to overlying lean zones. The Douglas Creek Member contains some of the thickest (1+ m) and well-formed stromatolites in the section, as well as the largest carbonate grainstones (oncolites). The siliciclastic input fluctuated both laterally and temporally, but overall was at its highest and accommodation at its lowest point in the study interval during the deposition of the Douglas Creek Member (Fig. 9.19).

During deposition of the R2 to middle R6 units, the system records some fluctuation in absolute lake level illustrated by the dominance of interpreted littoral to sublittoral facies, but also the presence of some profundal facies. The bulk volume of these units is littoral to sublittoral, indicating that the lake system was fairly consistent, but the presence of some profundal facies suggests periods of higher lake level. These units record fluctuations in accommodation, which is controlled by tectonic subsidence and tectonically and climatically driven siliciclastic sediment supply and delivery (Figs. 9.16 and 9.17). The available accommodation, however, fluctuated during this interval, increasing during the organic-rich periods and decreasing during organic-lean periods, with aggradation to retrogradation and progradation, respectively (Fig. 9.19). The siliciclastic input also fluctuated, resulting in higher siliciclastic material in the lean zones and lower siliciclastics in the organic-rich zones (Fig. 9.19). In the organic-rich zones, there does seem to be substantial lake level changes based on the presence of organic-rich carbonate mudstone as well as microbialite facies present. These are a result of slight vertical lake level fluctuations in low angle ramp, shallow lake environments that result in significant lateral shoreline translations and hence abrupt facies changes from the profundal to sublittoral or even littoral realm.

A rise in absolute lake level is interpreted above the sandstone in the upper R6 unit, as evidenced by a significant facies change from dominantly shallow littoral and sublittoral to dominantly deeper sublittoral and profundal facies (Figs. 9.16 and 9.17). At this stratigraphic boundary, available accommodation began an increasing trend, whereas siliciclastic input began to decrease. The B-Groove indicates a small shallowing event, with a thin interval of more sublittoral facies. The base of the Mahogany zone (R7) represents another rise in absolute lake level marking the transition from sublittoral to profundal to exclusively profundal facies (Figs. 9.16 and 9.19). The highest lake level is within the Mahogany zone, near the Mahogany bed. The A-Groove indicates another shallowing event, with a decrease in organic matter production or preservation. Within the R8 unit, at the base of the middle R8, the absolute lake level began to fall again and salinity increased dramatically, creating a hyper-saline lake environment. There were no outlets from the lake system besides evaporation, resulting in stratification of the water column. Dense, supersaturated brines accumulated at the bottom of the lake, where saline minerals precipitated.

Figure 9.19 illustrates two patterns in absolute lake level changes: (1) the longer term absolute lake level stability from the R2 through the upper R6 units, with alternating rich and lean zones reflecting fluctuations in accommodation and siliciclastic input, and (2) the increase in absolute lake level that occurred midway through the upper R6 and R7 units, providing a shift from dominantly shallow to dominantly profundal lake facies.

9.5.3 Lake Phases

The studied interval of the Douglas Creek and Parachute Creek Members at the Evacuation Creek outcrop and Asphalt Wash-1 core illustrate the long-term evolution of Lake Uinta in the Uinta Basin from a fluctuating "freshwater" lake with high fluvial input, to a rising, deep lake, and finally to a terminal lake system with hypersaline conditions. The facies present demonstrate this evolutionary pattern and correspond to facies associations defined by Carroll and Bohacs (1999), as well as fit their model of lake phase

evolution from an overfilled to balanced-fill to underfilled lake basin. These lake phases are defined by the balance between the influx of water and sediment fill and potential accommodation present in the basin.

The Douglas Creek Member to the base of the upper R6 is interpreted as an overfilled lake basin consisting of fluvial-lacustrine facies. In an overfilled basin, the influx rate of water plus sedimentation is greater than potential accommodation (Carroll and Bohacs 1999). During this overfilled time, the Uinta Basin was being supplied with sediment from the uprising mountains surrounding the basin, but was also spilling over the Douglas Creek Arch into the Piceance Creek Basin. Overall, accommodation was at its lowest in this lower stratigraphic interval (Fig. 9.19). Overfilled basins have high amounts of inflows and outflows, but they are in relative equilibrium. These systems are described as freshwater lakes that are closely related to fluvial systems due to the high amount of siliciclastic, fluvial influx (Carroll and Bohacs 1999). Since the inflows and outflows are relatively equal, any lake-level fluctuations are minimal and are climatically driven (Carroll and Bohacs 1999). As evidenced above, in low-gradient carbonate ramp settings, minimal lake-level fluctuations can have a profound impact on the facies deposited.

Carroll and Bohacs (1999) describe "fluvial-lacustrine" facies as prograding parasequences, about 10 m thick that grade from mudstone or siltstone, to shelly coquina, to small sandy deltas. Similar parasequences are observed throughout these lower siliciclastic units, but there is much more variability in parasequence style and stacking patterns than described by the Carroll and Bohacs (1999) model. Progradation is recorded in these lower lean zones, but in the rich zones, aggradational or even retrogradational stacking patterns dominate. Although this entire interval can be termed "fluvial-lacustrine" and overfilled, there is a significant amount of additional detailed information about lake evolution that is preserved.

The Douglas Creek Member through the L3 zone, termed here lake phase 1a, is highly variable, stratigraphically (and laterally), in terms of lithology, and units are thinner relative to the overlying interval from the base of the R4 to the top of the upper R6 sandstone, termed here lake phase 1b, (Figs. 9.12, 9.15, 9.16, 9.17). Below the R4 unit in lake phase 1a, there is a strong presence of fluvial facies as well as littoral lacustrine facies, but the architectural relationships between the two are highly heterogeneous and complex. The individual rich and lean zones in this interval are more difficult to define based on this high degree of variability in both the vertical and horizontal directions. High variability suggests fluctuations in siliciclastic input and accommodation were frequent and periods between fluctuations short-lived (Fig. 9.19). In contrast, facies in the interval from the base of the R4 unit to the top of the upper R6 sandstone, which comprise lake phase 1b, are relatively more homogeneous and laterally continuous within each zone (Figs. 9.12, 9.15, 9.16, 9.17). Within lake phase 1b, very clear organic-rich and lean zones can be defined by the lithology and stacking patterns. These zones are laterally continuous over the entire study area and stratigraphic boundaries between zones are easily defined. This suggests fluctuations in sediment supply and accommodation were less frequent and periods between fluctuations were longer-lived (Fig. 9.19). Both lake phases 1a and 1b contain fish scales/bones and, as such, suggest fresher-water conditions were dominant. Oil shale preservation in the rich zones required persistent water column stratification conditions, either through means of stagnant water mass circulation, temperature, oxygen, and/or salinity stratification. These conditions would be further encouraged by low siliciclastic sediment input.

Carroll and Bohacs' (1999) description for "fluctuating profundal" facies associations fits descriptions from Evacuation Creek and the Asphalt Wash-1 core from the top of the upper R6 zone up to the middle of the R8 zone. In a balanced-fill basin, water plus sediment influx is relatively equal to potential accommodation (Carroll and Bohacs 1999). This balance of inputs and available space causes lake level to rise and therefore corresponds to the "fluctuating profun-

dal" facies. Above the upper R6 unit, siliciclastic input decreases significantly and is absent altogether above the B-Groove. This fall in siliciclastic input is coupled with an increase in available accommodation. Above the upper R6 sandstone, absolute lake level increased, enough so that dominantly organic-rich carbonate mudstone (oil shale) was deposited. These facies are indicative of a deep lake environment. An absolute lake level rise is interpreted at the top of the upper R6 sandstone unit, and is marked by a shift in facies type from dominantly littoral/sublittoral to dominantly sublittoral/profundal facies (Figs. 9.12, 9.15, 9.16, 9.17, and 9.18) (Ryder et al. 1976). As a balance-filled lake basin, lake level was above the Douglas Creek Arch and the Uinta and Piceance Creek Basins were in communication. Preservation of abundant oil shale in this interval suggests long-lived water column stratification causing bottom water anoxia. Local preservation of saline minerals in cores outside of the study area within the Mahogany zone and the upper R6 suggest periodic salinity driven density stratification affected this system during this interval (Birgenheier and Vanden Berg 2011). This water column stratification may have enhanced organic preservation and encouraged further anoxia.

Notably, the interval between the upper R6 sandstone and the middle of the R8 can be further divided. Below the Mahogany zone (top of the upper R6 sandstone to the top of the B-Groove), termed here lake phase 2a, there is a higher amount of siliciclastic input into these "fluctuating profundal" facies (Figs. 9.12, 9.15, 9.16, 9.17, and 9.19).

Within the upper R6 zone and the B-Groove, there are more sandstones and siltstones, whereas from the base of the Mahogany zone to the Mahogany bed, termed here, lake phase 2b, there is no evidence of siliciclastic input. The base of lake phase 2b (the base of the Mahogany zone) is interpreted to represent another increase in absolute lake level and accommodation, whereas siliciclastic input decreased. Lake level was highest during the deposition of the Mahogany zone, and reached its highest mark near the Mahogany bed (Fig. 9.19). From the Mahogany bed to the base of the middle R8, termed here lake phase 3a, absolute lake level remained high and relatively stable outside of the A-Groove, which represents a slight shallowing event. Although this entire interval can be widely termed "fluctuating profundal," further subdivision of this interval based on facies variability helps to define a more precise model of lake evolution.

At the middle R8 unit of the Asphalt Wash-1 core, the organic-rich carbonate mudstones display abundant saline minerals at a distinct stratigraphic depth (336.3 ft), suggesting another shift in lake conditions (Figs. 9.16, 9.17, and 9.19). The saline zone is not exposed in the area of the measured sections along Evacuation Creek, although it is documented in outcrop further to the north (Vanden Berg et al. 2012).

The final phase in lake evolution, termed here lake phase 3b, is interpreted as an underfilled basin comprising "evaporative facies" (Carroll and Bohacs 1999). An underfilled basin is defined where potential accommodation is greater than water and sediment influx and evaporative facies dominate these hypersaline environments (Carroll and Bohacs 1999). This saline zone represents a time when Lake Uinta's only main outflow mechanism was evaporation and marked the transition to a terminal basin.

An interplay between climatic changes and tectonic activity drive the short and long term changes of lake evolution (Carroll and Bohacs 1999). Based on the dominance of littoral to sublittoral facies preserved below the upper R6, the overall absolute lake level is quite shallow, but there is a constant, steady rise in absolute lake level, with some, short-lived deepening events (Fig. 9.19). However, the stratigraphic section below the upper R6 sandstone does display facies changes and systematic stacking patterns in the alternation between siliciclastic dominated lean zones and carbonate dominated rich zones. The facies changes and stacking patterns are attributed to changes in climate, which affected the amount of fluvial sediment delivery into the lake system from the hinterland. Organic-lean zones record periods in which fluvial siliciclastic transport into the lake system was high. These zones are attributed to episodes of high precipitation that carried a high volume of siliciclastic material into the basin (Birgenheier et al. 2013; Plink-Bjorklund and Birgenheier 2012). Due to the

exceptionally high siliciclastic sedimentation rate, carbonates were unable to form and the available accommodation space on the shallow lake margin was quickly filled. The intermittent organic-rich carbonate zones resulted from a more stable climate between the periods of high siliciclastic input (Fig. 9.19). The rich zones are characterized by lower siliciclastic sediment supply that encouraged the uninterrupted formation of carbonates. The relative lake level between the rich and lean zones is very similar since both zones are dominated by littoral to sublittoral facies, but climate via the rate of fluvial sediment delivery, and lake-margin gradient are the driving factors that affects the short-term changes in lithology.

The meter-scale cyclic changes (stacked parasequences) in the rich and lean zones are an indication of the rates and types of lithologic deposition taking place. The lean zones are marked by prograding sandstones and siltstone dominated parasequences that are deposited in numerous pulses out into the basin. These sediment pulses are erosive and relatively short-lived. The progradational stacked parasequences imply that the sedimentation rate was greater than accommodation, allowing for shallowing cycles. The rich zones are marked by retrogradational or aggradational stacked carbonate parasequences. The retrogradational or aggradational stacking patterns imply that deposition rates in the rich zones could not keep up with accommodation, or subsidence. Since the accommodation rate is greater than the rate of carbonate precipitation, the cycles in the rich zones either progressively deepened or stayed relatively stable.

Longer-term evolutionary lake changes are more likely to have been driven by tectonic activities associated with basin formation and the interplay between basins (Carroll and Bohacs 1999). However, the shorter-term changes and minor relative lake level fluctuations within these phases were likely driven by climatic activity.

Recent studies in the Uinta Basin have established a relationship between lean zone deposition and early Eocene abrupt global warming events (hyperthermals) (Birgenheier et al. 2013; Plink-Bjorklund and Birgenheier 2012; Foreman et al. 2012). These events are well documented in the marine carbon isotope record, and are only recently documented in the terrestrial realm (Abels et al. 2012). Basin scale sedimentation events have previously been linked to Milankovitch-predicted periodicities with high confidence levels, but numerous non-Milankovitch periods are also observed (Aswasereelert et al. 2013). Foreman and others (2012) document a basin-scale shift to multistoried sheet-sandstones at the onset of the Paleocene/Eocene thermal maximum event. These sandstone deposits are dominated by upper flow regime sedimentary structures, indicating high-energy discharge events. Hyperthermal (global warming) events are characterized by increased precipitation intensities and seasonality, which cause an increase in weathering and sediment deposition (Birgenheier et al. 2013; Plink-Bjorklund and Birgenheier 2012 Birgenheier and Vanden Berg 2011; Foreman et al. 2012). The climatic drivers for these lean zones are thought to be caused by global warming events that exhibit overall arid climates, with highly seasonal, flashy discharge events such as monsoons that quickly deposit high volumes of siliciclastic material at high energy levels (Birgenheier et al. 2013; Plink-Bjorklund and Birgenheier 2012; Birgenheier and Vanden Berg 2011).

Additionally, Tänavsuu-Milkeviciene and Sarg (2012) have developed a detailed evolutionary model of the Green River Formation in the Piceance Creek basin of Colorado. This model is based on detailed facies analysis, but also uses gamma ray and Fischer assay data to generate a basin-scale correlation to help understand the formation and paleoevolution that formed the organic-rich deposits present in the Piceance Creek basin. Within an overall deepening-upward trend in lake evolution, Tänavsuu-Milkeviciene and Sarg defined six lake stages based on facies associations. These stages are summarized in Table 9.4 and then compared to the lake phases defined here for the Uinta basin.

Controls on the depositional trends in the Piceance Creek basin are also considered by Tänavsuu-Milkeviciene and Sarg (2012) to be

Table 9.4 Lake evolution of Piceance Creek Basin versus Uinta Basin

Piceance Creek Basin		Uinta Basin	
Lake stages	Facies	Lake phase	R/L Zones
Stage 6: Closing lake	Introduction of more siliciclastic deposits among profundal facies	3b	R8
Stage 5: High lake	No marginal lake deposits present, only thick laterally continuous organic-rich oil shale, includes Mahogany zone	3a	R8, A-Groove, R7 (above Mahogany marker)
Stage 5		2b	R7 (below Mahogany marker)
Stage 4: Rising lake	Laterally continuous, organic-rich oil shale deposits, indicating an overall increase in profundal facies	2a	B-Groove, Upper R6 (upper carbonate unit)
Stage 3: Highly fluctuating lake	Channelized deltaic deposits that alternate with littoral to sublittoral microbial carbonates or by littoral to sublittoral oil shales and thick profundal oil shale breccias	1b	Upper R6 (middle siliciclastic and lower carbonate units, Middle R6, Lower R6, L5, R5, L4, R4
Stage 2: Transitional lake	Numerous, laterally discontinuous deltaic sandstone deposits interbedded by microbial carbonates and littoral to sublittoral oil shales	1a	L3, R3, L2, R2, Upper Douglas Creek Member

This table compares lake stages from the Piceance Creek basin by Tanavsuu-Milkeviciene and Sarg (2012) to the lake stages developed in our study of the Uinta Basin

consistent with global Eocene climate patterns. During times of arid climates, depositional units are highly cyclic, with sediments that are laterally heterogeneous, whereas during humid climates depositional units are laterally continuous.

One aim of this study was to develop a predictable evolutionary model for the eastern side of the Uinta Basin that could be used to help facilitate prudent and economic development of Utah's oil shale resource. Since this model is based on outcrop and core from the extreme eastern part of the basin, it would be prudent to see if there are similar patterns and changes throughout the section in other parts of the basin. The prime zones for oil shale development are those with the most homogenous rich zones and the highest grade of organic-richness. In our evolutionary model, these would be lake phase 2b and 3a. These phases include the Mahogany zone and represent when lake level was at its highest, and the most economical oil shale was being deposited. We find that the rich zones below the Mahogany zone are comprised of both organic-rich and poor carbonate parasequences. This heterogeneity within the rich zones poorly impacts their overall organic-richness, and could have a negative impact on their economic potential. From a geochemical view, the organic-rich carbonate mudstone below and above the Mahogany zone (F2.4 and F2.5) are distinct (Fig. 9.14). These geochemical distinctions could impact geomechanical properties as well as chemical reactions during ex situ retorting or in situ heating. One benefit of studying such a laterally extensive and vertically complete section is the opportunity to study the heterogeneities within the different rich zones and to consider how they could affect development.

9.6 Conclusions

The Evacuation Creek outcrop and the Asphalt Wash-1 core provide an exceptional dataset for interpreting the sedimentologic and sequence stratigraphic changes that occur within the Uinta Basin's Green River Formation. The high degree of heterogeneity in these sections illustrates the complexity of the mixed siliciclastic-carbonate lacustrine depositional system, yet further exami-

nation of the succession reveals predictability to the facies and stratigraphic stacking patterns. Ten different facies were deposited in four different facies associations: siliciclastics, carbonates, saline deposits, and volcanic-derived deposits. The combination of short-term climatic changes and longer-term tectonic mechanisms shaped the evolution of Lake Uinta from an overfilled basin with frequent and short-lived fluctuations in sediment supply and accommodation (lake phase 1a), to an overfilled basin with less frequent and longer-lived fluctuations in sediment supply and accommodation (lake phase 1b), to a balance-filled basin with little siliciclastic input (lake phase 2a), to a balance-filled basin with virtually no sediment supply and an increasing lake level (lake phase 2b), to a stable, high lake level (lake phase 3a), to an underfilled basin with abundant saline minerals (lake phase 3b). Spectral gamma ray analysis provides evidence for changes in lithologic composition that reflect this lake evolution, while also exhibiting similar changes in stacking patterns between stratigraphic sections.

Short-term climatic changes influence variations in the sediment supply regime, specifically during Eocene hyperthermal events that were characterized by seasonal, flashy fluvial discharge, or monsoonal episodes. Lean zones were dominated by high fluvial and siliciclastic input, with lower accommodation. The base of the lean zones are marked by regionally extensive surfaces of erosion, overlain by progradationally stacked coarsening upwards mouthbar and terminal distributary channel packages. Rich zones are characterized by low siliciclastic input and higher rates of carbonate production and accommodation. Rich zones contain regionally extensive flooding surfaces at their base that record reduced siliciclastic input, increased accommodation, and relative lake level rise, and are overlain by aggradational to retrogradationally stacked shallowing upwards carbonate dominated packages. The regional lateral continuity of rich and lean zones and the stacking patterns of their comprising packages, as well as the regional extent of erosion and flooding surfaces support an allocyclic control on deposition. Specifically, the amount of fluvial sediment delivery into the lake from the hinterland varied systematically as a result of climate changes.

Longer-term tectonically induced subsidence determined accommodation space and interbasin lake communication. Identifying the role of climatic and tectonic drivers in deposition provides a genetic stratigraphic model and an understanding of lateral facies architecture that can be used to better evaluate the valuable resources of the Green River Formation in the Uinta Basin. If this stratigraphic model can be applied and correlated throughout the basin, then the most economic oil shale targets can be laterally traced and identified.

References

Abbott W (1957) Tertiary of the Uinta Basin: guidebook to the geology of the Uinta Basin; eighth annual field conference

Abels HA, Clyde WC, Gingerich PD, Hilgen FJ, Fricke HC, Bowen GJ, Lourens LJ (2012) Terrestrial carbon isotope excursions and biotic change during Palaeogene hyperthermals. Nat Geosci 5:326–329. doi:10.1038/ngeo1427

Andrews A (2006) Oil shale: history, incentives, and policy. Congressional Research Service, Library of Congress, Washington, DC, pp 1–32

Aswasereelert W, Meyers SR, Carroll AR, Peters SE, Smith ME, Feigl KL (2013) Basin-scale cyclostratigraphy of the Green River Formation, Wyoming. Geol Soc Am Bull 125:216–228. doi:10.1130/B30541.1

Bader JW (2009) Structural and tectonic evolution of the Douglas Creek arch, the Douglas Creek fault zone, and environs, northwestern Colorado and northeastern Utah: implications for petroleum accumulation in the Piceance and Uinta basins. Rocky Mt Geol 44:121–145

Bhattacharya JP, Giosan L (2003) Wave-influenced deltas: geomorphological implications for facies reconstruction. Sedimentology 50:187–210

Birgenheier L, Vanden Berg M (2011) Core-based integrated sedimentologic, stratigraphic, and geochemical analysis of the oil shale bearing Green River Formation, Uinta Basin, Utah, Oil and gas technology topical report. United States Department of Energy DE-FE0001243. National Energy Technology Laboratory, Morgantown, WV, pp 1–30

Birgenheier LP, Plink-Bjorklund P, Vanden Berg MD, Rosenberg M, Toms L, Golab J (2013) A genetic stratigraphic framework of the Green River Formation, Uinta Basin, Utah: the impact of climatic controls on lake evolution. In: American Association of Petroleum

Geologists annual meeting, Pittsburgh, PA, 22–25 May 2013
Blackstone DL Jr (1983) Laramide compressional tectonics, southeastern Wyoming: University of Wyoming. Contrib Geol 22:1–38
Blakey RC, Ranney W (2008) Ancient landscapes of the Colorado plateau. Grand Canyon Association, Grand Canyon, pp 1–156
Borer J, McPherson M, Henriquel P, Homewood P, Cross T (1998) Field guide: stepped shorelines and reservoir facies distribution of the northern Green River lacustrine deposits, Uintah Basin, Utah-Colorado
Carroll AR, Bohacs KM (1999) Stratigraphic classification of ancient lakes: balancing tectonic and climatic controls. Geology 27:99–102
Cashion WB (1967) Geology and fuel resources of the Green River Formation Southeastern Uinta Basin Utah and Colorado. United States Department of the Interior: Geological Survey Professional Paper, Washington, DC
Crews SG, Ethridge FG (1993) Laramide tectonics and humid alluvial fan sedimentation, Ne Uinta Uplift, Utah and Wyoming. J Sediment Petrol 63:420–436
DeCelles PG (1994) Late Cretaceous-Paleocene synorogenic sedimentation and kinematic history of the Sevier thrust belt, northeast Utah and southwest Wyoming. Geol Soc Am Bull 106:32–56
Dickinson WR, Klute MA, Hayes MJ, Janecke SU, Lundin ER, McKittrick MA, Olivares MD (1988) Paleogeographic and paleotectonic setting of Laramide sedimentary basins in the central Rocky Mountain region. Geol Soc Am Bull 100:1023–1039
Dyni JR (2006) Geology and resources of some world oil-shale deposits: USGS scientific investigations report 2005–5294, US Geological Survey, Reston, VA, pp 1–49
Fahey JJ (1962) Saline minerals of the Green River Formation. United States Department of the Interior: Geological Survey Professional Paper, Washington, DC
Foreman BZ, Heller PL, Clementz MT (2012) Fluvial response to abrupt global warming at the Palaeocene/Eocene boundary. Nature 1–4. doi: 10.1038/nature11513
Fouch TD (1975) Lithofacies and related hydrocarbon accumulations in tertiary strata of the Western and Central Uinta Basin, Utah. In: Bolyard DW (ed) Deep drilling frontiers in the central rocky mountains: rocky Mountain Association of Geologists symposium. Rocky Mountain Association of Geologists, Denver, pp 163–173
Fouch TD, Nuccio VF, Osmond JC, MacMillan L, Cashion WB, Wandrey CJ (1992) Oil and gas in uppermost cretaceous and tertiary rock, Uinta Basin, Utah. In: Fouch TD, Nuccio VF, Chidsey TC, Jr (eds) Hydrocarbon and mineral resources of the Uinta Basin, Utah and Colorado: Utah Geological Association. Guidebook, vol 20. Salt Lake City, pp 9–47
Hagen ES, Shuster MW, Furlong KP (1985) Tectonic loading and subsidence of intermontane basins: Wyoming foreland province. Geology 13:585–588
Johnson RC (1985) Early Cenozoic history of the Uinta and Piceance Creek Basins, Utah and Colorado, with special reference to the development of Eocene Lake Uinta. In: Flores RM, Kaplan SS (eds) Cenozoic paleogeography of west-Central United States, Society for sedimentary geology. Rocky Mountain Section SEPM, Denver, pp 247–276
Keighley D, Flint S, Howell J, Andersson D, Collins S, Moscariello A, Stone G (2002) Surface and subsurface correlation of the Green River Formation in central Nine Mile Canyon, SW Uinta Basin, Carbon and Duchesne Counties, East-Central Utah, Utah geological survey miscellaneous publication 02–1. Utah Geological Survey, Salt Lake City, pp 1–66
Keighley D, Flint S, Howell J, Moscariello A (2003) Sequence stratigraphy in Lacustrine Basins: a model for part of the Green River Formation (Eocene), Southwest Uinta Basin, Utah, U.S.A. J Sediment Res 73:987–1006
Moncure G, Surdam RC (1980) Depositional environment of the Green River Formation in the vicinity of the Douglas Creek Arch, Colorado and Utah: University of Wyoming. Contrib Geol 19:9–24
Moore J, Taylor A, Johnson C, Ritts BD, Archer R (2012) Facies analysis, reservoir characterization, and LIDAR modeling of an Eocene Lacustrine Delta, Green River Formation, Southwest Uinta Basin, Utah. In: Baganz OW, Bartov Y, Bohacs K, Nummedal D (eds) Lacustrine sandstone reservoirs and hydrocarbon systems, vol 95, AAPG Memoir. American Association of Petroleum Geologists, Tulsa, pp 183–208
Morgan CD, Chidsey TC Jr, McClure KP, Bereskin SR, Deo MD (2003) Reservoir characterization of the Lower Green River Formation, Uinta Basin, Utah, Open file report 411. Utah Geological Survey, Salt Lake City, pp 1–140
Olariu C, Bhattacharya JP (2006) Terminal distributary channels and delta front architecture of river-dominated delta systems. J Sediment Res 76:212–233. doi:10.2110/jsr.2006.026
Osmond JC (1965) Geologic history of site of Uinta Basin, Utah. AAPG Bull 49:1957–1973
Picard MD, High LR Jr (1972) Paleoenvironmental reconstructions in an area of rapid facies change, Parachute Creek Member of Green River Formation (Eocene), Uinta Basin, Utah. Geol Soc Am Bull 83:2689–2708
Plink-Bjorklund P, Birgenheier LP (2012) Extreme seasonality during early Eocene hyperthermals. American Geophysical Union annual convention, San Francisco, CA, paper GC21D-1005, 3–7 December 2012
Renaut RW, Gierlowski-Kordesch EH (2010) Lakes. In: James NP, Dalrymple RW (eds) Facies models 4. Geological Association of Canada, St. John's, pp 541–575
Ruble TE, Philp RP (1998) Stratigraphy, depositional environments and organic geochemistry of source-rocks in the Green River Petroleum System, Uinta Basin, Utah. In: Pitman JK, Carroll AR (eds) Modern and ancient lake systems. Utah Geologic Association Guidebook, vol 26. Salt Lake City, pp 289–321

Ryder RT, Fouch TD, Elison JH (1976) Early tertiary sedimentation in the western Uinta Basin, Utah. Geol Soc Am Bull 87:496–512

Schomacker ER, Kjemperud AV, Nystuen JP (2010) Recognition and significance of sharp-based mouthbar deposits in the Eocene Green River Formation, Uinta Basin, Utah. Sedimentology 57:1069–1087. doi:10.1111/j.1365-3091.2009.01136.x

Smith ME, Carroll AR, Singer BS (2008) Synoptic reconstruction of a major ancient lake system: Eocene Green River Formation, western United States. Geol Soc Am Bull 120:54–84. doi:10.1130/B26073.1

Smith ME, Chamberlain KR, Singer BS, Carroll AR (2010) Eocene clocks agree: coeval 40Ar/39Ar, U-Pb, and astronomical ages from the Green River Formation. Geology 38:527–530. doi:10.1130/G30630.1

Surdam RC, Stanley KO (1980) Effects of changes in drainage-basin boundaries on sedimentation in Eocene Lakes Gosiute and Uinta of Wyoming, Utah, and Colorado. Geology 8:135–139

Tänavsuu-Milkeviciene K, Sarg FJ (2012) Evolution of an organic-rich lake basin – stratigraphy, climate and tectonics: Piceance Creek basin, Eocene Green River Formation. Sedimentology 59:1735–1768. doi:10.1111/j.1365-3091.2012.01324.x

Taylor AW, Ritts BD (2004) Mesoscale heterogeneity of fluvial-lacustrine reservoir analogues: examples from the Eocene Green River and Colton Formations, Uinta Basin, Utah, USA. J Pet Geol 27:3–26

U.S. Geological Survey Oil Shale Assessment Team (2010) Oil shale resources of the Uinta Basin, Utah and Colorado, U.S. geological survey digital data series DDS–69–B. US Geological Survey, Reston

Vanden Berg M (2008) Basin-wide evaluation of the uppermost Green River Formation's oil-shale resource, Uinta Basin, Utah and Colorado, Utah Geological Survey special study 128. Utah Geological Survey, Salt Lake City, pp 1–19

Vanden Berg MD, Anderson P, Wallace J, Morgan CD, Carney S (2012) Water-related issues affecting conventional oil and gas recovery and potential oil-shale development in the Uinta Basin, Utah, United States Department of Energy DE-NT0005671. National Energy Technology Laboratory, Morgantown, pp 1–267

Williamson CR, Picard MD (1974) Petrology of carbonate rocks of the Green River Formation (Eocene). J Sediment Petrol 44:738–759

Witkind IJ (1995) Geologic map of the Price 1 × 2 quadrangle, Utah, U.S. Geological Survey miscellaneous information series, map I-2462. The Survey, Reston

Phosphatic Carbonate Shale of the "Bird's Nest Saline Zone", Upper Green River Formation, Uinta Basin, Utah

10

Dave Keighley

Abstract

In aqueous depositional systems, phosphorus (P) is highly mobile and is readily reworked back into the water column after initial sedimentation. As a result, during deposition of most lacustrine sedimentary successions, gross P sedimentation typically is not much greater than gross P release, leading to low net P abundance. Such low abundances predominate in a 200 m-thick lacustrine succession of variably shaley, evaporitic, and organic-rich carbonate mudstone from the upper member of the Green River Formation in the Uinta Basin of Utah. However, the succession also includes thin but highly enriched phosphatic horizons that represent marked aberrations in the prevailing depositional and immediate subsurface diagenetic environment. This contribution details one carbonate shale bed, containing calcite pseudomorphs, that is equated with the nahcolite-bearing "bird's-nest saline zone" of the upper Green River Formation. X-ray diffraction analyses and scanning electron microscopy record the P-enrichment as interstitial microcrystalline aggregates of calcium fluorapatite. The calcium fluorapatite also partly replaces precursor grains, forms a grain coating around some silicate grains and occurs alongside abundant displacive and pseudomorphing crystals of calcite, and rhombic dolomite.

At high pH, which would have promoted nahcolite precipitation in the deeper part of the lake, the presence of dissolved Mg^{2+} would have kinetically inhibited calcium fluorapatite precipitation even if P was at saturation. But, during evaporitic pumping adjacent to a sabkha environment, and possibly mediated by methanogenic bacteria, the formation of ferroan dolomite, and smectite, Mg^{2+} was removed from porewaters allowing calcium fluorapatite to crystallize.

D. Keighley (✉)
Department of Earth Sciences, University of New Brunswick, Fredericton, NB E3B 5A3, Canada
e-mail: keig@unb.ca

M.E. Smith, A.R. Carroll (eds.), *Stratigraphy and Paleolimnology of the Green River Formation, Western USA*, Syntheses in Limnogeology 1, DOI 10.1007/978-94-017-9906-5_10

10.1 Introduction

Phosphorus (P) can be preserved in the sedimentary record as a component of detrital mineral phases, fossil bone and shell. It is also released from dead and decaying organic matter, rarely from soluble inorganic phases, ultimately to be incorporated into the sediment pile of productive lakes and oceans as diagenetic mineral phases. However, most sedimentary successions have low phosphate content because much of what initially accumulates in sediment is continuously recycled back into the water column. Although the recycling mechanisms may temporarily break down, allowing for accumulation of sedimentary phosphate, there are few recorded examples of phosphatic beds in ancient lake strata.

This paper focuses on one example of elevated P in the variably shaley, variably marly mudstone (for brevity: "carbonate shale") of the upper Green River Formation (upper GRF), of the Uinta Basin in Utah (Fig. 10.1a). The example in question is associated with the uppermost occurrences of laminae-disruptive, coarsely crystalline calcite pseudomorphs that mark the Bird's Nest Saline Zone (BNSZ) in Gate Canyon, ~152 m above the base of the Mahogany Oil Shale Zone (MOSZ; Fig. 10.1b, c). The P occurs as aggregates of microcrystalline calcium fluorapatite (CFA) that infill interstices and replace detrital grains. The origin of this CFA is best interpreted to be the result of early diagenetic successions precipitating from hypersaline fluids in the shallow substrate, conditions not previously explained in detail for producing ancient lacustrine phosphates.

10.2 Previous Work

There are few, but varied, reports and interpretations of ancient lacustrine strata enriched in phosphatic minerals such as anapaite, $Ca_2Fe(PO_4)_2.4H_2O$; bradleyite, $Na_3PO_4.MgCO_3$; britholite, $(Ce,Ca)_5SiO_4(PO_4)_3(OH,F)$; fairfieldite $Ca_2(Mn,Fe)(PO_4)_2.2H_2O$; hydroxylapatite, or "hydroxyapatite", $Ca_5(PO_4)_3OH$; mitridatite $Ca_6(H_2O)_6[Fe_9O_6(PO_4)_9].3H_2O$; vivianite, $Fe_3(PO_4)_2.8H_2O$; and carbonate fluorapatite (CFA), or "francolite", $Ca_{10\text{-}a\text{-}b\text{-}c}\ Na_a\ Mg_b\ (PO_4)_{6\text{-}x}\ (CO_3)_{x\text{-}y\text{-}z}\ (CO_3,F)_y\ (SO_4)_z\ F_2$, where $2c = x - y - a$ = vacancies in the Ca site. In the Pliocene Glenns Ferry Fm. of Idaho, francolite is described replacing ooid and oncoid cortices and as a fibrous isopachous cement. These phosphatic ooidal sandstones are considered to have formed beneath an oxic microzone present at the sediment surface at times of lake transgression over nearshore sediment (Swirydczuk et al. 1981). In the Carboniferous Albert Formation of New Brunswick, phosphate enrichment mostly occurs in dolomitic oil shale but also in concretionary sandstone and fish-scale-bearing grey shale (Mossman et al. 1987). Britholite and anapaite have been identified and related to breakdown of algal matter with released P involved in mineral replacement (e.g. of calcite). Mudstone of the Miocene Cerdanya Basin of Spain contains veins, sphaerulite beds and septarian-like nodules of anapaite and fairfieldite. Precipitation of phosphate was determined to have occurred in open lacustrine mud with Ca-poor, circumneutral pH porewater fluctuating between oxic and anoxic (de las Heras et al. 1989). Phosphorite nodules in the Precambrian Diabaig Fm. of W Scotland contain microcrystalline francolite replacing detrital grains and infilling pores of silt laminae that also contain algal filaments and other eukaryotes and prokaryotes (Rodd and Stewart 1992; Strother et al. 2011). The preferred interpretation was that the francolite replaced micritic calcite below the oxic boundary (Rodd and Stewart 1992). The Štínik Fm. (Permian) of the Southern Gemeric Unit, Slovakia, contains CFA intraclasts and matrix within fining-upward sandstone–mudstone cycles. Turbidites are thought to have reworked stratabound phosphate that originally formed by the iron redox pump mechanism (Vozárová and Rojkovič 2000). In clayey diatomites from the Miocene of Thessaly, Greece, various phosphates occur as leaf and fecal replacements, veins and irregular concretions. The interpretation is that deep-lake sediment with anoxic circumneutral pH porewaters originally precipitated vivianite that was mostly altered to anapaite and hydroxylapatite as pore-

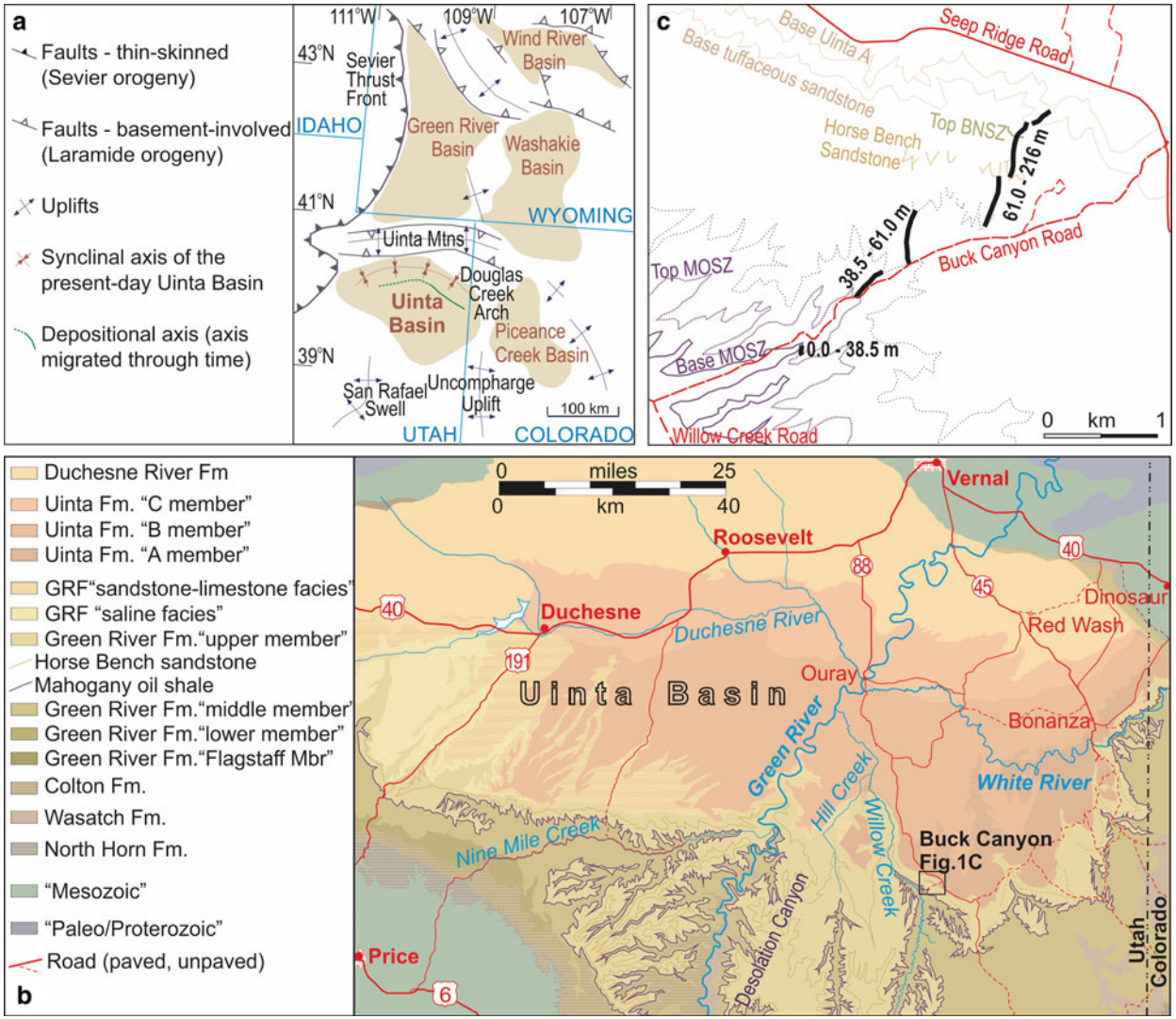

Fig. 10.1 (**a**) General location map of the major Laramide Basins in western United States (after Dickinson et al. 1988). Location of structural and depositional axes equate to Cashion (1995). (**b**) Geologic map for the Uinta Basin, adapted from Keighley (2013). (**c**) Location of the measured section at Buck Canyon

waters became more Ca-enriched; mitridatite was the result of recent weathering (Stamatakis and Koukouzas 2001). In all cases, anoxic decay of organic material in the substrate was thought to be a major contributor of dissolved P into porewaters. Abundant P has been identified in other lacustrine strata, but the host mineral and, or, its form or occurrence has not been detailed. For example, at Lake Manyara, Tanzania, Pleistocene bentonite clays interbed with phosphate. Fluorapatite was identified from XRD analyses but its diagenetic origin was not detailed (Mutakyahwa 2002). Phosphate minerals have also been reported in Eocene oil shale from Messel (Dietrich 1978); mid-Holocene sapropel from Lake Bosumtwi in West Africa (Talbot and Kelts 1986); Miocene marl of the Hula Basin, Jordan (Bein 1986); and Permian marl of the Ville Graben, France (Carasco 1989).

There have also been several studies from the Paleogene Laramide Basins of the western USA. The US Geological Survey's geochemical reference material, SGR-1, which is from part of the MOSZ of the adjacent Piceance Creek Basin, records an abundance of P at 0.328 ± 0.066 wt% (USGS website 2010; values always given as P_2O_5); the average in shale-rock composites is slightly less, ranging from 0.13 wt% (NASC, Gromet et al. 1984) to 0.16 wt% (PAAS, Taylor and McLennan 1985). In contrast, Tuttle (2009) encountered values of between 0.88 and 3.8 wt% P in seven of her ~150 sampled oil shale beds from above, below, and within the MOSZ, yet no other studies from this basin have encountered such anomalous values (Love 1964; Desborough et al. 1976; Saether et al. 1981). Phosphorus values of up to 18.2 wt% have been identified in interfingering sandstone, shale, and evaporite beds (that in core contain bradleyite) of the Wasatch Formation and GRF in the Greater Green River Basin of Wyoming (Fahey 1962; Love 1964; Mott and Drever 1983; Tuttle 2009). Bradley (in Fahey 1962, p. 62) suggested the "thin phosphate-rich zones in the Wilkins Peak Member may simply represent times when calcium carbonate precipitation was very rapid and swept out the phosphorus from the lake water, depositing it as tricalcium phosphate". Love (1964) proposed that the phosphates precipitated directly from periodically highly stratified hypersaline water columns.

In the Uinta Basin, most sampling has failed to encounter significant P-enriched horizons (Swanson 1960; Fabbi and Espos 1976; Tuttle 2009). Prior to Keighley (2013) and this paper, anomalously high values of P, at >8 wt% and >1 wt%, have been recorded only at stratigraphically unknown levels adjacent to Desolation Canyon, west of the Green River, and in a tributary of Hill Creek, ~12 km due west of the Buck Canyon study area (Love 1964); and as ~6 % apatite from XRD analysis of an oil shale close to Highway 191 (Bristow et al. 2012).

10.3 Geological Setting

10.3.1 Tectonic Setting of Paleogene Laramide Basins

The early Cenozoic Laramide Orogeny produced a series of extensive, primarily internally drained, nonmarine depositional basins in the western USA (Dickinson et al. 1988; Fig. 10.1a). N–S trending domal uplift of Mesozoic strata produced the saddle-like Douglas Creek Arch that formed a spill point between the Piceance Creek Basin and the Uinta Basin. Major uplift of E–W trending, thrust-fault-bounded basement rocks formed the Uinta Mountains (Bradley 1995) that separated these basins from the Greater Green River Basin to the north. The major erosional remnant of the Uinta Basin now forms a gentle asymmetrical syncline located in eastern Utah and westernmost Colorado; the fold axis, which also approximates with the depositional axis, is preserved toward the northern margin of the basin (Fig. 10.1a, b) in what, during the orogeny, was equivalent to a foreland-basin type setting.

10.3.2 Stratigraphy and Depositional Setting of the Uinta Basin

A typical lacustrine, tripartite vertical succession (Lambiase 1990) occurs in the Paleocene–Eocene of the Uinta Basin (Fig. 10.2). At the base, a predominantly coarse-clastic succession (Colton

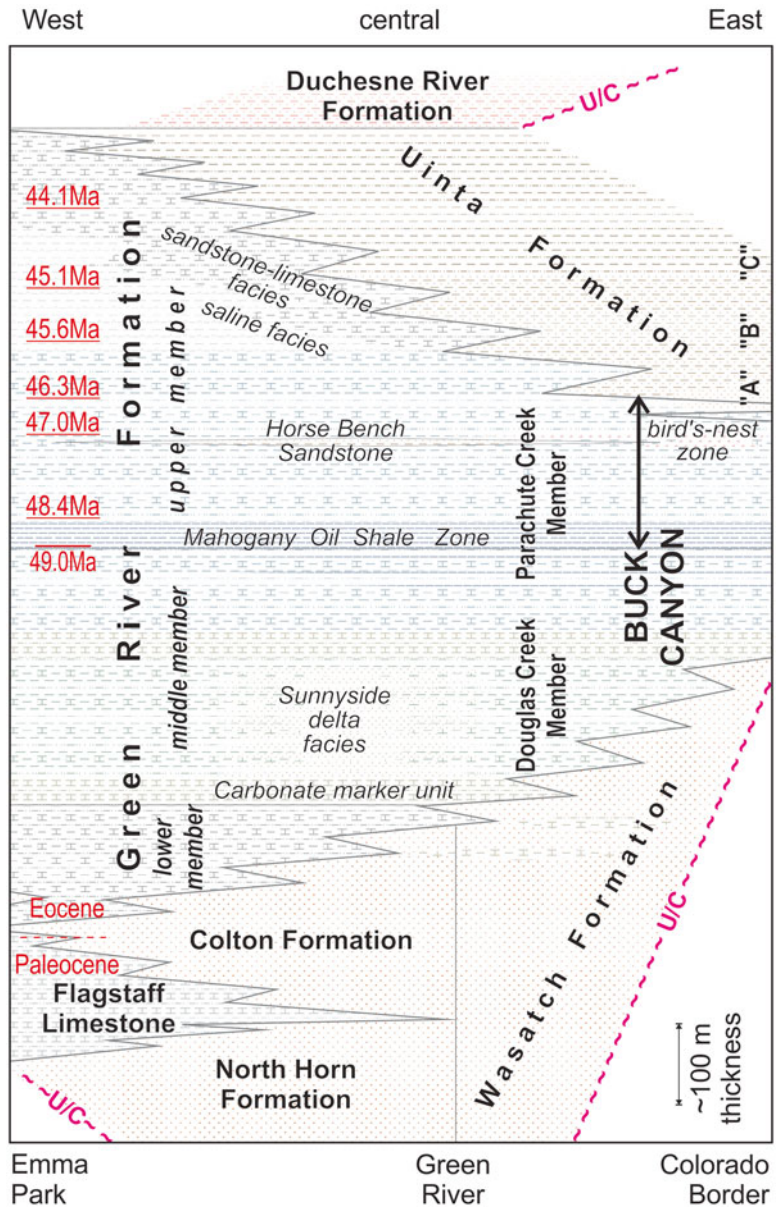

Fig. 10.2 Paleogene lithostratigraphic terminology for the lacustrine phases of the Uinta Basin (Adapted from Keighley 2013)

and Wasatch formations) is interpreted to be the initial alluvial inputs into the developing basin (Morris and Richmond 1992). Progressively upsection, variably shaley, variably carbonate-, evaporite-, and organic-rich mudstone, assigned to the GRF, cyclically onlaps toward the basin margin as the basin continued to deepen and the lake fluctuated, but generally expanded, in size (Keighley et al. 2003a). Oil shale is present at various stratigraphic levels with the richest oil shale beds concentrated within the approximately 30 m-thick MOSZ (Cashion 1967). The MOSZ is considered to mark the base of the informal upper member of the GRF (Morgan et al. 2002) and is traceable across most of the Uinta Basin. It is also correlated eastward into the Piceance Creek

Basin of Colorado. The MOSZ is interpreted to represent deepwater deposition during or immediately following the most prolonged period of merged lakes that periodically filled both depressions (as "Lake Uinta"), during and following the Early Eocene Climatic Optimum (Cashion 1967; Keighley et al. 2003b; Keighley and Flint 2008; Smith et al. 2008; Birgenheier and Vanden Berg 2011).

There are a few tuff beds present in the upper GRF. Sourced from numerous volcanic centers active in the western US at the time, they have been radiometrically dated and correlated across several kilometers of outcrop (Fig. 10.2; Smith et al. 2008). There is also one mappable sandstone interval, the Horse Bench Sandstone (HBS), which is most prominent west of the Green River and ~150 m above the MOSZ (Dane 1954; Dyni 1976; Remy 1992). In Willow Creek, the HBS lies ~120 m above the MOSZ but increasingly difficult to trace eastward. Eastward and northeastward across the basin, there is also a reduction in the variety and abundance of clay minerals in the upper GRF, along with less calcite, more dolomite and evaporite minerals (Dyni 1976). Near the White River southeast of Bonanza (Fig. 10.1), an interval with many (in outcrop, leached or altered to calcite) bedded nahcolite ($NaHCO_3$) nodules in a dolomitic shale matrix (Milton and Eugster 1959) was first described as the BNSZ by Cashion (1967). Birgenheier and Vanden Berg (2011) and Vanden Berg et al (2013) recently have also identified fracture-filling shortite ($Na_2Ca_2(CO_3)$), and described the BNSZ in core from north of Willow Creek. These authors note that near the basin depocenter the BNSZ is >110-m thick with nodules concentrated in two ~20-m thick intervals (termed the lower and upper saline zone) that are separated by an intervening succession rich in oil shale (termed the middle R-8 zone). Keighley (2013) correlates the interval to outcrop in Buck Canyon (Fig. 10.1c). The authigenic minerals identified in the BNSZ, and other saline units noted below, point to a lake that was evolving, cyclically, from a brackish into a hypersaline system, with evaporative phases containing warm (20–35 °C), sodic-carbonate dominated, low sulfate, high alkalinity waters (Bradley 1929; Milton and Eugster 1959; Tuttle and Goldhaber 1993; Dyni 1996; Smith et al. 2008; Vanden Berg et al. 2013).

Interbedded sandstone and mudstone of the Uinta Formation progressively caps the upper GRF, the contact being stratigraphically higher in the west than the east (Cashion 1967). This is due to pinch-outs of medium- to fine-grained sandstone (characteristic of the informal "A" member), which represent fluvial-deltaic deposits that gradually infilled both the Piceance Creek Basin and then the Uinta Basin from the northeast (Johnson 1981; Donnell 2009). To the west and upsection, finer grained sandstone and variegated mudstone (Uinta Fm., member "B") interfingers with a succession of mudstone, limestone, and yet more evaporite beds known as the "Saline Facies" and "Sandstone and Limestone Facies". Although included as part of the Uinta Fm. by Dane (1954) these facies intervals, along with thin tongues of Uinta Fm.-type sandstone, have been included by subsequent workers as part of the upper GRF (Fig. 10.2).

10.4 Methods

Detailed methodology is outlined in Keighley (2013). Briefly, at Buck Canyon (Fig. 10.1c), the exposed section has been logged at the bed (cm) scale (Fig. 10.3) with beds ascribed to one of four broad, end-member lithofacies, with more detailed lithofacies components identified where outcrop was of sufficient quality and extent (Table 10.1). For the original purpose of a chemostratigraphic study, samples were collected throughout the upper GRF, from the base of the MOSZ, through the BNSZ (including the calcite-pseudomorph bed, 152 m above MOSZ), and up into the basal Uinta A sandstone at the top of Seep Ridge (vertical thickness ~216 m). Sampling was systematic (every 4 m where there was outcrop, n = 52) with additional material collected at beds of particular interest (n = 37; total = 89 samples).

The elemental composition of all these samples was analyzed by Activation Laboratories,

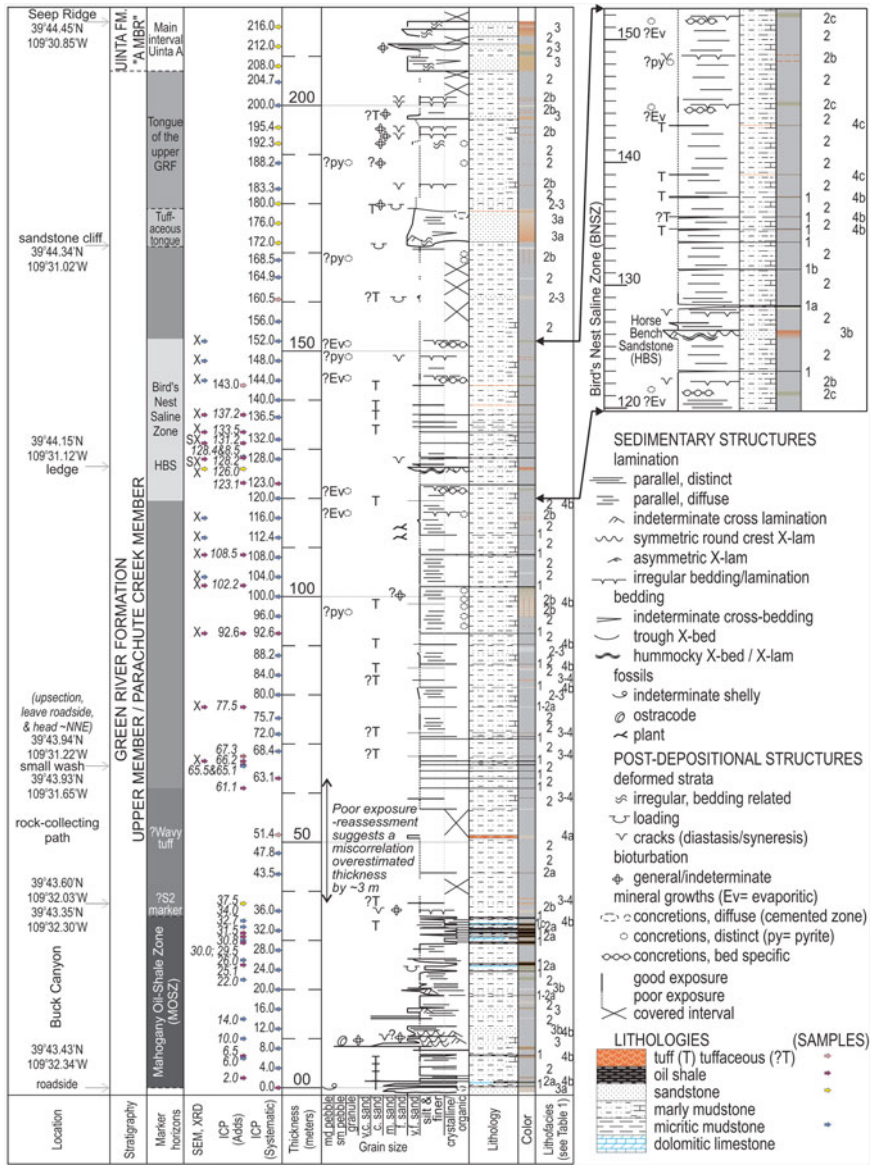

Fig. 10.3 Summary sedimentary log for the upper member of the Green River Formation, from the base of the Mahogany Oil Shale Zone up into the base of the Uinta Formation, adjacent to Buck Canyon (Adapted from Keighley 2013). See Table 10.1 for lithofacies codes

Canada, using a Varian Vista ICP-OES, calibrated using 7 prepared USGS and CANMET certified reference materials, and a Perkin Elmer SCIEX ELAN ICP/MS, all to a standard defined by ISO 17025. Selected samples were also analyzed by a Bruker AXS D8 solid state powder diffraction X-Ray Diffraction (XRD) system (at the University of New Brunswick) to determine major mineral phases present in the rock. Phase identification was made with a combination of windows-based software Bruker Eva and MDI Jade. Remaining sample chips from samples of greatest interest were split in half. One half was further cut and polished as a standard thin section along a cross-sectional surface. The other half was cut, polished and carbon coated along

Table 10.1 Lithofacies classifications for Buck Canyon (Adapted from Keighley 2013)

Lithofacies	Description	Interpretation	Occurrence
1. Oil shale	Typically 10–150 mm thick, purplish-black, to brown to dark gray, whitish weathering, micro- laminated to massive, commonly within one bed. Some paper shale. Interbedded and gradational with lithofacies 2, rarely with 4.	Settling of organic-rich detritus with minor (cyclic) clastic/evaporite input under eutrophic, no flow lacustrine conditions.	Most common in MOSZ (0–37.5 m) but sporadic up to 137.5 m.
	Component lithofacies identified where better exposed:		
	1a: Light-gray weathering, slightly domal caps (?stromatolitic).	1a: relatively shallow (photic) lake	1a not identified in the BNSZ
	1b: Angular crystals, ~2 mm diameter of (?pseudomorphing) carbonate	1b: evaporative, deep or (shallow) lake	
	1c: Internal micro-slumping ± microfaults	1c: remobilized, slumped, deep lake.	
2. Mudstone	Variably shaley, marly or variably calcareous/dolomitic, micro-laminated to apparently massive, can be variably colored (e.g., brown, olive, greenish gray, mid to light gray, and buff). Commonly soft-sediment deformed. Interbedded and gradational with all other lithofacies.	Cyclic suspended and washload deposition during low/no flow conditions with varied evaporite precipitation when minimal/no clastic input. Lacustrine low energy (offshore and low energy nearshore).	Common throughout. Predominant below 170 m.
	Component lithofacies identified where (rarely) better exposed:		
	2a: mostly massive, brown, dolomitic (micritic), whitish weathering	2a: clastic-starved lake	
	2b: rusted ?pyrite nodules ± cracks (diastasis) disrupting lamination, often in siltier strata, orange weathering	2b: anoxic shallow-water	
	2c: mm- to cm-scale calcite crystals (pseudomorphs) disrupting lamination in olive/ greenish grey shaley marlstone (evaporitic shale)	2c: evaporative conditions, likely shallow-water.	2c restricted to rare beds from 120 to 152.5 m

(continued)

Table 10.1 (continued)

Lithofacies	Description	Interpretation	Occurrence
3. Sandstone	Beds generally thin, very fine grained, buff, brown, orange or yellowish gray in color and variably calcareous. Diffuse low-angle cross beds and cross-laminations. Interbedded and gradational with lithofacies 2 and 4.	Suspended/saltating load deposition under waning aqueous flow.	Common above 200 m (Uinta A).
	Component lithofacies identified where better exposed:		
	3a: Lateral and vertical stacked lenticular beds occurs in fine-medium grained sandstone of the Uinta A. Asymmetric ripple cross-lamination, low-angle and planar cross bedding, and soft-sediment deformation structures.	3a: fluvial – sheetflood, possibly deltaic	3a occurs below the MOSZ and in the Uinta A.
	3b: Laterally extensive, tabular sandbodies of silty, highly calcareous, very-fine grained sandstone that quite sharply coarsen up from marly mudstone. Parallel lamination, wavy and hummocky cross-lamination.	3b: prograding lacustrine shoreface (offshore transition to nearshore)	3b Uncommon (but includes HBS at 126 m)
4. Tuff	Mostly massive, 10–450 mm thick, weather to a variably yellow to rusty-orange surface color, interbedded with lithofacies 2 or 3, and rarely capping or grading from lithofacies 1.	Volcanic ash falls	Sporadic throughout.
	Component lithofacies identified where better exposed:		
	Coarser-grained tuffs can be a dark gray color whereas others have		
	4a: light yellowish gray, dolomitic groundmass with occasional weathered (rusty) phenocrysts and irregular/wavy lamination	4a: Reworking/slumping/loading in shallow lacustrine conditions	4a not found in the BNSZ.
	4b: dark grey, fine to coarsely crystalline	4b, 4c: sub-aqueous settling in low-flow lacustrine conditions	
	4c: as for b, distinctly jointed "piano-key" structure.		

the counterface cross-section and on a bedding surface and analyzed with a Hitachi SU 70 FEG-SEM (resolution: 1.0 nm at 15 kV) with attached Oxford Instruments INCA solid-state EDS (also at UNB). The sample from 152 m required additional heating to 100 °C to eliminate problems in the vacuum chamber caused by degassing. Initial mapping of contiguous/adjoining ~300 µm by ~400 µm areas from top to bottom of each cross-sectional sample used the INCA mapping tool with 5 min acquisition times (~2 million counts), complemented with a BSE image of the same area. Selected INCA elemental maps were color coded and, using Corel software, overlain on the BSE image before being cropped, and montaged to help identify mineral phases. Areas or mineral associations of greater interest were mapped at greater resolution or spot analyzed. Spot size and interaction volume are dependent on the atomic number of the material being examined and the energy of the incident electron beam.

10.5 Buck Canyon Measured Section

10.5.1 General Description

A detailed description of the entire upper GRF in Buck Canyon is provided in Keighley (2013). In summary, and illustrated in Fig. 10.3, the MOSZ is ~35 m thick and comprises carbonate shale (lithofacies 2) irregularly interbedded with several <20 cm-thick beds of the other lithofacies (Table 10.1). Oil shale beds (lithofacies 1) are thickest and most common near the top of the MOSZ. The overlying 20–25 m is very poorly exposed on very gentle slopes, but is dominated by marly mudstone with only isolated ledges of tuffaceous sandstone and oil shale. A series of 5–20 cm-thick oil shale beds, typically spaced 0.5–2 m apart, mark the start of the better exposed section (starting ~60 m above base MOSZ). Thin beds of lithofacies 1 and 4 continue to outcrop at irregular intervals upsection, but lithofacies 2 still predominates. Keighley (2013) identifies the BNSZ, described in more detail below, between ~120 and ~152 m above base MOSZ. Upsection, lithofacies 2 continues to dominate, with rare lithofacies 4, until a 3–8 m thick, convolutely laminated, tuffaceous sandstone (lithofacies 3), with a deformed basal contact, is encountered ~171 m above base MOSZ. Overlying this sandstone is another interval dominated by lithofacies 2. The section is capped at the top of Buck Canyon by two stacked sandbodies (~207–216 m above base MOSZ) considered to form the basal beds of the main body of the Uinta Fm. "A member".

10.5.2 Description of the BNSZ

The base of the BNSZ is taken ~120 m above base MOSZ at an ~1 m-thick succession of olive-green weathering, laminated, carbonate shale that is variably disrupted by mm-scale, angular, displacive and pseudomorphed crystal aggregates now comprising calcite and rare dolomite: "mealstone" of Dyni (1996) (=lithofacies 2c). Two similar ~1 m-thick beds with calcite pseudomorphs occur at 144 and 152 m above base MOSZ. The top of the latter bed marks the top of the BNSZ at this locality. Most of the intervening BNSZ comprises variably exposed, gray, laminated carbonate shale (lithofacies 2). Sporadically, the carbonate shale contains intervals where laminae exhibit numerous lenticular, non-polygonal cracks filled with similar muddy sediment. Commonly in association with these cracks are variably spherical nodules, <1 cm diameter, that are highly rusted from surface weathering; rarely the nodule's core is pyritic (e.g., 148 m = lithofacies 2b). Variably brown, micritic, and diffusely laminated dolomitic mudstone (lithofacies 2a) is also present and locally grades into variably thin beds of oil shale (lithofacies 1) at several horizons, representing the middle R-8 zone. The uppermost 3 oil shale beds at 134.7, 135.7 and 137.2 m above base MOSZ are <5 cm-thick and are associated with similarly thin, gray, tuffaceous beds (lithofacies 4b). At 126 m above base MOSZ is the HBS, represented by a ~0.7 m-thick ledge of orange weathering, light gray, symmetrically rippled, coarsening-upward silty to very-fine-grained, and slightly tuffaceous calcareous sandstone (Fig. 10.4).

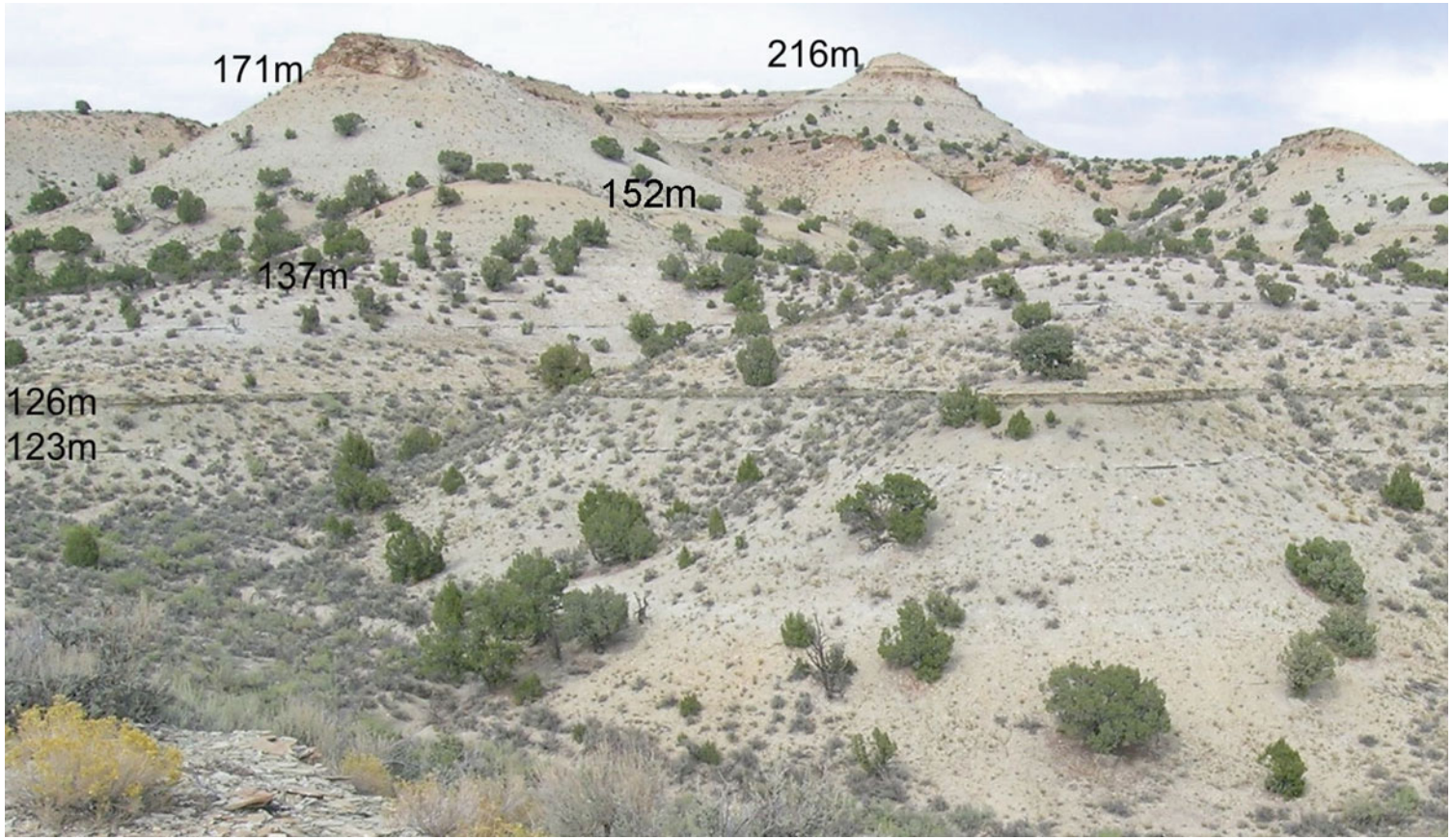

Fig. 10.4 The *upper* part of the measured section, including the bird's nest saline zone (BNSZ), is exposed west of Seep Ridge on the north side of Buck Canyon. The major ledge at 126 m is considered an eastern extension of the Horse Bench Sandstone. The tuffaceous sandstone at 171 m is highly deformed and locally can be loaded down into underlying carbonate shale by over 5 m

10.6 Sample Analyses

For the entire ICP dataset in Buck Canyon (n = 89), median P abundance is 0.08 wt%, whereas the mean is 0.72 wt% due to numerous anomalies. One such anomaly is the calcite-pseudomorph bed at 152 m that contains P at 5.57 wt%. Other anomalies, to be discussed in another paper, reach up to 9.47 wt% P, are distributed unevenly through the section, and represent samples from some of the oil shale beds (Fig. 10.5). For the entire dataset, the element additionally shows a high correlation co-efficient with uranium ($r = +0.78$, significant at $\alpha = 0.01$). Also of note, the Ca content is relatively constant throughout the section, but Mg values display an overall decline upsection (Fig. 10.5).

It should be noted that it is unlikely the above data will be inclusive of all phosphatic beds in the section: some beds may have been overlooked in the systematic sampling program (several were caught only in the additional sampling program, Fig. 10.5) and, since the phosphatization appears highly localized, the P abundance may have been diluted in some cases by inclusion in the sample of non-phosphatic horizons within a particular bed.

Nine samples from the BNSZ were further investigated by whole-rock XRD analysis. Table 10.2 shows that the fine-grained deposits of the BNSZ comprise a predominance of carbonate phases, with the silicon-bearing minerals collectively subordinate, and clay minerals (included in the sheet-silicates column of Table 10.2) generally negligible, i.e., compositionally the strata are mostly carbonate mudstone. The presence of CFA as the main P mineral is confirmed for the 152 m sample (Table 10.2; note that the calculated CFA percentage reflects the abundance exclusive of the organic phase). Zeolite occurs only in the 152 m sample, as the mineral faujasite. No pyrite was evident in this sample.

In hand specimen, angular crystals extensively and irregularly disrupt the mm-scale lamination. From thin-section optical petrography, these crystals are confirmed to be calcite, but their occasional orthorhombic-pyramidal cross-section indicates that at least some of the calcite is a pseudomorphic phase (Fig. 10.6). Most likely, the calcite is a replacement of shortite since this mineral has the appropriate precursor crystal form (orthorhombic hemimorphic, see fig 12 in Fahey 1962).

In SEM, typically sub-angular to sub-rounded grains of ~20–60 μm size (rarely exceeding 100 μm) map as combinations of Na, K, Al, and, or, Si (Fig. 10.7) and are considered to represent the silicate phases identified in XRD. Oriented elongate silicate grains and medium to coarse silt-sized silicate grains interlayer, at the ~0.25 mm scale, with larger (~100 μm) interlocking crystals to define the lamination. The latter include subpoikilotopic, subhedral crystals that map as Ca, O, and C (calcite), and euhedral-subhedral rhombic crystals containing Ca, Mg, with occasional minor Fe (high-Mg calcite or dolomite). No sodic (bi-) carbonates, siderite, pyrite or kerogenous stringers were identified by EDS, but very rare grains map as pure carbon (interpreted as coalified plant matter).

The matrix is generally an indistinguishable mix of crystals of Ca, P, F, Si, Al, Mg, minor Na, K, Fe, Ti, and rare traces of rare earth elements. Admixed sub-micron oblate hexagonal crystals may be a smectite or zeolite. The main CFA components, Ca, P and F, concentrate as rare detrital grains (Figs. 10.7 and 10.8a), along stringers (Fig. 10.8b), grain rims on selected silicate (mostly quartz) particles (Fig. 10.8c, d), and variably concentrated in scattered grain-shaped masses that might indicate variably altered precursor grains, possibly multi-mineralic (Fig. 10.8e, f).

Poikilotopic calcite encloses and post-dates the aforementioned phosphatized multi-mineralic grains (Fig 10.8f) and zoned, pitted rhombic dolomite (Fig. 10.9). Four transects of point spectra additionally indicate that the Fe content typically varies in the rhombs, with the cores in Fig. 10.9a and c being non-ferroan, their rims ferroan. High Mg content is characteristic of the rhombs, with lower values occasionally found toward the rims. The enclosing late-stage calcite is non-ferroan, and similarly contains minimal Mg. Pitted rhombs, particularly the one shown in Fig. 10.9b, have higher levels of impurities than pure rhombs, suggesting encapsulation of aluminum silicates

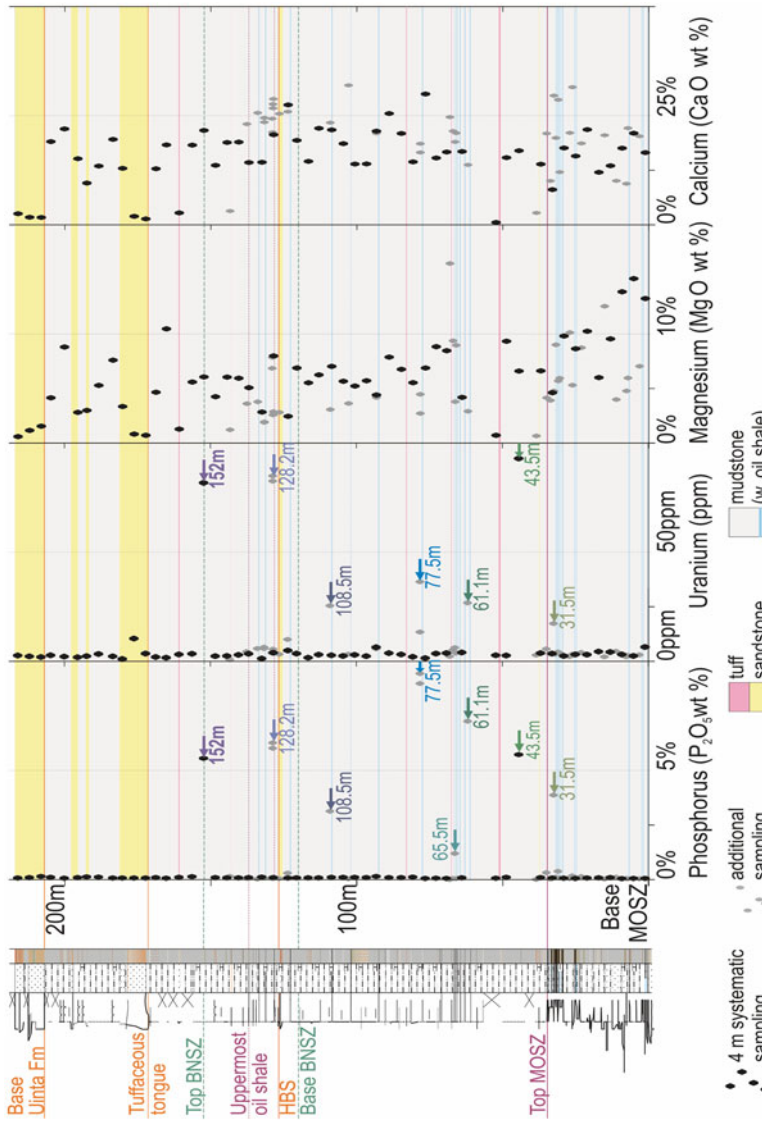

Fig. 10.5 Raw wt% as oxide and ppm data for various elements as determined from ICP analysis of samples from the upper GRF at Buck Canyon. Data from the systematic sampling, every 4 m, is shown by *black diamonds*. Additional (focussed) sampling of selected beds are shown by *gray diamonds*. The relative standard deviation from replicate analyses is <5 % for major elements and <10 % for the minor element, and uncertainty associated with various determinations is ±15 % at ten times, and ±5 % at 100 times the detection limits (limits: P_2O_5, CaO, MgO = 0.01 %; U = 0.1 ppm)

Table 10.2 XRD Analyses of 9 samples from the BNSZ of the upper GRF at Buck Canyon

Sample Horizon	Lithofacies	Quartz	Feldspar	Mica	Calcite	Dolomite	Zeolite	Phosphate
152 m	2	15	11	–	19	38	2	15
144 m	2	11	21	6	21	41	–	–
140 m	2	14	21	–	28	37	–	–
137.2 m	1	12	14	–	40	35	–	–
133.5 m	1	10	13	–	56	21	–	–
131 m	1	11	16	14	33	26	–	–
128.2 m	1	16	30	–	33	3	–	18
128.1 m	1	1	14	–	58	27	–	–
126 m	3	29	14	–	28	29	–	–

The reference-intensity-ratio method was used to estimate the weight fractions of the different phases. Errors are generally ±5 %, but increase with more diverse sample mineralogy, lower abundance of a mineral, overlapping peaks, and increasing presence of clays and salts

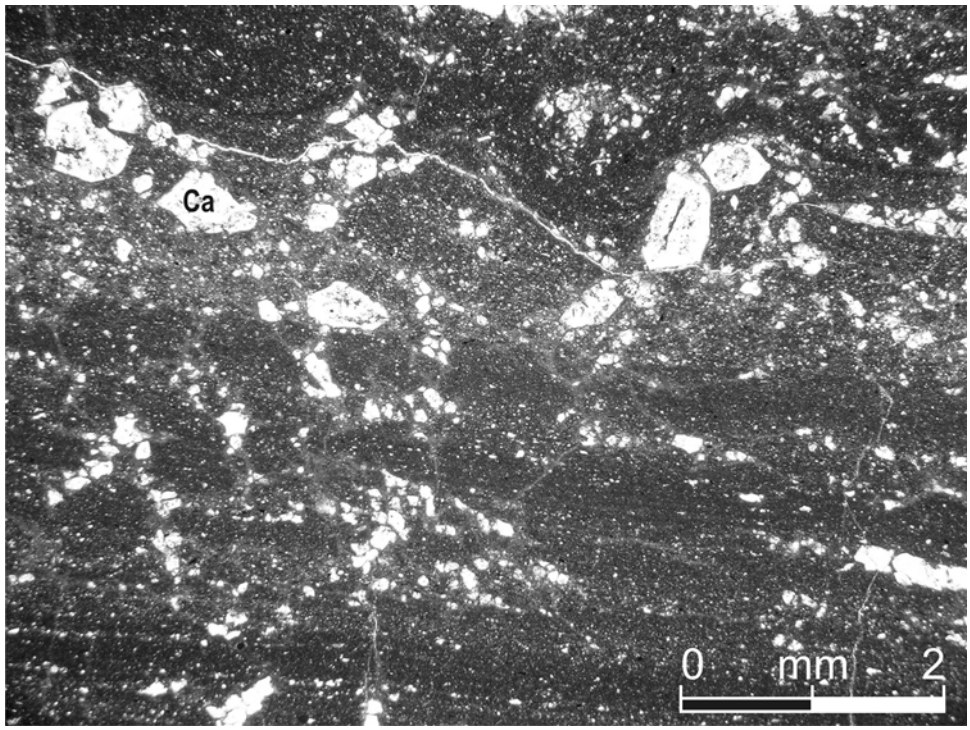

Fig. 10.6 Thin section photomicrograph of the carbonate shale at 152 m exhibits a lamination disrupted by variably sized nodules and microfractures. The shape of several crystals is closer to the form of shortite, suggesting the calcite (Ca) now present is a pseudomorphic phase. The original mineral is considered to have grown in situ because of the numerous inclusions of carbonate shale still embedded in the crystal form

by the growing dolomite crystal. Where P is recorded (e.g., rhombs in Fig. 10.9b, c) it occurs adjacent to the dolomite–calcite contact, or even enclosing the dolomite rhombs (Fig 10.9b). EDS data provide ambiguous evidence as to whether the P represents the element substituting in the carbonate lattice or that the calcite grew around and enveloped microcrystalline CFA.

10.7 Interpretations

10.7.1 Depositional Environments of the BNSZ

Facies models of evaporative lakes (e.g., Renaut and Gierlowski-Kordesch 2010) consider irregular and discontinuous, displacive and often pseudomorphed crystals in weakly laminated mudstone to form marginally, such as within saline mudflats during lake regressions, with cumulative, bedded evaporites typically forming near the basin/lake center. This model is appropriate for the BNSZ. In Buck Canyon, the lower and upper saline intervals (lithofacies 2c) are of a very limited thickness and identified only by pseudomorphing calcite crystals disrupting (brecciating) bedding (e.g., 152 m), suggesting a marginal setting. In the upper saline zone, interbedded lithofacies 2b may provide another indication of shallow water conditions. Lenticular cracks in the GRF have previously been considered related to subaqueous physical stresses associated with wave activity (Picard 1966; "diastasis" of Cowan and James 1992). However, subaqueous salinity changes affecting muds containing minor quantities of swelling clays ("synaeresis" of Plummer and Gostin 1981) cannot be ruled out. In strata below 152 m, the association of diagenetic pyrite (outcrop only) indicates that low Eh porewaters containing abundant dissolved ferrous iron and sulfide were present in the substrate (Hesse 1990) but not necessarily that the shallow lake waters were anoxic. The two saline intervals are considered to represent lateral facies transitions from the nodular nahcolite beds (Keighley 2013). Bedded nahcolite nodules increase in size and occur over greater stratal thicknesses toward the northeast, which indicates the direction to the evaporitic lake depocenter (Cashion 1967; Vanden Berg et al. 2013).

In the broader picture, occurrences of lithofacies 1 and its components within the BNSZ of Buck Canyon are interpreted as lateral facies extensions of the middle R-8 zone of the cores, and to represent anoxic-lake highstands (Desborough 1978). Interbeds of lithofacies 2a, and lithofacies 2 in general, ambiguously record either more oxic lake conditions that allowed for the breakdown of organic detritus or a lower productivity lake that might have existed under the saline conditions. The high carbonate content of the interbedded lithofacies 1 and 2 successions indicates a mostly clastic-starved setting, likely an offshore location.

Lithofacies 3b in the HBS exhibits a coarsening upward profile that, together with the contained wave-influenced sedimentary structures, indicates a prograding shoreface. The HBS thickens westward, where planar cross-strata additionally interbed to indicate a fluvio-deltaic source for the shoreface sandstone. Lying within the BNSZ, the HBS has previously been interpreted to be a lake low-stand succession (Brownfield et al. 2010) although at a higher resolution, it lies stratigraphically between two oil shale beds (lithofacies 1) and so could be considered a stand-still deposit during the transgressive phase that followed deposition of the lower saline interval.

In summary, although there was an overall trend upsection from an anoxic, balanced-fill, deep lake during deposition of the MOSZ to a predominantly underfilled, restricted evaporative basin during deposition of the BNSZ, lake transgressions and anoxic deep lake conditions still occurred periodically (i.e., the cyclicity noted by Smith et al. 2008). Within this context, the BNSZ at Buck Canyon would occupy a proximal position to the southerly, fluctuating but mostly closed-lake shoreline and to have formed during prolonged regressive lake stages as quiet, shallow water deposits close to marginal mud-flats. The P-enriched bed at 152 m is equated with a prolonged saline event accompanying a lake low stand.

10.7.2 Cause of Phosphorus Anomalies in the BNSZ

The basic P cycle for lakes is reviewed in detail elsewhere (e.g., Föllmi 1996; Wetzel 2001, and see Fig. 10.10) but usually the cycle leads to the epilimnion becoming a major P sink. Reserves of available P in the epilimnion are ultimately

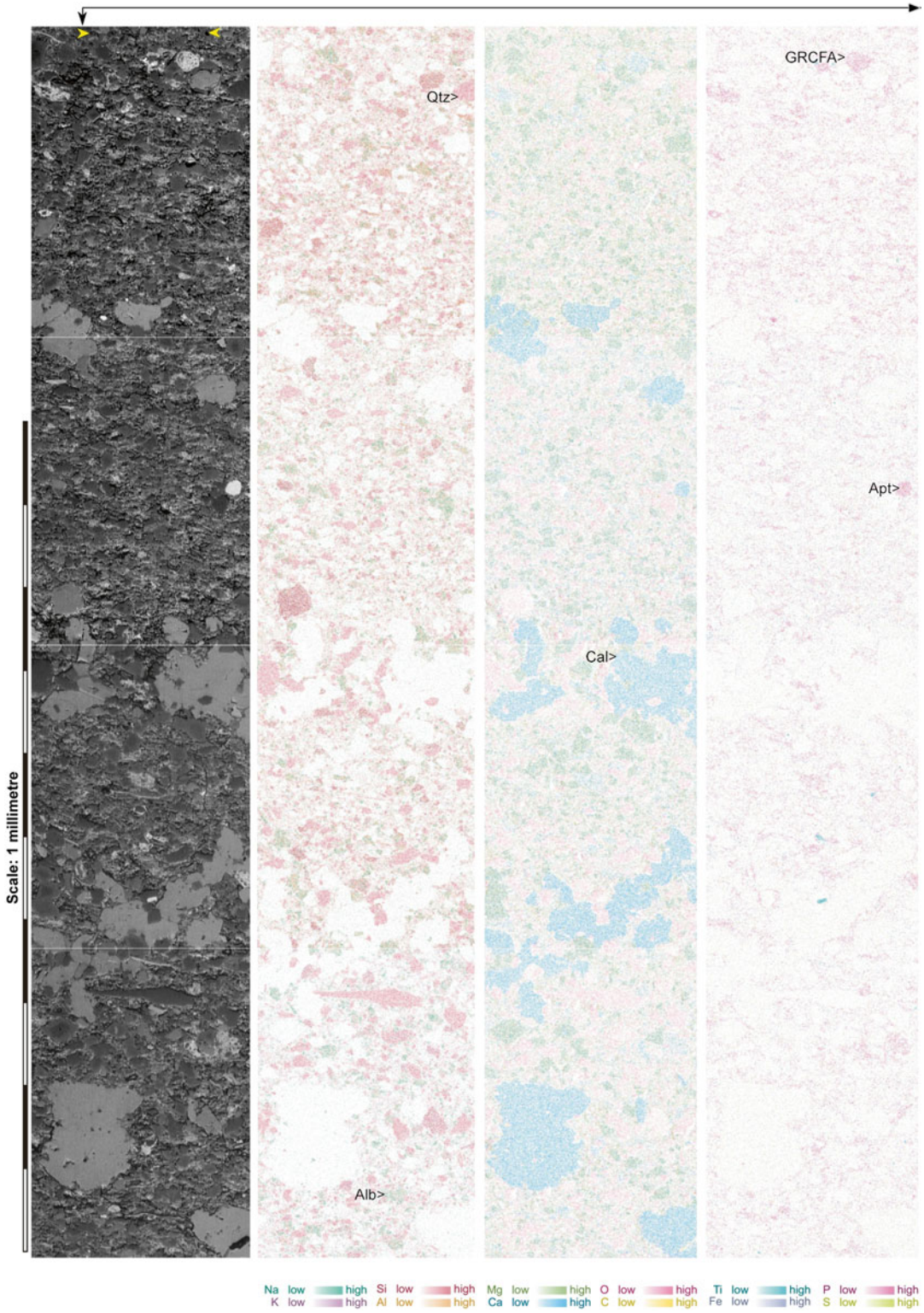

Fig. 10.7 SEM images of the carbonate shale at 152.0 m. For each sample, the first column is a montage of Back-Scattered Electron (BSE) images, with the other three columns being color-coded maps for selected elements to give a general indication of sample mineralogy. *Alb* albite, *AlkF* alkali feldspar, *Apt* apatite (detrital grain), *Cal* calcite, *Dol* dolomite, *GRCFA* grain-replacive calcium fluorapatite, *Qtz* quartz, *RFF* resin-filled fracture, *Rut* rutile, *ShS* sheet silicate

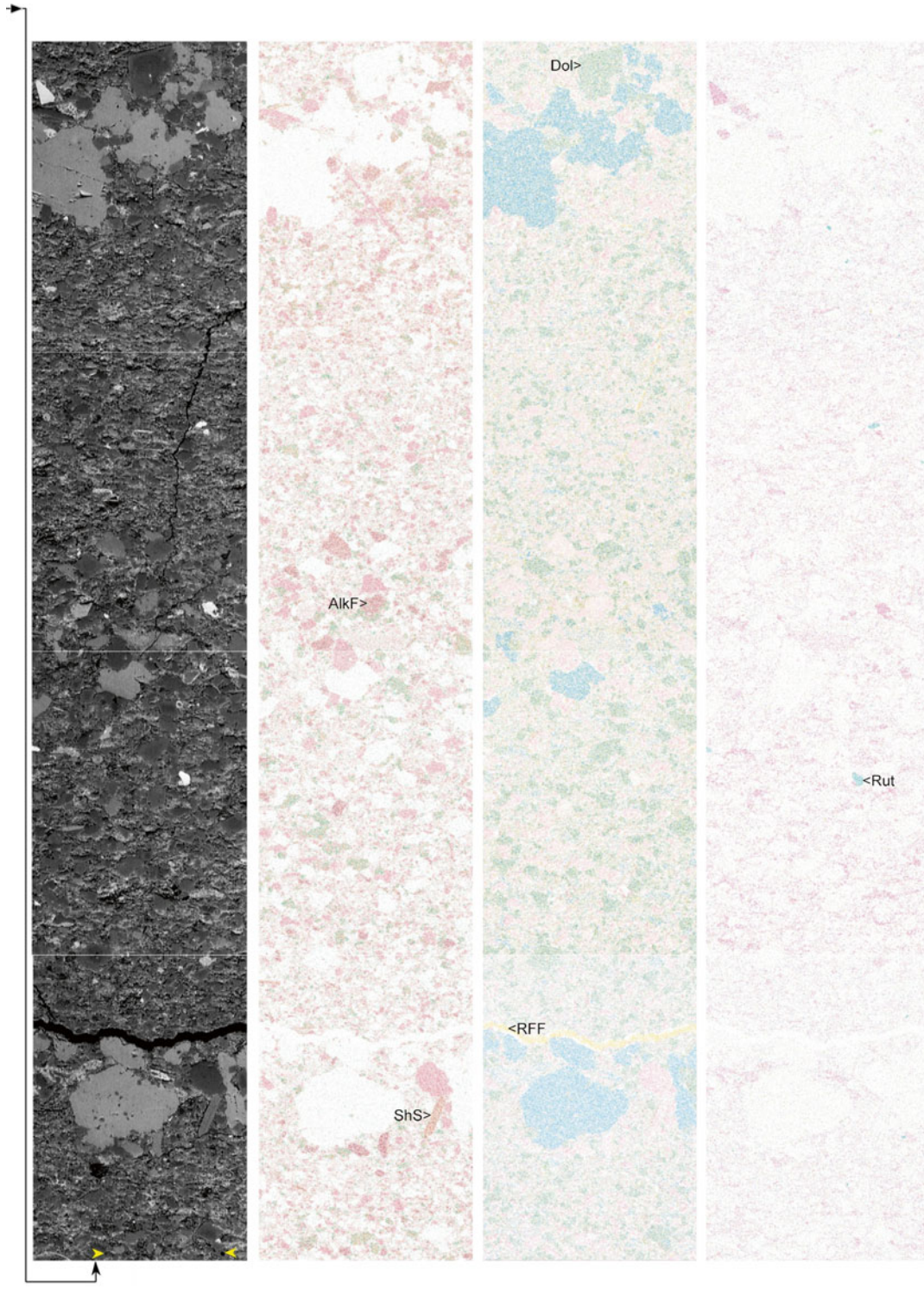

Fig. 10.7 (continued)

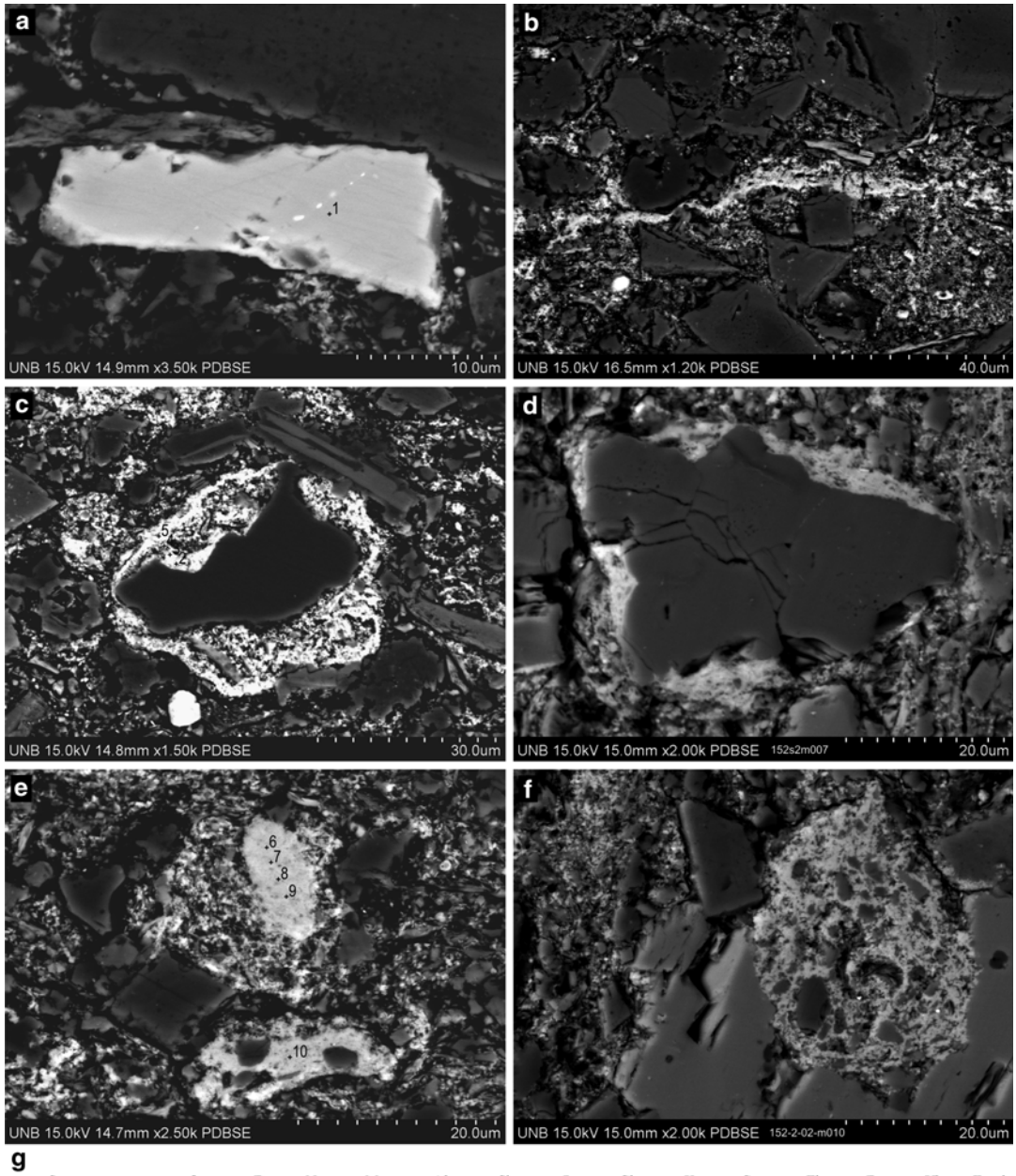

g

Spectrum	O	F	Na	Mg	Al	Si	P	Cl	K	Ca	Ti	Fe	Yb	Total
Spectrum(1)	39.12	7.87					19.90	0.20		38.25		0.26	0.00	105.59
Spectrum(2)	29.41	4.11	0.68	0.58	1.14	4.71	15.32		0.67	30.79	0.90	0.75		89.06
Spectrum(3)	40.45	4.94	0.81	1.54	2.33	8.58	14.90		1.21	28.11		1.14		104.01
Spectrum(4)	21.41	1.83	0.45	1.08	1.44	7.81	13.22		1.00	26.05	0.23	1.27		75.80
Spectrum(5)	27.59	3.31	0.62	1.11	1.65	7.15	15.71		0.89	27.79		1.08		86.90
Spectrum(6)	10.72	1.33	0.33	0.16	0.19	0.98	16.42		0.24	31.15		0.39	0.00	61.91
Spectrum(7)	40.16	5.68	1.14	0.48	0.43	1.96	17.02			33.93				100.79
Spectrum(8)	8.51	1.07	0.30	0.12	0.61	3.37	15.10		0.53	27.86		0.40		57.88
Spectrum(9)	7.98	0.91	0.20	0.10	0.15	0.83	14.11		0.22	28.57		0.47	0.00	53.53
Spectrum(10)	16.72	2.06	0.59	0.35	0.75	2.94	16.58		0.56	30.86		0.74		72.15

depleted only when the P-bearing dead biota is able to permanently sink down through the hypolimnion in stratified (meromictic) lakes (Levine et al. 1986). The biotic detritus is then able to settle out onto the substrate, to join detrital inorganic P phases and phases precipitated from solution (gross P sedimentation). Ultimately the detritus and P is buried and lithified in the sediment pile prior to later uplift for renewed weathering. However, a major complication to the cycle exists because, even after initial sedimentation, P may recycle back into the hypolimnion by remobilization from particulate stores into dissolved interstitial P by various mechanisms under anaerobic conditions (Boström et al. 1988; and discussed below). Where there is no well-established and permanent hypolimnion, a significant P-concentration gradient can then be present between the interstital and lake waters, promoting molecular diffusion into the overlying water column (gross P release). From a steady-state viewpoint, P retention (net P sedimentation) = gross P sedimentation – gross P release (Hupfer and Lewandowski 2008). For much of the BNSZ, ICP analyses (Fig. 10.5) indicate low background P concentrations and hence gross P sedimentation ≥ gross P release. Exceptionally, the sample from 152 m indicates a situation where gross P sedimentation ≫ gross P release. As reviewed earlier, such enrichment is rare in the known lacustrine geologic record and requires an explanation.

Temporary increased net P sedimentation may result from increased gross P sedimentation and, or, reduced gross P release. For the 152 m sample, increases in gross P sedimentation do not appear to be directly responsible for several reasons. Even though the drainage basin would have included apatite-bearing outcrops of the Phosphoria Formation (e.g., Hendrix and Byers 2000) and fresh volcanic ash falls (e.g., Smith et al. 2008), refractory P-bearing grains are rare (Fig. 10.7). Although outcrop is poor, carbonate shale overlies the phosphatic bed, so there is no evidence for increased dissolved-P influx via deposition of overlying tuffaceous or coarse clastic layers (Fig. 10.3). Also absent are skeletal hard parts and evidence of hardground reworking: the bed can be considered a "pristine phosphate" (Föllmi 1996). Gross P sedimentation may well have been enhanced by way of influxes of adsorbed inorganic-P on calcite or clays such as smectite (e.g., Ruttenberg and Berner 1993; Song et al. 2006; Holmkvist et al. 2010). Detrital Fe-oxides are absent from the strata and are unlikely to have been a common source of adsorbed P because the BNSZ was deposited when Lake Uinta likely had predominantly high pH, and sorption capacities for Fe-oxides decrease as pH levels increase above 6.5 (Stumm and Morgan 1996) and in the presence of dissolved sulfate (Katsev et al. 2006). Most importantly, the element is not present in its original organic or adsorbed inorganic phosphate phase, but as crystalline (precipitated) CFA.

Love (1964) and Swirydczuk et al. (1981) have proposed that phosphates in ancient lakes in Utah could have precipitated directly from periodically highly stratified hypersaline water columns (e.g., caused by a sudden drying of the

Fig. 10.8 Detailed BSE images with selected EDS analyses of CFA phases from 152 m. (**a**) Possibly an angular detrital grain of relatively pure CFA (Cl can substitute for F in the CFA lattice). (**b**) Ca and P are mapped as variably abundant in the matrix, and can concentrate (*brighter gray* – reflecting elements with higher atomic number) along irregular stringers, possibly related to precursor organic-rich laminae. (**c**, **d**) Variably thick coatings of sub-micron-scale crystals (EDS indicates an admixture of clays and/or carbonates, and CFA: the complexity of the matrix makes definitive EDS analysis of the CFA composition problematic due to limitations in the focus and penetration of the electron beam), each surrounding a silicate grain. (**e**) Variably dense, somewhat fibrous microcrystalline CFA and admixed clay/silicate/carbonate that may itself be diagenetic replacement or residual material of a precursor grain. The CFA bottom center may be replacing the groundmass of a multi-minerallic grain. (**f**) Another potentially phosphatized multi-mineralic grain is mostly enclosed by late-stage pseudomorphic calcite exhibiting the highly pitted morphology typical of this phase. (**g**) Tabulation of EDS spot analyses located in 8a, c, and e

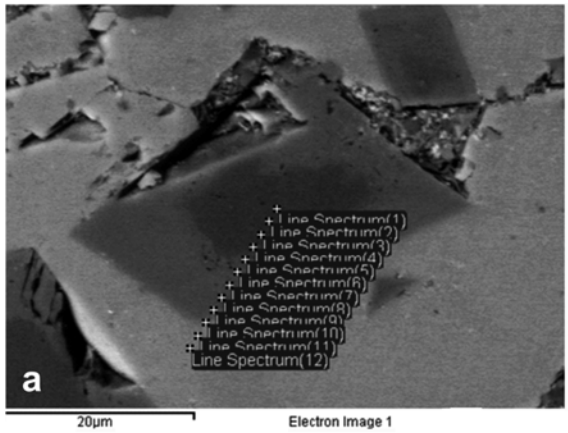

SAMPLE 152A

Spectrum	Mg	Ca	Fe	O	Al	Si	Na	K	Mn	P	Total
Line Spectrum(1)	11.23	21.41		29.80							62.44
Line Spectrum(2)	11.96	21.55		27.73							61.24
Line Spectrum(3)	11.82	21.41	0.39	27.32							60.94
Line Spectrum(4)	11.95	21.98	0.87	27.53					0.19		62.51
Line Spectrum(5)	5.63	20.48	2.12	11.69					0.18		40.10
Line Spectrum(6)	7.85	22.09	2.10	21.08	0.14	0.31					53.57
Line Spectrum(7)	10.36	23.59	2.83	27.40							64.17
Line Spectrum(8)	9.61	24.69	2.89	25.14							62.33
Line Spectrum(9)	5.22	29.97	2.28	14.26							51.72
Line Spectrum(10)	4.86	35.68	1.87	30.71							73.12
Line Spectrum(11)	0.21	32.66	0.42	14.22							47.52
Line Spectrum(12)	0.17	40.22	0.26	23.32							63.98
Max.	*11.96*	*40.22*	*5.27*	*30.71*	*0.14*	*0.31*			*0.19*		
Min.	*0.17*	*20.48*	--	*11.69*	--	--			--		

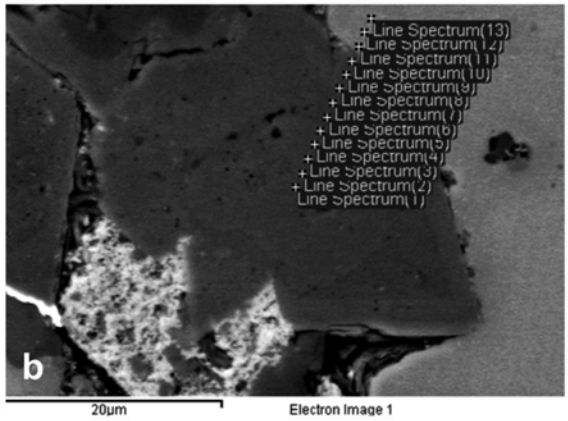

SAMPLE 152B

Spectrum	Mg	Ca	Fe	O	Al	Si	Na	K	Mn	P	Total
Line Spectrum(1)	9.09	20.18	4.22	18.42							51.91
Line Spectrum(2)	5.30	19.61	3.68	13.00		0.11					41.70
Line Spectrum(3)	9.85	21.92	4.29	19.07			0.11				55.25
Line Spectrum(4)	4.56	20.83	2.67	8.84	0.10	0.50					37.49
Line Spectrum(5)	8.39	21.47	1.76	19.97		0.19			0.23		52.01
Line Spectrum(6)	7.71	21.27	1.04	18.31							48.34
Line Spectrum(7)	12.12	23.82	2.14	31.07							69.15
Line Spectrum(8)	6.08	20.99	2.85	11.47		0.11					41.50
Line Spectrum(9)	7.27	24.04	2.62	19.21	0.33	1.45		0.25	0.18	0.67	56.01
Line Spectrum(10)	3.26	32.71	1.69	34.44	1.55	4.36		0.28		0.73	79.03
Line Spectrum(11)	0.15	34.17	0.34	13.37		0.16				0.12	48.30
Line Spectrum(12)	0.11	31.99	0.48	12.76		0.10				0.18	45.63
Line Spectrum(13)		27.24	0.31	8.02		0.14				0.20	35.90
Max.	*12.12*	*34.17*	*4.29*	*34.44*	*1.55*	*4.36*	*0.11*	*0.28*	*0.23*	*0.73*	
Min.	--	*19.61*	*0.31*	*8.02*	--	--	--	--	--	--	

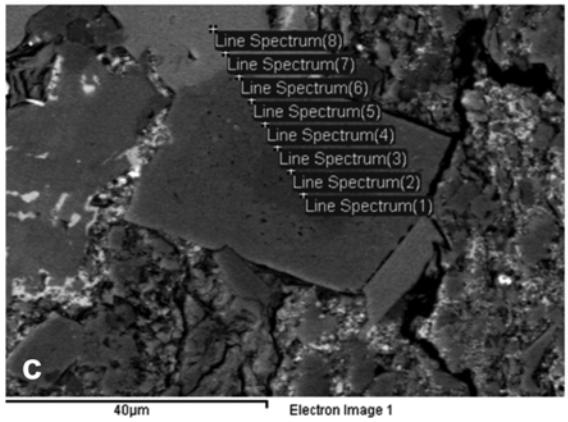

SAMPLE 152C

Spectrum	Mg	Ca	Fe	O	Al	Si	Na	K	Mn	P	Total
Line Spectrum(1)	4.60	17.67	0.28	13.16							35.70
Line Spectrum(2)	8.44	20.24		22.06							50.74
Line Spectrum(3)	3.72	17.14	1.07	5.98		0.12			0.46		28.48
Line Spectrum(4)	6.99	19.53	1.95	13.52					0.23		42.21
Line Spectrum(5)	5.07	18.83	2.75	11.12							37.77
Line Spectrum(6)	5.00	21.46	3.41	14.85						0.79	45.51
Line Spectrum(7)	0.16	37.07		23.24							60.47
Line Spectrum(8)		33.75	0.26	18.51							52.53
Max.	*8.44*	*37.07*	*3.41*	*23.24*		*0.12*			*0.46*	*0.79*	
Min.	--	*17.14*	--	*5.98*		--			--	--	

Fig. 10.9 BSE images and tabulated EDS analyses from 152 m detailing the zoning and diagenetic relationships in carbonates. (**a**) The EDS analyses are from a transect that runs from a core of NF dolomite through zoned Fe dolomite and out into late stage calcite. (**b**) A zoned Fe dolomite is post-dated by bright CFA microcrystalline aggregates (*lower left*) and large blocky calcite (*right*). Note that P is recorded only in the outermost five spectra, further indicating that the core had precipitated prior to P coming out of solution. (**c**) The EDS analyses again indicate a zoned dolomite, non-ferroan at its core with P recorded close to the rim (spectrum 6) and the contact with the low-Mg calcite (spectra 7 and 8). All results in weight percent. Processing option: all elements analyzed (values for carbon omitted: sample was carbon coated)

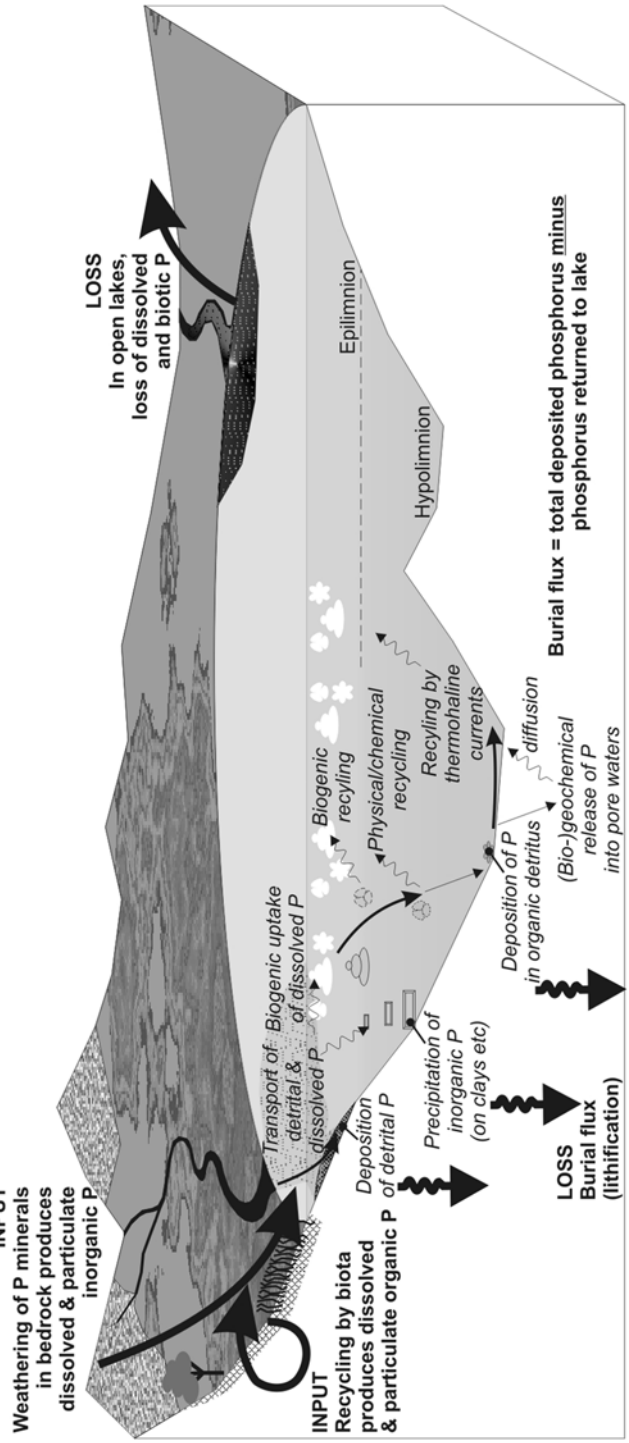

Fig. 10.10 The phosphorus cycle in lakes (Adapted from Keighley 2013)

climate) with the development of a chemocline that could act as a phosphate trap, inhibiting recycling into surface waters. However, in this sample the CFA is considered diagenetic because (i) settling of precipitated platy crystals in a low-energy environment would be expected to impart a preferred orientation, (ii) localized concentration of CFA as grain coatings, and (iii) P is recorded in SEM at the contact between authigenic dolomite and later calcite. The chemocline simply may have limited upward diffusion gradients, allowing P to accumulate and reach saturation in substrate pore waters.

Increased net P sedimentation is therefore considered the result of lowered gross P release due to initial substrate remobilization, by methods outlined in Boström et al. (1988), followed by its precipitation as diagenetic CFA. Jahnke (1984) and Van Cappellen and Berner (1988, 1991) identify CFA as the thermodynamically stable apatite phase that precipitates early and rapidly from high-carbonate, high pH solutions in the very shallow substrate. It remains uncertain whether CFA precipitates directly, or via precursor phosphate-mineral phases (e.g., Emerson 1976; House 1999; Song et al. 2002), or as a phosphatic gel (e.g., Slansky 1986).

As noted by Van Cappellen and Berner (1991) for oceans, and for example Kleeberg and Dudel (1997) and Anshumali (2007) for geochemically more variable lakes, the kinetics of apatite precipitation are influenced by numerous interlinked controlling parameters including dissolved-ion abundance (NO_3^-, CO_3^{2-} SO_4^{2-}, O^{2-}) and dissolved organic molecules, as well as temperature, salinity, alkalinity, pH, and Eh. Furthermore, redox reactions, adsorption, mineral phase solubility, and mineralization of organic matter are all mechanisms that have been invoked for bringing the primary CFA ions (F, Ca, and PO) to concentrations probably well above equilibrium (Knudsen and Gunter 2002). None of these mechanisms is universally dominant (e.g., Van Cappellen and Berner 1991; Kaiserli et al. 2002; Katsev et al. 2006) and, in particular, the long-held paradigm that redox, particularly involving Fe-oxides, is the major mechanism has now been shown to be valid only under special circumstances for lakes (Hupfer and Lewandowski 2008).

If all major components of CFA were at saturation, the main limiting control would have been the presence of Mg^{2+} in solution. At neutral pH, CFA growth is limited if the Ca:Mg ratio drops below 1.2:1, but at a pH of 7.5–8, CFA is limited if the ratio drops below 5.2:1 (Knudsen and Gunter 2002). The Mg^{2+} ion either may be incorporated into the apatite crystal, resulting in lattice distortion that limits crystal growth (Gulbrandsen et al. 1984), or the Mg^{2+} may block crystal growth sites simply by its adsorption onto the crystal (Van Cappellen and Berner 1991). High Ca:Mg ratios can be attained by removal of Mg^{2+}, by enrichment of Ca^{2+}, such as by dissolution of calcite or gypsum (Nathan and Lucas 1972), or by authigenesis. The diagenetic succession of phosphate post-dating the abundant rhombic dolomite crystals (Fig. 10.9) suggests that only once the Mg^{2+} was incorporated into the dolomite cement in the substrate – this reaction also liberates F^- ions from MgF complexes, aiding fluoride saturation – could phosphogenesis commence.

The dolomite in question can be considered a primary, penecontemporaneous dolomite, and its rhombic form directs interpretation toward the evaporative pumping sabkha model of dolomite formation (Morrow 1990). Even so, dolomite precipitation is itself problematic, with poorly understood kinetic effects where there are temperatures below 50 °C and low dissolved sulfate (e.g., Machel 2004; Armenteros 2010). The formation of nahcolite, rather than the trona common in the Wyoming lakes, suggested to Milton and Eugster (1959) that moderate lake temperatures of 35 °C or less persisted in the possibly deeper water Uinta Basin (lower with higher atmospheric CO_2: Lowenstein and Demicco 2006). However, despite low sulfate concentrations in Lake Uinta, if any organic matter was breaking down in the substrate, the presence of methanogenic bacteria may have promoted progressively Fe-enriched dolomites with biogenic sulfate reduction being suppressed (Mazzullo 2000). The lack of pyrite at 152 m is further support. Whereas Fe^{2+} was forming from the breakdown of limited

Fe-silicates, oxides, and highly reactive organic iron compounds by Fe-reducing bacteria, any H_2S that was generated slightly deeper in the substrate and that diffused upward would be kinetically inhibited from reacting with the Fe^{2+} due to high porewater pH (Tuttle and Goldhaber 1993). Iron was thus increasingly available for incorporation into a dolomite lattice provided methanogenesis maintained high pH and carbonate alkalinity (Mazzullo 2000).

The localized concentration of CFA as grain coatings and partial grain replacements (Fig. 10.8) suggests they were the preferred CFA nucleation sites. Both Mg-bearing smectite and zeolite are considered effective adsorption sites for P (e.g., Ruttenberg and Berner 1993; Sakadevan and Bavor 1998; Stamatakis and Koukouzas 2001), and their precipitation as clay rims or partial alterations of volcanic grains could also have contributed to lower Mg^{2+} levels. Authigenic zeolite and smectite can form by evaporative pumping around volcanic-influenced saline lake margins (e.g., Renaut 1993; Hay and Kyser 2001). Smectite has not been verified either in XRD or SEM for this sample, but was noted in the upper GRF further east by Dyni (1976) and Bristow et al. (2012) who found that dolomite abundance was related to the inverse of Mg-smectite abundance.

10.8 Conclusions

Low background concentrations of P are recorded from ICP analyses of 89 samples from the upper GRF of the Uinta Basin, Utah, and indicate that a minor amount of phosphate was continuously accumulating during the deposition of over 200 m of Eocene lacustrine strata. However, in the BNSZ one carbonate shale containing calcite pseudomorphs (as well as an oil shale bed not detailed herein), phosphorus peaks at values of over 5 wt% of the oxide. XRD analysis of 9 samples from the BNSZ confirms CFA as the major P-bearing mineral. Thin section and SEM observations identify the CFA as microcrystalline aggregates, with EDS recording the presence of sodium and sulfate that would have substituted into the CFA crystal lattice. Diagenetic calcite is considered to pseudomorph large shortite crystals as well as to enclose rhombic zoned ferroan dolomite in precipitate-dominated laminae.

The establishment of a chemocline in a high pH, high alkalinity, saline lake of low organic productivity may have caused dissolved P to reach saturation in lake and pore waters. However, CFA would not normally precipitate because at high pH, Mg^{2+} in solution effectively inhibits CFA precipitation. Evaporative pumping to the adjacent sabkha, potentially also with the activity of methanogenic bacteria, led to the precipitation of rhombic, zoned ferroan dolomite, reducing dissolved Mg^{2+} content, and permitting CFA to then precipitate, possibly also in association with smectite diagenesis.

Acknowledgments Manuscript reviewers and editors provided detailed and constructive comments. D. MacIsaac assisted with logging and sampling. V. Reddy (UNB Earth Sciences) undertook the XRD analyses. Sample chips and thin sections were produced by A. Murphy and C. Nash (UNB Earth Sciences). SEM analysis was courtesy of S. Boonsue and J. Spray (UNB Earth Sciences). Field and stratigraphic discussions with M. Vanden Berg, D. Sprinkel and C. Morgan (Utah Geological Survey) were very constructive. Funding for this project was provided in part by an NSERC Discovery Grant and by a Utah Geological Survey, State of Utah Petroleum Research Grant.

References

Anshumali RAL (2007) Phosphorus fractionation in surficial sediments of Pandoh Lake, Lesser Himalaya, Himachal Pradesh, India. Appl Geochem 22:1860–1871

Armenteros I (2010) Diagenesis of carbonates in continental settings. In: Alonzo-Zarza AM, Tanner LH (eds) Carbonates in continental settings: geochemistry, diagenesis and applications, vol 62, Developments in sedimentology. Elsevier Science, Amsterdam/London, pp 61–151

Bein A (1986) Stable isotopes, iron and phosphorus in a sequence of lacustrine carbonates – paleolimnic implications. Chem Geol 59:305–313

Birgenheier LP, Vanden Berg MD (2011) Core-based integrated sedimentologic, stratigraphic, and geochemical analysis of the oil shale bearing Green River Formation, Uinta Basin, Utah. United States Department of Energy and National Energy Technology Laboratory, Topical report, 19 p

Boström B, Andersen JM, Fleischer S, Jansson M (1988) Exchange of phosphorus across the sediment-water interface. Hydrobiologia 170:229–244

Bradley WH (1929) The occurrence and origin of analcite and meerschaum beds in the Green River Formation of Utah, Colorado, and Wyoming, U.S. Geological Survey, professional paper 158-A. U.S. Government Printing Office, Washington, DC, p 7

Bradley MD (1995) Timing of the Laramide rise of the Uinta Mountains, Utah and Colorado. In: Jones RW (ed) Resources of Southwestern Wyoming. Wyoming Geological Association, Casper, Wy, pp 31–44

Bristow TF, Kennedy MJ, Morrison KD, Mrofka DD (2012) The influence of authigenic clay formation on the mineralogy and stable isotopic record of lacustrine carbonates. Geochim Cosmochim Acta 90:64–82

Brownfield ME, Johnson RC, Dyni JR (2010) Sodium carbonate resources of the Eocene Green River Formation, Uinta Basin, Utah and Colorado. U.S. Geological Survey, Digital data series DDS-69-BB, Ch. 2, 13 p

Carasco B (1989) Lacustrine sedimentation in a Permian intermontane basin: the Villé Graben (Vosges, France). Palaeogeogr Palaeoclimatol Palaeoecol 70:179–186

Cashion WB (1967) Geology and fuel resources of the Green River Formation, southeastern Uinta Basin, Utah and Colorado, vol 548, U.S. Geological Survey, professional paper. U.S. Government Printing Office, Washington, DC, p 48

Cashion WB (1995) Stratigraphy of the Green River Formation, eastern Uinta Basin, Utah and Colorado—a summary. In: Averett WR (ed) The Green River Formation in Piceance Creek and Eastern Uinta Basins field trip 1995. Grand Junction Geological Society, Grand Junction, Co, pp 15–21

Cowan CA, James NP (1992) Diastasis cracks: mechanically generated synaeresis-like cracks in Upper Cambrian shallow water oolite and ribbon carbonates. Sedimentology 39:1101–1118

Dane CH (1954) Stratigraphic and facies relationships of the upper part of the Green River Formation and lower part of the Uinta Formation in Duchesne, Uintah, and Wasatch counties, Utah. AAPG Bull 38:405–425

De las Heras X, Grimalt JO, Albaigés J (1989) Origin and diagenesis of the organic matter in Miocene freshwater lacustrine phosphates (Cerdanya Basin, eastern Pyrenees). Org Geochem 14:667–677

Desborough GA (1978) A biogenic-chemical stratified lake model for the origin of oil shale of the Green River Formation: an alternative to the playa-lake model. Geol Soc Am Bull 89:61–971

Desborough GA, Pitman JK, Hufman C (1976) Concentration and mineralogical residence of elements in rich oil shales of the Green River Formation, Piceance Creek Basin, Colorado, and the Uinta Basin, Utah – a preliminary report. Chem Geol 17:13–26

Dickinson WR, Klute MA, Hayes MJ et al (1988) Paleogeographic and paleotectonic setting of Laramide sedimentary basins in the central Rocky Mountain region. Geol Soc Am Bull 100:1023–1039

Dietrich R (1978) Das Messelitproblem: Messelit und Anapait aus dem Olschiefervorkommen bei Messel. Der Aufschluss Sonderheft 29:229–233

Donnell JR (2009) Intertonguing of the lower part of the Uinta Formation with the upper part of the Green River Formation in the Piceance Creek Basin during the late stages of Lake Uinta. U.S. Geological Survey, scientific investigations report 2008–5237, 25 p

Dyni JR (1976) Trioctahedral smectite in the Green River Formation, Duchesne County, Utah, vol 967, U.S. Geological Survey, professional paper. U.S. Government Printing Office, Washington, DC, p 14

Dyni JR (1996) Sodium carbonate resources of the Green River Formation, U.S. Geological Survey, open-file report 1996–729. U.S. Dept. of the Interior, U.S. Geological Survey, Denver, p 39

Emerson SE (1976) Early diagenesis in anaerobic lake sediments: chemical equilibria in interstitial waters. Geochim Cosmochim Acta 40:925–934

Fabbi BP, Espos LF (1976) X-ray fluorescence analysis of 21 selected major, minor, and trace elements in eight new USGS standard rocks. In: Flanagan FJ (ed) Description and analyses of eight new USGS rock standards, vol 840, U.S. Geological Survey, professional paper. U.S. Dept. of the Interior, U.S. Geological Survey, Reston, p 192

Fahey JJ (1962) Saline minerals of the Green River Formation, vol 405, U.S. Geological Survey, professional paper. U.S. Government Printing Office, Washington, DC, p 50

Föllmi KB (1996) The phosphorus cycle, phosphogenesis and marine phosphate-rich deposits. Earth-Sci Rev 40:55–124

Gromet LP, Dymek RF, Haskin LA, Korotev RL (1984) The "North American Shale Composite": its compilation, major, and trace element characteristics. Geochim Cosmochim Acta 48:2469–2482

Gulbrandsen RA, Robertson CE, Neil ST (1984) Time and crystallization of apatite in seawater. Geochim Cosmochim Acta 48:213–218

Hay RL, Kyser TK (2001) Chemical sedimentology and paleoenvironmental history of Lake Olduvai, a Pliocene lake in northern Tanzania. Geol Soc Am Bull 113:1505–1521

Hendrix MS, Byers CW (2000) Stratigraphy and sedimentology of Permian strata, Uinta Mountains, Utah: allostratigraphic controls on the accumulation of economic phosphate. In: Glenn CR, Prévôt-Lucas L, Lucas J (eds) Marine authigenesis: from global to microbial, vol 66, SEPM Special Publication. SEPM (Society for Sedimentary Geology), Tulsa, pp 349–367

Hesse R (1990) Early diagenetic pore water/sediment interaction: modern offshore basins. Geosci Canada Reprint Ser 4:277–316

Holmkvist L, Arning ET, Küster-Heins K et al (2010) Phosphate geochemistry, mineralization processes, and *Thioploca* distribution in shelf sediments off central Chile. Mar Geol 277:61–72

House WA (1999) The physico-chemical conditions for the precipitation of phosphate with calcium. Environ Technol 20:727–733

Hupfer M, Lewandowski J (2008) Oxygen controls the phosphorus release from lake sediments – a long-lasting paradigm in limnology. Int Rev Hydrobiol 93:415–432

Jahnke RA (1984) The synthesis and solubility of carbonate fluorapatite. Am J Sci 284:58–78

Johnson RC (1981) Stratigraphic evidence for a deep Eocene Lake Uinta, Piceance Creek Basin, Colorado. Geology 9:55–62

Kaiserli A, Votusa D, Samara C (2002) Phosphorus fractionation in lake sediments – Lakes Volvi and Koronia, N. Greece. Chemosphere 46:1147–1151

Katsev S, Tsandev I, L'Heureux I, Rancourt DG (2006) Factors controlling long-term phosphorus efflux from lake sediments: exploratory reactive-transport modeling. Chem Geol 236:127–147

Keighley D (2013) Outcrop chemostratigraphic correlation of the upper Green River Formation (Mahogany oil shale zone—Uinta Fm. boundary) in the Uinta Basin, Utah. Utah Geological Survey, Salt Lake City, Ut

Keighley D, Flint S (2008) Models of fluvial sandbody geometry and connectivity in the middle Green River Formation, Nine Mile Canyon, SW Uinta Basin. In: Longman MW, Morgan CD (eds) Hydrocarbon systems and production in the Uinta Basin, Utah, vol 37, Rocky Mountain Association of Geologists – Utah Geological Association, Special Publication. Rocky Mountain Association of Geologists/Utah Geological Association, Denver/Salt Lake City, pp 101–119

Keighley D, Borer J, Morgan C et al (2003a) Facies asymmetry in alluvial-lacustrine basins: a transect across the Uinta basin, eastern Utah and western Colorado. AAPG Annual Convention, Salt Lake City. 77 + xxxiii p, May 2003

Keighley D, Flint S, Howell J, Moscariello A (2003b) Sequence stratigraphy in lacustrine basins: a model for part of the Green River Formation (Eocene), southwest Uinta Basin, Utah. J Sediment Res 73:987–1006

Kleeberg A, Dudel GE (1997) Changes in extent of phosphorus release in a shallow lake (Lake Großer Müggelsee; Germany, Berlin) due to climatic factors and load. Mar Geol 139:61–75

Knudsen AC, Gunter ME (2002) Sedimentary phosphorites – an example: phosphoria formation, Southeastern Idaho, U.S.A. In: Kohn MJ, Rakovan J, Hughes JM (eds) Phosphates: geochemical, geobiological, and materials importance, vol 48, Reviews in mineralogy and geochemistry. Mineralogical Society of America, Washington, DC, pp 363–389

Lambiase JJ (1990) A model for tectonic control of lacustrine stratigraphic sequences in continental rift basins. In: Katz BJ (ed) Lacustrine basin exploration – case studies and modern analogs, vol 50, AAPG, memoir. American Association of Petroleum Geologists, Tulsa, pp 265–276

Levine SN, Stainton MP, Schindler DW (1986) A radiotracer study of phosphorus cycling in a eutrophic Canadian Shield lake, experimental lake 227, northwestern Ontario. Can J Fish Aquat Sci 43:366–378

Love D (1964) Uraniferous phosphatic lake beds of Eocene age in intermontane basins of Wyoming and Utah, U.S. Geological Survey, professional paper 474-E. U.S. Government Printing Office, Washington, DC, pp 1–66

Lowenstein TK, Demicco RV (2006) Elevated Eocene atmospheric CO_2 and its subsequent decline. Science 313:1928

Machel HG (2004) Concepts and models of dolomitization: a critical reappraisal. In: Braithwaite CJR, Rizzi G, Darke G (eds) The geometry and petrogenesis of dolomite hydrocarbon reservoirs, vol 235, Geological Society special publication. Geological Society, London, pp 7–63

Mazzullo SJ (2000) Organogenic dolomitization in peritidal to deep-sea sediments. J Sediment Res 70:10–23

Milton C, Eugster HP (1959) Mineral assemblage of the Green River Formation. In: Abelson PH (ed) Researches in geochemistry. Wiley, New York, pp 118–150

Morgan CD, Chidsey TC, McClure KP et al (2002) Reservoir characterization of the lower Green River Formation, southwest Uinta Basin, Utah. Utah Geological Survey – U.S. Department of Energy DOE/BC/15103-4 OSTI No. 805237, 140 p

Morris TH, Richmond DR (1992) A predictive model of reservoir continuity in fluvial sandstone bodies of a lacustrine deltaic system, Colton Formation, Utah. In: Fouch TD, Nuccio VF, Chidsey TC (eds) Hydrocarbon and mineral resources of the Uinta Basin, Utah and Colorado, vol 20, Utah Geological Association publication. Utah Geological Association, Salt Lake City, pp 227–236

Morrow DW (1990) Dolomite—Part 1: the chemistry of dolomitization and dolomite precipitation. Geoscience Canada, Reprint Series 4, pp 113–123

Mossman DJ, Macey JF, Lemmon PD (1987) Diagenesis in the lacustrine facies of the Albert Formation, New Brunswick, Canada: a geochemical evaluation. Bull Can Pet Geol 35:239–250

Mott LV, Drever JI (1983) Origin of uraniferous phosphatic beds in Wilkins Peak Member of Green River Formation, Wyoming. Am Assoc Pet Geol Bull 67:70–82

Mutakyahwa MKD (2002) Mineralogy and chemistry of bentonite (?) deposits at Minjingu, Lake Manyara, North Tanzania. J Afr Earth Sci 34:213–221

Nathan Y, Lucas J (1972) Synthèse de l'apatite à partir du gypse: application au problème de la formation des apatites carbonates par precipitation directe. Chem Geol 9:99–112

Picard MD (1966) Oriented, linear-shrinkage cracks in Green River Formation (Eocene), Raven Ridge area, Utah. J Sediment Petrol 36:1050–1057

Plummer PS, Gostin VA (1981) Shrinkage cracks: desiccation or synaeresis? J Sediment Petrol 51: 1147–1156

Remy R (1992) Stratigraphy of the Eocene part of the Green River Formation in the south-central part of the Uinta basin, Utah. U.S. Geological Survey, Bulletin B 1787-BB, pp BB1–BB69

Renaut RW (1993) Zeolitic diagenesis of late Quaternary fluviolacustrine sediments and associated calcrete formation in the Lake Bogoria basin, Kenya Rift Valley. Sedimentology 40:271–301

Renaut RW, Gierlowski-Kordesch EH (2010) Lakes. In: James NP, Dalrymple RW (eds) Facies models 4, vol 6, Geotext. Geological Association of Canada, St. John's, pp 541–575

Rodd JA, Stewart AD (1992) Geochemistry, weathering and diagenesis of the Diabaig Formation (Torridon Group) in NW Scotland. Scott J Geol 28:27–35

Ruttenberg KC, Berner RA (1993) Authigenic apatite formation and burial in sediments from non-upwelling, continental margin environments. Geochim Cosmochim Acta 57:991–1007

Saether OM, Runnells DD, Ristinen RA, Smythe WR (1981) Fluorine: its mineralogical residence in the oil shale of the Mahogany Zone of the Green River Formation, Piceance Creek Basin, Colorado, U.S.A. Chem Geol 31:169–184

Sakadevan K, Bavor HJ (1998) Phosphate adsorption characteristics of soils, slags, and zeolite to be used as substrates in constructed wetland systems. Water Resour 32:393–399

Slansky M (1986) Geology of sedimentary phosphates. Elsevier, New York

Smith ME, Carroll AR, Singer BS (2008) Synoptic reconstruction of a major ancient lake system: Eocene Green River Formation, western United States. Geol Soc Am Bull 120:54–84

Song Y, Hahn HH, Hoffmann E (2002) The effect of carbonate on the precipitation of calcium phosphate. Environ Technol 23:207–215

Song Y, Weidler PG, Berg U et al (2006) Calcite-seeded crystallization of calcium phosphate for phosphorus recovery. Chemosphere 63:236–243

Stamatakis MG, Koukouzas NK (2001) The occurrence of phosphate minerals in lacustrine clayey diatomite deposits, Thessaly, Central Greece. Sediment Geol 139:33–47

Strother PK, Battison L, Brasier MD, Wellman CH (2011) Earth's earliest non-marine eukaryotes. Nature 473:505–509

Stumm W, Morgan JJ (1996) Aquatic chemistry: chemical equilibria and rates in natural waters, 3rd edn. Wiley, New York

Swanson VE (1960) Oil yield and uranium content of black shales. U.S. Geological Survey, professional paper 356-A, Washington, DC, pp 1–44

Swirydczuk K, Wilkinson BH, Smith GR (1981) Synsedimentary lacustrine phosphorites from the Pliocene Glenns Ferry Formation of southwestern Idaho. J Sediment Petrol 51:1205–1214

Talbot MR, Kelts K (1986) Primary and diagenetic carbonates in the anoxic sediments of Lake Bosumtwi, Ghana. Geology 14:912–916

Taylor SR, McLennan SM (1985) The continental crust: its composition and evolution. Blackwell, London

Tuttle MLW (2009) A collection of chemical, mineralogical, and stable isotopic compositional data for Green River Oil Shale from depositional center cores in Colorado, Utah, and Wyoming. U.S. Geological Survey, Reston, Va

Tuttle MLW, Goldhaber MB (1993) Sedimentary sulfur geochemistry of the Paleogene Green River Formation, western USA: implications for interpreting depositional and diagenetic processes in saline alkaline lakes. Geochim Cosmochim Acta 57:3023–3039

United States Geological Survey (2010) USGS geochemical reference materials and certificates: USGS certificate of analysis, Green River Shale, SGR-1. http://minerals.cr.usgs.gov/geo_chem_stand/shale.html. Accessed 3 July 2010

Van Cappellen P, Berner RA (1988) A mathematical model for the early diagenesis of phosphorus and fluorine in marine sediments: apatite precipitation. Am J Sci 288:289–333

Van Cappellen P, Berner RA (1991) Fluorapatite crystal growth from modified seawater solutions. Geochim Cosmochim Acta 55:1219–1234

Vanden Berg MD, Lehle DR, Carney SM, Morgan CD (2013) Geological characterization of the Bird's Nest Aquifer, Uinta Basin, Utah: assessment of the aquifer's potential as a saline water disposal unit. Utah Geological Survey, special study 147, CD-ROM

Vozárová A, Rojkovič I (2000) Permian lacustrine phosphatic sandstone in the Southern Gemeric Unit, Western Carpathians, Slovakia. Geol Carpath 51:265–278

Wetzel RG (2001) Limnology: lake and river ecosystems, 3rd edn. Academic, San Diego

11 Evaporites of the Green River Formation, Bridger and Piceance Creek Basins: Deposition, Diagenesis, Paleobrine Chemistry, and Eocene Atmospheric CO_2

Elliot A. Jagniecki and Tim K. Lowenstein

Abstract

Sedimentary structures and petrographic textures of evaporites and associated sediments of the Green River Formation, together with evaporite phase equilibria, provide information on depositional and diagenetic conditions. Volumetrically important trona ($NaHCO_3 \cdot Na_2CO_3 \cdot 2H_2O$) and shortite ($Na_2CO_3 \cdot 2CaCO_3$) occur in the Wilkins Peak Member, Bridger Basin, WY, whereas nahcolite ($NaHCO_3$) occurs in the saline facies of the time equivalent Parachute Creek Member, Piceance Creek Basin, CO. The saline facies of the Parachute Creek Member was deposited in a relatively deep perennial hypersaline lake. In contrast, deposition of the Wilkins Peak Member, Bridger Basin, occurred in shallower perennial saline lakes that periodically desiccated. Trona from the Bridger Basin and nahcolite from the Piceance Creek Basin are stratigraphically associated with oil shale, suggesting evaporite deposition in perennial, density stratified saline lakes. Primary textures in bedded trona and nahcolite indicate that they formed at the air-water interface as microcrystalline cumulate needles. Halite formed concurrently with trona and nahcolite as cumulate layers, and as basin floor crusts. Shortite formed diagenetically during burial of the Wilkins Peak Member in the Bridger Basin as displacive crystals, pseudomorphous replacements of precursor Na-Ca-carbonate minerals, and fracture filling cements.

Precipitation of trona and nahcolite necessitates that the inflow waters that fed the Green River lakes contained total carbonate ($HCO_3^- + CO_3^{2-}$) greater than $Ca^{2+} + Mg^{2+}$. During evapoconcentration, lake waters evolved into Na^+-CO_3^{2-}-HCO_3^--Cl^- brines. The formation of trona versus nahcolite

E.A. Jagniecki (✉) • T.K. Lowenstein
Department of Geological Sciences and
Environmental Studies, Binghamton University,
Binghamton, NY 13902, USA
e-mail: ejagnie1@binghamton.edu;
lowenst@binghamton.edu

M.E. Smith, A.R. Carroll (eds.), *Stratigraphy and Paleolimnology of the Green River Formation, Western USA*, Syntheses in Limnogeology 1, DOI 10.1007/978-94-017-9906-5_11

can be explained by variations in brine pH, Na^+ concentration, temperature, or pCO_2. Nahcolite is the stable mineral at elevated atmospheric pCO_2 (>1,125 ppm); trona is also stable at high pCO_2, but at higher temperatures. Nahcolite formed under elevated atmospheric pCO_2 during the Early Eocene Climatic Optimum.

11.1 Introduction

The early and middle Eocene Green River Formation of Wyoming, Colorado, and Utah, consists of lacustrine deposits with vast reserves of oil shale and the world's largest deposit of sodium carbonate evaporites (Fig. 11.1) (Bradley and Eugster 1969; Dyni 1998). Economically important oil shales (organic-rich carbonate and siliceous mudstones) and sodium carbonate evaporites accumulated together in the Wilkins Peak Member, Greater Green River Basin, and Parachute Creek Member, Piceance Creek Basin 51.3–49.6 million years ago and later in the Uinta Basin 48.0–46.5 million years ago (Smith et al. 2003, 2008a) (Fig. 11.1).

The depositional environments of the evaporites and organic-rich carbonate mudstones of the Wilkins Peak Member and equivalents, whether stratified perennial lakes or ephemeral playas, have been debated for decades. The depositional settings of the Green River evaporite facies have been controversial, in part because of the lack of detailed sedimentological studies (exceptions are Beard et al. 1974; Dyni 1981; Birnbaum and Radlick 1982; Boni and Atkinson 1998). Bedded trona ($NaHCO_3 \cdot Na_2CO_3 \cdot 2H_2O$), halite (NaCl), and carbonate mudstone of the Wilkins Peak Member of the Bridger Basin have been interpreted as perennial saline lake deposits (Bradley 1966; Bradley and Eugster 1969; Eugster and Surdam 1973) or, alternatively, as saline pan and mudflat deposits, where shallow alkaline saline lakes formed and commonly dried out, analogous to modern Lake Magadi, Kenya (Eugster and Hardie 1975; Birnbaum and Radlick 1982; Roehler 1993; Carroll and Bohacs 1999; Pietras and Carroll 2006). The ephemeral saline lake model has also been applied to the bedded nahcolite ($NaHCO_3$), halite, and oil shale of the Parachute Creek Member, Piceance Creek Basin (Lundell and Surdam 1975). In contrast, perennial saline lake conditions for deposition of the Piceance Creek Basin bedded mudstone-nahcolite-halite are suggested by fine scale lamination, turbidites (Dyni and Hawkins 1981; Johnson 1981; Tänavsuu-Milkeviciene and Sarg 2012), the gradually rising Br^- profile (measured from halite) in stratigraphic sections (Dyni et al. 1970), and the ^{34}S enrichment in sulfide minerals and organic matter (Tuttle and Goldhaber 1991, 1993).

Advances in our understanding of evaporite deposition and early diagenesis in modern and Pleistocene arid closed basins (Casas and Lowenstein 1989; Smoot and Lowenstein 1991; Li et al. 1996; Schubel and Lowenstein 1997) and thermodynamic data on sodium carbonate mineral equilibria (Eugster 1966; Bradley and Eugster 1969; Harvie et al. 1984; Monnin and Schott 1984; Plummer et al. 1988; Risacher and Clement 2001; Jagniecki et al. 2013) have set the stage for new sedimentological, petrographic, and geochemical interpretations of the Green River evaporites. Because a significant portion of the high grade Green River oil shale lies in the evaporative facies of the Parachute Creek Member, Piceance Creek Basin, new knowledge about deposition and diagenesis of the Green River evaporites has implications regarding the origin of oil shale in hypersaline environments.

The objectives of this paper are to: (1) document the timing of formation, whether synsedimentary or burial diagenetic, of the principal saline minerals of the Green River Formation,

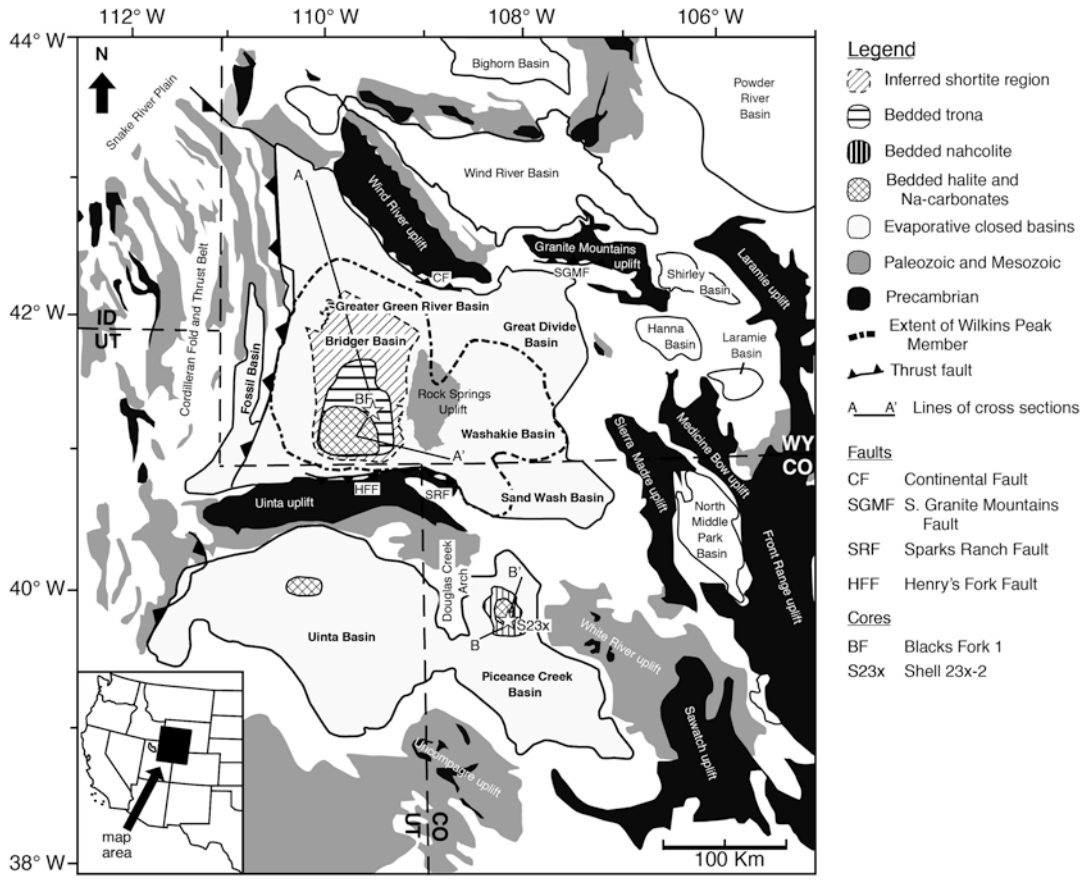

Fig. 11.1 General geologic map of Eocene basins and associated uplifts, and extent of Green River Formation saline deposits and Wilkins Peak Member (*dashed line*) (Modified from Roehler 1992; Smith et al. 2008a). Distribution of saline deposits is from Culbertson (1970) and Dyni (1996). Line marked A-A' is the location of cross section shown on Fig. 11.2 and B-B' is cross section shown on Fig. 11.4

including nahcolite, trona, halite, and shortite ($Na_2CO_3 \cdot 2CaCO_3$), and to determine the paleoenvironmental conditions that controlled their distribution, (2) develop depositional models for the primary lacustrine evaporites and associated oil shales including approximate water depths and major ion brine chemistries, and (3) calculate atmospheric CO_2 concentrations from the equilibrium assemblage of sodium carbonate minerals, which has paleoclimate significance because the early Eocene was the longest prolonged warm period of the last 65 million years (Zachos et al. 2001). Paleoenvironmental information about the Green River basin center evaporites has implications for better understanding the physicochemical conditions of evaporite and oil shale accumulation in hypersaline environments, and can help solve the following questions: Why is nahcolite common in the Piceance Creek Basin whereas trona is the dominant Na-carbonate in the Bridger Basin and modern alkaline saline systems? Does the present distribution of nahcolite in the Piceance Creek Basin reflect elevated pCO_2 in the early Eocene (Lowenstein and Demicco 2006)?

11.2 Geological Background and Previous Work

Green River sediments were deposited over an area > 65,000 km^2 in the Laramide-age Bridger, Washakie, and Sand Wash Basins to the north and in the Uinta and Piceance Creek Basins to the south (Dyni 2006; Smith et al. 2008a) (Fig. 11.1). The Tipton Shale and Laney Shale Members of the Green River Formation, Greater Green River Basin, were deposited during expanded lake stages and consist of carbonate and siliceous mudstones, siltstones and sandstones, limestones, and oil shales (Bradley 1963, 1966) (Fig. 11.2). Between these two members lies the Wilkins Peak Member, which formed in an underfilled, evaporative, hydrologically-closed basin during the latter stages of the Early Eocene Climatic Optimum (Bradley 1963, 1966; Eugster and Surdam 1973; Eugster and Hardie 1975; Lundell and Surdam 1975; Smoot 1978, 1983; Zachos et al. 2001; Pietras and Carroll 2006; Smith et al. 2008a, b) (Fig. 11.2). Wilkins Peak Member sediments consist of oil shale, fluvial-alluvial siltstone and sandstone, dolomitic mudstone, and sodium carbonate evaporites, the latter interpreted as alkaline saline lake and/or saline pan deposits (Culbertson 1966; Eugster and Surdam 1973; Dyni 1996; Pietras and Carroll 2006). The Wilkins Peak Member is ~180 to 400 m thick in the Bridger Basin and contains >127 billion tons of trona that occurs in 40 beds, 25 of which are 1 m or more in thickness (Dyni 1996); it also hosts the world's largest deposit of disseminated shortite (>10,500 km^2 in Wyoming) (Culbertson 1966, 1971; Smoot 1983; Wiig et al. 1995; Dyni 1996) (Fig. 11.1). In the southern portion of the Bridger Basin, halite was deposited with bedded trona in trona beds 1–18 (Culbertson 1966; Wiig et al. 1995) (Fig. 11.1; Plate 11.1a, c, d). After deposition of trona bed 18, the depocenter of the Bridger Basin shifted northward, and halite-free trona beds 19–25 were deposited (Culbertson 1966, 1971; Leigh 1991; Wiig et al. 1995). Other saline minerals in the Wilkins Peak Member are gaylussite ($Na_2CO_3 \cdot CaCO_3 \cdot 5H_2O$), pirssonite ($Na_2CO_3 \cdot CaCO_3 \cdot 2H_2O$), northupite ($Na_2CO_3 \cdot MgCO_3 \cdot NaCl$), and minor nahcolite ($NaHCO_3$) (Fahey 1962; Culbertson 1971; Robb and Smith 1976).

Evaporites in the Wilkins Peak Member, Bridger Basin, were examined in borehole cores and in a ~4 m-thick section of trona bed 17 exposed in the Solvay trona mine. This report focuses on the lower-middle portion of the Wilkins Peak Member [317–402.3 m] from the ERDA Blacks Fork 1 core, where trona beds 13–18 occur with dolomitic mudstones and oil shales (Fig. 11.3). This section of the Blacks Fork 1 core contains the well-known Wilkins Peak lake expansion-contraction cycles (Smoot 1983; Roehler 1992; Pietras et al. 2003; Pietras and Carroll 2006; Smith et al. 2008a). Clastic marker beds A-D, interpreted as fluvial-deltaic deposits that accumulated during low lake levels, also occur in this portion of the Blacks Fork 1 core (Culbertson 1961; Smoot 1983; Carroll and Bohacs 1999). These deposits are interpreted to have formed as sheet deltas and birdfoot distributary deltas; soil overprints formed during periods of desiccation (Smoot 1983; J.P. Smoot, personal communication 2013).

The lower and middle Eocene lacustrine deposits of the Piceance Creek Basin record the long-term progression from open lake, to closed-basin, and then a return to open lake conditions (Moncure and Surdam 1980; Cole 1985; Smith et al. 2008a; Tänavsuu-Milkeviciene and Sarg 2012) (Fig. 11.4). The Piceance Creek Basin contains the following members and formations: the Wasatch Formation, the Cow Ridge, Douglas Creek, Anvil Points, Garden Gulch, and Parachute Creek Members of the Green River Formation and the Uinta Formation (Bradley 1931; Dyni et al. 1970; Beard et al. 1974; Dyni 1981; Pitman 1996; Johnson et al. 2010; Tänavsuu-Milkeviciene and Sarg 2012) (Fig. 11.4).

In the center of the Piceance Creek Basin, the Cow Ridge Member overlies the Wasatch Formation and consists of limestone, sandstone, and shale with freshwater molluscs (Johnson 1984; Smith et al. 2008a; Johnson et al. 2010). The Douglas Creek Member lacustrine limestones, oil shales, and sandstones (fluvial dominated)

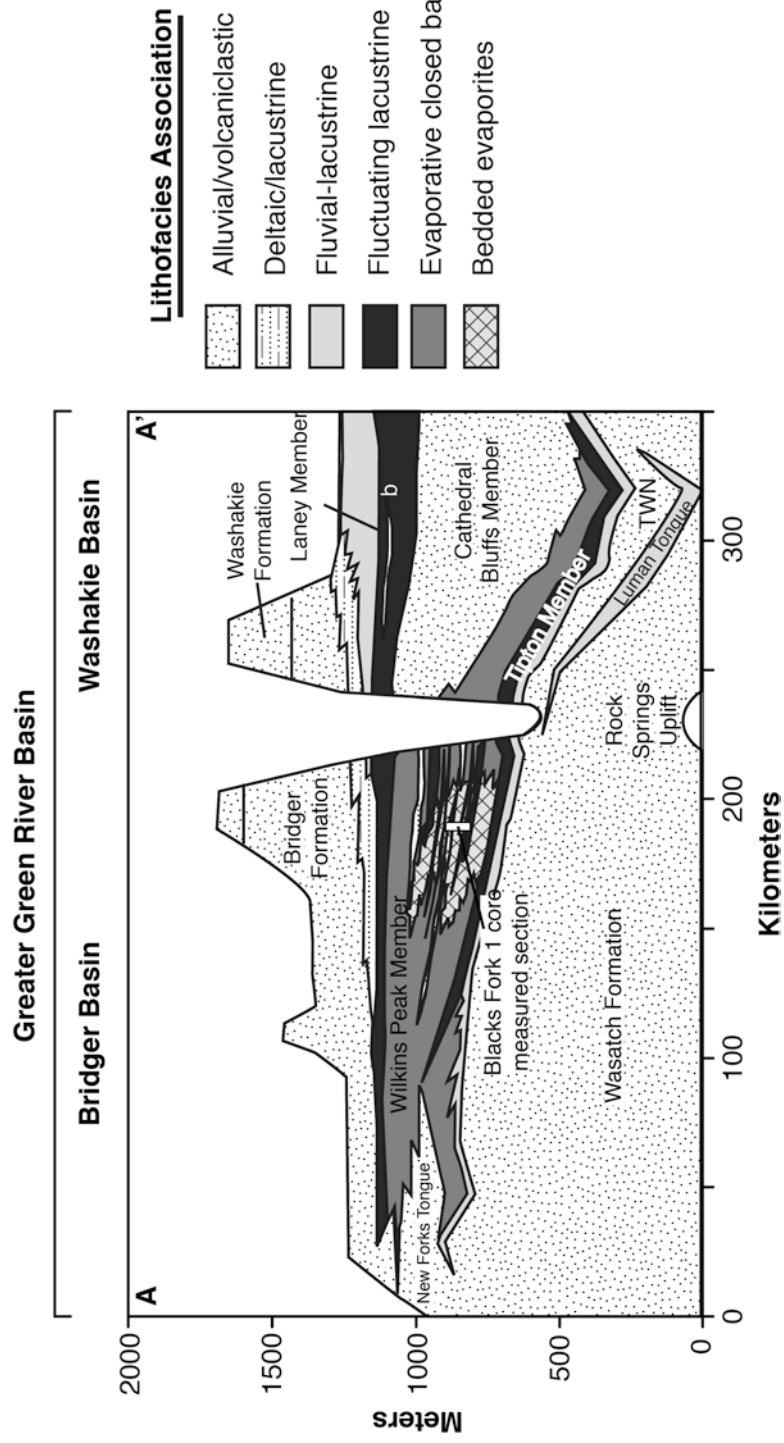

Fig. 11.2 Simplified cross section through the Green River Formation from northwest to southeast, Bridger and Washakie Basins, WY. *Abbreviations*: *b* Buff marker bed, *TWN* Niland Tongue of the Wasatch Formation (Adapted from Smith et al. (2008a) and Chetel and Carroll (2010))

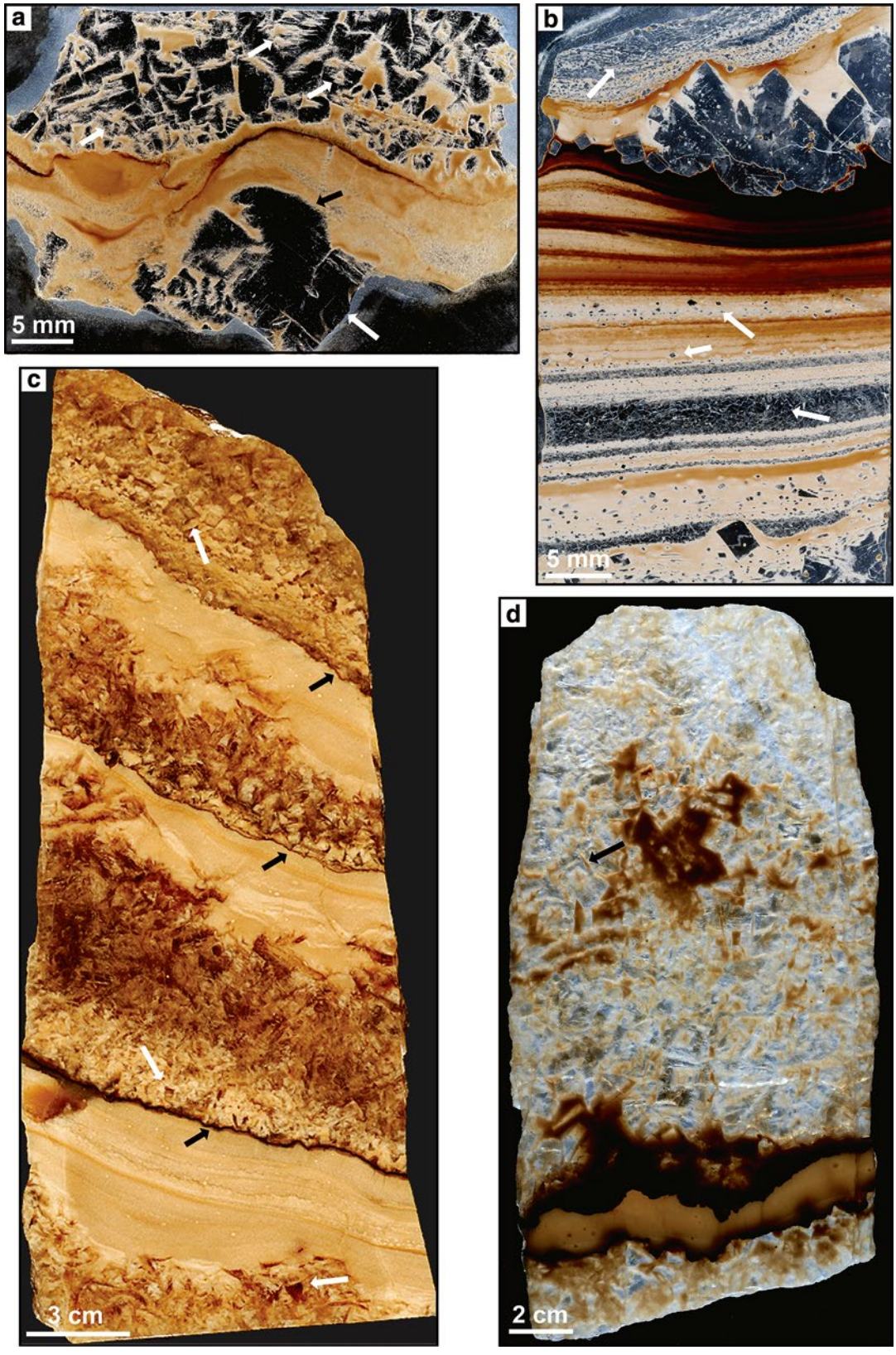
a
5 mm
b
5 mm
c
3 cm
d
2 cm

occur above the Cow Ridge Member on the western and southwestern margins of the basin along the Douglas Creek arch (Johnson et al. 2010). Anvil Points Member sandstones overlie the Cow Ridge Member along the eastern and northern margins of the Piceance Creek Basin (Johnson et al. 2010). Directly above the Cow Ridge Member is the Garden Gulch Member, which consists of argillaceous mudstone and no mollusc fossils (Bradley 1931; Tänavsuu-Milkeviciene and Sarg 2012). Above the Garden Gulch Member is the evaporative Parachute Creek Member (~900 m thick) with dolomitic and siliceous mudstones, including oil shale, and bedded and disseminated evaporites that formed contemporaneously with the saline facies of the Wilkins Peak Member (Dyni et al. 1970; Roehler 1992; Dyni 1996; Smith et al. 2008a; Boak and Poole, Chap. 8, this volume). Nahcolite, halite, dawsonite ($NaAl(OH)_2CO_3$), and minor wegscheiderite ($Na_2CO_3 \cdot 3NaHCO_3$), shortite ($Na_2CO_3 \cdot 2CaCO_3$), northupite ($Na_2CO_3 \cdot MgCO_3 \cdot NaCl$), and searlesite ($NaBSi_2O_6 \cdot H_2O$) occur in the lower portion of the saline facies (~340 m thick) (Hite and Dyni 1967; Dyni et al. 1970; Young and Smith 1970; Beard et al. 1974; Dyni 1981, 1996). The total amount of nahcolite in the lower saline facies is estimated to be >32 billion tons where it occurs as bedded units (Greeno Bed), nodules, and interbedded with halite (LS and US, Lower and Upper Salt zones) (Fig. 11.4) (Dyni 1996). Dissolution contacts occur in nahcolite and halite beds which indicate that the top and lateral portions of the saline facies have been dissolved by groundwater (Fig. 11.4) (Dyni 1996). This "leached zone", with evaporite cavities and solution breccias, extends into the lower part of the Mahogany Zone, a 20–60 m thick high-grade oil shale that is traceable across the Piceance Creek and Uinta Basins (Cashion and Donnell 1972). Lake deposits above the Mahogany Zone interfinger with alluvial/volcaniclastic sediments of the Uinta Formation (Trudell et al. 1970; Smith et al. 2008a).

Evaporites from the lower saline facies of the Parachute Creek Member were examined in borehole cores of which the Shell Oil 23x-2 core is a representative example (Fig. 11.5). A stratigraphic section from the Parachute Creek Member (518.1–594.4 m) contains the lower halite-bearing evaporite facies (Dyni et al. 1970; 2006) in the R-5 rich oil shale zone (Cashion and Donnell 1972, 1974) (Fig. 11.5). Organic-rich dolomitic and siliceous mudstone (oil shale), both laminated and brecciated, occur with bedded evaporites (nahcolite and halite). Microcrystalline dawsonite (<2 μm) and iron sulfides are also widely disseminated throughout the section (Beard et al. 1974; Dyni 1998; Tänavsuu-Milkeviciene and Sarg 2012).

Plate 11.1 Green River Formation trona, nahcolite, and halite. (**a**) Thin section photomicrograph from Trona bed 17, Grierson 1 core, Wilkins Peak Member, Bridger Basin (539.8 m) showing microcrystalline trona draping clear, bottom growth halite (*bottom white arrow*). Top half of section shows upward widening fabric of bottom growth halite and microcrystalline trona at halite crystal boundaries. Note partial replacement of halite by trona (*top white arrows*). Large bottom growth halite cube (*bottom white arrow*) appears to be rounded (partially dissolved) at trona-halite boundary (*black arrow*). (**b**) Thin section photomicrograph, Shell 23x-2 core (561.4 m) showing microcrystalline nahcolite and halite cumulates draping clear, vertical bottom growth halite (top) and flat layers of nahcolite and halite cumulates (*arrows*), Parachute Creek Member, Piceance Creek Basin. (**c**) Slab photograph from Solvay mine, Trona bed 17, showing alternations of bedded bottom growth halite and microcrystalline trona laminae. "Root beer" colored layers are halite replaced by trona. Note cubic structure and upward widening fabric of bottom growth halite (*white arrows*). Dark, stylolitic layers at boundary between laminated trona and bottom growth halite (*black arrows*) are composed of dolomite and organic matter. Wilkins Peak Member, Bridger Basin. (**d**) Slab from Solvay mine, Trona bed 17, showing halite cumulates (*black arrows*) replaced by trona. Cores of cumulate halite show remnant fluid inclusion banding now replaced by trona needles. Bottom shows microcrystalline trona bordered by dark, organic-rich trona

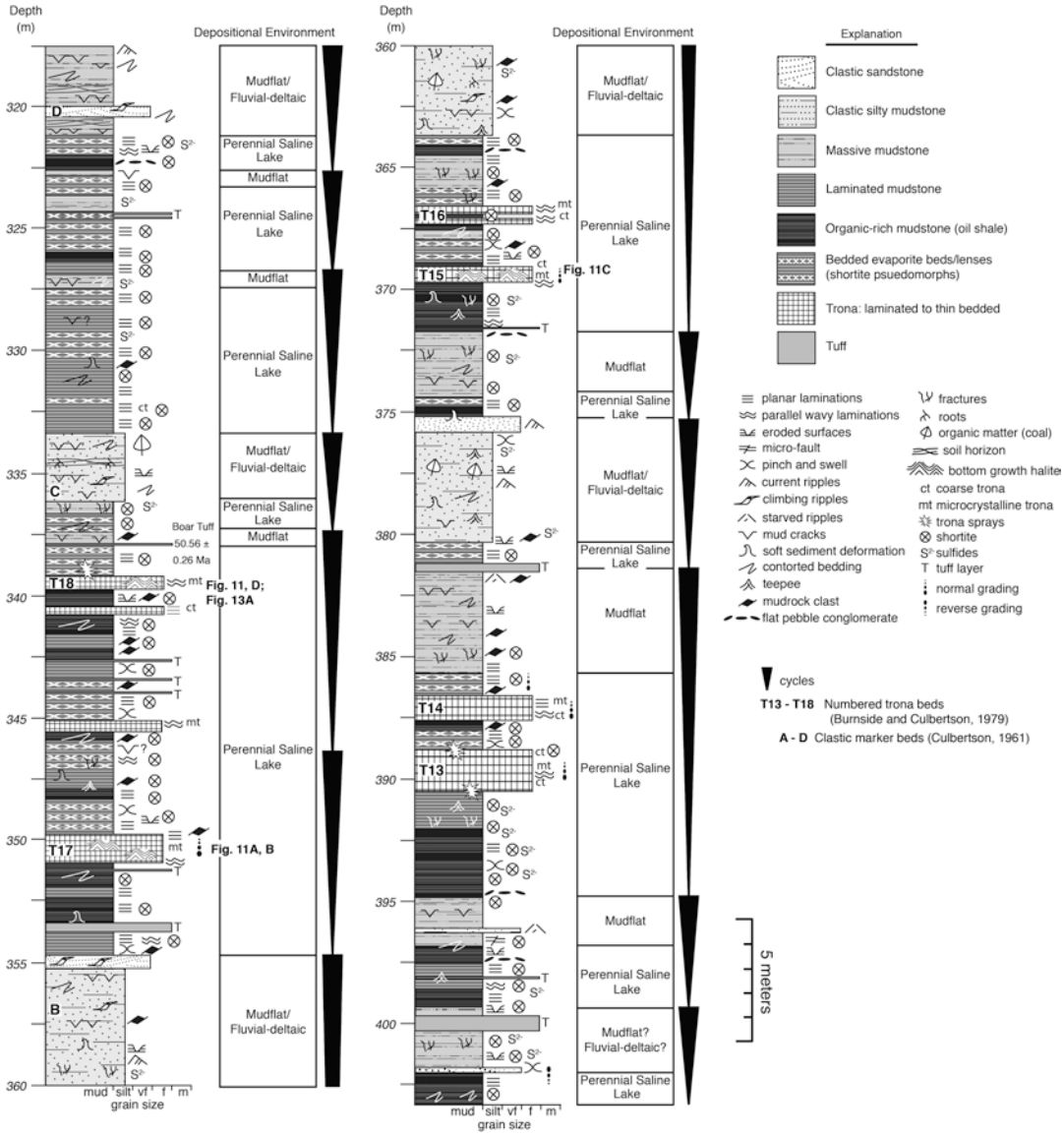

Fig. 11.3 Measured section from the lower-middle interval of the Wilkins Peak Member, Blacks Fork 1 core, Bridger Basin, WY (Figs. 11.1 and 11.2). Note meter-scale lacustrine expansion-contraction cycles (*black arrow symbols*). Subaerial and fluvial-deltaic deposits (i.e., mudcracks, roots, paleosols) represent lowest lake levels. Bedded trona and oil shale were deposited in perennial hypersaline lakes. Numbered trona beds from Burnside and Culbertson (1979); letters *A–D* are clastic marker beds (Culbertson 1961). Photographs in Figs. 11.11 and 11.13 are keyed to stratigraphic section

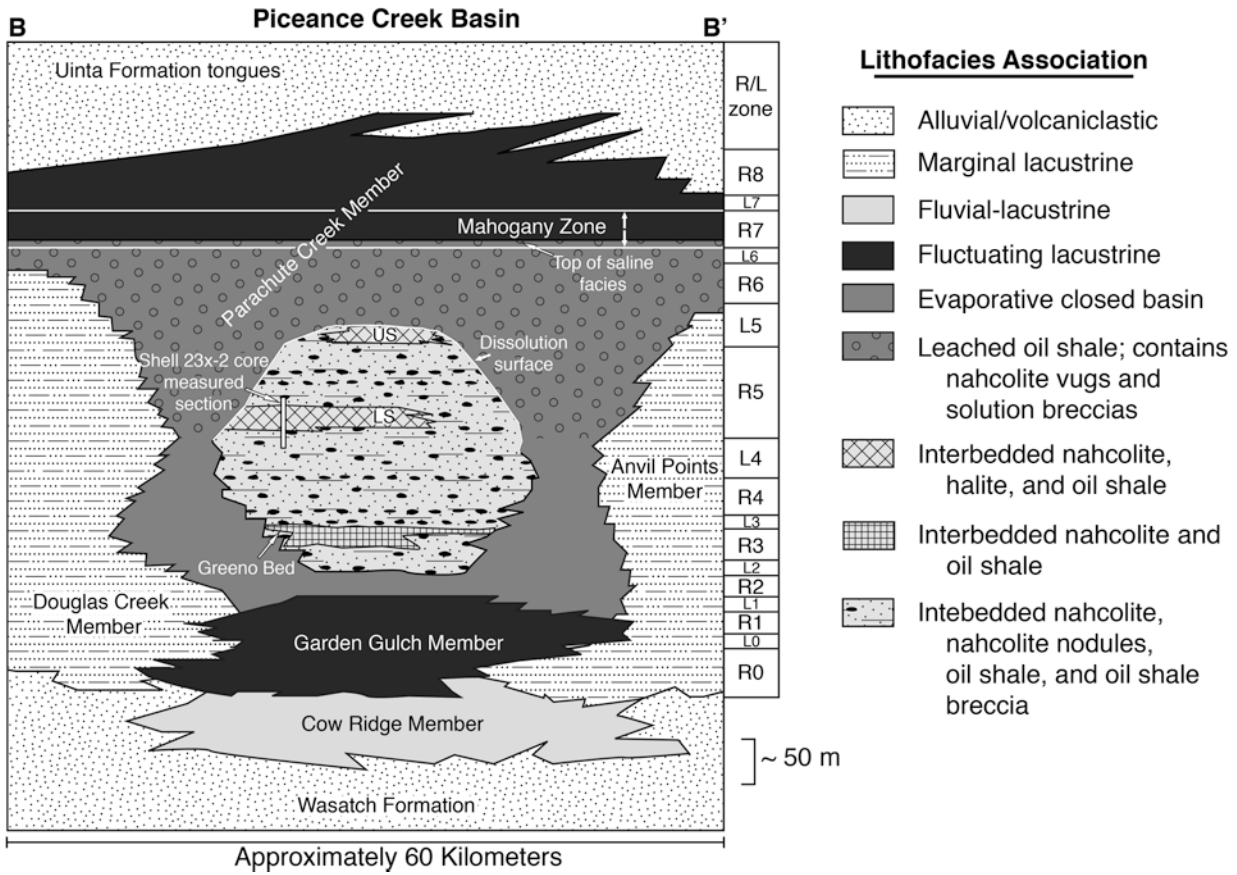

Fig. 11.4 Generalized stratigraphic relationships in the Green River Formation from southwest to northeast, and correlation with kerogen rich and lean zones in Piceance Creek Basin, CO. Greeno Bed includes numbered nahcolite units 1–3. Rich (R0-R8) and lean (L0-L7) oil shale zones after Cashion and Donnell (1972, 1974) and Dyni (2006). Upper (US) and lower (LS) salt zones after Dyni (1981) and Dyni (1996) (Adapted from Pitman (1996), Dyni (1981), Dyni (2006), Smith et al. (2008a), and Johnson et al. (2010))

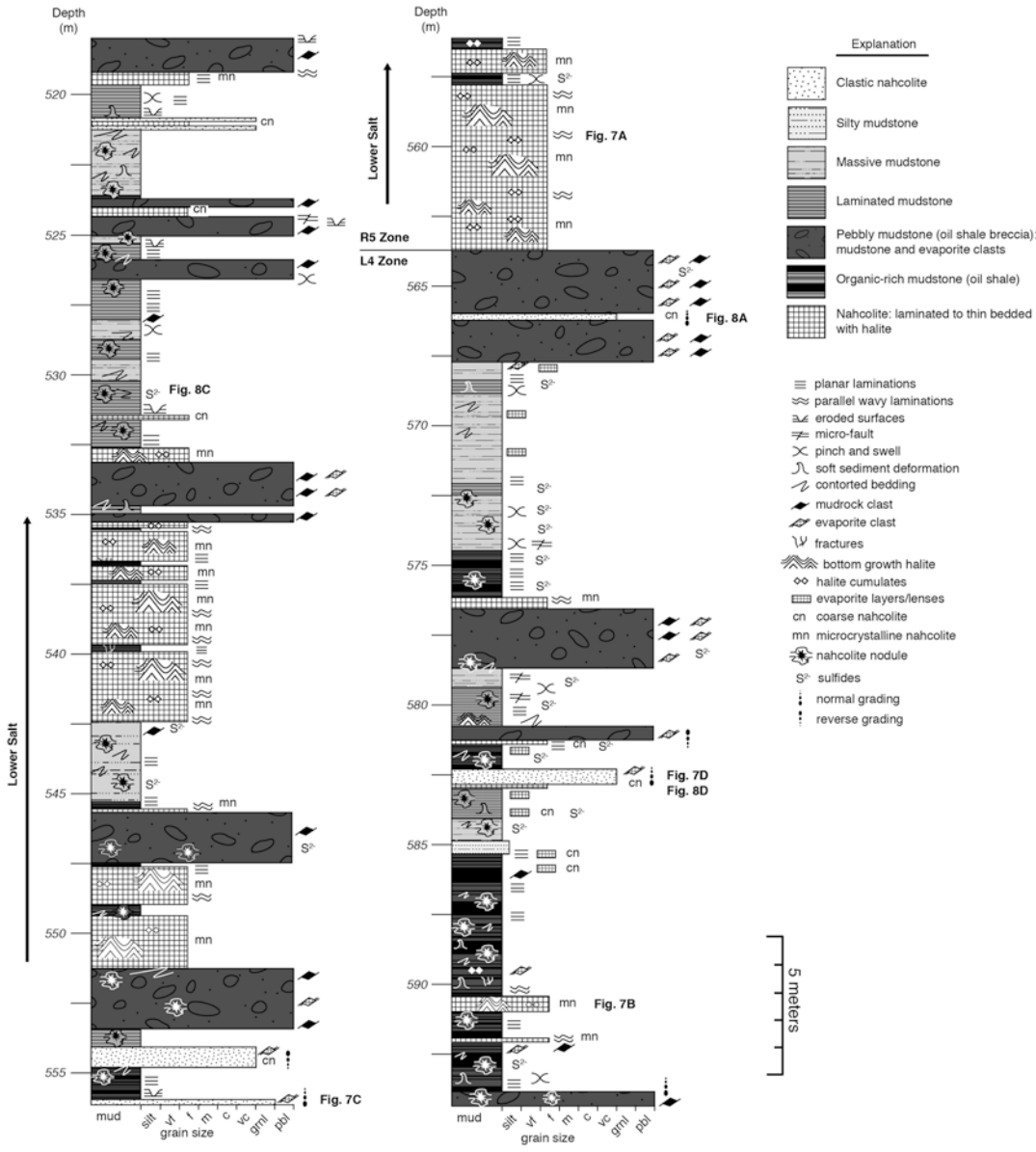

Fig. 11.5 Measured section from the middle interval of the Parachute Creek Member, Shell 23x-2 core, Piceance Creek Basin, CO (see Figs. 11.1 and 11.4 for location). Depositional environment for entire stratigraphic section is interpreted as a perennial saline lake. Bedded nahcolite is associated with oil shale and oil shale breccia. Intervals with transported clasts of nahcolite, mudstone, and oil shale breccia, are interpreted as subaqueous debris flows or turbidites. Rich and lean oil shale zones (R5 and L4) after Cashion and Donnell (1972, 1974). Stratigraphic position of photographs in Figs. 11.7 and 11.8 are shown

11.3 Evaporite Sedimentology/ Petrography and Interpretation of Paleoenvironments

Sedimentological and petrographic analysis can help distinguish primary sedimentary evaporites in the Green River Formation, formed in surface environments, from those saline minerals formed during burial diagenesis (Hardie et al. 1985). Primary syndepositional features include sedimentary structures (i.e., bedding, graded bedding), detrital settle out textures, competitive crystal growth textures, and dissolution-precipitation features (Hardie et al. 1985). These contrast with diagenetic features including displacive growths, cements, mineral replacements, and recrystallization mosaic textures. Diagenetic features, however, can form syndepositonally or during burial, which complicates their interpretation. Petrographic textures and fabrics are used here to distinguish deposits that formed in perennial saline lakes from those formed in saline pans (Lowenstein and Hardie 1985; Smoot and Lowenstein 1991; Schubel and Lowenstein 1997). Comparison with modern and Pleistocene evaporites (for example, Owens Lake, Searles Lake and Death Valley, California, and Lake Magadi, Kenya) facilitated interpretations of depositional conditions and syndepositional diagenetic overprints (Smoot and Lowenstein 1991).

11.3.1 Parachute Creek Member, Piceance Creek Basin, CO

11.3.1.1 Synsedimentary Nahcolite and Halite

Nahcolite, the major sodium carbonate mineral of the Piceance Creek Basin, occurs in bedded deposits (1 cm and up to 8.6 m thick), in places finely layered with halite (Figs. 11.5 and 11.6) (Beard et al. 1974; Dyni 1981). Nahcolite laminae are made of microcrystalline chemical "mud" (nahcolite prisms ~10 μm and up to 150 μm in length) and sorted halite "cumulate" rafts and plates (~5 μm and up to 7 mm in length), textures diagnostic of precipitation at the air-water interface of a hypersaline lake (Fig. 11.7a, b; Plate 11.1b) (Lowenstein and Hardie 1985; Lowenstein and Demicco 2006). These nahcolite and halite cumulates settled out from suspension to the brine bottom where they formed layered deposits. Nahcolite and halite cumulates that overlie halite crystal crusts that grew at the bottom of a hypersaline lake (Fig. 11.7a; Plate 11.1b) form crystal drapes that thicken between halite crystals and thin at their tops, as would be expected of deposits that settled-out from suspension. Rarely, nahcolite needles occur within primary fluid inclusions in both cumulate and bottom growth halite, which indicates that nahcolite formed as a primary mineral concurrently with cumulate halite growth and/or settled on top of bottom growth halite, and was trapped during the next increment of halite crystal growth (LaClair and Lowenstein 2007, 2010). Oil shale, comprised of alternating dark and light laminations, rich and poor in organic matter, is commonly interbedded with nahcolite-halite. Light colored laminae are predominantly carbonate minerals (calcite and dolomite), whereas dark colored organic-rich laminae also contain siliciclastic minerals (quartz, feldspar, and clays) (Pitman 1996; Tänavsuu-Milkeviciene and Sarg 2012; Boak and Poole, Chap. 8, this volume).

Bottom growth halite crusts exhibit vertical, widening upward fabrics, indicating growth into an open, halite-saturated brine body (Fig. 11.7a; Plate 11.1b). Bottom growth halite is commonly clear and lacks the dense fluid inclusion banding typical of chevron halite that crystallizes rapidly (days) in shallow brine pools (Smoot and Lowenstein 1991; Li et al. 1996; Lowenstein et al. 1999) (Fig. 11.7a; Plate 11.1b). This suggests slow halite growth (years?) at the bottom of a perennial brine pool, analogous to Pleistocene bottom growth halite from the Death Valley DV93-1 core, Badwater Basin (Li et al. 1996; Lowenstein et al. 1999). In that core, black mud and halite layers composed of fine crystal cumulates and clear, vertically oriented bottom grown crusts, were deposited in a perennial saline lake up to ~90 m deep. Similar centimeter size bottom growth halite cubes were also recovered at water

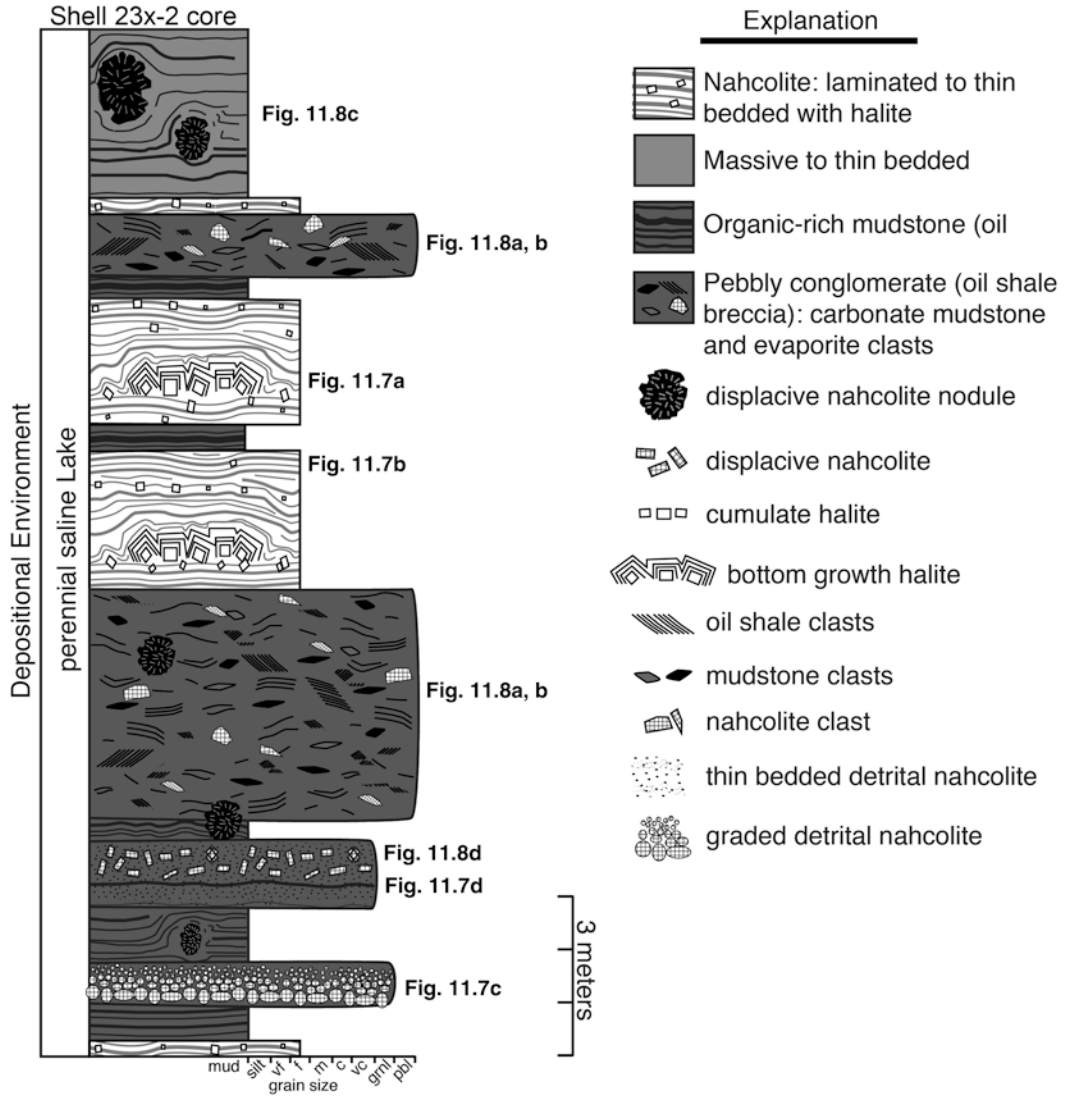

Fig. 11.6 Generalized illustration of perennial saline lake section from Shell 23x-2 core, Parachute Creek Member, Piceance Creek Basin, showing common stratigraphic relationships, sedimentary structures, and textures. Figure numbers on right correspond to images in Figs. 11.7 and 11.8. From bottom to top: laminated microcrystalline nahcolite and halite cumulates overlain by oil shale that may contain graded, rounded nahcolite clasts, displacive nahcolite nodules, and thin beds of fine clastic nahcolite. Above this unit, oil shale breccia with carbonate mudstone matrix and carbonate mudstone, oil shale, and nahcolite clasts and rare displacive nahcolite nodules. Above is bedded nahcolite, bottom growth halite, and halite cumulates interbedded with oil shale. Oil shale breccia occurs above the bedded evaporite-oil shale sequence. At top is massive to thin-bedded mudstone with nahcolite nodules

depths of 50–250 m in the Dead Sea (Neev and Emery 1967; Beyth 1980; Herut et al. 1998).

Bedded nahcolite-halite completely lacks syndepositional dissolution features, which indicates that deposition occurred in a density stratified lake, where deposits were protected from undersaturated surface waters by dense bottom brines. This type of deposition requires that the rate of evaporation exceed the rate of inflow. Evaporation of lake surface waters led to: (1) concentration of surface brines, and nucleation of evaporites that settled through the water

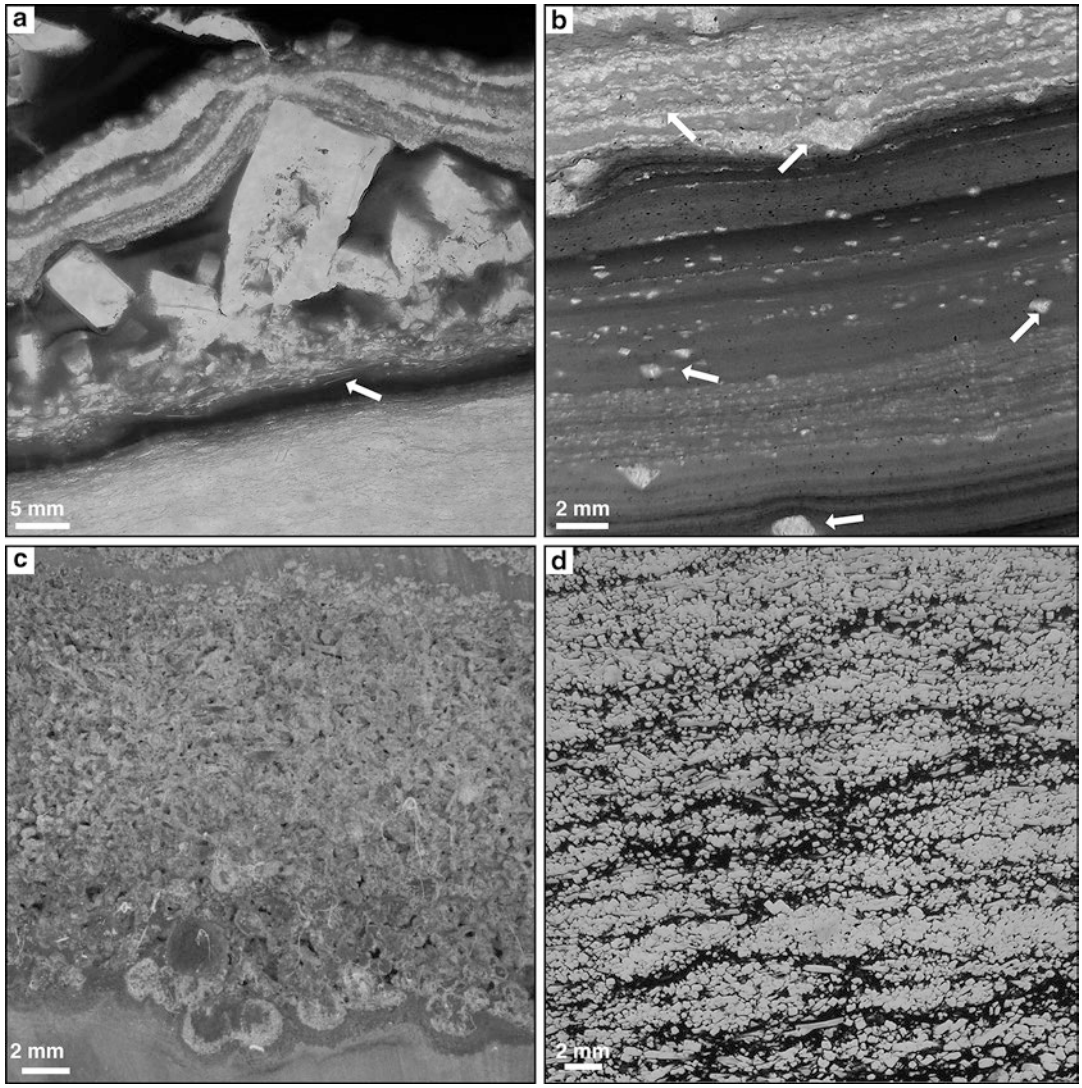

Fig. 11.7 Representative sedimentary features, Shell 23x-2 core, Parachute Creek Member, Piceance Creek Basin. Stratigraphic position of samples is shown on Figs. 11.5 and 11.6. (**a**) Thin section photomicrograph of halite with vertical bottom growth fabric draped by microcrystalline nahcolite (*grey*) and halite cumulates (*white*). Dark gray to black layers are organic-rich nahcolite with microcrystalline dolomite and halite rafts (*white arrow*). Bottom of thin section contains nahcolite and halite cumulates. Note bottom growth halite crystals widen upward and contain faint fluid inclusion banding (559 m). (**b**) Thin section of laminated microcrystalline nahcolite (*light to dark grey*) with halite cumulates (*white with arrows*), indicating co-deposition of both minerals. Dark gray layers are organic-rich nahcolite; black specks are sulfides (591 m). (**c**) Core slab of graded nahcolite layer composed of rounded clasts. Top of layer contains subrounded to angular crystals suggesting less reworking (556 m). (**d**) Thin section of detrital nahcolite crystals in organic-rich carbonate mudstone. Crystals are subrounded and angular, some with point-contacts between crystals. Note lenses of nahcolite crystals (*center*) produced by mechanical working (583.5 m)

column, and (2) eventual sinking of surface brines, made denser than underlying waters by evaporative concentration, which displaced less dense brines in the water column; the brine ceased to sink when its density equaled that of the surrounding waters. During step 1 the settling evaporite crystals may have dissolved in the water column. Continuous evaporative concentration of

the surface waters, and mixing with the lower brine body, eventually caused the entire water column to become supersaturated with halite and nahcolite (chemically holomictic). The absence of bedded nahcolite-halite on the margins of the Piceance Creek Basin implies that: (1) evaporites deposited in shallower marginal areas of the lake were dissolved by inflow waters, (2) evaporite deposition occurred when lake levels were low and basin margin areas were subaerially exposed, or (3) evaporites were leached and dissolved by much later migration of groundwaters (Dyni 1996).

The Dead Sea illustrates brine stratification, where inflow waters from the Jordan River form a surface layer above denser halite-saturated waters. However, in recent decades inflow from the Jordan River has been dramatically reduced, which has reduced brine stratification and caused the entire water column of the Dead Sea to become saturated with halite (Steinhorn and Gat 1983; Steinhorn 1985; Gavrieli et al. 1989). Other modern examples of density stratified (meromictic) hypersaline lakes include Mono Lake, California and Lake Bogoria, Kenya (Renaut and Gierlowski-Kordesch 2010).

Nahcolite also occurs as two types of transported and reworked clasts. One type is found as centimeter scale graded layers of rounded nahcolite clasts (~200 μm to 3 mm) (Fig. 11.7c) or as well sorted grainstones made of subhedral to rounded crystal clasts (~100 μm to 2 mm) (Fig. 11.7d). Lake bottom turbidity currents may have transported these types of nahcolite grains (Dyni and Hawkins 1981). The second type of clastic nahcolite consists of large crystalline aggregates that occur with mudstone clasts in oil shale breccia (Fig. 11.8a) (Tänavsuu-Milkeviciene and Sarg 2012). Oil shale breccia contains matrix-supported oil shale and dolomitic mudstone clasts (5 mm to ≥5 cm), commonly flattened, contorted and smeared by compaction (Fig. 11.8b), and here interpreted as subaqueous debris flow deposits. Most clasts are composed of fine-grained dolomite mudstone; the organic-rich matrix also contains dolomite, dawsonite, quartz, and feldspar (Dyni and Hawkins 1981). Oil shale breccias were interpreted as turbidite deposits by Dyni and Hawkins (1981) because in some occurrences, larger clasts grade upward into smaller clasts. Oil shale clasts may exhibit internal lamination, in places intricately folded by soft sediment deformation (Fig. 11.8b). Finely laminated clasts may have originally formed in deep water, whereas non-laminated clasts may have originated in much shallower water (Dyni and Hawkins 1981). Regardless, the abundance of oil shell breccia suggests the Piceance Creek Basin had unstable slopes that, at times, slumped and caused turbid underflows that deposited sediment in deeper parts of the lake (Dyni and Hawkins 1981; Johnson 1981; Tänavsuu-Milkeviciene and Sarg 2012). Clastic nahcolite in the basin center was derived from more marginal deposits, analogous to the lake margin gypsum crusts of the Dead Sea that have been eroded, transported and deposited on the basin floor (Neev and Emery 1967).

11.3.1.2 Diagenetic Nahcolite

Nahcolite occurs in dolomitic and siliceous mudstones as nodules, composed of radiating crystal rosettes (~0.5 to 30 cm) (Fig. 11.8c) and as randomly oriented euhedral crystals (1 mm to 1 cm) (Fig. 11.8d). In both occurrences, nahcolite grew displacively by pushing aside surrounding muds. The timing of intrasediment nahcolite growth, however, is ambiguous – it may have occurred during or shortly after deposition of the host lacustrine muds or during burial. Two arguments support the early syndepositional origin of displacive nahcolite: (1) Surrounding laminae are commonly deformed around nahcolite nodules and euhedra, indicating crystallization occurred before significant compaction or lithification and (2) nahcolite-saturated brines existed in overlying lake waters.

11.3.1.3 Parachute Creek Member Paleoenvironments

The basin center saline zone of the Parachute Creek Member lacks sedimentary structures indicative of deposition in shallow water, such as cross-bedding, and exposure features, such as mudcracks (Dyni et al. 1970; Dyni and Hawkins 1981; Dyni 1996; Pitman 1996;

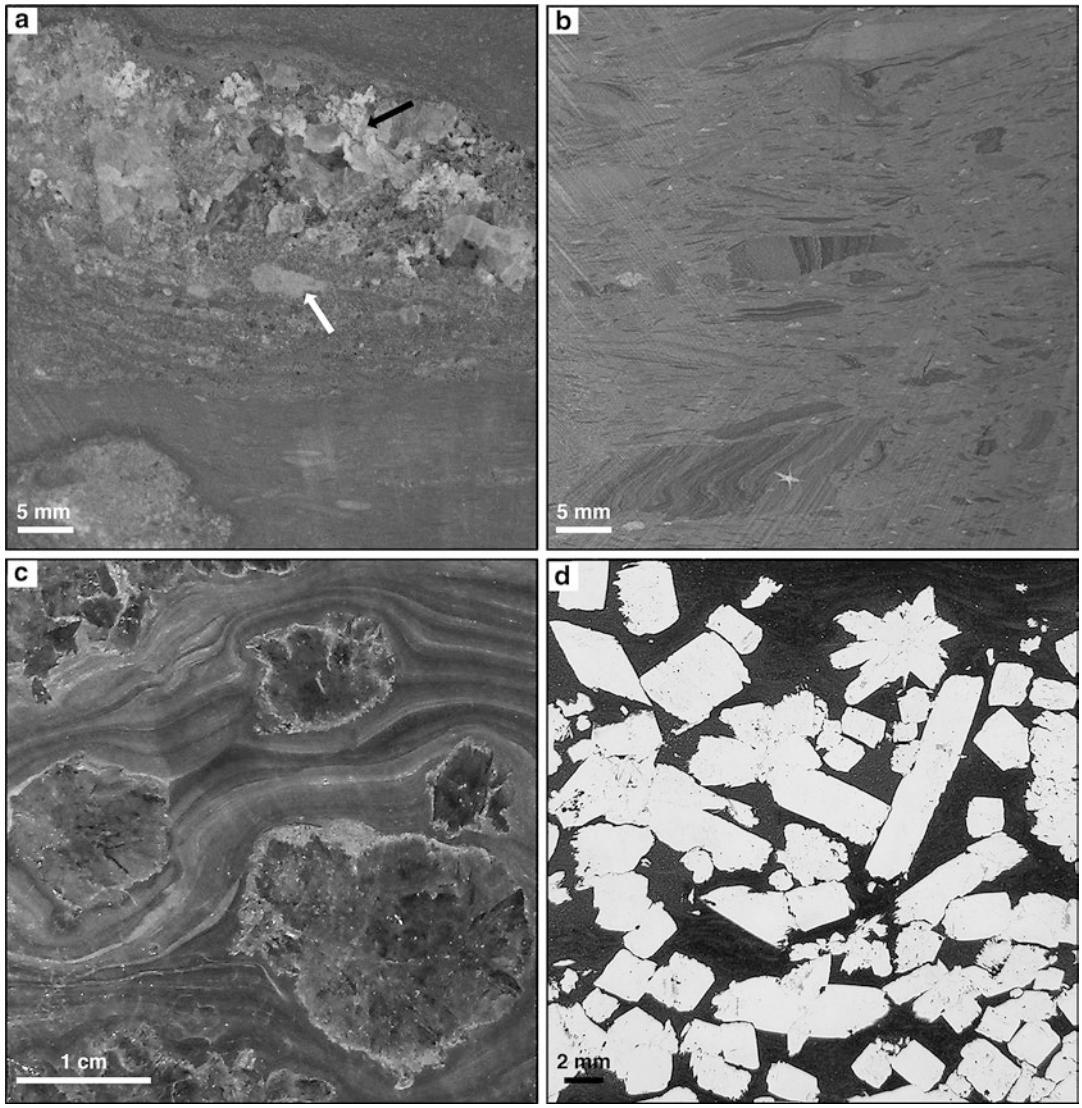

Fig. 11.8 Representative sedimentary features, Shell 23x-2 core, Parachute Creek Member, Piceance Creek Basin. Photographs correspond to letters on Fig. 11.6. (**a**) Core slab of oil shale breccia with large composite clast made of dolomitic mudstone (*bottom arrow*) and nahcolite crystals (*top arrow*). Clast in lower left corner is comprised of fine nahcolite crystals (567.5 m). (**b**) Core slab of oil shale breccia composed of randomly oriented, compacted, oil shale clasts in an organic-rich dolomitic mudstone matrix (623.7 m). (**c**) Core slab of nahcolite nodules, composed of radiating crystal sprays. Surrounding laminated mudstone is compacted and contorted indicating displacive growth of nahcolite in soft sediment (531.6 m). (**d**) Thin section of euhedral displacive nahcolite in laminated mudstone. Note laminae at top are compacted around star shaped nahcolite rosette (583.7 m)

Tänavsuu-Milkeviciene and Sarg 2012). Oil shale laminae preserved on the sub-millimeter scale are interpreted to have been deposited by the settling of fine grained sediments in a perennial lake. The preservation of organic matter and sulfides, and the absence of burrowing in laminated oil shale indicate that paleolake bottom waters were anoxic and saline (Dyni and Hawkins 1981; Johnson 1981; Tänavsuu-Milkeviciene and Sarg 2012). Nahcolite and halite interbedded with oil shale indicate accumulation in a density stratified saline lake (Dyni and Hawkins 1981;

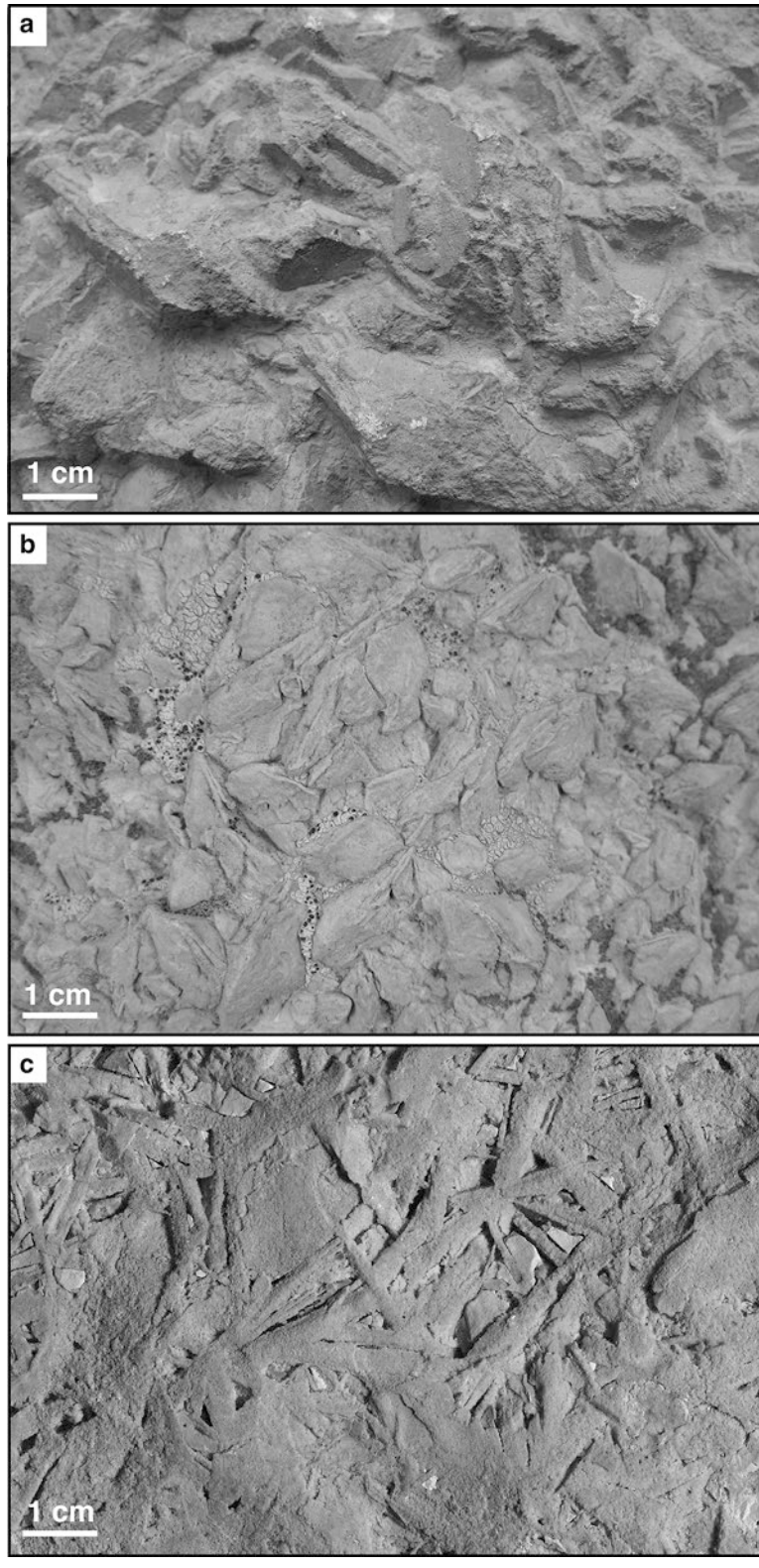

Fig. 11.9 Evaporite casts from lake margin deposits of Douglas Creek Member, Piceance Creek Basin, CO (**a**) and Wilkins Peak Member, Bridger Basin, WY (**b** and **c**). (**a**) Outcrop sample from Douglas Creek Arch, CO, showing large monoclinic-dipyramidal evaporite casts (gaylussite?) in peloidal mudstone. Sample is associated

Dyni 1996). Perennial saline lake conditions also produced the progressive increase of Br^- in halite from the base of the lower salt zone to the upper salt zone (15–182 ppm) (Dyni et al. 1970).

The evaporites of the Parachute Creek Member are equivalent to basin margin outcrops of the upper Anvil Points and Douglas Creek Members, which consist of channelized fluvial-deltaic deposits and littoral to sublittoral oil shale, siliciclastics and mudstones, and boundstones (Moncure and Surdam 1980; Johnson et al. 2010; Tänavsuu-Milkeviciene and Sarg 2012). Strata on the Douglas Creek arch contain evaporite casts (gaylussite?) and subaerial exposure features (mudcracks) that may be contemporaneous with evaporites in the basin center (Fig. 11.9a) (Moncure and Surdam 1980; Cole 1985). These lake margin deposits record fluctuating lake levels in an evaporative underfilled basin (Carroll and Bohacs 1999; Smith et al. 2008a; Tänavsuu-Milkeviciene and Sarg 2012).

In the Shell 23x-2 core, alternating nahcolite-halite and oil shale, on the centimeter to meter scale, record fluctuating lake levels in a perennial saline lake (Fig. 11.6). Oil shale laminae, composed of organic matter, dolomite/calcite and fine siliciclastics, are interpreted to reflect periods when inflow waters supplied sediment and provided favorable conditions for algal blooms and carbonate precipitation (Bradley and Eugster 1969; Tänavsuu-Milkeviciene and Sarg 2012). Bedded nahcolite-halite reflect lower lake levels in response to low inflow and high evaporation rates.

About half of the oil shale cored in the saline facies of the Parachute Creek Member is composed of oil shale breccia, as 0.4–6.5 m thick beds (Fig. 11.5) (Dyni and Hawkins 1981). Transport of oil shale mudstone and nahcolite clasts likely began on unstable slopes that slumped and triggered subaqueous debris flows (Dyni and Hawkins 1981; Tänavsuu-Milkeviciene and Sarg 2012). Turbidity currents also developed following slumping of sediments on oversteepened slopes or from debris flows as they accelerated downslope (Dyni and Hawkins 1981). The accumulation of oil shale breccia in the center of the Piceance Creek Basin suggests that a relatively steep-sided deep lake existed during Parachute Creek Member time (Dyni and Hawkins 1981; Tänavsuu-Milkeviciene and Sarg 2012). Oil shale breccia occurs below and directly above bedded nahcolite-halite which indicates that breccia deposition occurred before or shortly after evaporites precipitated, and suggests lake level changes triggered their deposition.

In summary, nahcolite and halite, along with oil shale and oil shale breccia in the Parachute Creek Member were deposited in a perennial saline lake with margins steep enough to produce numerous mass flow deposits. Paleolake depths fluctuated and may have been similar to the Dead Sea (300 m) or the Pleistocene perennial lakes of Badwater Basin, Death Valley (<90 m) (Lowenstein et al. 1999). Dyni and Hawkins (1981) suggested paleolake depths between 50 and 100 m could generate slump structures and produce turbidity currents in the center of the basin. Johnson (1981) measured the relief of lake-margin progradational delta complexes and from them, estimated maximum paleolake depths of ~300 m.

11.3.2 Wilkins Peak Member, Bridger Basin, WY

11.3.2.1 Synsedimentary Trona and Halite

Trona, the major sodium carbonate mineral in the Bridger Basin, occurs in bedded deposits, mainly as microcrystalline laminae in trona beds 1–18

Fig. 11.9 (continued) with stromatolite mounds, similar to modern gaylussite crystals found on sublacustrine tufa blocks at Mono Lake, CA (David Herbst, personal communication 2011; Bischoff et al. 1991). Photo courtesy of Lauren Ricketts. (**b**) Outcrop photograph of bladed evaporite casts, similar to those in Fig. 11.9A, collected from Slate Canyon. Evaporite crystals occur in burrowed carbonate mudstone. (**c**) Outcrop photograph showing bedding plane view of monoclinic tabular-bladed evaporite casts (gaylussite? trona?) from Firehole Canyon. The tops of individual crystals are typically smooth or truncated by dissolution

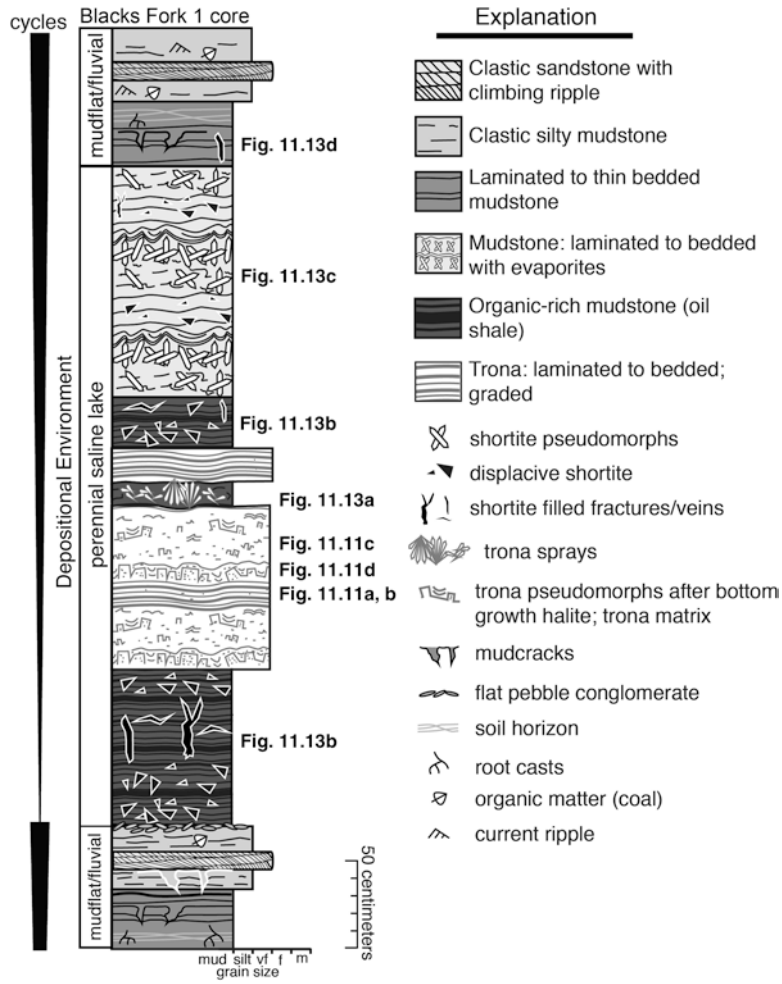

Fig. 11.10 Generalized section from the Blacks Fork 1 core, Bridger Basin, Wilkins Peak Member, showing sedimentary features and interpreted depositional environments. Figure numbers correspond to Figs. 11.11 and 11.13. Laminated oil shale and bedded trona-halite are perennial saline lake deposits. Oil shale was deposited during relatively high lake levels; inflow waters carried fine sediments and solutes into the lake. Bedded trona-halite formed during lower lake levels, lower inflow and higher evaporation. Perennial saline lake deposits also include laminated to thin-bedded mudstone with bedded shortite psuedomorphs. The original mineral (gaylussite? pirssonite?), now replaced by shortite, grew as bottom crusts and displacive crystals. Mudcracks and soil horizons indicate subaerial exposure in mudflat and fluvial-deltaic deposits

(Figs. 11.3 and 11.10), and as coarse, radiating bladed crystals in the upper trona beds 19–25. Microcrystalline trona consists of sorted, needle-shaped crystals (50–200 μm) arranged parallel to bedding in ~2 mm to 1 cm thick layers (Leigh 1991; Boni and Atkinson 1998) (Fig. 11.11a–c; Plate 11.1a, c). In some cases, trona crystals within individual laminae are graded, which suggests a cumulate settle-out origin for these layers (Leigh 1991; Boni and Atkinson 1998) (Fig. 11.11a). Fining upward textures indicate that larger trona crystals settled out of suspension first and finer crystals settled later. The overlying organic-rich dolomite may represent a slow "rain" of particles after the trona crystallization event. Trona cumulates above halite crystal crusts form crystal drapes that thicken between halite crystals and thin at their tops (Plate 11.1a, c).

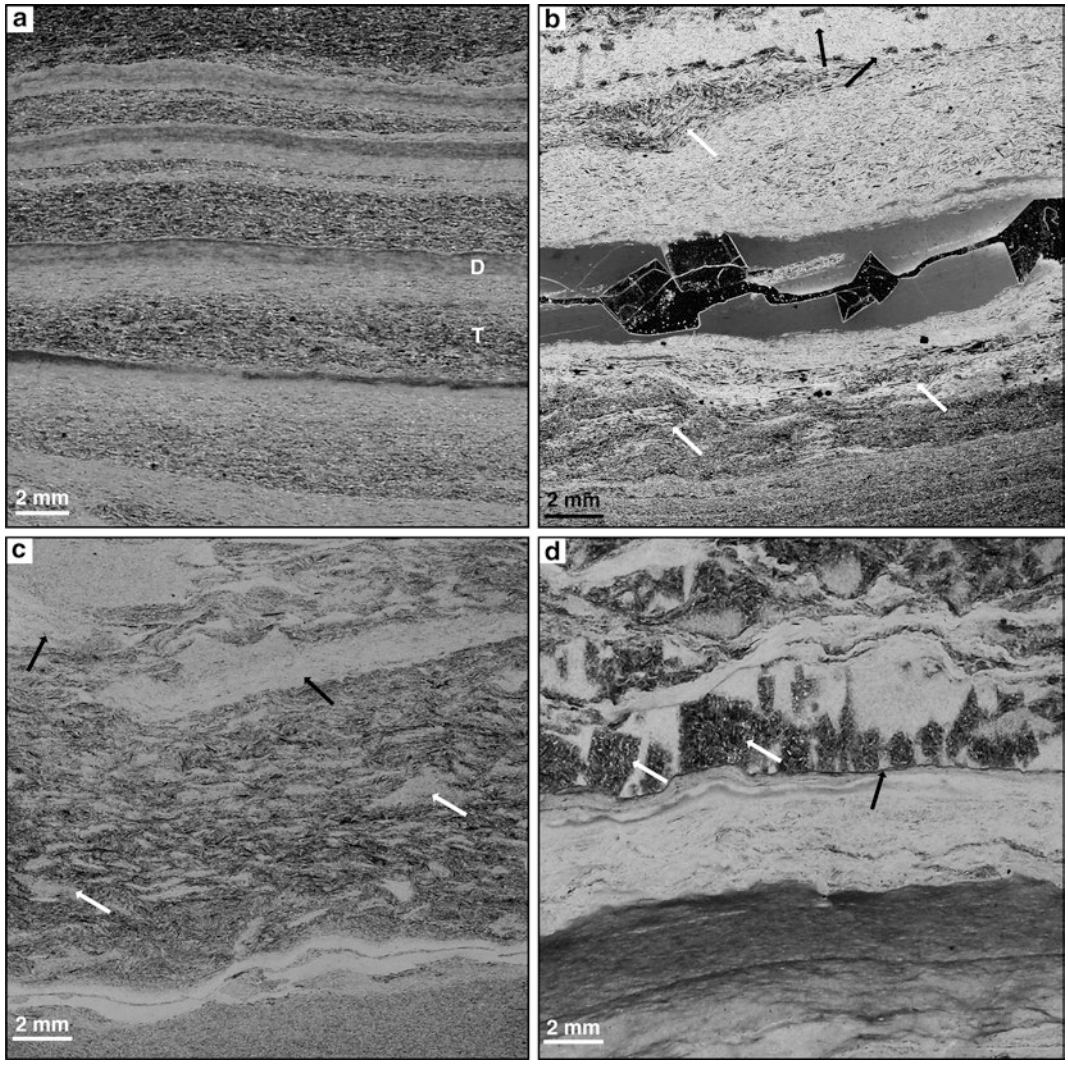

Fig. 11.11 Representative sedimentary features, Wilkins Peak Member, Blacks Fork 1 core, Bridger Basin. Photographs correspond to letters on Figs. 11.3 and 11.10. (**a**) Thin section photomicrograph from trona bed 17 (349.9 m). Perennial lacustrine trona cumulate needles (*T*), oriented parallel to bedding, fine upward and grade into organic-rich dolomite (*D*). (**b**) Thin section photomicrograph from trona bed 17 (349.8 m) showing trona cumulate needles oriented parallel to bedding (*bottom*) and trona crystals that are randomly oriented or deformed (*white arrows*). Randomly oriented trona needles are interpreted as early diagenetic in origin. *Black arrows* point to halite cumulates, now replaced by trona. Black blebs are sulfides. Thin bed of dolomitic mudstone with displacive shortite (dark euhedral crystals) in middle; dark horizontal fracture-like feature is thin-section artifact. (**c**) Thin section photomicrograph from trona bed 15 (368.8 m). Bottom is layered cumulate microcrystalline trona. Middle is microcrystalline trona clasts (*white arrows*) in a matrix of trona cement (dark). Top shows a fragmented trona cumulate layer (*black arrows*). (**d**) Thin section photomicrograph of trona bed 18 (340.5 m) showing vertical, widening upward bottom growth halite replaced by trona (*white arrows*). Thin organic-rich dolomitic parting (<10 μm) (*black arrow*) separates cumulate trona (below) from bottom growth halite (above)

Trona bed 17 displays cycles of bottom growth halite (now replaced by trona, see below) draped by laminated microcrystalline trona (Plate 11.1a, c). Organic-rich dolomitic partings sharply separate the laminated microcrystalline trona from the overlying bottom growth halite crusts (Fig. 11.11d; Plate 11.1c, d). Boni and Atkinson (1998) suggested that these dolomitic partings formed when dilute waters entered the basin during flooding events and re-supplied lake waters with calcium and magnesium.

Microcrystalline trona precipitated at the air-water interface of a hypersaline lake and settled from suspension to the lake bottom where it formed layered deposits (Lowenstein and Hardie 1985; Smoot and Lowenstein 1991). Trona cumulates from the Wilkins Peak Member resemble the laminated trona deposited at Owens Lake, CA, after flooding in 1938–1939 and 1968–1969 (Smith et al. 1987; Alderman 1985; Brown et al. 2003) (Fig. 11.12). Following the 1968–1969 flooding, Owens Lake was ~2.4 m deep; trona was deposited as laminated cumulates in 1970 and 1971. Smith et al. (1987) reported trona precipitation during summer afternoons when lake water temperatures and salinities reached their maxima from evapoconcentration. Smith et al. (1987) also observed natron precipitation during cold nighttime periods which was later converted to trona when temperatures rose.

Bottom growth halite from the Bridger Basin exhibits vertical, widening upward fabrics that lack fluid inclusion banding and syndepositional dissolution surfaces (Fig. 11.11d; Plate 11.1a, c, d). The vertical, widening upward growth fabric and the lack of fluid inclusion banding indicates that halite grew slowly in a permanent brine body (Smoot and Lowenstein 1991; Li et al. 1996; Lowenstein et al. 1999). The absence of syndepositional dissolution surfaces indicates that deposition occurred in a density stratified lake, where evaporites on the brine floor were protected from undersaturated surface waters by dense bottom brines (Smoot and Lowenstein 1991; Li et al. 1996; Lowenstein et al. 1999). In that density stratified system, dilute floodwaters would collect as a surficial layer above the bottom brines.

11.3.2.2 Diagenetic Trona

Trona "spar", predominant in upper trona beds 19–25 and rare in the lower trona beds, lacks primary sedimentary fabrics. Earlier descriptions of trona spar include two types: (1) randomly oriented bladed, coarsely crystalline mosaics, and (2) satin spar that fills fractures (Birnbaum and Radlick 1982; Leigh 1991; Wiig et al. 1995; Boni and Atkinson 1998). Birnbaum and Radlick (1982) and Leigh (1991) show that type-1 trona spar is a diagenetic crystalline mosaic lacking primary crystal growth textures and fabrics. Trona satin spar consists of clear, fibrous crystals that fill vertical and horizontal fractures and so is diagenetic in origin. Birnbaum and Radlick (1982) and Leigh (1991) thought satin spar trona formed postdepositionally from hydraulic fracturing, when trona-saturated brines filled open fractures.

Diagenetic trona also occurs as displacive needles and needle sprays in dolomitic organic-rich layers (Fig. 11.13a). Some trona needles exhibit asymmetric upward or downward growth textures, but most are randomly oriented and bent, and contain inclusions of organic material, pyrite, and dolomite. The absolute timing of diagenetic crystal growth, syndepositional or burial, cannot be ascertained, but crystallization did occur when sediments were still soft.

There are many examples of pseudomorphous replacement of halite by trona (Figs. 11.11d and 11.13a; Plate 11.1a, c, d). Layers composed of halite exhibiting vertical growth fabrics are partially to completely replaced by trona crystals, ~ 200 μm to 6 mm in length. Rarely, trona replaces cumulate halite (Fig. 11.11b, Plate 11.1d). Trona crystals initially grew across primary halite crystal boundaries (Plate 11.1a, d) and eventually formed crystalline mosaics that completely replaced halite (Figs. 11.11d and 11.13a).

Replacement of halite by trona may be explained by increases in temperature that occurred during burial of brine-saturated halite-trona deposits in the Bridger Basin. To illustrate, we modeled variations in the solubility of halite and Na-carbonates with temperature in concentrated Na-Cl-HCO_3-CO_3 brine (Fig. 11.14). Brine

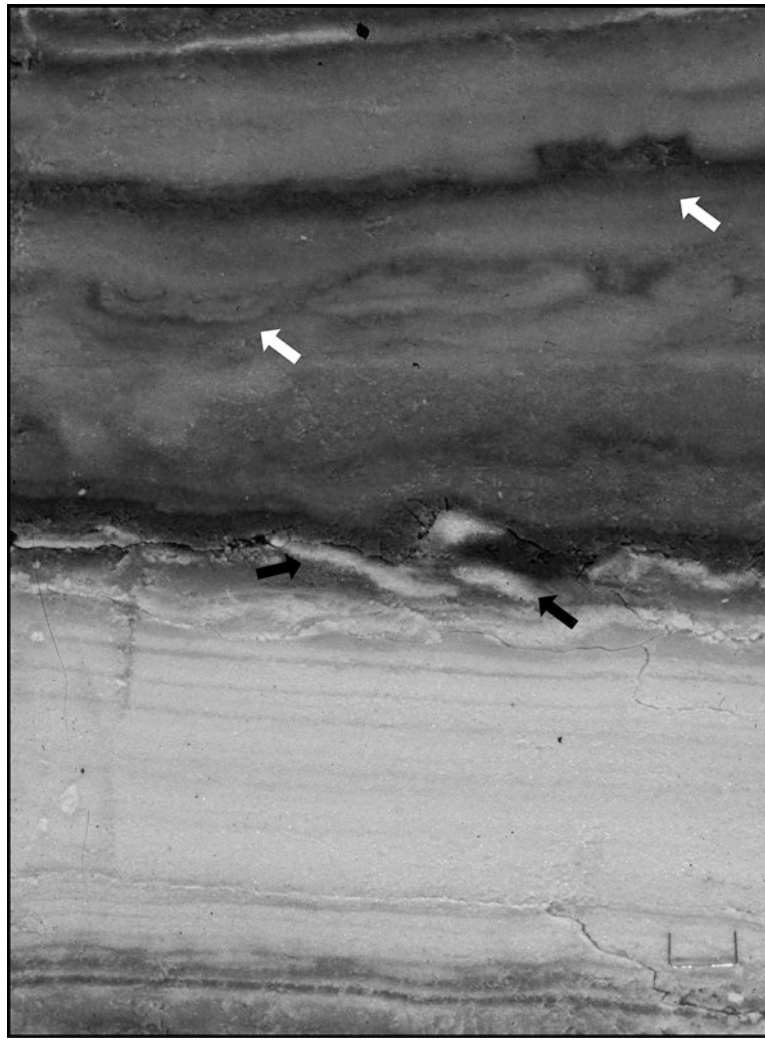

Fig. 11.12 Core slab of modern bedded microcrystalline trona, shallow subsurface, Owens Lake, California. Lower half consists of flat, parallel laminated trona cumulates deposited before the 1967–1968 flood. Middle contains a dark clay-rich layer with trona flat pebbles (*black arrows*) above a dissolution surface produced by the 1967–1968 flood. Top smeared trona layers (*white arrows*) are interpreted as sodium carbonate (natron?), precipitated during winter, and converted to trona during summer. Staple at lower right is 7 mm wide (Photo and interpretation courtesy of Joe Smoot)

from Lake Magadi, Kenya (Jones et al. 1977) (Table 11.1) was evaporated to trona and halite saturation at 25 °C using the computer program PHRQPITZ (Plummer et al. 1988) (left side of Fig. 11.14 where the trona and halite saturation state, Q/K, ion activity product/equilibrium constant, = 1). When temperature is raised to 100 °C, Magadi brine remains saturated with trona (Q/K ~ 1) but becomes undersaturated with respect to halite. When applied to the bedded halite and trona of the Bridger Basin, the modeling predicts that some halite will dissolve during burial. In such an alkaline Na-Cl-HCO_3-CO_3 brine, the addition of Na^+ from halite dissolution will lead to supersaturation and precipitation of trona.

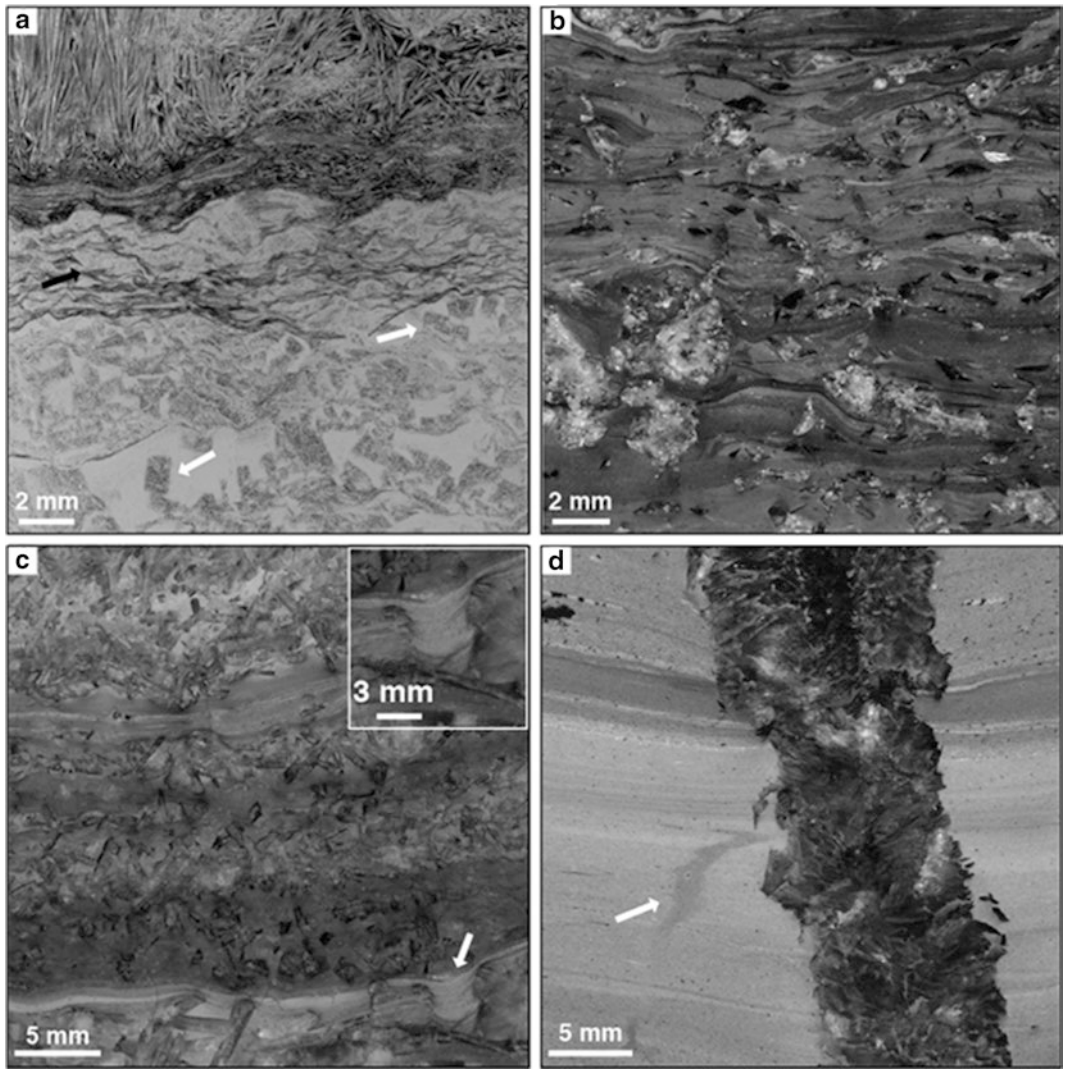

Fig. 11.13 Representative sedimentary features, Wilkins Peak Member, Blacks Fork 1 core, Bridger Basin. Photographs correspond to letters on Figs. 11.3 and 11.10. (**a**) Thin section photomicrograph from trona bed 18 (340.1 m) showing cumulate trona and bottom growth halite (*arrow*). Halite is now replaced by trona. The top of the thin section shows upward (*left*) and random (*right*) displacive growth of trona needles in organic-rich mud. (**b**) Core slab (262.7 m) showing organic-rich mudstone with laminae compacted around displacive crystals and crystal aggregates of shortite that contain organic matter and pyrite. Black bladed shapes are sulfide crystals. (**c**) Core slab (260.9 m) of thin-bedded to laminated dolomitic mudstone with shortite pseudomorphs after precursor Na-Ca carbonate mineral. Shortite pseudomorphs show bottom growth fabrics draped by carbonate mud (*bottom*), and displacive crystal growth fabrics that crosscut and disrupt primary layering. *Inset* is an enlarged view (*arrow*) showing where carbonate mud thickens between pseudomorph crystals and thins at their tops. (**d**) Core slab (423.9 m) of bedded carbonate mudstone with shortite-pyrite cement-filled fracture (~10 mm wide, > 30 mm long). Edges of fracture are irregular and contain shortite crystals that grew outward into the sediment. Scattered tiny black crystals are sulfide minerals. *Arrow points* to mudcrack showing that lake deposits were periodically subaerial exposed

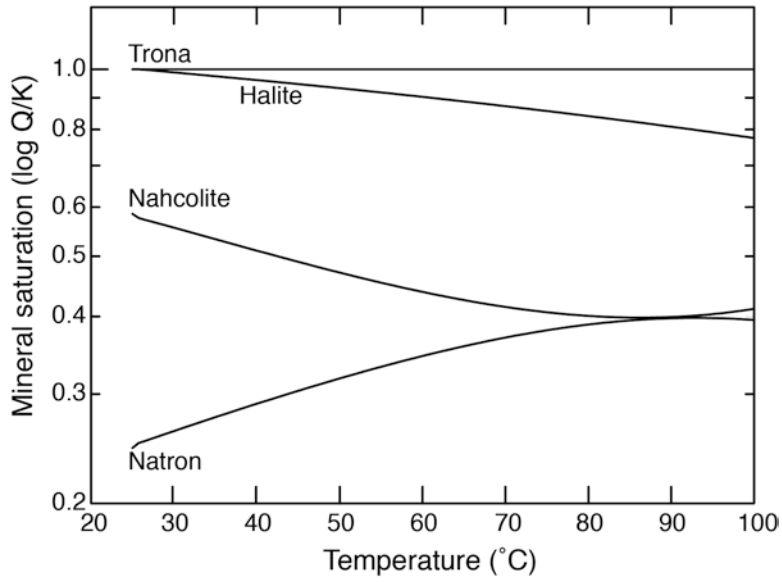

Fig. 11.14 Solubility of halite and Na-carbonate minerals versus temperature in Na^+-Cl^--HCO_3^--CO_3^{2-}-rich brines. Lake Magadi, Kenya, surface brine [chemical analysis from Jones et al. (1977); Table 11.1] was evaporated at 25 °C and pCO_2 of $10^{-3.4}$ using the computer program PHRQPITZ until trona and halite saturation was reached. That is shown on diagram at 25 °C where trona and halite are at saturation and Q/K = 1 (ion activity product, Q, divided by equilibrium constant, K, = 1). That same brine is undersaturated with respect to nahcolite and natron (Q/K for each mineral < 1). PHRQPITZ was then used to test mineral saturation states of the evaporated Magadi brine at temperatures >25 °C. Trona solubility is not strongly dependent on temperature so Q/K for trona is 1 and brines remain saturated with trona from 25 to 100 °C. Halite solubility, on the other hand, is strongly dependent on temperature; increasing temperature produces brines undersaturated with respect to halite. Increased pore fluid temperatures during normal burial diagenesis can produce brines saturated with respect to trona but undersaturated with respect to halite, which may explain pseudomorphous replacement of halite by trona

Table 11.1 Selected water compositions (mg/kg), Lake Magadi, Kenya

Water sampled	Na	K	Ca	Mg	HCO_3	CO_3	SO_4	Cl	SiO_2	pH
Rim (highland) streams (average)	19	5	9.6	4.7	74	N.D.	11	8.8	30	7.6
Hot springs (>50 ° C) (average)	11,400	204	N.D.	N.D.	12,800	4,180	171	5,430	87	9.3
Warm springs (<50 ° C) (average)	10,400	122	N.D.	N.D.	7,680	5,560	197	5,300	64	9.7
Main lake, surface brines (average)	106,000	1,580	N.D.	N.D.	5,000	83,600	1,680	64,500	819	10.5

From Jones et al. (1977) and Drever (1988)
N.D. not determined/below detection limit

11.3.2.3 Diagenetic Shortite

Shortite occurs in the Bridger Basin in the lower and upper portions of the Wilkins Peak Member in dolomitic mudstones, organic-rich oil shale, and trona-bearing mudstone (Fahey 1939; Milton and Eugster 1959; Bradley and Eugster 1969; Leigh 1991; Roehler 1992; Wiig et al. 1995; Dyni 1996). Shortite occurs as (1) euhedral displacive crystals and crystalline aggregates, (2) pseudomorphs after tabular Na-Ca carbonate minerals (gaylussite or pirssonite?), and (3) vein and fracture-fills (Fig. 11.13b–d) (Jagniecki et al. 2013).

Euhedral displacive shortite crystals have an orthorhombic-pyramidal crystal structure that may be triangular in cross section (Fig. 11.11b). Displacive crystals incorporate inclusions of the host sediment, including organic matter and dolomite. Displacive shortite also occurs as crystal aggregates that typically contain pyrite (Fig. 11.13b). Displacive shortite crystals and crystal aggregates crosscut sedimentary layers; surrounding layers are commonly compacted around shortite. The absolute timing of displacive shortite growth is ambiguous, but some must have formed prior to significant compaction (Fig. 11.13b).

Shortite pseudomorphs have a different crystal habit than primary displacive shortite (Fig. 11.13c). Shortite pseudomorphs are comprised of bedded, elongated tabular crystals (1 mm to >6 mm) that are typically twinned and commonly form thin crystalline beds in grey-green and brown laminated to thin-bedded mudstones. The precursor mineral originally grew displacively and as a crystalline crust at the brine bottom. Identification of the parent mineral on the basis of crystal habit is difficult because the Na-Ca-carbonates gaylussite and pirssonite share similar morphologies. It is likely that gaylussite, pirssonite, or both, were the precursor mineral(s) because: (1) they form today as bottom crusts or displacively in sediments in modern alkaline lakes (i.e. gaylussite in Mono Lake, CA, and pirssonite in subsurface sediments, Searles Lake, CA) and (2) gaylussite and pirssonite dehydrate to shortite during burial (Bury and Redd 1933; Jagniecki et al. 2013).

Shortite-filled fractures are composed of interlocking crystal mosaics that commonly contain pyrite (Fig. 11.13d). Fracture boundaries are irregular which shows that shortite crystals grew into the surrounding sediment. Sedimentary layering is cross-cut and commonly compacted around shortite-filled fractures.

All occurrences of shortite indicate that it formed diagenetically. Sediment layers cross-cut by shortite and sediment compacted around shortite crystals suggest that some crystallized before significant compaction (Bradley and Eugster 1969; Jagniecki et al. 2013). Jagniecki et al. (2013) show that shortite only forms at temperatures >52 °C from Na_2CO_3 saturated pore fluids (>1.1 *m* Na_2CO_3). They concluded that shortite psuedomorphs formed during burial from dehydration of gaylussite or pirssonite:

$$Na_2CO_3 \cdot CaCO_3 \cdot 2H_2O_{(pirssonite)} + CaCO_3 = Na_2CO_3 \cdot 2CaCO_{3(shortite)} + 2H_2O \quad (11.1)$$

where pirssonite loses $2H_2O$ to form shortite at temperatures >52 °C. Similarly, shortite may form from dehydration of gaylussite (loss of $5H_2O$), but experiments by Bury and Redd (1933) showed that gaylussite dehydrates to pirssonite (loss of $3H_2O$) first, at temperatures >40 °C. The gaylussite to pirssonite transition is preserved in subsurface sediments, KM-3 core, Searles Lake, CA, where gaylussite and traces of pirssonite occur at shallow depths (20–120 m) but at greater depths (166–258 m) pirssonite dominates (Eugster and Smith 1965; Smith et al. 1983). Shortite is not found in Searles Lake subsurface sediments implying they have not reached temperatures >52 °C. Shortite is also found in the Miocene Na_2CO_3 deposits of Beypazari, Turkey (Suner 1994; García-Veigas et al. 2013) and shortite psuedomorphs, now calcite, are interpreted from the Cambrian alkaline playa deposits of Lake Parakeelya, Officer Basin, South Australia (White and Young 1980). In Beypazari, shortite occurs stratigraphically below gaylussite and pirssonite-bearing strata, which bolsters the argument that these Na-Ca carbonates formed sequentially at increasing burial depths and temperatures.

11.3.2.4 Wilkins Peak Member Paleoenvironments

Trona beds 1–18 of the Wilkins Peak Member are commonly associated stratigraphically with oil shale, which lacks sedimentary structures diagnostic of shallow water deposition (Figs. 11.3 and 11.10). Fine scale laminae in oil shale composed of organic matter and dolomite micrite are interpreted as settle-out deposits, although Smoot (1983) suggested organic-rich laminae may have formed as cohesive lake bottom mats because they occur as reworked flat pebble intraclasts. The presence of sulfides, absence of burrows, and preservation of organic matter indicate that bottom waters were probably saline and anoxic. The majority of trona and trona-halite beds are interlayered with oil shale which suggests the Wilkins Peak paleolakes were commonly density stratified with hypersaline bottom waters. The progressive increase in Br^- in halite from trona beds 6, 9, 10, 11, 15, and 16 supports the interpretation that a perennial brine body existed during evaporite deposition (Higley 1983). Biomarkers from organic-rich oil shales also suggest saline, anoxic conditions (Carroll and Bohacs 2001).

The lower to middle Wilkins Peak Member in the Blacks Fork 1 core displays repetitive, meter-scale, lake expansion-contraction cycles, 4–17 m thick (Figs. 11.3 and 11.10). These cycles record high-frequency lake level fluctuations in an evaporative underfilled basin (Eugster and Hardie 1975; Smoot 1983; Carroll and Bohacs 1999; Pietras and Carroll 2006; Smith et al. 2008a). Cycles consist of alternating deeper, perennial lake deposits and shallow lake, mudflat, and fluvial deposits (Figs. 11.3 and 11.10). Lake expansion is marked by flat pebble conglomerates composed of dolomitic mudstone intraclasts that overlie mudcracked mudstones (Figs. 11.3 and 11.10) (Smoot 1983; Pietras and Carroll 2006). Mudstone intraclasts are interpreted as rip-up clasts derived from exposed lake margins and transported into lake waters by floods or wave action (Eugster and Hardie 1975; Smoot 1983; Pietras and Carroll 2006). Overlying oil shale beds (0.1–2.5 m thick), traceable laterally >10 km in the Bridger Basin, were deposited during maximum lake expansion and in the deepest lakes (Eugster and Hardie 1975; Smoot 1983; Pietras and Carroll 2006). Trona-halite beds associated with oil shale formed in perennial hypersaline lakes that shrank from maximum depths by evaporoconcentration. Thin-bedded dolomitic mudstones with shortite psuedomorph layers are also interpreted as perennial saline lake deposits (Figs. 11.3 and 11.10).

Lake contraction and desiccation is best indicated by mudcracked mudstones (Smoot 1983; Pietras and Carroll 2006) (Figs. 11.3 and 11.10). Lake contraction is also indicated by clastic marker beds, such as sandstone and mudstone marker beds A to D (Fig. 11.3). These marker beds, with ripple cross stratification, mudcracks, intraclasts, soil horizons, carbonaceous plant material, and root structures, are fluvial channel and floodplain deposits (Smoot 1983; Pietras and Carroll 2006). Their occurrence near the center of the Bridger Basin must mean lake levels were low.

Meter-scale cycles in the Wilkins Peak Member indicate that the Bridger Basin had relatively low relief so that lake expansion and contraction produced major shifts in shoreline position (Smoot 1983; Pietras and Carroll 2006). Saline lakes in the Bridger Basin were shorter lived (~10^4 years, Pietras and Carroll 2006) than the perennial saline lake system that continually occupied the Piceance Creek Basin during deposition of the Parachute Creek Member. We speculate that the hypersaline lakes in the Bridger Basin during deposition of trona beds 1–18 were deep enough (~10 m) to protect trona and halite at the basin floor from dissolution by dilute floodwaters. Saline bottom crusts were protected from dissolution because winds cannot mix surface waters with bottom brines at those depths. A modern analog is Great Salt Lake with shallow basin relief and depths over the past 50 years of 7–14 m.

11.4 Green River Brine Geochemistry and Evolution

The geochemical evolution of closed basin brines is controlled by the chemical composition of stream and spring inflow, evaporative concentration, and the selective removal of solutes during

evaporite precipitation (Eugster and Smith 1965; Hardie and Eugster 1970; Eugster and Jones 1979; Eugster 1980; Smoot and Lowenstein 1991; Lowenstein and Risacher 2009). The inflow waters that fed the alkaline saline lakes of the Green River Formation are interpreted to have derived their solutes from low temperature weathering reactions involving silicate mineral bedrock and meteoric water containing carbonic acid (Bradley and Eugster 1969; Eugster and Hardie 1975; Dyni 1998; Carroll et al. 2008; Smith et al. 2008b). In particular, the weathering of volcanic rocks from the Absaroka and Challis volcanic provinces to the north and northwest of the Green River basins, the large volume of volcanic detritus derived from the erosion of those volcanics, and the numerous tuffs and authigenic zeolites found in the Green River Formation, all suggest volcanic influences on the chemical composition of inflow waters (Eugster and Hardie 1975; Smith et al. 2008a, b; Doebbert et al. 2010; Chetel and Carroll 2010). The main solutes derived from chemical weathering of such parent materials are Na^+, SiO_2, and HCO_3^- with subordinate K^+, Ca^{2+}, Mg^{2+}, SO_4^{2-} and Cl^-.

The trona and nahcolite deposits of the Green River Formation required alkaline parent brines (pH >10), which, in turn, required that inflow waters feeding the Green River lakes contained total carbonate ($HCO_3^- + CO_3^{2-}$) greater than $Ca^{2+}+Mg^{2+}$ (Figs. 11.15 and 11.16). When calcite (or dolomite) formed during evaporative concentration of such waters, Ca^{2+}-Mg^{2+} and CO_3^{2-} were removed in a 1:1 ratio, Ca^{2+}-Mg^{2+} became depleted, and $HCO_3^- + CO_3^{2-}$ became enriched in the evolved brines. This "$CaCO_3$" chemical divide, defined by the initial amounts of $Ca^{2+}+Mg^{2+}$ and total carbonate in the water at the point of calcite or dolomite precipitation, determines its chemical fate (Hardie and Eugster 1970; Smoot and Lowenstein 1991; Lowenstein and Risacher 2009) (Figs. 11.15 and 11.16). The $CaCO_3$ chemical divide and the original low ratio of Ca^{2+}/HCO_3^- in inflow waters due to the weathering of volcanic rocks are believed to have been responsible for the production of Green River alkaline waters. Mass balance calculations by Smith et al. (2008b) show that during Wilkins Peak Member time high rates of physical erosion, chemical weathering, and denudation "rivaled the highest documented non-glacial Quaternary rates for crystalline bedrock" (Smith et al. 2008b, p. 1). Elevated atmospheric pCO_2 and high temperatures may have enhanced silicate-weathering rates during the Early Eocene Climatic Optimum (Smith et al. 2008b).

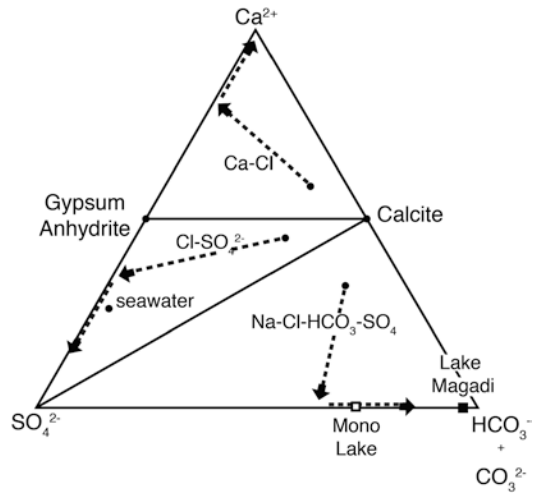

Fig. 11.15 Ternary phase diagram illustrating how inflow waters evolve into brines. Solid lines illustrate the concept of chemical divides. These lines from Calcite to SO_4 and Calcite to Gypsum-Anhydrite separate waters that that will evolve (*dashed lines* and *arrows*) upon evaporation and precipitation of calcite and gypsum into Ca-Cl brines, Cl-SO_4-rich brines, and Na-Cl-HCO_3-SO_4-rich brines. Brine evolution pathways are dependent on relative equivalents of Ca, SO_4, and HCO_3 in inflow waters, which determines chemical evolution of the brine at the $CaCO_3$ and $CaSO_4$ chemical divides (Adapted from Smoot and Lowenstein (1991))

11.4.1 Green River Spring Inflow?

Spring discharge and groundwater seepage may have contributed to the formation of alkaline brines in the Green River lakes. Discharge from springs and mixing with lake waters may cause precipitation of carbonates, either subaerially or subaqueously. This is commonly observed in modern and Pleistocene alkaline lake systems, for example Mono Lake, CA, Pyramid Lake, NV, and Lake Bogoria, Kenya, where travertine and

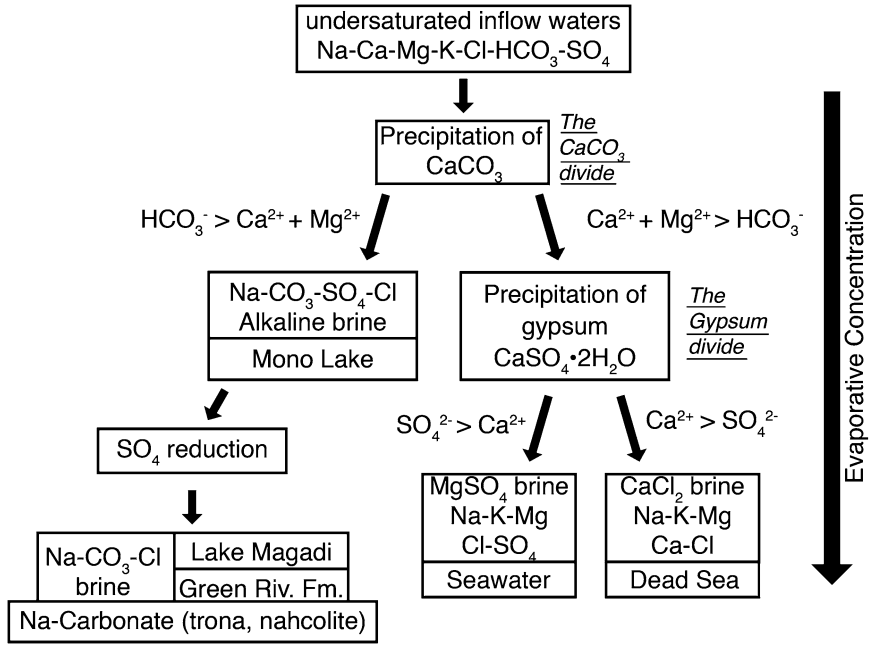

Fig. 11.16 Diagram illustrating the principle of chemical divides and the evolution of three major brine types. Lake Magadi and Green River brines lie on the left side of the diagram because of their low Ca^{2+}/CO_3^{2-} ratios. In this case, Ca^{2+} is removed from the brine during carbonate precipitation at the $CaCO_3$ chemical divide; continued evaporative concentration produces an alkaline brine dominated by HCO_3^--CO_3^{2-} at pH > 10. Sulfate reduction in Magadi and Green River brines removes SO_4^{2-}, producing a Na-CO_3-Cl water from which sodium carbonate minerals precipitate (Adapted from Hardie (2003))

tufa deposits form at zones of mixing between spring and lake waters. Carbonate precipitation in these lakes effectively removes the small amounts of Ca^{2+} carried into the basins by rivers and springs. Relatively large volumes of hydrothermal alkaline spring discharge, rich in $HCO_3^- + CO_3^{2-}$, and depleted in Ca^{2+} and Mg^{2+}, at Lake Magadi and Lake Bogoria are responsible for producing the extremely low Ca^{2+}/ CO_3^{2-} ratio in lake waters there (Table 11.1; Eugster 1970; Jones et al. 1977).

Recently, Earman et al. (2005) proposed that given the relatively common occurrence of volcanic rocks in closed arid basins, and the relative rarity of trona deposits in the geologic record, the standard surface weathering model of Eugster and Hardie (1975) may not be entirely correct. Earman et al. (2005) suggested that an extra pulse of CO_2 is an "important pre-condition for the formation of trona deposits". In order to form thick sodium carbonate deposits, thus, CO_2 beyond that derived from chemical weathering is required. They proposed magmatic sources of CO_2 and noted the association of alkaline waters relatively rich in $HCO_3^- + CO_3^{2-}$ and depleted in Ca^{2+} in areas of active volcanism (for example, Lake Magadi, Table 11.1). In summary, spring inflow and groundwater seepage, with or without magmatic CO_2 sources, may have contributed solutes to the Green River lakes.

11.4.2 Bacterial Sulfate Reduction

Sulfate reduction under anoxic conditions may have influenced brine evolution in the Green River lakes. The absence of sulfate minerals and the abundance of sulfides (pyrite with minor marcasite and pyrrhotite) in the Green River Formation suggest that sulfate reduction was a syndepositional process and occurred in the lake water column. Indeed, S is found in amounts up

to 4.9 weight percent in the Parachute Creek Member, northern Piceance Creek Basin (Dyni 1983; Tuttle and Goldhaber 1993). Anoxic environments preserve organic carbon in oil shales and would favor reduction of sulfate and precipitation of iron sulfides. Sulfate reduction can be represented by:

$$SO_4^{2-} + 2C_{organic} + 2H_2O = H_2S + 2HCO_3^- \quad (11.2)$$

where SO_4^{2-} and organic carbon react to produce H_2S and HCO_3^- (Drever 1988). Bicarbonate produced from bacterial sulfate reduction then added to the total alkalinity of the Green River brines. H_2S may escape to the atmosphere or react to form iron sulfides (now pyrite) or organosulfur compounds. These processes are thought to account for the low sulfate concentrations in some modern saline lakes, such as Lake Magadi (Table 11.1, Jones et al. 1977), and the absence of sulfate minerals in some ancient saline lake deposits.

11.4.3 Geochemical Modeling of Green River Brine Evolution

To better understand the evolution of Green River paleobrines, we used the surface water composition from Lake Magadi as a modern analog. Lake Magadi is appropriate for this analysis because trona and halite actively precipitate there today. Magadi lake waters have high concentrations of Na^+, HCO_3^-, and Cl^- and relatively low K^+, Ca^{2+}, Mg^{2+}, and SO_4^{2-}, due to Na^+-HCO_3^- rich spring inflow and stream inflow waters that have weathered volcanic rocks (Table 11.1). Evaporation simulations of Lake Magadi waters were done using the computer program EQL/EVP, based on Pitzer's ion interaction model (Risacher and Clement 2001). Simulations were carried out at equilibrium in an open system at 25 °C and at pCO_2 of 398 ppm (log −3.4 pCO_2) and 1,995 ppm (log −2.7 pCO_2) (Fig. 11.17). Evaporation begins at log concentration factor of 0 and progresses to the right. Minerals precipitated are shown as bars at the top; the amounts of the various minerals formed are shown in the middle, in millimoles (assuming 1 kg of parent water). Brine evolution is shown on the bottom plot of concentration factor (i.e., evaporation) versus concentration of each solute, in millimoles per kg H_2O. Lake Magadi waters, with extremely low Ca^{2+}/HCO_3^- ratios, precipitate negligible amounts of alkaline earth carbonate (not shown on diagram). Lake Magadi brines are supersaturated with amorphous silica, which precipitates at the beginning of the simulation (vertical "Am. Si" and "Si" lines on diagram). At Lake Magadi, Si precipitation occurs as amorphous gels, magadiite, and chert (Eugster 1967; Bradley and Eugster 1969; Eugster and Jones 1968; Surdam and Eugster 1976). Chert layers and nodules in the Wilkins Peak and Parachute Creek Members (Eugster and Surdam 1973) may have formed similarly.

The next mineral to precipitate from Magadi waters as they become more concentrated by evaporation is trona, which forms in large amounts. Halite precipitates next in larger amounts than trona (Fig. 11.17a). The mineral sequence of trona-halite is the same as observed in the Wilkins Peak Member of the Green River Formation. Brines at this point in the evaporation sequence are rich in Na^+, K^+, CO_3^{2-}-HCO_3^-, and Cl^-. Continued evaporation produces the potassium bearing minerals glaserite ($K_3Na(SO_4)_2$) and sylvite (KCl), but they are not observed at Lake Magadi because brines are never that highly evaporated. Potassium-bearing salts are not found in the Green River Formation again because evaporative concentration never reached the potash facies or because brines were depleted in K^+ during syndepositional formation of clay minerals (i.e. illite) or authigenic K-feldspar (Boak and Poole, Chap. 8, this volume).

The above simulations show that Green River lake waters evolved into Na^+- CO_3^{2-}-HCO_3^--Cl^- rich brines that precipitated trona and halite. The absence of sulfate minerals in the Green River Formation suggests that SO_4^{2-} was removed by sulfate reduction (reaction (11.2); Fig. 11.16). The occurrence of dolomite/ferroan dolomite interbedded with trona and halite suggests Ca^{2+} and Mg^{2+} were supplied by periodic influxes of new water into the lake system.

11.5 Discussion

11.5.1 Green River Evaporites and Eocene Atmospheric pCO_2

Understanding the origin of the bedded trona and nahcolite of the Green River Formation is significant because the equilibrium assemblage of sodium carbonate salts depends on pCO_2 (Eugster 1966; Lowenstein and Demicco 2006) (Figs. 11.17 and 11.18). In particular, experiments by Eugster (1966) showed that nahcolite only forms under high pCO_2 concentrations, >1,330 ppm, and at >1,125 ppm in halite saturated brine (Fig. 11.18). Trona is stable over a wide range of pCO_2; at high temperatures it forms at elevated pCO_2.

Computer simulations of evaporative concentration and brine evolution underscore the importance of atmospheric pCO_2 in controlling the precipitation of nahcolite versus trona (Fig. 11.17). At modern atmospheric pCO_2

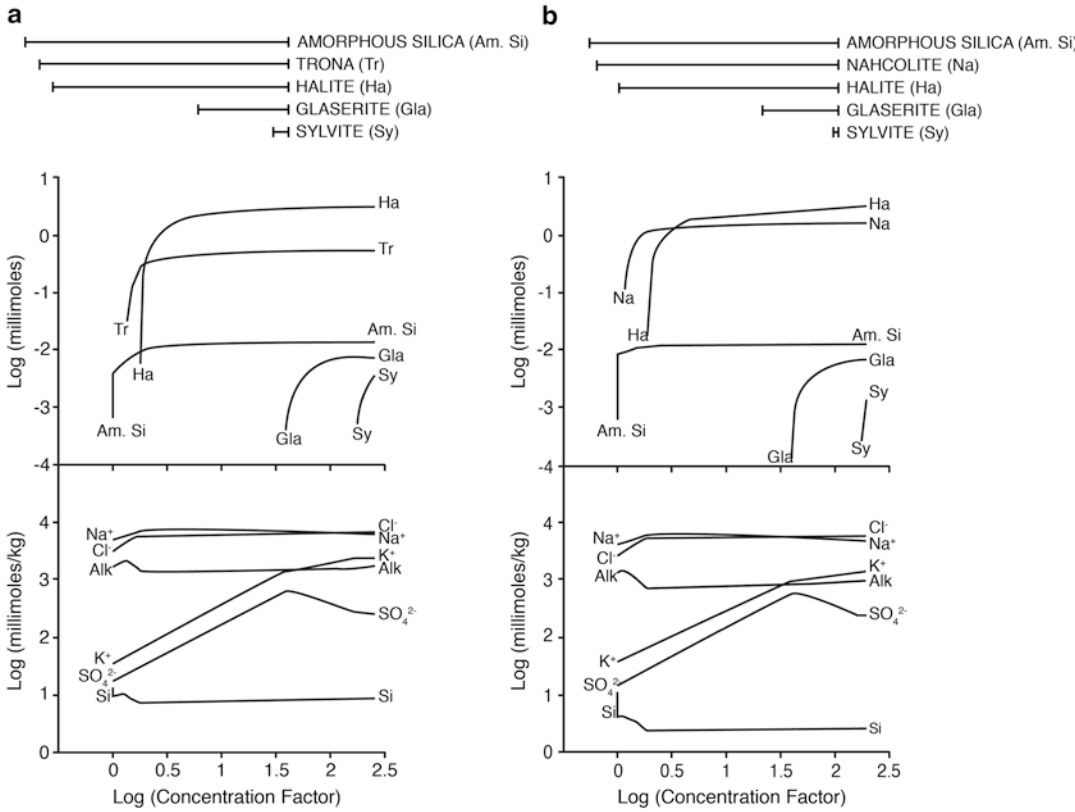

Fig. 11.17 Model of brine evolution, Lake Magadi, Kenya (Table 11.1), using the EQL/EVP computer program (Risacher and Clement 2001) under open system conditions at 25 °C and varying pCO_2 concentrations. (**a**) Simulated evaporation of lake water with present-day atmospheric pCO_2 concentrations of $10^{-3.4}$. (**b**) Simulated evaporation of lake water with elevated Eocene atmospheric pCO_2 concentration of $10^{-2.4}$. Concentration factor increases to the right during progressive evaporation and brine evolution. The *top* of the diagrams show the sequence of salts precipitated, middle shows the amount of salts precipitated (as log millimoles per kg of H_2O), and the *bottom panel* shows the evolution of major ions during evaporation (log millimoles per kg of H_2O)

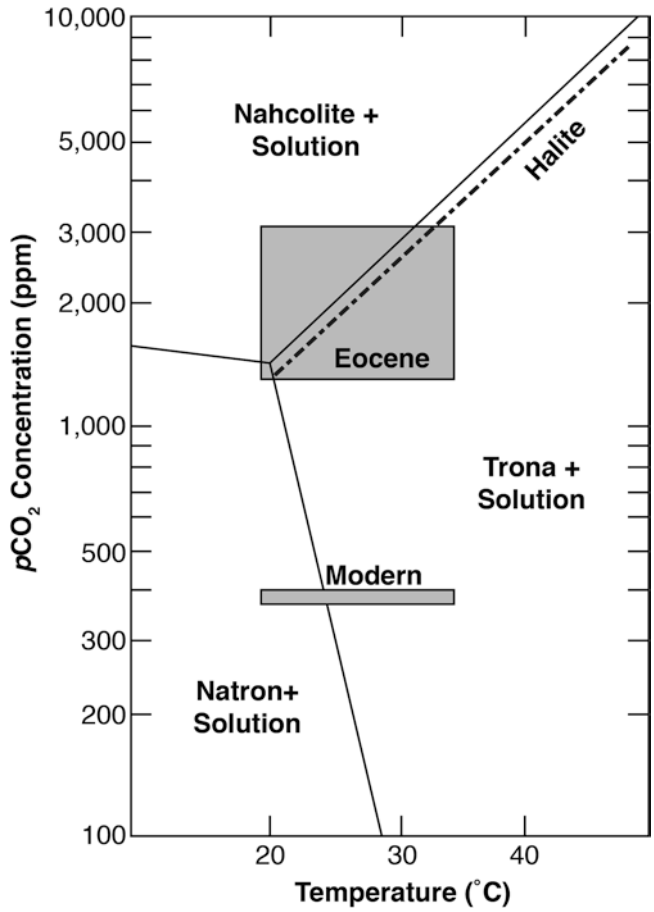

Fig. 11.18 Phase diagram showing stability fields of sodium carbonate minerals as a function of partial pressure of CO_2 and temperature. Minerals and solution are in equilibrium at 1 atm total pressure (From Eugster 1966). *Shaded boxes* show modern and interpreted Eocene lake temperatures and atmospheric pCO_2. The lower limit of nahcolite stability is ~1,330 parts per million. Addition of NaCl (*dashed line*, halite saturation) lowers the pCO_2 concentration in equilibrium with nahcolite and trona to 1,125 ppm at 20 °C (Adapted from Lowenstein and Demicco (2006))

(398 ppm), 25 °C, trona precipitates during evaporation of Lake Magadi brine (Fig. 11.17a). A second simulation, done at the same temperature, 25 °C, and using the same Lake Magadi brine chemistry but higher pCO_2 (1,995 ppm) produced nahcolite, not trona (Fig. 11.17b). A third simulation run at high pCO_2 (1,995 ppm), 30 °C, resulted in precipitation of trona.

Petrographic studies show that nahcolite in the Piceance Creek Basin co-precipitated with cumulate halite, the latter in places as relatively large "rafted" crystals that were held at the air-water interface by surface tension. Such surface tension controlled features suggest that co-precipitation of halite and nahcolite occurred at the surface of a perennial saline lake, rather than at the chemocline (Plate 11.1b; Lowenstein and Demicco 2006). Fluid inclusions in cumulate halite from the Piceance Creek Basin that contain trapped nahcolite microcrystals add additional evidence that nahcolite formed as a primary mineral at the air-water interface (LaClair and Lowenstein 2007, 2010). Precipitation from surface brines in contact with air suggests that nahcolite formed in

equilibrium with atmospheric CO_2 and that the early Eocene atmosphere had elevated pCO_2, at least 1,125 ppm, which is ~4 times preindustrial concentrations (Lowenstein and Demicco 2006) (Fig. 11.18). Other pCO_2 proxies also suggest that the early Eocene had elevated atmospheric pCO_2 (Pearson and Palmer 2000; Berner and Kothavala 2001; Demicco et al. 2003; Royer et al. 2004; Yapp 2004; Pagani et al. 2005; Fletcher et al 2008; Beerling et al. 2010; Breecker et al. 2010; Hyland and Sheldon 2013). These results are significant because the early Eocene was the longest prolonged warm period of the last 65 million years (the Early Eocene Climatic Optimum, EECO, of Zachos et al. 2001). Elevated pCO_2 and global warmth thus suggest a causal connection between greenhouse gases and climate during the EECO.

Trona, not nahcolite, is the dominant sodium carbonate mineral in the coeval Wilkins Peak Member of the Green River Formation, Bridger Basin. The enigma of finding trona and nahcolite in deposits of the same age may be explained by variations in (1) brine chemistry, (2) temperature, and (3) pCO_2.

11.5.1.1 Brine Chemistry

The reaction:

$$2NaHCO_3\left(\text{nahcolite}\right)+2H_2O+Na^+ \leftrightarrow NaHCO_3\cdot Na_2CO_3\cdot 2H_2O\left(\text{trona}\right)+H^+ \qquad (11.3)$$

indicates that trona forms instead of nahcolite at high activity of Na^+ (a_{Na+}) and high pH. Simultaneous formation of trona and nahcolite in the Bridger and Piceance Creek Basins may therefore indicate different brine compositions. Bradley and Eugster (1969) suggested that the solubilities of trona and nahcolite are dependent on the sodium content in solution and the bicarbonate quotient, $HCO_3^-/(HCO_3^- + CO_3^{2-})$. Trona is less soluble (more stable) at high concentration of Na^+ and low bicarbonate quotient, whereas nahcolite is stable at lower Na^+ concentration and high bicarbonate quotient.

11.5.1.2 Temperature

At elevated pCO_2, temperature controls the stability of trona and nahcolite, with trona favored at high temperatures and nahcolite at lower temperatures (Fig. 11.18). Fluid inclusion homogenization temperatures from Parachute Creek Member halites suggest average bottom and surface brine temperatures of 16–22 °C, and 21–28 °C, respectively, not unlike the modern Dead Sea (LaClair and Lowenstein 2010). At elevated pCO_2, these temperatures fall in the nahcolite stability field (Fig. 11.18). If the Piceance Creek Basin was at higher elevation than the Bridger Basin, and lapse rates were 3–6 ° C/km (Norris et al. 1996; Wolfe et al. 1998), then nahcolite precipitation would have been favored in the higher elevation Piceance Creek Basin but trona could have formed in the lower, warmer, Bridger Basin, all at the same elevated atmospheric pCO_2. But north to south regional paleodrainage patterns and spillover to the south are suggested by the overfilled, freshwater lakes of the Laney Member, Greater Green River Basin, and the time equivalent (~49 Ma) evaporative Mahogany Zone of the Parachute Creek Member, Piceance Creek Basin (Carroll et al. 2008; Smith et al. 2008a). These relationships imply lake spillover from north to south and that the Greater Green River Basin was at a higher elevation than the Piceance Creek Basin at ~49 Ma. Thus, the scenario that trona formed in a hotter, lower elevation Bridger Basin is unlikely. But paleobasin altitudes may have changed over the 2 million year interval between the main phase of evaporite deposition in the Bridger Basin (~51.4–50.8 Ma, Smith et al. 2008a) and Laney-Mahogany Zone deposition. It is also possible that the site of trona accumulation, the southern Bridger Basin, was at a lower elevation than other Greater Green River subbasins.

11.5.1.3 Microbially Influenced pCO_2

High pCO_2 concentrations needed to form nahcolite may have been produced in lake waters and

bottom sediments by organic processes operating in the Piceance Creek saline lake system. CO_2 may be generated in brines by microbially-mediated processes, including respiration, denitrification, methanogenesis, and reduction of sulfate, iron, and manganese (Boehrer and Schultze 2008). Positive $\delta^{13}C$ values, between +0.09 and +20 ‰ obtained from nahcolite in the Piceance Creek Basin, suggest possible carbon sources from anaerobic decomposition of organic matter by methanogenic bacteria, or photosynthesis, which removes carbon enriched in ^{12}C, leaving lake waters with high $\delta^{13}C$, especially in lakes with long residence times (Reitsema 1980; Pitman 1996; Mees et al. 1998). But ^{13}C enrichment in nahcolite may also result from inorganic processes such as evaporative concentration of lake waters and degassing of CO_2 concurrent with evaporation (Smith et al. 1987; Mees et al. 1998). Thus, positive carbon isotopic values from bedded nahcolite in the Piceance Creek Basin do not resolve the issue of whether the high pCO_2 needed to form and preserve nahcolite was generated by organic processes. Microbially-mediated processes may explain the even higher positive $\delta^{13}C$ values (+8 to +20 ‰) found in nahcolite nodules that grew displacively in organic-rich sediments during early diagenesis (Reitsema 1980; Pitman 1996). But for the bedded sodium carbonate minerals, their segregation in separate thick stratigraphic sections (bedded trona in the Bridger Basin and bedded nahcolite in the Piceance Creek Basin) is not consistent with local biological controls of CO_2-enriched microenvironments, which change dramatically in time and space. Organic rich "oil shale" exists in both basins, which also argues against a strong biological control on the pCO_2 at which nahcolite or trona precipitated.

11.6 Conclusions

1. The lower to middle Wilkins Peak Member contains repetitive, meter-scale lake expansion-contraction cycles that consist of alternating deeper, perennial lake deposits and shallow lake, mudflat and fluvial deposits. Trona from trona beds 1–18 is associated with oil shale, and formed in perennial hypersaline lakes. Mudcracked mudstones and fluvial-deltaic deposits cap cycles and record lake contraction and desiccation.
2. Shortite formed diagenetically during burial at temperatures >52 °C. Shortite crosscuts depositional cycles in the Wilkins Peak Member and occurs in perennial saline lake mudstones and evaporites, oil shale, and subaerially exposed mudstones.
3. Evaporites and associated deposits of the Parachute Creek Member, Piceance Creek Basin, were deposited in relatively deep perennial lakes. Bedded nahcolite and halite are associated with oil shale and oil shale breccia and accumulated in density stratified perennial saline lakes. Oil shale breccias are mass flow deposits generated along relatively steep basin margins.
4. Brines from which trona, nahcolite, and halite precipitated indicate that inflow waters contained relatively high proportions of Na^+, HCO_3^-, and Cl^- and lower K^+, Ca^{2+}, Mg^{2+}, and SO_4^{2-}. During evapoconcentration, parent waters evolved into Na^+-HCO_3^--CO_3^{2-}-Cl^- brines; sulfate was reduced to sulfide by sulfate reduction. Major solutes Na^+ and HCO_3^- were probably derived from chemical weathering of volcanic rocks in the northern Absaroka and Challis volcanic provinces. Additional solutes from spring inflow waters may have been important in producing alkaline saline lake waters.
5. Primary syndepositional textures of trona from the Bridger Basin and nahcolite from the Piceance Creek Basin suggest they formed at the air-brine interface in contact with the atmosphere. Experimental data and geochemical modeling shows that nahcolite only forms at high pCO_2 concentrations, >1,125 ppm; trona also precipitates at high pCO_2 but only at elevated temperatures and high activities of Na^+ and high pH. We conclude that nahcolite and trona formed in equilibrium with the elevated atmospheric CO_2 concentrations of the early Eocene. This implies that varying major ion brine chemistry, pH, or surface water temperatures controlled the precipitation of trona versus nahcolite.

Acknowledgments We extend our appreciation to Solvay Chemicals Inc. and FMC Industrial Chemicals for access to trona mines, with special thanks to Larry Refsdal, Matteo Paperini, John Kolesar and Rich Kramer. We thank R.V. Demicco, L. Ricketts, D. LaClair, A.R. Carroll, M.E. Smith, K. Tänavsuu-Milkeviciene, and J.R. Dyni for discussions and interpretations; J. P. Smoot, and J. Boak for their helpful reviews of this manuscript; David Tuttle for preparing photographs, and the USGS Core Research Center for providing core data. This work was supported by a Geological Society of America Research Grant, the American Association of Petroleum Geologists Grants-in-aid program, and the Center for Oil Shale Technology and Research (COSTAR) at Colorado School of Mines.

References

Alderman SS (1985) Geology of the Owens Lake evaporite deposit. In: Schreiber BC, Harner HL (eds) Sixth international symposium on salt, vol 1. Salt Institute, Alexandria, pp 75–83

Beard TN, Tait DB, Smith JW (1974) Nahcolite and dawsonite resources in the Green River Formation, Piceance Creek Basin, Colorado. In: Murray DK (ed) Guidebook to the energy resources of the Piceance Creek basin, Colorado 25th field conference. Rocky Mountain Association of Geologists, Denver, pp 101–109

Beerling DJ, Fox A, Anderson CW (2010) Quantitative uncertainty analyses of ancient atmospheric CO_2 estimates from fossil leaves. Am J Sci 309:775–787

Berner RA, Kothavala Z (2001) Geocarb III: a revised model of atmospheric CO_2 over Phanerozoic time. Am J Sci 301:182–204

Beyth M (1980) Recent evolution and present stage of Dea Sea brines. In: Nissenbaum A (ed) Hypersaline brines and evaporitic environments, vol 28. Elsevier, Amsterdam, pp 155–165

Birnbaum SJ, Radlick TM (1982) A textural analysis of trona and associated lithofacies, Wilkins Peak Member, Eocene Green River formation, southwestern Wyoming. In: Handford CR, Loucks RG, Davies GR (eds) Depositional and diagenetic spectra of evaporites – a core workshop. SEPM, Tulsa, pp 75–99

Bischoff JL, Herbst DB, Rosenbauer RJ (1991) Gaylussite formation at Mono Lake, California. Geochim Cosmochim Acta 55:1743–1747

Boehrer B, Schultze M (2008) Stratification of lakes. Rev Geophys 406:27

Boni PL, Atkinson WW (1998) A mineralogic and stratigraphic profile of trona bed 17 in the Solvay trona mine near Green River, Wyoming. In: Dyni J R, Jones RW (eds) Proceedings of the first international Soda Ash conference, Public Information Circular No. 40, Rock Springs, June 1997. Wyoming State Geological Survey, Laramie, pp 21–32

Bradley WH (1931) Origin and microfossils of the oil shale of the Green River Formation of Colorado and Utah. US Geol Surv Prof Pap 168:58

Bradley WH (1963) Paleolimnology. In: Frey DG (ed) Limnology in North America. University of Wisconsin Press, Madison, pp 621–652

Bradley WH (1966) Paleolimnology of the trona beds in the Green River Formation of Wyoming. In: Rau JL (ed) Symposium on salt. Northern Ohio Geological Society, Cleveland, pp 160–164

Bradley WH, Eugster HP (1969) Geochemistry and paleolimnology of the trona deposits and associated authigenic minerals of the Green River Formation of Wyoming. US Geol Surv Prof Pap 496-B:71

Brown N, Lamos P, Scarr I (2003) Present-day features related to the deposition of trona at Owens Lake, California, and a comparison with the trona deposits of the Green River Basin. In: Proceedings of the 39th forum on geology of industrial minerals, Special Publication, vol 33. Nevada Bureau of Mines and Geology, pp 36–40

Breecker DO, Sharp ZD, McFadden LD (2010) Atmospheric CO2 concentrations during ancient greenhouse climates were similar to those predicted for A.D. 2100. Proc Natl Acad Sci U S A 107:576–580

Burnside MJ, Culbertson WC (1979) Trona deposits in the Green River Basin, sweetwater, Unita and Lincoln Counties, Wyoming. US Geol Surv Open-File Rep 79–737:10

Bury CR, Redd R (1933) The system sodium carbonate-calcium carbonate-water. J Chem Soc Lond 272:1160–1162

Carroll AR, Bohacs KM (1999) Stratigraphic classification of ancient lakes: balancing tectonic and climatic controls. Geology 27:99–102

Carroll AR, Bohacs KM (2001) Lake-type controls on petroleum source rock potential in nonmarine basins. AAPG Bull 85:1033–1053

Carroll AR, Doebbert AC, Booth AL, Chamberlain CP, Rhodes-Carson MK, Smith EM, Johnson CM, Beard BL (2008) Capture of high altitude precipitation by a low altitude Eocene lake, western U.S. Geology 36:791–794

Casas E, Lowenstein TK (1989) Diagenesis of saline pan halite: comparison of petrographic features of modern, Quaternary, and Permian halites. J Sed Petrol 59:724–739

Cashion WB, Donnell JR (1972) Chart showing correlation of selected key units in the organic-rich sequence of the Green River Formation, Piceance Creek Basin, Colorado, and Uinta Basin, Utah. US Geol Surv Oil Gas Invest Chart OC-65

Cashion WB, Donnell JR (1974) Revision of nomenclature of the upper part of the Green River Formation, Piceance Creek Basin, Colorado, and Eastern Uinta Basin, Utah. US Geol Surv Bull 1394-G:9

Chetel LM, Carroll AR (2010) Terminal infill of Eocene Lake Gosuite, Wyoming, U.S.A. J Sed Res 80:492–514

Cole RD (1985) Depositional environments of oil shale in the Green River Formation, Douglas Creek arch, Colorado and Utah. In: Picard MD (ed) Geology and energy resources. Utah Geological Association Publication, Uinta Basin of Utah, pp 211–224

Culbertson WC (1961) Stratigraphy of the Wilkins Peak member of the Green River formation, Firehole Basin quadrangle, Wyoming. US Geol Surv Prof Pap 424D:170–173

Culbertson WC (1966) Trona in the Wilkins Peak member of the Green River formation, southwestern Wyoming. US Geol Surv Prof Pap 550-B:B159–B164

Culbertson WC (1971) Stratigraphy of the trona deposits in the Green River Formation, southwest Wyoming. Rocky Mt Geol 10:15–23

Demicco RV, Lowenstein TK, Hardie LA (2003) Atmospheric pCO_2 since 60 Ma from records of seawater pH, calcium and primary carbonate mineralogy. Geology 31:793–796

Doebbert AC, Carroll AR, Mulch A, Chetel LM, Chamberlain CP (2010) Geomorphic controls on lacustrine istotopic compositions: evidence from the Laney member, Green River Formation, Wyoming. Geol Soc Am Bull 122:236–252

Drever JI (1988) The geochemistry of natural waters, 2nd edn. Prentice Hall, Inc., New Jersey

Dyni JR (1981) Geology of the nahcolite deposits and associated oil shales of the Green River Formation in the Piceance Creek Basin, Colorado. Dissertation, University of Colorado

Dyni JR (1983) Distribution and origin of sulfur in Colorado oil shale. In: 16th Oil Shale symposium proceedings. Colorado School of Mines Press, Golden, pp 144–159

Dyni JR (1996) Sodium carbonate resources of the Green River Formation in Utah, Colorado, and Wyoming. US Geol Surv Open-File Rep 96–729:42

Dyni JR (1998) Prospecting for Green River-type sodium carbonate deposits. In: Dyni JR, Jones RW (eds) Proceedings of the first international Soda Ash conference, Public Information Circular No. 40, Rock Springs, June 1997. Wyoming State Geological Survey, Laramie, pp 37–47

Dyni JR (2006) Geology and resources of some world oil-shale deposits. US Geol Surv Sci Invest Rep 2005–5294:42

Dyni JR, Hawkins JE (1981) Lacustrine turbidites in the Green River Formation, northwestern Colorado. Geology 9:235–238

Dyni JR, Hite RJ, Raup OB (1970) Lacustrine deposits of bromine-bearing halite, Green River Formation, northwestern Colorado. In: Rau JL, Dellwig LF (eds) Third symposium on salt. Northern Ohio Geological Society, Cleveland, pp 166–180

Earman S, Phillips FM, McPherson BJOL (2005) The role of "excess" CO_2 in the formation of trona deposits. Appl Geochem 20:2217–2232

Eugster HP (1966) Sodium carbonate-bicarbonate minerals as indicators of P_{CO_2}. J Geophys Res 71:3369–3377

Eugster HP (1967) Hydrous sodium silicates from Lake Magadi, Kenya: Precursors of bedded chert. Science 157:1177–1180

Eugster HP (1970) Chemistry and origin of the brines of Lake Magadi, Kenya. Mineral Soc Am Spec Pap 3:213–235

Eugster HP (1980) Geochemistry of evaporitic lacustrine deposits. Annu Rev Earth Planet Sci 8:35

Eugster HP, Hardie LA (1975) Sedimentation in an ancient playa lake complex: the Wilkins Peak Member of the Green River Formation of Wyoming. Geol Soc Am Bull 86:319–334

Eugster HP, Jones BF (1968) Gels composed of sodium-aluminum silicate, Lake Magadi, Kenya. Science 161:160–163

Eugster HP, Jones BF (1979) Behavior of major solutes during closed-basin brine evolution. Am J Sci 279:609–631

Eugster HP, Smith GI (1965) Mineral equilibria in the Searles Lake evaporites, California. J Petrol 6:473–522

Eugster HP, Surdam RC (1973) Depositional environment of the Green River Formation of Wyoming: a preliminary report. Geol Soc Am Bull 84:1115–1120

Fahey JJ (1939) Shortite, a new carbonate of sodium and calcium. Am Mineral 24:514–518

Fahey JJ (1962) Saline minerals of the Green River formation, with a section on X-ray powder data for saline minerals of the Green River Formation by M.E. Mrose. US Geol Surv Prof Pap 405:50

Fletcher BJ, Brentnall SJ, Anderson CW, Berner RA, Beerling DJ (2008) Atmospheric carbon dioxide linked with Mesozoic and early Cenozoic climate change. Nat Geosci 1:43–48

García-Veigas J, Gündoğan İ, Helvaci C, Prats E (2013) A genetic model for Na-carbonate mineral precipitation in the Miocene Beypazari trona deposit, Ankara province, Turkey. Sed Geol 294:315–327

Gavrieli I, Starinsky A, Bein A (1989) The solubility of halite as a function of temperature in the highly saline Dead Sea brine system. Limnol Oceanogr 34:1224–1234

Hardie LA (2003) Evaporites. In: Middleton GV (ed) Encyclopedia of sediments and sedimentary rocks. Kluwer Academic Publishing, Dordrecht, pp 584–585

Hardie LA, Eugster HP (1970) The evolution of closed-basin brines. Mineral Soc Am Spec Pub 3:273–290

Hardie LA, Lowenstein TK, Spencer RJ (1985) The problem of distinguishing between primary and secondary features in evaporites. In: Schreiber BC, Harner HL (eds) Sixth international symposium on salt, vol 1. Salt Institute, Alexandria, pp 11–39

Harvie CE, Moller N, Weare JH (1984) The prediction of mineral solubilities in natural waters: the Na-K-Mg-Ca-H-Cl-SO4-OH-HCO3-CO3-CO2-H2O system to high ionic strengths at 25°C. Geochim Cosmochim Acta 48:723–751

Herut B, Gavrielli I, Halicz L (1998) Coprecipitation of trace and minor elements in modern authigenic halites from the hypersaline Dead Sea brine. Geochim Cosmochim Acta 62:1587–1598

Higley DK (1983) Distribution of bromine in bedded halite in the Green River Formation, Southwestern Wyoming. US Geol Surv Open-File Rep 83–726:49

Hite RJ, Dyni JR (1967) Potential resources of dawsonite and nahcolite in the Piceance Creek Basin, northwest Colorado. Q J Colorado Sch Min 62:25–38

Hyland EJ, Sheldon ND (2013) Coupled CO_2-climate response during the Early Eocene Climatic Optimum. Palaeogeogr Palaeoclimatol Palaeoecol 369:125–135

Jagniecki EJ, Jenkins DM, Lowenstein TK, Carroll AR (2013) Experimental study of shortite ($Na_2CO_3 \cdot 2CaCO_3$) formation and application to the burial history of the Wilkins Peak Member, Green River Basin, Wyoming, USA. Geochim Cosmochim Acta 115:31–45

Johnson RC (1981) Stratigraphic evidence for a deep Eocene Lake Uinta, Piceance Creek Basin, Colorado. Geology 9:55–62

Johnson RC (1984) New names for units in the lower part of the Green River Formation, Piceance Creek Basin, Colorado. US Geol Surv Bull 1529-I:20

Johnson RC, Mercier TJ, Brownfield ME, Pantea MP, Self JG (2010) An assessment of in-place oil shale resources in the Green River Formation, Piceance Basin, Colorado. US Geol Surv Digital Data Series DDS-69-Y:187

Jones BF, Eugster HP, Rettig SL (1977) Hydrochemistry of the Lake Magadi basin, Kenya. Geochim Cosmochim Acta 41:53–72

LaClair D, Lowenstein TK (2007) Eocene Green River evaporites: depositional environment and paleoclimate. Paper presented at the Geological Society of America annual meeting, Abstracts with Programs, Denver, 28–31 Oct 2007

LaClair D, Lowenstein TK (2010) Using microthermometry and laser Raman spectroscopy and evaporites to reconstruct the paleoclimate of the Eocene Green River Formation, Colorado, USA. Paper presented at the 10th Biennial Pan-American Current Research on Fluid Inclusions conference, Las Vegas, 7–10 June 2010

Leigh RT (1991) Wyoming trona: an overview of the geology and economic utilization. In: Wyoming Geological Association Guidebook, 42nd field conference, pp 103–120

Li J, Lowenstein TK, Brown CB, Ku TL, Luo S (1996) A 100 ka record of water tables and paleoclimates from salt cores, Death Valley, California. Palaeogeogr Palaeoclimatol Palaeoecol 123:179–203

Lowenstein TK, Demicco RV (2006) Elevated Eocene atmospheric CO_2 and its subsequent decline. Science 313:1928

Lowenstein TK, Hardie LA (1985) Criteria for the recognition of salt-pan evaporites. Sedimentology 32:627–644

Lowenstein TK, Risacher F (2009) Closed basin brine evolution and the influence of Ca-Cl inflow waters: Death Valley and Bristol Dry Lake California, Qaidam Basin, China, and Salar de Atacama, Chile. Aquat Geochem 15:71–94

Lowenstein TK, Li J, Brown CB, Roberts SM, Ku TL, Luo S, Yang W (1999) 200 k.y. paleoclimate record from Death Valley salt core. Geology 27:3–6

Lundell LL, Surdam RC (1975) Playa-lake deposition, Green River Formation, Piceance Creek basin, Colorado. Geology 3:493–497

Mees FM, Reyes E, Keppens E (1998) Stable isotope chemistry of gaylussite and nahcolite from deposits of the crater lake at Malha, northern Sudan. Chem Geol 146:87–98

Milton C, Eugster HP (1959) Mineral assemblages of the Green River Formation. In: Abelson PH (ed) Researches in geochemistry. Wiley, New York, pp 118–150

Moncure G, Surdam RC (1980) Depositional environment of the Green River Formation in the vicinity of the Douglas Creek Arch, Colorado and Utah. Contrib Geol Univ Wyoming 19:9–24

Monnin C, Schott J (1984) Determination of the solubility products of sodium carbonate minerals and an application to trona deposition in Lake Magadi (Kenya). Geochim Cosmochim Acta 48:571–581

Neev D, Emery KO (1967) The Dead Sea. Geol Surv Israel Bull 41:147

Norris RD, Jones LS, Corfield RM, Cartlidge JE (1996) Skiing in the eocene Uinta Mountains? Isotopic evidence in the Green River Formation for snow melt and large mountains. Geology 24:403–406

Pagani M, Zachos JC, Freeman KH, Tripple B, Bohaty S (2005) Marked decline in atmospheric carbon dioxide concentrations during the Paleogene. Science 309:600–602

Pearson PN, Palmer MR (2000) Atmospheric carbon dioxide concentrations over the past 60 million years. Nature 406:695–699

Pietras JT, Carroll AR (2006) High-resolution stratigraphy of an underfilled lake basin: Wilkins Peak Member Eocene Green River Formation, Wyoming, U.S.A. J Sed Res 76:1197–1214

Pietras JT, Carroll AR, Rhodes MK (2003) Lake basin response to tectonic drainage diversion: eocene Green River Formation, Wyoming. J Paleolimnol 30:115–125

Pitman JK (1996) Origin of primary and diagenetic carbonates in the lacustrine Green River Formation (Eocene), Colorado and Utah. US Geol Surv Bull 2157:1–17

Plummer LN, Parkhurst DL, Fleming GW, Dunkle SA (1988) PHRQPITZ- a computer program incorporating Pitzer's equations for calculation of geochemical reactions in brines. US Geol Surv Water-Res Invest Rep 88–4153:309

Reitsema RH (1980) Dolomite and nahcolite formation in organic rich sediments: isotopically heavy carbonates. Geochim Cosmochim Acta 44:2045–2049

Renaut RW, Gierlowski-Kordesch EH (2010) Lakes. In: Dalrymple RW, James NP (eds) Facies models, vol 6, 4th edn, Geological Association of Canada IV Series. GEOtext, Toronto, pp 541–575

Risacher F, Clement A (2001) A computer program for the simulation of evaporation of natural waters to high concentration. Comp Geosci 27:191–201

Robb WA, Smith JW (1976) Mineral profile of Wyoming's Green River Formation-sampled by Blacks Fork core. Wyom Geol Assoc Earth Sci Bull 9:1–7

Roehler HW (1992) Correlation, composition, areal distribution, and thickness of Eocene stratigraphic units, greater Green River basin, Wyoming, Utah, and Colorado. US Geol Surv Prof Pap 1506-E:E1–E49

Roehler HW (1993) Eocene climates, depositional environments, and geography, greater Green River basin, Wyoming, Utah, and Colorado. US Geol Surv Prof Pap 1506-F:F1–F74

Royer DL, Berner RA, Montañez IP, Tabor NJ, Beerling DJ (2004) CO_2 as a primary driver of Phanerozoic climate. GSA Today 14(5):4–10

Schubel KA, Lowenstein TK (1997) Criteria for the recognition of shallow perennial saline lake halites based on recent sediments from the Qaidam Basin, western China. J Sed Res 67:74–87

Smith GI, Barczak J, Moulton GF, Liddicoat JC (1983) Core KM-3, a surface-to-bedrock record of Late Cenozoic sedimentation in Searles Valley, California. US Geol Surv Prof Pap 1256:24

Smith GI, Friedman I, McLaughlin RJ (1987) Studies of Quaternary saline lakes-III. Mineral, chemical, and isotopic evidence of salt solution and crystallization processes in Owens Lake, California, 1969–1971. Geochim Cosmochim Acta 51:811–827

Smith ME, Singer B, Carroll A (2003) $^{40}Ar/^{39}Ar$ geochronology of the Eocene Green River Formation, Wyoming. Geol Soc Am Bull 115:549–564

Smith ME, Carroll AR, Singer BS (2008a) Synoptic reconstruction of a major ancient lake system: Eocene Green River Formation, western United States. Geol Soc Am Bull 120:54–84

Smith ME, Carroll AR, Mueller ER (2008b) Elevated weathering rates in the Rocky Mountains during the Early Eocene Climatic Optimum. Nat Geosci 1:370–374. doi:10.1038/ngeo205

Smoot JP (1978) Origin of the carbonate sediments in the Wilkins Peak Member of the lacustrine Green River Formation (Eocene) Wyoming, U.S.A. Int Assoc Sedimentol Spec Publ 2:109–127

Smoot JP (1983) Depositional subenvironments in an arid closed basin; the Wilkins Peak Member of the Green River Formation (Eocene), Wyoming, U.S.A. Sedimentology 30:801–827

Smoot JP, Lowenstein TK (1991) Depositional environments of non-marine evaporites. In: Melvin JL (ed) Evaporites, petroleum, and mineral resources. Developments in sedimentology. Elsevier, Amsterdam, pp 189–347

Steinhorn I (1985) The disappearance of the long term meromictic stratification of the Dead Sea. Limnol Oceanogr 30:451–472

Steinhorn I, Gat JR (1983) The Dead Sea. Sci Am 249:102–109

Surdam RC, Eugster HP (1976) Mineral reactions in the sedimentary deposits of the Lake Magadi region, Kenya. Geol Soc Am Bull 87:1739–1752

Suner F (1994) Shortite formation in Turkey: its geochemical properties. In: Proceedings of the 29th international geological congress Kyoto, Japan, Part A. VSP International Science Publishers, Zeist, Netherlands, pp 237–244

Tänavsuu-Milkeviciene K, Sarg JF (2012) Evolution of an organic-rich lake basin – stratigraphy, climate and tectonics: Piceance Creek basin, Eocene Green River Formation. Sedimentology 59(6):1735–1768

Trudell LG, Beard TN, Smith JW (1970) Green River Formation lithology and oil-shale correlations in the Piceance Creek Basin, Colorado. US Bur Mines Rep Invest 7357:14

Tuttle ML, Goldhaber MB (1991) Sulfur geochemistry and isotopy of the Green River Formation, Wyoming, Utah, and Colorado. US Geol Surv Bull 1973B:B1–B20

Tuttle ML, Goldhaber MB (1993) Sedimentary sulfur geochemistry of the Paleogene Green River Formation, western USA: Implications for interpreting depositional and diagenetic processes in saline alkaline lakes. Geochim Cosmochim Acta 57:3023–3039

White AH, Young BC (1980) Cambrian alkali playa-lacustrine sequence in the northeastern officer basin, South Australia. J Sed Petrol 50:1279–1286

Wiig SV, Grundy WD, Dyni JR (1995) Trona resources in the Green River Basin, southwest Wyoming. US Geol Surv Open-File Rep 95–476:88

Wolfe JA, Forest CE, Molnar P (1998) Paleobotanical evidence of Eocene and Oligocene paleoaltitudes in midlatitude western North America. Geol Soc Am Bull 110:664–678

Yapp CJ (2004) $Fe(CO_3)OH$ in goethite from a mid-latitude North American Oxisol: estimate of atmospheric CO_2 concentration in the Early Eocene "Climatic optimum". Geochim Cosmochim Acta 68:935–947

Young NB, Smith JW (1970) Dawsonite and nahcolite analyses of Green River Formation oil-shale section, Piceance Creek Basin, Colorado. US Bur Mines Rep Invest 7445:22

Zachos J, Pagani M, Sloan L, Thomas E, Billups K (2001) Trends rhythms, and aberrations in the global climate 65 Ma to present. Science 292:686–693

Trace Fossils of the Eocene Green River Lake Basins, Wyoming, Utah, and Colorado

12

Jennifer Jane Scott and Michael Elliot Smith

Abstract

Trace fossils produced by insects, annelids, molluscs, birds, mammals, reptiles, amphibians, and fish are diverse in the Green River and roughly correlative formations, and provide clues to interpret sedimentary environments, stratigraphy, and paleoecology of continental organisms during the Early to middle Eocene (~53–43 Ma). The Green River Formation represents an excellent case study to better understand the composition and distribution of trace fossil assemblages in continental lake basins with dynamic tectonic and climatic histories. Bioturbation representing the subaerial exposure and pedogenesis of lacustrine and lake-margin sediments is useful for the recognition of mappable stratigraphic surfaces. The traces are mainly produced by air-breathing organisms in lake-margin terrestrial environments. In shallow water deposits of the freshwater and saline Green River lakes, trace fossil assemblages include simple trails and burrows, and are generally low diversity and have high bioturbation intensities. In saline to hypersaline lakes, moderate to high diversity assemblages are concentrated in areas with freshwater input to lake-margin settings, such as the distal delta plain or shallow water areas lakeward of fluvial input. In hypersaline lake sediments deposited in shallow littoral areas and mudflats, trace fossils are typically associated with subaerial exposure, and include meniscate backfilled burrows that that cross-cut sediments deposited in shallow water. Vertebrate trace fossils are most commonly preserved in mudflat environments of the saline lakes, and include footprints of birds, mammals, and reptiles.

J.J. Scott (✉)
Department of Earth Sciences, Mount Royal University, Mount Royal Gate 4825, T3E 6K6 Calgary, AB, Canada
e-mail: jescott@mtroyal.ca

M.E. Smith
School of Earth Science and Environmental Sustainability, Northern Arizona University, 602 S. Humphreys, Flagstaff, AZ 86011, USA

M.E. Smith, A.R. Carroll (eds.), *Stratigraphy and Paleolimnology of the Green River Formation, Western USA*, Syntheses in Limnogeology 1, DOI 10.1007/978-94-017-9906-5_12

12.1 Introduction

Animal and plant trace fossils in the Early to middle Eocene (~53–43 Ma) Green River and roughly correlative formations are abundant and diverse. They can be used as tools for the paleoenvironmental and stratigraphic interpretation of lacustrine to terrestrial settings in the Green River basins of Wyoming, Colorado, and Utah. This chapter provides a summary of the types of trace fossils present, their typical associations with depositional environments, and the types of environmental conditions they represent. The majority of the trace fossils were produced in shallow lacustrine and lake-margin environments, and many of the traces were produced by air-breathing organisms (e.g., insects, mammals, birds). The distributions of different trace fossil assemblages and their stratigraphic applications are considered in the context of the lake-type basin model (Bohacs et al. 2000, 2007; Scott et al. 2012a). Examples are presented from several localities in the Green River basins to summarize the known trace fossil assemblages, and to illustrate their utility for interpreting environmental conditions and environments (Fig. 12.1). The trace fossils can also be used for the more detailed sequence stratigraphic interpretation of lacustrine and lake-margin deposits, and are helpful for recognizing progradational cycles in successions that represent both lowstand and highstand lake levels (Scott 2010).

Sedimentation rate is the dominant control on the degree of overprinting and cross-cutting of trace fossils in both continental and marine settings, and is an important consideration for the stratigraphic application of trace fossils of the Green River and associated formations (Scott et al. 2012a). In continental basins, different trace fossil assemblages, or suites, can be closely associated because traces produced subaqueously in lacustrine or riverine areas are often cross-cut by traces produced by a different set of organisms after exposure of the substrate. In some examples, evidence of subaerial exposure is not recorded by the sediments themselves. Instead, the evidence is provided by trace fossil assemblages that grade into the next as a substrate dries. The degree of overprinting by burrows increases with substrate stability through time, and can correspond to increases in water-table depths. Conceptually, this gradational association between trace fossil assemblages representing substrate moisture conditions (e.g., Hasiotis 2007) is similar to the lateral transitions between shallow marine ichnofacies. For example, the *Cruziana* and *Zoophycus* ichnofacies in the lower shoreface to offshore transition in marine basins are not discrete assemblages but instead grade into one another as environmental conditions change across sedimentary profiles (Pemberton et al. 2012).

Traces produced by terrestrial invertebrates in pedogenically modified sediments may also provide insights into the climatic conditions prevalent in basin margin areas during the Early to middle Eocene (Smith et al. 2008a; Golab 2010). Changes in climatic conditions during the Early to middle Eocene (e.g., Zachos et al. 2001, 2008; Smith et al. 2014) may also have indirectly influenced the composition of vertebrate footprint assemblages through time due to the probable relationship between climate and the rapid evolution of mammals and birds at this time (e.g., Woodburne et al. 2009a, b; Dutchak 2010). The distribution of vertebrate footprints may also be indirectly related to climate through the control of climate on sedimentary environments and the dominant conditions that contribute to the preservation of tracks, such as in arid lake-margin mudflats.

Numerous authors have documented and interpreted the significance of trace fossils in the Green River and correlative formations of Wyoming, Utah, and Colorado (Table 12.1; Fig. 12.2). Vertebrate trackways of mammals and birds and invertebrate trails in lake margin carbonates surrounding Lake Uinta have been studied by Curry (1957), Erickson (1967), Moussa (1968, 1970), D'Alessandro et al. (1987), Greben and Lockley (1992), Foster (2001), Yang et al. (1995), Hamblin et al. (1998, 1999), Lockley et al. (1999), Sarjeant et al. (2002), and Olson (2014). Trace fossils produced in terrestrial environments in the Green River and correlative formations in Wyoming and

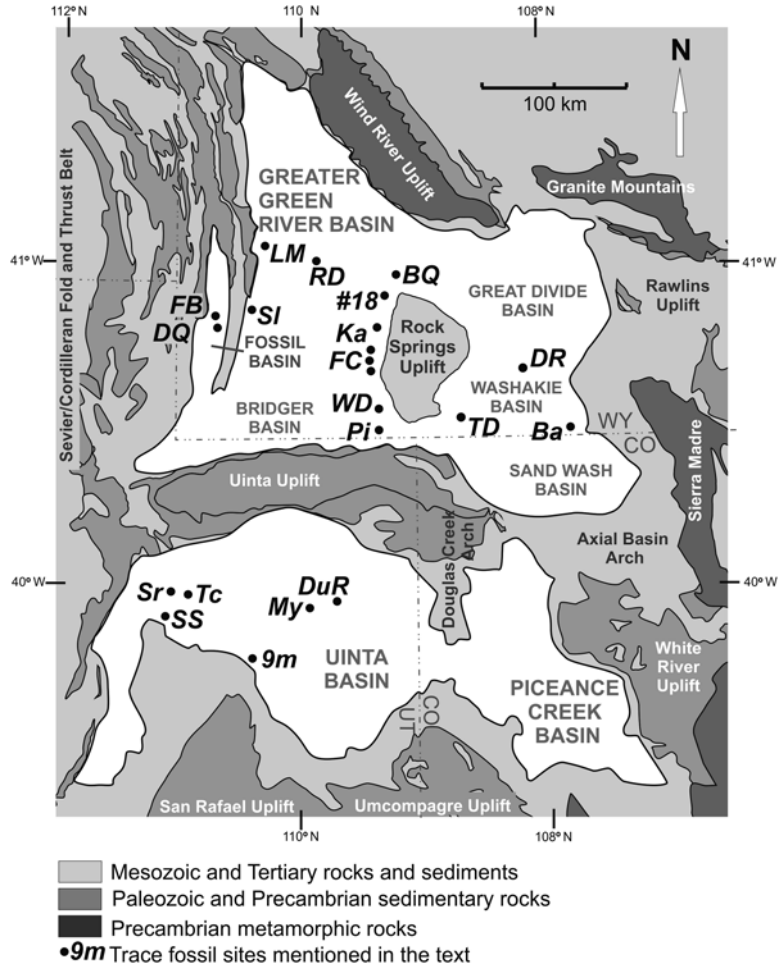

Fig. 12.1 Map showing the Green River lake basins in southwest Wyoming, northeast Utah, and northwest Colorado. Trace fossil sites mentioned in the text and Table 12.1 are figured. **Wyoming:** *#18* White Mountain at #18 crossing, *Ba* Baggs area, *BQ* Bird Quarry in the Jack Morrow Hills, *DQ* Dayvault Quarry, *DR* Delaney Rim (near Wamsutter; includes North Barrel Springs), *FB* Fossil Butte National Monument, *FC* Firehole Canyon area (includes Firehole Canyon, Middle Firehole Canyon, Sage Creek, and Chicken Springs Draw), *Ka* Kanda, on White Mountain, *LM* Little Mesa, near LaBarge, *Pi* Pipeline area, *RD* Reardon Draw, *Sl* Slate Creek, *TD* Trail Dugway, *WD* Wildhorse Draw. **Utah:** *9 m* Nine Mile Canyon, *DuR* Duchesne River, *My* Myton area, *Sr* Strawberry Reservoir area, Strawberry Canyon, *SS* Soldier Summit, *Tc* Timber Creek

Utah have been studied by D'Alessandro et al. (1987), Hasiotis and Honey (2000), Zonneveld et al. (2006), and Golab (2010). Leggitt and Cushman (2001), Leggitt and Loewan (2002), and Leggitt et al. (2007) studied caddisfly larval cases associated with bioherms of the freshwater Tipton Member in Wyoming. Lamond and Tapanila (2003) reported "embedment cavities" of invertebrates in lacustrine stromatolites. Leggitt and Cushman (2003) reported flamingo-like nest mounds from the Wasatch Formation in Wyoming. Roehler (1988) reported abundant burrows in deltaic deposits of the Cottonwood Creek Delta, Tipton Member in the Washakie subbasin, Wyoming. Deeper lacustrine trace fossils such as fish swimming traces have been studied by Martin et al. (2010) from Fossil Lake in Fossil Basin, Wyoming.

Table 12.1 Trace fossils in the Green River and correlative formations of Wyoming, Utah, and Colorado. Numbering corresponds with stratigraphic position shown in Fig. 12.2

Reference	Age	Stratigraphy	Location	Traces (general)	Ichnogenera
1. Bohacs et al. 2007	Early-middle Eocene	Green River Formation (Tipton, Wilkins Peak, Laney); Wasatch Formation (Lumen Tongue, Niland Tongue, Cathedral Bluffs)	Greater Green River basin	Bird, insect, mammal trackways; annelid, insect burrows, arthropod nests	*Steinichnus*, *Scoyenia*, *Planolites*, *Palaeophycus*, *Scolicia*, *Fuersichnus*, *Edaphichnium*, *Haplotichnus*, *Eatonichnus*, AMB, insect and bird trackways, insect nests, spider traces
2. Curry 1957	Middle Eocene	Green River Formation (Parachute Creek Member)	Timber Creek, Uinta basin	Bird, insect/nematode, lizard, mammal	Shorebird tracks, cf. *Presbyorniformipes*, lizard tracks, cf. *Cochlichnus*, mammal tracks
3. D'Alessandro et al. 1987	Late Eocene	Duchesne River Formation	Duchesne River, near Vernal, Uinta basin	Insect burrows, annelid and other arthropod burrows	*Ancorichnus*, *"Muensteria"*, *Palaeophycus*, *Scoyenia*, *Skolithos*, rhizoliths
4. Erickson 1967	Middle Eocene	Green River Formation	Tucker (Soldier Summit area), Uinta basin	Bird trackway and feeding traces	*Presbyornis* tracks and feeding traces, cf. *Presbyorniformipes*
5. Foster 2001	Middle Eocene	Cathedral Bluffs Member, Wasatch Formation	Jack Morrow Hills, "Bird Quarry", GGRB	Salamandar trackway	*Ambystomichnus*
6. Golab 2010	Early Eocene	Colton Formation and Green River Formation (Lower, Sunnyside Delta)	Nine Mile Canyon area, Uinta basin	Insect trails, burrows and nests; crayfish burrows, rhizoliths	*Celliforma*, *Camborygma*, *Cochlichnus*, *Ancorichnus*, rhizoliths, "AMB", *Macanopsis*, *Scoyenia*, *Steinichnus*, *Haplotichnus*
7. Hamblin et al. 1998, 1999	Middle-Late Eocene	Duchesne River Formation and Uinta Formation	Myton, Uinta basin	Mammal tracks	Perissodactyl tracks, uintathere tracks
8. Lamond and Tapanila 2003	Early-mid Eocene	Green River Formation (Tipton Member)	Delaney Rim, Washakie basin	"Embedment cavities"	Embedment cavities in stromatolites, produced by brine shrimp or insects
9. Moussa 1968, 1970	Middle Eocene	Green River Formation (Parachute Creek)	Soldier Summit, Uinta basin	Bird, insect/nematode	cf. *Cochlichnus*, bird tracks, mammal (perissodactyl) tracks
10. Hasiotis and Honey 2000	Early Eocene	Wasatch Formation (Main Body)	Washakie basin	Crayfish	*Camborygma*

11. Leggitt and Cushman 2001; Leggitt and Loewan 2002; Leggitt et al. 2007	Early-middle Eocene	Green River Formation (Tipton Member)	Essex Mountain, Big Sandy, Little Mesa, GGRB	Caddisfly larval cases	n/a
12. Lockley et al. 1999	Eocene	Green River Formation	Strawberry Canyon, Uinta basin	Mammal trackways	Perissodactyl, bird, lizard, carnivore (creodont)
13. Martin et al. 2010	Early-middle Eocene	Green River Formation (Fossil Butte Member)	Dayvault Quarry, Fossil basin	Fish swimming and feeding traces	*Undichna*
14. Olson 2014	Middle Eocene	Green River Formation	Tucker (Soldier Summit area), Uinta basin	Bird (stilt-like) tracks	*Juncitarsus* trackway
15. Roehler 1988	Early-middle Eocene	Green River Formation (Cottonwood Creek Delta, Tipton Member)	Baggs, Washakie basin	"Worm burrows"	cf. *Planolites*
16. Sarjeant et al. 2002	Early Eocene	Wasatch Formation	Baggs, Sand Wash basin	Mammal tracks (carnivore)	creodont trackway
17. Scott 2010	Middle Eocene	Green River Formation (Wilkins Peak Member)	Bridger basin	Bird, mammal, and reptile tracks; insect trackways and burrows	*Taenidium*, *Ancorichnus*, *Skolithos*, *Scoyenia*, *Helminthoidichnites*, *Macanopsis*, *Planolites*, *Palaeophycus*, *Steinichnus*, *Arenicolites*, *Lockeia*, perissodactyl, bird, carnivore tracks, rhizoliths
18. Yang et al. 1995	Middle Eocene	Green River Formation (Parachute Creek)	Timber Creek, Uinta basin	Bird trackway	*Presbyorniformipes*
19. Zonneveld et al. 2006	Early Eocene	Wasatch Formation (Main Body)	Fossil basin	Terrestrial burrows	*Lunulichnus*

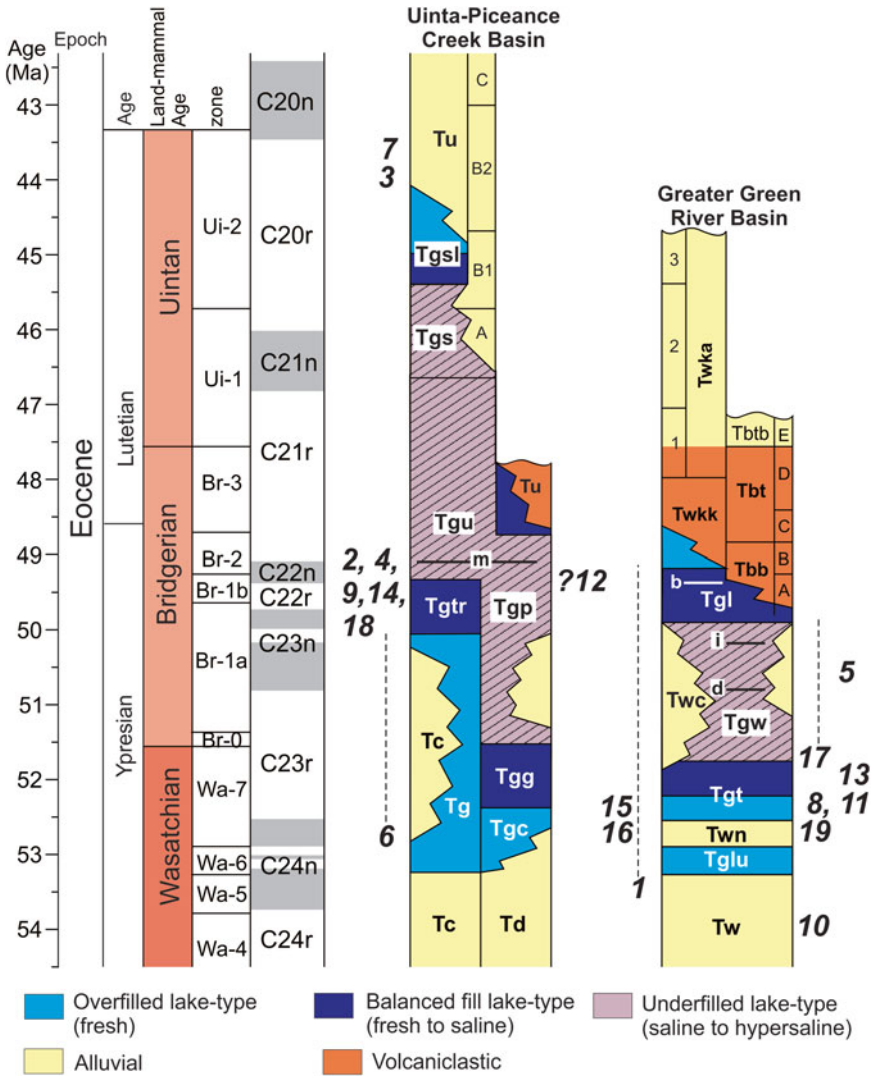

Fig. 12.2 Eocene stratigraphy of the Green River lake basins in southwest Wyoming, northeast Utah, and northwest Colorado. Geochronology of Smith et al. (2014). Stratigraphic units after Smith et al. (2008c): *Tg* Green River Formation, *Tglu* Lumen Tongue, *Tgt* Tipton Member, *Tgw* Wilkins Peak Member, *Tgl* Laney Member, *(Tgl)b* buff marker; *Tgc* Cow Ridge Member, *Tgg* Garden Gulch Member, *Tgtr* transitional interval; *Tgp* Parachute Creek, *Tgu* upper member, *Tgs* saline facies, *Tw* Wasatch Formation, *Twn* Niland Tongue, *Twc* Cathedral Bluffs Tongue, *Tb* Bridger Formation, *Tbb* Blacks Fork Member, *Tbt* Twin Buttes Member, *Tbtb* Turtle Bluff Member, *Twkk* Washakie Formation, Kinney Rim Member, *Twka* Washakie Formation, Adobe Town Member, *Tc* Colton Formation, *Td* Debeque Formation, *m* Mahogony Zone, *Tu* Uinta Formation. Number scheme follows order of authors in Table 12.1, and illustrates general stratigraphic range of cited studies. *1* – Bohacs et al. 2007; *2* – Curry 1957; *3* – D'Alessandro et al. 1987; *4* – Erickson 1967; *5* – Foster 2001; *6* – Golab 2010; *7* – Hamblin et al. 1998, 1999; *8* – Lamond and Tapanila 2003; *9* – Moussa 1968, 1970; *10* – Hasiotis and Honey 2000; *11* – Leggitt and Cushman 2001; Leggitt and Loewan 2002; Leggitt et al. 2007; *12* – Lockley et al. 1999; *13* – Martin et al. 2010; *14* – Olson 2014; *15* – Roehler 1988; *16* – Sarjeant et al. 2002; *17* – Scott 2010; *18* – Yang et al. 1995; *19* – Zonneveld et al. 2006

Bohacs et al. (2007) were the first to consider the trace fossils of the Greater Green River basin in Wyoming as a tool for interpreting water tables and soil moisture content of lake-margin settings in the different lake-type basins. Scott (2010) used the evaporitic Wilkins Peak Member of the Green River Formation and correlative Cathedral Bluffs Member of the Wasatch Formation in Wyoming to develop a model for the distribution of vertebrate and invertebrate trace fossils in underfilled lake-type basins. Sato et al. (2014) focused on the use of terrestrial and lake-margin traces for the stratigraphy of the fluvio-lacustrine Duchesne River and Uinta formations in the Uinta basin, Utah. Each of the ichnological case studies presented by these authors contributes to a better understanding of the paleoecology of vertebrates and invertebrates known from the Green River basins. Each study can also be applied to understanding changes in environmental conditions, as they were related to changing climate, tectonics, and/or drainage patterns as recorded by the dynamic sedimentary fill of each of the Green River basins.

12.2 Lake-Type Basins and Trace Fossils in the Green River Formation

The lake-type basin model (Carroll and Bohacs 1999; Bohacs et al. 2000) can be successfully integrated with the ichnofacies model for lake basins to help simplify interpretations of environmental conditions that influenced the preserved trace fossil assemblages in different localities (Buatois and Mángano 2004, 2009; Bohacs et al. 2007; Scott et al. 2012a). Factors controlling sedimentation (e.g., energy levels), hydrochemical conditions (e.g., salinity, oxygenation, mixing regime), and the behavior of trace-producing organisms, combine to determine the assemblage of trace fossils. The distribution and composition of lithofacies associations and their stratigraphic packaging reflects the lake-type basin, whether it was overfilled with respect to water and sediment input, in balance with the input, or underfilled with respect to the flux of water and sediment (Carroll and Bohacs 1999; Bohacs et al. 2000). The types of sedimentary environments associated with these different lake-type basins, environmental conditions, and trace fossil assemblages are also dependant on the relationship between the accommodation in the basin and if the water can overspill the bounding sill(s) (Buatois and Mángano 2004, 2009; Bohacs et al. 2007).

Overfilled lake-type basins are characterized by lakes that are open, spill into an adjacent basin, and receive an abundant influx of water and sediment deposited in progradational fluvial to deltaic deposits (Bohacs et al. 2000). Water tables are expected to be shallow and sedimentary substrates soft, contributing to a trace-fossil association assemblage containing soft-ground burrows (e.g., *Planolites*) produced in subaqueous substrates (Buatois and Mángano 2004). Balanced fill and underfilled lake-type basins both are characterized by trace fossil assemblages produced in subaerial lake-margins containing burrows produced in soft (e.g., *Planolites*) and firm or cohesive substrates (e.g., *Taenidium*, *Steinichnus*). In underfilled lake-type basins, these assemblages (i.e. *Scoyenia* ichnofacies) can be found in the basin center and basin margin, but in balanced fill lake-type basins, these assemblages are found only at the basin margins (Scott et al. 2012a). Terrestrial trace types, or those formed in pedogenically modified sediments, are most abundant towards the basin margins where topographic gradients are relatively steep and water tables are relatively low.

Underfilled lake-type basins can contain subaerially exposed alluvial facies and terrestrial trace fossils near the basin center, such as in the Wilkins Peak Member in the central Bridger subbasin (Scott 2010). The stratigraphic packaging of distinct lithofacies macroassociations can be sharply juxtaposed in underfilled lake-type basins, with very different sets of sedimentary and hydrochemical conditions represented by a sharp contrast between stacked lithofacies assemblages (Smith et al. 2014). Sharp contrasts in the vertical packaging of sediments and trace fossils assemblages are present in underfilled basins because the entire sediment and solute load in the

basin accumulates, and any changes in the amount of water input to the basin are reflected in the sedimentary record. Shorelines fluctuate at a variety of scales in underfilled basins, and their movement across the basin floor can be followed using by trace fossils (e.g., *Skolithos*, *Taenidium*).

In contrast, the shorelines of lakes in overfilled lake-type basins are relatively stable and lake-margin areas are typically wet and poorly drained (Bohacs et al. 2000). The lakes are fresh because water and solutes are able to spill over the lake-bounding sill. Sedimentation is dominated by siliciclastic deposition, and terrestrial, lake-margin, and lacustrine facies associations contain very little carbonate sediments (Bohacs et al. 2000). Trace fossil assemblages in these lake-type basins are thus dominated by burrows produced in sandy soft substrates by organisms that are most abundant in freshwater habitats, such as gastropods, bivalves, ostrocodes, and oligochaetes (Buatois and Mángano 2004, 2009; Bohacs et al. 2007). The trace fossil assemblages are associated with freshwater shallow lacustrine and siliciclastic lake margin environments, such as those present in the Luman Tongue of the Wasatch Formation, Wyoming (Bohacs et al. 2007) and the lower portion of the Tipton Member in the Greater Green River basin (Fig. 12.3). Shorelines remain near the basin margins in overfilled lake-type basins, and terrestrial trace fossils are not present in basin center deposits.

The aerial extent of lakes in balanced-fill lake-type basins fluctuates between expanded water bodies that nearly fill the basin when lake waters are at the bounding sill, and restricted water bodies during times of decreased rates of water and sediment input or subsidence in the basin (Bohacs et al. 2000). These types of lakes preserve thick packages of lacustrine oil shales in basin margin and basin center areas, such as the Rife Bed of the Tipton Member and the LaClede Bed of the Laney Member of the Green River Formation in Wyoming. The balanced fill lakes were probably deeper than underfilled lakes, and were stratified, saline, and oxygen-poor. Trace fossils are not typically observed in oil shales, and during times of expanded balanced fill lake-types, trace fossil assemblages are thus limited to lake-margin environments at the basin margins (Fig. 12.4). During times of restricted lakes, such as the evaporitic shallow lacustrine and lake-margin facies of the Buff Marker of the Laney Member in the Washakie subbasin, simple traces were produced in soft substrates (e.g., *Planolites*). Possible vertebrate footprints maybe preserved in very shallow water or emergent sediments. This trace fossil assemblage is similar to the evaporitic mudflats of the underfilled Wilkins Peak Member, but with substrates relatively soft and wet. Lake-margin deposits from the transition of balanced fill to underfilled lake-type in the Uinta basin, as in the Soldier Summit area (Fig. 12.5), contain trace fossils characteristic of emergent, but not hypersaline, settings.

Basin center areas in balanced fill lake-type basins typically remain filled with water until the basins are eventually filled with sediment from progradational deltaic sediments, such as the Sand Butte Bed of the Laney Member, Wyoming (Smith et al. 2008c; Chetel and Carroll 2010). Trace fossils may be lacking from entire sedimentary successions of basin center deposits in balanced fill lake-type basins if the lakes remained stratified and oxygen-poor, as seen in the majority of the LaClede Bed of the Laney Member. Fossil Lake in Fossil Basin, Wyoming, however, provides an example demonstrating that oxygenation events in balanced-fill lake-type basin can contribute to the formation and preservation of fish swimming and feeding traces on horizons that are interbedded with fish body fossils (Martin et al. 2010).

12.3 Environmental Conditions Influencing Trace Fossils in the Green River Lake Basins

12.3.1 Subaerial Exposure

Some types of trace fossils are good indicators of very shallow water depths or the subaerial exposure of a substrate (e.g., vertebrate footprints, *Taenidium baretti*), but many of the trace types present in lake basins are simple in form and are

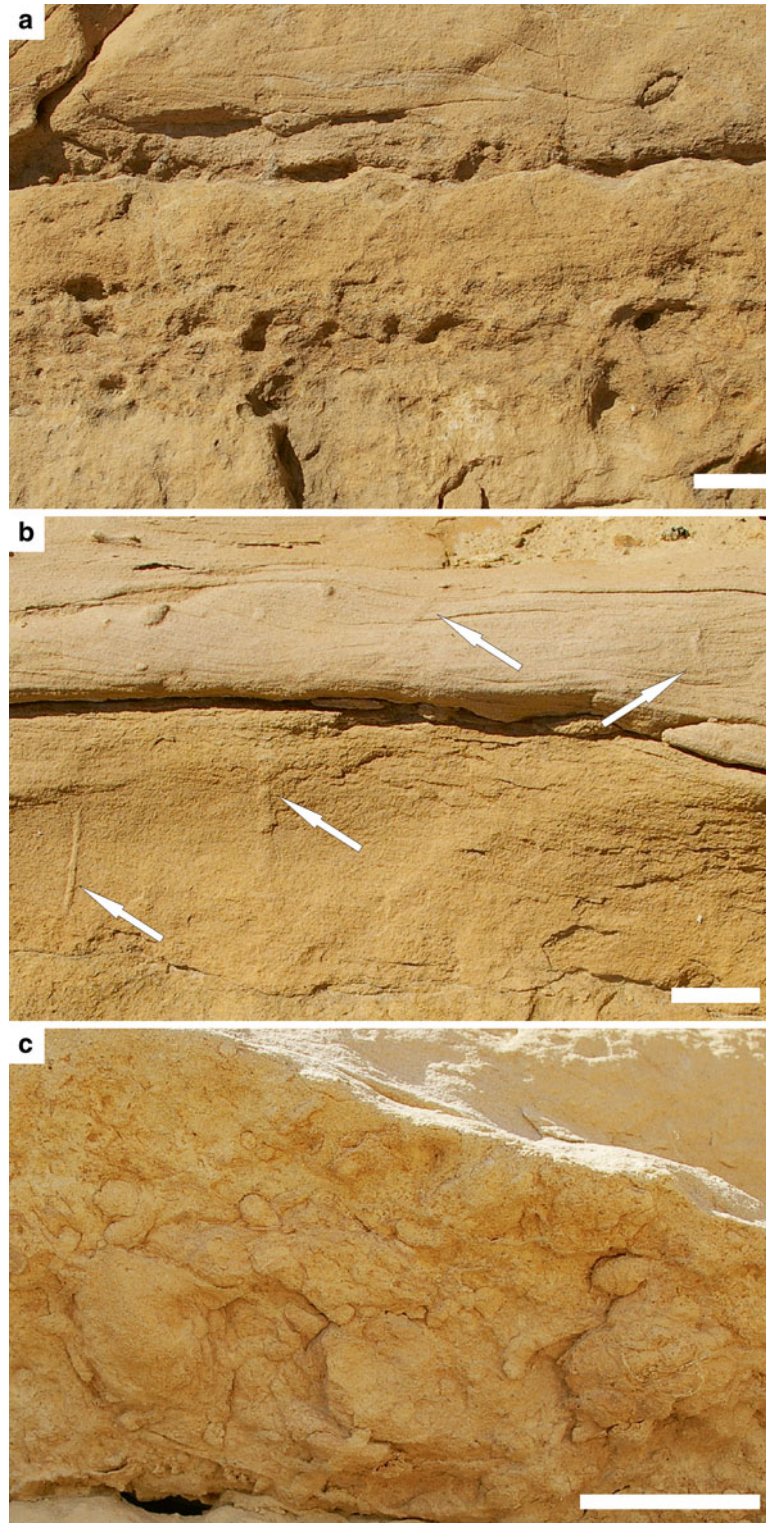

Fig. 12.3 The overfilled Tipton Member in the southern Bridger subbasin (Pipeline east section). All scale bars 2 cm. (**a**) Heavily burrowed horizons with simple burrows in soft substrates (*Planolites* and *Palaeophycus*); note bivalve shell at top right. (**b**) Simple vertical to oblique burrows (*Skolithos*) in soft sandy substrate (*arrows*). (**c**) Bivalve resting traces (*Lockeia*) and simple burrows in soft substrate on the base of heavily bioturbated horizon

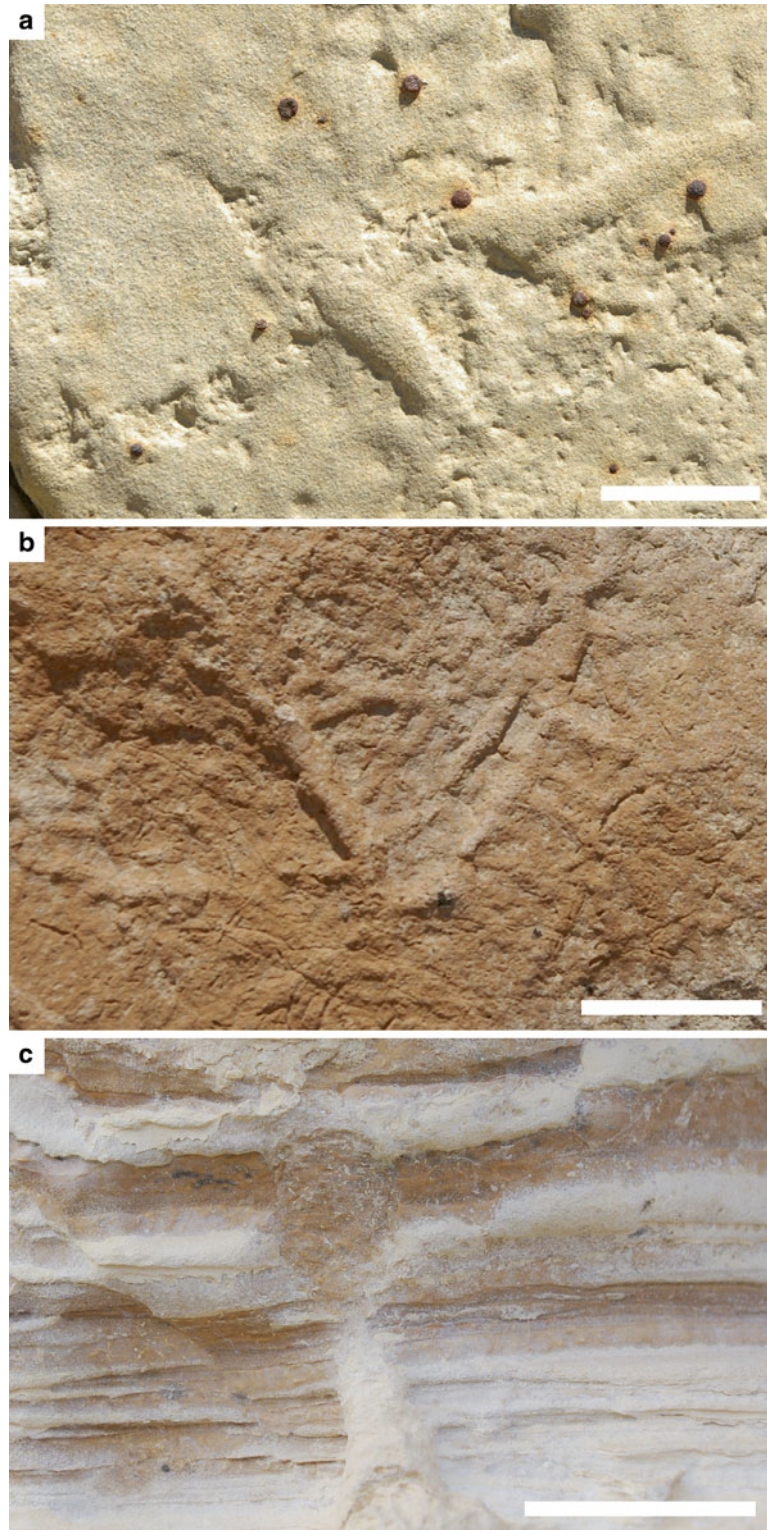

Fig. 12.4 The balanced fill Laney Member in the Greater Green River Basin, Wyoming. All scale bars 2 cm. A-C, fluvio-lacustrine facies at North Barrel Springs on Delaney Rim, Washakie subbasin. D-E, Buff Marker at Trail Dugway on Kinney Rim, Washakie subbasin. F, Lower LaClede Bed at Wildhorse Draw, southern Bridger subbasin. (**a**) Cross-cutting backfilled burrows in soft sand substrate, with poorly defined bioturbation. (**b**) High density cross-cutting simple horizontal burrows in soft substrate (*Planolites*). (**c**) Heterolithic organic-rich and organic-poor shallow lacustrine carbonates burrowed by vertically oriented meniscate backfilled burrow (*Taenidium*)

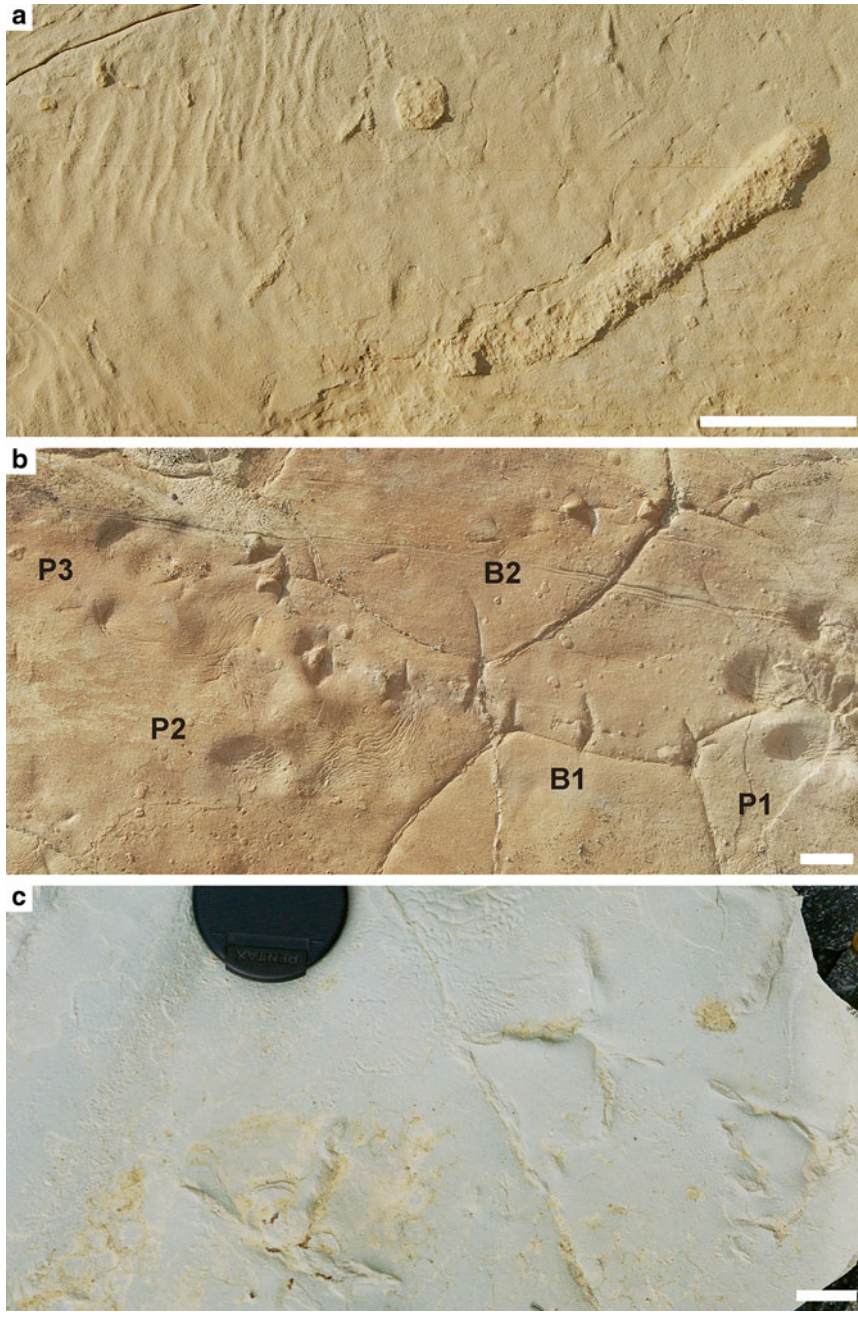

Fig. 12.5 The balanced fill to underfilled basin transition in the Soldier Summit area, Utah. Scale bars all 2 cm. (**a**) Field photo of very thin carbonate mudstone bed with surface texture similar to "elephant skin", showing cohesiveness of muddy substrate. Traces on surface include tiny invertebrate trails and backfilled burrows cross-cutting surface. (**b**) Field photo of well preserved vertebrate footprints on desiccated mudstone bed, including two trackways of a plover-like bird (numbered B1 and B2), and one trackway of 3-toed perissodactyl (3 footprints on slab, numbered P1, P2, and P3). (**c**) Deeply impressed bird footprints in carbonate mudstone bed

not diagnostic of either subaerial or subaqueous depositional environments (e.g., *Planolites*, *Skolithos*). It is important to consider the detailed morphology of the traces, such as the sharpness of the burrow margins (e.g., sharp or soft) and any preservation of ornamentation (e.g., scratch traces), the type of fill (e.g., aggregate backfilled), and cross-cutting relationships between traces and other sedimentary features (e.g., desiccation cracks). For example, *Skolithos* produced in soft-substrate sandstones of the Tipton Member of the southern Bridger subbasin are associated with high-intensity burrowed horizons with *Planolites* (Fig. 12.3). The traces originate from several horizons within a ~4 m thick sandstone package and are interpreted to have been produced in shallow lake waters and preserved in fluvio-deltaic deposits. In contrast, sharp-walled *Skolithos* burrows are present in thin bedsets of calciclastic sandstones (~1 m) interpreted as storm deposits of the Wilkins Peak Member in the southern Bridger subbasin (Scott et al. 2012a, fig 10b). The traces originate only from the uppermost horizon of the bedset, and extend downwards into a wave-ripple-laminated substrate. All evidence within this thin sedimentary package together shows that lake-levels dropped, and that the burrows were probably produced on the freshly subaerially exposed substrate, possibly by tiger beetle larvae.

12.3.2 Substrate Consistency

Details in the morphology of vertebrate footprints and invertebrate burrows, trails, and trackways provide clues to the degree of water saturation in substrates at the time of trace formation, and help to interpret the drainage of subaerially exposed substrates (e.g., Laporte and Behrensmeyer 1980; Davis et al. 2007). The trace morphology can indicate whether or not the traces were produced in saturated substrates of lacustrine environments, or in subaerially exposed, firm and moist substrates (e.g., Genise et al. 2009). Microbially bound or clay-rich substrates preserve a greater degree of morphological detail than substrates lacking some way of stabilization before preservation (e.g., Marty et al. 2008; Scott et al. 2010; Carmona et al. 2012). Determining the substrate consistency at the time of trace formation can be useful for interpreting whether the traces were produced syn-depositionally or whether the traces were formed post-depositionally under different conditions than those affecting the deposition of the sediment. Recognizing this gap in time is especially important for using terrestrial trace fossils for stratigraphy.

Vertebrate footprints can be used to interpret substrate consistency (e.g., Scrivner and Bottjer 1986) using four main categories: (1) soft, soupy and fully saturated sandstones; (2) wet to saturated, partially stabilized sandstones; (3) wet to saturated, partially stabilized carbonate mudstones; and (4) firm, desiccating carbonate mudstones, siltstones, and sandstones. In the Wilkins Peak Member of Wyoming, deeply impressed and poorly formed mammal footprints preserved in cross-section (Category 1) in the basin-center arkosic sandstones of delta-plain environments show that the sands were saturated or were within very shallow water when the footprints were produced (Fig. 12.6a–b). Mammal and bird footprints and reptile swimming marks in similar environments retain some morphological features of the producers (Category 2) and show that the traces were produced in substrates that were stabilized in some way, either by slightly desiccated clays or by microbial mats (Fig. 12.6c–d and 12.7a–b). Examples of footprints in Category 2 are often associated with sedimentary features characteristic of very shallow standing water, such as low-amplitude symmetrical ripples. Deeply impressed bird footprints that preserve the original morphology of the impressions (Category 3) were observed near Soldier Summit, Utah, and are interpreted to have been produced in wet, soupy substrates of mudflats and muddy pools on lake margins (Fig. 12.5c). It appears that the carbonate mud was sufficiently cohesive to retain the original morphology of the tracks. Mammal and bird footprints that are shallowly impressed and retain some morphological detail of the original tracks (Category 4) were produced in firm and moist substrates, and/or were

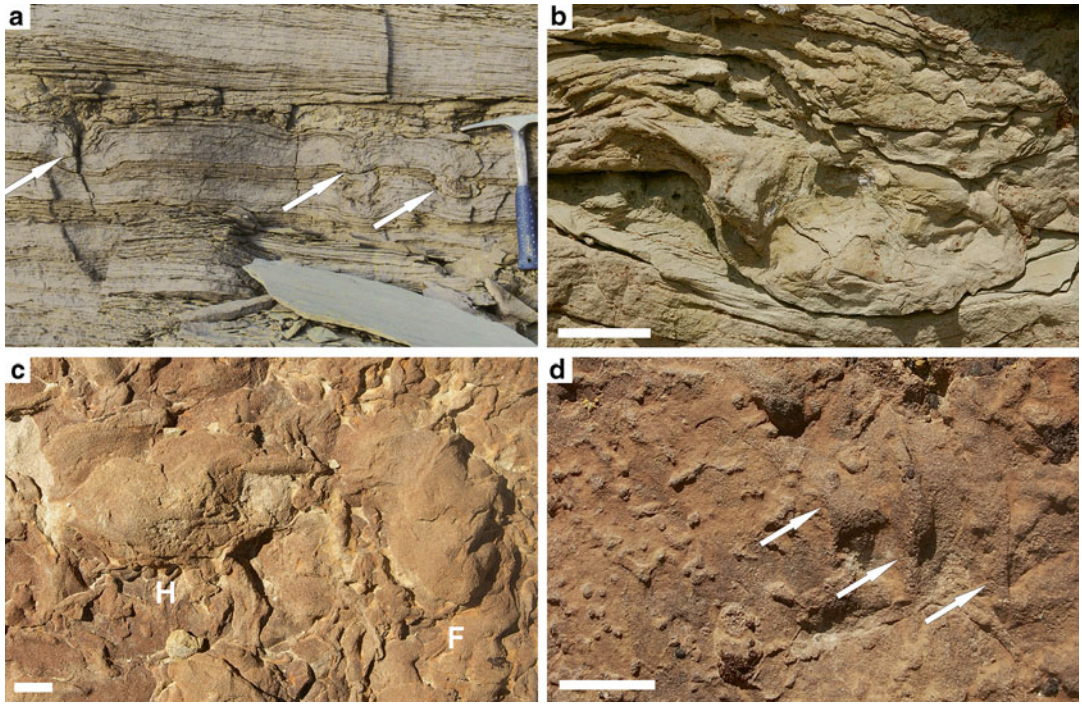

Fig. 12.6 Mammal footprints in saturated sandy substrates of the basin center clastic units of the Wilkins Peak Member in the Bridger subbasin. All scale bars 2 cm. (**a**) Multiple deeply impressed small mammal footprints (*arrows*) into rippled and thinly bedded arkosic sandstone unit "D" at Kanda, White Mountain. Hammer for scale. (**b**) Close-up longitudinal section of mammal footprint in the lower part of the arkosic sandstone unit "D" at Firehole Canyon. (**c**) Reptile footprints in the arkosic sandstone "D" at Firehole Canyon. F – front, H – hind. (**d**) Reptile claw marks (*arrows;* swimming traces) with simple burrows (*Planolites*) in substrate possibly stabilized with clay and organic film, in "D" sandstone at Firehole Canyon

underlain by packed sediment (Fig. 12.5b and 12.8a–b), or in tuffs (e.g., the "Strawberry Slab", Lockley et al. 1999). Environments of deposition associated with this morphological category include shoreline areas on low-gradient evaporitic mudflats or small, drying pools on lake-margin plains. Shallowly impressed mammal footprints that are associated with evaporite pseudomorphs are typically poorly preserved in substrates that may have been disrupted by salt efflorescence (Fig. 12.8; cf. Scott et al. 2010).

12.3.3 Drainage

The depth and orientation of burrows produced by air-breathing invertebrates, whether they are horizontal, vertical, or three dimensional burrow networks, can be used to interpret the position of the water table and the drainage of a substrate (e.g., Hasiotis 2007). In particular, meniscate backfilled burrows (e.g., *Taenidium barretti*, "adhesive meniscate burrows"; Smith et al. 2008b) appear to be the most useful indicator of drainage in the Green River and correlative formations. Small (~4 mm diameter) and medium-sized (~7 mm diameter) meniscate backfilled burrows with dominantly horizontal orientations are associated with sedimentary features that indicate a moist to wet substrate, typically interpreted as being near the lake shoreline (Fig. 12.9). In contrast, the larger meniscate backfilled forms (~2 cm diameter) may be present in horizontal orientations at shallow depths from the paleosurface from which the burrows originated, or they may be dominantly vertical up to ~1.5 m depth

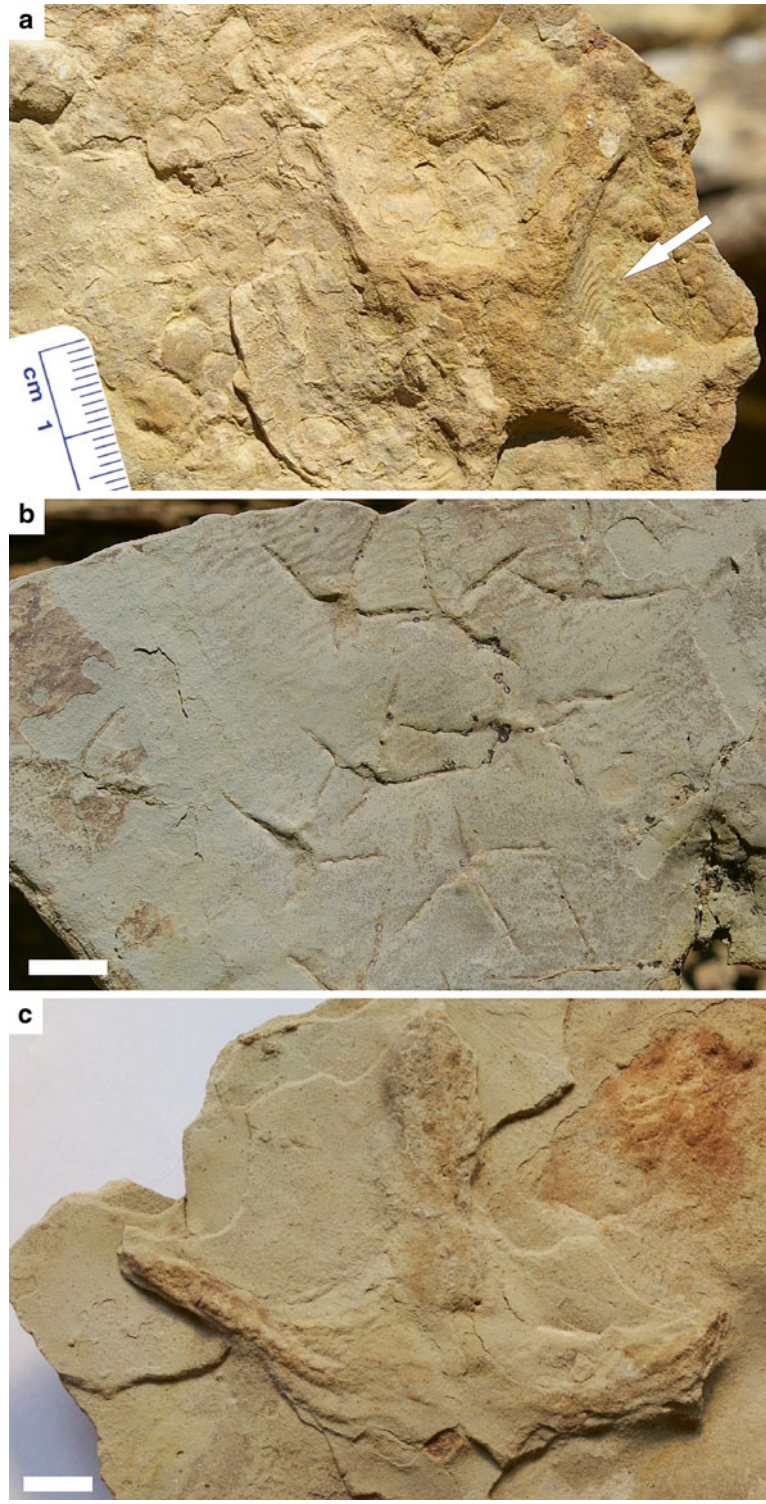

Fig. 12.7 Bird footprints in the basin center clastic unit "A" of the Wilkins Peak Member in the Bridger subbasin at Firehole Canyon. All scale bars 1 cm. (**a**) Cast of bird footprint preserving skin impressions on footprint wall (*arrow*). (**b**) Several plover-like bird footprints preserving micro-ripples or "elephant skin" texture showing clay stabilization of substrate. (**c**) Cast of large *Presbyornis*-like bird footprint

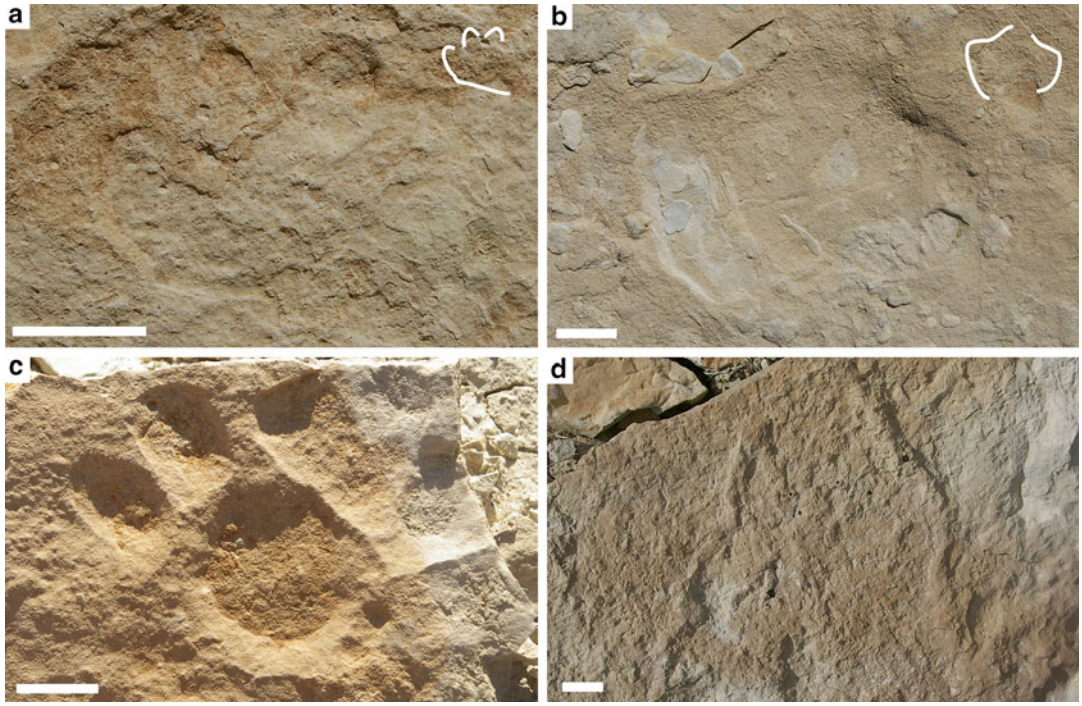

Fig. 12.8 Trace fossils from the evaporative mudflat facies in the basin center Wilkins Peak Member, Bridger subbasin, Wyoming. All scale bars 2 cm. Line drawings showing interpretations of footprints. A-D – at Firehole Canyon above the "D" sandstone. (**a**) Plan view of 4-toed (probable perissodactyl) footprint into firm substrate with possible salt efflorescence. (**b**) Plan view of relatively well preserved 3-toed footprint (probable perissodactyl). Note broken mudchips on surface. (**c**) Plan view of carnivore footprint showing 4 digits and metatarsal pad. Note that margins of footprint are sharp but fine details are not preserved, possibly due to salt efflorescence. (**d**) Plan view of two large invertebrate tunnels on top surface of bed. Irregular morphology is attributed to salt efflorescence

(Fig. 12.9). Examples of these deeply penetrating burrows were observed in several places in fluvio-deltaic sandstone deposits with trough cross-stratification or climbing ripples (e.g., Slate Creek, western Bridger subbasin). Simple vertical burrows (*Skolithos*) are also sometimes more than half a meter in depth, such as in the rippled sandstones of splay-like fans near the shoreline in the underfilled basin center (Fig. 12.10a–d; e.g., Wilkins Peak Member, Bridger subbasin) or at the balanced fill basin margin (Fig. 12.10e; e.g., Tipton Member, southern Bridger subbasin). These large burrows were probably produced by tiger beetles or spiders once the substrate was exposed. Deep, vertically oriented examples of *Taenidium* and *Skolithos* are common in laminated and rippled sandstones beds more than ~50 cm thick, which are interpreted to be well drained. In contrast, the smaller, horizontally oriented examples are preserved in siltstones and carbonates, and are interpreted to signify that the water table was relatively high when bioturbation took place and substrates were poorly drained.

12.3.4 Sedimentation Rate and Hiatuses

Burrow intensity and the vertical distribution of trace fossils from marine and lacustrine deposits can be used to interpret sedimentation rates, and they can also show whether or not deposition was episodic or continuous (Buatois and Mángano 2007; Gingras et al. 2011). In the arkosic sandstones of the basin center Wilkins Peak Member, Wyoming, for example, sedimentary structures

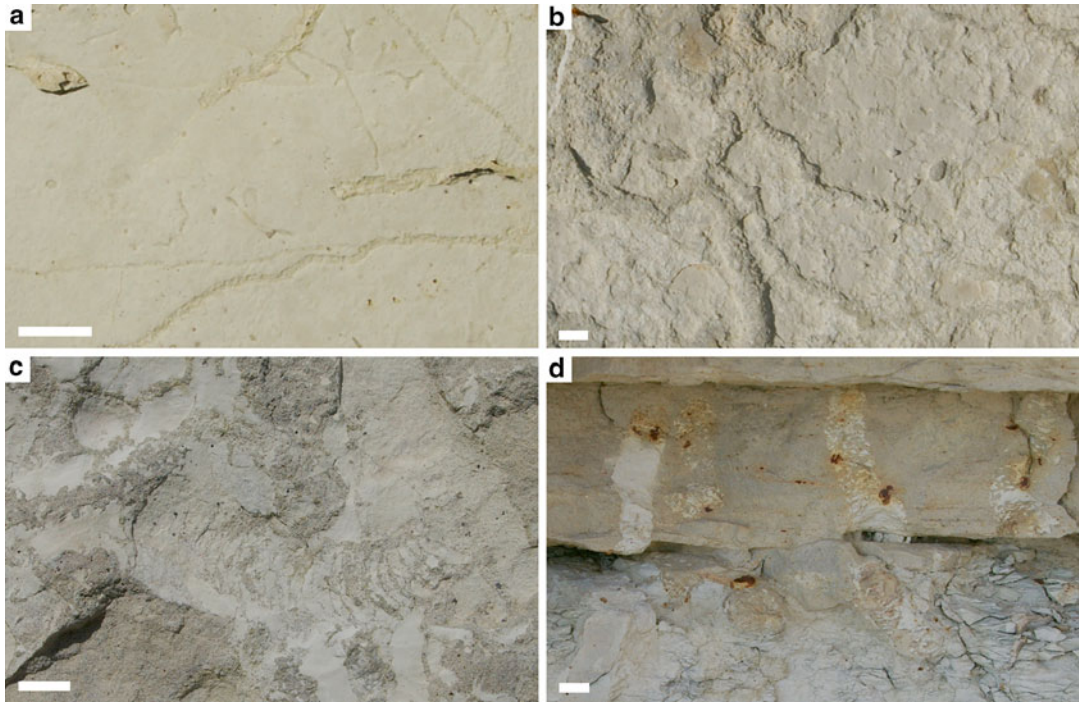

Fig. 12.9 Backfilled burrows in lake-margin deposits at Slate Creek on the western margin of the Bridger subbasin. All scale bars 1 cm. (**a**) Small-sized (~3–4 mm diameter) backfilled burrows and trails (~1–2 mm diameter) in laminated carbonate mudstone from emergent very shallow lacustrine sediments. (**b**) Dominantly horizontal medium-sized (~7–10 diameter) backfilled burrow networks in desiccating mudflat sediments. (**c**) Horizontally oriented large-sized (~25 mm diameter) meniscate backfilled burrow cross-cutting carbonate mud drape deposited on mudflat/very shallow lake. (**d**) Vertically oriented large-sized (~18 mm diameter) meniscate backfilled burrows penetrating through fluvial sandstones into underlying mudstones. Note muddy fill of burrows. Burrows extend for another meter into substrate below

such as climbing ripples in very fine- to fine-grained sandstones, dune-scale cross bedding, and large-scale trough cross-stratification are associated with the progradation of clastics into the lake. The sedimentary structures alone are not diagnostic of continuous or episodic deposition or of any particular depositional environment. However, when ichnology is used in conjunction with sedimentology, sedimentation rates and episodic deposition is recognized and used to interpret the arkosic sandstone units as delta-front clinothems, sheet floods, or channel bars. Trace fossils such as *Skolithos*, *Helminthoidichnites*, *Taenidium barretti*, and *Planolites* mark horizons within the sandstone successions that represent standing water or waning flow during periods of slow deposition in channels on the delta plain.

In some thick packages (up to 5 m thick) of climbing rippled very fine- to fine-grained sandstones interpreted as mouth bars in the basin center arkosic sandstones, trace fossils are lacking, and the association with water escape structures and sheared rippled crests help to demonstrate that the deposition was continuous and within the lake (Fig. 12.10a). In contrast, some packages with climbing rippled fine-grained sandstones lack water escape structures and contain deep vertical burrows produced by terrestrial organisms (Fig. 12.10d). Although deposition was likely nearly continuous, there were periods of quiescence in these distal splays or sheet flood deposits onto the delta-plain (Fig. 12.10b–d). These examples illustrate the utility of invertebrate burrows to help recognize variable sedimentation

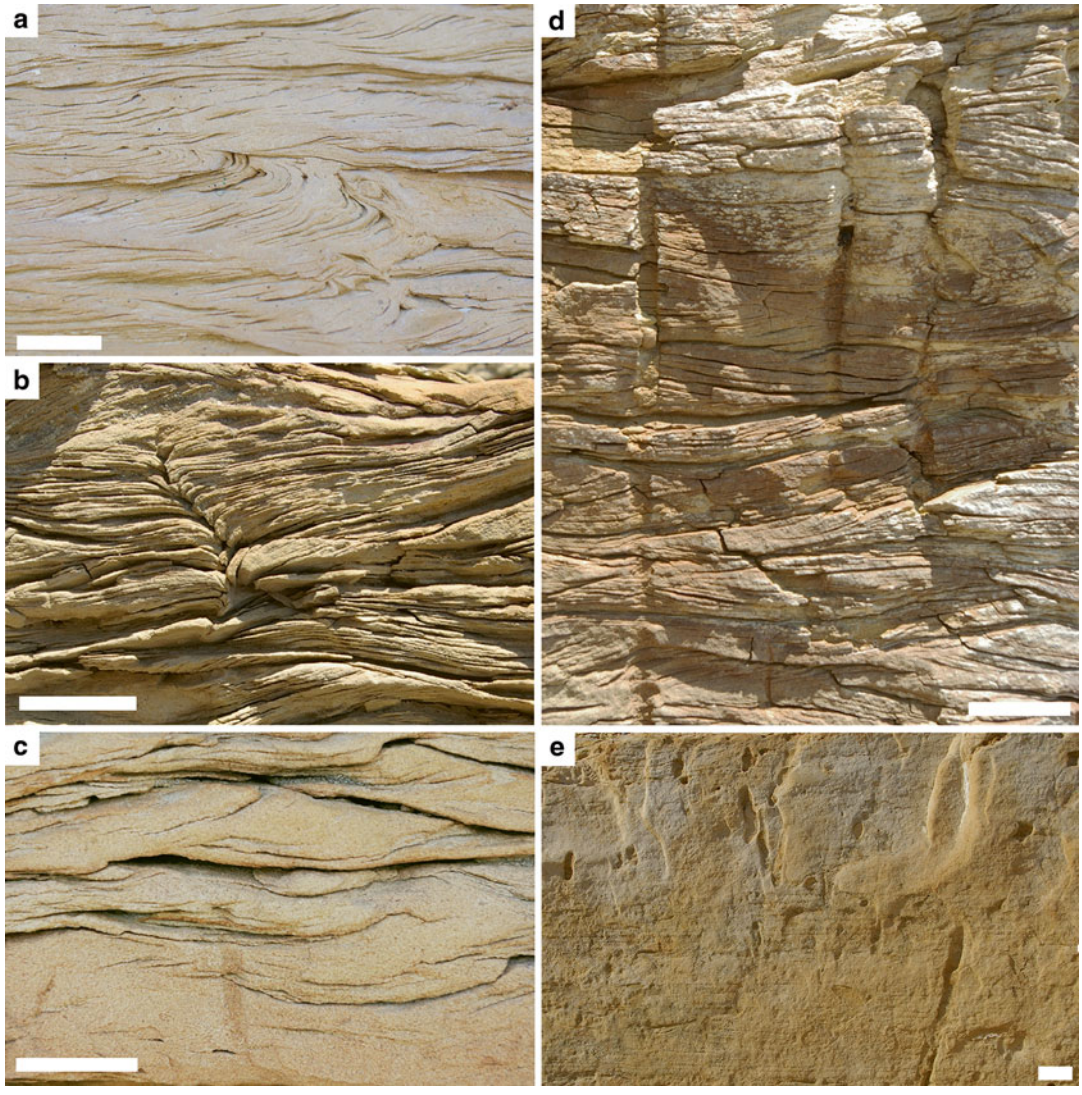

Fig. 12.10 Vertical burrows as evidence of sedimentation rate and subaerial exposure in fluvio-lacustrine and deltaic sandstones of the basin center Wilkins Peak Member (A-D) and basin margin Tipton Member, Bridger subbasin (E). All scale bars 2 cm. (**a**) Sheared ripple crests in climbing rippled bedset of the deltaic sandstone "D" at Chicken Springs Draw in the Firehole Canyon area, basin center Wilkins Peak Member. Sedimentation rate high; no bioturbation. (**b**) Downward-deflected laminae of "escape trace" in rippled sandstones of the delta-plain sandstone "A" in Middle Firehole Canyon. Sedimentation rate high but periodic. (**c**) Small-sized *Skolithos* vertical burrow in rippled sandstone of fluvio-lacustrine facies at top of "A" sandstone in Middle Firehole Canyon. Sedimentation rate lower and periodic. (**d**) Medium-sized vertical burrows (*Skolithos*) through rippled sandstone on delta-plain of "A" sandstone at Middle Firehole Canyon. Subaerial exposure following deposition. (**e**) Vertical to oblique burrows (*Psilonichnus*-like, *Skolithos*) in exposed foreshore sandstones of the basin margin Tipton Member in the Pipeline area

rates (e.g., escape traces), as well as to help determine if deposition occurred within Lake Gosiute or on the surrounding delta plain.

In terrestrial deposits, trace fossils typically do not reflect the sedimentation rate of the substrate because they are produced during the pedogenic modification of the substrate after its deposition. However, terrestrial traces can be used together with other pedogenic features (e.g., degree of ped formation) to approximate the time represented by the paleosol, and to infer how long the deposit was stable before deposition of overlying sediment (Genise 2004; Hasiotis 2007; Bedatou et al. 2009). Well developed social insect nests require extended periods of time to become established (e.g., Hasiotis 2007). In the uppermost beds of the progradational arkosic sandstones in the basin center Wilkins Peak Member for example, a small social insect nest, possibly produced by ants, demonstrates that the paleosurface was stable and exposed to the air for at least a year or two (Fig. 12.11a). Deeper, larger ant

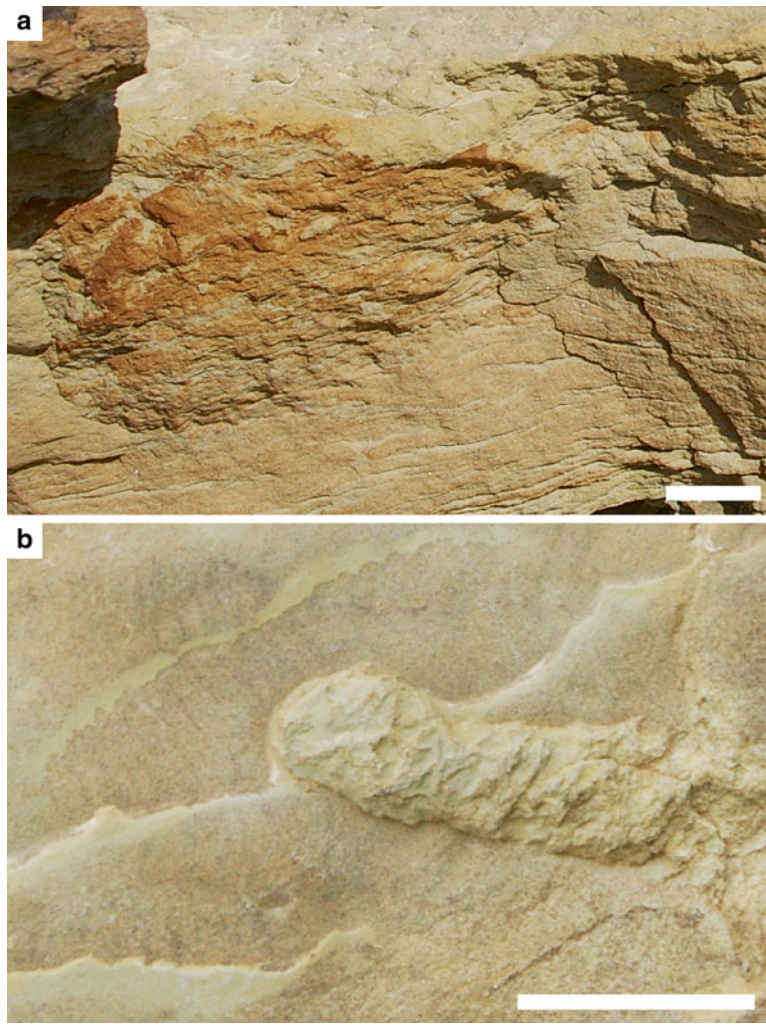

Fig. 12.11 Terrestrial trace fossils of the underfilled basin center in the sandstone unit "A" at Middle Firehole Canyon, Wilkins Peak Member, Bridger subbasin. All scale bars 2 cm. (**a**) Insect nest, possibly produced by ants, in rippled fluvial sandstones at the top of the "A" sandstone. Note sharp margins of nest and high density simple burrows within nest area. (**b**) Well preserved backfilled burrow with scratch marks in clayey sand substrate (*Steinichnus*)

nests in the paleosols of the Colton Member of the Wasatch Formation in the Uinta basin show that the paleosols there were stable for an extended length of time (Golab 2010). Other examples of bee nests (e.g., *Celliforma*) and beetle brood cells (cf. *Coprinisphaera*) in weakly developed sandy paleosols in the Uinta basin (Golab 2010) and the southern Bridger subbasin help to demonstrate that those substrates were stable and exposed to the air for at least a year.

12.3.5 Salinity

The Green River lakes varied in their salinity from freshwater to saline to hypersaline in different parts of the lake system at different times (e.g., Smith et al. 2008c). Evidence for paleosalinities includes evaporite minerals (e.g., Bradley and Eugster 1969; Deardorff and Mannion 1971) and stable isotopes (Doebbert et al. 2014). Gastropod and ostracode body fossils (e.g., Roehler 1988) and caddisfly larval cases (e.g., Leggitt et al. 2007) are present in the freshwater environments of the different lake-types (Fig. 12.12). In the saline to hypersaline lakes of underfilled basins however, body and trace fossils are rare except in isolated areas with localized freshwater input (Leggitt 2007; Scott 2010). Trace fossils are commonly lacking in and around the saline and hypersaline lakes, probably due to hydrochemical stresses that preclude bioturbation or high interstitial salinities that lead to salt efflorescence and the poor preservation of burrows (cf. Scott et al. 2010).

The Wilkins Peak Member in the Bridger subbasin records fluctuating salinities in Lake Gosiute and climate-related periods of clastic and freshwater input (e.g., Smith et al. 2014). Trace fossils are preserved in saline to hypersaline lake-margin deposits (e.g., evaporitic mudflats) or in the areas where there was freshwater input into the lake (e.g., fluvio-deltaic areas and adjacent shallow lacustrine; Fig. 12.13a). The trace fossil assemblage typical of very shallow saline lacustrine environments is limited to simple forms of invertebrate traces present in high densities (e.g., cross-cutting *Helminthoidichnites*), and in some cases include diminutive vertical burrows (e.g., *Skolithos*, *Polykladichnus*) that were probably produced by insect larvae (Fig. 12.13b–c; Scott 2010). A moderately diverse assemblage of poorly preserved vertebrate footprints is also characteristic of these settings, including medium- to large-sized perissodactyls, as well as some medium to large-sized carnivores (Fig. 12.8). In deposits laterally or vertically adjacent to sites of freshwater input

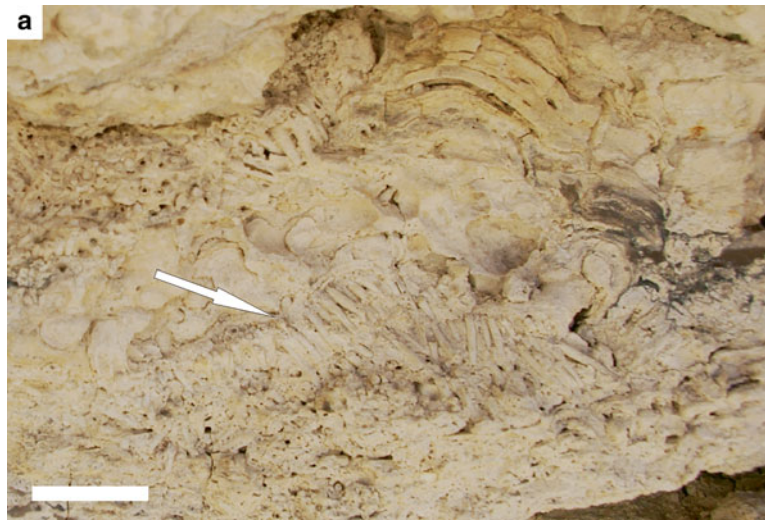

Fig. 12.12 Lacustrine caddisfly cases in freshwater shallow lacustrine facies at Reardon Draw in the Northern Bridger subbasin. Scale bar 2 cm. (**a**) Interbedded oriented caddisfly cases with laminar stromatolite

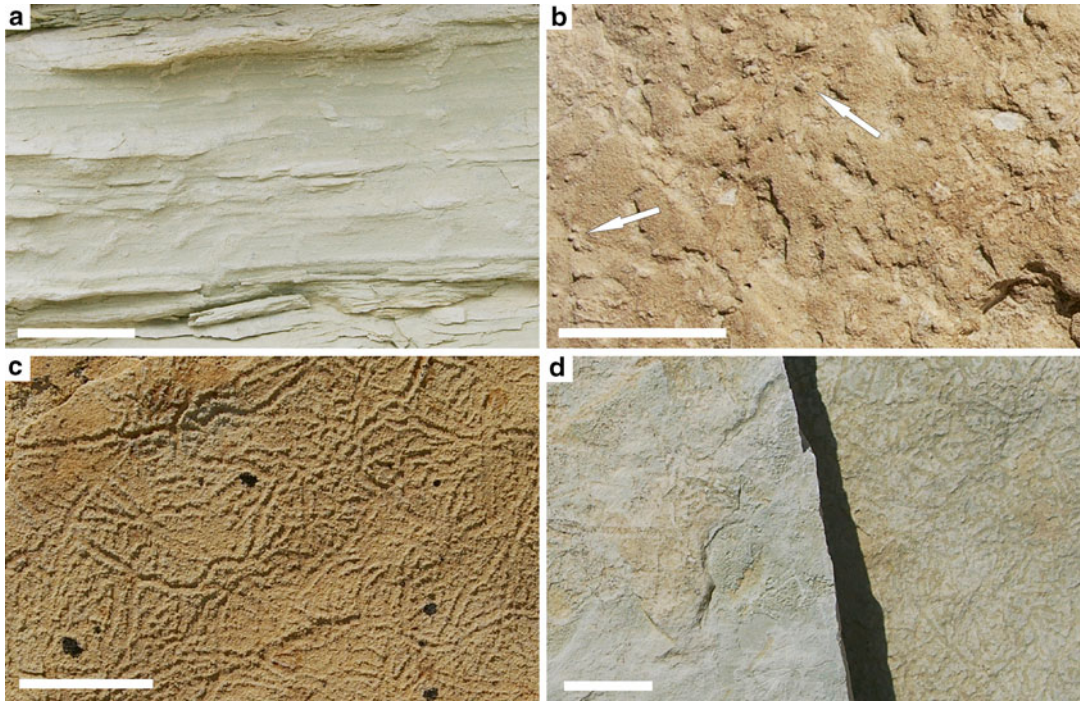

Fig. 12.13 Shallow saline lacustrine trace fossils in the Wilkins Peak Member in the Bridger subbasin. All scale bars 2 cm. (**a**) Laminated organic-rich lacustrine marl within the "A" sandstone in Middle Firehole Canyon with vertical and oblique simple burrows (*Skolithos*, *Planolites*). (**b**) Plan view of very small vertical burrows (*Skolithos*, *Polykladichnus*) and horizontal burrows (*Planolites*) in carbonate siltstone. (**c**) Bedding plane view of dense cross-cutting trails (*Helminthoidichnites*) in calcitic very shallow lacustrine unit above the "D" sandstone at #18 Crossing on White Mountain. (**d**) Densely cross-cutting simple trails (*Helminthoidichnites*) on bedding planes of dolomitic mudstone in sublittoral facies above the "E" sandstone at Firehole Canyon

(e.g., arkosic fluvio-deltaic sandstones), structureless carbonate siltstones and mudstones deposited in lake marginal areas also preserve mm-scale iron-stained root marks and impressions of sedges or grass stems. These areas are interpreted as paludal marshes surrounding the lake. Deeper, sublittoral lacustrine deposits (e.g., kerogen-poor dolomitic mudstones) preserve rare and low-density simple trails (e.g., *Helminthoidichnites*) on bedding planes (Fig. 12.13d), but stagnant profundal environments that preserve oil shales do not contain trace fossils. These associations are typical of underfilled lake-types, which are well represented by the Wilkins Peak Member in Wyoming, and are also typical of some facies in of balanced fill lake-types, as represented by the Laney Member in Wyoming.

In contrast, freshwater lacustrine deposits represented by the overfilled Schegg's Bed of the Tipton Member in the Greater Green River basin preserve an assemblage of burrows (e.g., *Planolites*, *Palaeophycus*, *Skolithos*, *Arenicolites*, *Lockeia*) in soft sandy substrates within the lake (Fig. 12.3). This relatively diverse trace fossil assemblage demonstrates that the lacustrine conditions were not stressful environments for the trace-producing organisms, which probably included oligochaetes, insects, and/or molluscs. In many cases, these burrows are associated with gastropod and bivalve shells, which further support this interpretation for the trace fossils. Vertebrate footprints have only rarely been found in lake margin areas associated with the freshwater Green River lakes.

12.3.6 Oxygenation

Kerogen-rich oil shales almost certainly represent lacustrine environments that lacked oxygen, and which were below the chemocline/thermocline. The preservation of the oil shales does not necessarily mean that the lakes were deep, but that they were stratified. Stratification of lakes occurs when the shallow waters are lower in density than the deeper waters, which can be due to higher salinities or lower temperatures in deeper waters (e.g., Cohen 2003). In modern tropical areas for example, air temperatures do not vary sufficiently between seasons to cause water bodies to overturn, and bottom waters become increasingly saline and oxygen-poor due to continued evaporation and lack of mixing with the atmosphere (e.g., Cohen 2003). Profundal facies associations are associated with these meromictic stratified lakes and also with high organic contents in lake sediments (e.g., Bohacs et al. 2000). With increasing salinity, water is capable of holding a decreasing amount of oxygen (Williams 1998). This association may have played a role in the preservation of widespread oil shale deposits, and also the lack of trace fossils in these facies.

Examples of trace fossils in sublittoral to profundal facies of the Green River Formation include fish swimming trails in lacustrine dolomitic shales of Fossil Lake, Wyoming (Loewen and de Gibert 1999; Martin et al. 2010), which demonstrate that oxygenation events affected the lake bottom waters. Fish body fossils are extremely abundant in the profundal lake deposits, which suggests that there were some freshwater areas in the lake, or that the epilimnion was fresh above the chemocline/thermocline. During mixing and oxygenation events, fish such as suckers (*Notogoneus*) swam to the lake floor to feed on detritus and possibly also on dead fish. The trace fossil evidence shows feeding marks of the suckers (Martin et al. 2010), and swimming marks circling in laminae just overlying fish body fossils (A. Aäse, pers. comm. 2013).

12.3.7 Taphonomic Processes

Environmental conditions that influence the taphonomy of trace fossils in the Green River basins are mainly related to: (1) high sedimentation rates and/or high flow velocity in fluvial channels; (2) the disruption of subaerially exposed substrates by salt efflorescence; (3) desiccation and repeated wetting and drying; and/or (4) the presence of roots. The effects of salt efflorescence are especially apparent on the poorly preserved mammal footprints of hypersaline lake margins in the Wilkins Peak Member in the central Bridger subbasin (Fig. 12.8). Evaporite (e.g., trona) pseudomorphs are also present. Rare examples of horizontally oriented insect burrow systems in these same deposits also show signs of disruption by efflorescence, which leads to the break-up of the burrow margins (Fig. 12.8d). A consideration of taphonomic processes is necessary before making inferences on the composition of the trace-producing community. For example, the trace fossil assemblage associated with evaporitic mudflats in the hypersaline Wilkins Peak Member does not contain bird footprints, but because of the poor preservation of the larger mammal tracks, it is possible that the lack of bird tracks may be due to destruction by taphonomic processes.

The original morphology of invertebrate and vertebrate trace fossils is partly controlled by the degree of substrate saturation with water, and whether or not the underlying sediments were soft or hard (Laporte and Behrensmeyer 1980; Scrivner and Bottjer 1986; Scott et al. 2010). Carbonate- and clay-rich sediments may retain the original morphology of vertebrate footprints or burrows with sharper burrow margins than clean sandstones. Soupy carbonates, for example, preserve sharp margins of footprints not disrupted later by efflorescence or other processes that lead to the break-up of the most surficial sediments such as desiccation. In contrast, mammal footprints deeply impressed into soupy sandstones have soft, indistinct margins. Sandstones stabilized by clays and/or microbial mats apparently behave similarly to wet carbonate muds by retaining the original

morphology of the traces with distinct boundaries and fine details, such as the tracksites in the Uinta basin (Fig. 12.5; cf. Marty et al. 2008).

12.4 Sedimentary Environments and Trace Fossils in the Green River Basins

12.4.1 Lake Margins to Terrestrial Environments

Most of the trace fossils described from the Green River and correlative formations were produced by air-breathing organisms, such as insects (e.g., D'Alessandro et al. 1987; Bohacs et al. 2007; Scott 2010; Golab 2010) and mammals and birds (e.g., Curry 1957; Moussa 1968, 1970), and possibly gastropods. Trace fossils produced in very shallow water at the lake margins, subaerially exposed mudflats, and other marginal settings such as delta-plains and pools adjacent to the lake typically have moderate to high diversity, although the assemblages show pronounced heterogeneity. They contain vertebrate footprints (e.g., Foster 2001) and several types of burrows, including network-like burrow systems and terrestrial insect nests (Figs. 12.7, 12.11, 12.14; Scott 2010). Terrestrial deposits, outside of the typical range of lake-level rise-and-fall, preserve trace fossils produced in fluvial channels and overbank paleosols in the Wasatch (e.g., Zonneveld et al. 2006; Bohacs et al. 2007) Duchesne River (D'Alessandro et al. 1987), and Colton formations (Golab 2010). Some examples include: (1) large burrows probably produced by crayfish (e.g., *Camborygma*, *Lunulichnus*) in pedogenically modified mudstones that underlie

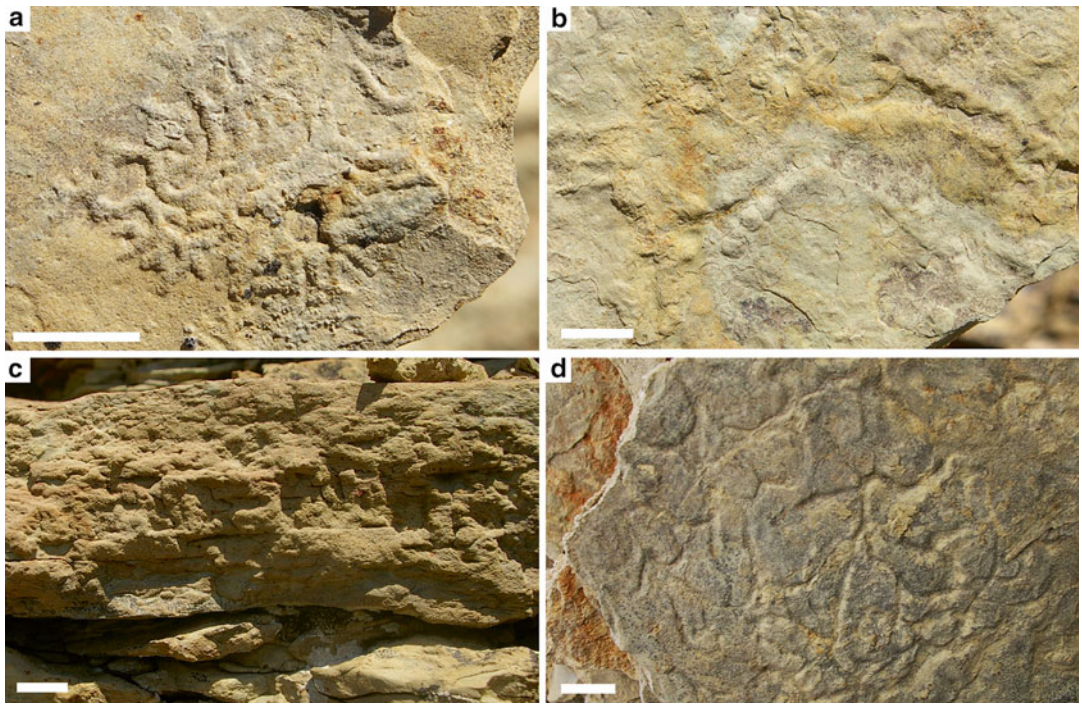

Fig. 12.14 Invertebrate trace fossils in the basin center clastic unit "A" of the Wilkins Peak Member in the Bridger subbasin at Firehole Canyon. All scale bars 1 cm. (**a**) Branching and cross-cutting invertebrate tunnels on top of bed. (**b**) Arthropod trackway in soupy mud showing displaced sediment on top of bed and median furrow. (**c**) High density bioturbation with simple soft-ground burrows (*Planolites* ichnofabric). (**d**) Branching tunnel network (cf. *Vagorichnus*) on base of bed

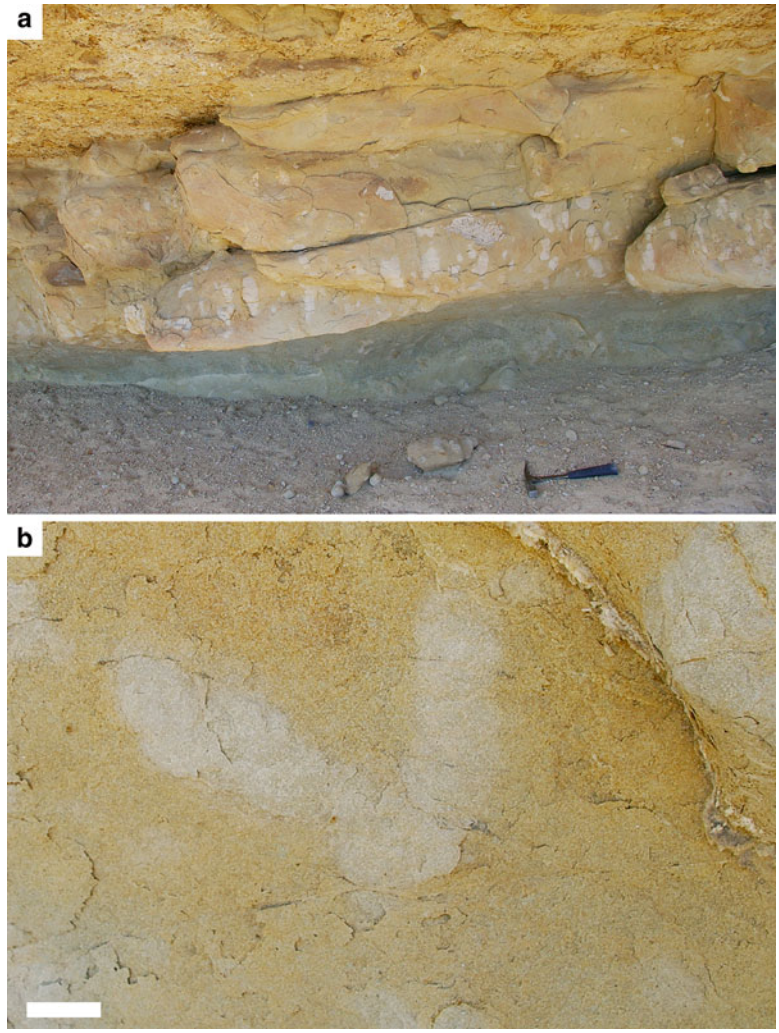

Fig. 12.15 Terrestrial trace fossils in paleosols and alluvial fan deposits at the southern margin of the Bridger subbasin. (**a**) View of trace fossils probably produced by crayfish (*Camborygma*) at the base of the sandstone shown in (a). (**b**) Close-up of branching burrow in sandstone shown in (**b**). Scale bar is 2 cm

channel deposits (Hasiotis and Honey 2000; Zonneveld et al. 2006) and alluvial fans (Fig. 12.15); (2) large carbonate-filled rhizoliths; and (3) insect brood cells and pupation chambers (e.g., *Celliforma*) (Golab 2010). Large (~2 cm diameter) meniscate backfilled burrows (e.g., *Taenidium baretti*) are common in fluvial and crevasse splay sandstones that are intercalated with paleosol mudstones. Some examples show that these burrows originate from paleosurfaces ~ 1–2 m above the bioturbated horizons, such as in the Cathedral Bluffs Member on the western margin of the Bridger subbasin at Slate Creek (Fig. 12.9d). The vertical orientation and great depth of the burrows, produced by air-breathing organisms, demonstrate that the water tables were at or below these levels at the time, and that the substrates were probably well drained.

12.4.2 Deltas

Deltas and delta plains in the Green River Formation are characterized by: (1) siliciclastic sediments containing evidence of trunk channels; (2) crevasse splays and sheet flood deposits; (3) weakly developed paleosols on overbank areas of the proximal to distal delta plain; and (4) mouth bars and bays in the proximal delta front (Culbertson 1961; Bohacs et al. 2007; Schomacker et al. 2010; Scott 2010; Smith et al. 2014). Deltas of overfilled lake-types (e.g., Farson Delta and other Schegg's Bed equivalents, Tipton Member), balanced fill lake-types (e.g., Bitter Creek Delta, Laney Member), and underfilled lake-types (e.g., arkosic sandstones, Wilkins Peak Member) represent Gilbert deltas and shallow water deltas. The facies associations in the different types of deltas are determined by the shoreline stability and depth of lake waters, as well as the amount of sediment input and rate of subsidence. Like the sedimentary facies, the trace fossil assemblages of deltas and delta plains also represent factors such as sediment input and sedimentation rates, stability of shorelines, and the inferred salinity of the lake waters.

Trace fossils are represented by a high diversity of types on delta plains, including: vertebrate footprints (e.g., bird, mammal) and swimming traces (e.g., crocodile, turtle); invertebrate traces produced in well drained subaerial areas (e.g., insect burrows and nests); and invertebrate traces produced in saturated substrates or in areas with thin films of standing water (e.g., insect trails and burrows, oligochaete burrows). Due to the variety of depositional environments in both subaerial and subaqueous settings of deltas, together with freshwater input into saline or hypersaline lacustrine areas, deltas are the most bioturbated setting of the Green River lake system, in overfilled, balanced fill, and underfilled lake-type basins (Fig. 12.16; Scott 2010).

Progradational packages (~5–25 m thick) of arkosic sandstones in Wilkins Peak Member in the central Bridger subbasin provide an example of how trace fossils can reflect an increasing degree of subaerial exposure of the sediments upwards within stacked shallowing upwards successions (Scott 2010). The clastic wedges prograded into the basin center during times of increased sediment input and relatively low lake levels, at times apparently controlled by changing precipitation to evaporation ratios and seasonality as related to eccentricity cycles (Smith et al. 2014). Each of the arkosic sandstone wedges contains two or more shallowing upwards successions separated by lacustrine flooding surfaces (Fig. 12.17). These packages are essentially parasequences, which represent the progradational stacking of clastic wedges deposited in the basin center during lowstands of Lake Gosiute. The units are overlain by lacustrine carbonates that have either sharp contacts with overbank deposits, or gradational contacts with fining upwards beds of siliciclastics deposited in flooded channels during lacustrine transgressions. The trace fossils are helpful for recognizing substrate conditions, for approximating the salinity of lake waters, and they are helpful for recognizing short-term and longer-term subaerial exposure.

Simple lacustrine trace fossils (e.g., *Planolites*, *Helminthoidichnites*) are more common in sublittoral and littoral facies associated with the arkosic sandstones of the Wilkins Peak Member than with lacustrine facies of the saline to hypersaline lake not influenced by freshwater input (Fig. 12.13a). Less extreme conditions would have characterized the areas of freshwater input into Lake Gosiute. Typically, the trace fossil diversity within lacustrine deposits of the saline to hypersaline Lake Gosiute is very low, and traces are simple in morphology (e.g., *Helminthoidichnites*), typically with high density (Fig. 12.13). Tunnel networks (e.g., *Vagorichnus*) and microbial mat textures were observed at the base of some coarsening-upwards sandstones (Fig. 12.14d). Mammal footprints produced in soupy, saturated substrates are often present within rippled very fine-grained sandstones of the subaerially exposed portions of the successions (Fig. 12.6). This facies also preserves very small (~1 mm) iron-stained root marks, and is interpreted to represent the marshy paludal zone where siliciclastics initially built out into the lake or into areas on the surrounding plain with

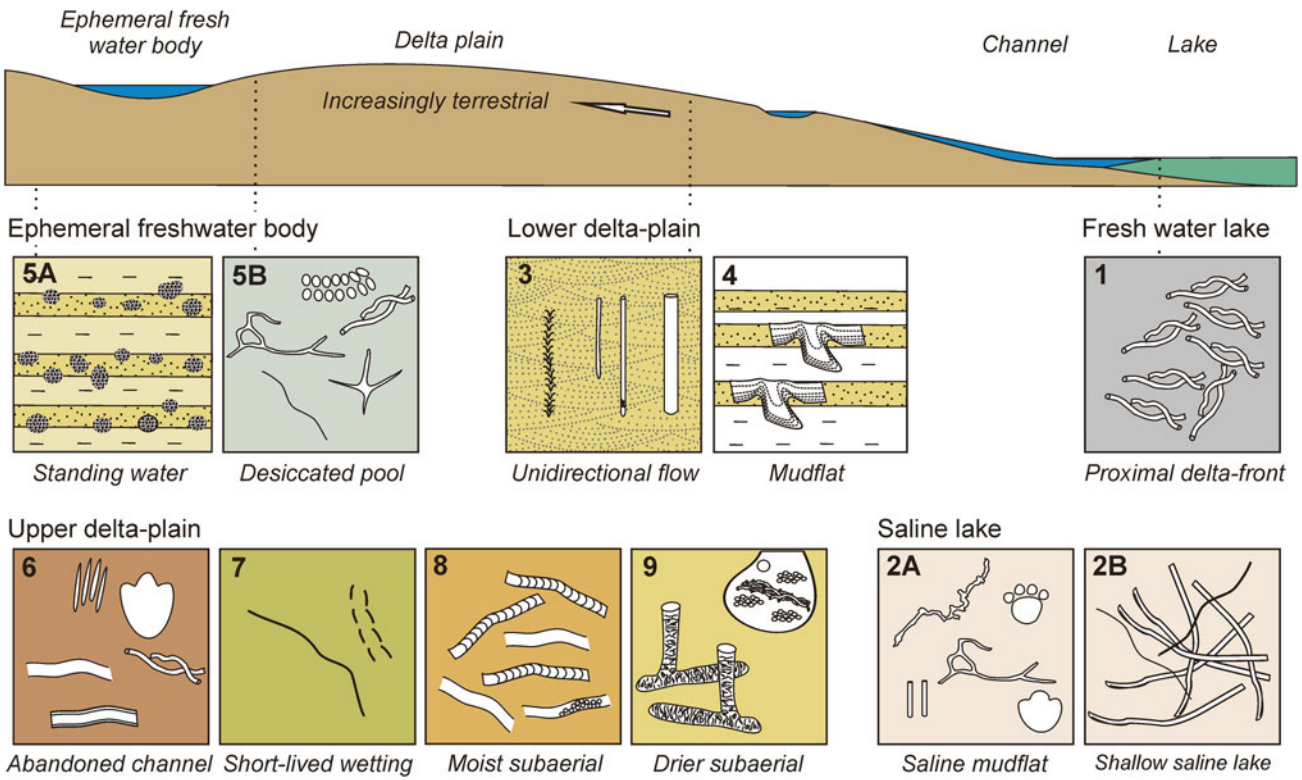

Fig. 12.16 Schematic representation of trace fossil suites in lacustrine and deltaic facies of the underfilled Wilkins Peak Member in the Bridger subbasin. Trace suite numbers correspond to those represented in the stratigraphic sections in Fig. 12.16 and Fig. 12.19. See (Scott 2010) for full description of the trace types

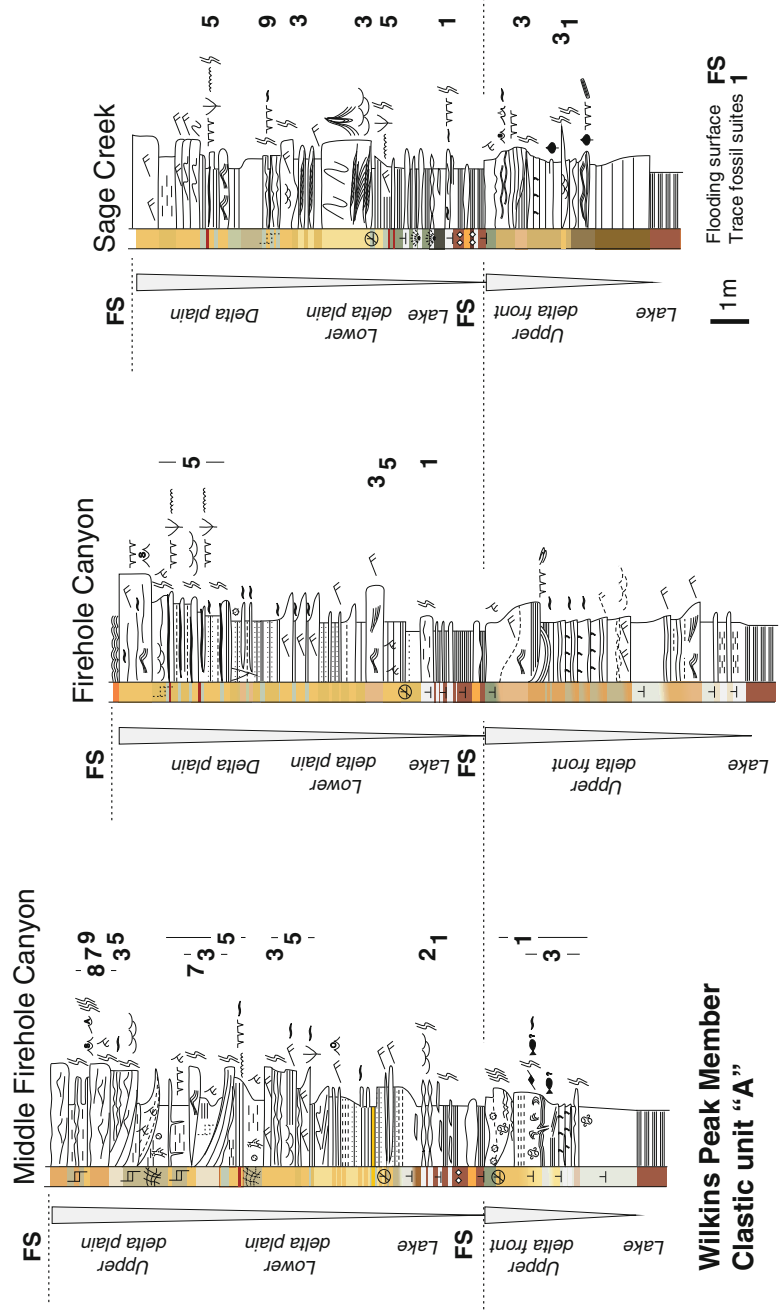

Fig. 12.17 Measured stratigraphic sections of the deltaic "A" sandstone unit in the basin center Wilkins Peak Member in the Bridger subbasin. Trace suite numbers correspond to those shown in Fig. 12.15. See Scott (2010) for a full description of the trace types and lithofacies. Colors shown represent actual color

standing water, distal to the trunk channels that supplied the arkosic sediment.

The uppermost parasequences in the arkosic sandstones preserve terrestrial trace fossils near the lake center in the Bridger subbasin, and provide evidence of well drained substrates possibly related to high topographical gradients in the uppermost portions of fans (Fig. 12.11). Meniscate backfilled burrows in three size modes (e.g., ~4, ~7, and ~15–25 mm diameter) were probably produced by insects (cf. Counts and Hasiotis 2009), and are the most common traces in these settings. Other traces, also likely produced by insects, include *Ancorichnus*, *Steinichnus* (Fig. 12.11b), and *Planolites*. In rare examples, social insect nests, probably produced by ants, are preserved in the uppermost portions of the clastic wedges (Fig. 12.11a). Some facies interpreted to represent small pools of standing water on the delta plain preserve a trace fossil assemblage typically composed of bird footprints, simple burrows produced in soft substrates (e.g., *Planolites*; Fig. 12.14c), insect trackways in soupy substrates (Fig. 12.14b), and high-density tunnel networks, probably produced by insect larvae (Fig. 12.14a; Scott 2010).

12.4.3 Evaporitic Lake Margins and Mudflats

At the Soldier Summit area of southwestern Lake Uinta in Utah, mudflat facies composed of thinly wavy bedded carbonate mudstones with some desiccation cracks preserve beautiful examples of bird (probably produced by *Presbyornis* or *Juncitarsus*) and mammal footprints (produced by perissodactyls), along with insect trails (e.g., *Cochlichnus*) (Fig. 12.5; Curry 1957; Erickson 1967; Moussa 1968, 1970; Olson 2014). Greben and Lockley (1992) found four main types of bird tracks in this area. Vertebrate tracks are common in the Uinta basin, and in general they are much better preserved than those from similar environments in the Greater Green River basin, where evaporate pseudomorphs are present and demonstrate that the mudflats there may have been covered in salt crusts.

Mudflats and paludal marsh areas that surrounded the central parts of saline to hypersaline Lake Gosiute of Wyoming when lake levels were low are composed of calcitic sandstones and siltstones, and dolomitic siltstones and mudstones of the Wilkins Peak Member. Evidence of desiccation, reed impressions, and mm-scale iron-stained root marks accompany a low-diversity trace fossil assemblage dominated by poorly preserved vertebrate footprints (Fig. 12.8; e.g., mammal) and simple, high density trails probably produced by insect larvae (e.g., *Helminthoidichnites*; Fig. 12.13c–d). Other traces sometimes present include high density diminutive (1–2 mm diameter) vertical burrows (e.g., *Skolithos*, *Polykladichnus*; Fig. 12.13b) and large (10 mm diameter), poorly preserved horizontal, branching tunnel systems (Fig. 12.8d). Sedimentary structures provide evidence of shallow flooding of mudflats and subsequent desiccation, including wavy bedding with calcite sands and dolomitic mudstone drapes, lenticular bedding, intraclast mudchip conglomerates, and desiccation crack polygons with mudchips preserved on bedding planes.

At several localities in Wyoming, particularly in the upper Wilkins Peak Member in basin margin areas of the Bridger subbasin, lacustrine and lake-margin mudstones and siltstones preserve a low diversity, high density trace fossil assemblage dominated by horizontal meniscate backfilled burrows (e.g., *Taenidium*; Fig. 12.9a–c). In most examples, the smaller-sized (~4 mm, ~7 mm) meniscate backfilled burrows have a horizontal orientation, and are found in sediments that are very closely associated with shallow lacustrine sedimentary structures (e.g., wavy bedding). In contrast, the larger forms (~15–25 mm) typically have a vertical component and show that the substrates had been drained to approximately 0.5–1 m depths. It is these larger forms that overprint lacustrine sediments, including oil shales and organic-poor mudstones that contain no other trace fossils. In cases where only the terrestrial traces are preserved in lacustrine sediments, the lacustrine environments are interpreted to have not been suitable for burrowing organisms due to environmental stresses such as

low oxygen levels, hypersalinity, or high turbidity. Examples of this association also include the Lower LaClede Member in the southern Bridger subbasin (Fig. 12.4c), and in Lake Uinta from Colorado (cf. Tänasvuu-Milkeviciene and Sarg 2015, *this volume*).

In subaerially exposed sand flat deposits of the Buff Marker, Lower LaClede Bed, Laney Member, Washakie subbasin, Wyoming, a low-diversity, low-density trace fossil assemblage is preserved, together with reverse-graded sandstones, wavy bedded and desiccation-cracked sandstones, evaporitic horizons, synaeresis cracks, low-amplitude symmetrical ripples, and microbial-mat surface textures (e.g., gas escape structures, wrinkle marks). The traces were produced in saturated and probably microbially bound substrates adjacent to the lake, and include *Planolites*, *Helminthoidichnites*, and *Cochlichnus* (~4 mm diameter).

12.4.4 Shallow Evaporitic Lacustrine

A low diversity assemblage of trace fossils characterizes shallow lacustrine areas in the evaporitic carbonate and dolomite lakes. In basin center areas of underfilled basins, high density simple trails are typically associated with wavy bedded siltstones and mudstones of the low-gradient littoral zone, and form an assemblage very similar to the subaerially exposed mudflats to which they are adjacent (Fig. 12.13c–d). In these settings, dolomitic mudstones may also contain a variety of different "shrinkage" or synaeresis cracks. Although these cracks appear similar to trace fossils, their origin is uncertain and they are likely best attributed to the shrinkage of the dolomitic muds or clays in saline waters, or to the shrinkage of microbial mats, or, in many cases, may be ascribed to evaporate pseudomorphs of bladed evaporates such as trona. These enigmatic structures are also present throughout these facies in the Green River basins (B. Töro, personal communication 2013).

The southern margin of the Bridger subbasin contains quartzose sandstones sourced from the Uinta Uplift, which were deposited in marginal lacustrine, shallow lacustrine, and fluvio-deltaic environments in Tipton and Wilkins Peak members. Shorelines of the expanded Lake Gosiute during Wilkins Peak time reached the southern margin of the underfilled lake-type, but were nevertheless saline to hypersaline except in areas where fluvial systems fed the lake. In shoreline areas with small channels at the southern basin margin, the trace fossil assemblage is relatively diverse for underfilled basins (Figs. 12.18, 12.19), and includes: (1) high density *Planolites* (~3 mm diameter) associated with microbial mat textures (wrinkle marks); (2) large branching burrows with burrow wall ornamentation (similar to *Scoyenia*); (3) vertical burrows up to 10 mm in diameter, soft walled burrow networks (cf. *Thalassinoides*); (4) vertebrate footprints produced in soft substrates (probably by rhinos or small uintatheres); and (5) medium-sized (~7–10 mm diameter) meniscate backfilled burrows that overprint the assemblage following lake-level drop. The sedimentary evidence, such as high amplitude symmetrical ripples also suggest that the depositional gradient may have been relatively high, allowing for increased fetch (Fig. 12.19d).

Trace fossils help to demonstrate the different salinities of the lake at different times and in laterally heterogeneous lake-margins. Higher in the section at the southern Bridger subbasin, shallow lacustrine deposits in the Wilkins Peak Member show evidence of sheet flooding from low-gradient areas into the lake (Smoot 1983). The trace fossil assemblage is low diversity, and is represented by large vertically oriented meniscate backfilled burrows (*Taenidium baretti)* that penetrate lacustrine sediments from subaerially exposed lake margin areas following lake level drop. In this example, no soft-substrate traces produced contemporaneously with initial deposition were observed, and the assemblage may signify that the lake waters were relatively saline (Fig. 12.20).

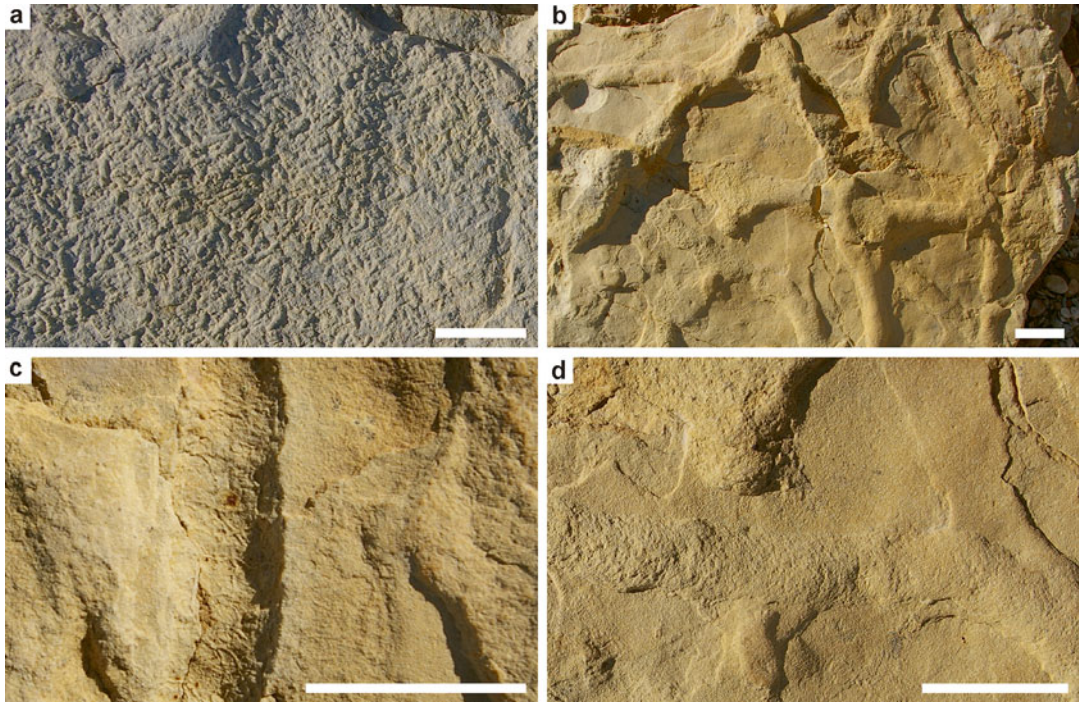

Fig. 12.18 Expanded lake facies and trace fossils at the southern basin margin in the underfilled Wilkins Peak Member of the Bridger subbasin (Pipeline area). All scale bars 2 cm. (**a**) High density cross-cutting simple horizontal traces (*Planolites*) on rippled bedding plane. Traces associated with microbial mat textures. (**b**) Branching horizontal burrow systems (cf. *Thalassinoides*) produced in soft substrates. (**c**) Linear features preserved on burrow wall with relatively sharp margins produced in soft substrate (cf. *Scoyenia*; compare with D'Alessandro et al. 1987). (**d**) Meniscate backfilled burrow (*Taenidium*) cross-cutting burrow network in (C)

12.4.5 Shallow Freshwater Lacustrine

Shallow freshwater lacustrine deposits, characterizing the overfilled lake-type and expanded lakes of balanced fill basins, have been investigated for trace fossils in a small number of localities (e.g., Bohacs et al. 2007). Examples show the preservation of *Planolites* and *Palaeophycus*, vertical burrows (*Skolithos*), escape traces, U-shaped burrows (*Arenicolites*), and resting or locomotion traces of bivalves (e.g., *Lockeia*), all produced in soft substrates. The producers likely include insects (e.g., mayfly larvae), oligochaetes, gastropods, and/or bivalves. Quartzose sandstones forming fluvio-lacustrine deposits of the Tipton Member in the southern Bridger subbasin contain abundant plant material along horizons that are entirely bioturbated with *Planolites* and *Palaeophycus* (Fig. 12.3). The Cottonwood Creek Delta of the Tipton Member in the Washakie subbasin also preserves soft-substrate burrows that were interpreted to have been produced by crustaceans and worms by Roehler (1988).

12.4.6 Sublittoral to Profundal Lacustrine

Sublittoral to profundal lacustrine trace fossils are uncommon, although fish swimming trails (e.g., *Undichna*), branching tunnel networks (e.g., *Vagorichnus*-like), and tiny sinuous trails

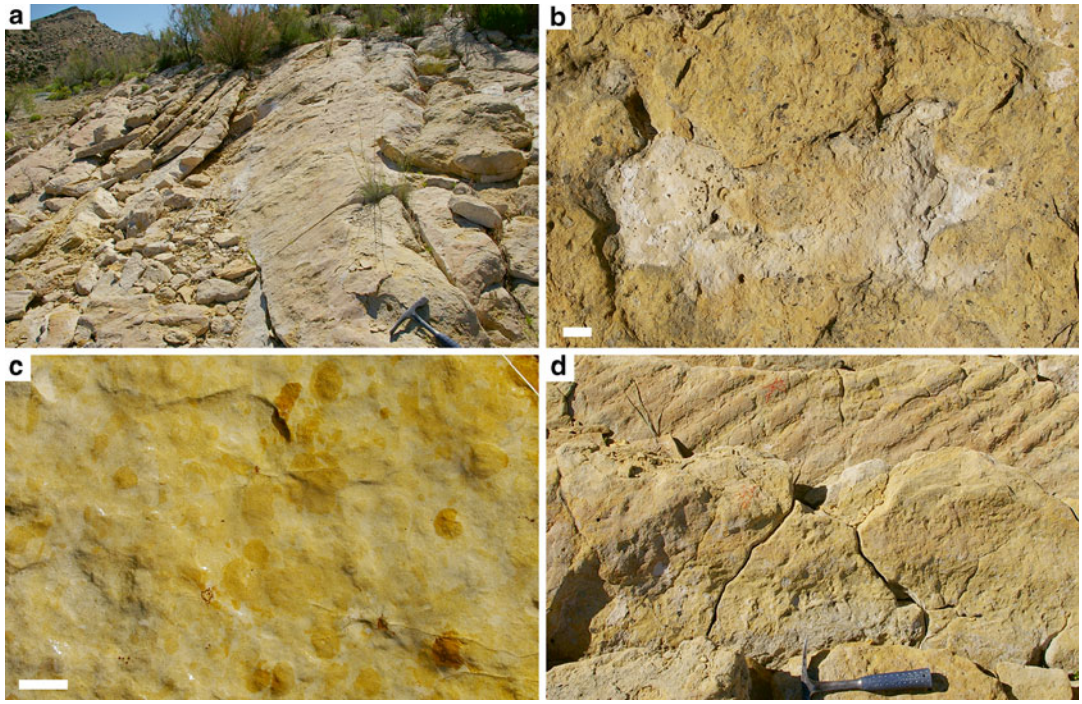

Fig. 12.19 Expanded lake facies and trace fossils at the southern basin margin in the underfilled Wilkins Peak Member of the Bridger subbasin (Pipeline area). All scale bars 2 cm. (**a**) Structureless, bioturbated quartzose sandstone unit overlain by wave-rippled beds. Hammer for scale. (**b**) Mammal footprints (perissodactyl) in soft sandy substrate. Note 3-toed footprint towards right and 3-toed footprint at left. (**c**) Entirely bioturbated sandstone shown in (F). Most burrows have structureless fill; some have meniscate fill. (**d**) View of symmetrical ripples in sandstones shown in (F). Hammer for scale. Note burrow networks, including meniscate backfilled burrows, in wave-rippled sandstones shown in foreground

(*Cochlichnus*) likely produced by insects and/or nematodes are found in the fish-fossil beds of Fossil Lake, Fossil Basin, Wyoming (e.g., Loewen and de Gibert 1999; Martin et al. 2010; A. Äase, personal communication 2013). Some of the fish swimming marks show feeding impressions on the sediment surface, and were produced by the sucker-like *Notogoneus* (Martin et al. 2010). Thin sandstone beds intercalated with oil shales below the Mahogany Zone in the Soldier Summit area of the Uinta basin contain large branching networks on the base of several beds, which are similar to *Thalassinoides* and may have been produced by crustaceans. Small bilobed trails (~5 mm diameter), possibly produced by aquatic insects, are associated with the larger networks (A. Martin, pers. comm. 2007). Very small (~2 mm diameter) simple trails (e.g., *Helminthoidichnites*) are preserved in sublittoral deposits of laminated organic-rich wavy-bedded dolomitic siltstones overlain by deltaic siliciclastics in the Wilkins Peak Member of the Bridger subbasin (Fig. 12.13d).

Very thinly laminated oil shales, such as in the Rife Bed of the Tipton Member and the lower LaClede Bed of the Laney Member in the Greater Green River basin, have not revealed trace fossils preserved in these profundal facies. If trace fossils are preserved in sublittoral facies (e.g., thin wavy bedded and laminated siltstones and organic-rich mudstones), they signify that the bottom waters of the lakes were not anoxic, although they may have been oxygen-poor. Most of the trace fossils found in these facies are small (less than 5 mm diameter), are present on bed-

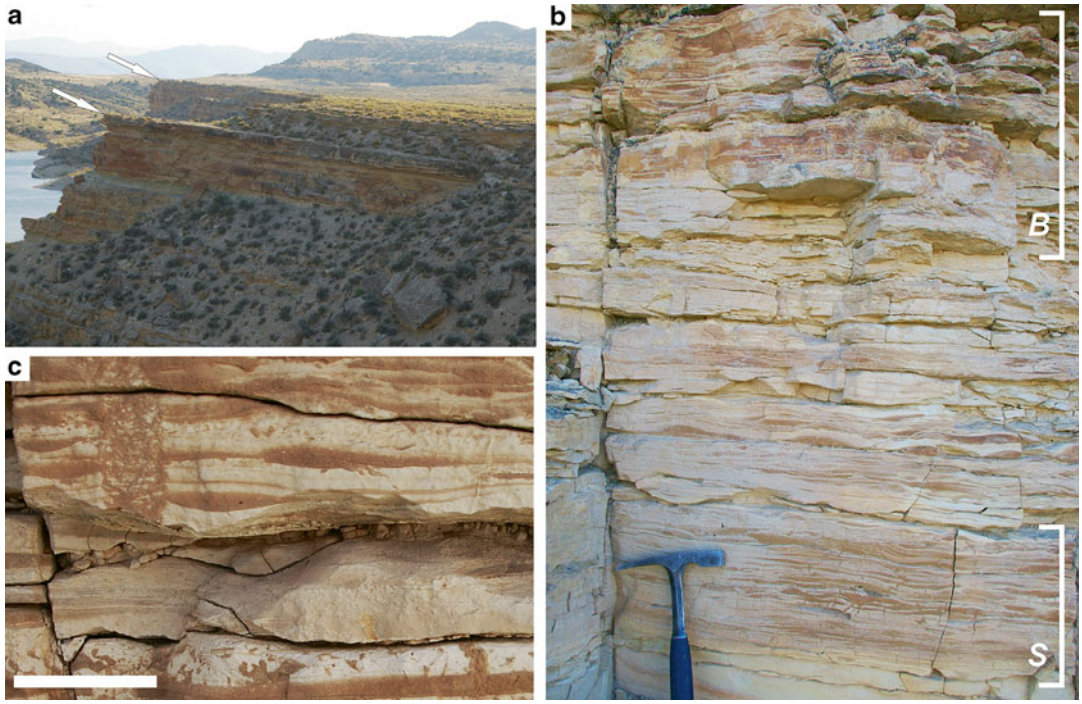

Fig. 12.20 Stratigraphic surface with trace fossils at the southern margin of the Bridger subbasin, Pipeline area. (**a**) Two shallowing upwards units (*arrows*) bioturbated by meniscate backfilled burrows from upper surfaces. (**b**) Upper part of top unit, showing laminated carbonate mudstones at base, wavy bedded carbonates and clastics, and bioturbated uppermost beds. Hammer for scale. (**c**) Close-up of vertically oriented burrow (*Taenidium barretti*) with angular aggregate fill. Shrinkage cracks in white carbonate bed below

ding planes, and are not easily observed in vertical sections or core. In some cases, larger (up to 2 cm diameter), meniscate backfilled burrows (e.g., *Taenidium*) are preserved within lacustrine oil shales (e.g., Tänasvuu-Milkeviciene and Sarg this volume), but they probably represent the subaerial exposure of the shales or overlying beds.

12.5 Utility of Trace Fossils for Stratigraphy and the Reconstruction of Environments

Trace fossil assemblages can be applied to the interpretation of environmental conditions prevalent in sedimentary paleoenvironments because animals and plants respond to these conditions (e.g., salinity, water saturation, substrate drainage). The composition of the assemblages tends to be recurrent in different environments, where animal and plant communities repeatedly co-occur. The distribution of different trace fossil assemblages, whether heterogeneous or relatively homogeneous along a lake margin for example, is a useful consideration for the interpretation of lateral changes in environmental conditions. Heterogeneity is typically more pronounced in more extreme settings (e.g., Scott et al. 2009), such as those around saline to hypersaline Lake Gosiute during the deposition of the Wilkins Peak Member (Scott 2010). Morphological features of individual traces, such as those that provide clues to substrate conditions (e.g., degree of water saturation), are also tools that can be used together with sedimentology to interpret environmental conditions (e.g., substrate

drainage). The bioturbation intensity and depth of burrowing from a horizon are also important for interpreting sedimentation rate, depth of the water table, and hiatuses in sedimentation. The examples in the Green River and correlative formations given in this chapter illustrate the utility of trace fossils for recognizing these parameters and using them for environmental interpretations.

In settings with limited accommodation, the overprinting of more than one trace fossil assemblage on a single horizon represents a discontinuity surface useful for correlation and the sequence stratigraphic interpretation of the basin fill. Two examples of contrasting vertical packaging of sedimentary facies and trace fossil assemblages from the basin margin and basin center areas during deposition of the Wilkins Peak Member illustrate contrasting scenarios for the application of trace fossils to basin analysis and interpretation of subsidence rates in underfilled lake-type basins.

First, resistant and laterally extensive surfaces that are bioturbated by meniscate backfilled burrows illustrate this application to the stratigraphy of the Green River Formation, including a ~2.5 m-thick coarsening upwards succession of the Wilkins Peak Member in the southern Bridger subbasin (Fig. 12.20). The succession shallows upwards from laminated lake-beds, to rippled sandstones interpreted as underflows, to wavy bedded shallow water deposits, to desiccation cracked interbedded mudstones and sandstones interpreted as the eulittoral zone. The uppermost horizon is the colonization surface for the burrowers producing the meniscate backfilled burrows (*Taenidium baretti*). The monospecific trace fossil assemblage in this example shows that the conditions within the lake were not suitable for burrowers, but that upon subaerial exposure of the lacustrine sediments and water table drop, air-breathing organisms could colonize the substrate. Bioturbation intensity is highest (BI = 3–5) at the uppermost horizon and burrows are oriented both horizontally and vertically to depths of up to ~1.5 m. The horizon is relatively indurated and resistant to erosion, and forms a surface that can be traced towards the lake center for almost 2 km in outcrop. The lakeward extension of this surface preserves an unusual texture interpreted as being produced by the trampling of birds, possibly the flamingo-like *Juncitarsus* or *Presbyornis* (cf. Scott et al. 2012b) and large mammal footprints with symmetrical ripples (Fig. 12.21).

Second, progradational stacking patterns of shallow evaporitic lacustrine to delta plain environments of the basin center are recognized by their closely associated lithofacies and trace fossil assemblages (Scott 2010; see "Deltas" section above). The building out of the clastic units onto exposed evaporitic mudflats shows that siliciclastic deposition into the carbonate lake may be related to an increase in precipitation, which contributed to the transport of clastics into an otherwise solute-dominated lake basin (Smith et al. 2014). Each progradational succession comprises two or more shallowing upwards cycles (parasequences) representing progradation during lacustrine lowstands (Figs. 12.17, 12.22). These stacked successions are overlain by sharp flooding surfaces to kerogen-rich oil shales in topographically higher areas, or they are gradationally overlain by rippled lacustrine deposits in flooded channels (Fig. 12.22). Towards the tops of each of the progradational cycles, an abundance of terrestrial burrow types help to show increasing water table depths and terrestrialization of the deposits below the next carbonate lake flooding surface.

In the basin center, gradual facies changes from lacustrine to terrestrial environments in these siliciclastic packages up to 25 m in thickness represent the net accumulation of sediments and the vertical stacking of gradually changing trace fossil assemblages (Scott 2010). Rare overprinting of trace fossils produced in different sedimentary environments is observed in these basin-center deposits, which suggests that it was a high accommodation potential setting with abundant sediment supply during lacustrine lowstands. The uppermost subaerial facies of these clastic units could thus be considered as maximum regressive surfaces, marking the changes from lowstands to expanded lakes. In the basin margin examples in contrast, burrows produced by air-breathing terrestrial organisms overprinted

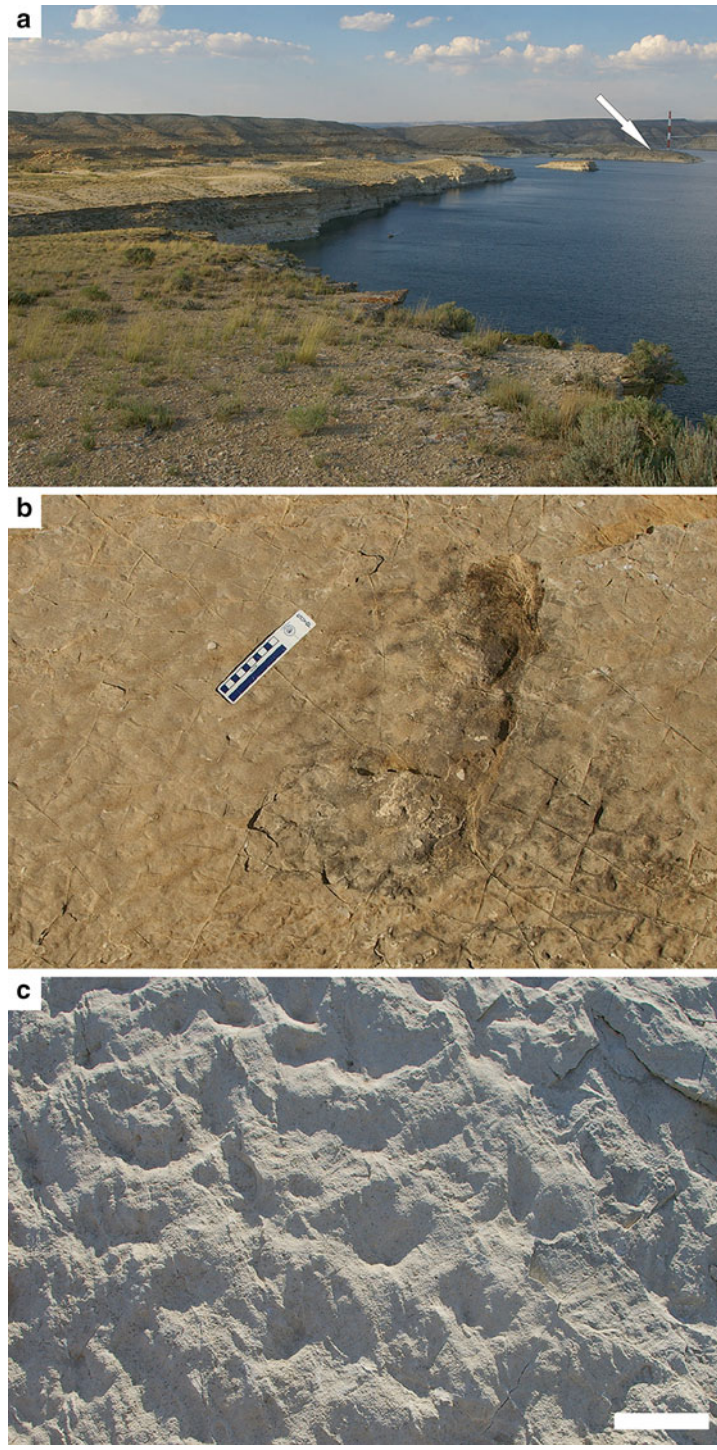

Fig. 12.21 Stratigraphic surface with trace fossils at the southern margin of the Bridger subbasin, Pipeline area. (**a**) The surface shown in Fig. 12.20a can be traced in outcrop for almost 2 km (*arrow*) towards basin center. (**b**) Large mammal footprints (produced by *Uintatherium*) in rippled substrate at basinward locality (*arrow in e*). Scale is in cm. (**c**) Surface texture at basinward locality (*arrow in e*) interpreted as soupy lacustrine muds trampled by gregarious birds such as *Presbyornis* or *Juncitarsus*. Compare with modern flamingo-trampled surface at Lake Bogoria (Scott et al. 2012b). Note moon-shaped morphology of posterior part of tracks showing movement of birds in one direction, and linear oriented "splash marks". Scale bar is 5 cm

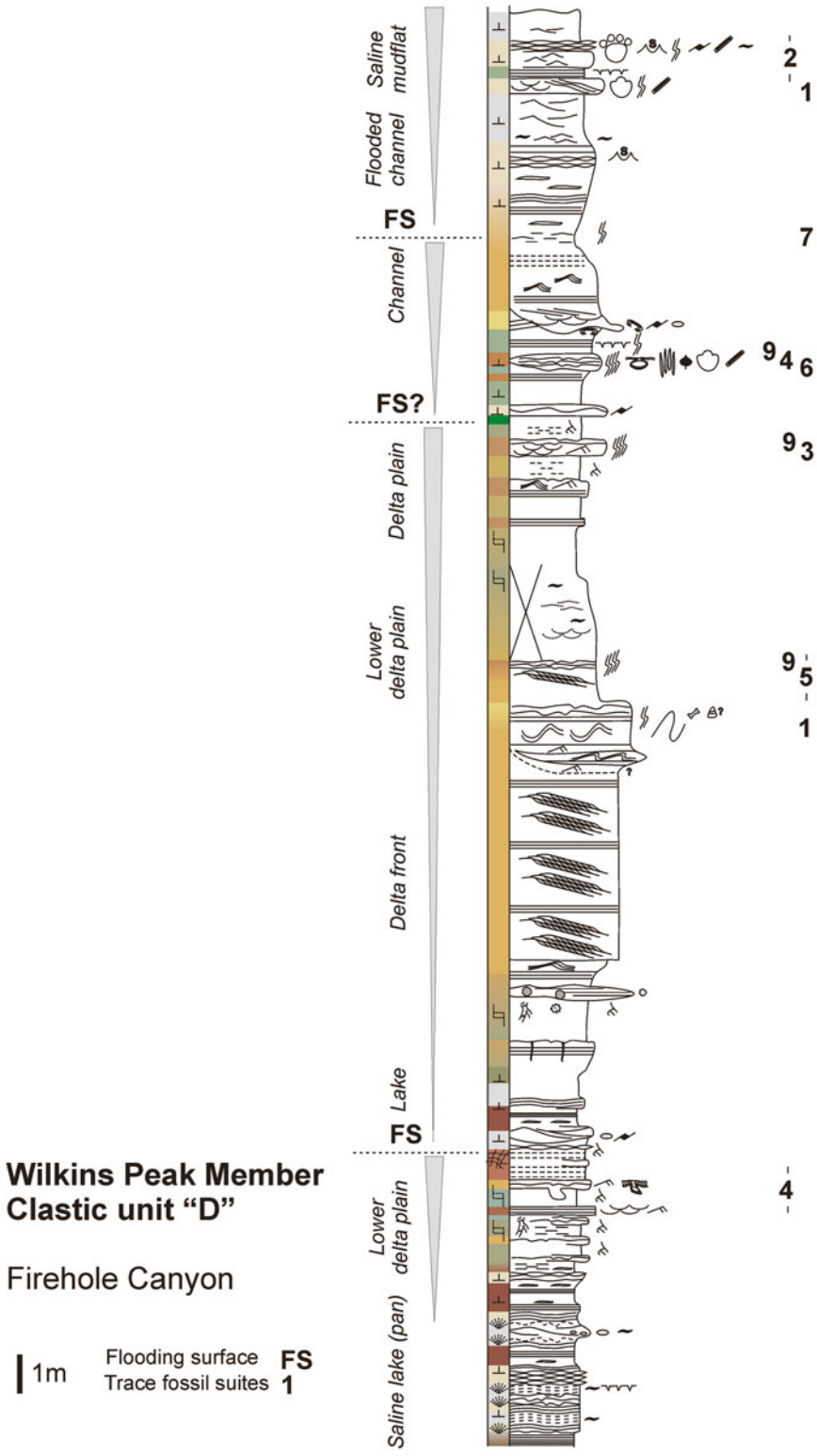

Fig. 12.22 Measured stratigraphic section of the deltaic "D" sandstone unit in the basin center Wilkins Peak Member in the Bridger subbasin. Trace fossil suite numbers correspond to those shown in Fig. 12.15. See Scott (2010) for a full description of the trace types and lithofacies. Colors shown represent actual color

lacustrine deposits when lake-level dropped, but were not accompanied by an influx of sediment. This may signify a decrease in precipitation leading to lake-level drop at the transition from lacustrine highstand to lowstand, and the basin margin bioturbated surface could thus be considered a sequence boundary.

12.6 Conclusions

Trace fossil assemblages in the Green River and correlative formations, like marine and other continental assemblages, represent the response of organisms to the environmental conditions prevalent in different depositional settings. Lacustrine sediments also provide evidence of environmental conditions such as hydrochemistry (e.g., evaporite deposits). Depositional environments such as fluvial channels and deltaic areas, bringing freshwater to otherwise saline lake margins, for example, are typically associated with trace fossil assemblages that are distinct from adjacent evaporitic areas, as described here for deltaic and evaporitic lake margin environments. In the Green River and correlative formations, there is a close relationship between the processes affecting deposition and the processes affecting the trace fossil assemblage in lacustrine and lake-margin settings. With pedogenically modified terrestrial deposits, however, the trace fossil assemblages are more closely related to the pedogenic conditions than to the original environment of deposition.

Terrestrial and lacustrine trace fossils have great potential as tools for paleoenvironmental interpretations of sedimentary deposits, and as important markers of stratigraphically useful horizons. Most ichnological research that focuses on the basin-scale distribution of trace fossil assemblages and integration with the lake-type model has been conducted in the Greater Green River basin of Wyoming and Colorado (e.g, Hasiotis and Honey 2000; Bohacs et al. 2007; Scott 2010). Most of the work done in the Lake Uinta basins has focused on vertebrate footprints (e.g., Curry 1957; Erickson 1967; Moussa 1968; Olson 2014), although some research has incorporated invertebrate trace fossils and facies analyses (D'Alessandro et al. 1987; Golab 2010; Sato et al. 2014). The stratigraphic application of the trace fossils in the Green River and correlative formations has been investigated by some authors (Bohacs et al. 2007; Scott 2010). Much work remains, however, to continue to describe case studies and develop models that improve the methodology and application of trace fossils to understanding the Green River lakes systems, as well as paleoecology in these basins during the Early to middle Eocene.

Acknowledgments This work has benefited from discussions and/or fieldwork with Arvid Aäse, Kevin Bohacs, Luis Buatois, Paul Buchheim, Alan Carroll, Terri Graham, Leroy Leggitt, Martin Lockley, Gabriela Mángano, Tony Martin, Robin Renaut, Balazs Töro, and Eric Williams. We are very grateful for their contributions. J.J.S. was supported by NSERC grants to Robin Renaut (Research Grant RG629-03) and Luis Buatois (Discovery Grant # 311726–05 and –08), a NSERC PGS-D scholarship and a NSERC Post-Doctoral Fellowship, by graduate student field research grants from the AAPG, GSA, and IAS, and by a research grant from Mount Royal University. National Science Foundation grants EAR-0230123, EAR-0114055 and EAR-0516760, the Donors of the Petroleum Research Fund of the American Chemical Society, Chevron, ConocoPhillips, summer research grants from GSA, AAPG, and Sigma Xi, and the Bailey Distinguished Graduate Research Fellowship provided funding for M.E. Smith. We are grateful for the comments and suggestions by reviewer Tony Ekdale, which improved the text, content, and presentation of the manuscript.

References

Bedatou E, Melchor RN, Genise JF (2009) Complex palaeosol ichnofabrics from Late Jurassic-Early Cretaceous volcaniclastic successions of Central Patagonia, Argentina. Sediment Geol 218:74–102

Bohacs KM, Carroll AR, Neal JE, Mankiewicz PJ (2000) Lake-basin type, source potential, and hydrocarbon character: an integrated sequence-stratigraphic–geochemical framework. In: Gierlowski-Kordesch EH, Kelts KR (eds) Lake Basins through space and time, vol 46, AAPG studies in Geology. American Association of Petroleum Geologists, Tulsa, Oklahoma, pp 3–34

Bohacs KM, Hasiotis ST, Demko TM (2007) Continental ichnofossils of the Green River and Wasatch Formations, Eocene, Wyoming: a preliminary survey, proposed relation to lake-basin type, and application

to integrated paleo-environmental interpretation. Mt Geol 44:79–108

Bradley WH, Eugster HP (1969) Geochemistry and paleolimnology of the trona deposits and associated authigenic minerals of the Green River Formation of Wyoming, USGS professional paper 496B. United States Geological Survey, Denver, Colorado, p 71

Buatois LA, Mángano MG (2004) Animal-substrate interactions in freshwater environments: applications of ichnology in facies and sequence stratigraphic analysis of fluvio-lacustrine successions. In: McIlroy D (ed) The application of ichnology to palaeoenvironmental and stratigraphic analysis, Geological society special publications, v. 228. The Geological Society Publishing House, Bath, UK, pp 311–333

Buatois LA, Mángano MG (2007) Invertebrate ichnology of continental freshwater environments. In: Miller W (ed) Trace fossils: concepts, problems, prospects. Elsevier, Amsterdam, pp 285–323

Buatois LA, Mángano MG (2009) Applications of ichnology in lacustrine sequence stratigraphy: potential and limitations. Palaeogeogr Palaeoclimatol Palaeoecol 272:127–142

Carmona NB, Ponce JJ, Wetzel A, Bournod CN, Cuadrado DG (2012) Microbially induced sedimentary structures in Neogene tidal flats from Argentina: palaeoenvironmental, stratigraphic and taphonomic implications. Palaeogeogr Palaeoclimatol Palaeoecol 353–355:1–9

Carroll AR, Bohacs KM (1999) Stratigraphic classification of ancient lakes: balancing tectonic and climatic controls. Geology 27:99–102

Chetel LM, Carroll AR (2010) Terminal infill of Eocene Lake Gosiute, Wyoming, U.S.A. J Sediment Res 80:492–514

Cohen AS (2003) Paleolimnology. Oxford University Press, Oxford, p 500

Counts JW, Hasiotis ST (2009) Neoichnological experiments with masked chafer beetles (Coleoptera: Scarabaeidae): implications for backfilled continental trace fossils. Palaios 24:74–91

Culbertson WC (1961) Stratigraphy of the Wilkins Peak Member of the Green River Formation, Firehole Basin Quadrangle, Wyoming. In: Short papers in the geological and hydrologic sciences, U.S. geological survey professional paper 424-D. United States Geological Survey, Denver, Colorado, pp 170–173

Curry HD (1957) Fossil tracks of Eocene vertebrates, southwestern Uintah Basin. In: Eighth annual field conference, Intermountain Association of Petroleum Geologists, Utah, pp 42–47

D'Alessandro A, Ekdale AA, Picard MD (1987) Trace fossils in fluvial deposits of the Duchesne River Formation (Eocene), Uinta Basin, Utah. Palaeogeogr Palaeoclimatol Palaeoecol 61:285–301

Davis RB, Minter NJ, Braddy SJ (2007) The neoichnology of terrestrial arthropods. Palaeogeogr Palaeoclimatol Palaeoecol 255:284–307

Deardorff DL, Mannion LE (1971) Wyoming trona deposits. In: Contributions to geology, vol 10, Trona issue. University of Wyoming, Laramie, pp 25–38

Dutchak AR (2010) Mammalian faunal change during the early Eocene climatic optimum (Wasatchian and Bridgerian) at Raven Ridge in the Northeastern Uinta Basin, Colorado and Utah. PhD dissertation, University of Colorado, Boulder

Erickson BR (1967) Fossil bird tracks from Utah: science museum of Minnesota. Mus Obs 5:140–146

Foster JR (2001) Salamander tracks (*Ambystomichnus*) from the Cathedral Bluffs Tongue of the Wasatch Formation (Eocene), northeastern Green River basin, Wyoming. J Paleontol 75:901–904

Gingras MK, MacEachern JA, Dashtgard SE (2011) Process ichnology and the elucidation of physico-chemical stress. Sediment Geol 237:115–134

Golab JA (2010) Ichno-pedological facies of the Colton and lower-middle Green River formations: implications for continental paleoclimate studies. M.Sc thesis, Colorado School of Mines

Greben R, Lockley M (1992) Vertebrate tracks from the Green River Formation, eastern Utah: implications for paleoecology: abstracts with programs, Geological Society of America, Rocky Mountain section, vol 24, p 16

Hamblin AH, Sarjeant WAS, Spalding DD (1998) A remarkable mammal trackway in the Uinta Formation (late Eocene) of Utah. Brigham Young Univ Geol Stud 43:9–18

Hamblin AH, Sarjeant WAS, Spalding DAE (1999) Vertebrate footprints in the Duchesne River and Uinta Formations (middle to late Eocene), Uinta Basin, vol 99–1. Utah Geological Survey, Miscellaneous Publications, Salt Lake City, pp 443–454

Hasiotis ST (2007) Continental ichnology: fundamental processes and controls on trace fossil distribution. In: Miller W (ed) Trace fossils: concepts, problems, prospects. Elsevier, Amsterdam, pp 268–284

Hasiotis ST, Honey JG (2000) Paleohydrologic and stratigraphic significance of crayfish burrows in continental deposits: examples from several Paleocene Laramide basins in the Rocky Mountains. J Sediment Res 70:127–139

Lamond RE, Tapanila L (2003) Embedment cavities in lacustrine stromatolites: evidence of animal interactions from Cenozoic carbonates in U.S.A. and Kenya. Palaios 18:445–453

Laporte LF, Behrensmeyer AK (1980) Tracks and substrate reworking by terrestrial vertebrates in Quaternary sediments of Kenya. J Sediment Petrol 50:1337–1346

Leggitt VL (2007) Freshwater facies of the saline Wilkins Peak Member of the Green River Formation. 4th international limnogeology congress, Barcelona, Spain, Abstracts, p 115

Leggitt VL, Cushman RA (2001) Complex caddisfly-dominated bioherms from the Eocene Green River Formation. Sediment Geol 145:377–396

Leggitt VL, Cushman RA (2003) Flamingo nest mounds from a crocodilian nesting site in the Eocene Wasatch Formation: Lincoln County, Wyoming. J Vertebr Paleontol 23(3):71A

Leggitt VL, Loewan MA (2002) Eocene Green River Formation "*Oocardium* tufa" reinterpreted as complex arrays of calcified caddisfly (Insecta: Trichoptera) larval cases. Sediment Geol 148:139–146

Leggitt VL, Biaggi RE, Buchheim HP (2007) Palaeoenvironments associated with caddisfly-dominated microbial-carbonate mounds from the Tipton Shale Member of the Green River Formation: Eocene Lake Gosiute. Sedimentology 54:661–699

Lockley MG, Ritts BD, Leonardi G (1999) Mammal track assemblages from the early tertiary of China, Peru, Europe and North America. Palaios 14:398–404

Loewen MA, Gibert JM de (1999) The first occurrence of Cenozoic fish trails (*Undichna*) from Eocene Fossil Lake, Wyoming. 59th annual meeting, Society of Vertebrate Paleontology. J Vertebr Paleontol 19(3):59A

Martin AJ, Vazques-Prokopec GM, Page M (2010) First known feeding trace of the Eocene bottom-dwelling fish *Notogoneus osculus* and its paleontological significance. PLoS One 5:1–8

Marty D, Strasser A, Meyer CA (2008) Formation and taphonomy of human footprints in microbial mats of present-day tidal flat environments: implications for the study of fossil footprints. Ichnos 16:127–142

Moussa MT (1968) Fossil tracks from the Green River Formation (Eocene) near Soldier Summit, Utah. J Paleontol 42:1433–1438

Moussa MT (1970) Nematode fossil trails from the Green River Formation (Eocene) in the Uinta Basin, Utah. J Paleontol 44:304–307

Olson SL (2014) Tracks of a stilt-like bird from the Early Eocene Green River Formation of Utah: possible earliest evidence of the Recurvirostridae (Charadriiformes). Waterbirds 37:340–345

Pemberton SG, MacEachern JA, Dashtgard SE, Bann KL, Gingras MK, Zonneveld J-P (2012) Shorefaces. In: Knaust D, Bromley R (eds) Trace fossils as indicators of sedimentary environments, Developments in sedimentology 64. Elsevier, Amsterdam, pp 563–603

Roehler HW (1988) Geology of the Cottonwood Creek Delta in the Eocene Tipton Tongue of the Green River Formation, southeast Washakie Basin, Wyoming. US Geol Surv Bull 1669-A:14

Sarjeant WAS, Reynolds RE, Kissel-Jones MM (2002) Fossil creodont and carnivore footprints from California, Nevada and Wyoming. In: Reynolds RE (ed) Between the Basins: exploring the Western Mojave and Southern Basin and Range Province, Desert studies consortium. California State University, Fullerton, pp 37–50

Sato T, Chan MA, Ekdale AA (2014) Fluvial-lacustrine ichnofacies of the Eocene Uinta and Duchesne River formations, northern Uinta Basin. In: Annual meeting, Abstracts. Geological Society of America Abstracts with Programs, v. 46, p. 773

Schomacker ER, Vestheim Kjemperur AV, Nystuen JP, Jahren JS (2010) Recognition and significance of sharp-based mouth-bar deposits in the Eocene Green River Formation, Uinta Basin, Utah. Sedimentology 57:1069–1087

Scott JJ (2010) Saline lake ichnology: Kenya Rift Valley and Eocene Green River Formation, Wyoming. PhD dissertation, University of Saskatchewan

Scott JJ, Renaut RW, Buatois LA, Owen RB (2009) Biogenic structures in exhumed surfaces around saline lakes: an example from Lake Bogoria, Kenya Rift Valley. Palaeogeogr Palaeoclimatol Palaeoecol 272:176–198

Scott JJ, Renaut RW, Owen RB (2010) Taphonomic controls on animal tracks at saline, alkaline Lake Bogoria, Kenya Rift Valley: impact of salt efflorescence and clay mineralogy. J Sediment Res 80:639–665

Scott JJ, Buatois LA, Mangano MG (2012a) Lacustrine environments. In: Knaust D, Bromley R (eds) Trace fossils as indicators of sedimentary environments, Developments in sedimentology 64. Elsevier, Amsterdam, pp 379–417

Scott JJ, Renaut RW, Owen RB (2012b) Impacts of flamingos on saline lake margin and shallow lacustrine sediments in the Kenya Rift Valley. Sediment Geol 277–278:32–51

Scrivner PJ, Bottjer DJ (1986) Neogene avian and mammalian tracks from Death Valley National Monument, California: their context, classification, and preservation. Palaeogeogr Palaeoclimatol Palaeoecol 57:285–331

Smith JJ, Hasiotis ST, Kraus MJ, Woody DT (2008a) Relationship of floodplain ichnocoenoses to paleopedology, paleohydrology, and paleoclimate in the Willwood Formation, Wyoming, during the Paleocene-Eocene thermal maximum. Palaios 23:683–699

Smith JJ, Hasiotis ST, Kraus MJ, Woody DT (2008b) *Naktodemasis bowni*: new ichnogenus and ichnospecies for adhesive meniscate burrows (AMB), and paleoenvironmental implications, Paleogene Willwood Formation, Bighorn Basin, Wyoming. J Paleontol 82:267–278

Smith ME, Carroll AR, Singer BS (2008c) Synoptic reconstruction of a major ancient lake system: Eocene Green River Formation, western United States. Geol Soc Am Bull 120:54–84

Smith ME, Carroll AR, Scott JJ, Singer BS (2014) Early Eocene negative isotopic carbon excursions and landscape destabilization triggered by eccentricity minima. Earth Planet Sci Lett 403:393–406

Smoot JP (1983) Depositional subenvironments in an arid closed basin: the Wilkins Peak Member of the Green River Formation (Eocene), Wyoming, U.S.A. Sedimentology 30:801–827

Tänasvuu-Milkeviciene K, Sarg JF (2015) Sedimentology of the world class organic-rich lacustrine system, Piceance basin, Colorado. In: Stratigraphy and paleolimnology of the Green River Formation, Western U.S. Springer, Dordrecht, pp 153–181

Williams WD (1998) Salinity as a determinant of the structure of biological communities in salt lakes. Hydrobiologia 381:191–201

Woodburne MO, Gunnell GF, Stucky RK (2009a) Climate directly influences Eocene mammal faunal dynamics in North America. Proc Natl Acad Sci 106(32): 13399–13403

Woodburne MO, Gunnell GF, Stucky RK (2009b) Land mammal faunas of North America rise and fall during the Early Eocene Climatic Optimum, vol 1. Denver Museum of Nature & Science, Denver, Colorado, pp 1–74

Yang S-Y, Lockley MG, Greben R, Erickson BR, Lim S-K (1995) Flamingo and duck-like bird tracks from the Late Cretaceous and Early Tertiary: evidence and implications. Ichnos 4:21–34

Zachos JC, Pagani M, Sloan L, Thomas E, Billups K (2001) Trends, rhythms, and aberrations in global climate 65 Ma to present. Science 292:686–693

Zachos JC, Dickens GR, Zeebe RE (2008) An early Cenozoic perspective on greenhouse warming and carbon-cycle dynamics. Nature 451:279–283

Zonneveld J-P, Lavigne JM, Bartels WS, Gunnell GF (2006) *Lunulichnus tuberosus Ichnogen. and Ichnosp. Nov.* from the early Eocene Wasatch Formation, Fossil Butte National Monument, Wyoming: an arthropod-constructed trace fossil associated with alluvial firmgrounds. Ichnos 13:87–94

Index

M.E. Smith, A.R. Carroll (eds.), *Stratigraphy and Paleolimnology of the Green River Formation, Western USA*, Syntheses in Limnogeology 1, DOI 10.1007/978-94-017-9906-5